

---

Dépôt Institutionnel de l'Université libre de Bruxelles /  
Université libre de Bruxelles Institutional Repository  
**Thèse de doctorat/ PhD Thesis**

**Citation APA:**

Tison, J.-L. (1976). *Ice-ocean interactions in antarctica : The marine ice perspective* (Unpublished doctoral dissertation). Université libre de Bruxelles, Faculté des sciences, Bruxelles.

**Disponible à / Available at permalink :** <https://dipot.ulb.ac.be/dspace/bitstream/2013/214338/3/b3f60844-c1bf-44c1-81b4-f9daf2903a8c.txt>

---

(English version below)

Cette thèse de doctorat a été numérisée par l'Université libre de Bruxelles. L'auteur qui s'opposerait à sa mise en ligne dans DI-fusion est invité à prendre contact avec l'Université (di-fusion@ulb.be).

**Dans le cas où une version électronique native de la thèse existe, l'Université ne peut garantir que la présente version numérisée soit identique à la version électronique native, ni qu'elle soit la version officielle définitive de la thèse.**

DI-fusion, le Dépôt Institutionnel de l'Université libre de Bruxelles, recueille la production scientifique de l'Université, mise à disposition en libre accès autant que possible. Les œuvres accessibles dans DI-fusion sont protégées par la législation belge relative aux droits d'auteur et aux droits voisins. Toute personne peut, sans avoir à demander l'autorisation de l'auteur ou de l'ayant-droit, à des fins d'usage privé ou à des fins d'illustration de l'enseignement ou de recherche scientifique, dans la mesure justifiée par le but non lucratif poursuivi, lire, télécharger ou reproduire sur papier ou sur tout autre support, les articles ou des fragments d'autres œuvres, disponibles dans DI-fusion, pour autant que :

- Le nom des auteurs, le titre et la référence bibliographique complète soient cités;
- L'identifiant unique attribué aux métadonnées dans DI-fusion (permalink) soit indiqué;
- Le contenu ne soit pas modifié.

L'œuvre ne peut être stockée dans une autre base de données dans le but d'y donner accès ; l'identifiant unique (permalink) indiqué ci-dessus doit toujours être utilisé pour donner accès à l'œuvre. Toute autre utilisation non mentionnée ci-dessus nécessite l'autorisation de l'auteur de l'œuvre ou de l'ayant droit.

----- English Version -----

This Ph.D. thesis has been digitized by Université libre de Bruxelles. The author who would disagree on its online availability in DI-fusion is invited to contact the University (di-fusion@ulb.be).

**If a native electronic version of the thesis exists, the University can guarantee neither that the present digitized version is identical to the native electronic version, nor that it is the definitive official version of the thesis.**

DI-fusion is the Institutional Repository of Université libre de Bruxelles; it collects the research output of the University, available on open access as much as possible. The works included in DI-fusion are protected by the Belgian legislation relating to authors' rights and neighbouring rights. Any user may, without prior permission from the authors or copyright owners, for private usage or for educational or scientific research purposes, to the extent justified by the non-profit activity, read, download or reproduce on paper or on any other media, the articles or fragments of other works, available in DI-fusion, provided:

- The authors, title and full bibliographic details are credited in any copy;
- The unique identifier (permalink) for the original metadata page in DI-fusion is indicated;
- The content is not changed in any way.

It is not permitted to store the work in another database in order to provide access to it; the unique identifier (permalink) indicated above must always be used to provide access to the work. Any other use not mentioned above requires the authors' or copyright owners' permission.

---

A 00121

UNIVERSITE LIBRE DE BRUXELLES – FACULTE DES SCIENCES  
DEPARTEMENT DES SCIENCES DE LA TERRE ET DE L'ENVIRONNEMENT (DSTE)  
GLACIOLOGIE

# ICE-OCEAN INTERACTIONS IN ANTARCTICA: The Marine Ice Perspective



J.-L. TISON,  
Mai, 2002

Universite Libre de Bruxelles



THESE PRE

003167887

D'AGREGE DE L'ENSEIGNEMENT SUPERIEUR



**UNIVERSITE LIBRE DE BRUXELLES – FACULTE DES SCIENCES  
DEPARTEMENT DES SCIENCES DE LA TERRE ET DE L'ENVIRONNEMENT (DSTE)  
GLACIOLOGIE**

# **ICE-OCEAN INTERACTIONS IN ANTARCTICA: The Marine Ice Perspective**

**J.-L. TISON,  
Mai, 2002**

**THESE PRESENTEE POUR L'OBTENTION DU GRADE LEGAL D'AGREGE DE L'ENSEIGNEMENT SUPERIEUR**

*To my wife and twin daughters,  
for their patience,  
understanding,  
and unconditional support.*

Brussels, May 2002

## Table of contents

Acknowledgments	5
Foreword	7
1. Framework and Motivation	8
1.1. The role of ice shelves in the Antarctic Ice Sheet System	9
1.2. Modelling the response of the Antarctic Ice Sheet to climate forcing : the ice shelves status	11
1.3. Marine ice: a major by-product of Ice-Shelf/Ocean interactions	16
2. A Suitable Setting for Shallow Depths Studies of Marine Ice Properties	21
2.1. The Terra Nova Bay area	22
2.2. The Nansen Ice Sheet	24
2.3. The Hells Gate Ice Shelf	25
2.4. The Campbell Ice Tongue	30
Paper 1: <i>The Glaciological map of Hells Gate Ice Shelf (Terra Nova Bay, Antarctica)</i>	33
Paper 2: <i>A dynamical approach to explain ice structures and complex morainic genesis on a partially grounded ice shelf (Hells Gate Ice Shelf – Victoria Land, Antarctica)</i>	37
Paper 3: <i>On the use of static GPS measurements to record the tidal response of a small Antarctic ice shelf (Hells Gate Ice Shelf, Victoria Land)</i>	43
3. The Marine Ice Diversity	51
3.1. Diversity of marine ice properties	52
3.1.1. Spatial variability	52
3.1.2. Textural variability	55
3.2. Diversity of marine ice genetic processes	62
3.2.1. Crack metamorphism at grounding lines	62
3.2.2. Double diffusion between basal continental fresh melt water and sea water in (re-) grounding areas	64
3.2.3. Deep and Shallow Thermohaline Circulation	66
3.2.4. Rift Thermohaline Convection	75
3.3. What can we learn from landfast sea ice studies?	78
3.3.1. The Georges VI Ice Shelf case (Antarctic Peninsula)	79
3.3.2. Evans Cove (Hells Gate Ice Shelf, Victoria Land)	82
3.4. A peculiar property of marine ice: its very low salinity as compared to sea ice	89
Paper 4: <i>Stratigraphy, Stable isotopes and salinity in multi-year sea ice from the rift area, South George VI Ice Shelf, Antarctic Peninsula</i>	96
Paper 5: <i>Ice composition evidence of marine ice transfer along the bottom of a small Antarctic ice shelf</i>	108

<b>Paper 6:</b> <i>Low salinity frazil ice generation at the base of a small Antarctic ice shelf</i>	<b>113</b>
<b>Paper 7:</b> <i>Investigating processes of marine ice formation in a floating ice tongue by a high resolution isotopic study</i>	<b>128</b>
<b>Paper 8:</b> <i>Preliminary results from 60 shallow cores and from one 45-m deep marine ice core at Hells Gate Ice Shelf (Victoria Land, Antarctica)</i>	<b>136</b>
<b>Paper 9:</b> <i>Ice shelf/ocean interactions at the front of Hells Gate Ice Shelf (Terra Nova Bay - Antarctica)</i>	<b>142</b>
<b>Paper 10:</b> <i>Linking landfast sea ice variability to marine ice accretion at Hells Gate Ice Shelf, Ross Sea</i>	<b>147</b>
<b>Paper 11:</b> <i>Significant marine ice accumulation in the ablation zone beneath an Antarctic ice shelf</i>	<b>181</b>
<b>Paper 12:</b> <i>A two-phase approach to the simulation of the combined isotope/salinity signal of marine ice</i>	<b>192</b>
<b>4. Perspectives and Future Work</b>	<b>208</b>
<b>4.1. Foreword</b>	<b>209</b>
<b>4.2. Implications for ice shelf mass-balance and stability in a global warming perspective</b>	<b>209</b>
4.2.1. Dielectric properties of marine ice, radio-echo soundings and ice shelf mass-balance	209
4.2.2. $\delta^{18}\text{O}$ as a geochemical tracer of the contribution of ice shelf melting to the ice shelf mass balance	210
4.2.3. Effect of impurities on ice rheology and potential rift welding efficiency in grounding and calving areas	211
4.2.4. Marine ice production in a warmer climate	214
<b>4.3. Implications for sediment export during glacial vs. interglacial times</b>	<b>214</b>
<b>4.4. Similarities with lake environments under large ice-sheets: the Vostok case</b>	<b>218</b>
<b>4.5. Challenge for the future</b>	<b>222</b>
4.5.1. Field work	222
4.5.2. Experimental work	222
4.5.3. Modelling work	223
<b>Paper 13:</b> <i>Freezing at the grounding line in east Antarctica: possible implications for sediment export efficiency</i>	<b>224</b>
<b>Paper 14:</b> <i>Ice formation in subglacial lake Vostok, Central Antarctica</i>	<b>230</b>
<b>5. Conclusions</b>	<b>241</b>
<b>6. References</b>	<b>244</b>



## Acknowledgements

*I would first like to express my warmest thanks to Professor Roland Souchez for introducing me to the exciting world of glaciological research. His overwhelming scientific enthusiasm has been the ideal ferment for my research career. His exceptional ability to bridge glaciology to other environmental disciplines and to integrate our specific research effort in a wider global context has been the secret recipe for the international recognition of our Laboratory. It will be a challenging task to maintain our research activity at the level of excellence he has brought it to.*

*I also gratefully acknowledge the "Fonds National de la Recherche Scientifique" (F.N.R.S.) for having supported my research activity for all these years. Its additional recurrent support from equipment and travel grants has allowed an optimal development of my research activities.*

*Antarctic field project are logistically and financially heavy. This project has been successful largely thanks to the efficient support of the four consecutive Antarctic research initiative of the Belgian Scientific Research Programme on Antarctica initiated by the Belgian Prime Minister's Services Science Policy Office (SPPS, now SSTC). We are equally grateful to the Italian Progetto Nazionale di Ricerche in Antartide and to the British Antarctic Survey for welcoming our field activity without reservation in their Antarctic research infrastructure.*

*Antarctic research is also an ideal setting for international collaboration. In this regard, I would like to address my very special thanks to Dr. E. Morris, Dr. J. Paren, Dr. K. Nicholls, Dr. A. Jenkins, Prof. G. Orombelli, Dr. M. Frezzotti, Prof. M. Meneghel, Prof. A. Bondesan, Dr. M. Dini, Dr. M. Stiévenard for their unrestricted involvement in the field, the precious support in the lab and their constructive contribution to our publications. A special mention goes to Prof. J. Jouzel for his long-running friendly support and expertise on isotopic matters, Prof. H. Eicken for exciting reviewings of papers dealing with isotopic and chemical fractionation, Prof. M. Jeffries for introducing me to the world of Antarctic sea ice and Dr. A. Khazendar for sharing my enthusiasm for ice-ocean interactions and developing the fundamental modelling effort.*

*And then there is our "working family" at the Glaciology Unit:*

*My colleague and special friend, Prof. Reginald Lorrain who I am so grateful to have brought me back to glaciological research, who supported me all along the way, and excels in tempering enthusiast scientific fights between "the boss" and myself,*

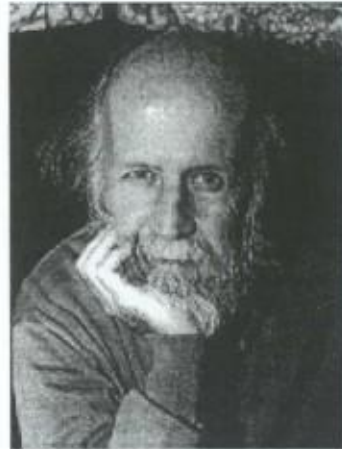
*Michèle Lemmens for faithful support and feminine diplomacy,*

*Jaquie Haren, Claire Lelouchier and Elmie Devos for endlessly providing the technical and administrative support, and keep on smiling,*

*Véronique Verbeke, Suzanne Sleewaegen and Denis Samyn, our "new blood", for reacting instantaneously to scientific, technical or logistic matters and efficiently sealing my memory leaks,*

*And all our DES and DEA students who patiently invested time and efforts in contributing to our research activity in the framework of their Master These,*

*Last, but certainly not least, I would like to thank my family and friends for caring and healing wounds. Special thanks to Mum and Dad for making me what I am and providing the ticket to the University and to Daddy and Granny for friendship and baby sittings support for the sake of Science.*



Notre époque cherche de nouveaux maîtres à penser et de nouvelles certitudes. Les intellectuels ont perdu leur prestige. Les curés ne sont plus écoutés. On demande donc aux scientifiques de les remplacer.

Il faut résister.

Mieux vaut apprendre aux gens à vivre dans l'incertitude quand il s'agit de grandes questions : le sens de la Vie et celui de l'Univers.

Chacun doit atteindre l'état adulte, c'est-à-dire élaborer lui-même sa propre vérité.

C'est pourquoi les scientifiques doivent refuser d'être des Gourous.

Il faut mettre le public en face de ses connaissances et de ses doutes.

Faire comprendre que le discours scientifique n'est pas un discours de vérité, mais une démarche en cours d'élaboration toujours passible de changements, si de nouvelles observations l'y obligent...

*Hubert Reeves, le vif l'express, 1990.*



## Foreword

This thesis investigates ice-ocean interaction processes in Antarctica, in the perspective of better understanding how the ongoing climate warming will interact with the mass balance of ice shelves and floating ice tongues, the fast moving regulating "taps" of the whole Antarctic Ice Sheet.

Using a multi-parametric analytical approach, we demonstrate the spatial and genetic diversity of what we refer to as "marine ice", a typical by-product of these ice shelf-ocean interactions. Then we show how these various ice-ocean interaction processes can potentially contribute to the sensitivity of these key polar areas to global warming. We suggest that, taking into account those processes explicitly in large-scale models of the dynamical behaviour of the Antarctic Ice Sheet might solve the apparent discrepancy between the model results showing a fairly robust ice sheet (in the context of the present-day global temperature rise) and the recent observed increase of regional ice shelf collapsing, particularly in the fairly sensitive Antarctic Peninsula.

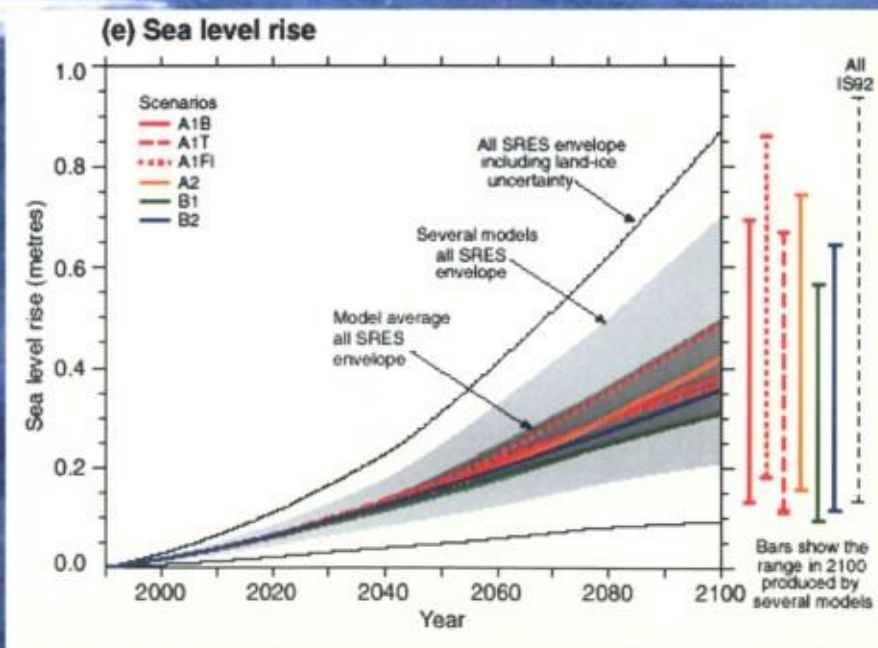
This work summarizes the results of more than 10 years of active Antarctic field research, mainly in the Ross Sea District (Terra Nova Bay area, South Victoria Land), but also in the Antarctic Peninsula. In accordance with the spirit of the "Agrégation de l'Enseignement Supérieur", as defined in our University statutes, we have written this thesis with the main objective to show how we believe our research activity in a given field has significantly contributed to the progress of science. This is a tough exercise since science, by definition, is in perpetual evolution (see our reference to H. Reeves interview). This thesis will indeed not deliver any final statement on the ice shelf role in ice sheets stability...the more we progress, the more unanswered questions we ask, making previous assertions obsolete, the more challenges we set for the future. Be it in the "marine ice genetic processes" or the "processes of marine ice desalination" our mind has constantly re-adjusted with time, and is still looking for verifying concepts: it is a "tooth-saw" progression, like the temperature signal of global warming since the industrial revolution!

Probably the most important message that I hope this thesis will pass to younger generations is that research is like education, a thrilling profession, with lots of moments of doubt, but also moments of intense excitement and satisfaction when undeniable progress is made, even if we know it is only the next brick in a very complex building. Research is certainly a wonderful job, but also a permanently destabilizing activity which, as for psychoanalysts, requires a serious contribution of optimism and self-confidence!

As a final word, we have designed our manuscript in what we believe is the fundamental rationale behind the "Agrégation de l'Enseignement Supérieur", that is to demonstrate our ability to communicate our knowledge and experience to University students. It is therefore deliberately that we have included some general glaciological concepts in the manuscript, and adapted the level of complexity to a wider scientific audience.



# 1. Framework and Motivation





### 1.1. The role of ice shelves in the Antarctic Ice Sheet System

One of the great scientific advances in the 1970-1980s was the development of the capability to recover (among others) paleo-temperatures (from the stable isotopes signal  $\delta^{18}\text{O}$  and  $\delta\text{D}$  of the ice) and  $\text{CO}_2$  content of ancient air trapped in deep polar ice cores. The amazing co-variation between these two paleo-climatic indicators, recently proved to be valid for the past four glacial-interglacial cycles (Vostok ice core, Antarctica – Petit et al., 1999), has raised a major concern in the scientific community and beyond. Considering this apparently simple relationship from the pre-industrial period as a rule for the  $\text{CO}_2$ -driven greenhouse global warming process, how would the Earth system cope with the tremendous (never observed in the last 500.000 years, at least) anthropogenic rate of increase of greenhouse gases since the late nineties? What would be the consequences in terms of potentially rapid climatic changes and sea level rise? These fundamental questions have boosted the scientific developments of the last decades in the field of global environmental studies, in terms of data acquisition, process studies as well as global climate modelling.

We now know that the actual temperature increase since 1860, although quite real, is only of about 0.5 to 0.7°C, far below expectations from a simple linear relationship based on the natural  $\text{CO}_2$  and temperature co-variation of the last glacial-interglacial transition. This is obviously the expression of a very complex system that has also proved to be potentially highly non-linear in its responses, with short-term instabilities generated above certain thresholds.

From the very beginning, the scientific community has been aware of the crucial role that the Antarctic Ice Sheet, and its seasonally ice-covered surrounding ocean, was playing in the climate system. Primarily because of its size (14 millions  $\text{km}^2$ , extending to 34 millions each winter, with the seasonal sea ice cover build-up), nature (more than 90% of the Earth's freshwater stored as ice, slowly flowing from the centre to the coast) and location, the Antarctic plays a major role in regulating surface energy exchanges, sea levels fluctuations through icebergs discharge and phase changes, bottom and intermediary water masses production, ocean-atmosphere gaseous exchanges, biological activity in surface waters a.s.o. However, partly because of its remoteness and inaccessibility, there still are considerable gaps in our knowledge of the Antarctic Ice Sheet System. As, an example, looking at the prospects of one of the first international Workshops dealing with the impact of  $\text{CO}_2$  enhanced (x2) scenarii on sea level changes (Seattle Workshop, 1985, Table 1), one can clearly see how much uncertainty affected the Antarctic contribution forecast at the time (ranging from 10 cm lowering to 1 meter rising of the global sea level), as compared to the contribution from small glaciers and ice caps or from the Greenland Ice Sheet.

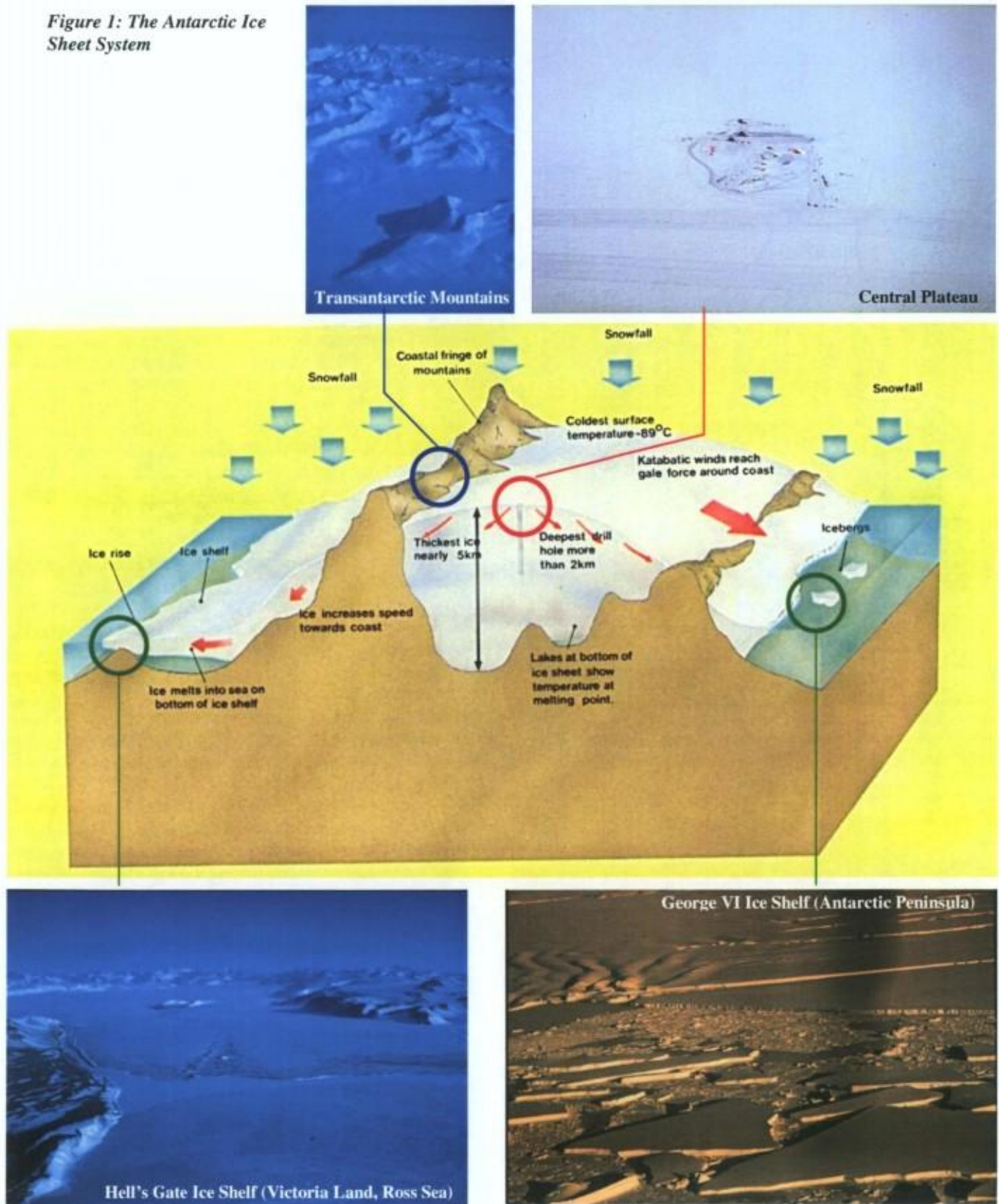
Ice Mass	Annual Probable Contribution to Sea Level With Steady-State 2 x $\text{CO}_2$ Atmosphere (mm/yr)	Range of Estimated Contribution to Total Sea-Level Change to Year 2100 (m)
Glaciers and small ice caps	2 to 5	0.1 to 0.3
Greenland Ice Sheet	1 to 4	0.1 to 0.3
Antarctic Ice Sheet	-3 to 10	-0.1 to 1 <sup>b</sup>

Table 1: Estimates of the contribution to sea-level rise by ice wastage in a  $\text{CO}_2$ -enhanced environment (from Report on the Seattle Workshop, 1985)



To understand better how ice shelves (the focus of the present dissertation) are a key parameter to the stability of the Antarctic Ice Sheet in the context of a warming climate, it is important to briefly summarise how the whole system works (Figure 1). Snow falls on the whole continent, including the Central Plateau, where it piles up and slowly increases its density by dry compaction, under the weight of overlying new snow layers. It turns into firn (density: 400 to 830  $\text{kgm}^{-3}$ ), then into ice when bubbles close-off (density: 830 to 917  $\text{kgm}^{-3}$ ). The ice slowly starts moving under gravity towards the coast, with

*Figure 1: The Antarctic Ice Sheet System*





most of the deformation concentrated close to the ice-bedrock interface. As it encounters the coastal mountain chains, it forms individual ice streams that eventually start floating on the ocean, downstream of the mountains crests, when the buoyancy criteria is fulfilled. Ice streams often meet again to form ice shelves (otherwise they turn into individual floating ice tongues) that spread over the sea surface because of the loss of friction when they get ungrounded. The area where the ice gets afloat is usually called the grounding line, although it is very often more likely to be a “grounding zone”. At that stage, the only control on increasing velocity of the ice is the friction against bedrock faces, be it what is known as “pinning points” (islands or “ice rises”, depending if the bedrock is visible at the surface or not) or the sides of coastal embayments. When the flow is no more restricted by these various back stresses, the ice expands further and eventually reaches the threshold for calving, the process by which vertical fractures in the ice shelf form, turn into larger rifts, finally isolating icebergs that start drifting and melting into the open sea.

Ice shelves are thus the natural “taps” of the Ice Sheet System, regulating the flow of continental ice towards the ocean, and, correlatively, the amount of freshwater added to the ocean, eventually contributing to sea level rise. It is intuitively easy to surmise that an increase of the ocean’s temperature, in a global warming scenario, will enhance basal melting of the ice shelves. This in turn would result in reduced back stresses, increased continental ice flow rates at the grounding line, and, potentially, destabilization of the whole ice sheet mass balance. This would be specially true for the Western Antarctic Ice Sheet, most of which lies below sea level, at depths sometimes greater than 2000 meters (Figure 2). However, as we will show in this dissertation, the rationale above (and sketched in Figure 1) is again quite an oversimplified view of reality, that doesn’t take into account other important ice-ocean interaction processes occurring below ice shelves and floating ice tongues.

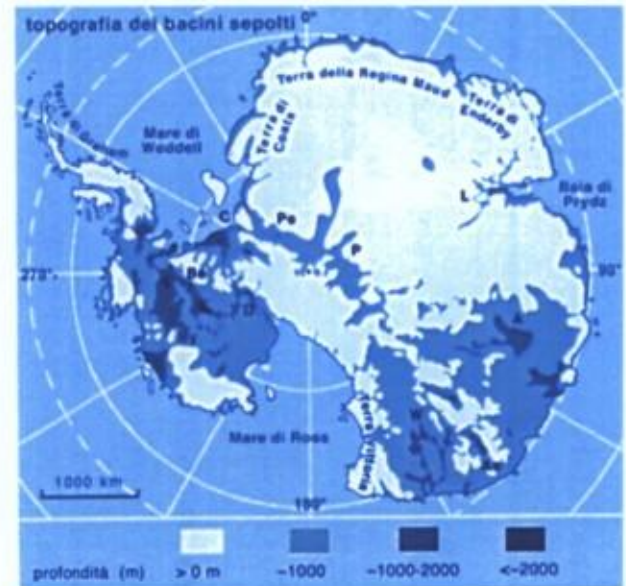


Figure 2: Areas below sea level under the Antarctic Ice Sheet. Areas at or above sea level are shown in light blue (Manzoni, 2000).

## 1.2. Modelling the response of the Antarctic Ice Sheet to climate forcing: the Ice Shelves status

The first modelling efforts of large ice masses date back to the mid 1950’s, where glaciologists were mainly concerned with finding a theoretical explanation of the observed temperature profiles in ice sheets (e.g. Robin, 1955, Weertman, 1968, Philbert and Federer, 1971). Starting from simple one-dimensional (vertical) steady-state models, they progressively evolved into pseudo-2D models (moving-column models, e.g. Budd et al., 1971), 2-D and finally 3-D models. Initially these models were either concerned with temperature distributions, independently of horizontal advection of ice (thermodynamic models), or with the modelling of ice flow in the isothermal case (ice deformation depends of the stress field alone and is independent of the temperature, dynamic models).

The first dynamic antarctic models were developed by Oerlemans (1982a,b) and Budd and Smith (1982), and were both “pseudo-3D” models in which changes in the horizontal domain were modelled using a geometric construction. In these models, grounding lines and ice shelves were already crudely considered. In Oerlemans (1982a), the ice at the prescribed grounding line is first redistributed over neighbouring grid points according to a prescribed snout steepness (using plastic flow theory), before a floatation criterion is applied. In a subsequent version (Oerlemans, 1982b) ice shelves were modelled



using a diagnostic procedure, giving ice thickness as a function of distance to grounding line and ice thickness at the grounding line. Budd and Smith (1982) improved the ice shelves treatment slightly by prescribing a constant horizontal strain rate (creep thinning), derived from freely floating ice shelves. In any of these cases, no special treatment was included for the flow in the transition zone between grounded and floating ice.

However, in polar ice sheets (far from isothermal state) the flow is, to a large extent, a temperature-dependent problem. A considerable step forward was made by Jenssen (1977) who designed a three-dimensional model incorporating the mutual interaction between ice flow and its thermodynamics and applied it to the Greenland Ice Sheet. However, numerical instabilities occurred, likely due to the use of a coarse grid (200x100 km and 10 layers in the vertical) and a crude approach to modelling the ice boundary. Formulation and analysis of thermo-mechanically coupled ice sheets further improved with a number of studies for two-dimensional cases (e.g. Hutter et al., 1986; Hindmarsh and Hutter, 1988; Hindmarsh et al., 1989, Dahl-Jensen, 1989). It is Huybrechts (1992) that proposed the first complete and detailed thermo-mechanically coupled 3-D model of the Antarctic ice sheet (see structure in Figure 3).

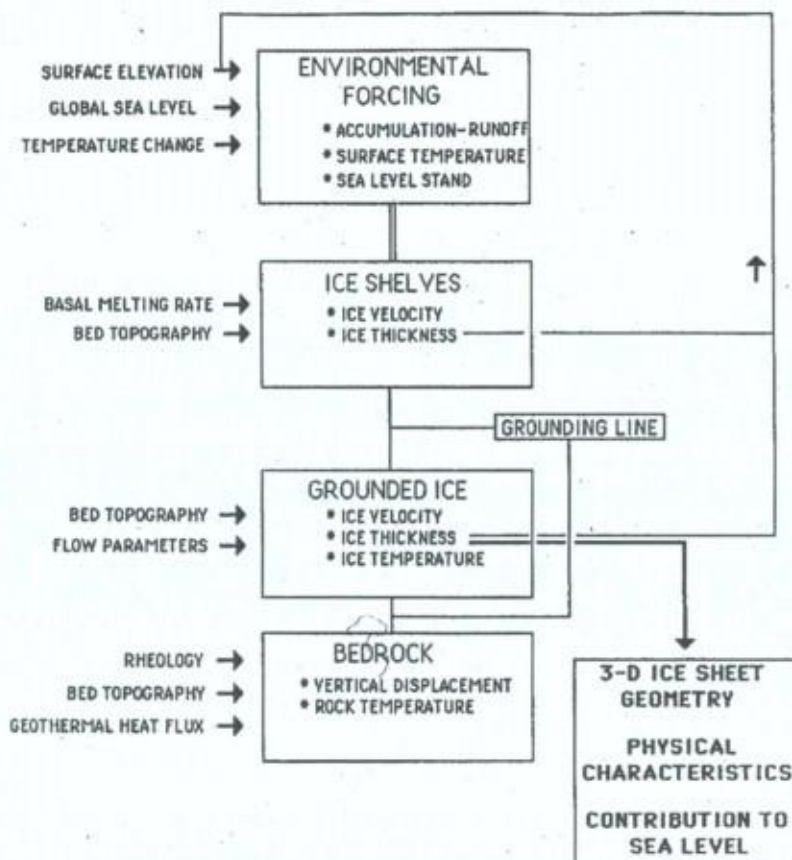


Figure 3: Schematic structure of the Huybrechts model (from Huybrechts, 1992). Inputs are given on the left-hand side. Prescribed environmental variables drive the model, which has ice shelves, grounded ice and bed adjustment as major components. The position of the grounding line is not prescribed, but internally generated. The model essentially outputs the time-dependent three-dimensional ice sheet geometry and the coupled temperature and velocity fields.



The Huybrechts model is time-dependent and computes the full set of coupled thermomechanical equations for ice flow in three dimensions (with the only restriction that the horizontal velocity vector cannot change direction with depth), as well as the geographical distribution of the ice mass. The horizontal grid point distance is 40 km and there are 10 layers in the vertical, which have closer spacing towards the bedrock surface where the shear concentrates.

The primary difference between this model and those used in earlier studies is a rigorous treatment of the flow across the grounding line and in the ice shelf, so that the grounding line position can be traced during the calculation by means of a floatation criterion. This is done by allowing for different velocity solutions in grounded and floating ice and by defining a stress transition zone in between, at the grounding line. At the seaward margin, however, the calving physics are not considered explicitly, and the ice shelf is actually made to extent all the way to the edge of the numerical grid. Boundary conditions are then applied for unconfined, freely floating and uniformly spreading ice shelves. Velocity components then follow from the flow law, where an expression can be found for the deviatoric stresses from the condition that the net total force on the ice shelf front must be balanced by the horizontal force exerted by the seawater.

The model also includes basal sliding, which is restricted to regions that are at the pressure melting point. It considers the response of the underlying bedrock to changing ice load, taking into account both the rigidity of the lithosphere and the viscosity of the asthenosphere, and including a temperature calculation.

This sophisticated model has been efficiently used in the last decade, particularly to test the sensitivity of the Antarctic Ice Sheet to Global warming. In his Thesis work, Huybrechts (1992) had already included two scenarios of greenhouse warming (Figure 4): a "low" scenario used the temperature increase predicted by the 1990 (Houghton et al., 1990) "business as usual" IPCC (Intergovernmental Panel on Climate Change) Working Group I Report, and a "high" scenario simulated a temperature rising by twice as much, to take into account larger temperature increases in the polar regions.

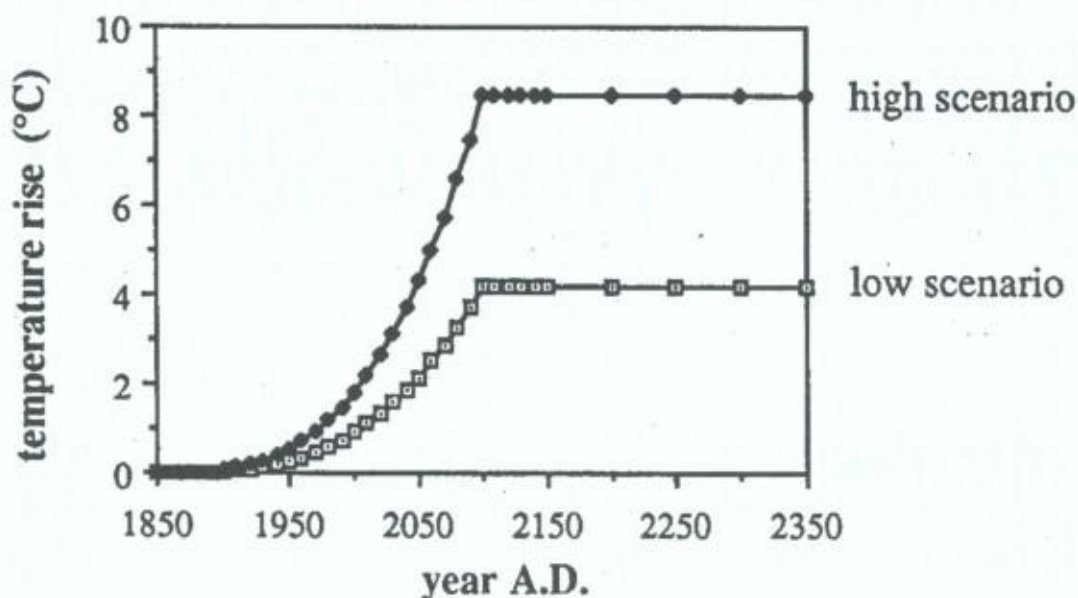


Figure 4: The temperature scenarios used to force the "static" and "dynamic" models in greenhouse warming experiments (Huybrechts, 1992). The "low scenario" is the 1990 IPCC predictions and the "high scenario" corresponds to a temperature increase by twice as much.

Impacts of the two scenarios on the global sea level are shown in Figure 5a, where a distinction is made between the *static response* (changes with respect to the present mass balance are accumulated forward in time whilst velocity field remains unchanged, keeping the amount of ice transported across the grounding line constant) and the *dynamic response* (the ice sheet shows a dynamical response to the substantial changes in ice thickness).

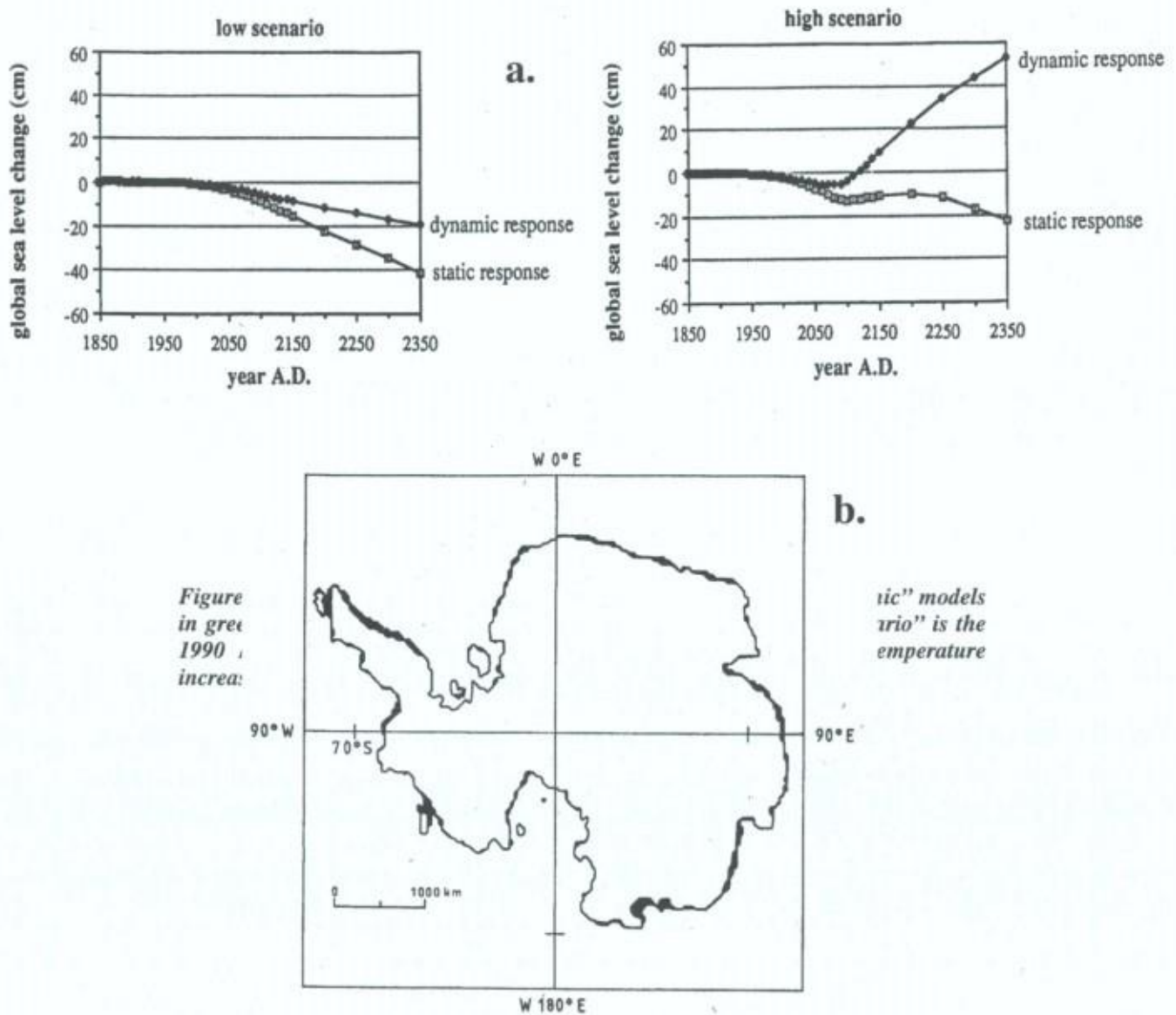
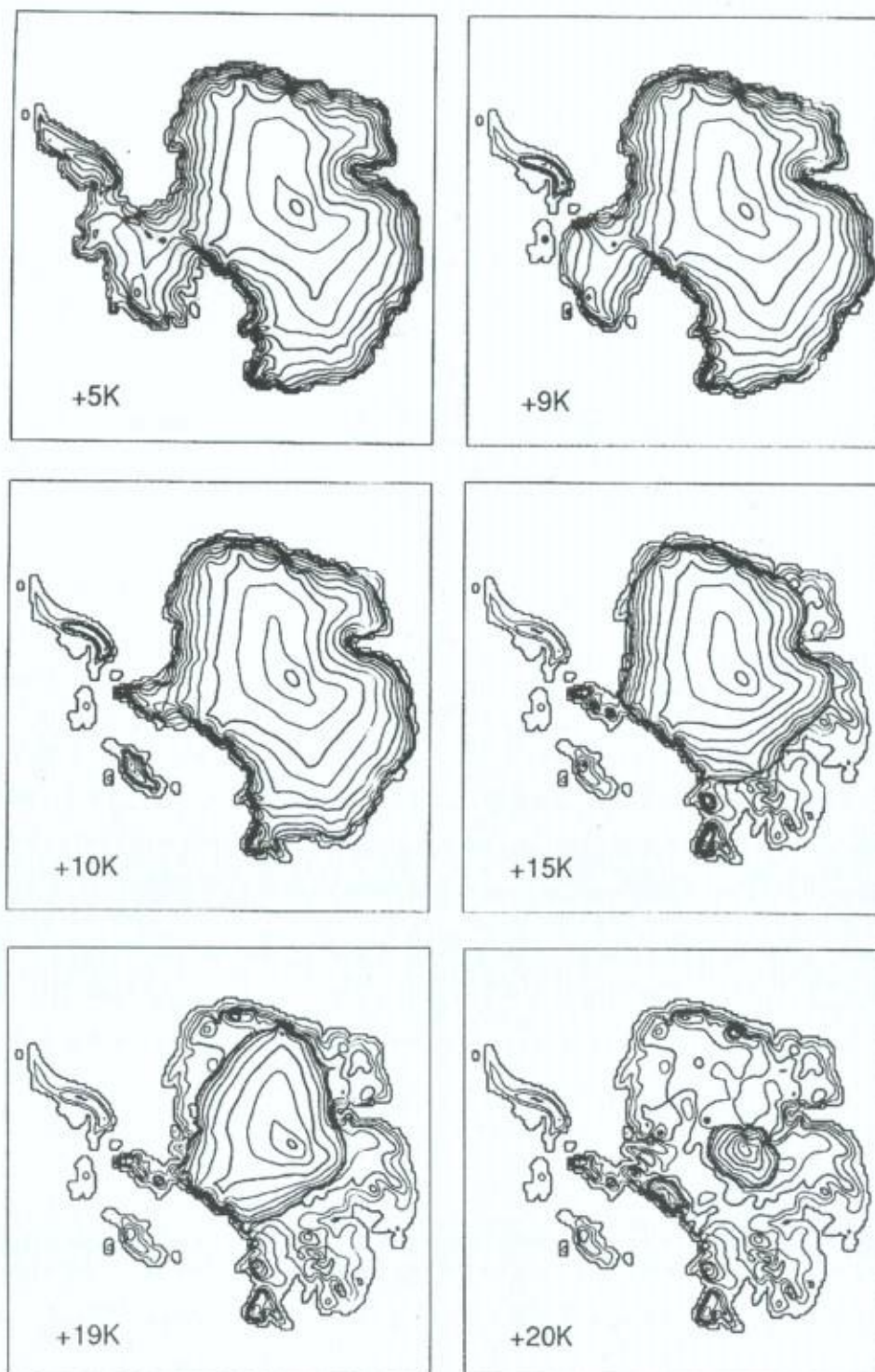


Figure 5: a) Response of the ice sheet expressed in global sea level changes for the high and the low scenario (Huybrechts, 1992); b) Grounding line retreat for the "high scenario" experiment. The black areas indicate where grounded ice has been replaced by ice shelf by the year 2500 (Huybrechts, 1992)

It is clear that neglecting the dynamic response of the ice sheet strongly underestimates its possible contribution to the global sea level rise. Another striking result from these simulations, that were both ended in year 2500, is the relatively moderate impact of considerable temperature changes on sea level changes. In the low scenario case, even the dynamic model still shows an actual storage at the ice sheet surface, because of the increased surface mass balance. It is only when the warming exceeds 5-6°C (after 2060-2070 in the "high scenario"), that a positive contribution to global sea level is recorded. Thinning at grounding lines becomes larger and significant grounding line retreat sets in. However, as shown in Figure 5b, grounding-line recession is still insignificant along the major ice shelves (Ronne-Filchner, Ross), because, even with a warming of 8.4°C, the number of positive degree-days (that allow actual melting of the ice surface) at these locations is still too low for runoff to take place.



In a later study, Huybrechts (1993) explored the necessary conditions for destabilisation of the Antarctic Ice Sheet, by imposing increasingly warmer mean annual temperatures ( $+5^{\circ}\text{K}$  to  $+20^{\circ}\text{K}$  - Figure 6).



*Figure 6: Steady-state ice-sheet geometries for the temperature perturbations above the present level, as indicated. Isolines are for surface elevation. Contour interval is 333m, the thick lines are every 1000 meters (Huybrechts, 1993).*

The first major changes in the ice sheet geometry occur at  $+9^{\circ}\text{K}$ , where the Antarctic Peninsula turns into an island with a small localized ice cap. It takes between  $10$  and  $15^{\circ}\text{K}$  of temperature increase to get rid of the marine-based (see Figure 2) West Antarctic Ice Sheet and it is only for temperature increases of up to  $20^{\circ}\text{C}$  that the East Antarctic ice Sheet is reduced to a local ice cap.

These few examples illustrate that the major outcome of Huybrechts model, is a fairly stable Antarctic ice Sheet, with respect to a  $+5^{\circ}\text{C}$  Global Warming. However, the recent developments of satellite imagery have drawn our attention to repeated disintegration events of some of the ice shelves (e.g., the Larsen Ice Shelf) fringing the Antarctic Peninsula, a regionally sensitive sector which has recorded mean annual air temperature increases of  $2$  to  $4^{\circ}\text{C}$  during the last 40 years. *We will show, in the coming sections, that complex ice-shelf/ocean interaction processes, that are not included in the present day Antarctic Ice Sheet models, are worth considering to improve our predictive capabilities of its response to anthropogenic climatic changes.*

### 1.3. Marine ice: a major by-product of Ice-Shelf/Ocean interactions

It is in the early 1970's that the first glaciological Antarctic field investigations unveiled the potential importance of ice-ocean interactions in the mass-balance and stability of ice shelves. Gow and Epstein (1972) provided the first demonstration that refrozen seawater existed at the bottom of the Koettlitz Ice Tongue in Antarctica. The same year, in the 350-m long G1 ice core drilled at the surface of the Amery Ice Shelf (Figure 7a), Morgan (1972) described, on a much larger scale, the existence of a peculiar ice mass located below 270 meters of ice of meteoric origin. With a total ice shelf thickness of about 428 meters, this 158-m bottom ice layer showed distinct physico-chemical properties (Figure 7b).

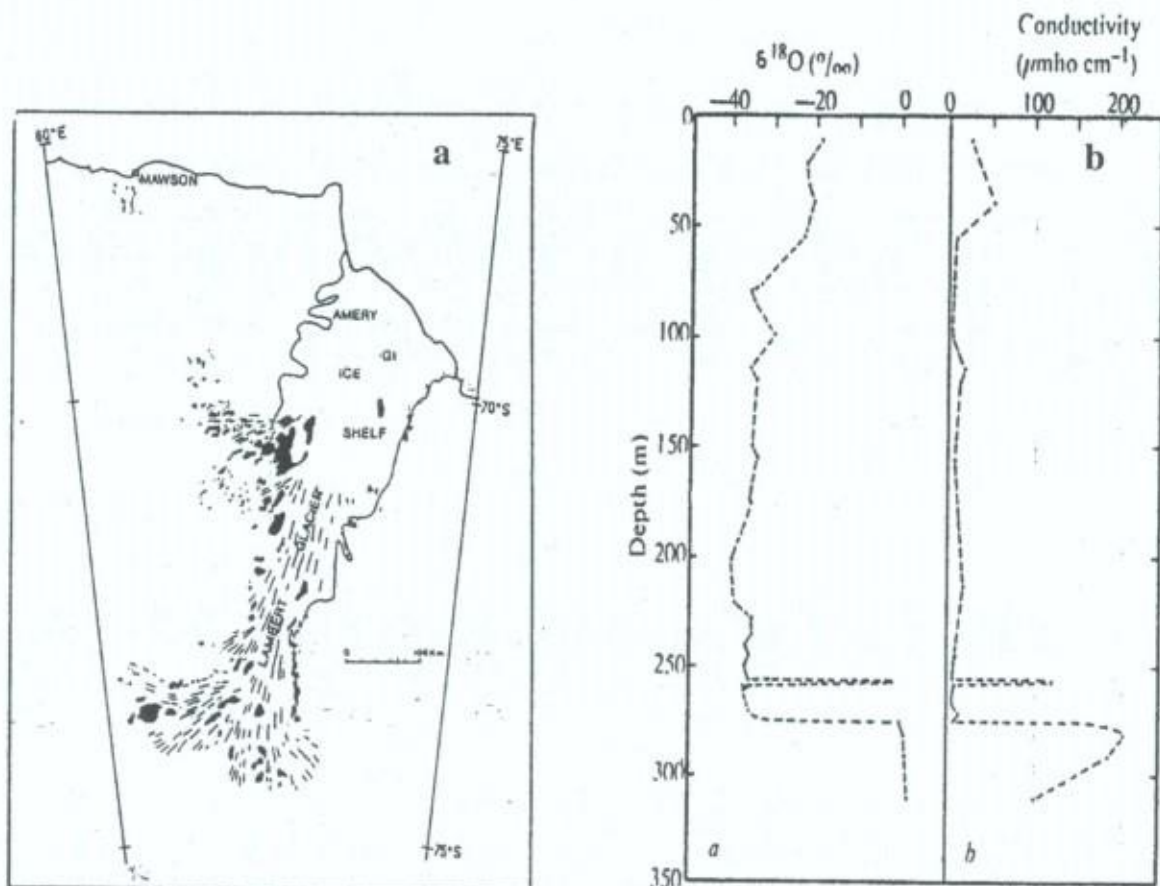


Figure 7: a) Location of ice drilling G1 on the Lambert Glacier-Amery Ice Shelf system in Antarctica and b)  $\delta^{18}\text{O}$  and conductivity profiles at G1 (Morgan, 1972)



The very sharp transition in the  $\delta^{18}\text{O}$  value towards values close to 0 ‰ indicate ice resulting from the freezing of sea water<sup>1</sup>, and this is confirmed by the electrical conductivity profile, a measure of the soluble impurity content of the ice. While the meteoric ice shows very low conductivity values (<50  $\mu\text{S}$ ), the signal increases by a factor of 10 at least when crossing the transition, suggesting the origin from sea water.

Zotikov et al. (1980) reported 6 meters of refrozen seawater at the bottom of a 416-m ice core recovered from the Ross Ice Shelf (Core J9). In that case, the accretion rate at the location was estimated to be of the order of  $2\text{ cm y}^{-1}$  by these authors. This value was in good agreement with what Robin (1979) had already theoretically suggested for the Ross Ice Shelf.

For obvious reasons, drilling for refrozen seawater at the bottom of ice shelves is confronted with the necessity of having first to penetrate hundreds of meters of meteoric ice. This explains why only two other major attempts have been made in this respect, both on the Filchner-Ronne ice shelf (Figure 8a - e.g. Oerter et al., 1992, Oerter et al. 1994, Eicken et al., 1994).

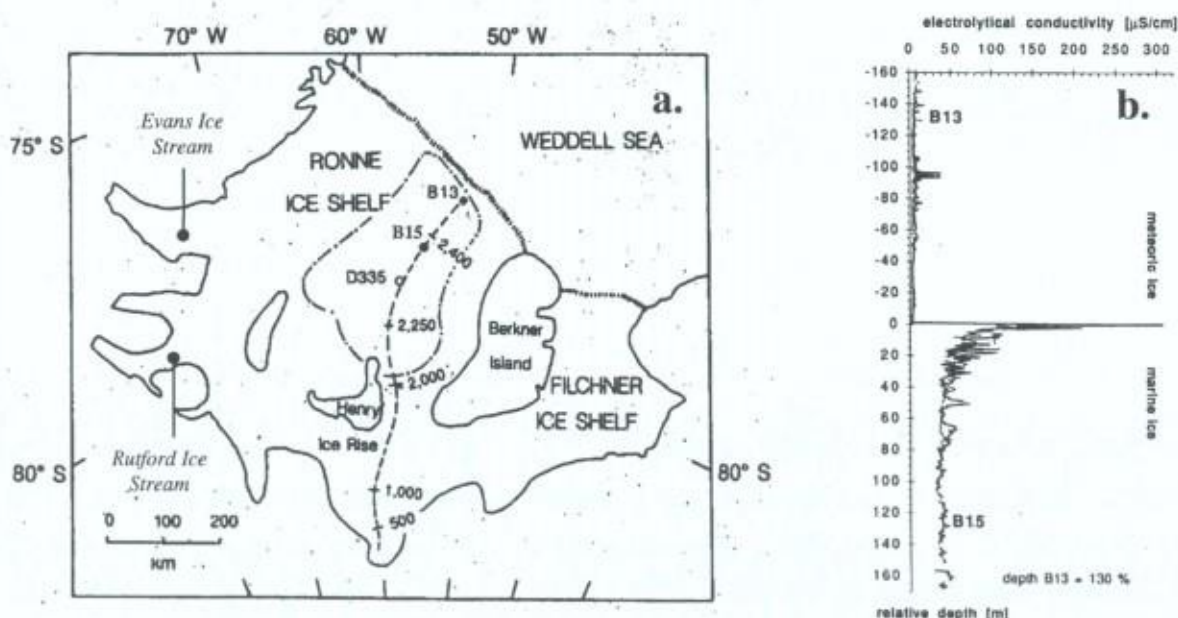


Figure 8: a) Location of ice drilling B13 and B15 on the Ronne Ice Shelf in Antarctica and b) conductivity profiles at B13 (thin line) and B15 (thick line) (Oerter et al., 1994). The depth scale of B13 is elongated by 30% to count for thinning due to strain. Rutford and Evans Ice Streams are also shown.

Bottom accretion has been found to form the lower 62 meters of the 215-meter core drilled in the Filchner-Ronne ice Shelf at site B13 (Oerter et al. 1992). Another 320-meter core, recovered further upstream from the same ice shelf at site B15, revealed the presence of a 167-meter thick accretion at the bottom (Oerter et al., 1994). The conductivity profile (Figure 8b) is very similar in B13 and B15, and it clearly shows a sharp conductivity increase at the transition to sea water ice, reproducing the pattern

<sup>1</sup> In the commonly used  $\delta$  scale, stable isotope data on natural waters are reported in terms of the ratio  $R$  between the concentrations of heavy and light isotopes ( $^{18}\text{O}/^{16}\text{O}$ , here). The  $\delta$  value of a given sample is the relative difference between the  $R$  ratio in the sample and the  $R$  ratio in a standard. The usual standard is termed SMOW i.e. Standard Mean Ocean Water.

$$\text{Thus } \delta^{18}\text{O} = \frac{^{18}\text{O}/^{16}\text{O}(\text{sample}) - ^{18}\text{O}/^{16}\text{O}(\text{SMOW})}{^{18}\text{O}/^{16}\text{O}(\text{SMOW})} \times 1000, \text{ in } \text{‰}$$

Since maximum fractionation on freezing is +3‰, frozen sea water will always show values close to 0‰, as opposed to meteoric ice which will display noticeably negative values because of the enrichment in light isotopes occurring during the initial evaporation process at the sea surface and of the successive partial condensation events in the clouds.

described at G1 on the Amery Ice Shelf. It is Oerter et al. (1992) that first introduced the "marine ice" term to qualify these bodies of sea water ice, and we will use that terminology from now on.

The isotopic composition and the conductivity are not the only properties that differ between the meteoric ice and the marine ice. Mean cross section of the crystals in B13 and B15 (one of the proxy to crystal size) also shows a sharp transition towards smaller values (Figure 9). At the same time, bubble inclusions that are the rule in meteoric ice give way to a perfectly bubble-free marine ice. In both ice cores, the occurrence of horizontal layers enriched in particle inclusions is reported in the first meters of marine ice below the transition. These inclusions, that were also described in the Amery ice core (Wakahama, 1974) are millimetre-sized pellets made of aggregates of clay- and silt-fraction minerals and biogenic material. They are probably responsible for inhibition of crystal growth in the topmost layers.

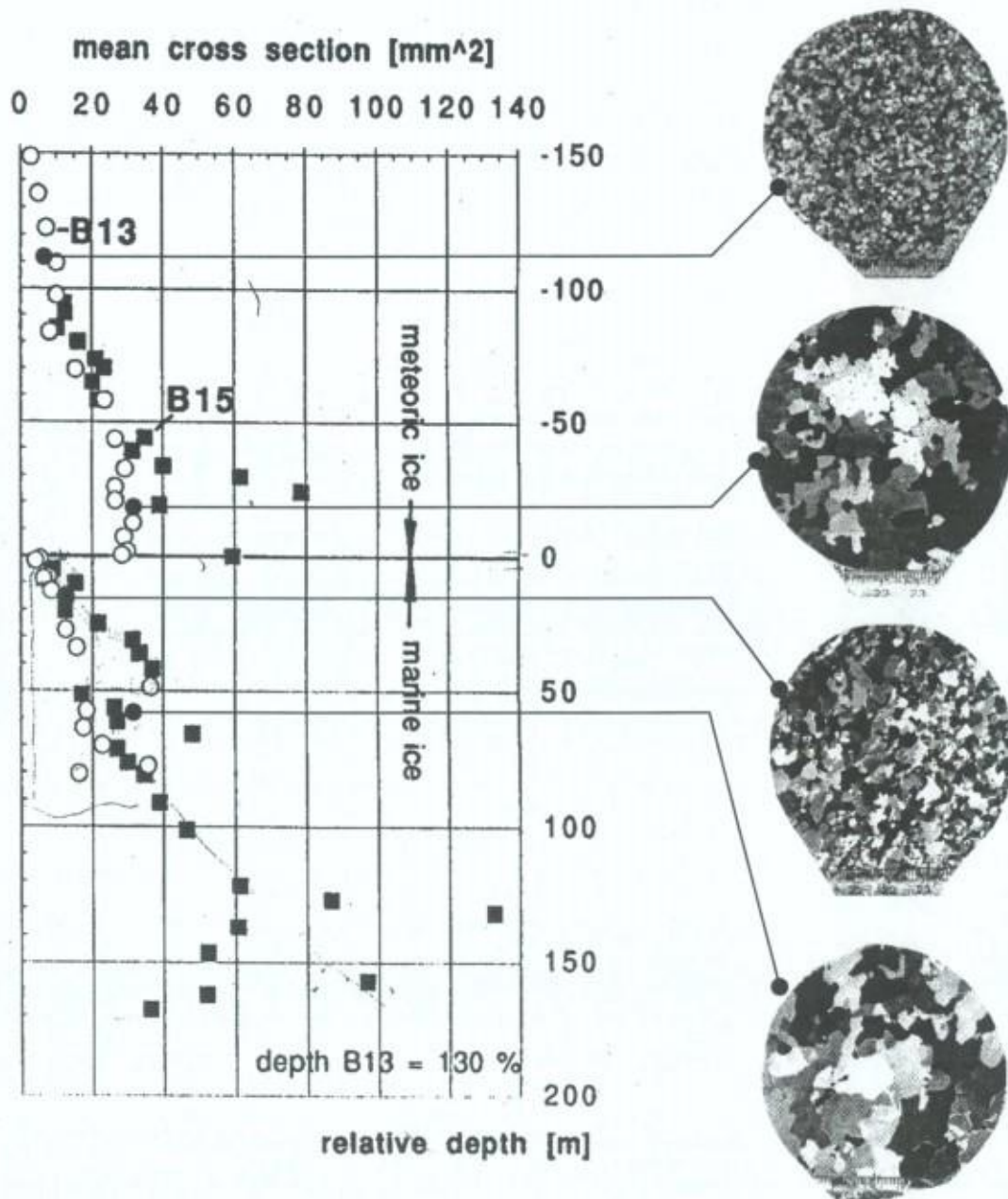


Figure 9: mean cross section of ice crystals in the B13 and B15 ice core (Eicken et al., 1994) and exemplanatory horizontal thin-sections between crossed polarizers (Oerter et al., 1994)



If Zotikov's observation of a few meters of marine ice accreting at the bottom of J9 can be reasonably understood by a direct freeze-on process of sea water at the bottom of the meteoric ice, the slow rate of this conduction-driven process makes it inadequate to be the only mechanism at play where several tens of meters of ice need to be accreted like in G1, B13 or B15. Hence, a second mechanism was introduced when Robin (1979) linked, for the first time, the formation of marine ice at G1 with ocean water circulation patterns in front and below the ice shelf. The overall circulation pattern, often referred to as the Deep Thermohaline Circulation (DTC), leads to new ice production in the water column below the ice shelf, following a process known as the "ice pump" mechanism, the theoretical elaboration of which was made by Lewis and Perkins (1986). Figure 10 illustrates the main components of the DTC and associated ice pump mechanism as one (mode 1) of the 3 major circulation modes of ice-shelf/ocean interactions described by Jacobs et al. (1992). Sea ice formation in front of the ice shelf, mainly under the recurrent activity of strong katabatic winds, produces a cold and saline (because of the salt rejection by the growing ice) surface water, often described as Winter Water. Because of its enhanced density, this water, now referred to as High Salinity Shelf Water (HSSW), "sinks" towards the continental shelf, where it either flows towards the continental shelf slope, or flows inland into the sub-ice-shelf cavity, towards the ice shelf grounding line, generally several hundred meters below the surface. Since this transfer is mainly adiabatic, the HSSW temperature is still close to the surface pressure melting point, the water mass therefore carrying extra latent heat that will be used to melt the ice shelf meteoric ice at depth. This produces less dense Ice Shelf Water that rises again towards the front of the ice shelf. It then becomes supercooled at shallower depths, therefore re-adjusting thermodynamically by generating individual ice crystals in the water column, know as "frazil" (hence the "ice pump" terminology). These crystals accumulate at the ice shelf-ocean interface under buoyancy and later consolidate to form marine ice. Ice Shelf Water will emerge at the front of the ice shelf in a depth range depending on the density

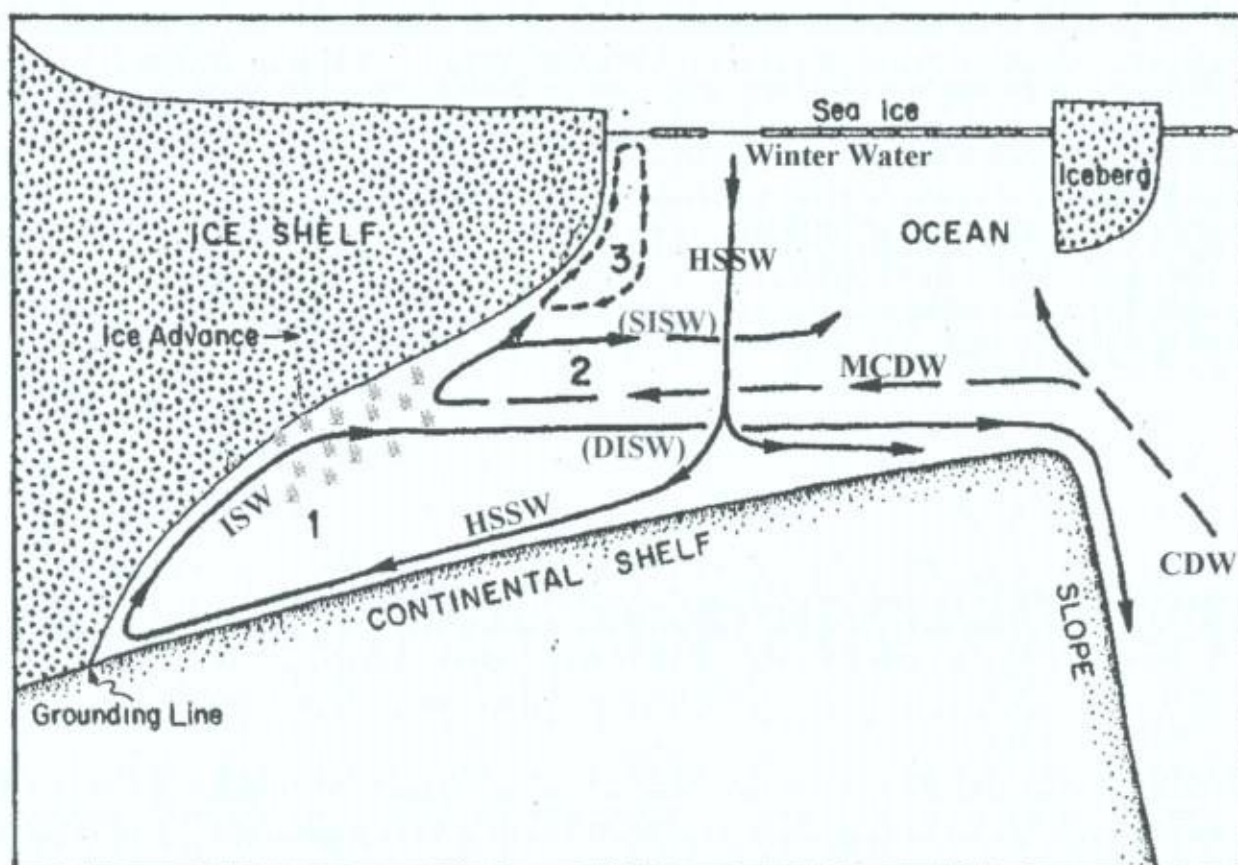


Figure 10: Ocean circulation patterns in the vicinity of ice shelves (Jacobs et al., 1992)



contrast. Frequently, frazil ice is still actively forming for some distance away from the ice shelf front, resulting in clouds of platy crystals (often ambiguously called "platelet ice") detected by remote sensing (Dieckmann et al., 1986).

The second circulation mode (2 in Figure 10) is linked to intermediate depth "warm" inflow (Modified Circumpolar Deep Water, MCDW) from the slope region. This mode ranges between two extremes: either the warmer water fills most of the sub-ice cavity resulting in greater melting (Potter and Paren, 1985), or the inflows are restricted in area or have much of their heat re-circulated to the ocean (Jacobs, 1991). Jacobs et al. (1979) suggested that, in the case of the Ross Ice Shelf, such a "warm core" flows beneath the ice shelf and undergoes cooling, dilution and lateral mixing. As the ice shelf thickens, the boundary layer moves to deeper levels and lower freezing temperatures that facilitate mixing. Eventually, it rises again, with some freezing possible (and thus production of marine ice), and emerges in the Ross sea as the shallower, low salinity Ice Shelf Water (SISW). Finally, the third mode (3 in Figure 10) is associated with the relatively shallow bases and walls within 100 km of the ice fronts, where melting is high due to tidal pumping and the seasonally warmer waters of the coastal currents (Jacobs and others, 1985).

Models of the DTC and its associated frazil ice production were initiated by Hellmer and Olbers (1989, 1991) and Jenkins and Doake (1991), and are constantly in the process of refinement (Hellmer and Jacobs, 1992; Determann and Gerdes, 1994; Jenkins and Bombosch, 1995; Bombosch and Jenkins, 1995; Grosfeld et al., 1997; Williams et al., 1998).

Fortunately, detection of marine ice bodies is not solely constrained to punctual deep drilling efforts. Remote sensing techniques, for example, are another means of investigation. These techniques must however be used in conjunction with each other to avoid serious misinterpretation biases, as we will discuss in more details in further sections. Some authors (Warren et al., 1993; Grosfeld et al., 1998) have shown that "green icebergs" are probably the drifting remnants of marine ice bodies. These are however, for obvious reasons, difficult to use for understanding marine ice "in situ" genetic processes. Finally, specific climatic conditions, at certain locations in Antarctica where intense katabatic winds activity lead to high surface ablation rates, give investigators the opportunity to sample bodies of marine ice nearer to the surface, thereby circumventing the difficulty of deep drilling logistics. Although it generally has the disadvantage not to record a full depth profile, this type of setting gives a much better access to the spatial variability of marine ice in the ice shelf system. As we will show in the next sections, the data sets presented in this work originated from such environmental settings and benefited from this spatial diversity to demonstrate that "direct freeze-on" or "frazil ice generation associated to a Deep Thermohaline Circulation" are only two of a larger set of mechanisms responsible for the contribution of marine ice bodies to the mass-balance of ice shelves.



## 2. A Suitable Setting for Shallow Depth Studies of Marine Ice Properties





## 2.1. The Terra Nova Bay area

The data sets discussed in this work were obtained from multiple series of shallow to medium depth ice cores retrieved in the framework of an active collaboration with the Italian PNRA (Programma Nazionale di Ricerche in Antartide, Drs. Orbelli, Meneghel, Bondesan, Frezzotti, Maggi, Capra) under the auspices of the Belgian Antarctic Program, funded by the Federal Science Policy Office of the Prime Minister (SSTC, OSTC). Fieldwork took place in the Terra Nova Bay area during several campaigns stretching between 1989 and 1997.

Figure 11 shows a mosaic of satellite photographs covering the area of interest: the Terra Nova Bay coast, in Southern Victoria Land, Ross Sea, Antarctica. Three main floating ice bodies were studied

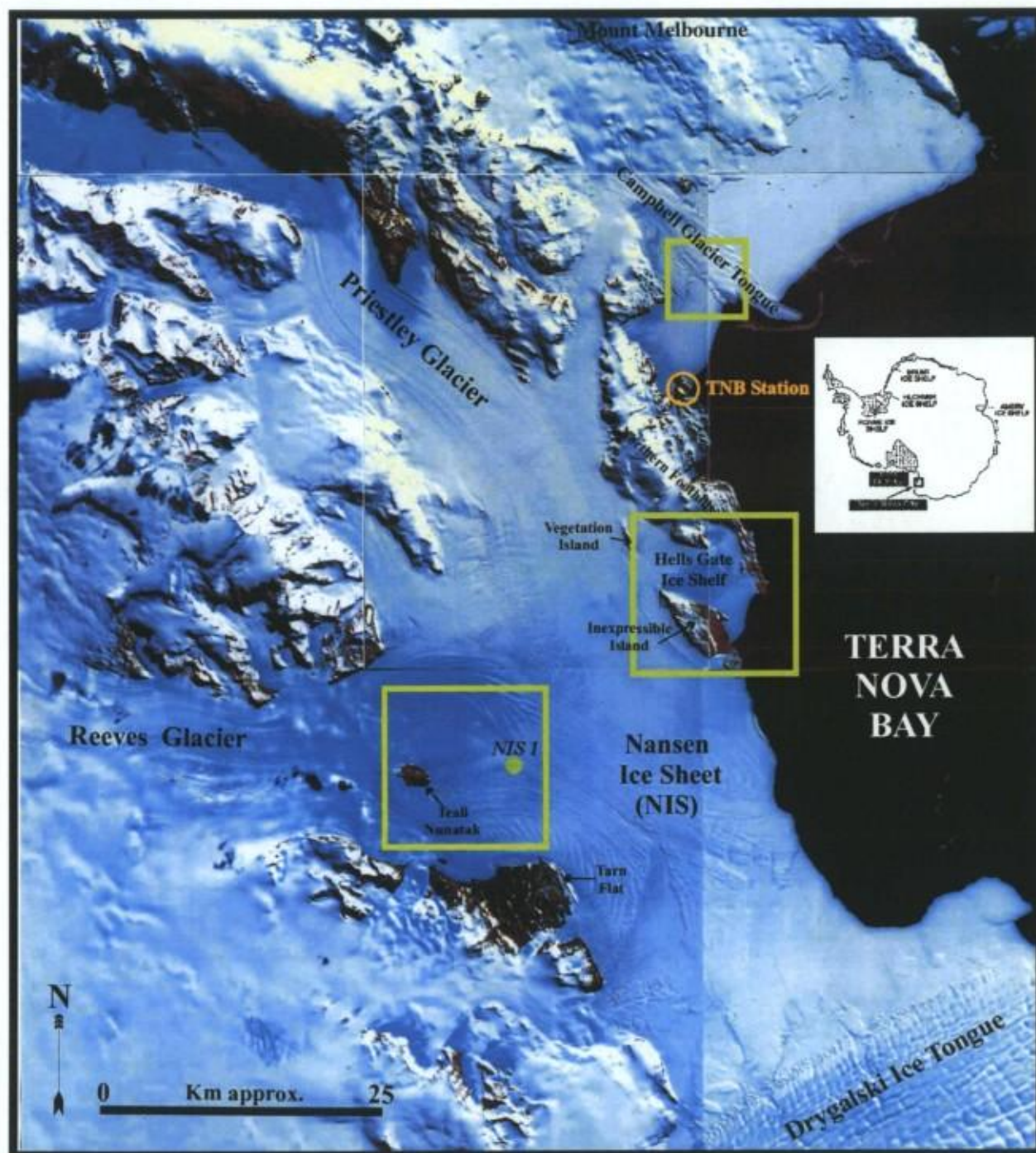


Figure 11: Satellite mosaic of the Terra Nova Bay area of interest (ENEA DIGITAL IMAGERY, PAS-ISP-GEOL). The main study areas are framed in green.



(green symbols in Figure 11), namely, from South to North: the Nansen Ice Sheet (which has been erroneously named, since it is actually an ice shelf), the Hells Gate Ice Shelf and the Campbell Ice Tongue.

The Terra Nova Bay area is renown for the persistence and intensity of the katabatic winds blowing from the Antarctic Plateau, across the TransAntarctic Mountains. Wind velocity measurements are available from the automatic weather station AWS 8931 (PAT - 74°53'S, 163°00'E), very close to the NIS1 drilling location (Figure 11). For the years 1989 and 1990, 41.2% of the wind blew from the Northwest (see also map of Figure 12), with wind speeds exceeding 28 knots ( $52 \text{ km h}^{-1}$ ) for more than 39% of the time (Baroni, 1996). This undoubtedly contributed to enhance surface ablation rates in the area, estimated by Frezzotti et al. (2000) to be between  $56 \pm 11$  and  $44 \pm 9 \text{ cm y}^{-1}$ . In turn, this major contribution to a negative surface mass balance induces an upward vertical velocity component of the ice, which brings the lower marine ice strata towards the surface, making it available for spatial inventory and shallow coring.

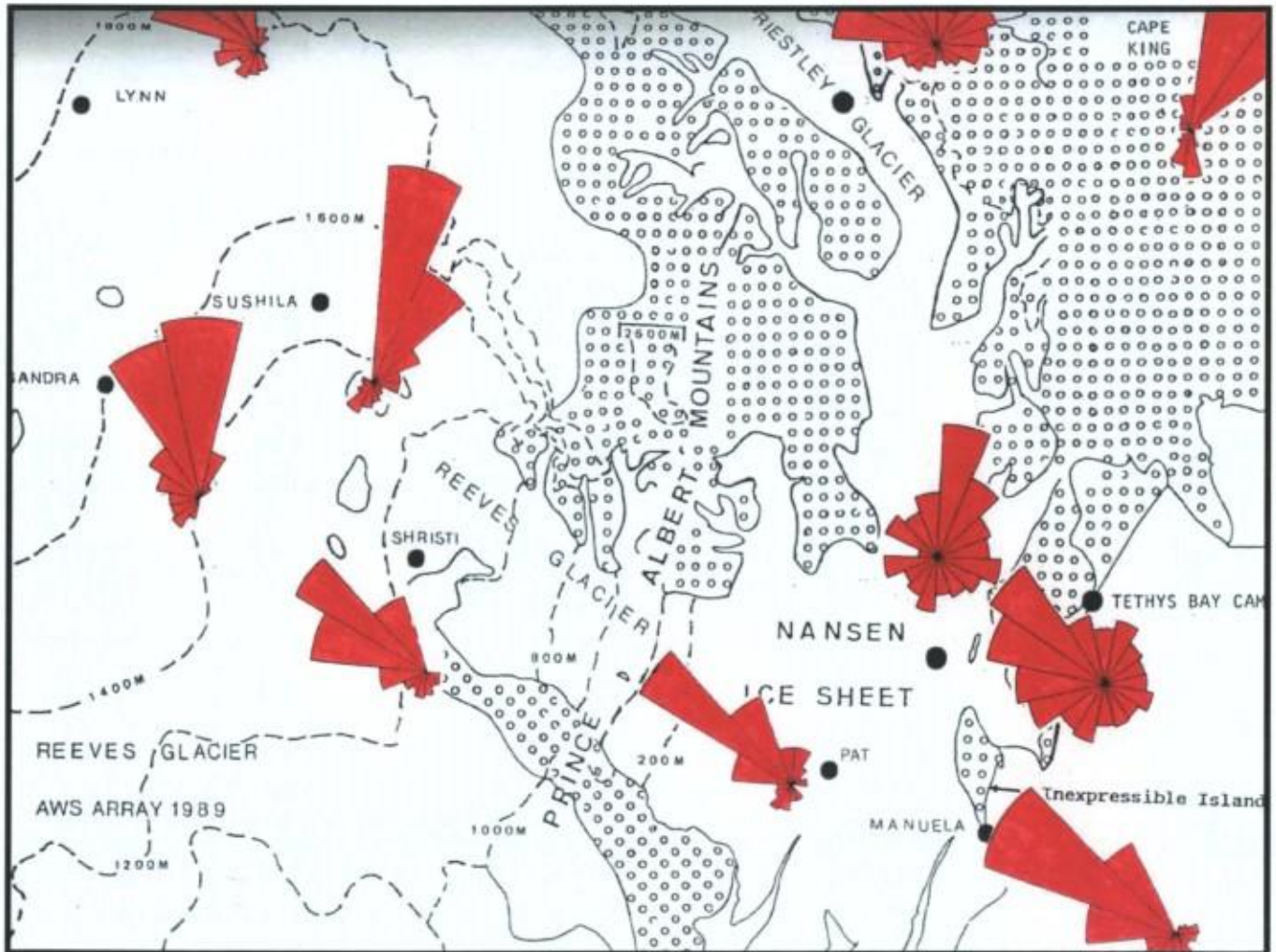


Figure 12: Sketch of the wind directions for all the AWS in the Terra Nova Bay area of interest, showing the yearly percentage of wind blowing in each sector (Ronveaux, 1992).



## 2.2. The Nansen Ice Sheet

As stated above, the Nansen Ice Sheet is actually an ice shelf, the grounding line of which runs in a roughly south-north direction across Reeves Glacier (Figure 13a), along the eastern side of Teall Nunatak (Frezzotti et al., 2000). The area we have focused our interest on is the branch of the Reeves Glacier flow, which passes North of Teall Nunatak. In that section, surface velocities at the grounding line vary between  $<50 \text{ m y}^{-1}$ , near Teall Nunatak, and  $100\text{--}150 \text{ m y}^{-1}$  further North (Frezzotti et al., 2000). Radio-echo soundings provided by the same authors show that ice thickness ranges from 120–150 m, in the highly crevassed area located halfway through (Figure 13b), to 600 m further North. In addition to crevasses, rifts have opened near the grounding line. Some contain “islands” of continental ice chunks that have been frozen in place by the surrounding sea/marine ice. From that point the shelf flows out into Terra Nova Bay for about 35 km to the front and it is about 25 km across between Tarn Flat and Inexpressible Island. These two bedrock features, together with the Northern Foothills laterally constrain the flow. The NIS 1 ice core (Figure 13c) was taken at  $74^{\circ}50.9'S$ ,  $162^{\circ}51.3'E$ , as close as was logistically possible to the grounding line, about 7.5 km downstream from it. Typical ice-flow horizontal velocities in the vicinity of the core site were measured by Frezzotti et al. (2000) to be about  $160 \text{ m y}^{-1}$ . These authors estimate that the ice shelf covers an area of approximately  $1800 \text{ km}^2$ , which make it a small to medium-sized ice shelf.

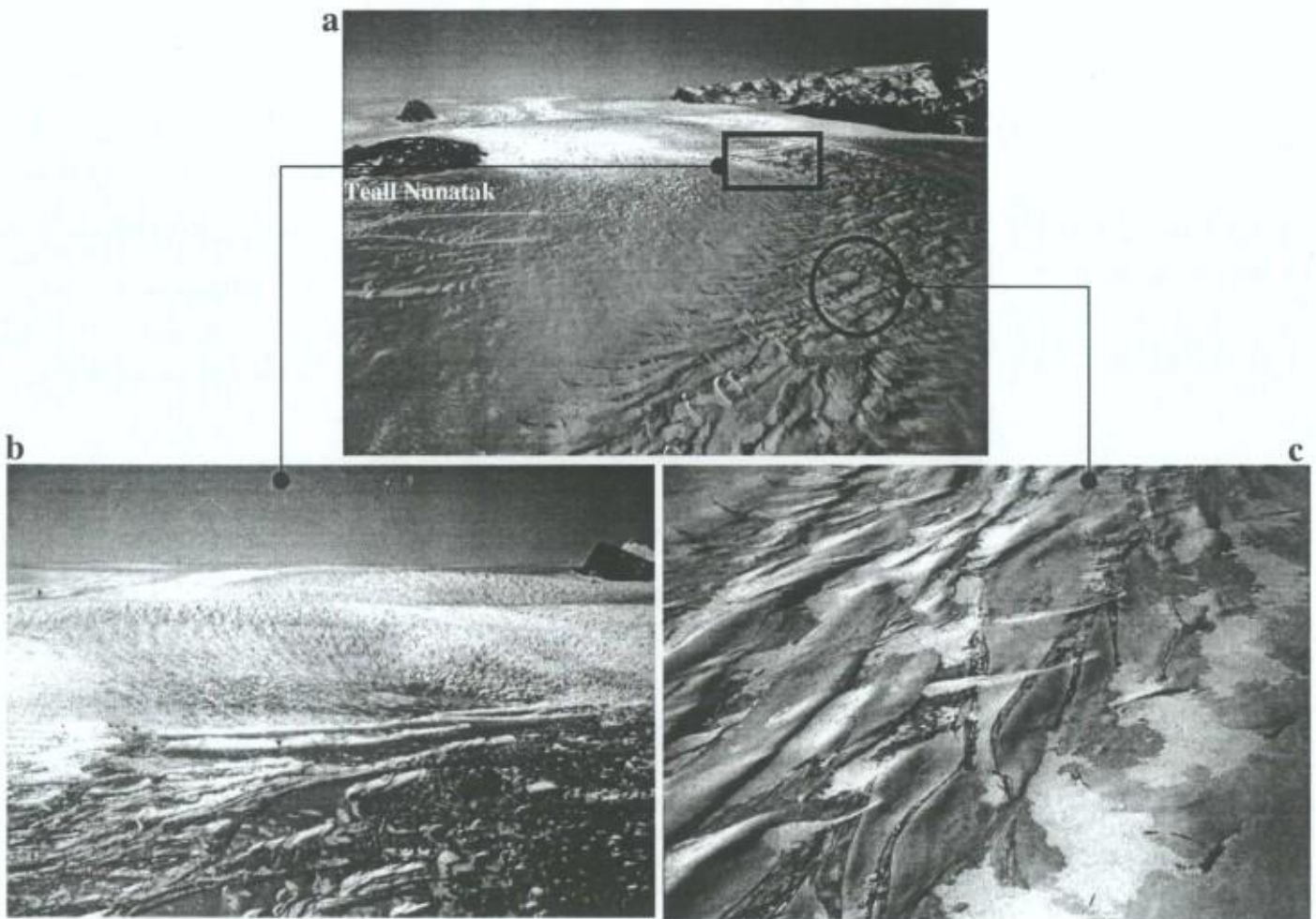


Figure 13: a) view of Nansen Ice Sheet towards Reeves Glacier; b) enlargement of rift and crevasses opening at the grounding line, North of Teall Nunatak; c) location of NIS1 drilling site



### 2.3. The Hells Gate Ice Shelf

Hells Gate Ice Shelf (HGIS - Figure 11, 14, 15 and 16) is a small Antarctic ice shelf located in Terra Nova Bay (Victoria Land, lat. 74°50'S, long. 163°50'E). It is derived from the larger Nansen Ice Sheet (NIS) and reaches the sea near Cape Russell. HGIS extends from North to South for 16.6 km with a maximum width of 9.8 km. It is composed of three main sectors (western, central, eastern) separated by two medial moraines stretching roughly North-South.



*Figure 14: view of Hells Gate Ice Shelf towards Priestley Glacier: note Vegetation Island (middle left), the Northern Foothills (middle right) and the two medial moraines. The front of the ice shelf is about 11 meters high and seen as a thin white line. Landfast sea ice is seen at the front, with a snow apron at the foot of the ice shelf cliff.*

A detailed glaciological study of the surface outcrops at HGIS (Bondesan and Tison, 1997) reveals a very complex interlacing of different ice types (Figure 15). *Snow* (light-brown/yellow areas in Fig. 15) covers the upstream half of the ice shelf, whilst it has been deflated from the lower half by the strong katabatic wind regime. In this downstream half, the main *meteoric ice* body of continental origin (light blue in Fig. 15, light grey in reality) is regularly covered by small patches of *lake ice* resulting from the freezing of summer surface meltwaters (orange in Fig. 15, light blue in reality). These concentrate in the local small surface depressions. *Marine ice* (light brown in Fig. 15, green-grey in reality) forms most of the frontal zone of the ice shelf, but also occurs as patchy outcrops generally organised in longitudinal or arched structures modelled by the complex dynamical behaviour of the ice shelf (see below). It is sometimes covered by a *veneer of sediments* (purple areas in Figure 15) that can participate in the development of ice-cored mounds 5-10 meters in height, typical of the western moraine. When the solid impurity load of the marine ice is higher, its green-greyish colour turns darker (dark blue in Figure 15). Evans Cove, the embayment in front of the ice shelf, is generally covered with seasonal landfast sea ice



until February. Finally, there is a narrow band of multi-year landfast sea ice fringing the ice shelf front, probably fed both from above (by the snow blown at the front) and from below (by the frazil escaping from the ice shelf-ocean interface).

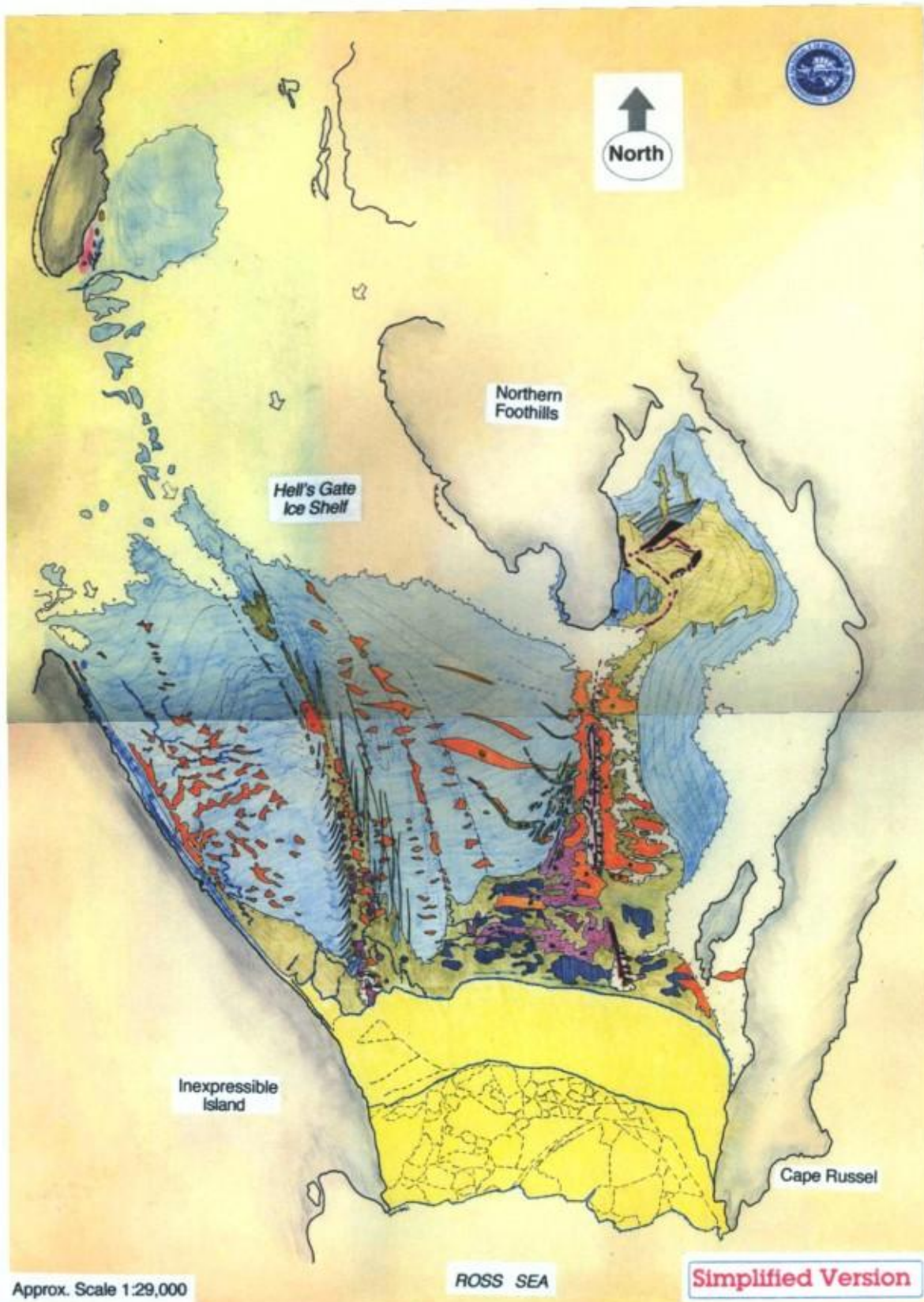


Figure 15: Glaciological map of Hells Gate Ice Shelf (courtesy of Prof. A. Bondesan): Snow = white, Meteoric ice = light blue, Lake ice = orange, Marine ice = light brown, debris covered ice = purple, debris-rich marine ice = dark blue (Bondesan and Tison, 1997)

Early radio-echo sounding (RES) profiles (Souchez et al., 1991) obtained about 1.5 km inland

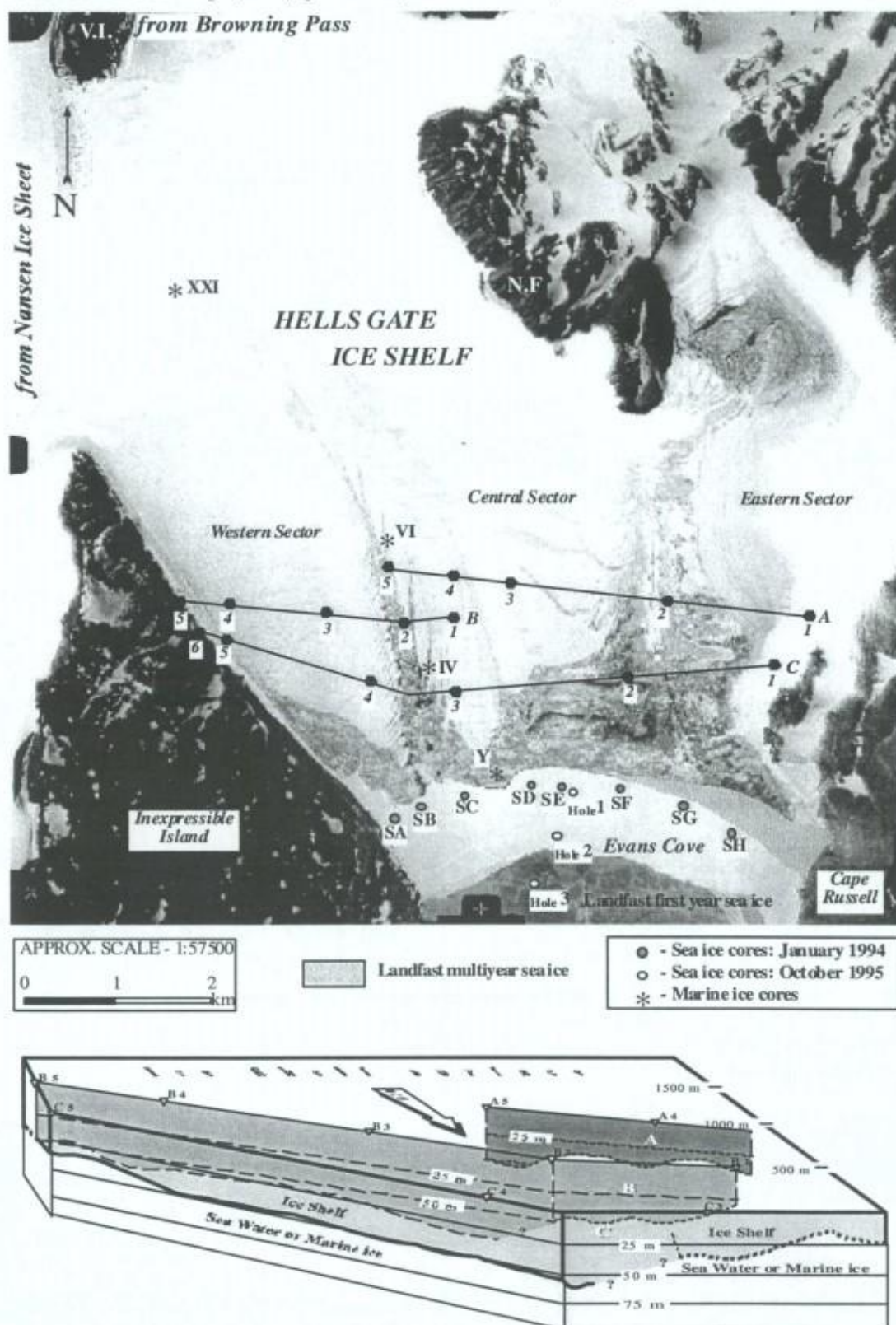


Figure 16: Top: Main features of Hells Gate Ice Shelf showing the position of the 1991 RES profiles (see text for details) and the location of the marine and sea ice cores (discussed in the following sections). Bottom: 3-D sketch of ice shelf thickness deduced from the 1991 echo-soundings. Aerial photograph in the background is: Terra Nova Bay - 11.06.1985 - FL 152.27 - TMA-2851-V. V.I. = Vegetation Island; N.F. = Northern Foothills (Tison et al., 1998).



from the ice front (Figure 16), showed a maximum ice shelf thickness of 70 m in the western sector reducing to only 20 m in some areas of the central sector. Furthermore, the interface picked-up by the RES was typically undulating in the central sector (A5-A3, B2-B1, C4-C3 in Figure 16 bottom), in phase with the clear-cut surface boundary between light-grey ice upstream and green-grey ice downstream. These data must, however, be treated carefully since, in several instances (especially in the central sector), the return signals were quite weak. It is, therefore, not known, in these cases, if the depth obtained corresponds to the ice-ocean interface, or to the continental meteoric ice-marine ice interface. Several arguments favour the latter hypothesis. First, seismic investigations (F. Merlanti, personal communication, May 1997) performed in the same area systematically provide higher ice thickness (22% higher in the western sector, 33% to 55% higher in the central sector). Secondly, isotopic ( $\delta^{18}\text{O}$ ,  $\delta\text{D}$ ) and crystallographic investigations of the surface clear-cut boundary indicate that it delimits continental meteoric ice (light gray, upstream) from marine ice (green-gray, downstream) (Lorrain et al., 1997; Tison et al., 1993). Finally, core Y (Figure 16, top), obtained downstream of line C within a few tens of meters of the ice front, reached a depth of 44 m, clearly in contradiction of the RES data from C3-C2. For the same reasons, more recent RES data from further upstream are somewhat discordant (Tison et al., 1997a and A. Lozej, personal communication). However, measurements agree on a thickness of about 150 m some 6 kilometers inland from the front. A maximum value of 250 m has been measured nearly 10 kilometers from the front, in the central part of the flow between Vegetation Island and the Northern Foothills (Figure 16, top).

The specific lay-out of the meteoric ice/marine ice boundary near the front, the shape of the marine ice outcrops visible upstream in the eastern part of the central sector, the large scale foliation patterns and the RES return from the central sector all suggest that the ice shelf results from the coalescence of several individual ice flows of different sizes, marine ice accreting in the upstream area (near the grounding area or around a pinning point) acting as a "welding unit" between these various ice flows (Tison et al., 1997a; Tison et al., 1998). This is a situation similar to the one detected, at a much larger scale (Figure 17), beneath the Ronne Ice Shelf by Corr et al. (1995). Comparing RES data to precise GPS/pressure determination of ice thickness at Ronne Ice Shelf revealed large discrepancies due to considerable lateral accumulation of marine ice between the Rutford and the Evans ice streams. These accumulations could only have formed as the two ice streams were ungrounding and joining together, upstream of the measured profiles.

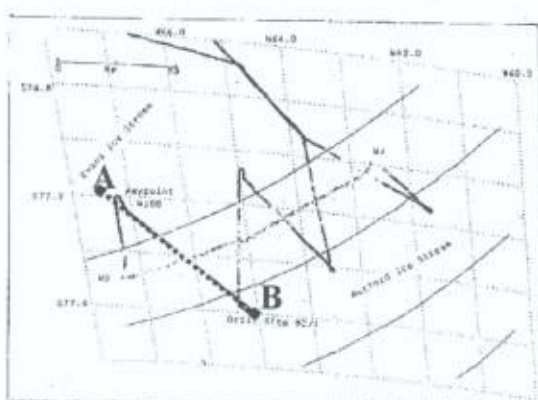
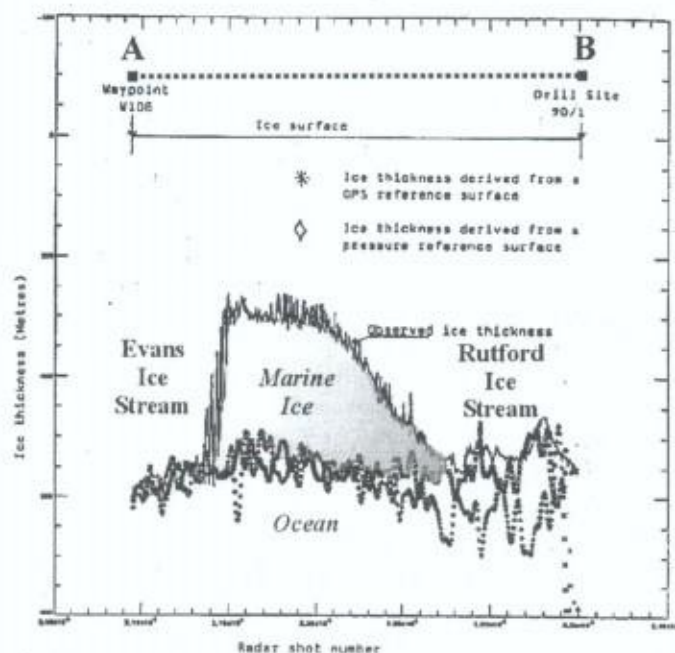
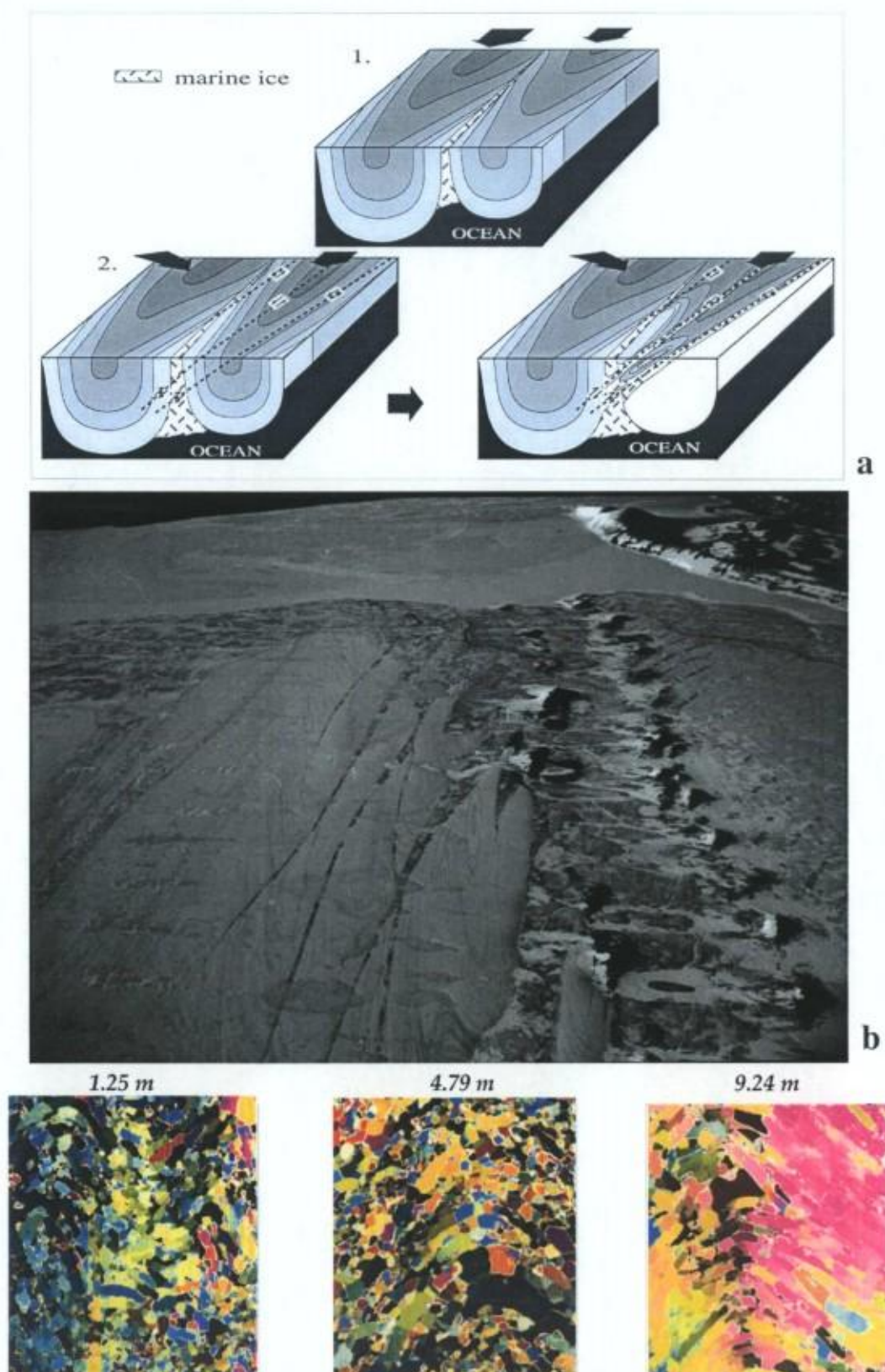


Figure 17: Marine ice detection between Evans Ice Stream and Rutford Ice Stream (Filchner-Ronne Ice Shelf) by combined remote sensing methods ("observed ice thickness" is the RES trace, compared to GPS and Pressure reference derived thickness) – Corr et al. 1995. See Figure 8 for location.







**Figure 18:** Deformational structures at Hells Gate Ice Shelf: a) Diagram illustrating the process of shearing at the junction of two individual ice flows with different flow directions (2); b) oblique aerial photograph of the western-central sector of HGIS, close to the ice shelf front (note the similarity of patterns with diagram a); c) three examples of folds and crystal bending in the marine ice at HGIS – thin sections are shown at scale 1:1 in the vertical plane between crossed polarizers (Tison et al., 1997a, 1998)



Large-scale morphological patterns (e.g. twin alignments of morainic dirt cones), marine ice outcropping patterns and ice foliation patterns also suggest a complex dynamical behavior of converging flow in the Hells Gate Ice Shelf. Side effects considerably affect the flow patterns in some areas (Tison et al., 1997a). An oblique component of the flow in the western sector brings the ice in compression against the central sector, and results in shearing of part of the marine ice initially accreted between the two flows (Figure 18a). This results in the typical outcropping and foliation patterns of Figure 18b. At a smaller scale, this compressive regime affects the crystal structure, which develop curved alignment of rectangular crystals and folded patterns. Similar features were successfully modeled and experimentally produced by Wilson et al. (1986) and Wilson and Zhang (1994).

Horizontal surface velocity were estimated using two independent techniques by Baroni (1990), Baroni et al. (1991a), Baroni et al. (1991b), and Frezzotti (1993). The western medial moraine is associated with marine ice forming at the southern tip of Vegetation Island (V.I. in Figure 16), where the flows from NIS and from Browning Pass meet. This moraine is composed of twin dirt cones that contain shells, worm tubes (serpulids) and sponges spicules, some in "living" position. Hypothesizing that these biogenic materials were incorporated into the marine ice at the ice-bedrock interface around Vegetation Island, dating of the shells (Baroni, 1990) provided estimates of surface velocities varying between 10.4 and 17.4 m y<sup>-1</sup>. Similarly, on the eastern moraine, velocities of 3 to 3.7 m y<sup>-1</sup> were obtained. These values are in good agreement with those calculated from comparison of aerial photographs taken in 1956 and 1985 giving 2.9 to 3.8 m y<sup>-1</sup> and 8.8 to 11.9 m y<sup>-1</sup> for the eastern and western sectors respectively (Frezzotti, 1993).

Marine ice accretion rates are difficult to assess from mass balance calculations, since these require surface strain rates measurements that are not available at present for HGIS. A crude estimate can, however, be made on the basis of shell dating and thickness estimates near the front. Baroni (1990) obtained a range of 0.122 to 0.250 m y<sup>-1</sup>, depending on the method used to correct the <sup>14</sup>C ages BP. These values are, however, minimum estimates, since the shells might have been brought to the surface further upstream in the ablation area, where thickness is higher. Another calculation can be made considering the surface velocity range obtained from aerial photographs for the western moraine, and the (minimum) seismic ice thickness of 126 m (F. Merlanti, personal communication, May 1997) measured at the location of marine ice core XXI. As clearly seen on Figures 15 and 16, this ice core is located on the most upstream outcrops of the marine ice body that formed at the southern tip of Vegetation Island. A somewhat higher range of 0.43 to 0.58 m y<sup>-1</sup> is obtained. These marine ice accretion rates are also higher than the surface ablation rates of 0.17 to 0.28 m y<sup>-1</sup> calculated by Baroni (1990) from dirt cone build-up rates or 0.20 to 0.30 m y<sup>-1</sup> estimated from bamboo poles ablation measurements (A. Bondesan, personal communication, June 1996). Finally, it should be underlined that all these estimated values are hypothesizing a constant accretion rate with time, which is not demonstrated.

Despite the obvious dynamical features described above, comparison of high precision static GPS measurements to local maregraphs indicate that most of the Hells Gate Ice Shelf reacts fully hydrostatically to the tidal forcing. Only in the strait between Vegetation Island and the Northern Foothills (Figure 15 and 16) does the ice shelf show departure from the hydrostatic equilibrium, in accordance with a scheme of bedrock valley sides' effects and periods of micro-seismic activity during part of the day (Bondesan et al., 1994).

## 2.4. The Campbell Glacier Ice Tongue

Campbell Glacier has its accumulation zone in the Transantarctic Mountains; it flows in a NNW-SSE depression carved into the Precambrian and Palaeozoic basement rocks (Carmignani et al., 1987). Being deviated by Mount Melbourne, which is a Cenozoic volcano, it acquires a more or less north-south direction, and shows a steeper gradient (Figure 11). The presence of small rock outcrops at this level indicates that the base of the glacier is above sea level. Then, Campbell Glacier reaches the sea where it terminates as a protruding glacier tongue.



The grounding line, usually defined as a line across the glacier where it first goes afloat, is thought to be located just south of the zone with the steeper gradient (Frezzotti, 1993). Radio-echo-sounding fails to detect it. The reflector is characterized by a weak energy contrast. This could be due to a change in the physical characteristics of the ice, the electromagnetic energy being absorbed because of the conductivity of a lower ice unit. Precise radio-echo-sounding is moreover difficult to perform in this crevassed area. Although the precise depth of the grounding line is not known, an approximate value can be given. A bathymetric survey in front of the ice tongue (Angrisano, 1989) gives a depth of about 160 m for the sea bottom. Over-deepening under the Campbell Glacier Tongue is a possibility but the grounding line depth should be around this value. The sampling site is about 3km downglacier from the presumed position of the grounding line.

The role of katabatic winds in the Campbell Glacier trough is much reduced, as opposed to the NIS-HGIS area. The winds are relatively weak so that the entire glacier is accumulating snow on its surface and, even at the terminus of the floating tongue, a substantial part of the ice cliff is made of ice derived from snow deposited on the tongue. As a result, there is no upward movement of ice and therefore marine ice, if present at the bottom, is not likely to outcrop at the terminus of the floating tongue. However, the southwestern part of the ice tongue near Gondwana Station has impinged on bedrock promontories or protuberances. Consequently, basal ice containing debris layers is visible and can be sampled. At the sampling site (Figure 19 left), a stacked sequence, a few meters thick, dipping 60° towards the centre of the glacier tongue shows two distinctive types of ice interbedded with bubbly glacier ice (Figure 19 right). A first type located in the upper part of the basal sequence consists of bands

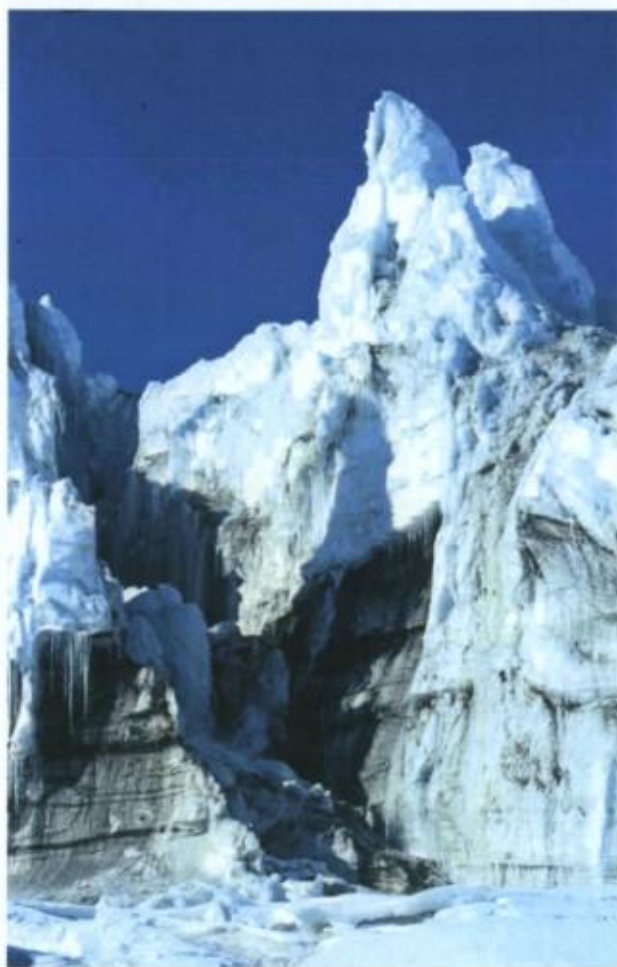


*Figure 19: Left – The sampling site at Campbell Glacier Tongue. Right – Close up of the sampling site, showing the two different types of ice (1 and 2) described in the text.*



of bubble-free ice with a thickness of the order of a few centimetres. The second type, located in the lower part of the basal sequence, shows bands of thin clear ice layers and layers of fine debris sometimes appearing folded with a few occasional pebbles. The proportion of bubbly glacier ice layers is much lower in this case. Debris consists mainly of quartz grains with rounded shapes and smooth edges (60%), volcanic glasses with elongated bubbles (30%) and lithic fragments. A few sponge spicules and shell fragments are also present. The heavy minerals mainly consist of pyroxenes (80%) indicating a major volcanic component and a few olivine, garnet and epidote minerals. The SEM (X-ray energy dispersion probe) analysis of the volcanic glass gives a dispersion in a  $\text{SiO}_2$  versus alkali diagram similar to that of rocks from the nearby Shield Nunatak complex (Worner et al., 1989), thus suggesting a local origin.

**Paper 1**

**The Glaciological Map of Hells Gate Ice Shelf  
(Terra Nova Bay, Antarctica)**

**Authors**

**A. Bondesan, J.-L. Tison**

**Journal**

**Terra Antarctica Reports, Vol. 1**

**Year**

**1997**





## **The Glaciological Map of Hells Gate Ice Shelf (Terra Nova Bay, Antarctica)**

A. BONDESAN<sup>1</sup>, J.-L. TISON<sup>2</sup>

<sup>1</sup>Dipartimento di Geografia "G. Morandini", Università di Padova, Via del Santo 26,  
35123 Padova - Italy

<sup>2</sup>Département des Sciences de la Terre et de l'Environnement, Université Libre de  
Bruxelles, Avenue F. D. Roosevelt 50, B-1050, Bruxelles - Belgium

The Hells Gate Ice Shelf (HGIS) is located in Terra Nova Bay, south of the Italian Antarctic Station. It extends 16.6 km north to south and has a maximum width of 9.8 km; the total area is more than 70 km<sup>2</sup>. It is nourished by the Priestley Glacier and by the ice flow from Browning Glacier. The HGIS is bounded by the northern Foothills to the east, Vegetation Island and Nansen Ice Sheet to the north, Inexpressible Island to the west and the Ross Sea to the south.

The glaciological map of HGIS is based on the field research carried out during the 1993-1994 Italian Antarctic Expedition as part of the Italo-Belgian joint glaciological research program. Data from former studies by Italian and Belgian researchers also greatly contributed to the making of this map.

Since the only available topographical map of this region is the U.S. Geological Survey 1:250 000 sheet "Mt. Melbourne", the cartographic basis that was adopted for the glaciological map of HGIS is an uncontrolled mosaic (approximate scale 1:25 000) derived from the black and white aerial photographs of the TMA 6-11-85 flight. The GPS geodetic measurements performed in 1994 (10 points) will allow the geometric georeferencing of topographical and morphological features in the area. The recent 1993 flight, especially programmed above HGIS, is also expected to bring new lights to the photointerpretation of the HGIS surface.

The glaciological map combines the photointerpretation of aerial photographs (1956-57 and 1985) with field survey performed during the 1993-94 Italian Antarctic Expedition. The great detail of the high-quality aerial images and the opportunity that we had to study and check the various glacial features directly in the field, under different climatic conditions, allowed us to identify properly the different glacial subsets and covers. Problematic cases were eventually investigated through ice corings and field studies of the ice textural characteristics.

The data covered by the map can be organized in the following forms:

- a) *snow and firn*. The borders between snow and ice were traced taking into account the strongly conservative snow patches and coverages; snow cover due to occasional snow precipitations were not mapped;
- b) *glacier ice*. It is easily recognized on aerial photographs and in the field; it shows a smooth surface, often with very clear foliation patterns, wide topographical undulations and a whitish color;
- c) *marine ice*. It forms at the ice/ocean interface at the base of the ice shelf and it is carried to the surface due to intense surficial ablation by katabatic winds. It is characterized by a greyish



A. Bondesan & J.-L. Tison

- color, rough surface, higher susceptibility to degradation during the warm season, presence of abundant marine debris and marine specimen remnants;
- d) *sea ice*. It extends seaward of the ice shelf cliff. In some places it turns into multiyear fast ice. It breaks up annually and frees the bay (Evans Cove) of ice. It is one of the most variable features of the map and therefore it was referred to a single date (from aerial photographs);
  - e) *lake ice*. During the seasonal increase in air temperature, melt water lakes form over a large part of the ice shelf surface. Afterwards, water freezes inside the topographical depressions and the lakes are easily recognized even during colder seasons. They develop both on glacier ice and on marine ice. Their position is very stable through the years;
  - f) *cones*. These are the most elevated and remarkable forms on the ice shelf. Other features linked to glacial deposits are: *supraglacial debris*, *erratic boulders*, *perched blocks*, *sinking stones* and *salt cones*, represented with their usual symbols;
  - g) the *ice cliff* existing at the front of the ice shelf was reconstructed according to its height above sea level, with the date of the observation; where it exists, the ramp in glacial front is traced;
  - h) regarding the *hydrography*, we mapped the main *melt water streams* (*bédières*) and the *melt water lakes*;
  - g) referring to the glacial dynamics and the related surficial forms, we mapped *pressure ridges*, *ice bulges* and *domes*, and the *sausage-like ridges* formed by the ice shelf movement against the rock border of Inexpressible Island;
  - h) using geophysical and topographical surveys, remote sensing and stable isotope analyses of the ice samples, it will be possible to individualize the *glacial flows* and the *flow directions*. The main *foliations* were identified by photointerpretation, and studied later in the field and from a helicopter. In certain conditions of visibility, we observed from the air more detailed and fine structures, hardly mappable without a suitable cartographic control;
  - i) only the main *crevasses* are traced (or series of crevasses), usually not clearly visible; *cracks* in fast ice, even though not fundamental, are shown. Other existing features are the *ice foot*, the *fast ice margin* and the *hummocked ice*. Where outcropping among the marine debris, the *marine specimens* are traced on the map. Also the approximate *floating area* and the *grounding line* will be traced on the map, if determined by recent research data;
  - j) last, regarding the *aeolian forms and processes*, we mapped: *snowdrifts*, *snowbarchans*, *sastrugi*, *wind scoops*, *snow deflation* and *corrasion* and the *wind direction*, as shown by aeolian morphology. Also the *thermokarst ablation* will be shown;
  - k) some supplementary and important information will also be added, including, for example, *geochronological dating* (with age, method and material), *ice drillings performed* (with depth), *geophysical surveys* (with method used), *stable isotope analyses*, *ice depth*, *snow accumulation and ablation*, *GPS measurements*, *mean annual temperature*, *wind direction* and *velocity*.

The glaciological map of Hells Gate was compiled as part of the geomorphological survey carried out in the boundary areas of the Northern Foothills and Inexpressible Island by A. Bondesan, M. Meneghel & M.C. Salvatore.

The map (scale 1:50 000), which is descriptive in many aspects, is designed as a basis for future interpretation of the dynamical behaviour of the ice shelf.

#### ACKNOWLEDGEMENTS

This work was carried out with the financial support of the Italian *Programma Nazionale di Ricerche in Antartide (P.N.R.A.)*.



## The Glaciological Map of Hells Gate Ice Shelf

## REFERENCES

- Baroni C., 1990. The Hells Gate and Backstairs Passage Ice Shelves, Victoria Land, Antarctica. *Mem. Soc. Geol. It.*, **43**, 123-144.
- Baroni C., Frezzotti M., Giraudi C. & Orombelli G., 1991. Ice flow and surficial variation inferred from satellite image and aerial photograph analysis of Larsen Ice Tongue, Hells Gate and Nansen Ice Shelves (Victoria Land, Antarctica). *Mem. Soc. Geol. It.*, **46**, 69-80.
- Baroni C. & Orombelli G., 1991. Holocene raised beaches at Terra Nova Bay, Victoria Land, Antarctica. *Quat. Res.*, **36**, 157-177.
- Baroni C., Stenni B. & Jacumin P., 1991. Oxygen isotopic composition of the ice samples from the Hells Gate and Backstairs Passage Ice Shelves (Victoria Land, Antarctica): evidence of bottom freezing. *Mem. Soc. Geol. It.*, **46**, 45-48.
- Caneva G., Lozej A., Merlanti F. & Tabacco I., 1994. Risultati preliminari della prospezione geoelettrica sulla piattaforma di Hells Gate, this volume.
- Chinn T. J. H., Whitehouse I. E. & Hofle H. C., 1989. Report on a reconnaissance of the glaciers of Terra Nova Bay Area. *Geol. Jb.*, **E38**, 299-319.
- Frezzotti M., 1992. Fluctuation of ice tongues and ice shelves derived from satellite images in Terra Nova Bay, Victoria Land, Antarctica. In: Yoshida Y. et al. (eds), *Recent progress in Antarctic Earth Science*, Terra Scientific Publishing Company, Tokyo. 733-739.
- Frezzotti M., 1993. Glaciological study in Terra Nova Bay, Antarctica, inferred from remote sensing analysis. *Annals of Glaciology*, **17**, 63-71.
- Frezzotti M., 1993. Analisi delle piattaforme e delle lingue di ghiaccio galleggianti della Terra Vittoria (Antartide) tramite immagini da satellite e fotografie aeree. *Geogr. Fis. Dinam. Quat.*, **15**, 107-109.
- Priestley R.E., 1923. British (Terra Nova) Antarctic Expedition 1910-13. Physiography (Robertson Bay and Terra Nova Bay regions). Harrison & Sons, London, 1-95.
- Souchez R., Meneghel M., Tison J.L., Lorrain R., Ronveaux D., Baroni C., Lozej A., Tabacco I. & Jouzel J., 1991. Ice composition evidence of marine ice transfer along the bottom of a small Antarctic ice shelf. *Geophys. Res. Lett.*, **18**, 849-852.
- Souchez R., Tison J.L., Fléhoc C., Stiévenard M., Jouzel J. & Maggi V., 1995. Investigating processes of marine ice formation in a floating ice tongue by a high resolution isotopic study. *J. Geophys. Res.* (in press).
- Tison J.L., Ronveaux D. & Lorrain R., 1993. Low salinity frazil ice generation at the base of a small antarctic ice shelf. *Antarctic Science*, **5** (3), 309-322.

## **Paper 2**

**A Dynamical Approach to Explain Ice Structures and Complex Morainic Genesis on a Partially Grounded Ice Shelf (Hells Gate Ice Shelf - Victoria Land, Antarctica)**

## **Authors**

**J.-L. Tison, A. Bondesan, G. Delisle, A. Lozej, F. Merlanti, L. Janssens**

## **Journal**

**Terra Antarctica Reports, Vol. 1**

## **Year**

**1997 (a)**





*Terra Antarctica Reports*  
1997, 1, 33 - 37

## **A Dynamical Approach to Explain Ice Structures and Complex Morainic Genesis on a Partially Grounded Ice Shelf (Hells Gate Ice Shelf - Victoria Land, Antarctica)**

J.-L. TISON<sup>1</sup>, A. BONDESAN<sup>2</sup>, G. DELISLE<sup>3</sup>, A. LOZEJ<sup>4</sup>,  
F. MERLANTI<sup>5</sup>, L. JANSSENS<sup>1</sup>

<sup>1</sup>Département des Sciences de la Terre et de l'Environnement,  
Université Libre de Bruxelles; 50, Av. F.D. Roosevelt, 1050 Bruxelles - Belgium

<sup>2</sup>Dipartimento di Geografia, Università di Padova, Via del Santo 26, 35123 Padova - Italy

<sup>3</sup>Bundesanstalt für Geowissenschaften und Rohstoffe, Stilleweg 2,  
30655 Hannover 51 - Germany

<sup>4</sup>Dipartimento Scienze della Terra, Sez. Geofisica, Università di Milano, Via Cicognara 7,  
20129 Milano - Italy

<sup>5</sup>Dipartimento Scienze della Terra, Università di Genova, Viale Benedetto XV 5,  
16132 Genova - Italy

### **INTRODUCTION**

The Hells Gate Ice Shelf (HGIS), a small Antarctic ice shelf of about 70 km<sup>2</sup> surface area, has always been a source of attraction in the Terra Nova Bay region (Fig. 1). It displays a unique collection of glaciological features that raise many questions, not only for glaciologists, but also geologists, oceanographers, biologists and paleo-climatologists. Its peculiar meteorological regime, with strong katabatic winds sustaining large ablation rates, makes it a unique site to study ice shelf mass balance and marine ice accretion processes (Souchez et al., 1991; Tison et al., 1993; Lorrain et al., 1995 - this volume and Tison et al., 1995 - this volume). Although static GPS measurements indicate free response of the ice shelf to the tidal forcing in its lower part (Bondesan et al., 1995 a, b - this volume), glaciological features at the ice shelf surface call for partial grounding (*sensu lato*) and/or significant side effects on the flow patterns.

### **GLACIOLOGICAL FEATURES AND FIELD MEASUREMENTS**

Large scale morphological patterns (ice shelf morphology south of Vegetation Island (Figs. 1 and 2) including: active and fossil crevasses - topographical height where the Nansen Ice Sheet feeds into HGIS - topographical low between the Western and Central sector of HGIS, upstream of the twinned Western dirt cone moraine), marine ice differentiated outcropping patterns, complex ice foliation patterns, morphology of the Western (dirt cones) moraine and bathymetry near the ice shelf front have been brought together to propose a model for the HGIS flow.

Preliminary "helicopter-borne" radar measurements were also performed at the end of the 1993-1994 field season (IX Italian Antarctic expedition) to discriminate grounded and floating areas



J. L. Tison et al.

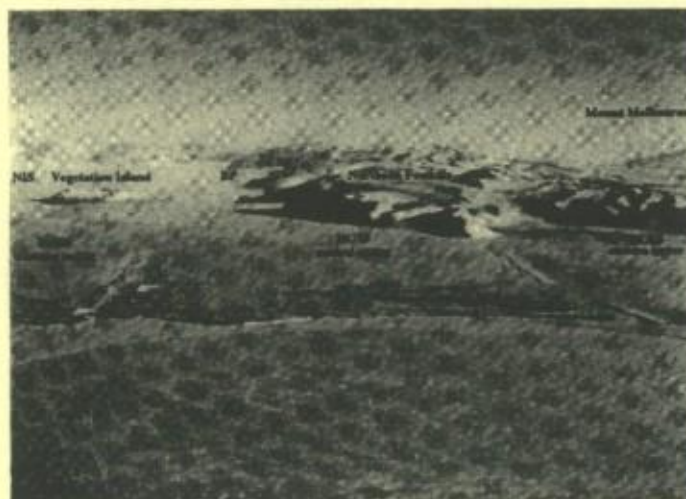


*Fig. 1* - General view of Hells Gate Ice Shelf (HGIS), looking North. Note from West to East (left to right on the photograph) Topographical height where the flow from Nansen Ice Sheet (NIS) feeds into HGIS, Vegetation Island in the background, S-shaped (darker) topographical low between the two major inflows from NIS and Browning Pass area (BP), twinned Western dirt cones moraine in the foreground, inversed V-shaped foliation pattern A (Fig. 3a) between two distinct flows of the Central sector, Eastern twin-crested moraine running South of Cape Confusion, the Northern Foothills in the background and the tip of Mount Melbourne in the far East.

at HGIS. Thirty punctual "in-flight" radar measurements were performed using a frequency of about 35 MHz. The broken flight line ran approximately as follows : across the Browning Pass ice inflow from the Northern Foothills to the southern tip of Vegetation Island - to Cape Confusion - to the northern tip of Inexpressible Island - to the southern tip of Vegetation Island again and, finally, to the ice shelf front in the direction of Cape Russell. The distinction between floating ice and ground based ice was made on the basis of the amplitude and form of the reflected EM-wave. Floating ice (or a water layer in ice) produces one strong high amplitude reflection. From ground based ice one expects a whole sequence of weaker reflections, the usually bumpy sub-ice surface offers numerous reflecting surfaces that all contribute to the returning signal.

### PROPOSING A DYNAMICAL MODEL FOR HGIS

Figure 2 sketches a tentative dynamical model for HGIS as it can be inferred from the data collection enumerated above. Numbers on the figure refer to the following steps :

- 1) flow from the Nansen Ice Sheet (NIS) comes into HGIS with a relatively "steep" slope (see also Fig. 1)
- 2) ice from Browning Pass and, possibly, partially from the Priestley Glacier, flows in-between Vegetation Island and the Northern Foothills
- 3) as it approaches the grounding line and/or the contact line with the flow from the NIS, the flow from Browning Pass (BP) develops a major active crevasse quickly filled with blown snow. Fossil scars of this major accident can easily be tracked down glacier as topographical lows extending across the HGIS upstream section (see also Fig. 1)
- 4) where the two flows meet along the grounding line in the western part, frazil ice accumulates in the sub-ice shelf inverted depression, eventually entraining organic fragments in "live" position. The S-shaped surface topographical low observed upstream of the western moraine,



## Ice Structures and Complex Morainic Genesis, Hells Gate Ice Shelf



Fig. 2- Proposed dynamical model for HGIS (see text for explanation)

between the two major feeding flows (see also Fig. 1), can be the result of either the transition to a floating regime (?), or the reduced ice thickness there (?) or the increased density due to the marine ice component (?)...

- 5) the eastern part of the Browning Pass composite flow appears to unground further downstream. Each flow keeps its structural properties (see foliation pattern A in figure 3a and natural equivalents in Fig. 1 and 4-left), and frazil accumulates at the flow junctions
- 6) as the composite flow from Browning Pass hits the bedrock shoulder visible in the bathymetry in front of the ice shelf, it grounds again
- 7) newly formed frazil accumulates in a pattern parallel to the ice-bedrock contact, forming thin lineated marine ice outcrops, similar to the one observed along Inexpressible Island and Vegetation Island
- 8) marine ice formed in-between individual flows (see 5) buckles on the obstacles, and the flow is diverted true South, towards the sea
- 9) two distinct bands of debris-rich marine ice crop out near the front, probably indicating large scale folding due to compression on the obstacle
- 10) as the overwhelming flow of the NIS meets the BP flow with an oblique component, new active shear planes can develop, provided that the ice shelf is partially grounded (*sensu lato*). The new foliation patterns expected (Fig. 3b) correspond to those observed (Fig. 4-right).

J. L. Tison et al.

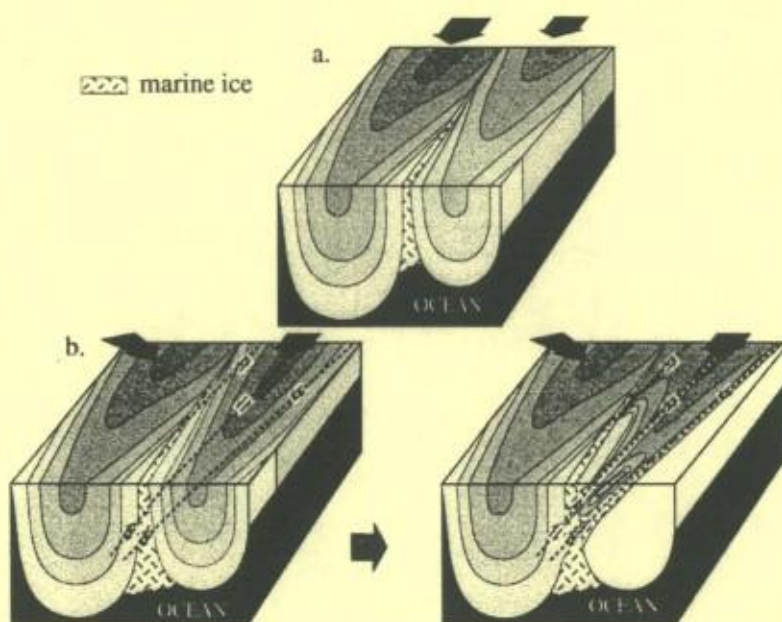


Fig. 3- Sketch of foliation patterns expected in different flow conditions (see text for explanation): a) parallel flow; b) oblique flow in partially grounded conditions..



Fig. 4 - Foliation patterns at HGIS, looking South-West. Foliation pattern A (Fig. 3a) resulting from sub-parallel flow, is visible at the extreme left of the picture. Foliation pattern B (Fig. 3b) is clearly illustrated on the Eastern (left) flank of the twinned Western dirt cones moraine visible at the right of the picture.



## Ice Structures and Complex Morainic Genesis, Hells Gate Ice Shelf

11. if a continuous debris layer inside the marine ice is cross-cut by these active shear planes, discrete amounts of debris will be delivered to the surface by ablation to the east of the initial debris layer position, and form the eastern row of dirt cones (Fig. 4). Since the active shear planes are discrete, the amounts of debris left in-between, will come to the surface later on along the initial position of the debris layer and form the western row of dirt cones (Fig. 4)

## FUTURE WORK

The model presented above is deliberately provocative. It partly relies on preliminary echo-sounding measurements that refute some data acquired from other techniques. For example, GPS measurements (Bondesan et al., 1995a, b) detect a freely floating ice shelf where echo soundings see it grounded. One could argue that punctual "in-flight" echo sounding measurements might be less reliable than continuous ground records, since the latter help discarding localized discontinuities. On the other hand, ice surface conditions were very bad at the time of measurement (extensive melting and abundance of bedières and melt water lakes). However, radio-echo soundings from the ground failed to succeed earlier in the season, and the data used here are the only one presently available for the Northern part of the ice shelf. Extensive ground echo sounding traverses were planned for the 1994-1995 field season together with new GPS measurements, and should therefore considerably improve our perception of grounded and floating areas at HGIS. The model nevertheless satisfactorily explains numerous glaciological features of HGIS and therefore should be of considerable help for further developments.

## ACKNOWLEDGEMENTS

The authors are greatly indebted to the Italian *Programma Nazionale di Ricerche in Antartide* (PNRA) and to the logistic team of Terra Nova Bay for unconditional and efficient support in the field. This paper is a contribution to the Belgian Antarctic Program (SSTC - Science Policy Office). J.-L. Tison is Research Associate at the Belgian National Fund for Scientific Research (F.N.R.S.).

## REFERENCES

- Bondesan A., Capra A., Gubellini A. & Tison J.-L., 1995a. Recording vertical movements of a small Antarctic ice shelf by static GPS measurements (Hells Gate Ice Shelf, Victoria Land), This volume.
- Bondesan A., Capra A., Gubellini A. & Tison J.-L., 1995b. On the use of static GPS measurements to record the tidal response of a small antarctic ice shelf (Hells Gate Ice Shelf - Victoria Land). *Geogr. Fis. Dinam. Quat.*, **17**(1994), 123-129.
- Lorrain R., Tison J.-L., Bondesan A., Ronveaux D. & Meneghel M., 1995. Preliminary results from 60 shallow cores and from one 45-m deep marine ice core at Hells Gate Ice Shelf, Victoria Land, Antarctica. This volume.
- Souchez R., Meneghel M., Tison J.-L., Lorrain R., Ronveaux D., Baroni C., Lozej A., Tabacco I. & Jouzel J., 1991. Ice composition evidence of marine ice transfer along the bottom of a small Antarctic ice shelf. *Geophys. Res. Lett.*, **18**, 849-852.
- Tison J.-L., Ronveaux D. & Lorrain R., 1993. Low salinity frazil ice generation at the base of a small antarctic ice shelf. *Antarctic Science*, **5** (3), 309-322.
- Tison, J.-L., Barbante, C., Bondesan, A., Lorrain, R. & Capra, A., 1995. Ice Shelf/Ocean interactions at the front of Hells Gate Ice Shelf (Terra Nova Bay - Antarctica). This volume.

### **Paper 3**

**On the Use of Static GPS Measurements to Record the Tidal Response of a Small Antarctic Ice Shelf (Hells Gate Ice Shelf, Victoria Land)**

### **Authors**

**A. Bondesan, A. Capra, A. Gubellini, J.-L. Tison**

### **Journal**

**Geografia Fisica Dinamica Quaternaria, Vol. 17**

### **Year**

**1994**



Geogr. Fis. Dinam. Quat.  
17 (1994), 123-129, 4 figg.

ALDINO BONDESAN (\*), ALESSANDRO CAPRA (\*\*), ALBERTO GUBELLINI (\*\*) &  
JEAN-LOUIS TISON (\*\*\*)

## ON THE USE OF STATIC GPS MEASUREMENTS TO RECORD THE TIDAL RESPONSE OF A SMALL ANTARCTIC ICE SHELF (HELLS GATE ICE SHELF, VICTORIA LAND)

**ABSTRACT:** BONDESAN A., CAPRA A., GUBELLINI A. & TISON J.L., *On the use of static GPS measurements to record the tidal response of a small antarctic ice shelf (Hells Gate Ice Shelf, Victoria Land)* (IT ISSN 0391-9838, 1994).

Recent developments of GPS (Global Positioning System) technology provide a new powerful tool to study ice shelf-ocean dynamical interactions. Here we present results from feasibility tests on the use of static GPS measurements to locate grounding zones and study their impact on the ice shelf mechanical response. The Hells Gate Ice Shelf has been chosen as a study case owing to its vicinity from Terra Nova Bay Station and to the peculiar problems it raises to glaciologists and geophysicists.

Technical and analytical problems are discussed and 5 short time lapse records, in various places at the ice shelf surface, are interpreted. Most of the survey stations appear to react fully hydrostatically to the tidal forcing, even during a secondary maximum of only a few centimeters amplitude. The most upstream station 4, located in a strait between Vegetation Island and the Northern Foothills, shows departure from hydrostatic equilibrium in accordance with a scheme of bedrock valley sides effects. The GPS curve recorded suggests that the ice shelf might not always behave elastically in grounding zones as also testified by periods of intense microseismic activity into the ice shelf during part of the day.

**KEY WORDS:** Global Positioning System, Ice shelf dynamics, Tidal forcing, Grounding zones.

**RIASSUNTO:** BONDESAN A., CAPRA A., GUBELLINI A. & TISON J.L., *Uso del GPS in modalità statica per registrare l'oscillazione di marea di una piccola piattaforma antartica di ghiaccio galleggiante (Hells Gate Ice Shelf, Terra Vittoria)* (IT ISSN 0391-9838, 1994).

Il recente sviluppo della tecnologia GPS (*Global Positioning System*) offre un nuovo potente strumento per studiare le interazioni dinamiche tra piattaforme di ghiaccio galleggiante e oceano. Qui vengono presentati i risultati dei test di fattibilità finalizzati all'uso delle misurazioni GPS in modalità statica per localizzare le zone di ancoraggio al fondo (*grounding zones*) e studiare il loro impatto sulla risposta meccanica delle piattaforme di ghiaccio galleggiante. La piattaforma di Hells Gate è stata scelta come area campione a causa della vicinanza alla Stazione Baia Terra Nova e alla particolare problematica di interesse glaciologico e geofisico.

Sono discussi i problemi tecnici e vengono interpretate 5 registrazioni a breve intervallo, effettuate in vari punti della superficie della piattaforma. La maggior parte delle stazioni di misura sembrano reagire idrostaticamente alle sollecitazioni di marea, perfino durante un massimo secondario di pochi centimetri di ampiezza. La stazione 4, localizzata più a monte di tutte, tra Vegetation Island e le Northern Foothills, mostra un allontanamento dalle condizioni di equilibrio forse per l'effetto generato dai versanti vallivi rocciosi. La curva GPS registrata suggerisce che la piattaforma potrebbe non sempre comportarsi elasticamente nelle *grounding zones*, come anche testimoniato dai periodi di intensa attività microsismica (*icequakes*) durante parte del giorno nell'area della stazione 4.

**TERMINI CHIAVE:** Global Positioning System, Dinamica delle piattaforme di ghiaccio galleggiante, Sollecitazioni di marea, Zone di ancoraggio al fondo.

(\*) Dipartimento di Geografia «G. Morandini», Università di Padova, Via del Santo, 26, 35123 Padova, Italy.

(\*\*) Istituto di Topografia, Geodesia e Geofisica Mineraria, Università di Bologna, Viale Risorgimento, 2, 40136 Bologna, Italy.

(\*\*\*) Département des Sciences de la Terre et de l'Environnement, Université Libre de Bruxelles, Avenue F. D. Roosevelt, 50, B-1050, Bruxelles, Belgium.

This work was carried out as part of the «Programma Nazionale di Ricerche in Antartide» (Italianantartide). The glaciological research frame, in which this note is included, is coordinated by Prof. G. Orombelli. The authors are grateful to the logistic staff of Terra Nova Bay for the constant and tireless support in field operations. We are also indebted to Prof. Carlo Stocchino for the tidal records he kindly provided and to the «geophysical team» of the Project «Glaciology and Paleoclimate», in particular F. Merlanti, for the geophysical data.

The authors are especially indebted to Prof. G.B. Castiglioni and Prof. G. Orombelli for their helpful and constructive comments as referees of the manuscript. A. Bondesan and J.-L. Tison planned the research and made the glaciological interpretations of the GPS data; A. Gubellini and A. Capra made the field measurements and the data analyses of GPS records. Every stage of the research is anyway the result of full collaboration among the authors.

## INTRODUCTION

Glaciological studies of the last decades have now well established the fundamental role played by ice-shelves in controlling ice-sheet mass balance. Boundary conditions at grounding lines (or pinning points), where the ice gets afloat (or regrounded), is still a critical step in simulating ice sheet sensitivity to climatic changes. Modelling needs testing against field evidences and therefore numerous attempts were made to localize grounding lines and to study their impact on ice shelf dynamics using various techniques.



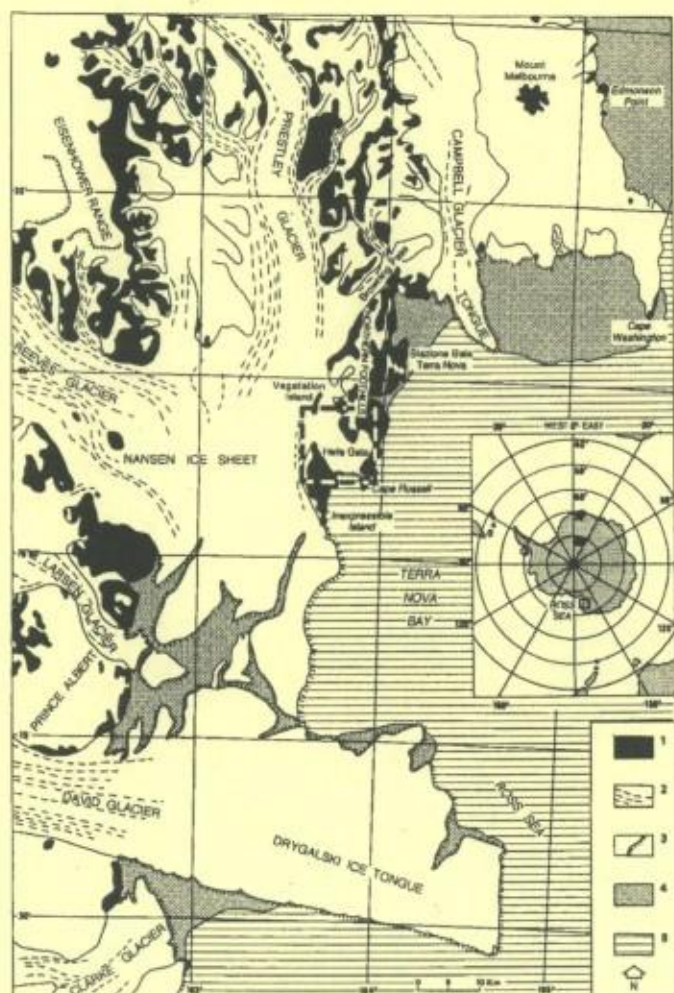


Fig. 1 - Index map of the Terra Nova Bay area (after OROMBELLI, 1986, modified). Legend: 1) Ice-free area, 2) Glacier, 3) Ice shelf and ice tongue, 4) Sea ice (Dec. 1963), 5) Sea.

Initially, before the recent development of GPS applications, the lack of any height reference on the ice shelf surface has required the use of unconventional techniques to detect the ice shelf response to tidal forcing (PEDLEY & *alii*, 1986). Gravity meters were most commonly used (after THIEL & *alii*, 1960) but also records of vertical movements of floating fast ice along the ice shelf (BISHOP & WALTON, 1977), tilt measurements of tidal flexure near grounding lines (STEFFENSON & *alii*, 1979), and pressure measurements on the sea floor (POTTER & *alii*, 1985; PEDLEY & *alii*, 1986) providing power spectrum records of tidal heights. These latter data have shown strong non-linear response to tidal forcing on the George VI Ice Shelf (Antarctic Peninsula) that were tentatively associated to an anelastic component in the deformation of the ice near the grounding line (PEDLEY & *alii*, 1986). Most recently, JACOBEL & *alii* (1994) tested the use of Landsat thematic mapper images to infer grounding line position against an array of field measurements, namely radar profiling, velocity measurements and tilt studies of ice flexure. Their

results point to the need of using several techniques in conjunction, to compensate weaknesses inherent to each individual type of measurement. Recently, repeated kinematic GPS measurements were used by VAUGHAN (1994) to locate the position of the grounding line under the Rutford Ice Stream and to analyze the mechanical response of the ice shelf to tidal forcing.

This work presents preliminary results from feasibility tests on the use of static GPS measurements to locate grounding zones under the Hells Gate Ice Shelf, a small antarctic ice shelf located in Terra Nova Bay, Victoria Land.

## THE HELLS GATE ICE SHELF

The Hells Gate Ice Shelf is located in Terra Nova Bay (Ross Sea), to the South of the Italian Antarctic Station, along the coastal belt of Transantarctic Mountains (lat.  $74^{\circ} 50' S$ , long.  $163^{\circ} 50' E$ , fig. 1). It can be considered as part of the Nansen Ice Sheet, from which it is separated along its western margin by the outcropping relief of Vegetation Island and Inexpressible Island. It extends from North to South for 16.6 km with a maximum width of 9.8 km, to the South of Cape Confusion, and its total area is more than 70 km<sup>2</sup>. It is fed by the ice flow from Browning Glacier, by some small glaciers outflowing from the Northern Foothills and, partially, by the Priestley Glacier. The Hells Gate Ice Shelf is surrounded by the Northern Foothills to the East, Vegetation Island and Nansen Ice Sheet to the North, Inexpressible Island to the West and the Ross Sea to the South (Evans Cove).

Owing to its peculiarities this ice shelf has been extensively studied by glaciologists and geophysicists during the last Italian antarctic expeditions, but still its glacial morphology and dynamics raise many unsolved questions.

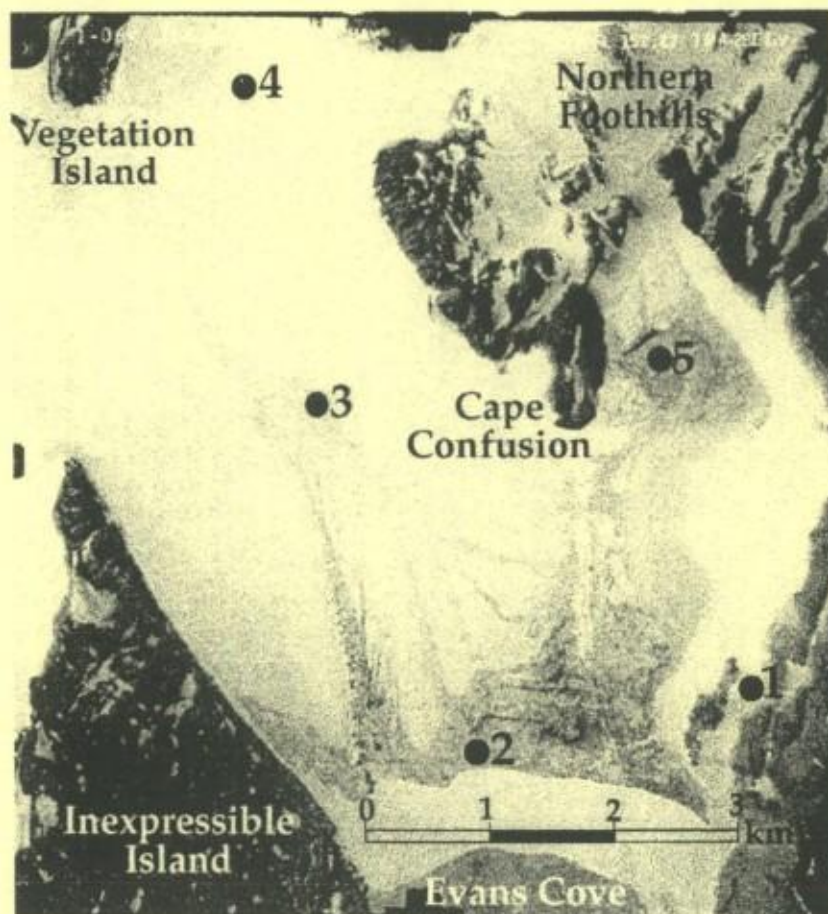
The ice shelf surface is conventionally divided into three sectors, separated to the East by a twin-crested morainic ridge and to the West by two alignments of ice-cored debris cones made of massive clast-supported diamict, locally showing a sandy matrix (supraglacial till). The supraglacial morainic deposits contain a great amount of marine subfossil specimens (Serpulids, Cirripedia and various shells) thought to have been incorporated into the marine ice accreting at the ice shelf bottom, close to the grounding line (BARONI, 1990). Other complex moraines outcrop near Cape Confusion and a composite lateral moraine develops to the East of Vegetation Island.

This ice shelf is also characterized by a strong uprise of its flow lines towards the surface, due to intense surficial ablation by the katabatic winds descending from the Antarctic Plateau and blowing with great intensity and frequency across the ice shelf (hence its name, given in 1912 by the «Northern Party» of the Scott Expedition).

Hells Gate Ice Shelf was described for the first time by PRIESTLEY (1923) in its study of Robertson Bay and Terra Nova Bay and it was reproduced very precisely in a



FIG. 2 - Main features of the Hells Gate Ice Shelf and survey stations location (after BONDE-SAN & *alii*, 1994a, b). Aerial photograph TMA-2851-V of 11-06-1985.



1:250.000 map. Later on, CAMPBELL & CLARIDGE (1975) focused on the study of the debris cones emerging between the western and central sector, and TISON & *alii* (1994b) recently proposed a dynamical model explaining the genesis of this morainic complex.

Paleoglaciological reconstruction from BARONI & OROM-BELLI (1991) showed an advance of the Hells Gate Ice Shelf following a glacio-eustatic uprise of the coastal margin in the area.

Several studies also dealt with evaluation of the surficial velocity of Hells Gate Ice Shelf, based either on  $^{14}\text{C}$  geochronological dating of subfossils remnants or on aerial photographs and satellite images studies (see for example, BARONI, 1990; BARONI & *alii*, 1991a, BARONI & *alii*, 1991c; FREZZOTTI, 1993). Both techniques provided similar values of about  $3.3 \text{ my}^{-1}$  for the eastern moraine. On the western dirt cones alignments, however, a slight discrepancy exists between the  $^{14}\text{C}$  derived velocities ( $10.4$  to  $17.4 \text{ my}^{-1}$  for shells incorporation around the southern part of Vegetation Island) and the photointerpretation ( $8.8$  to  $11.9 \text{ my}^{-1}$ ).

Stable isotopes measurements ( $\delta^{18}\text{O}$ ) of ice samples from the ice shelf (BARONI & *alii*, 1991b) revealed outcropping marine ice (ice resulting from the freezing of sea water accreting at the base of the ice shelf) in its frontal zone, thereby indicating basal freezing under the ice shelf. Co-isotopic (both in  $\delta\text{D}$  and  $\delta^{18}\text{O}$ ), chemical and crystallographic analyses shed more light on the processes involved in the formation of this marine ice (SOUCHÉZ & *alii*, 1991; RONVEAUX, 1992; TISON & *alii*, 1993; LORRAIN &

*alii*, 1994). These studies suggested contrasted depositional environments for the different types of marine ice observed, related to the morphology of the submerged portion of the ice shelf and to the ocean circulation in front and below the ice shelf (TISON & *alii*, 1994a). Topographical measurements performed on the debris cones (BARONI, 1990) also allowed to estimate the accumulation rates due to basal freezing ( $5\text{--}25 \text{ cm y}^{-1}$ ) and the surface ablation rates ( $16.5$  to  $36.5 \text{ cm y}^{-1}$ ), supposing hydrostatic equilibrium.

Finally, geophysical investigations (gravimetry surveys, geoelectrical measurements, active and passive seismic and radar measurements) are about to solve the complex problem of discriminating between continental ice/ marine ice/ ocean/ bedrock interfaces returns (CANEVA & *alii*, 1994a to c; LOZEJ & *alii*, 1994).

For the purpose of the experiments related to the present work, a small network of 5 GPS survey stations was settled to record the response of the ice shelf to tidal forcing. The stations were selected as follows (fig. 2):

- station 1: designed to be the altimetric reference point it was placed on a rocky outcrop near Cape Russell;
- station 2 to 4: positioned on a longitudinal transect from the ice shelf front to the strait between Vegetation Island and the Northern Foothills; these three stations were intended to record the transition from the freely floating part to the grounded part of the ice shelf;
- station 5: was chosen to detect any tidal influence in this highly sheltered zone, to the East of Cape Confusion.



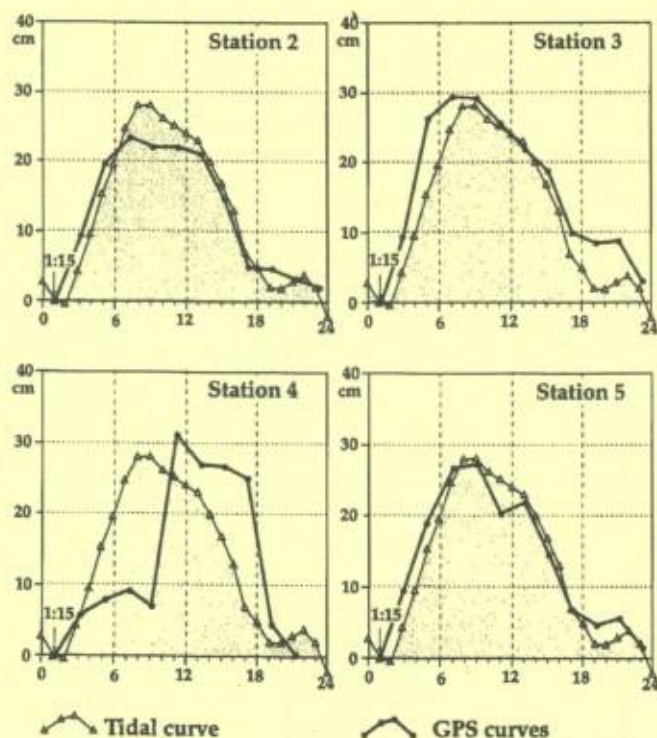


FIG. 3 - Relative vertical movement of Hells Gate Ice Shelf on 5th January 1994 as a function of time for GPS survey stations 2 to 5. The measured tidal curve for the same day near Terra Nova Bay (data from C. Stocchino) is also given as a background (see text for explanation).

## METHODOLOGY OF GPS MEASUREMENTS

The measurements were made simultaneously using four Trimble 4000 SSE and one 4000 SST GPS receivers on the five survey points.

In this experimental phase, kinematic GPS survey was discarded for logistic reasons, since the instruments batteries did not have the necessary stored energy to cover 24 hours of continuous measurements. A rapid static survey has alternatively been chosen, based on 12 measurements of 30 minutes duration each, at two hours intervals. This technique allows more precise measurements than the kinematic survey, however one must keep in mind the error associated to the movement of the survey station during the 30 minutes of observation. In the present case, this was verified to be in the precision range of the method. Kinematic GPS survey has the potential advantage to tackle the problem of possible high frequency ice shelf oscillations, given the continuous record of height changes. An experiment of kinematic survey measurement of ice shelf oscillations has been performed contemporaneously on Drygalski Glacier by FREZZOTTI & alii (1994).

Another important problem, that should be addressed for future measurements, is the possible vertical displacement of the receivers tripods due to ice melting under solar radiation. In the present case, tripods were simply laid on the ice surface and tripods sinking of 10 to 12 cm were

observed after the 24 hours measuring session. A mean sinking rate of 0.5 cm/hour was then used to correct the GPS measurements (except for station 1 that was settled on a bedrock promontory), hypothesizing a similar effect at all survey stations. One way to tackle this problem would be to design an instrument holder that could be firmly buried into the ice.

Two different softwares (*GPSurvey* and *Topas Turbo*) were used to elaborate the data. Where data acquisition was not much disturbed (points 2, 3, 5) the two softwares gave similar results. On point 4, however, where data acquisition was strongly disturbed, results were quite different. The noise in data acquisition is most probably linked with ionospheric effects, multipath effects and imaging phenomenon being difficult to invoke in this case. In a peculiar session, *Topas Turbo* gave a float solution, with 29 unresolved cycle slips, while *GPSurvey* gave a fixed solution, that assumes cycle slips resolution. However, the more regular trend of *Topas Turbo* solutions and the strange anomalies of *GPSurvey*, suggest that the *Topas Turbo* algorithm is probably more appropriate where the measurements are strongly disturbed. Therefore, in Antarctica, where a lot of cycle slips exist due to ionospheric noise, this software appears more reliable. The different effects of ionospheric noise on point 4 with respect to the other measurement points could be due to the use of different GPS receivers: a 4000 SST receiver was used on point 4, while 4000 SSE receivers were used on the other points. In fact, in the older 4000 SST receivers the signal squaring technique is used, while in the 4000 SSE receivers a cross-correlation procedure between the two signals, L1 and L2, enables to avoid the signal squaring, that amplifies the noise.

## RESULTS AND DISCUSSION

### *The tidal forcing curve*

In order to provide a base for the interpretation of ice shelf vertical movement curves, it is necessary to know the tidal forcing curve that they should mimic, in a pure hydrostatic equilibrium. Such a tidal curve for the 5<sup>th</sup> January 1994 was kindly provided by Prof. Carlo Stocchino on the basis of the tide-gauge recordings at Terra Nova Station, about 20 km to the North of Hells Gate Ice Shelf.

### *The GPS curves*

The relative vertical movement of the ice shelf as a function of time is plotted on figure 3 for points 2 to 5. The measured tidal curve is also given as a background. The main features of the curves can be summarized as follows:

- a) Curves 2, 3 and 5 show a similar pattern with:
  - synchronously peaking values between 7:15 and 9:15, in phase with the maximum of the tidal cycle;
  - dissymmetric profile, with a regular ascend and a step-like behaviour at the last stages of descend (17:15 to



21:15), in phase with the secondary maximum of the tidal curve.

b) On the longitudinal profile of points 2-3-4, the amplitude of the vertical movement clearly increases upstream.

c) Curve 4, unlike the others, shows:

- a 3-hours time-lag in the achievement of the maximum amplitude;
- a step-like behaviour in the ascending phase, that doesn't exist in the tidal curve;
- a plateau followed by a sharp decrease in the descending phase, whereas the tidal curve shows a more regular gradient.

#### *Interpretation limits*

Given the conditions of this experimental phase, one must take a certain number of limiting factors into account when interpreting the curves of fig. 3. For example, given the incertitude on the real rate of sinking of tripods at each survey point, differences in amplitude of less than 5 cm for simultaneous measurements on different stations should not be considered as significative. On the other hand, it should be noted that the tidal forcing curve is only strictly valid for Terra Nova Bay, and that coastal configuration, like engulfments and straits, can considerably affect the tidal curve both in amplitude and phase.

#### *Is the Hells Gate Ice Shelf in full hydrostatic equilibrium?*

Fig. 4 schematically illustrates possible effects of bedrock sides (like, for example, in a fjord or on the flanks of a pinning point) and of bottom topography in the vicinity of the grounding line, on the oscillation of an ice shelf in response to tides. Only the excess hydrostatic pressure due to the tidal forcing is taken into account in the drawings of fig. 4.

Away from any bedrock sides and from the grounding line, the ice shelf will react fully hydrostatically to the tidal forcing (HOLDSWORTH, 1977; PEDLEY & *alii*, 1986), and the recorded curve for altitudinal changes will mimic the tidal cycle (dashed line on the graphs of fig. 4). Close to bedrock sides, the excess hydrostatic pressure can be splitted into two components: a shear stress parallel to the local bedrock and a tensile (low to high tide) or a compressive (high to low tide) stress perpendicular to the bedrock. The build-up of stresses at the initial stages of ascending and descending tides will set up a delay in the mechanical response of the ice shelf to the tidal forcing. Once a critical value is reached, the energy is released through ice deformation. The GPS curve should then be typically dissymmetric with a step-like behaviour just after low tide and high tide. Depending on the geometry of the system (length to height ratio of the ice shelf's cross section; contact area with the bedrock sides) a possible phase-lag could also be observed between the two curves.

Where a hummocky bedrock topography exists, near the grounding line (lower fig. 4-(a)), the GPS curve of a

survey station nearby will reflect the combined effects of stress build-up on the local obstacle sides and increasing (low to high tide) or decreasing (high to low tide) decoupling of the glacier from its bed. At rising tide, the delay in the response to tidal forcing due to the stress build-up in the ice will be progressively compensated by the increasing surface area submitted to the excess hydrostatic pressure. Around high tide, full decoupling will eventually occur and the GPS curve will catch up with the tidal cycle. From high to low tide, stress build-up in the ice will slow down the ice shelf response shortly after contact has been recovered with the bedrock bottom topography. Eventually, the ice shelf sinking will follow on during the low tide period. As a result the full GPS curve should also be dissymmetric, with a concave rising limb (concavity depending on bedrock obstacles spectrum), a summit in phase with the tide and a multistep-like descending limb.

Curves 2, 3 and 5 from Hells Gate Ice Shelf are in good agreement with the tidal cycle and it can therefore be reasonably estimated that in these survey points the ice shelf is in hydrostatic equilibrium, a necessary condition for ice shelf mass balance calculations from simple dynamical models (BARONI, 1990). Interestingly enough, even the secondary maximum recorded at Baia Terra Nova is present in the three curves. Since this maximum is only a few centimeters high, it gives us confidence in the relatively small error range estimated for the field measurements. The hydrostatic behaviour of point 5 was also unexpected, given its location very close to the shore, in a small engulfment near Cape Confusion. The small size of the catchment feeding the floating ice in this area probably strongly reduces the ice thickness and favours buoyancy very close to the valley side.

On the longitudinal profile of survey stations 2-4, the amplitude of the vertical movement increases upstream. Although the total altitudinal difference of the maximum is only about 10 cm, and could therefore be very close to the interpretation limits, this is coherent with an engulfment increasing effect on the tidal amplitude. Much more striking is the difference in profiles between point 2-3 and point 4. The latter shows departure from an hydrostatic behaviour. This is not surprising given its location in a strait between Vegetation Island and the Northern Foothills. The GPS profile is similar to the one predicted for bedrock side effects (fig. 4-above), adding a phase delay between high tide and maximum ice shelf altitude. However this latter effect could be the expression of tide retardation inland, with regard to the Terra Nova Bay prediction; this may also depend on the *establishment of the port* due to the shape of the Evans Cove engulfment in which the Hells Gate Ice Shelf flows, combined with a *river tide* effect. The GPS curve nevertheless ends up in phase again with the low tide from Terra Nova Bay. The geophysical team working on Hells Gate Ice Shelf placed over the shelf surface, at survey site 4, a microseismic station to test the microseismic activity into the glacial body for a period of 3 days (CANEVA & *alii*, 1994a to c; LOZEJ & *alii*, 1994; MERLANTI, personal communication). Intense icequakes activity was detected in restricted periods (about 8 hours) of the day and these result might well be



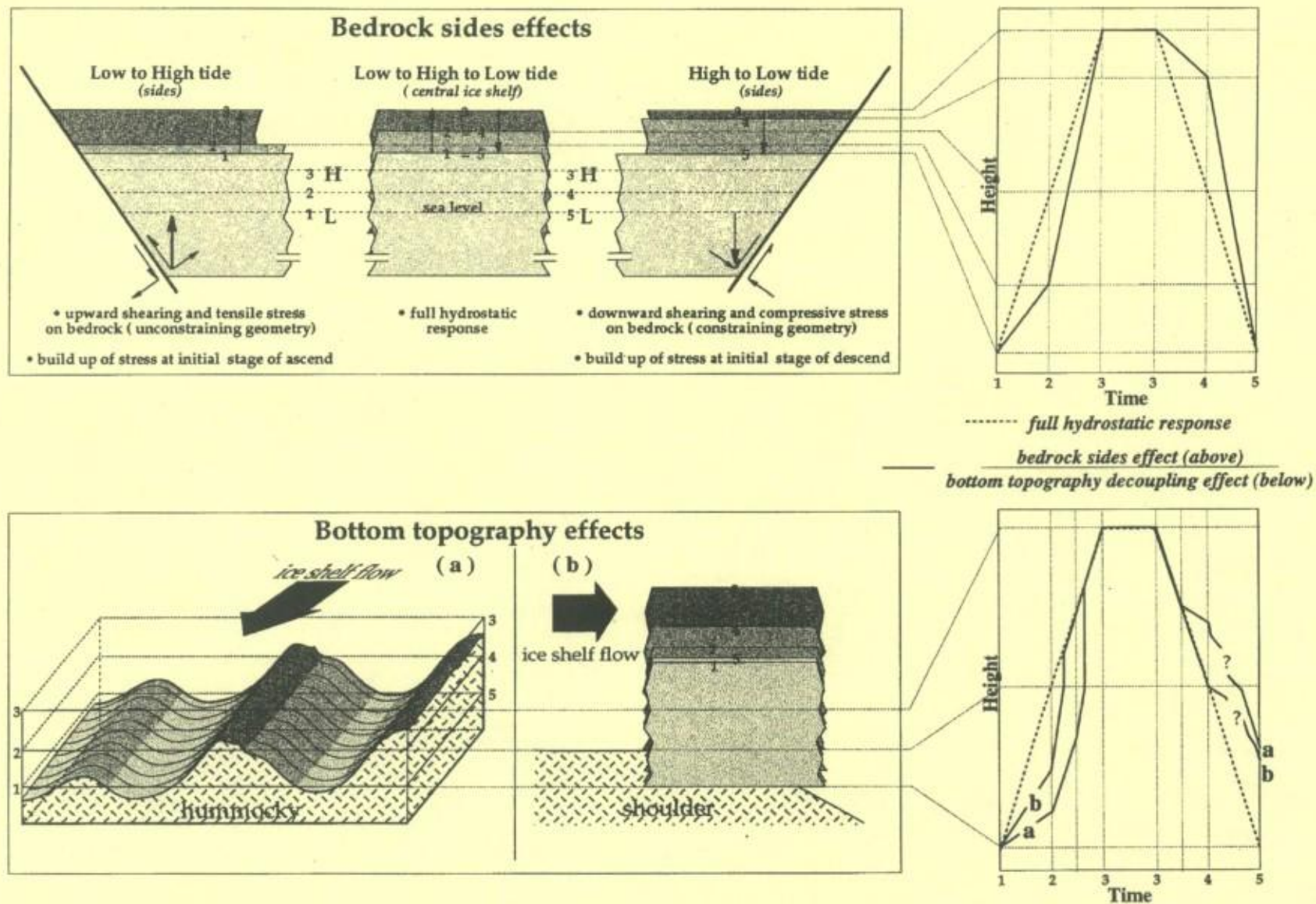


FIG. 4 - Schematic representation of hypothesized bedrock sides and bottom topography effects on the ice shelf's vertical movement. Numbers refer to time steps (1 and 5 = middle of low tide, 3 = middle of high tide, 2 = half time between 1 and 3, 4 = half time between 3 and 5). Shaded areas on the «hummocky bottom topography» correspond to successive areas that would be freed by the ice if there was no mechanical delay.



linked with the stress build-up episodes in the ice. Similar concentrated icequakes activities were reported between high tide and low tide by VAN DER OSTEN-WOLDENBURG (1990) around an ice rumple on Ekström Ice Shelf (Akta Bay, Antarctica).

Vegetation Island thus apparently acts as a pinning point at the level of survey station 4, and the real grounding zone should probably be searched for further upstream in this area.

## CONCLUSION

GPS altitudinal changes records provide us with better insights into the mechanical response of ice shelves to tidal forcing. Beside the possible location of a grounding line where ice shelf oscillation simply breaks down, it shows that there are several possible situations where the ice shelf does not freely respond to hydrostatic pressure changes linked with tides. This would favour the larger concept of grounding «zones» or «areas», as opposed to grounding «lines». GPS studies, coupled with microseismic measurements, could provide valuable informations on the type of dynamic response of the ice shelf to the excess hydrostatic stress applied. The case study of GPS survey station 4 at Hells Gate Ice Shelf suggests that the ice shelf might not always behave elastically in grounding areas, as suggested by PEDLEY & *alii* (1986) but not detected by VAUGHAN (1994).

Future static GPS surveys should rely on improved survey station settings to avoid receivers drift, and test runs should be designed to accurately evaluate advantages and disadvantages of kinematic and rapid static methods. These tests should also focus on a better understanding of software performances in highly disturbed data acquisition situations that seem to occur in Antarctica.

## REFERENCES

- BARONI C. (1990) - *The Hells Gate and Backstairs Passage Ice Shelves, Victoria Land, Antarctica*. Mem. Soc. Geol. It., 43, 123-144.
- BARONI C., FREZZOTTI M., GIRAUDI C. & OROMBELLI G. (1991a) - *Ice flow and surficial variation inferred from satellite image and aerial photograph analysis of Larsen Ice Tongue, Hells Gate and Nansen Ice Shelves (Victoria Land, Antarctica)*. Mem. Soc. Geol. It., 46, 69-80.
- BARONI C. & OROMBELLI G. (1989) - *Glacial geology and geomorphology of Terra Nova Bay (Antarctica)*. Mem. Soc. Geol. It., 33, 171-193.
- BARONI C. & OROMBELLI G. (1991) - *Holocene raised beaches at Terra Nova Bay, Victoria Land, Antarctica*. Quat. Res., 36, 157-177.
- BARONI C., STENNI B. & JACUMIN P. (1991b) - *Oxygen isotopic composition of the ice samples from the Hells Gate and Backstairs Passage Ice Shelves (Victoria Land, Antarctica): evidence of bottom freezing*. Mem. Soc. Geol. It., 46, 45-48.
- BARONI C., STENNI B. & LONGINELLI A. (1991c) - *Isotopic composition of Holocene Shells from raised beaches and ice shelves at Terra Nova Bay (Northern Victoria Land, Antarctica)*. Mem. Soc. Geol. It., 46, 93-102.
- BISHOP J.F. & WALTON J.L.W. (1977) - *Problems encountered when monitoring tidal movement in extremely cold conditions*. Polar Record, 18 (116), 502-505.
- BONDESAN A. & TISON J.L. (1994a) - *Glaciological Research on Hells Gate Ice Shelf (Terra Nova Bay, Antarctica)*. Field Data Reports, IX ItaliAntartide Expedition, 54-56.
- BONDESAN A. & TISON J.L. (1994b) - *The glaciological map of Hells Gate Ice Shelf (Terra Nova Bay, Antarctica)*. Incontro di Studio del Progetto di Ricerca Glaciologia e Paleoclima, Roma, 20-21 Giugno 1994, Enea. (Abstract).
- CAMPBELL J.B. & CLARIDGE G.G. (1975) - *Occurrence of dirt cones in Antarctica (note)*. New Zealand Jour. Geol. Geoph., 18, 349-355.
- CANEVA G., LOZEJ A., MERLANTI F. & TABACCO I. (1994a) - *Integrated geophysical surveys of the Hells Gate Ice Shelf and the Enigma Lake Basin (Nern Victoria Land)*. Field Data Reports, IX ItaliAntartide Expedition, 59-60.
- CANEVA G., LOZEJ A., MERLANTI F. & TABACCO I. (1994b) - *Risultati preliminari della prospezione geoelettrica sulla piattaforma di Hells Gate*. Incontro di Studio del Progetto di Ricerca Glaciologia e Paleoclima, Roma, 20-21 Giugno 1994, Enea. (Abstract).
- CANEVA G., LOZEJ A., MERLANTI F. & TABACCO I. (1994c) - *Sperimentazione di metodologie per lo studio della dinamica delle piattaforme galleggianti: l'esempio di Hells Gate*. Incontro di Studio del Progetto di Ricerca Glaciologia e Paleoclima, Roma, 20-21 Giugno 1994, Enea. (Abstract).
- FREZZOTTI M. (1993) - *Glaciological study in Terra Nova Bay, Antarctica, inferred from remote sensing analysis*. Ann. Glaciol., 17, 63-71.
- FREZZOTTI M., VITTUARI L. & MAGGI V. (1994) - *Dynamics of David Glacier and Drygalski Ice Tongue*. Incontro di Studio del Progetto di Ricerca Glaciologia e Paleoclima, Roma, 20-21 Giugno 1994, Enea. (Abstract).
- HOLDSWORTH G. (1977) - *Tidal interaction with ice shelves*. Ann. Geophys., 33, 133-146.
- JACOBEL R.W., ROBINSON A.E. & BINDSCHADLER R.A. (1994) - *Studies of the grounding line location on Ice Streams D and E, Antarctica*. Ann. Glaciol., 20, 39-42.
- LOZEJ A., MERLANTI F., PAVAN M. & TABACCO I. (1994) - *Risultati preliminari delle prospezioni sismiche a rifrazione e riflessione sulla piattaforma di Hells Gate*. Incontro di Studio del Progetto di Ricerca Glaciologia e Paleoclima, Roma, 20-21 Giugno 1994, Enea. (Abstract).
- LORRAIN R., TISON J.L., BONDESAN A., RONVEAUX D. & MENEGHEL M. (1994) - *Preliminary results from 60 shallow cores and from one 45 m deep marine ice core at Hells Gate Ice Shelf, Victoria Land, Antarctica*. Incontro di Studio del Progetto di Ricerca Glaciologia e Paleoclima, Roma, 20-21 Giugno 1994, Enea. (Abstract).
- OROMBELLI G. (1986) - *La prima spedizione del Programma Nazionale di Ricerche in Antartide. Osservazioni geomorfologiche*. Riv. Geogr. It., 93, 129-169.
- PEDLEY M., PAREN J.G. & POTTER J.R. (1986) - *The tidal spectrum underneath antarctic ice shelves*. Journ. Geophys. Res., 91, C11, 13001-13009.
- POTTER J.R., PAREN J.G. & PEDLEY M. (1985) - *Tidal behaviour under an antarctic ice shelf*. Br. Antarct. Surv. Bull., 68, 1-8, 1985.
- PRIESTLEY R.E. (1923) - *British (Terra Nova) Antarctic Expedition 1910-13. Physiography (Robertson Bay and Terra Nova Bay regions)*. Harrison, London, 1-95.
- RONVEAUX D. (1992) - *The dynamics of a small antarctic ice shelf as indicated by an ice composition study*. Univ. Libre de Bruxelles, Ph.D. Thesis, 1-391, unpublished.
- SOUCHEZ R., MENEGHEL M., TISON J.L., LORRAIN R., RONVEAUX D., BARONI C., LOZEJ A., TABACCO I. & JOUZEL J. (1991) - *Ice composition evidence of marine ice transfer along the bottom of a small Antarctic ice shelf*. Geophys. Res. Lett., 18, 849-852.
- STEPHENSON S.N., DOAKE C.S.M. & HORSFALL J.A.C. (1979) - *Tidal flexure of ice measured by tiltmeter*. Nature, 282, 496-497, 1979.
- THIEL E., CARY A.P., HAUBRICH R.A. & BEHRENDT J.C. (1960) - *Gravimetric determination of ocean tide, Weddell and Ross seas, Antarctica*. Journ. Geophys. Res., 65, 629-639.
- TISON J.-L., BARBANTE C., BONDESAN A., LORRAIN R. & CAPRA A. (1994a) - *Ice Shelf/Ocean interactions at the front of Hells Gate Ice Shelf*. Incontro di Studio del Progetto di Ricerca Glaciologia e Paleoclima, Roma, 20-21 Giugno 1994, Enea. (Abstract).
- TISON J.L., BONDESAN A., DELISLE G., LOZEJ A., MERLANTI F. & JANSSENS L. (1994b) - *A Dynamical approach to explain ice structures and complex morainic genesis on a partially grounded ice shelf (Hells Gate Ice Shelf, Victoria Land, Antarctica)*. Incontro di Studio del Progetto di Ricerca Glaciologia e Paleoclima, Roma, 20-21 Giugno 1994, Enea. (Abstract).
- TISON J.L., RONVEAUX D. & LORRAIN R. (1993) - *Low salinity frazil ice generation at the base of a small antarctic ice shelf*. Antarctic Sc., 5 (3), 309-322.
- VON DER OSTEN-WOLDENBURG H. (1990) - *Ice quakes on Ekström ice shelf near Akta Bay, Antarctica*. Journ. Glaciol., 36 (122), 31-36.
- VAUGHAN D. (1994) - *Investigating tidal flexure on an ice shelf using kinematic GPS*. Ann. Glaciol., 20, 372-376.



### 3. Marine Ice Diversity





### 3.1. Diversity of marine ice properties

#### 3.1.1. Spatial variability

It is clear, from the field descriptions in Section 2 that the peculiar environment of the Terra Nova Bay coast has enabled us to demonstrate a significant variability in the marine ice spatial distribution that had never been revealed before. Briefly, one can group the various location of marine ice occurrence along the following scheme:

(a) *Between the individual flows of meteoric continental ice forming the ice shelf*

This is typically the case for the upstream patchy outcrops of marine ice organised in longitudinal or arched structures at HGIS (Figure 15). There, the arched structures result from buckling of the longitudinal marine ice fillings between the individual continental ice streams, as the general northwestern flow hits a submarine crest (-200 to -150 m, see bathymetry in Figure 56, top) developing at the southern tip of the Northern Foothills. The same crest is at the origin of the eastern morainic ridge. Apart from the special case where the ice is thin enough to allow the development of transverse rifts close to the grounding line (see (c), below), it is the same pattern of accretion between individual continental ice flows that governs marine ice occurrences on a larger scale at the Nansen Ice Sheet. It is also the same pattern that was detected locally by Corr et al. (1995, our Figure 17) and, very recently, at the scale of the whole Amery Ice Shelf by Fricker et al. (2001). Figure 20 summarizes the results from these authors who computed marine ice thickness (Figure 20c) from the hydrostatic height anomaly  $\delta h'$  (Figure 20 b), defined as the difference between the measured satellite radar altimeter surface height and the surface height calculated from measured ice thickness using airborne RES and the hydrostatic equation:

$$H = \frac{Z(\rho_w - \rho_i)}{\rho_w} \quad (1)$$

where  $H$  is the surface height relative to sea level,  $Z$  is the ice thickness and  $\rho_i$  and  $\rho_w$  are the column-averaged densities of ice and sea water respectively. As mentioned before, RES

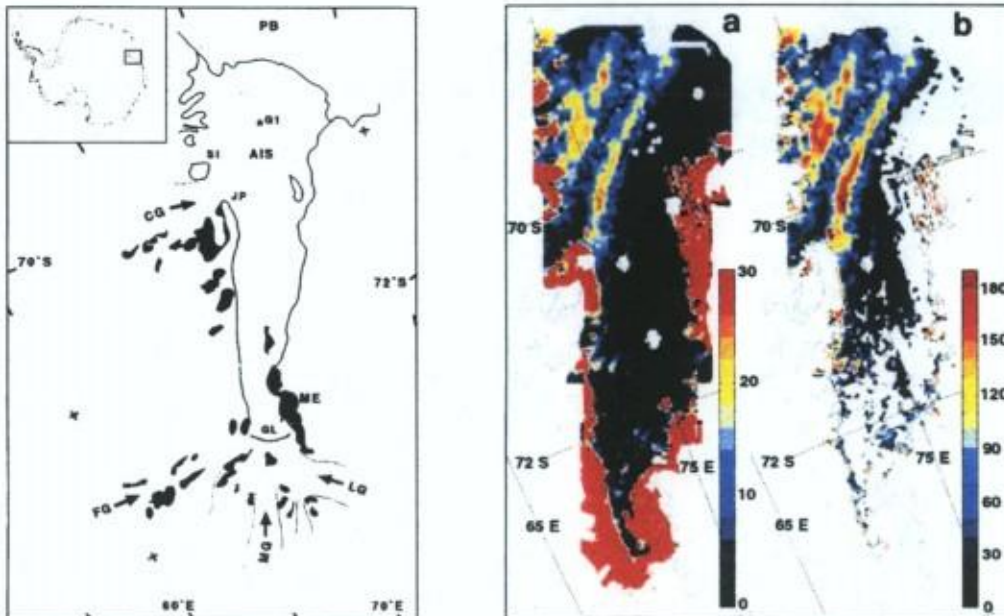


Figure 20: left) Map of Amery Ice Shelf - right) Distribution of a) hydrostatic height anomaly ( $\delta h'$  in meters) and b) computed thickness of marine ice (meters) – see text for details (from Fricker et al., 2001)



systems typically detect the meteoric-marine ice, since it exhibits a moderate dielectric contrast but the signal may not penetrate the marine ice layer itself because of high absorption of electromagnetic energy within (Blindow, 1994).  $\delta n'$  can thus be used to provide an estimate of the thickness and extent of marine ice that underlies meteoric ice masses that are known to be floating.

The thickest marine ice occurs in two longitudinal bands, oriented along the ice flow direction. These are located each side of the Charybdis/Scylla glacier (CG in Figure 20a) inflow where this stream merges with the Amery Ice Shelf downstream of Jetty Peninsula (JP), and with an unnamed stream from north of Single Island (SI).

Fricker et al. (2001) actually followed the path of previous work at the Filchner Ice Shelf (Thyssen, 1988; Thyssen et al, 1993, Grosfeld et al., 1998). Figure 21 (left) shows deduced marine ice thickness in the northern half of the Filchner Ice Shelf, using a similar approach. Clearly, the marine ice accretes following a longitudinal pattern centred on the limit between the Foundation Ice Stream and the Support Force Glacier. Its pattern is fairly well reproduced by a 3-D ocean circulation model (Figure 21, right) in which basal freezing is hypothesized whenever the ocean temperature is below the local pressure melting point at the ice-ocean interface.

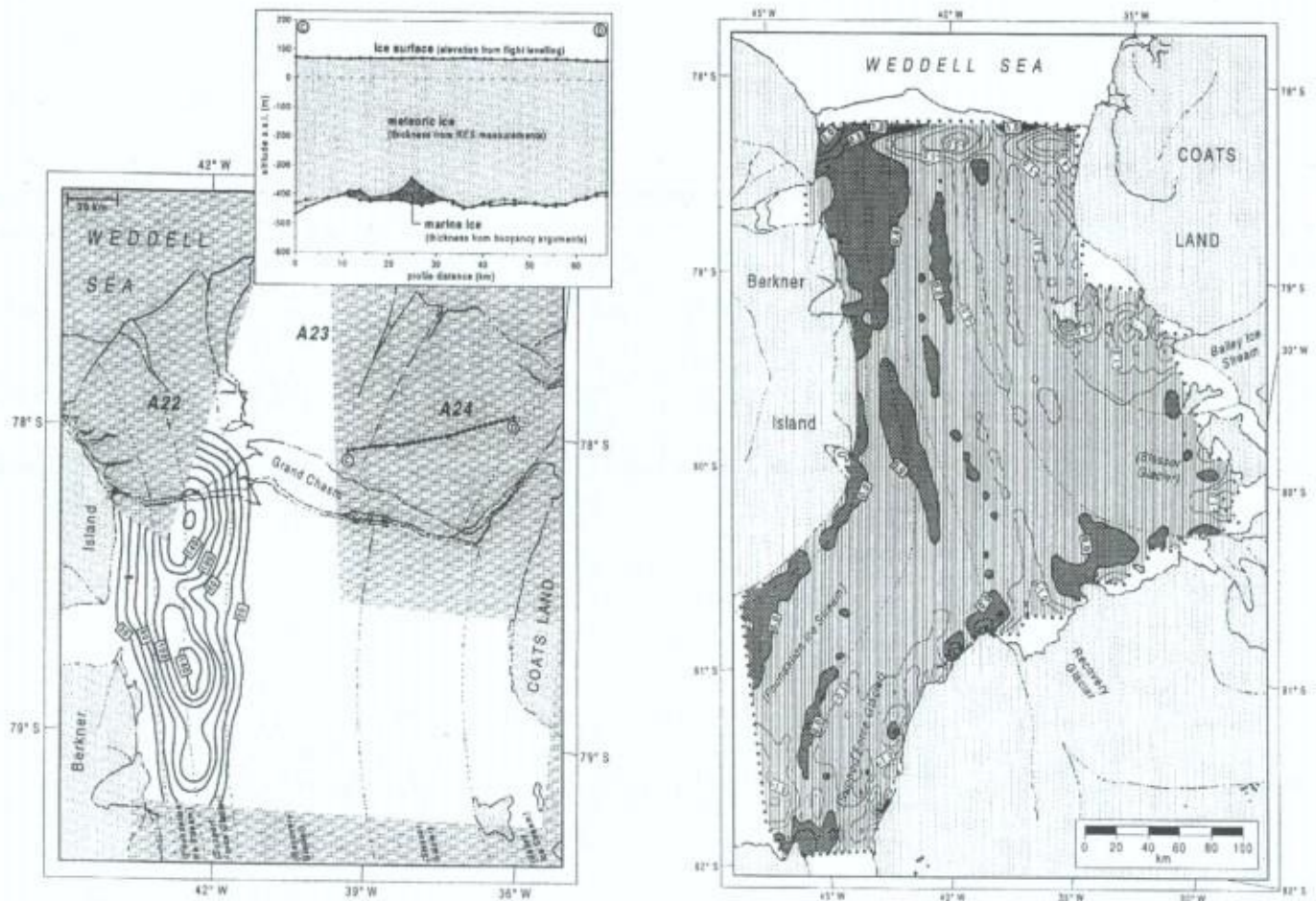


**Figure 21:** left) Thickness of the marine ice layer beneath the north-western part of the Filchner Ice Shelf. The map includes later (calving in 1986 along the rift "Grand Chasm") tabular icebergs A22, A23 and A24. Contours are from standard interpolation software (Thyssen et al., 1993); right) Basal melt/freezing rates (freezing positive, crosshatching) in  $m_{ice} y^{-1}$  beneath the Filchner Ice Shelf derived from a 3-D ocean circulation model. Melt-freezing rates are the result of heat flux across the ice shelf/ocean boundary, which is controlled by the temperature difference between the ice shelf base and the adjacent ocean (Grosfeld et al., 1998).



**(b) In frontal parts of ice shelves**

This location has only been observed at Hells Gate Ice Shelf (Figure 15), because of the combination of strong katabatic winds and moderate ice shelf thickness at the front (Figure 16, bottom). It however, does not preclude that marine is also present at depth in the frontal part of other ice shelves. Figure 20c clearly shows light blue and yellow colours at the front of the Amery Ice Shelf, indicating marine ice thickness of 50 to 100 meters, and Warren et al. (1993) report “green icebergs” from the Amery Ice Shelf, the colour of which is due to their lower section made of marine ice (often revealed after the icebergs have capsized). Thyssen et al. (1993) report that a warm sub-shelf current melts the marine ice layer at the Filchner-Ronne Ice Shelf, before it reaches the calving front. However, Thyssen et al. (1993) indicate marine ice up to a few tens of kilometres from the front, even in the rifted area preparing the major iceberg calving of 1986 (see, for example, transect C-D in inset of Figure 21 left). It is also interesting to note, in the 3-D ocean circulation model of Figure 21 (right), the occurrence of a narrow fringe (a few kilometres wide) where intense basal accretion occurs right at the front of the ice shelf.

**(c) In transversal rifts**

The Nansen Ice Sheet has provided us with a unique opportunity to study marine ice formation in crevasses and rifts forming as transversal features where the continental ice crosses the grounding line (Figure 13). But this is not the only place where such a pattern occurs. Indeed, transversal rifts are the common preliminary stage of large tabular iceberg calving events, and frequently develop in the frontal zone of ice shelves. Although there is no direct evidence of marine ice forming in the late Grand Chasm of the Filchner Ice Shelf (Figure 21, left), a “green” iceberg has been identified as having originated from the easternmost iceberg among the three that resulted from the calving event of 1986. Therefore, Grosfeld et al. (1998) explicitly proposed the idea that the Grand Chasm has provided an ideal environment for a local ice pump to take place (see Section 1.3, p. 19), which produced the marine ice under the northeastern Filchner Ice Shelf, otherwise prone to intense melting, in 3-D ocean models where rift geometry is not included (Figure 21, right).

**(d) Along bedrock outcrops**

This is the typical situation encountered at Campbell Glacier Tongue. The marine nature of the ice is there more difficult to spot, given the usually complex dynamical environment in which it is mixed with debris layers and bubbly glacier ice of meteoric origin (Figure 19). High-resolution textural and isotopic analyses are a pre-requisite in those cases. In the

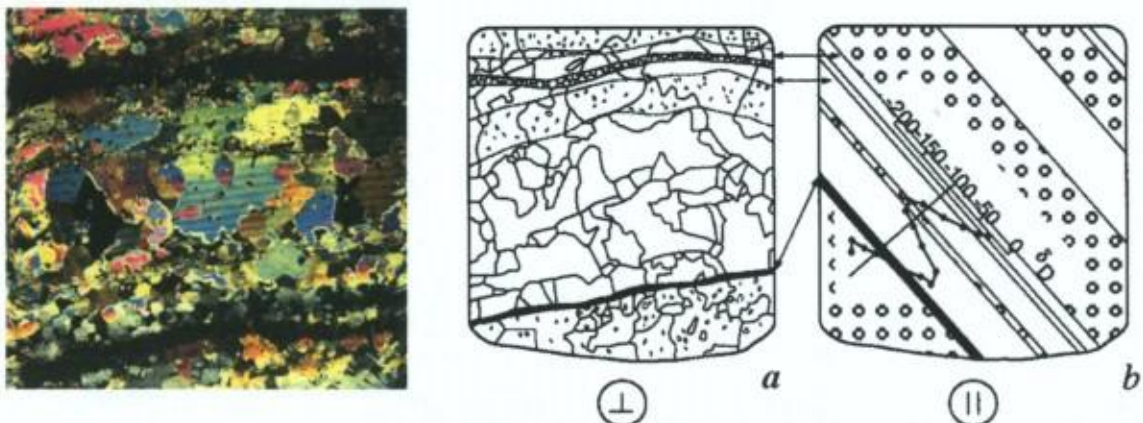


Figure 22: left) Vertical thin-section of a sample from the basal part of the Campbell Glacier Tongue, seen between crossed polarizers; right) (a) detailed “rubbing” (crystal boundaries are enhanced and transcribed on a transparent sheet by rubbing with a pencil) of a slice of the same block, some 10 cm further inside and (b) profile of isotopic sampling for  $\delta D$  seen in a plane perpendicular to the plane where the rubbing was made (Souchez et al., 1995).



example of Figure 22, marine ice layers a few centimetres thick can only be detected as a nearly positive  $\delta D^2$  peak, as opposed to the surrounding (highly negative) glacier ice values, thanks to a millimetric sampling procedure running parallel to the layering.

(e) *Along discrete planes inside continental ice*

This is probably the least conspicuous type of occurrence, which also requires a detailed scanning of the ice properties to be detected. Marine ice generally occurs there as a finer grained crystalline texture devoid of bubbles, “sandwiched” between two layers of continental meteoric bubbly ice (Figure 23). It often displays, in its central plane, a thin layer of microparticules (Figure 23).

### 3.1.2. Textural variability

Marine ice diversity not only resides in its spatial distribution, but also in its various textural facies. These are often associated to the genetic processes, as we will see in the next section. Marine ice



Figure 24: Retrieval of a translucent bubble-free marine ice core at Hells Gate Ice Shelf

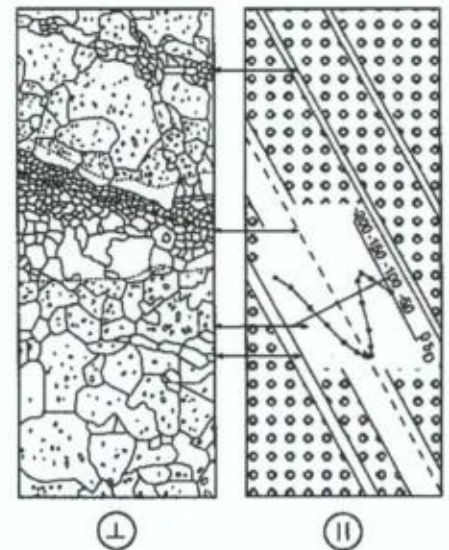


Figure 23: (left) detailed “rubbing” (crystal boundaries are enhanced and transcribed on a transparent sheet by rubbing with a pencil) of a slice of basal ice at Campbell Glacier; (right) profile of isotopic sampling for  $dD$  seen in a plane perpendicular to the plane where the rubbing was made (Souchez et al., 1995).

studies are fairly recent and, therefore, no attempt had been made until Tison et al. (1998) to develop a proper nomenclature. Initially textural facies in marine ice cores should not differ from those observed in sea ice given the similarity of the source environment. However, it should be kept in mind that marine ice accretes at the bottom of large ice shelves, therefore at very slow consolidation rates generally precluding bubble inclusions, resulting in the typical translucent bubble-free aspect of most of the marine ice cores (Figure 24). Also, marine ice is likely to undergo much larger post-depositional cumulative strains than sea ice, and these can lead to considerable alterations of the original texture. Similarly, the impact of shearing on the ice shelf margins and/or converging flow in smaller ice shelves (as is the case in this study) can also partially alter the textures in the marine ice producing patterns that should not be expected in sea ice (even when deformed during rafting events or pressure ridging).

<sup>2</sup>  $\delta D$  is the equivalent of  $\delta^{18}O$  (see footnote 1, page 17), but for the ratio between light and heavy hydrogen isotopes (the latter being usually called Deuterium).



## (a) Columnar ice

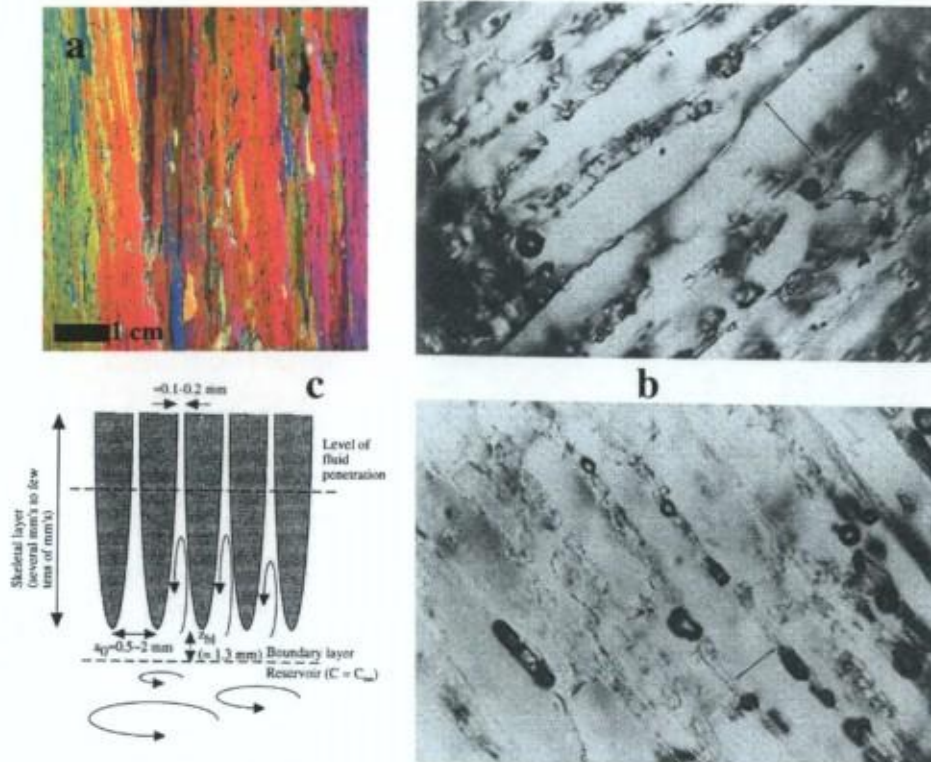


Figure 25: a) vertical thin section of columnar ice between crossed polarizers; b) horizontal thin sections of columnar ice showing the intra-crystalline substructure with brine layers and air pockets (darker areas) - (from Weeks and Ackley, 1986); c) schematic drawing of the structure and exchange processes in the bottommost layers of sea ice (from Eicken, 1998). Double arrows in 25b are about 0.6 mm long.

This typical texture shows vertically elongated crystals, often several centimetres long (Figure 25a). Each crystal contains numerous micro-inclusions of brines and bubbles, organized in a pattern of parallel alignments called intra-crystalline brine-layer-ice plate substructure (Figure 25 a and b). It is the trademark of ice grown from the progression of a freezing front in a seawater reservoir, known as *congelation sea ice*. The intra-crystalline substructure is the expression of the ice-water interface geometry (Figure 25c), which is not planar, because of supercooling induced by the rejection of salts at the ice-sea water interface.

This type of texture is only seldomly encountered in marine ice cores. We have only seen it twice, at Hells Gate Ice Shelf: once at the meteoric-glacier ice interface in a core drilled below the western medial moraine and once at the limit between two very contrasted marine ice types in core IV (see Figure 16, top). We will discuss this latter occurrence later on.

## (b) Platelet ice

The terminology was initially introduced by Lange (1988), to describe a texture made of elongated acicular crystal (spicules), both in horizontal and vertical thin sections (Figure 26 left). These crystals, as opposed to columnar ice crystals, are generally devoid of intra-crystalline substructure. However, the platelet ice facies is rarely seen alone. It generally occurs as a mixed platelet-congelation facies (Figure 26 right) with a wide range of proportions between the two components. In that case, the crystals are less angular and



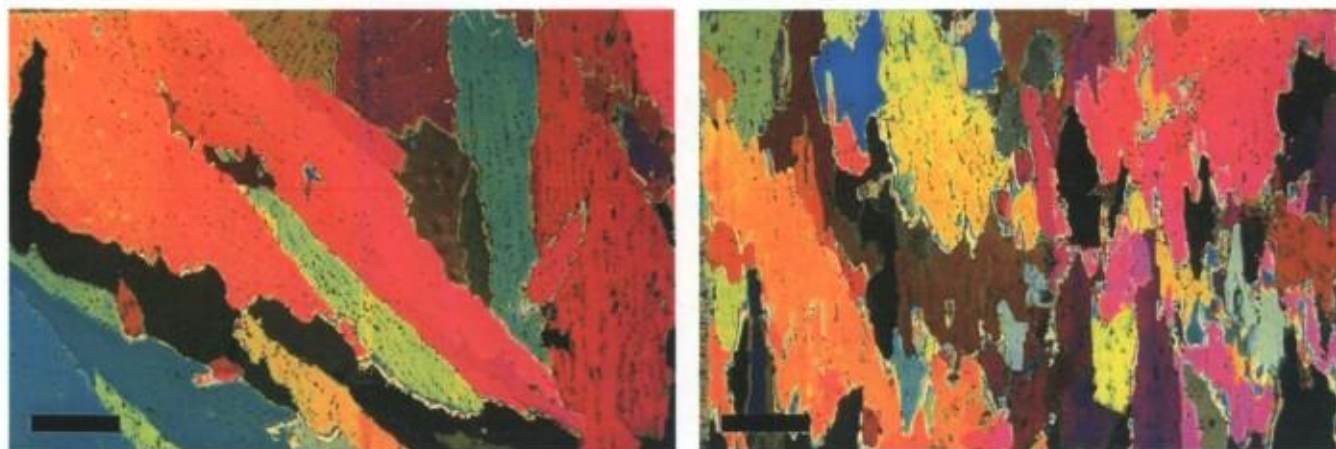


Figure 26: Vertical thin section of platelet ice (left) and of mixed platelet/congelation ice (right) as seen between crossed polarizers. The horizontal black mark is 1 cm.

show wavy uneven edges, a reason why it is sometimes called the “draped facies” (Jeffries et al., 1993).

Since it has generally only be observed close to ice shelf fronts, it has been attributed (e.g. Eicken and Lange, 1989; Kipfstuhl, 1991) to unrestrained frazil ice nucleation and growth resulting from adiabatic supercooling in ascending Ice Shelf Water as part of the Deep Thermohaline Convection (DTC – mode 1 in Figure 10). Nucleation and growth of plate-like frazil ice crystals directly to the bottom of an existing ice sheet from an adiabatically supercooled water mass has also been invoked (Eicken and Lange, 1989; Gow et al., 1998). However, platelet ice is only observed in very small amounts in marine ice (only once in all the Terra Nova Bay cores of this study). Some authors (Eicken, 1994) suggest that the platelet facies is the original texture of all marine ice facies formed in the DTC under large ice shelves (where it has however never been described as such), and that it is eventually later reduced in size and shape under deviatoric buoyancy stress, as thick layers of loose platelets accrete at the bottom. Some debris-free granular marine ice facies observed at HGIS are, however, so fine grained that, in that case, a process of fragmentation under the deviatoric buoyancy stress is hard to envisage. Furthermore, these fine grained facies also occur as irregular pockets surrounded by populations with larger crystal sizes, and these structures are more easily explained in terms of heterogeneity of the loose frazil as it consolidates, rather than in terms of homogeneous large scale post-depositional deformation structures. Bombosch and Jenkins (1995) suggest, by modeling frazil ice production in Ice Shelf Water that the platelet ice facies could be associated with the evolution of ice crystals passively entrained in Ice Shelf Water as it levels off and exits at some depth in front of the ice shelf.

(c) *Granular Ice*



Figure 27: Vertical thin section in granular ice: a) fine-grained; b) medium-grained, c) coarse-grained as seen between crossed polarizers. The horizontal black mark is a 1 cm scale.



The granular texture is typically one of a polycrystalline aggregate of “grains” with no preferential elongation (equigranular). It is described as *orbicular* if the grains show rounded crystal boundaries or *polygonal* if the grains show sharp linear crystal contours. A further distinction can be made depending on the fact that the crystal boundaries show regular polygonal shapes (typically the case of firn, snow ice or superimposed ice) or complicated jagged *interlocking* contours.

The granular texture is by far the most frequently observed in marine ice cores (see also Figure 9). Grains however show a whole range of sizes (from sub-millimeter to several centimeters, Figure 27) depending on the amount of recrystallization generated under the cumulative strain as the ice travel in the spreading ice shelf. The medium- to coarse-grained marine ice is therefore generally of the granular type with interlocking grains.

When granular marine ice is submitted to strong compressive stresses (for example between two coalescent continental floating ice flows) it can develop fold structures underlined by

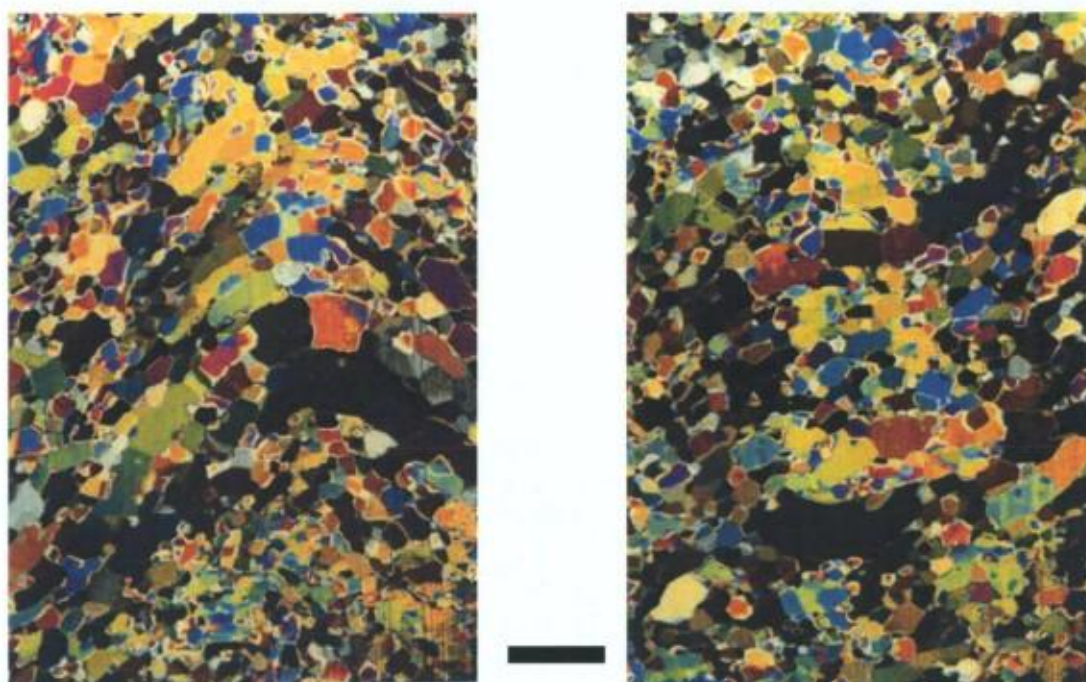


Figure 28: Examples of the “string lined” facies developing in the marine ice in the zone of strong compressive stresses at Hells Gate Ice Shelf (core IV, western moraine). Vertical thin-sections are seen between crossed polarizers. The black marker is a 1 cm scale.

rectangular crystals in arranged individual curved alignments. This was recently described by Tison et al. (1997, 1998) and called the “string-lined” facies (Figure 28).

#### (d) *Banded ice*

The banded ice facies (Figure 29) is typically composed of stacks of rectangular crystals of various sizes in vertical thin section, the limits of which are commonly underlined by trains of brine inclusions (Lorrain et al., 1997; Tison et al., 1993, Tison et al., 1998). It is characteristic of the marine ice occurring in the frontal zone of Hells Gate Ice Shelf (e.g. core Y, Figure 15 and 16 top). This facies shows strong similarities with the bottom layer of some of the southernmost sea ice cores (52 and 54) described by Gow et al. (1987) in the Weddell Sea. These authors describe it as “wafer-like” crystals (Figure 30) and note that “the crystals are so loosely bonded at the very bottom that it was often difficult to obtain competent core when drilling floes containing this kind of ice”. Ice fabrics in these layers exhibited vertical c-axes and the authors suggested that this type of ice might represent underwater ice as described by Russian observers at Antarctic coastal locations [e.g.



Serikov, 1963]. We will see later (section 3.3) that this facies is also found in the landfast sea ice accreting in front of HGIS. It should be noted that the banded facies strongly differs from the other frazil ice facies associated with adiabatic supercooling in DTC, i.e., platelet and draped facies. It shows no interstitial columnar ice, and the crystals appear rectangular in vertical thin sections, and platy (with shaded extinctions) in horizontal thin sections (Figure 31). Furthermore, c-axes are strongly concentrated in a single maximum roughly perpendicular to the plates instead of the random arrangement found in the platelet facies. As a matter of fact, this facies would probably better deserve the "platelet" denomination than the platelet facies which would, in turn, be better described as an "acicular facies" or "mixed acicular-columnar facies".

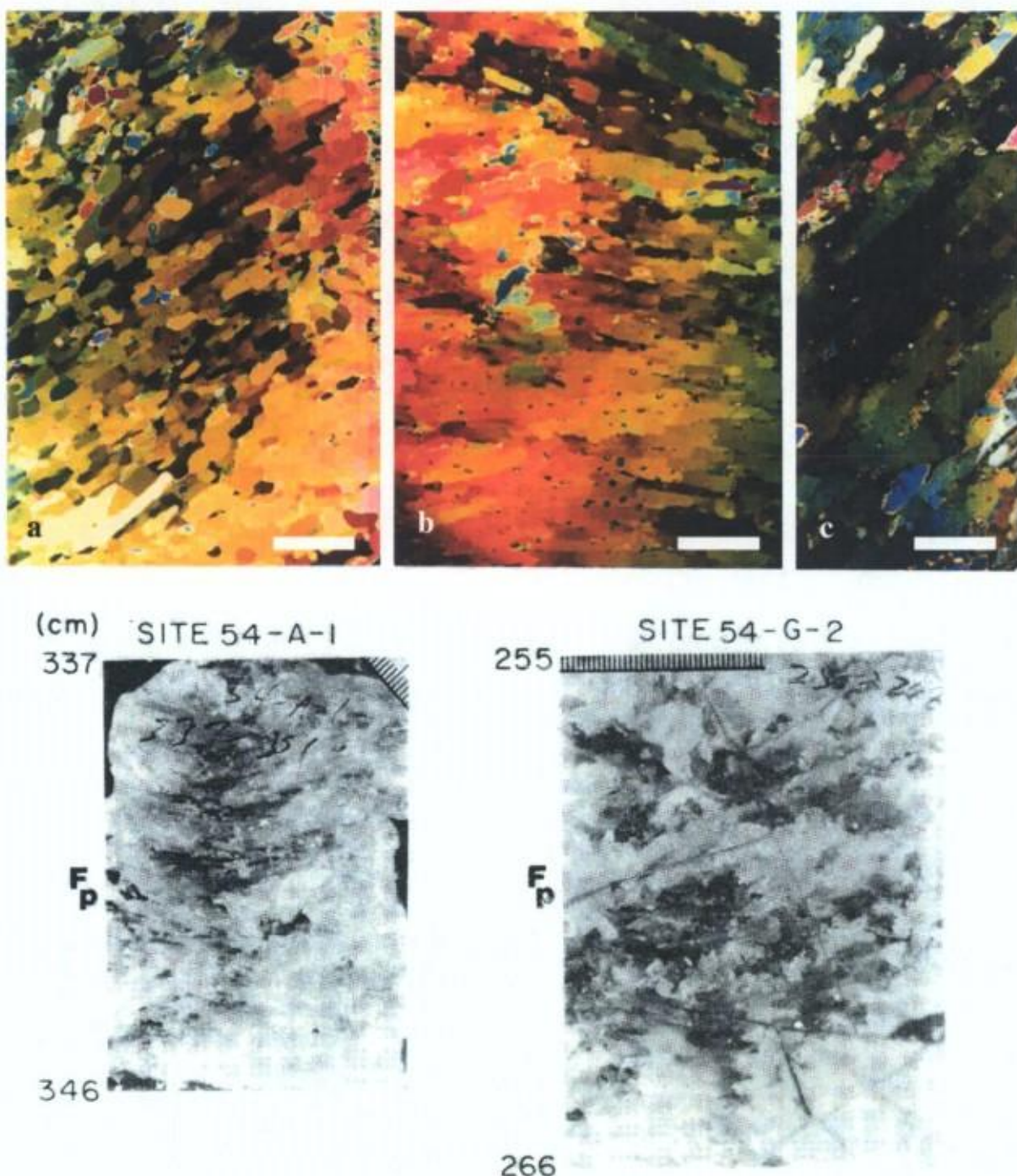


Figure 30: Vertical thick-sections of the "wafer-like" platy structure described by Gow et al. (1987) in the multi-year sea ice of the Weddell Sea.



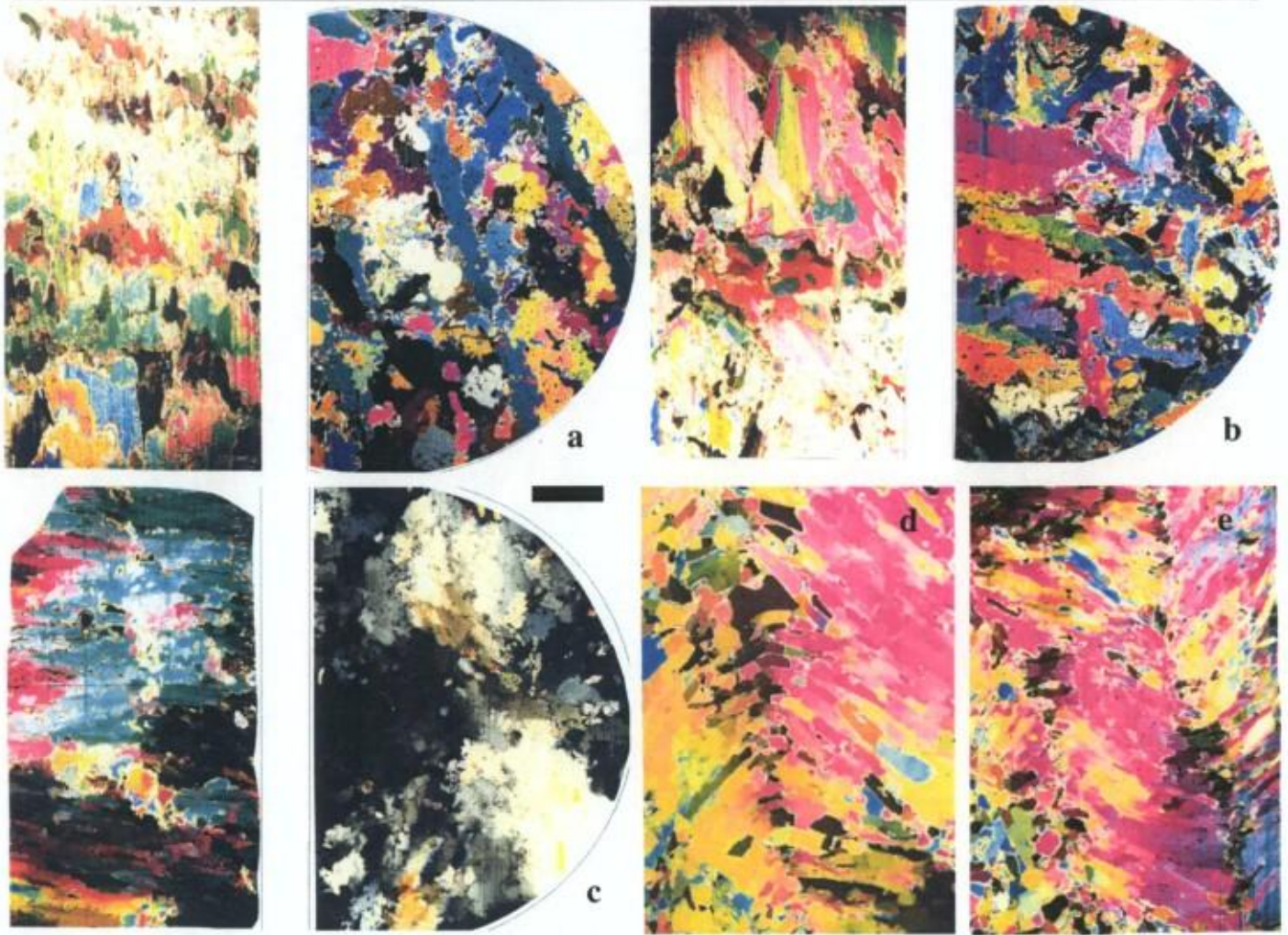


Figure 31: Comparison of the “draped” (a), platelet (b) and banded facies (c) in horizontal and vertical thin-sections of landfast sea ice in front of HGIS, as seen between crossed polarizers. When submitted to important compressive stresses the banded facies of marine ice displays a “wavy” texture (d and e). The black marker gives the 1 cm scale.

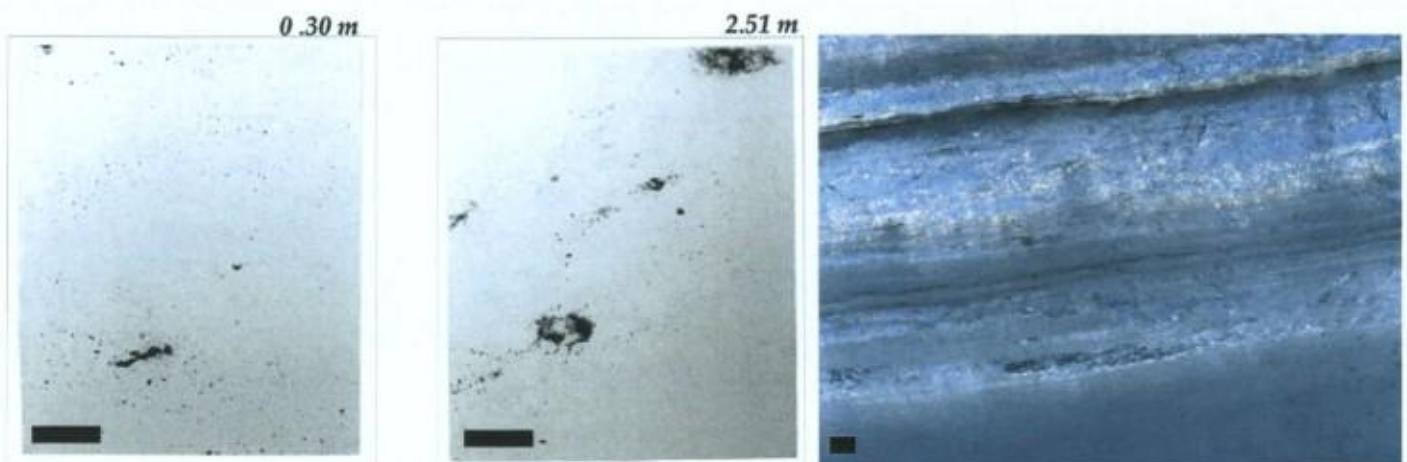


Figure 32: Solid inclusions occurrences at Hells Gate Ice Shelf (left and middle: vertical thick sections of core IV) and Campbell Glacier Tongue (right). Black mark is 1 cm scale.



(e) *Debris-rich ice*

Solid inclusions are found in some of the marine ice cores in the Terra Nova Bay area, but were also described in other deep marine ice cores, like G1 (Amery Ice Shelf - Morgan, 1972), B13 and B15 (Filchner-Ronne Ice Shelf - Oerter et al., 1992, Eicken et al., 1994). In the latter cases, they are essentially reported as thin discrete sub-horizontal layers occurring in the first meters below the contact with the continental meteoric ice. Debris-enriched ice was found throughout the whole of the 45 meters of the NIS1 core (Figures 11 and 13), with variable concentrations (from a few dispersed aggregates to distinct sediment layers, generally folded, occurring sometimes several tens of meters below the surface). It was also present in cores XXI, VI and IV (Figure 32 left and middle) at Hells Gate Ice Shelf, and as clear laminations in the basal ice studied at the Campbell Glacier Tongue (Figure 32 right). No debris was however seen in core Y at HGIS (>90% banded facies).

In all cases, the inclusions can be described as millimeter-sized pellets made of aggregates of clay-and silt-fraction minerals and biogenic material. A sample of the various components of these inclusions is given in Figure 33.

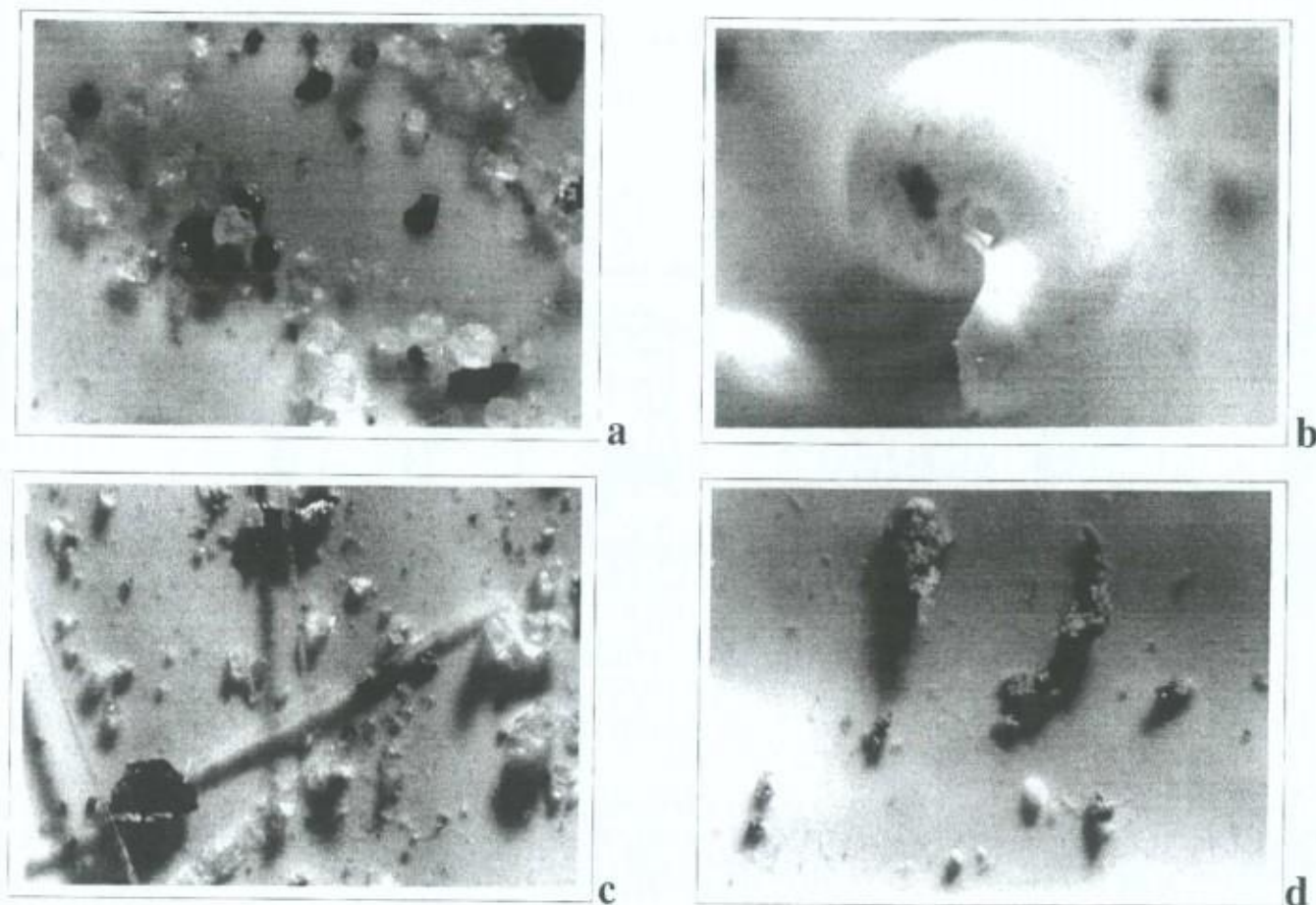


Figure 33: Solid inclusions of core IV at Hells Gate Ice Shelf, as seen under the binocular (enlargement 40x). (a) mineral inclusions; (b) entire shell; (c) sponge spicules; (d) faeces pellets.



### 3.2. Diversity of marine ice genetic processes

In this section, we will show how, combining our data sets on textures, structures, chemical composition, stable isotopes chemistry and solid impurities in the Terra Nova Bay area, we were able to decipher various mechanisms of marine ice formation below ice-shelves. As stated earlier on, we demonstrated that marine ice formation is not solely associated to the Deep Thermohaline Circulation.

#### 3.2.1. Crack metamorphism at grounding lines

We will first concentrate on the discrete, few centimetres thick, layers embedded in the meteoric continental ice at the Campbell Glacier Ice Tongue sampling site (Figures 11 and 23). As mentioned before, these are clear ice layers, with considerable spatial extension, consisting of very small crystals and showing maximum  $\delta D$  values close to 0‰ (sea water value) along their central plane. This is a clear signature for marine ice (see section 1.3, p. 17). Progressing towards both sides of the layer, isotopic values become increasingly negative (down to typical meteoric ice values in the area), at the same time crystal size increases and a sharp limit is crossed where the ice gets bubbly. It is frequent that a single crystal is actually split in two zones by this limit (Figure 23).

Plotting the co-isotopic values ( $\delta^{18}O$ - $\delta D$  diagram) of the high-resolution sample analyses from these layers gives further insights in the processes at play. In Figure 34, the marine ice samples under consideration are plotted as open circles (Marine ice type 1). Bubbly glacier ice samples derived from

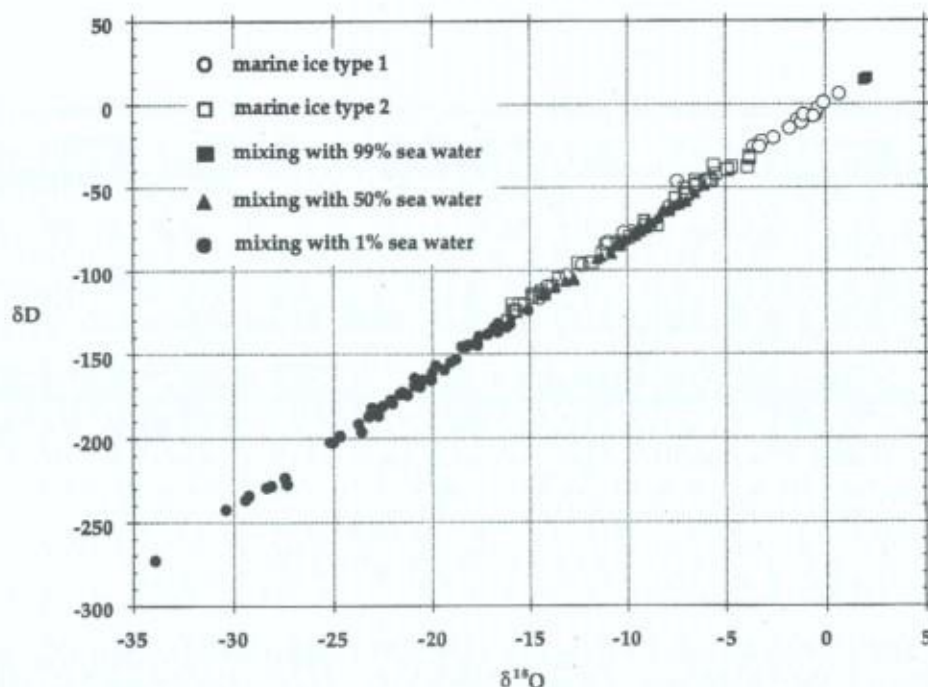


Figure 34: The  $\delta^{18}O$ - $\delta D$  relationship in the basal marine ice from Campbell Glacier Tongue compared with mixing computer simulations (Souchez et al., 1995).

snow of coastal origin and snow fallen in the Terra Nova Bay show  $\delta D$  values more negative than -130‰ and  $\delta^{18}O$  values more negative than -17‰. Together with bubbly glacier ice from the continental interior with even lower  $\delta$  values, they are aligned, in a  $\delta^{18}O$ - $\delta D$  diagram, on a precipitation line<sup>3</sup> with the

<sup>3</sup> Because of the differential isotopic fractionation between oxygen and hydrogen atoms in the water molecule during the evaporation and condensation processes leading to a precipitation event, samples of natural freshwater generally align on a line with a slope close to 8, called the *precipitation line* (or *Meteoric Water Line*, on a global scale) – see e.g. Craig, 1961; Dansgaard, 1964; Souchez and Lorrain, 1991.



equation  $\delta D = 7.92 \delta^{18}O + 2.76$ ; correlation coefficient  $r = 0.997$  ( $n=41$  samples). Points representing equilibrium freezing of a mixture between local sea water at Campbell Glacier (30 meters depth,  $-3.23\text{‰}$  in  $\delta^{18}O$  and  $-0.69\text{‰}$  in  $\delta D$ ) and the various (melted) meteoric ice sampled locally are shown in Figure 34 as black dots, triangles and squares, for 1%, 50% and 99% mixing ratios respectively. The samples of marine ice type 1 lie very close to the distribution of these theoretical points. They also show a large range of isotopic values (reaching values very close to those obtained by the freezing of normal sea water) and a slope of 7.86, which precludes that the whole thickness of the marine ice layer results from a simple, single freezing process (Jouzel and Souchez, 1982). Enrichment by isotopic exchange with clay minerals is able to produce important isotopic shifts, but on a much lower slope (Souchez et al., 1990), it is therefore also precluded in this case. The co-isotopic signature of the marine ice considered here can therefore be regarded as one of a mixing process. It should be noted, however, that this does not necessarily imply a "physical" mixture of continental water and sea water in various proportions.

Another typical feature of these marine ice layers is the occurrence of a thin solid impurity film, running parallel to the limits of the layer, usually where the isotopic maximum is located. This type of discontinuity underlined by impurities (debris, bubbles) is typically observed in refrozen cracks at the surface of temperate glaciers or in a sea ice cover.

The set of properties described above can be understood in a scenario where intrusion of water occurs in fissures freshly opened at the base of the floating glacier, with subsequent ice formation as depicted in Figure 35.

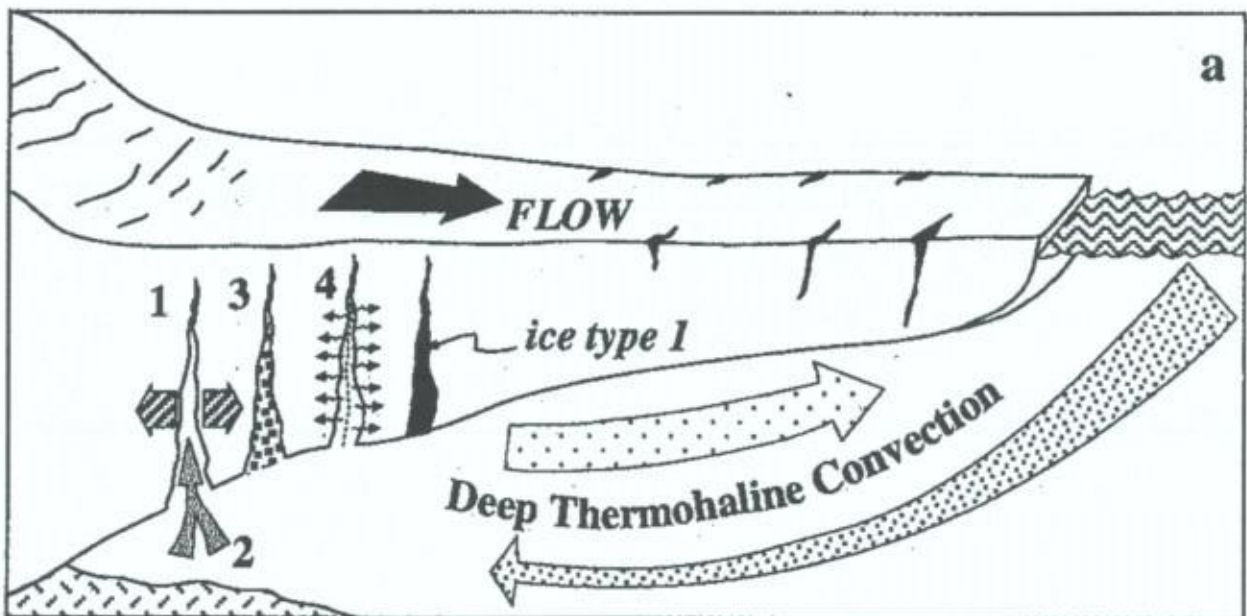


Figure 35: Schematic diagram for the formation of marine ice in bottom crevasses forming at grounding lines (Souchez et al., 1995)

Basal crevasses have been observed at the bottom of floating glaciers or ice shelves by means of radio-echo sounding (RES) methods. Several authors, such as Jezek et al. (1979) and Shabtaie and Bentley (1982) have detected them in the Ross Ice Shelf at numerous locations. Orheim (1986) observed many bottom crevasses in the Riiser-Larsen Ice Shelf. Grounding lines and pinning points (local re-grounding areas associated with islands) are favourable sites for the formation and opening of basal crevasses. Hellmer and Jacobs (1992) indicate that bottom crevasses are common near grounding lines where tidal bending occurs. Jezek and Bentley (1983) believe that most bottom crevasse fields are associated with rapid grounding or ungrounding of ice. As soon as these fractures will occur ([1] in Figure 35), they will fill up with sea water [2], and the sudden drop in ambient pressure will trigger frazil ice formation [3]. The heat sink provided by the colder ice surrounding the crack will help consolidating



the loose frazil from both sides [4], solid impurities being rejected in the central part of the former fracture (Figure 23). In the course of the consolidation process, recrystallization must have occurred, as indicated by the presence of ice crystals, which are bubble-free in their inner part and bubbly in their outer part at the meteoric ice-frazil ice contact. Diffusion of isotopes along the pathway represented by water films at the ice crystals limits during recrystallization must certainly be taken into account. It probably explains the gradual decrease in  $\delta$  values from the centre of the former fissure towards the sides. Clearly, in this case, the alignment of the samples on a mixing line (Figure 34) does not reflect the mixing of two water masses. Although it is not necessary for the process to occur, the existence of a Deep Thermohaline Circulation below the Campbell Glacier Tongue would increase the potential amount of frazil ice formed in the crevasse. Hellmer and Jacobs (1992) also explain the filling of bottom crevasses with marine ice by an ice pump mechanism driven by the pressure dependence of the freezing point.

The crevasses reported above all have dimensions of meters. The type 1 marine ice described here is typically only centimetres wide. Possibly these fissures could exist in the same location, but remain undetected by radio-echo soundings. They also might have formed at a larger scale and subsequently been subjected to strain thinning. The latter process is one of the possible reasons to explain the small grain size in the marine ice.

The fact that the observed grain size might result from post-genetic deformation processes, raises the possibility that the fracture actually filled up with larger crystals formed by direct freezing of congelation ice on the walls. This is however unlikely since (a) no intracrystalline brine layers, typical of congelation ice, are observed in the marine ice and (b) the isotopic signal increases towards the centre of the former fracture, a distribution opposite to the one expected to result from the progression of a freezing front in a closed water reservoir (Souchez and Jouzel, 1984).

### 3.2.2. Double diffusion between basal continental fresh melt-water and sea water in (re-) grounding areas

It is generally assumed that if the melting point is reached at the glacier base in the coastal region, subglacial meltwater loaded with sediments discharges into the sea at the grounding line. Zotikov (1986) has pointed out that if this subglacial meltwater reaches the sea, a layer of relatively freshwater will exist above normal sea water beneath the ice shelf. Since the freezing point of freshwater is higher than the freezing point of sea water, bottom freezing will probably occur and be responsible for a thickening of the ice shelf at or near the grounding line (Figure 36). However, no one until Souchez et al. (1995) had demonstrated the existence of ice resulting from such a freezing process close to grounding or re-grounding areas, neither was the freezing mechanism involved clearly understood.

Marine ice type 2 observed at the base of the Campbell Glacier Tongue, shows the same textural and (co-)isotopic features as marine ice type 1, apart from the fact that (a) it is associated with layers enriched in sediments (Figures 19, 22 and 37), some of which is undoubtedly of a marine origin (shell fragments and sponge spicules are found in the sediment layers) and (b) the isotopic maximum is generally lower, indicating a stronger influence of the meteoric

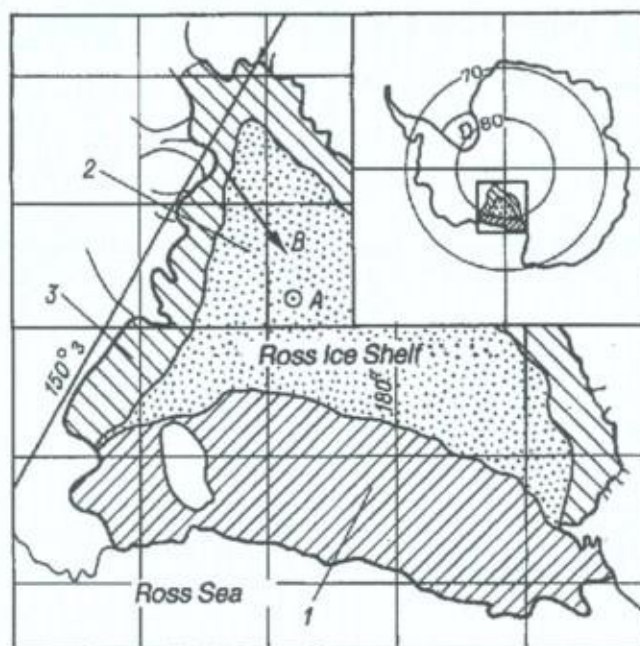


Figure 36: Theoretical distribution of zones of freezing and melting below the Ross Ice Shelf (Zotikov, 1986) - A) Site of Deep drilling J9; B) General glacier movement; 1) melting region; 2) region of bottom freezing caused by upward heat transport through the ice shelf; 3) region of bottom freezing enhanced by arrival of freshwater under shelf.



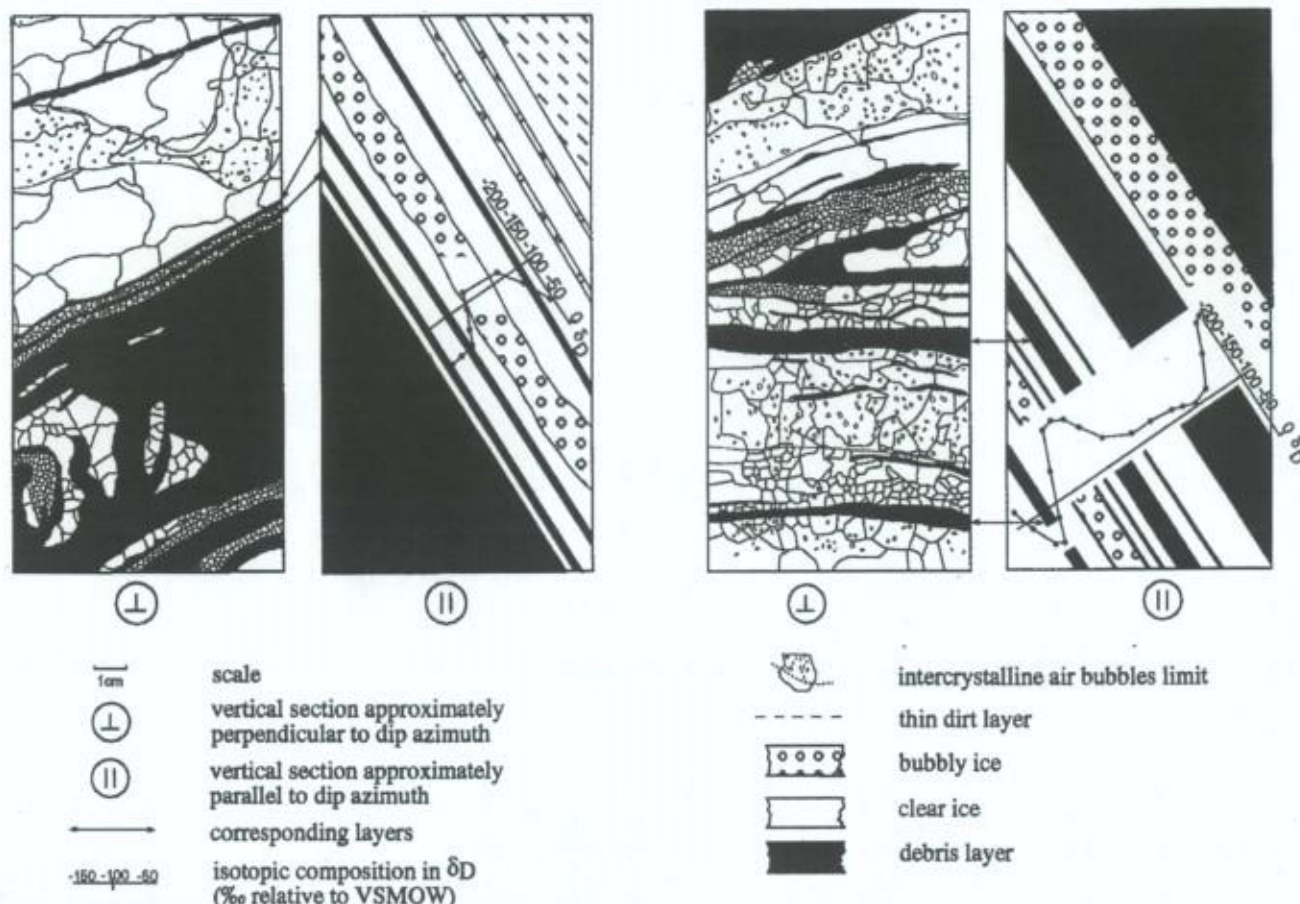


Figure 37: Rubbings and  $\delta D$  measurements in two examples of marine ice type 2 at Campbell Glacier Tongue (Souchez et al., 1995).

component in the mixing process (Figure 34 and 37). The freezing mechanism thus involves both a mixing process between isotopic signatures of sea water and continental meltwater and the presence of marine sediments. The best location candidate for this process to occur is therefore the ice-bedrock (sediment) interface near grounding lines or re-grounding areas around pinning points. However, whatever the mechanism involved, it requires the sea water to be at its local freezing point, which precludes areas under the influence of the Deep Thermohaline Circulation. Moreover, for freezing to occur in the area where the meteoric water of continental origin meets the sea water, it is imperious to preserve the salinity contrast, i.e. to prevent efficient mixing between the two water masses. Therefore, a double-diffusion process within the pores of subglacial sediments, in areas sheltered from the Deep Thermohaline Circulation and from the tidal mixing that prevails at grounding lines (MacAyeal, 1984) is worth considering (Figure 38, Souchez et al., 1998).

At some distance upstream from the actual decoupling of the glacier from its bed, sea water seeping through the sediments will come into contact with continental meltwaters. Because the freezing point of sea water is lower than that of continental meltwater, heat diffusion will occur. Heat will diffuse through both liquid and solid

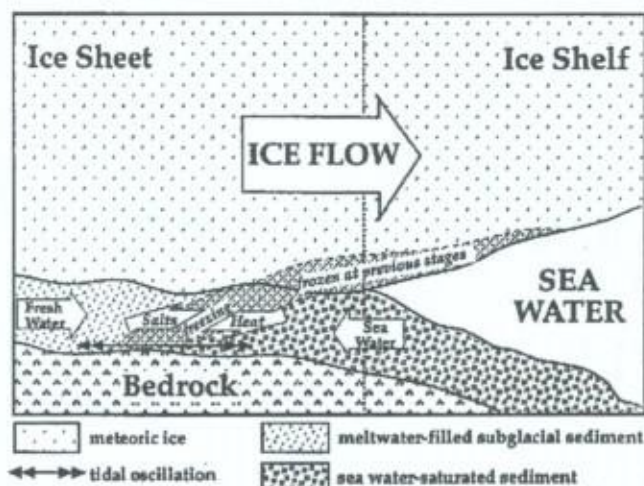


Figure 38: Schematic diagram for the formation of marine ice by a double-diffusion freezing process in sediments located at grounding lines or in regrounding areas (Souchez et al., 1995).



fractions from upstream to sea water. On the other hand, the salinity of sea water being higher than that of continental meltwater, salts will diffuse from the sea-water-saturated sediment into the meltwater-filled subglacial sediment. Salt can diffuse only through the liquid, unlike heat. Thermal diffusivity is also an order of magnitude higher than salt diffusion. The meltwater-filled sediment loses heat faster than it gains salt, and freezing occurs, welding the sediment to the bottom of the ice. Since this mechanism occurs within the subglacial sediment, rapid mixing between continental water and sea water is precluded.

If meteoric continental ice meltwater within the subglacial sediment enters into contact with sea water at the grounding line, diffusion will occur. Like salts, heavy isotopes of oxygen and hydrogen will diffuse from sea water, wherein they are less impoverished, to continental meltwater, where they are more depleted. Diffusion coefficients of stable isotopes and of salts in liquid water have the same order of magnitude, so that the double-diffusion mechanism described above also leads to isotopic diffusion. The isotopic composition of the debris-rich ice layers formed by freezing will depend on the magnitude of the diffusion process prior to freezing.

Marine ice with the same characteristics as the Campbell type 2 as also been encountered in some of the cores drilled below the western moraine at Hells Gate Ice Shelf. The detailed study of the ice shelf morphological features (section 2.3) indicates that the debris-rich marine ice forming the main part of the western moraine has originated at the Southern tip of Vegetation Island (Figures 14 to 16), a local pinning point. The occurrence of sponge remains in living position incorporated into the ice shelf, most probably as "anchor ice" lifted from the shallow depth sea-bottom under buoyancy (Dayton and others, 1969), and the CTD profiles in Evans Cove and along the Terra Nova Bay coast both demonstrate that active freezing has been possible there, near re-grounding zones, away from the influence of the Deep Thermohaline Circulation (no local input of HSSW, see section 3.3. - p. 87).

### 3.2.3. Deep and Shallow Thermohaline Circulation

Nearly ten years (1991-1999) of "in depth" study of the Hells Gate Ice Shelf have allowed us to show that a major fraction of the marine ice occurring in the area results from Thermohaline Circulation processes involving both the NIS and HGIS system. More importantly, we have been able to discriminate between a "classical" Deep Thermohaline Circulation, similar to the one described for all the deep marine ice cores performed elsewhere in the Antarctic, and what we identified as a "Shallow" Thermohaline Circulation resulting from the tidal forcing of summer surface waters below the frontal part of the ice shelf.

Figure 39 shows the result of sub-surface (2 meters depth) sampling for textural analyses at Hells Gate Ice Shelf (Lorrain et al., 1997). Marine ice appears in green symbols, as opposed to continental meteoric ice in blue and lake ice in red. This preliminary approach has the advantage to reveal the contrast in spatial distribution of two main textural facies at

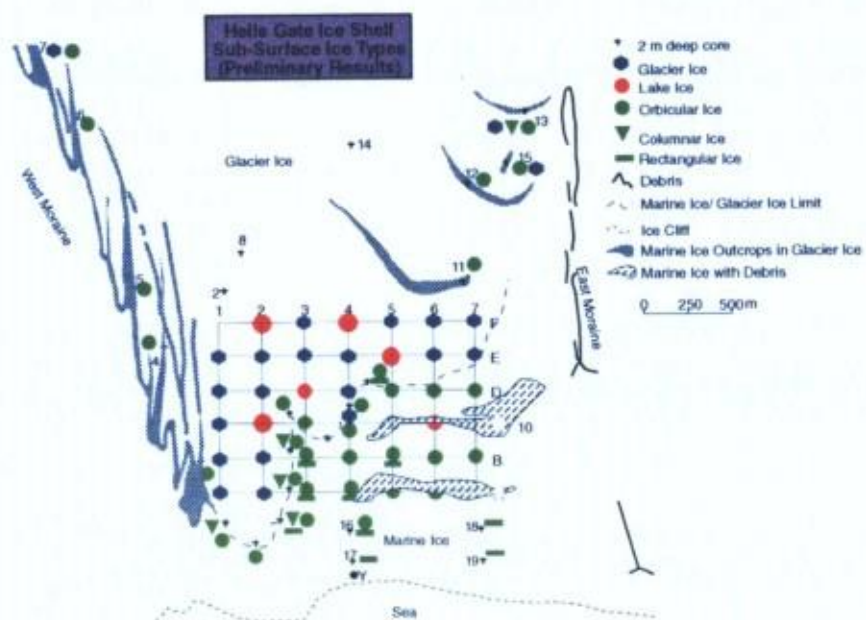


Figure 39: Sub-surface (2 meters depth) ice types at Hells Gate Ice Shelf (after Lorrain et al., 1997)



SCALE FOR ALL PHOTOGRAPHS :  = 1cm

Figure 40: Selected typical textural characteristics of cores XXI, VI, IV and Y at HGIS, shown in vertical thin-sections between crossed polarizers. Depths in meters are indicated to the right. Selection has been made to give a complete overview of textural variability inside the cores, rather than a true representation of the frequency of occurrence of the different facies.

HGIS: the *granular facies* (dots) is dominant upstream, where marine ice fills the inverted depressions between individual continental ice flows, whilst the *banded facies* (rectangles) builds most of the front of



the ice shelf. It is worth noting the limited occurrence of columnar/congelation ice (triangles), exclusively located, in small amounts (generally maximum a few tens of centimetres) at continental ice/marine ice or granular/banded ice contact interfaces.

This contrast in the spatial distribution of textures is confirmed by medium depth (10 to 45 meters deep) ice coring along a flow line (Tison et al., 1998). Figure 40 shows the textural characteristics of marine ice cores XXI, VI, IV and Y, roughly aligned along the flow line of the western medial moraine (Figure 16). Given that the marine ice thickness is already 126 m at the location of core XXI (seismic ice thickness), that the mean ablation rate is estimated to be between 0.20 and 0.30 m a<sup>-1</sup> and that the surface velocities are between 9 and 12 m a<sup>-1</sup> (see section 2.3) the cores are thought to adequately approximate what would be recorded with depth in a single ice core, close to the ice shelf front, supposing it had not been subjected to surface sublimation. Indeed, using the most conservative estimates for surface velocity (9 m a<sup>-1</sup>) and for ablation rate (0.20 m a<sup>-1</sup>) one can calculate that the amount of marine ice ablation between two successive core locations is 3 to 8 times higher than the core length at the most upstream site of each pair. It should be stressed, however, that this does not necessarily mean that the ice in core IV is younger than in core XXI, since this obviously depends on factors like the balance between horizontal velocities, surface ablation rates, marine ice accretion rates (of which we only have minimum estimates) and longitudinal extension of the marine ice depositional areas. Also, the dynamical characteristics of HGIS flow described above are likely to affect the original stratigraphy of the marine ice deposits to a certain extent, and this will have to be taken into account in the discussion below.

Nevertheless, the textural results from the studied cores (Figure 40) support the surface observations from previous work at HGIS. The two upstream cores (XXI and VI) show a granular facies exclusively, whilst core Y consists of 97% banded facies. The remaining 3% consists of granular ice, confined to discrete layers or pockets in the first 10 m of the core. Core IV, located about halfway between VI and Y (Figure 16), is of particular interest. Down to 5.35 m it shows a typical fine-grained granular texture. Below 6 m, core IV is exclusively banded, with the exception of the bottom-5 cm, which consist of granular ice. Between 5.35 and 6 m, a mixed columnar-platelet ice texture is observed.

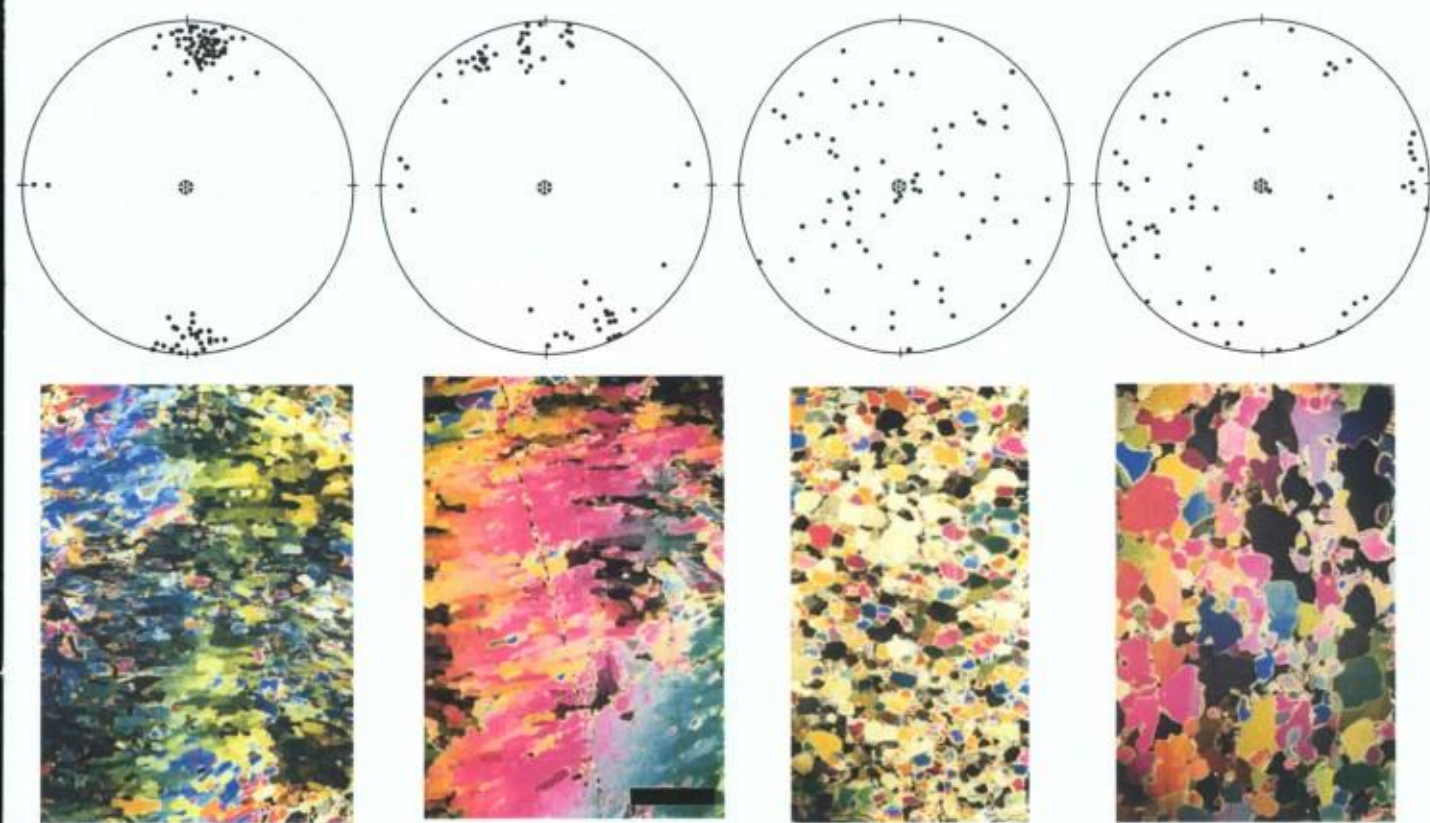


*Figure 41: Fabric (c-axes) contrast between the banded and the granular facies at HGIS. Photographs of thin-sections are seen in the vertical plane, between crossed polarizers. The black marker is a 1 cm scale.*

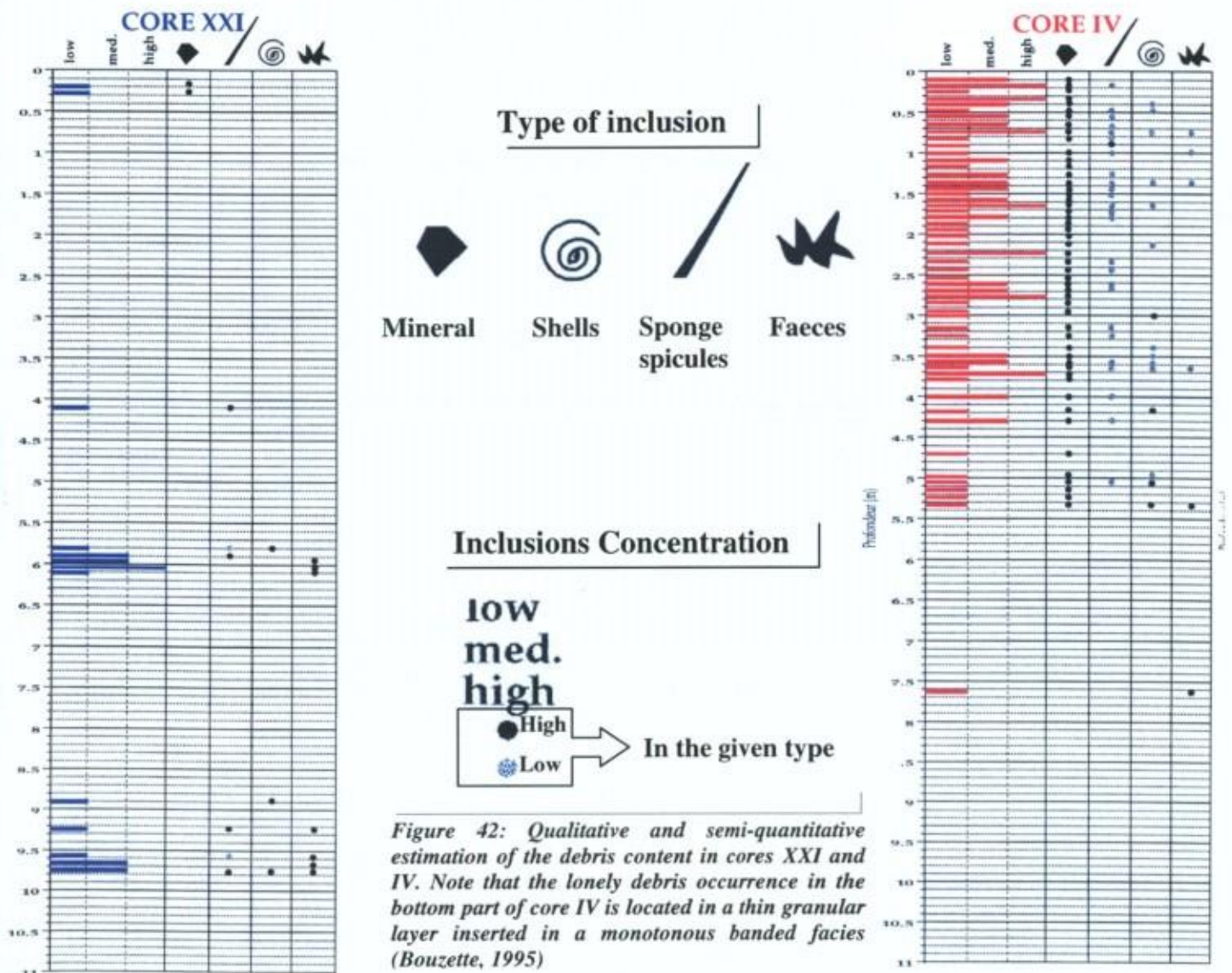


This spatial layout supports the assumption made above that the vertical juxtaposition of the four cores illustrates the large-scale (kilometre) distribution of the textural facies in a vertical plane oriented parallel to the mean flow line. The assumption, however, probably does not hold at the smaller metre to centimetre scales, owing to the complex dynamical behaviour of Hells Gate Ice Shelf (section 2.3). The sharp textural contrast occurring at 5.35 m and the re-occurrence of the granular facies at the bottom of core IV could, therefore, be the signature of shearing of a lower stratigraphic unit higher up in the core, in a process similar to the one depicted in Figure 18a. The tilting of the crystals might be a further argument in this respect.

The basic contrast discussed above is not limited to textures and spatial distribution, it also involves other physico-chemical properties, as shown here below:

(a) *Ice fabric*

Tison et al. (1993) have shown that there is a strong contrast in fabric between the granular and the banded facies (Figure 41), suggesting different depositional environments. The banded frazil shows strong c-axes concentrations at a maximum generally perpendicular to the crystal elongation. This suggests crystal growth in interface flowing conditions where differential shear favors rotation of the crystals parallel to the local ice-ocean interface. Local vortex structures in the banded facies also suggest a transition from laminar to turbulent flow on some occasions. On the contrary, the obvious lack of preferential





orientation in the granular frazil suggests an accretion process in calm conditions, with no effect of interfacial streaming, and sustained post-depositional recrystallization in the case of the medium- and coarse-granular facies.

**(b) Debris content**

Granular marine ice contains particulate matter inclusions, as shown in Figure 42, where both the type of inclusion and a semi-quantitative estimate of inclusions abundance are represented (Bouvette, 1995). These inclusions mainly consist of sponge tests and crustaceous faeces, sometimes showing peritrophic membrane, and, occasionally, echinoderm spicules and worm tubes fragments (G. Houvenaghel, personal communication). One out of 15 samples also contained diatoms fragments. The dominance of fragments of benthic origin indicates the proximity of the sea floor for the waters where the frazil ice formed. It also confirms the efficiency of the scavenging effect of rising frazil ice crystals on suspended matter, as was experimentally demonstrated by Reimnitz et al. (1990). On the contrary, no particulate matter was found in the banded facies of core IV (lower 4.5 meters) and hardly none in the whole 45 meters of core Y. Furthermore, in the rare case of debris occurrences in the banded facies, it was generally located in a thin layer of granular ice.

**(c) Bulk Salinity**

The composite bulk salinity profile for cores XXI, VI, IV and Y is shown in Figure 43.

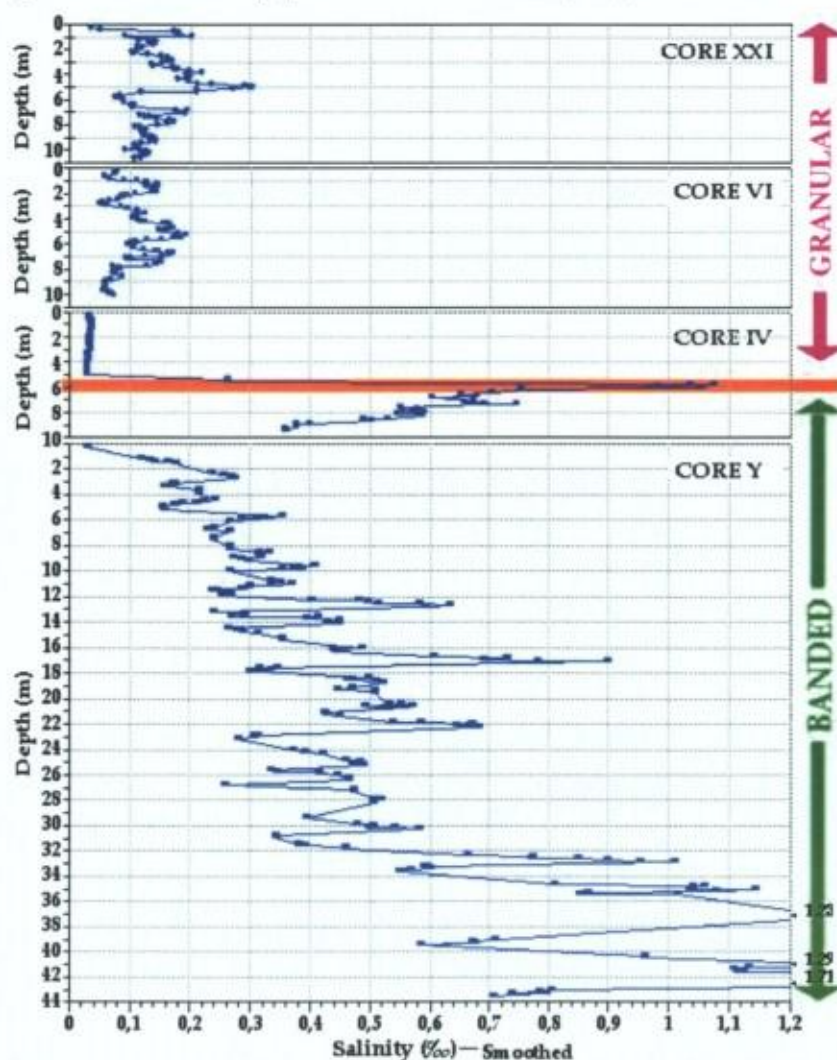


Figure 43: Bulk salinity profiles for cores located on a flow line centered on the western moraine at HGIS (Tison et al., 1998)



Although the top 50 centimeters of the cores were systematically discarded from the measurements to avoid surface contamination or alteration, there is obviously a recurrent pattern of increasing salinity from very low levels in the first meter of cores XXI, VI and Y. The pattern most probably results from superficial “washing” of the ice during the melting events frequently observed during the summer (see also the abundance of surface lake ice in Figure 15).

The salinity trend (Figure 43) in the granular facies corresponds to a decrease in a downstream direction, from maximum values of 0.3‰ in core XXI to values less than 0.03‰ in core IV. Both the trend and the minimum values are consistent with the observations in other deeper marine ice cores at Filchner Ronne Ice Shelf and Amery Ice Shelf (Eicken et al., 1994; Morgan, 1972; Oerter et al., 1992). There is a sharp increase of the salinity when entering the mixed platelet-congelation horizon in core IV, with values of up to 1.1‰.

In the banded facies of the bottom part of core IV and of core Y, salinities are noticeably higher and universally increase with depth, especially below 32 m, where water was first observed to invade the drill hole. The water level rose slowly in the hole in the next 24 hours, and stabilized at 11 m depth, which is equivalent to the ice-shelf freeboard in front of the drill site. Conductivity measurements on two water samples taken in the hole at the beginning and at the end of the process were equivalent to respectively 3 and 0.9 times the

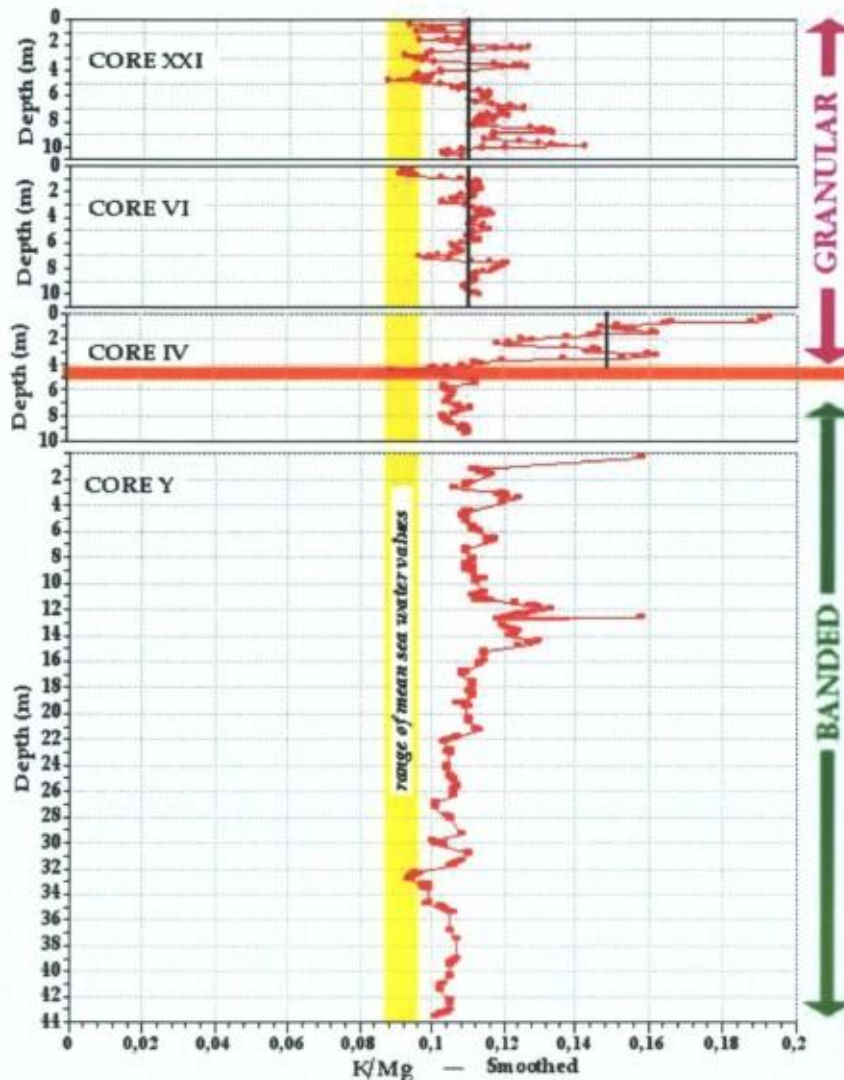


Figure 44: K/Mg profiles for cores located on a flow line centered on the western moraine at HGIS (Tison et al., 1998)



conductivity of normal sea water. This indicates that the bottom part of the banded facies is still thoroughly permeable to sea water and that the "in-situ" interstitial water in these layers is considerably enriched by the brine exclusion process resulting from the consolidation of the upper levels. This supports the idea that, in this case, freezing is actively taking place in the consolidation process (see section 3.4.).

(d) *K/Mg ratio*

Fig. 44 plots the composite profile of the K/Mg ratio (K and Mg being expressed in  $\text{meq l}^{-1}$  for charge and weight compatibility) in the four cores considered. This ratio has been chosen (Tison et al., 1993) since it is unlikely to be affected by salt precipitation in the HGIS environment. Indeed, Richardson (1976), in his study of the phase relations in sea ice as a function of temperature, indicates that  $\text{CaCO}_3 \cdot 6\text{H}_2\text{O}$  is the first salt to precipitate from sea water at a temperature close to the freezing point and that  $\text{Na}_2\text{SO}_4 \cdot 10\text{H}_2\text{O}$  and  $\text{CaSO}_4 \cdot 2\text{H}_2\text{O}$  soon follow, at temperatures of  $-8^\circ\text{C}$  and  $-10^\circ\text{C}$  respectively. Marine ice subjected to such a range of temperatures, as is probably the case for the HGIS when it is progressively brought up to the surface by ablation, is likely to show a greater variability in the ratios of elements forming salts under freezing conditions. Following Richardson (1976), concentrations in K and Mg ions in sea water at sub-freezing temperatures, under quasi equilibrium conditions, do not change until the temperature falls below  $-34^\circ\text{C}$ . This is confirmed by the observations of Cragin et al. (1986) in brine layers infiltrating the Mc Murdo ice shelf and progressively submitted to lower temperatures where, for Na/Mg as well as for Na/K, there is a good agreement between these ratios in sea water and those in the ice samples. This ratio in congelation ice (0.11) and platelet ice (0.10) from HGIS is close to the one in standard sea water (0.10), thereby confirming the absence of significant fractionation with regard to sea water for these ice types. Any departure from the sea water value is therefore a good indicator of active chemical fractionation below the ice shelf.

Again, there is here a marked contrast between the granular and the banded facies (Figures 43, 44 and 45): the saltier banded facies shows K/Mg ratios very close to the one of sea

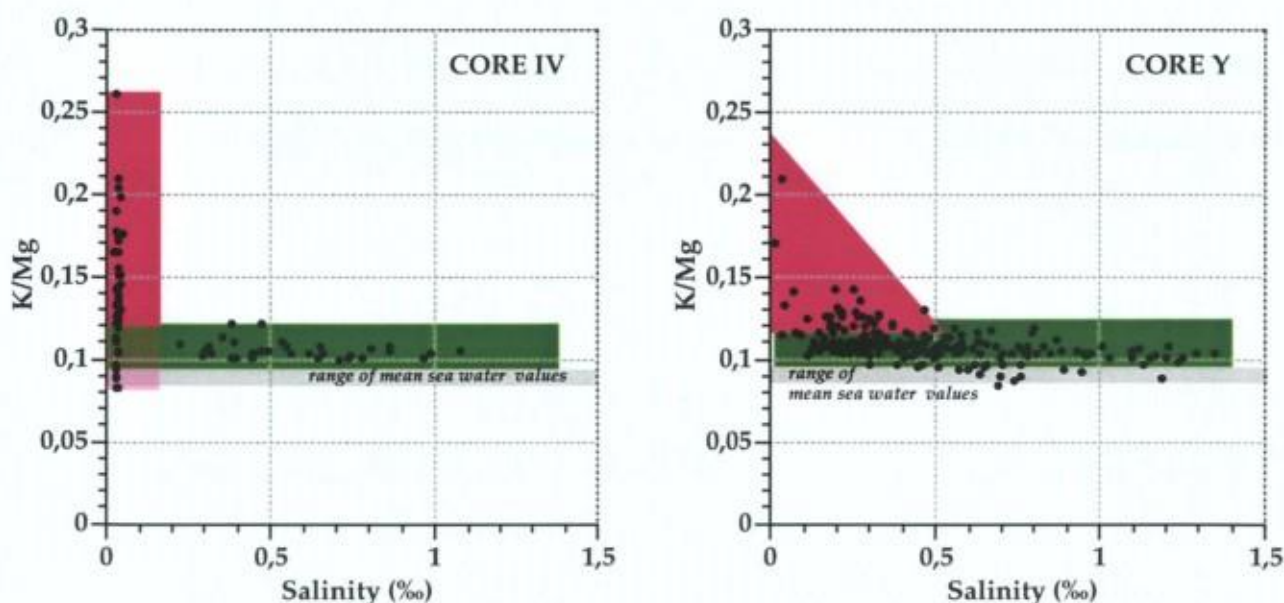


Figure 45: The K/Mg – Bulk salinity relationship for cores IV and Y at HGIS (Tison et al., 1998). The range of sea water values is indicated in grey. The purple area mainly groups granular ice samples and the green area banded, columnar and platelet ice samples.

water and, inversely, the low salinity granular ice samples display higher K/Mg ratios.



(e) Co-isotopic signature ( $\delta^{18}\text{O}$ ,  $\delta\text{D}$ )

Using early shallow depth ice core results, Souchez et al. (1991) demonstrated that downstream marine ice transfer must occur at Hells Gate Ice Shelf. Figure 46 summarizes their results. It plots the  $\delta\text{D}$ - $\delta^{18}\text{O}$  values for local sea water collected between 0 and 200 meters in front of the ice shelf together with those of columnar (congelation), platelet and frazil (no distinction was made at the time between the granular and the banded facies) ice samples. Sea water samples, congelation, platelet and frazil ice samples are aligned on a slope of 6.6 (correlation coefficient 0.93). This slope can be considered as a freezing slope. Indeed, the freezing slope on which ice samples due to water freezing are aligned in a  $\delta\text{D}$ - $\delta^{18}\text{O}$  diagram can be calculated using the equation:

$$S = \left( \frac{\alpha - 1}{\beta - 1} \right) \times \left( \frac{1000 + \delta_i\text{D}}{1000 + \delta_i^{18}\text{O}} \right) \quad (\text{Souchez and Jouzel, 1984}) \quad (2)$$

where  $\alpha$  and  $\beta$  are the respective equilibrium fractionation coefficients for Deuterium and Oxygen-18 (taken usually as  $\alpha=1.0208$  and  $\beta=1.003$ ),  $\delta_i\text{D}$  and  $\delta_i^{18}\text{O}$  are the respective  $\delta$  values for the initial water at the beginning of freezing. Taking  $\delta_i\text{D} = -4 \text{‰}$  and  $\delta_i^{18}\text{O} = -0.6 \text{‰}$  (mean values for sea water at ice shelf's edge), the calculated slope is 6.9, which is fairly close to the measured value. The difference between the  $\delta$  values of most frazil ice samples and sea water samples is higher than the maximum possible shift which can be obtained by a single freezing event, thus precluding this sea water as the parent water for the frazil ice. In their paper, Souchez et al. (1991) concluded that the best candidate for the

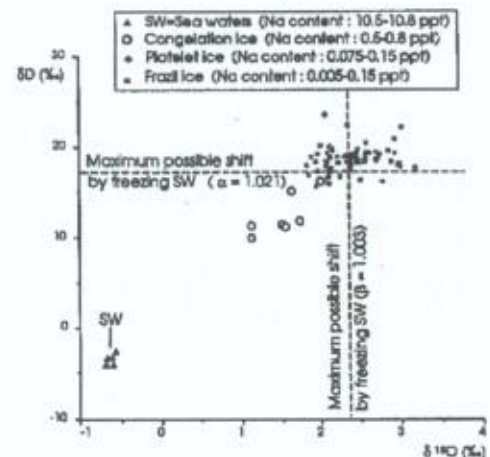


Figure 46:  $\delta\text{D}$ - $\delta^{18}\text{O}$  diagram for sea water and marine ice types of the Hells Gate Ice Shelf (Souchez et al., 1991)

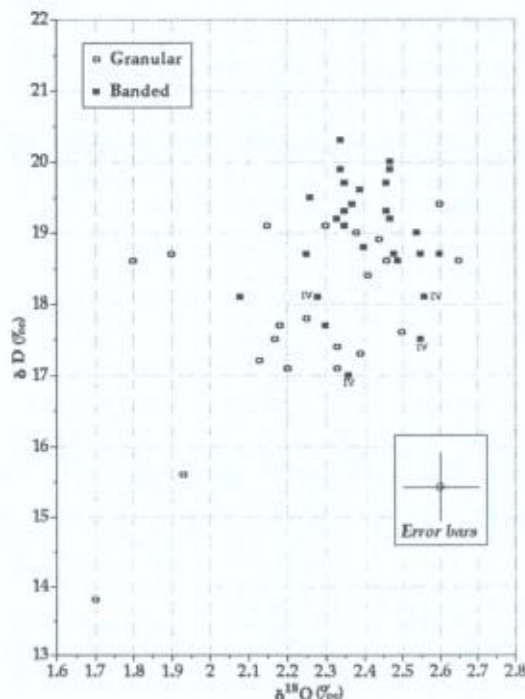


Figure 47:  $\delta^{18}\text{O}$ - $\delta\text{D}$  relationship for the two main marine ice facies at HGIS (cores XXI, IV and Y - Tison et al., 1998)

"parent water" in which the frazil ice has originated is a mixture between sea water and melted congelation sea ice produced at the bottom of the ice shelf, in the context of the Deep Thermohaline Circulation. These authors therefore demonstrated that downstream marine ice transfer occurs at the bottom of the ice shelf. It is however difficult to conceive by comparing the scarcity of the columnar ice facies to the great abundance of the marine ice facies at Hells Gate that the latter is fully inherited from melting and re-mixing of the first. Therefore, Tison et al. (1998) investigated for contrasts in the co-isotopic signature of the granular vs. the banded facies (Figure 47). This is a difficult task to achieve, if one keeps in mind all the cumulative steps involved in the build up of a consolidated marine ice layer. The final isotopic signature will depend on a number of factors: the signal of the "parent water" for individual frazil ice crystals, the apparent fractionation coefficient, the signal of the "host water" where individual frazil ice crystals accumulate, the



porosity of the loose frazil (proportion of water to ice) and the efficiency of fractionation during the consolidation process by freezing of the "host water". The slight increase of the isotopic signal in the water resulting from mixing of the granular ice meltwater with sea water, that will eventually form the parent water for individual crystals of the banded facies formed further downstream, could easily become lost in this multiple step process. Nevertheless, although, as foreseen, all the samples lie in the area of a few error bars in Figure 47, the pattern suggests that samples from the banded facies are slightly enriched with regards to those from the granular facies, especially if one does not consider the four samples from the banded facies occurring just below the transition zone in core IV.

To summarize, we have shown that two main facies of marine ice exist at Hells Gate Ice Shelf. Besides the widespread granular facies described in the literature for all other deep marine ice cores, a banded facies is dominant closer to the ice shelf front. In places where both facies are present on top of each other, a transition zone exists showing a mixed platelet-congelation facies indicating an episode of direct freezing of sea water at the interface driven by heat conduction through the ice shelf, previous to the deposition of the banded facies. The granular facies is characterized by the presence of debris inclusions (indicating the relative proximity of a grounding area), low salinities and moderate to high chemical fractionation, as far as the K/Mg ratio is considered. The co-isotopic signature of the banded facies, on the other hand, indicates that it could have been generated in a "parent water" partly diluted by the meltwater from the granular facies.

Simple experiments, where fresh-water ice blocks were melted in a sea water reservoir above its freezing point (Tison et al., 1993: their Table 1 and Figure 5), were shown to result in a 30% reduction of the salinity and a 125% increase of the K/Mg ratio in the interface water layer. This process, reflecting a selective diffusion mechanism from undiluted to diluted sea water had previously been demonstrated by Ben-Yaakov (1972) and shown to lead to an increase of K/Mg of up to 200% of its original value in sea water. Repeating the experiment described above with a gauge incising the bottom of the melting ice block, showed increased differences, thereby indicating accumulation of waters of least density in inverted depressions below the ice (Tison et al., 1993). It was then proposed that melting below an ice shelf would enhance dilution of the interstitial host water within the loose frazil accumulating underneath. It would also enhance chemical fractionation between sea water and this interstitial water, resulting in the original chemical signature of the granular facies.

The general trend in the granular ice of the composite profiles (Figures 43 and 44) is to a decrease in salinity and increase in fractionation downstream on the profile (i.e., as one gets closer to the ice shelf front), suggesting that the heat source requested for melting and dilution processes, hypothesized by Tison et al. [1993], is to be found in the frontal area of HGIS. A potential candidate for this is the tidal pumping in summer of warmer water of the coastal currents, described by Jacobs et al. (1992) as "circulation mode-3" (Figure 10, section 1.3).

The developments above suggest that the two main facies observed at Hells Gate Ice Shelf correspond to two different ice-ocean interaction modes:

- (a) The granular ice facies results from an ice pump mechanism active in a "classical" Deep Thermohaline Circulation" cell. The frazil ice produced in the supercooled outcoming Ice Shelf Water accumulates in relatively calm conditions, in inverted depressions located at the junction of individual continental meteoric ice flows and then consolidates. We will see later on, that, for reasons of bedrock geometry and mesoscale ocean circulation, the descending branch of this DTC is probably actually located under the Nansen Ice Sheet (3.3. - p.87)
- (b) The banded ice facies results from an ice pump mechanism associated with a "shallow" frontal Thermohaline Circulation, connected to the tidal forcing of surface waters below the ice shelf, in which the depositional environment for the frazil ice crystals is one of interfacial flow with local turbulences, intense mixing and, therefore, limited chemical fractionation.



We will see that landfast sea ice studies in front of HGIS bring support to the existence of such contrasted ice-ocean interaction patterns. It is also interesting to note that Grosfeld et al.'s (1998) 3-D oceanographic model for the Filchner Ice Shelf cavity predicts a zone of potentially enhanced freezing in a narrow frontal band, only a few kilometres wide. This could be the equivalent of our shallow frontal Thermohaline Circulation.

3.2.4. Rift Thermohaline Convection

We have seen in section 3.2.1 that basal crevasses are common features at the bottom of floating glaciers, particularly near grounding lines and pinning points. In some favourable circumstances, these crevasses can reach to the surface and eventually turn into rifts several hundred of meters wide. Very

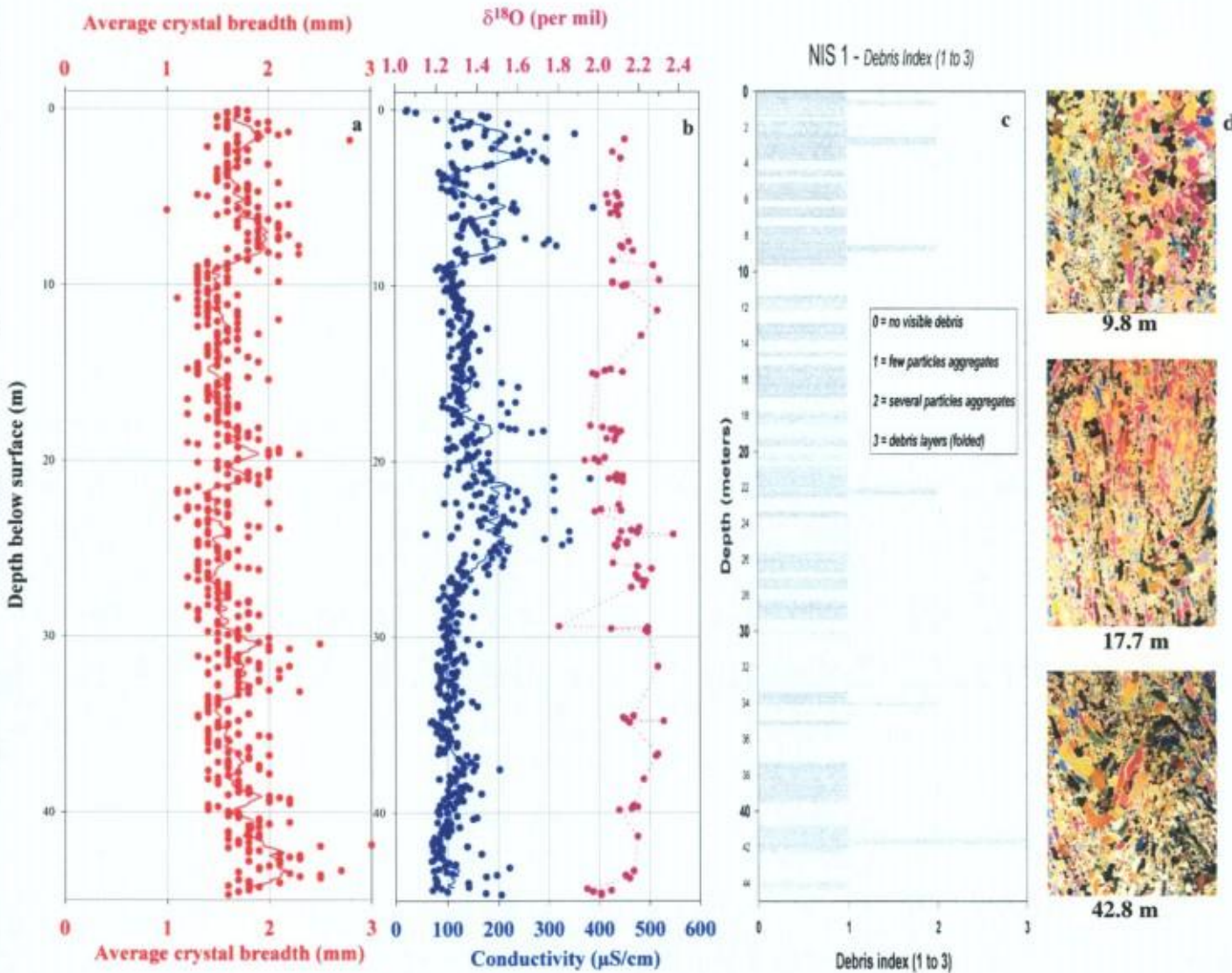


Figure 48: Main properties of the NIS1 core (see Figures 11 and 13 for location): a) Average crystal breadth (mm), b) Conductivity (a proxy to bulk salinity,  $\mu\text{Scm}^{-1}$ ), c) Debris content (semi-quantitative estimate from visual examination in transmitted light) and d) examples, in vertical thin sections seen through crossed polarizers, of granular, "stringlined" and folded textures in the core. Note that each texture type can be found at various depths (after Khazendar, 2000 and Khazendar et al., 2001).

quickly the rifts are filled with ice, which is transported downstream at the same time it is strongly compressed both laterally between joining individual continental ice flows and longitudinally between



the closing lips of the former rift (Figure 13). Khazendar (2000) and Khazendar et al. (2001) have made a detailed description of a 45 meters ice core (NIS1) drilled some seven and a half kilometres downstream of the open rift area developing at the grounding line of the Reeves Glacier, where it flows into the Nansen Ice Sheet (Figures 11 and 13). Figure 48 and Table 2 summarize their results.

*Table 2: Main results from the 45-m NIS1 ice core retrieved from the Nansen Ice Sheet (Victoria Land, Antarctica – Tison et al., 2001)*

	Crystal size (mm)	Conductivity ( $\mu\text{Scm}^{-1}$ )	Salinity (‰)	$\delta^{18}\text{O}$ (‰)
Mean	1.66	138.00	0.06	2.12
Minimum	1.00	22.30	0.005	1.80
Maximum	3.00	390	0.19	2.37
$\sigma$	0.27	54.01	0.02	0.09

Textural (no bubbles and granular/stringlined facies), isotopic (positive  $\delta$  values) and salinity (mean salinity about two orders of magnitude lower than sea ice and one order of magnitude higher than continental meteoric ice) properties of the samples from NIS1 are undoubtedly the signature of a marine ice body. The conductivity range (Table 2) does overlap the ranges of 40-200  $\mu\text{Scm}^{-1}$  for B13 on the Filchner-Ronne Ice Shelf (Oerter et al., 1992) and 100-210  $\mu\text{Scm}^{-1}$  for G1 on the Amery Ice Shelf (Morgan, 1972). Furthermore, the baseline trend of decreasing salinity with depth (Figure 48) echoes what has been observed in the above-cited studies. The oxygen isotope composition results correspond well with the slightly positive values reported for G1 by Morgan (1972) and the value of +2‰ for B13 measured by Oerter et al. (1992).

However, some striking differences exist between NIS1 and other marine ice cores of equivalent extension:

- (a) The mean crystal breadth is 1.7 mm (Table 2), which, if we use a rounded approximation, corresponds to an average crystal cross-sectional area of 2.7  $\text{mm}^2$ . This value is distinctly lower than those ranging between 5 and 60  $\text{mm}^2$  reported for B13 and B15 by Oerter et al. (1994). Furthermore, with most crystals having cross-sectional areas fluctuating between 1.1 and 3.8  $\text{mm}^2$ , NIS1 also exhibits a much more confined range. NIS1 core crystal size shows a slight tendency to increase with depth in the lower third of the core (Figure 48 - 11 points running mean smoothed profile). The B13 core, by contrast, shows a much clearer trend of increased crystal size with depth.

All these characteristics can easily be understood if one considers the age difference between marine ice in the NIS1 core as compared to B13 and B15. Because of its location very close to the grounding line and considering local surface velocity values, marine ice at NIS1 must be of the order of 50 years old, as compared to the hundreds of years estimated for the Filchner-Ronne cores by Eicken and others (1994). This would have given the NIS grains less time to recrystallize under normal Arrhenius-type crystal growth<sup>3</sup>, thus resulting in their relatively smaller size and lower range.

- (b) The abundance of the string-lined facies and of small scale folding features in the NIS1 core are another peculiarity that finds its explanation in the local ice dynamics, as illustrated in the drawing of Figure 49. Submitting the marine ice body to sub-horizontal stresses

<sup>3</sup> "Normal" (in the absence of stress) crystal growth takes the form  $D^2 - D_0^2 = kt$ , where  $D^2$  is the mean cross-sectional area of crystals at age  $t$  and  $D_0^2$  is the initial value of  $D^2$ . The crystal growth rate  $k$  varies with temperature according to the Arrhenius Equation  $k = k_0 \exp(-E/RT)$ ; where  $k_0$  is a constant,  $T$  is the absolute temperature,  $R$  is the gas constant ( $8.314 \text{ Jmol}^{-1}\text{K}^{-1}$ ) and  $E$  is the activation energy for grain-boundary self-diffusion (Paterson, 1994).



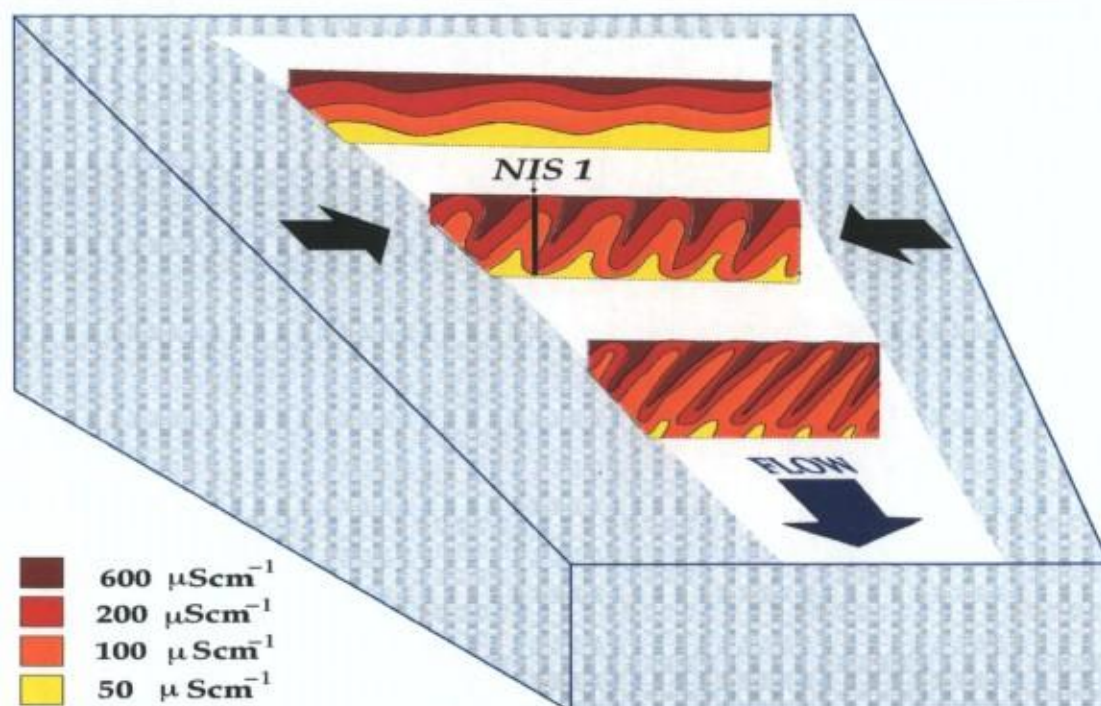


Figure 49: Schematic drawing of how folding features can affect the initial salinity stratigraphy in the marine ice body at Nansen Ice Sheet, under the compressive forces generated by the coalescence of neighbouring individual continental ice flows (Khazendar et al., 2001).

generated at the junction of coalescent floating ice tongues will result in localized grain recrystallization processes and tight folding with sub-vertical hinges, as observed.

- (c) The NIS1 core, with a maximum measured conductivity of  $390 \mu\text{Scm}^{-1}$ , generally exhibits higher salinities than B13, B15 and G1. The top 0.4 m of marine ice in the B15 core show conductivity values as high as  $390 \mu\text{Scm}^{-1}$  (Oerter et al., 1994), but interaction with particulate inclusions abundant in these layers could have occurred. Indeed, the B15 conductivity profile rapidly drops back to a baseline value of around  $40 \mu\text{Scm}^{-1}$ , similar to that of B13. The NIS1 core, by contrast, has a conductivity baseline value that falls from around  $140 \mu\text{Scm}^{-1}$  to  $90 \mu\text{Scm}^{-1}$  with increasing depth (Figure 48). Again this discrepancy is understandable if one considers that the rift marine ice starts consolidating much closer to the surface, i.e. under much stronger temperature gradients, and therefore much faster freezing rates. Since, as shown by Burton et al. (1953), the efficiency of impurity fractionation at the ice-water interface on freezing is inversely proportional to the freezing rate, higher freezing rates (closer to the surface) will result in saltier ice (see also section 3.4).
- (d) Another salient feature of the conductivity profile in Figure 48, is that severe higher salinity “accidents” are superimposed to the baseline, over a few meters of depth. This is to be expected if the original stratigraphy has been disturbed by large scale folding processes, bringing lower strata at higher levels (Figure 49). Although these are difficult to track in a 7.5 cm diameter core, we take the observed small scale folding and the local dynamical context as indirect proofs of their existence.

As for the crack metamorphism process at grounding lines described in section 3.2.1., there was no trace whatsoever in the NIS1 core of columnar-congelation ice that might have developed under direct freezing on the sidewalls of the rift. Although that process might have happened locally, it is in fact difficult to conceive that a whole rift, generally several hundreds of meters wide and deep, could be filled with ice by such a process. Direct freezing of surface water downwards, as occurs for sea ice, could be responsible for a few meters thickness, not several tens of meters. Furthermore, we have just



demonstrated that the overall properties of our NIS1 core are much closer to those of marine ice generated in a Deep Thermohaline Circulation cell than to sea ice properties.

In that context, Khazendar (2000) has developed a numerical model simulating a rift (or a basal crevasse) already wide open with a turbulent water plume active inside. Ice formation is mainly through the creation of frazil ice crystals, in addition to direct freezing on the portion of the wall of the cavity, where the water in the plume begins to be supercooled. In a general way, the model can be considered as another application of an ice pump mechanism: the process by which ice in contact with sea water is melted at depth and deposited higher in the water column. A detailed mechanism by which the transfer of ice through the water column takes place is however needed. The simulation of melting and freezing processes at the ice/ocean interface is therefore provided by a plume model (Jenkins, 1991; Jenkins and Bombosch, 1995; Bombosch and Jenkins, 1995), which is a central feature of Khazendar's (2000) rift model.

An important advantage of Khazendar's (2000) rift model is that it can easily be extended to all kinds of rifts opening in ice shelves, be it in the vicinity of ice rises, ice islands, on the side of large embayments or in the frontal zone of ice shelves where rifts often precede calving events. We will see the potential importance of this in section 4.

*Table 3: Total thickness of ice accumulated at the end of 100-year runs covering four experiments: Ronne rift with Ice Shelf Water (ISW) initially filling the cavity; Ronne rift with Modified Weddell Deep Water (MWDW) initially filling the cavity; and both these experiments repeated with a periodic, 12-months cycle, renewal of ambient water.*

Experiment description	Initial ambient temperature (°C)	Initial ambient salinity (psu)	Total ice accumulation (m) with no renewal of ambient water	Total ice accumulation (m) with renewal of ambient water
Ronne rift with ISW	-2.0800	34.6800	61.9516	129.7831
Ronne rift with MCDW	-1.5000	34.5000	56.0303	0.0425

Probably the major output of Khazendar's (2000) set of simulations applied to several documented real cases in the Antarctic, is that considerable amounts of marine ice will form in rifts only when they are filled by plumes of Ice Shelf Water, and even more so if these plumes are replenished on a regular base. This is illustrated in Table 3, for the case study of a rift located some 30 km inland from the front of the northwest corner of the Ronne Ice Shelf. The ice thickness in the rift has been roughly estimated to be more than 200 meters by seismic methods (King, 1994). Four runs of 100 years have been performed, two by initially filling the cavity with Ice Shelf Water (ISW) or with warmer and fresher Modified Circum Deep Water (MCDW), and two others by re-filling the cavity with these same initial waters every 12 months. The results are self-explaining: although comparable total ice thickness are observed when the water in the cavity is not renewed, the more realistic case where renewal occurs results in maximum marine ice thickness in the ISW case, and hardly no filling at all in the MCDW case.

### 3.3. What can we learn from landfast sea ice studies?

In section 1.3., we have pointed out that the relative scarcity of marine ice related work in the literature is partly due to its restricted accessibility for field studies. We have then shown that the Terra Nova Bay area environment provides a unique opportunity to increase our knowledge on the spatial



variability and diversity of genetic mechanisms for marine ice. In this section we will demonstrate, with two case studies, how landfast sea ice<sup>4</sup> can also be used as a short-term archive for ice-ocean interactions.

### 3.3.1. The Georges VI Ice Shelf case (Antarctic Peninsula)

Our first example illustrates the production of marine ice in an open rift close to the border of the southern George VI Ice Shelf in the Antarctic Peninsula (Figure 50). Landfast sea ice was sampled in March 1988 in a heavily rifted area located some 15 kilometres of the actively calving front of the southern George VI Ice Shelf. Figure 51 summarizes the textural, bulk salinity (of which Na concentration is used as a proxy) and  $\delta^{18}\text{O}$  data set recovered from a representative 5.54 m thick ice core.



Figure 50: Location and landsat image (9 January 1973) of the Southern George VI Ice Shelf. The rift area where the landfast sea ice was sampled is indicated by a square.



The combined analysis of these three parameters has been used by Tison et al. (1991) to reconstruct the growth history of the ice cover and to decipher the processes underlying its build-up. After the initial freezing of the ocean surface, the sea ice cover has grown both upward (mainly snow accumulation as indicated by the negligible salinity and the low  $\delta^{18}\text{O}$  values) and downward. The shape of the  $\delta^{18}\text{O}$  curve in the upper snow layer (suggesting a full annual cycle) and the recurrence of a transitional profile in the 500-554 cm depth range similar to the one observed in the 100-170 cm range are two major arguments to suggest that the ice is actually second-year ice<sup>5</sup>. The fact that the salinity (Na) and the  $\delta^{18}\text{O}$  curves show sympathetic behaviour can be interpreted as the signature of the parent water for the ice, as opposed to

<sup>4</sup> Landfast sea ice commonly stands for a part of the sea ice cover that is fasten to the land, be it a bedrock coastland or a floating ice body of continental origin (ice shelf or ice tongue).

<sup>5</sup> Second year ice commonly stands for a sea ice cover that has survived one full summer period



the effect of a decreasing freezing rate with depth that would result in the two curves going in opposite directions<sup>6</sup>.

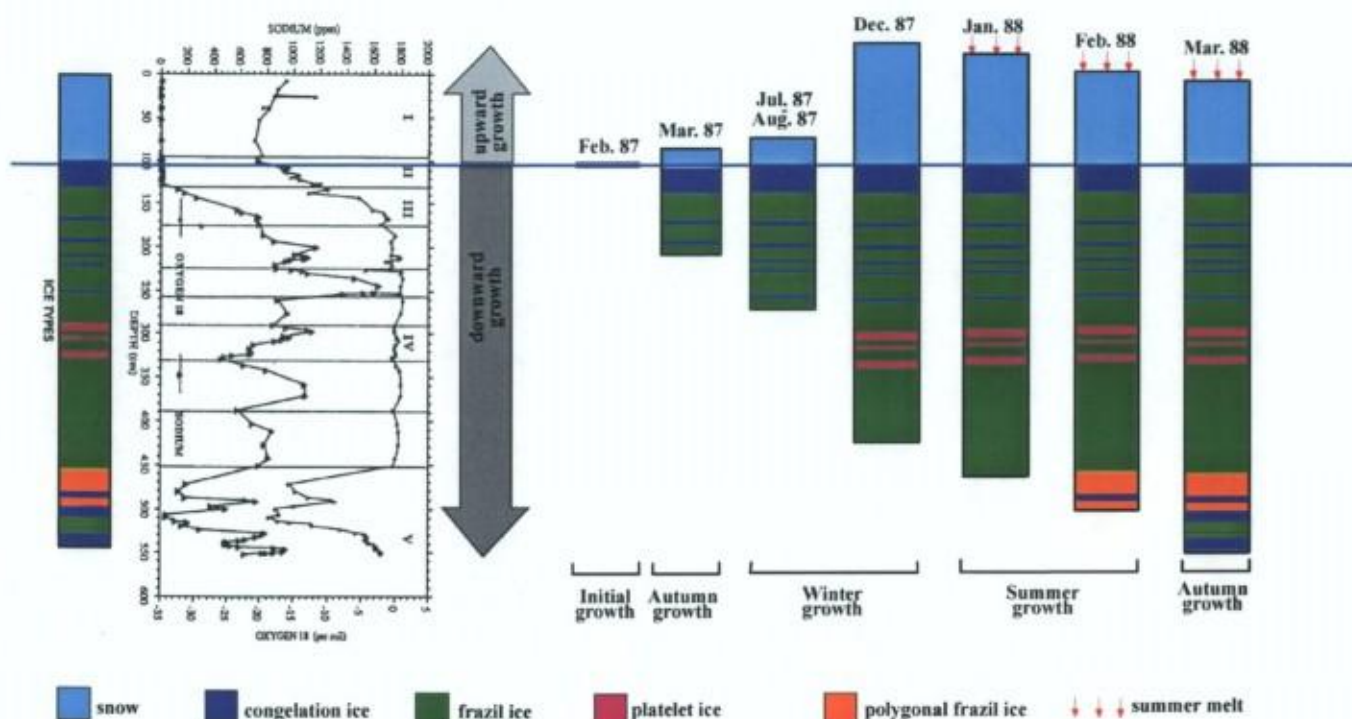


Figure 51: Schematic diagram summarizing the data set interpretation from Tison et al. (1991) study of a landfast sea ice core sampled in the rift area close to the southern front of the George VI Ice Shelf. The time scale is hypothetical and based on the data interpretation. Hydrostatic rebound has been neglected in the drawing.

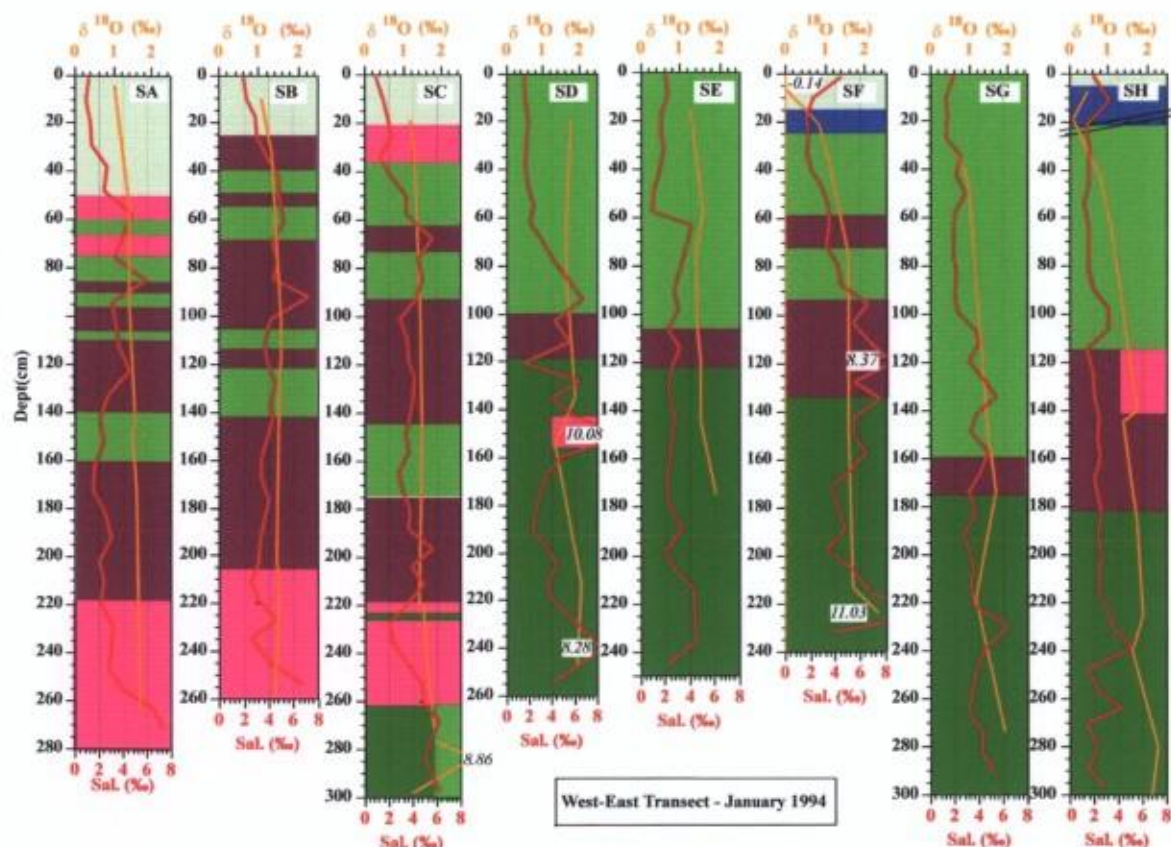
Half of the core consists of ice formed during the winter 1987. Although during that period, the parent water is close to normal sea water, the  $\delta^{18}\text{O}$  and Na curves show a few sympathetic fluctuations, indicating dilution events. Tison et al. (1991) compared the samples distribution in a  $\delta^{18}\text{O}$ /Na diagram with various mixing lines of pure sea water with either meltwater of surface snow or meltwater from the ice shelf walls, in an attempt to determine the freshwater source for the dilution process. For the winter accretion both sources were equally plausible. However, since surface melting is obviously precluded during the winter, the source must be found in the melting of the ice shelf walls. The nearly 3.5 meters of winter granular/frazil ice accumulation must therefore result from an active ice pump mechanism similar to the one modelled in the Khazendar's (2000) rift plume model. Another evidence that this process has been active is the occurrence, during 3 of the 5 dilution episodes, of platelet ice layers. We know from the available descriptions in the literature that this peculiar textural profile is always associated to ice production in thermohaline convection processes.

The summer 1988 has seen a strong dilution of the parent water for the ice accretion. Water properties actually returned to those prevailing during the initial build-up of the ice cover, the previous year. Comparison with the mixing lines mentioned above indicate, this time, that at least one third of the samples must have formed from a parent sea water diluted by melting of the ice shelf walls, with increased dilution intensity as compared to the winter. Ice formation in this brackish water has resulted in a polygonal granular ice facies. The very bottom of the ice cover typically reproduces the trend observed during the previous autumn.

<sup>6</sup> Decreasing the freezing rate will indeed improve the efficiency of the observed fractionation at the ice-water interface, i.e. building new ice that will be enriched in heavy isotopes and depleted in salts, hence the expected opposite trends in the Na and  $\delta^{18}\text{O}$  curves.



This study shows that the landfast sea ice forming in the south George VI Ice Shelf rifts is actually predominantly marine ice, demonstrating the efficiency of the process of rift filling through ice-ocean interactions, where ice melted at depth is redistributed at the ocean surface. This is a process very different from the classically invoked mechanism where the ice cover mainly builds up from the top, with concurrent participation of direct sea water freezing under heat conduction and drifting snow deposition. Although we do not know the detailed oceanography under the ice shelf at that location (and therefore if the water contributing to the plume filling the rift is Ice Shelf Water, Circumpolar Deep Water or even, though less likely, High Salinity Shelf Water), it is interesting to note that the net marine ice accumulation observed here during the first year of existence of the ice cover is compatible with the 3 to 5 meters obtained in Khazendar's (2000) simulations.



North - South Transect - October 1995

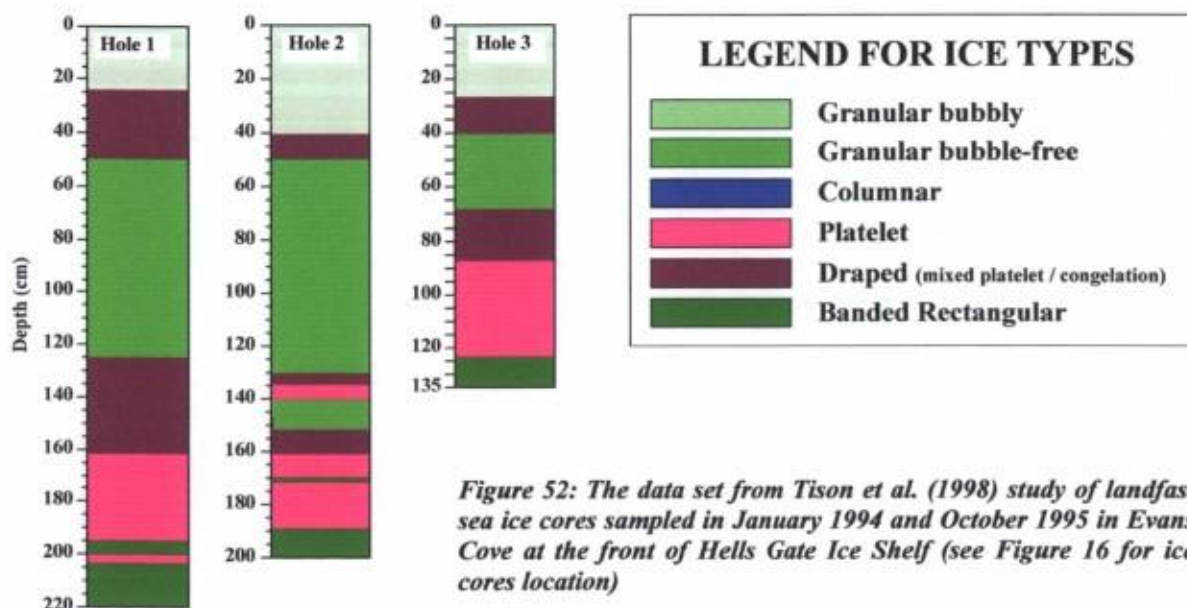
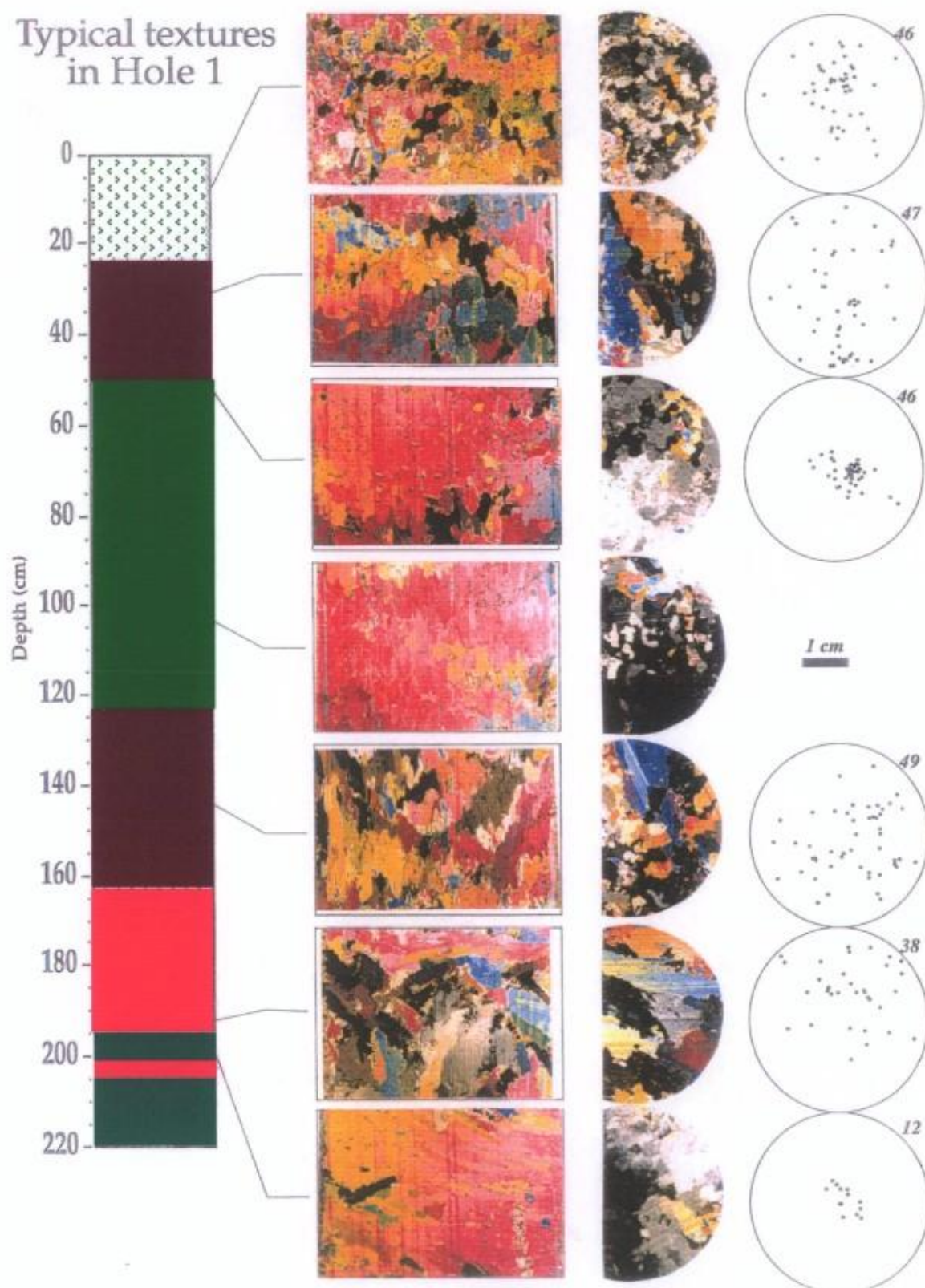


Figure 52: The data set from Tison et al. (1998) study of landfast sea ice cores sampled in January 1994 and October 1995 in Evans Cove at the front of Hells Gate Ice Shelf (see Figure 16 for ice cores location)



## 3.3.2. Evans Cove (Hells Gate Ice Shelf, Victoria Land)



**Figure 53: Textures and fabrics in Hole 1 (October 1995).** Rectangular photographs are vertical thin sections and circular photographs show horizontal thin sections at equivalent depths. The scale is valid for all pictures. C-axes are shown in the horizontal plane and plotted in the lower hemisphere of a Schmidt net and the number of c-axes measured is specified. Legend for ice types is as in Figure 52 (Tison et al., 1998).



This second example shows how landfast sea ice forming in front of ice shelves allows us to improve our understanding of ice-ocean interaction processes actually occurring below the ice shelves. Figures 52 and 53 summarize the results of Tison et al.'s (1998) study of landfast sea ice cores in Evans Cove, the small embayment in front of Hells Gate Ice Shelf (see Figure 16 for ice cores location). Figure 52 combines results from a spring (October 1995) transect, roughly perpendicular (North-South, Holes A to C in Figure 16) to the ice shelf front, with those from a summer (January 1994) transect, roughly parallel to it (East-West, Cores SA to SH in Figure 16). Figure 53 illustrates textures and fabrics in Hole 1.

Consolidation of wind- and wave-induced frazil ice produced in highly agitated surface sea water (strong katabatic winds), showing dilution effects by continental meltwaters (lower salinity, lower  $\delta^{18}\text{O}$ ), generally forms the initial sea ice cover in the beginning of the winter. This is indicated by the granular ice facies, the richness in air/brine inclusions and the random c-axes fabric (Figure 53).

In more than half of the cores, the surface layer is underlain by a platelet or a draped facies (Figures 52 and 53). Then, a lower granular facies develops, eventually in alternation with the draped facies. The crystallographic and textural contrasts between the granular facies forming the surface layer and the one occurring further below suggest different origins (Tison et al., 1998). The latter shows a slight elongation of the crystals in the vertical plane, denoting partial influence of a downward congelation process. However, instead of the usual concentration of c-axes in the horizontal plane typical of congelation sea ice, it displays a strong clustering along the vertical (Figure 53). This suggests that most of the winter accretion in front of HGIS consists of small individual discs of frazil ice crystals (with c-axes perpendicular to the disc), gently settling upward at the base of the existing sea ice cover in a calm environment, allowing orderly packing. Sweeping of wind- and wave-induced frazil ice crystals formed in the Terra Nova Bay polynya down to a maximum 1.70 m underneath the already existing fast ice cover in Evans Cove is improbable because of the steady south-eastward blowing katabatic winds. These are constantly "skimming" away the thin superficial buoyant layer of newly formed frazil. Moreover, the thickness of this granular facies tends to increase towards the ice shelf front in the 1995 cores (Figure 52). Dynamical thickening through rafting<sup>7</sup> is equally precluded given the maximum depth observed for this facies and the absence of typical signatures of the process (see, for example, Eicken, 1998). The most plausible source for these frazil ice crystals is, therefore, the active supercooling in the Deep Ice Shelf Water adiabatically rising below HGIS during the winter, that is also responsible for the granular marine ice facies described before. As shown below (p. 84-88), the structure of the water column in front of HGIS confirms the presence of large amounts of Deep Ice Shelf Water (DISW). Further, relatively fast consolidation of the host water leads to a slight elongation of the crystals, which, however, retain their original crystallographic signature.

The end of the winter season is dominated by platelet accretion (Hole 1 to 3 and SA to SC). This facies is nearly absent in the eastern cores, where the winter accretion is thinner. It is not clear, however, if the lack of platelet ice in the eastern cores results from a lower accretion of platelet ice compared to the western zone, or increased bottom melting in the beginning of the summer season.

Bottom accretion still occurs during the summer as a banded facies. This facies does not exist in front of the western sector (west of the western medial moraine) and forms between 44% and 54% of all consolidated ice cores in front of the central and eastern sector. There also, a thick layer (several meters) of unconsolidated loose rectangular frazil ice crystals exists at the base of the sea ice cover from the end of the winter through most of the summer. This banded rectangular facies is thus actively building preferentially in the eastern sector in the first half of the summer. The  $\delta^{18}\text{O}$  signal increases slightly in the second half of the core, as the banded facies starts to build up (Figure 52). This last observation is consistent with the suggestion made in section 3.2.3. that warm surface water is forced under HGIS by tidal action and partially melts marine ice previously accreted at the bottom. The meltwater produced is

<sup>7</sup> "Rafting" describes the dynamical process by which individual "pancakes" (consolidated aggregates of wind- and wave-induced frazil ice crystals), typically a few decimetres thick, thrust each other under heavy swell. It contributes to the thickening of the sea ice cover to a maximum of 50-60 centimetres, and generally results in oblique discontinuities in the cores.



likely to increase the  $\delta$ -value of the resultant sub-ice shelf top water layer, since marine ice has a slightly positive signature. This water mass will be the host water (and possibly the parent water, if further

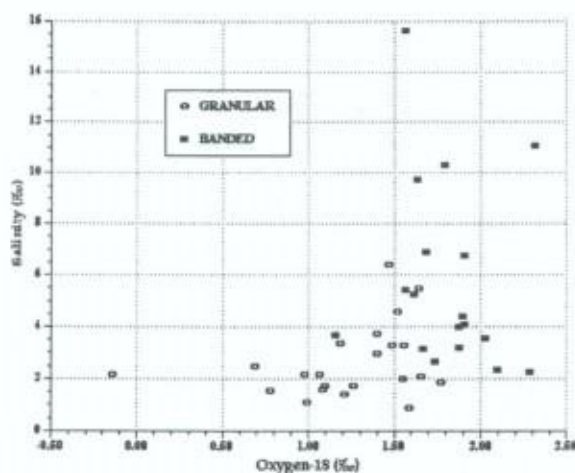


Figure 54:  $\delta^{18}\text{O}$  versus salinity for samples of the granular and banded facies in the landfast sea ice cores at HGIS (Tison et al., 1998)

result partly from grain sizes, shapes, and hence, porosity.

These complementary information we gathered from the landfast sea ice cores improve our insight into the complex ice-ocean interactions processes occurring in the Nansen Ice Sheet-Hells Gate Ice Shelf system (Figure 55).

The granular marine and landfast sea ice (set apart the surface wind- and wave-frazil) facies observed at HGIS must result from adiabatic supercooling in Ice Shelf water produced in a Deep Thermohaline Circulation (DTC) as it occurs beneath larger ice shelves (mode-1 in Figure 10). Referring to hydrological measurements during three Italian summer cruises in the Ross Sea (1995/95, 1995/1996 and 1997/1998) Budillon and Spezie (2000) describe summer water masses in the Terra Nova Bay polynya as relatively simple. A warmer and fresher (because of sea ice melt) Summer Surface Water (SSW) occupies the surface layer, that extends between 50 and 150 meters depth. Below this layer, High Salinity Shelf Water (HSSW) is found all the way down to the bottom, with a potential temperature close to surface freezing point and salinity  $> 34.7$  ‰. This HSSW is inherited from the surface production of cold and saltier sub-surface water during sea ice freezing (mostly in the winter, hence its name of Winter Water). In this quasi isothermal layer of HSSW, an Ice Shelf Water (TISW, Terra Nova Bay Ice Shelf Water), showing temperatures below the surface freezing point (a signature for ice-ocean interaction below the ice shelf) is widely detected in the whole of Terra Nova Bay, as shown by the distribution of maximum temperature anomaly between the *in-situ* temperature and the surface freezing point (Figure 56). It is clear from the isotherm patterns in Figure 56 that the NIS-HGIS system is the central area of production for this ISW.

growth or new crystal growth is allowed by adiabatic supercooling) for the loose crystals that will form the banded facies in the landfast sea ice (actually a down-flow “extension” of the banded marine ice facies), resulting in the higher  $\delta^{18}\text{O}$  values observed. Another way to visualize this process is to plot the granular frazil from winter accretion in the sea ice and the banded rectangular frazil from summer accretion, on a salinity- $\delta^{18}\text{O}$  diagram (Figure 54). The banded rectangular frazil is clearly shifted towards higher salinities and higher  $\delta^{18}\text{O}$  values. The isotopic trend is similar to the one observed for co-isotopic values in the marine ice cores (Figure 47). However,  $\delta^{18}\text{O}$  ranges in the sea ice are, in both facies, shifted towards less positive values. This can be clearly related to differences in freezing rates of the frazil host water during consolidation, which must be significantly higher below 1.50 m of first-year sea ice than below several tens of meters of shelf ice. Higher salinities in the banded rectangular facies probably

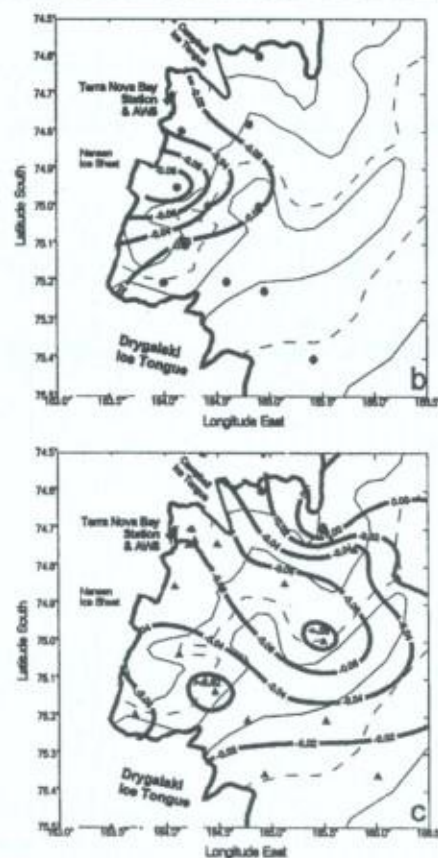
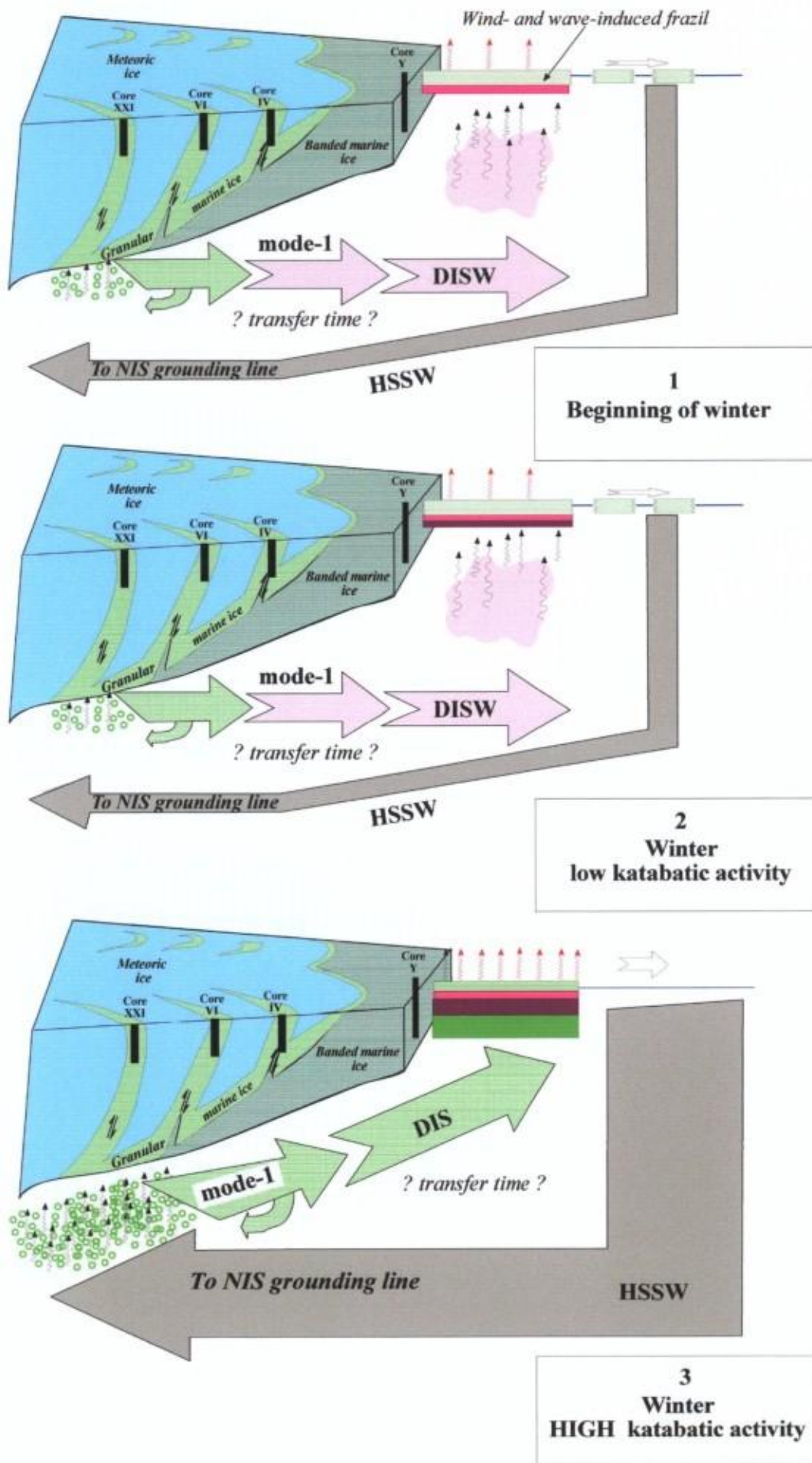


Figure 56: Distribution of the maximum anomaly ( $^{\circ}\text{C}$ ) between the *in-situ* potential temperature and the surface freezing point ( $S=34.85$ ) for the Dec. 1997 and Feb. 1998 CLIMA cruises (Budillon and Spezie, 2000)







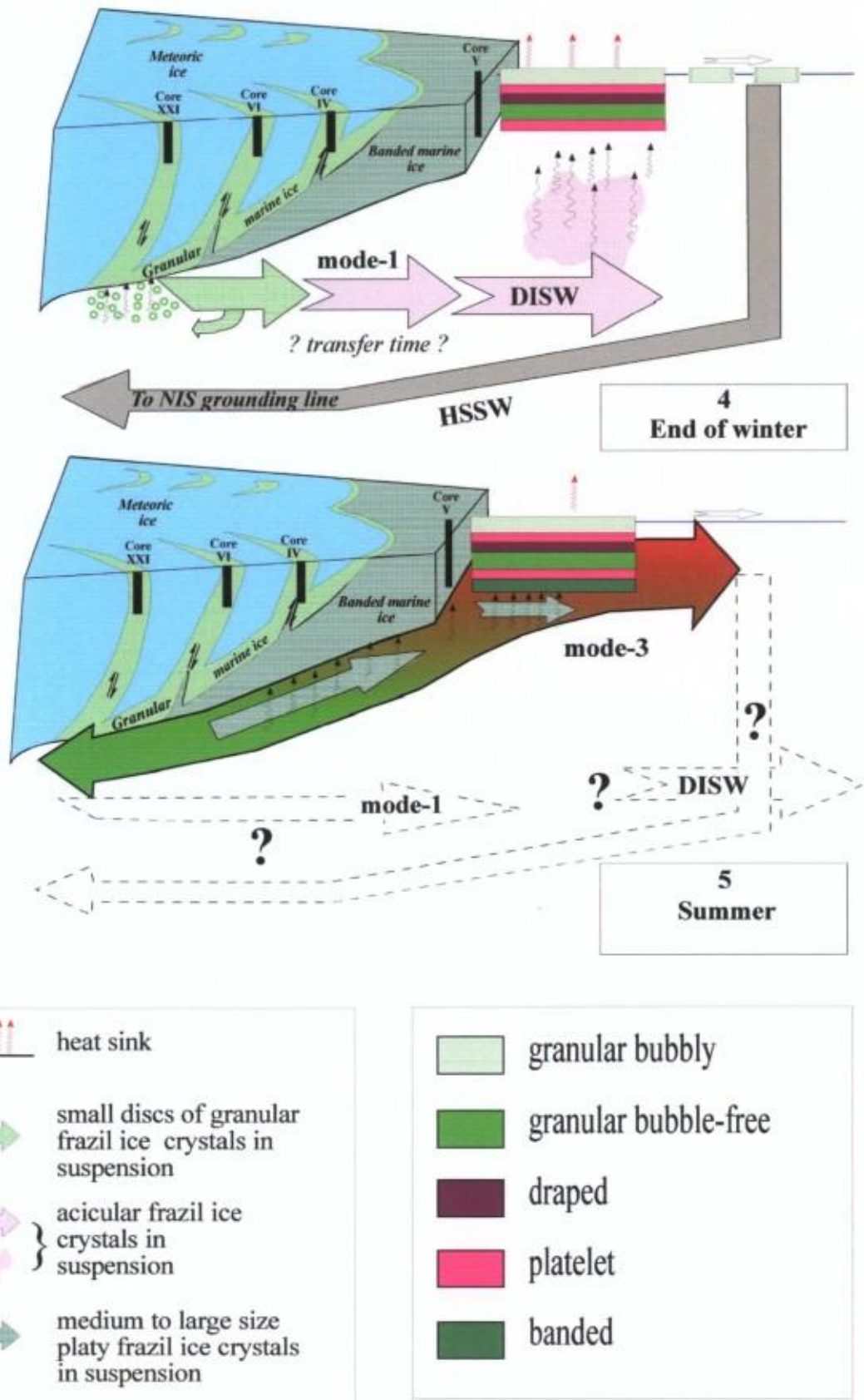


Figure 55: Schematic diagram illustrating the links between marine ice and landfast sea ice deposition processes, and how these potentially relate to ocean circulation and ice-ocean interaction patterns on a yearly time scale. Landfast sea ice deposition has been deliberately vertically exaggerated for readability. The drawing has to be perceived in 3-D, in- and out-flows not being meant to always occur on the same vertical (see details in text).



The only oceanic profile presently available in Evans Cove (Fabiano et al., 1991), shows Ice Shelf Water from 100 m deep to about 100 m above the sea floor, which consists of a narrow trough 700 m deep in the central part of Evans Cove, with depth increasing inland (Figure 56 top). The maximum ice thickness at HGIS as far as half way to the northern tip of Vegetation Island (Figure 16) is only 250 m, which implies a larger-scale circulation pattern in which HSSW produced in the Terra Nova Bay polynya, can access the Nansen Ice Sheet grounding lines (grey arrows in Figure 55), for example beneath Reeves and Priestley Glaciers (see section 3.2.4). Part of the Ice Shelf Water produced in those locations could recirculate along the eastern and western flanks of Vegetation Island, carrying with it loose frazil ice crystals formed by adiabatic supercooling. These crystals would accumulate in the depression formed at the southern tip of Vegetation Island, between the two merging flows as suggested previously.

Remnants of frazil ice crystals formed in this manner (hereafter DTC-granular facies) escape at the front of the ice shelf, where they accrete under the sea ice during the winter to form the granular facies with vertical c-axes fabrics (Figure 55). In all first-year sea ice cores that are thought to have retained the whole of the winter accretion (Hole 1, 2 and 3; SA, SB, SC in Figure 52), platelet ice bounds the lower limit of this winter accretion, while the upper limit (boundary with the initial wind- and wave- frazil ice accretion where it exists) consists of either the platelet (SA, SC) or the draped mixed congelation/platelet facies (Hole 1, 2 and 3 in Figure 52). We postulate that these observations can be interpreted as the expression of variable intensities of the DTC. Bombosch and Jenkins [1995], show that the large size of crystals in the platelet facies reflects slower frazil ice crystal growth rates in the Ice Shelf Water as it levels off and eventually escapes at depth in front of the ice shelf. Transition from a small-grained DTC-granular facies to a platelet or a draped facies in the landfast first-year sea ice could thus reflect variations in the degree of supercooling of the ISW where these crystals were formed. In early winter (Figure 55-1), enhanced freezing at the polynya surface is likely to increase HSSW production and speed up the DTC. At that time, the density contrast between ISW and HSSW should be moderate and supercooling weak. This would favor formation of the platelet facies or, probably more often, the draped mixed platelet-congelation facies, since congelation ice growth rates would still be competitive with the platelet crystal accretion rates beneath a thin sea ice cover.

In the mid-winter (Figure 55-3), the DTC may accelerate, resulting in higher density contrasts between ISW and HSSW and stronger supercooling producing the fine-grained matrix of the DTC-granular sea ice facies. At the end of the winter (Figure 55-4), a slower DTC would again favor larger crystal growth. The heat sink through the sea ice cover is also reduced, along with the consolidation rate. The latter part of this proposed cycle would result in the platelet ice facies observed at the bottom of the winter accretion of the cores where summer melting at the base of the ice was less important. In addition, large-scale fluctuations in the HSSW production related to katabatic wind activity during the winter could explain the alternations of the draped and the DTC-granular facies (Figure 55-2 and 55-3).

Several hypotheses can be formulated for the genesis of the banded marine and sea ice facies:

- (a) *Post-depositional deformation processes* leading to recrystallization of the original granular textures and fabrics. This is unlikely, as the marine banded facies is spatially confined to the frontal zone, and not developed in cores XXI and VI, where surface morphology and foliation show that the deformation is quite active. Also, discs or plates are seen to accrete in the water column below the sea ice cover and thin sections of these half frozen bottom deposits are identical to the banded facies observed at the base of the solid level sea ice cover above, where no evidence of deformation was found.
- (b) *Expression of a spatially changing environment* for the granular frazil ice crystals formed in the DTC, as the geometry of the base of the ice shelf switches from highly irregular (with transverse inverted depressions between individual flows close to the grounding line or around pinning points) towards a smoother interface closer to the front. In the first case, rapid lateral ascension of frazil crystals along steep slopes would favor the production of



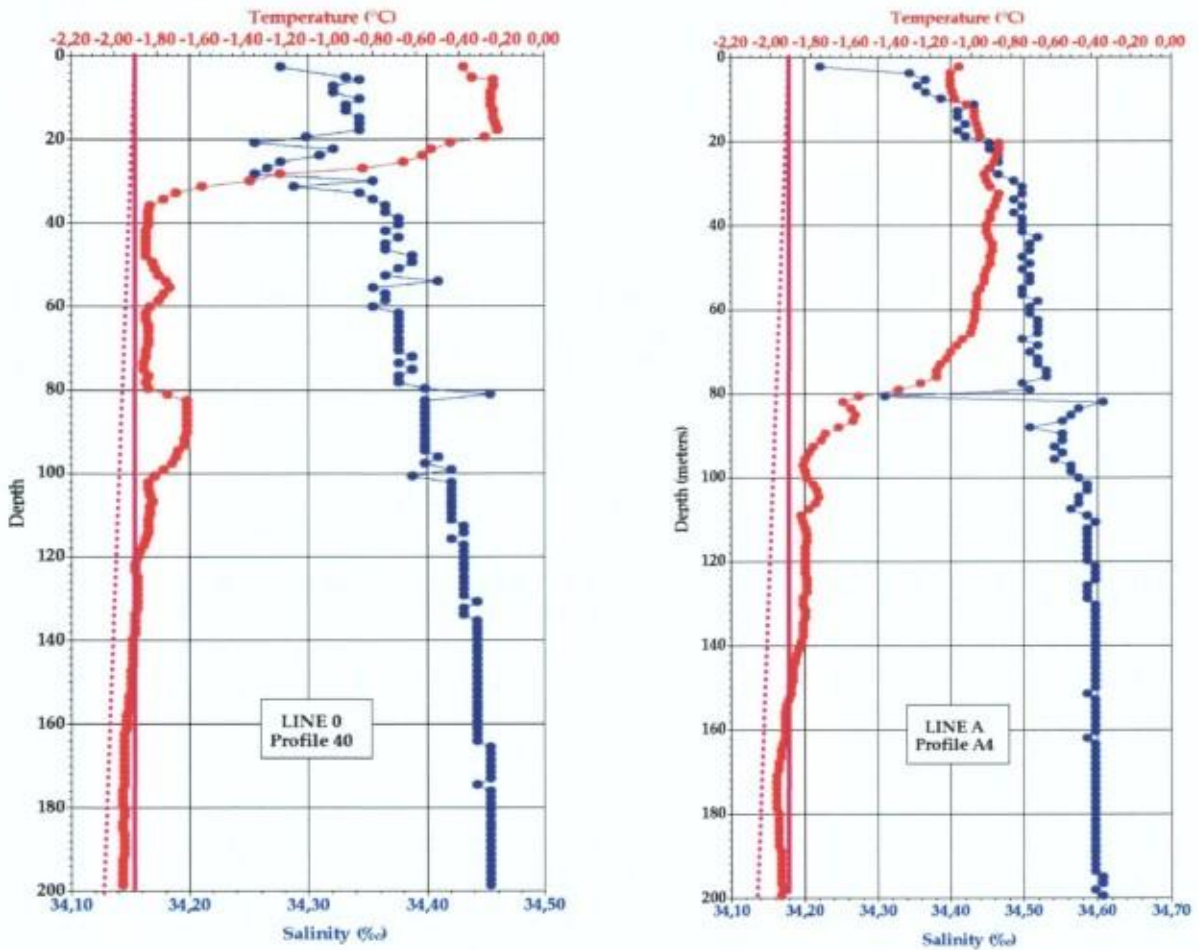
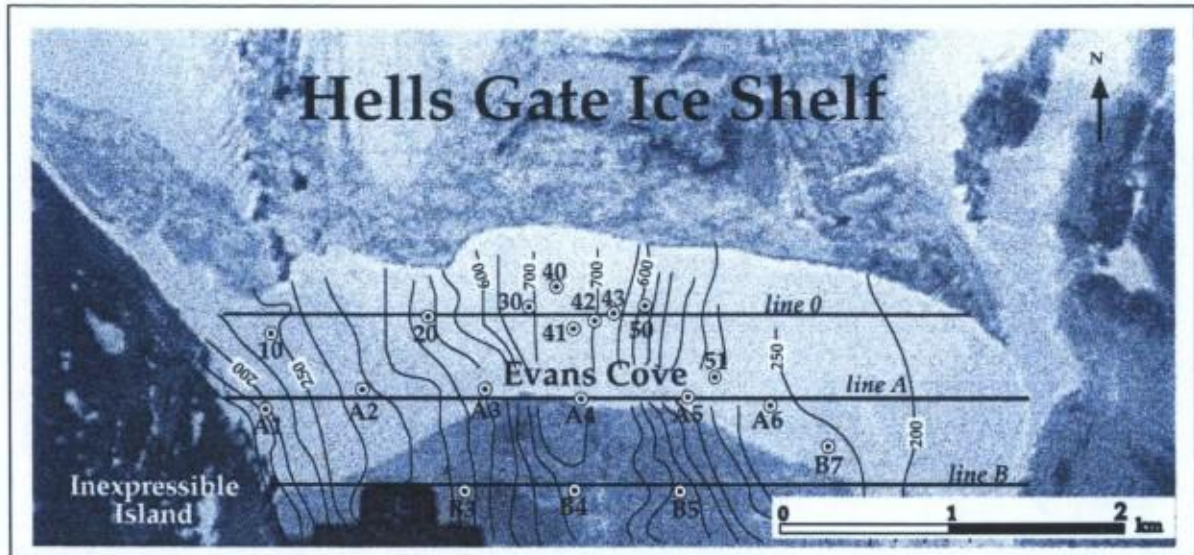


Figure 56: Results from preliminary CTD casts in front of Hells Gate Ice Shelf with location map. Also shown is the bathymetry in meters. Exemplative temperature and salinity profiles for Station 40 (close to the central part of the ice shelf front) and Station A4 (further seaward) are plotted together with the surface (solid line) and "in situ" (dotted line) calculated freezing point temperature lines.

small crystals accreting in a random fashion at the base of the ice shelf. In the latter case, slower ascension further away from the initial production site would favor slower growth of larger crystals, accreting in an orderly fashion at the bottom of the ice shelf. The lower



growth rates would result in higher isotopic values because of the higher fractionation efficiency. However, granular marine ice is observed up to several hundred meters downstream of the surface contact line between meteoric ice and marine ice (Figure 39). Moreover, if this hypothesis is correct, only the banded facies should be found in the first-year landfast sea ice in front of the ice shelf. Finally, Budillon and Spezie (2000), although they do not preclude functioning of the polynya during the summer with a small rate of surface wind- and wave-induced frazil ice production, reckon that owing to this modest rate and the absence of the preconditioning phase due to summer vertical stratification, it is not reasonable to suppose a HSSW formation in the strict sense for this period, which therefore remains a typical winter process. For those reasons, we favour the next hypothesis.

- (c) *Expression of a temporally changing environment.* The seasonal character of the banded facies accretion (summer only) suggests that it is linked to seasonal processes in the water column in front of or below the ice shelf. We have seen that the lower salinity and enhanced chemical fractionation in the granular marine ice consolidating closer to the ice shelf front (top of core IV, Figures 43 and 44) suggest tidal forcing of warm surface waters below HGIS during the summer (Figure 55-5). These waters would favor partial melting of the loose granular frazil and produce a water mass at local pressure melting point showing lower salinities and higher isotopic signatures. This water mass, perhaps mixed with water carrying DTC-granular frazil, would eventually exit at the front. The marine and sea ice banded facies, then represent either transformed granular frazil ice crystals initially formed in the DTC, or new crystals formed by adiabatic supercooling, or both.

Figure 56 shows preliminary results from CTD casts in front of Hells Gate Ice Shelf along its centreline (Tison et al., 1997b). Station 40 is located close to the ice front, whilst Station A4 is further seaward in Evans Cove. Both profiles show (1) a warmer and fresher surface sea water layer of thickness varying from 20 to 80 meters, (2) the top of the Deep Ice Shelf Water (below surface freezing point) layer between 120 and 140 meters and (3) alternation of two colder (close to surface freezing point) and two warmer (although less than the surface water) layers that we believe are reflecting the ice-ocean interactions of mode 3 (Figures 10 and 55-5). These results clearly come in support to the existence of both a Deep and a Shallow Thermohaline Circulation associated respectively with ocean circulation mode-1 and mode-3 at HGIS, as hypothesized from the ice studies.

### 3.4. A peculiar property of marine ice: its very low salinity as compared to sea ice

The occurrence of marine ice bodies in such a wide range of locations, most of it corresponding to weak points of ice shelves, suggests it might play a significant mechanical role, as a welding agent, contributing to ice shelf stability. The bulk salinity of marine ice (as low as 0.03‰) is an important factor in this regard, since it is known to considerably affect the rheological properties of the ice (e.g. Hooke et al., 1988; Thorsteinsson et al., 1999). It is indeed an order of magnitude higher than that of meteoric ice, but 2 orders of magnitude lower than those observed in granular sea ice (a few ‰) which, with the exception of snow ice, also results from frazil ice formation and consolidation in sea water. The reasons for such a stark contrast in bulk salinity between marine ice and granular sea ice are still a subject of debate in the literature. Eicken et al. (1994) have clearly demonstrated that none of the postgenetic desalination processes, summarized by Weeks and Ackley (1986) for sea ice, is strong or fast enough to explain the relative purity of marine ice. The anomalous low salinity in the marine ice can thus only be explained by the low initial salinity of newly consolidated ice layers.

Eicken et al. (1994), while noting the decreasing salinity with depth in the B13 core, exclude consolidation under the advancement of a freezing front as an explanation for the salinity profile and general salinity level arguing that conductive heat fluxes are too low in the central Ronne Ice Shelf and that an "anomalously" low salt distribution coefficient would be needed at the interface to explain the observed salinities. These authors suggested that consolidation under the deviatoric buoyancy stress



associated with the ten of meters of crystals accumulating beneath would lead to densification and expulsion of brine through fragmentation and settling of individual platelet crystals.

To test the plausibility of these alternative processes, we (Tison et al., 2001) have developed a simple model to attempt the reconstruction of the  $\delta^{18}\text{O}$ /salinity relationship observed at NIS1 and in other deep marine ice cores (Figure 57). Predicting the salinity and isotopic composition of marine ice as defined here is complicated by the fact that these properties reflect the contribution of two main processes (Figure 58):

- (a) The first process, which we refer to as the “frazil ice phase”, consists of the formation of individual frazil ice crystals in the oceanic sub-ice shelf cavity, as a result of supercooling. The “parent” water of these crystals (ice shelf water – ISW) is a mixture of High Salinity Shelf Water (HSSW) with glacial meltwater from the base of the ice shelf. As they are transported in the density-driven rising ISW plume, the crystals float upward due to their buoyancy and accumulate at the base of the ice shelf further downstream.
- (b) The second process, to which we refer to as the “consolidation phase”, is less well understood. As crystals rise under buoyancy and accumulate, they are surrounded by a water body that we call the “host” water. The proportion of water volume to the total volume of the ice/water mixture (“porosity”) varies depending on the local conditions. The porosity of loose frazil ice mixtures derived from laboratory experiments and field measurements, both for

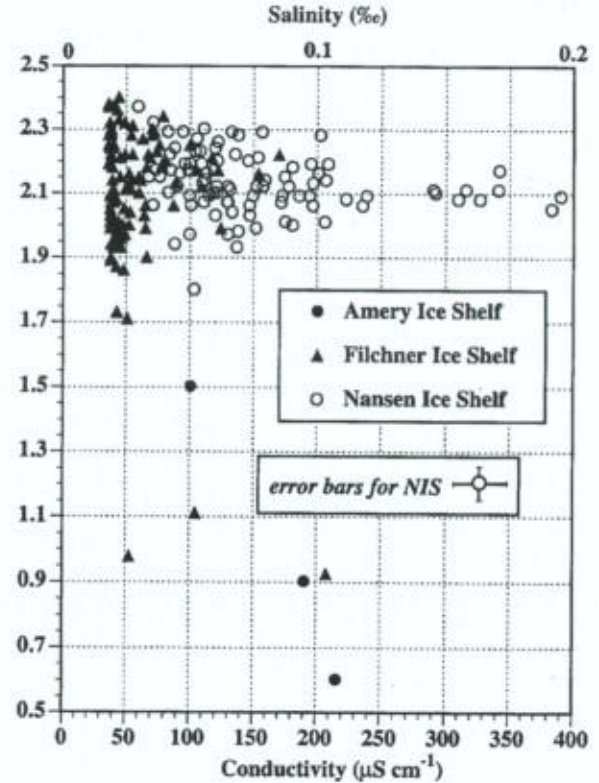


Figure 57: The  $\delta^{18}\text{O}$  relationship for 99 samples in the NIS1 45-m ice core from the Nansen Ice Shelf (dotted circles). Also plotted are the marine ice data from the B13 core (solid triangles, Filchner Ice Shelf, courtesy of H. Oerter and W. Graff, Alfred Wegener Institute) and the G1 core (black circles, Amery Ice Shelf, y 12 mon of V. Morgan, Australian Antarctic Division)

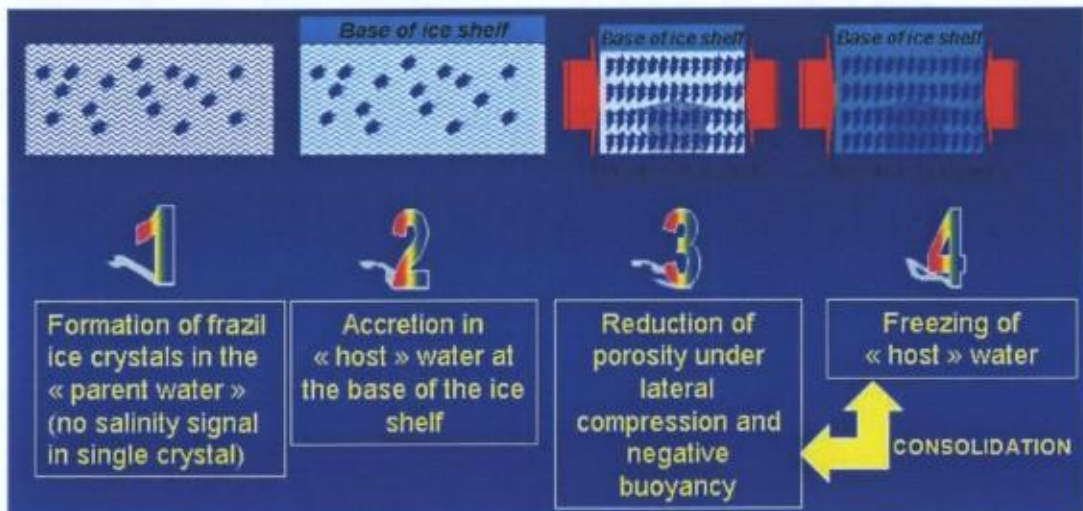


Figure 58: Marine ice...the “Making of”



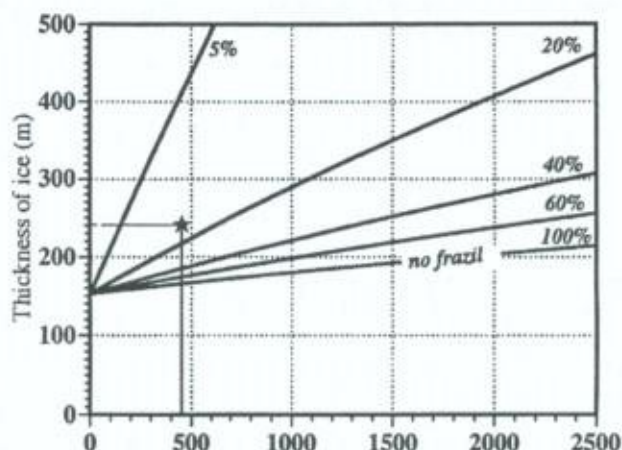


Figure 59: Cumulated consolidated ice thickness for various constant porosity values as a function of time in the case of the B13 ice core (Filchner Ice Shelf), calculated using a simple heat conduction model. Initial thickness is 153 m of meteoric ice, as observed at B13. Total ice thickness at B13 and estimated travel time from initiation of marine ice accretion to the B13 site (Oerter et al., 1992) are plotted as a star (see text).

freshwater ice and sea ice, ranges between 40% and 67% (Andersson and Daly, 1992; Daly, 1984; White, 1991). However, as suggested by Eicken et al. (1994), the deviatoric buoyancy stress exerted by the accumulation of tens of meters of loose frazil ice crystals could greatly increase the packing density. Similarly, the lateral compressive stresses induced by the converging flow of individual ice streams as they merge to form the ice shelf (or “reconstitute” it, around pinning points), as was observed at Hells Gate Ice Shelf (Tison et al., 1997a, 1998) and Nansen Ice Shelf (Khazendar et al., 2001), can also quite significantly reduce the porosity of the marine ice that has already accumulated. Obviously, for accumulated ice crystals to be “squeezed” by lateral compression, its mechanical behavior should have developed solid-like characteristics so it is no longer merely an aggregate of loose crystals in suspension. Experiments by Martin and Kauffman (1981) demonstrate that this is indeed already the case for slush of 30 to 40% ice concentrations. This packing process will contribute to the reduction of the bulk salinity (host water being

expelled from the mixture) and is a first step in the consolidation process.

Two major mechanisms could then be invoked to explain further consolidation of the marine ice body: (1) heat conduction across the ice shelf leading to the freezing of the interstitial water (either in a process of coarsening and joining of existing grains, or by the nucleation of new grains) and (2) local melt-regelation processes at contact points between grains in the compacting aggregate. The first mechanism has the potential to further reduce the impurity content of the ice by salt rejection and its subsequent diffusion toward the bulk sea water reservoir. The second mechanism will eventually alter the small-scale chemical properties of marine ice. Figure 59 shows the cumulated consolidated ice thickness for various constant porosity values as a function of time in the case of the B13 ice core (Filchner Ice Shelf). Consolidated ice thickness is calculated using a simple heat conduction model, based on the assumption that the heat conducted through the ice results solely in the freezing of the interstitial water. Plotting the total ice thickness at B13 (239 m - Oerter et al. 1992) versus the estimated travel time from initiation of marine ice accretion to B13 (450 years - Oerter et al., 1992) shows that consolidation through heat conduction is a plausible process (with a mean constant porosity slightly lower than 20%).

The discussion above shows a level of complexity difficult to simulate in the present state of knowledge. However, considerable insight can be gained into the processes at work by using a simplified approach where the final  $\delta^{18}\text{O}$ -salinity signal is modeled by combining the following two steps: (1) the formation of individual frazil crystals in the parent water and, (2) the freezing of interstitial host water (Figure 60). It is reasonable to assume, in the case of marine ice or granular sea ice, that the salinity of single ice crystals is negligible (see, e.g. Eicken, 1998; Tison et al., 1993). The isotopic signal of single frazil crystals (*frazil ice phase*), the isotopic and salinity signal of

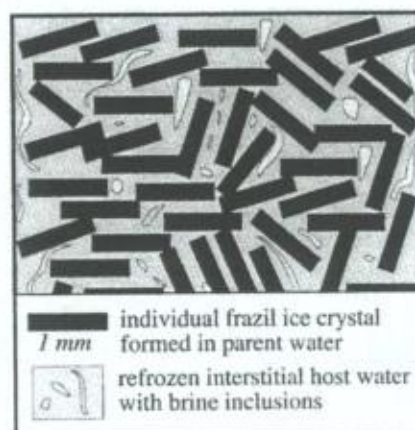


Figure 60: Sketch illustrating the model concept (see text for details)



the “frozen” host water (*consolidation phase*) are obtained using a “boundary layer” model approach (Tison et al., 1998):

As freezing progresses in a water reservoir, physico-chemical changes occur at the ice-water interface, which result in a differentiation of the chemical signals between ice and water. Depending on whether the chemical species under consideration is retained within microscopic inclusions in the host phase (e.g., sea-salt ions) or occurs as a true solid solution (e.g., water isotopes in ice) the differentiation process is called “segregation” or “fractionation”, respectively. The proportion of heavy isotopes (or salts) incorporated from the liquid into the solid at the interface is constant for a given temperature. For the stable isotopes it is described by the equilibrium fractionation factor:

$$\alpha_{eq} = \frac{R_s}{R_l}, \quad (3)$$

where  $R_s$  and  $R_l$  are the isotopic ratios  $^{18}\text{O}/^{16}\text{O}$  (or D/H) in the solid and liquid phases at the interface, under thermodynamic equilibrium conditions

For salinity, one similarly uses the equilibrium segregation factor:

$$k_{eq} = \frac{C_s}{C_l}, \quad (4)$$

where  $C_s$  and  $C_l$  are the impurity concentration in the solid and the liquid, respectively, at the interface.

As a result of this process, concentration on the liquid side of the interface differs from that of the bulk of the reservoir. Species transport therefore occurs, through molecular diffusion, convecto-diffusive fluxes and turbulent mixing in the melt. These processes are commonly integrated into a “boundary layer” concept (Figure 61), such that the concentration in the liquid takes on the reservoir value (in the case of a semi-infinite reservoir, e.g., for sea water) at a finite distance  $z_{bl}$  from the interface. Within this boundary layer, transport occurs by diffusion processes only. Depending on the freezing rate, the gradient in the boundary layer will vary and therefore so will the concentration in the liquid at the interface. As a result,  $\alpha_{eff}$ , the effective (apparent) fractionation factor (or  $k_{eff}$ , the effective segregation factor) will differ from the equilibrium fractionation factor  $\alpha_{eq}$  ( $k_{eq}$ ) that would be observed either in the case of near-zero growth rate or during forced convection ( $z_{bl}=0$ ).

For a given freezing rate, in the case of a semi-infinite reservoir, after a short “initial transient” the concentration in the ice remains constant since a steady state regime arises, where the flux of a given species into the ice is exactly compensated by the one at the base of the boundary layer. The effective fractionation factor for that steady state is given by Burton et al. (1953):

$$\alpha_{eff} = \frac{\alpha_{eq}}{\alpha_{eq} - (\alpha_{eq} - 1) e^{-\frac{z_{bl}v}{D}}}, \quad (5)$$

where  $v$  is the growth rate and  $D$  is the diffusion coefficient. A similar relationship is valid for the effective segregation factor, with  $k_{eff}$  and  $k_{eq}$  instead of  $\alpha_{eff}$  and  $\alpha_{eq}$  in (5). The initial transient marks the

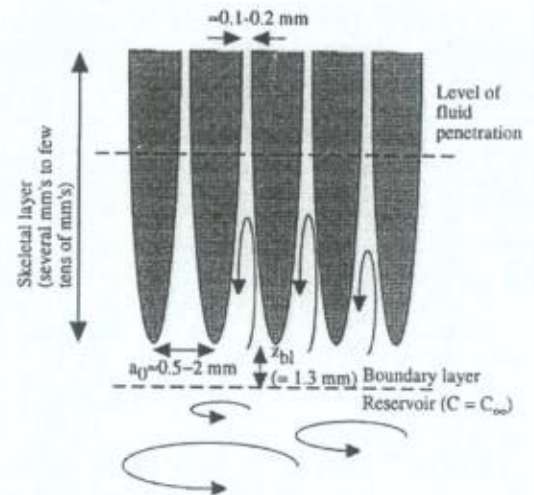


Figure 61: sketch illustrating the boundary layer concept in the case of columnar sea ice (Eicken, 1998)



transition from the equilibrium fractionation recorded in the initial ice increment toward the steady state value. It clearly must not be neglected in the case of growing individual frazil ice discs that are typically of the size of the order of a millimetre (Tison et al., 1998).

Souchez et al. (1987, 1988) used a box diffusion model to apply the boundary layer concept to isotopic fractionation in sea ice. In their approach the simulation of the stable-isotope distribution in the ice was performed in two steps: (1) freezing of an ice thickness during a time increment depending on the freezing rate, with associated fractionation, and (2) diffusion in the boundary layer and homogenization in the bulk of the reservoir during the appropriate time lapse. In nature, freezing and diffusion are simultaneous. Using an axis moving with the ice front, both processes can be described by the same partial differential equation:

$$\frac{\partial c}{\partial t} = D \frac{\partial^2 c}{\partial x^2} + V \frac{\partial c}{\partial x}, \quad (6)$$

(where  $c$  is the concentration,  $x$  is the space coordinate measured normal to the ice/water interface and  $V$  is the velocity of the ice front) applying the appropriate boundary conditions and using the equilibrium fractionation (3) or segregation (4) coefficients to calculate the concentrations on both sides of the interface. The model used by Tison et al. (1998) solves (6) numerically using the Crank-Nicolson method. At each time step, the solution of the resulting set of linear equations is obtained by Gaussian elimination using a simple algorithm for tridiagonal systems. These adjustments reduce the execution time considerably and improve the precision of the results.

Once the chemical signature of both the single frazil ice crystals and the frozen host water are known, the resulting mixed signal to be compared to observations is obtained as follows:

$$\text{Modelled signal} = \{[\text{signal of single frazil crystal} \times (1 - \text{porosity})] + [\text{signal of frozen host water} \times (\text{porosity})]\} \quad (7)$$

Different combinations of porosity and freezing rates could occur in nature. For example, a high freezing rate would be associated with high porosity at the top of the water column in an open rift where sufficient frazil discs had yet to accumulate and produce significant compaction. Lower in the water column, where accumulation is perhaps progressing faster than freezing, high compaction would produce a low-porosity slush subjected to a very slow freezing rate due to the insulating effect of overlying ice. The lateral stresses associated with converging ice streams or a closing rift would produce a situation where low porosity is combined with a large range of freezing rates depending on depth. We have taken this variety into account in our simulations by considering each porosity level for a range of plausible freezing rates.

Figure 62 summarizes the most interesting simulation results from Tison et al. (2001). Simulations parameters are indicated on top of each graph. A typical Ross Sea ISW  $\delta^{18}\text{O}$  value of  $-0.61\text{‰}$  (Jacobs et al., 1985) has been used both for the parent water and the host water in these examples. The following important conclusions can be drawn:

- (a) Initial transient characteristics have to be considered while estimating the  $\delta^{18}\text{O}$  signature of the small individual crystals forming in the "frazil ice phase." For a realistic range of growth rates, the  $\delta^{18}\text{O}$  signature of these frazil ice crystals ( $\delta^{18}\text{O}_{\text{frazil}}$  in Figure 62) will indeed be higher compared to parent water when the initial transient is considered,
- (b) Applying a boundary layer model concept to the "consolidation phase," with the parameter values used for sea ice or columnar/congelation marine ice (Figure 62 a), cannot explain the observed  $\delta^{18}\text{O}$ /salinity relationship, even for porosity close to the permeability limit (5% [Cox and Weeks, 1975; Golden et al., 1998; Weeks and Ackley, 1986]),



- (c) In the framework of the boundary layer concept used as an approximation for the consolidation process, the simulations compare well with the measured properties only when using a segregation factor value of  $k^*_{eq} = 0.005$  (Figure 62b). This value is an order of magnitude lower than the lowest observed value in columnar ice growing from sea water at equivalent depth. It reflects the fact that the actual process of consolidation does not allow the development of intracrystalline substructures, impurities being confined to intercrystalline location after saturation of the crystal lattice. Figure 63 proposes a schematic depiction of how processes that combine melting under compaction and refreezing under heat conduction might work. Starting at a stage where the aggregate of loose crystals begins to develop solid-like characteristics (approximately 30–40% porosity, see above) under lateral compression and deviatoric buoyancy stress, neighboring grains (solid line) will partially melt at contact points and feed fresh meltwater into the interstitial host water. This will (1) reduce the porosity (dotted lines) and (2) lower the salinity and enrich the  $\delta^{18}\text{O}$  of the interstitial water. Subsequent freezing of the host water under heat conduction will enrich the ice phase in  $\delta^{18}\text{O}$ , impoverish the remaining liquid in  $\delta^{18}\text{O}$ , increase its salinity and drive salt and isotopic diffusion through the interconnected interstitial water network. The process is likely to continue until the 5% porosity threshold is reached and closed system freezing occurs. The resulting texture is in accordance with that observed, lacking the intracrystalline cellular inclusions, and salt impurities remain located at grain boundaries once the ice lattice is saturated,
- (d) Since no intracrystalline substructure is developed in marine ice, one might wonder if different boundary layer thickness still apply to salinity and  $\delta^{18}\text{O}$ . Figure 62c is identical to Figure 62b, with the exception that the  $z_{blNa}$  and  $z_{bl\delta^{18}\text{O}}$  values are both set to 2.9 mm. Results from the model now better cover the range of the observed  $\delta^{18}\text{O}$  values, taking error bars into account. A major uncertainty nevertheless persists in the actual value of  $z_{bl}$ . However, Tison et al. (1998, simulation not included here) show that changing the value of  $z_{bl}$  to 1 mm

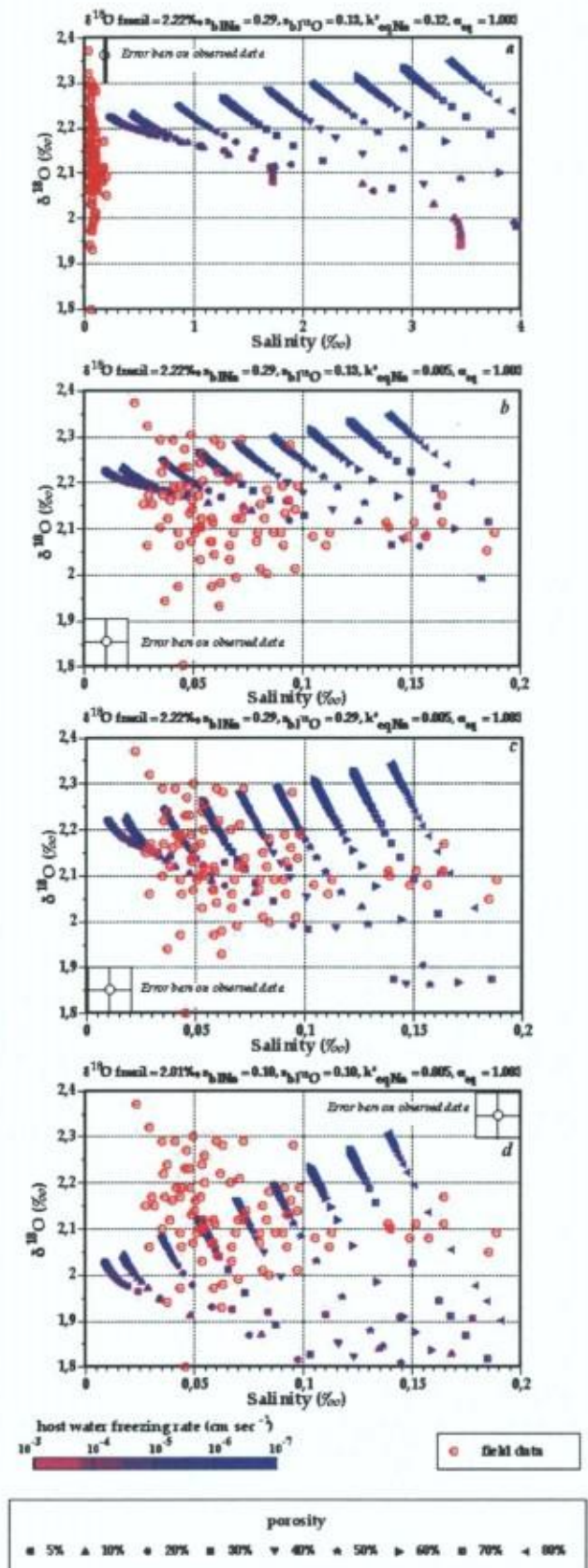


Figure 62: Representative results of  $\delta^{18}\text{O}$ /Salinity relationship simulations with Tison et al. (2001) model, as compared to observed values at NIS1. Parameters for each set of simulations are described at the top of each graph (see text).



does not alter the location of the simulation curves in the graph. The only change is that lower salinity and higher  $\delta^{18}\text{O}$  values are obtained for the same freezing rates and porosity,

- (e) It is obviously unrealistic to cover the isotope/salinity signal of all the observed data points in a single simulation with decreasing growth rate and a constant set of parameters. Porosity and water characteristics are also susceptible to change in the course of the process. For example, the small group of samples with the highest salinity could have resulted from a consolidation process at low porosity and relatively high freezing rates as a result of closure under high lateral compressive stresses, occurring relatively close to the surface. Choosing boundary layers of equivalent size (Figure 62c) and/or changing the isotopic signal of the individual frazil ice crystals (in accordance with the growth rates range in the water column, Figure 62d) would account for the extremes in the  $\delta^{18}\text{O}$  distribution in the consolidated marine ice.

However, closed system refreezing in the pores at low freezing rates and low porosity (i.e. in the low salinity range), in a process such as the one sketched in Figure 63, would also increase the small-scale isotopic variability, allowing both enrichment of the first refrozen layers and entrapment of depleted residual waters, as observed for our data points in Figures 57 and 62,

- (f) Although spanning a different range of salinity, because of their different depth location, the NIS and B13 cores show nearly identical  $\delta^{18}\text{O}$  ranges and a similar trend to increased  $\delta^{18}\text{O}$  variability at low salinity (Figure 57). This suggests that the same processes are controlling the isotope/salinity signature of the marine ice at both locations. As a first approximation, we might consider that the  $\delta^{18}\text{O}$  signature is mainly controlled by the one of the individual frazil ice crystals. Dispersion occurs through dissociation of the host water freezing products at lower freezing rates and porosity. Salinity is mainly controlled by the freezing rate (and thus the freezing depth) of the host water and by the porosity reduction in the consolidating medium.

Obviously, the model described here is only a crude description of the real world situation. Processes such as coarsening and sintering of discs, which are known to occur in bodies of consolidating frazil (e.g., Martin and Kauffman, 1981), are not explicitly included. However, sensitivity tests have allowed us to define several important variable settings, different from those used in sea ice growth models, that will have to be considered in future more sophisticated models for marine ice formation.

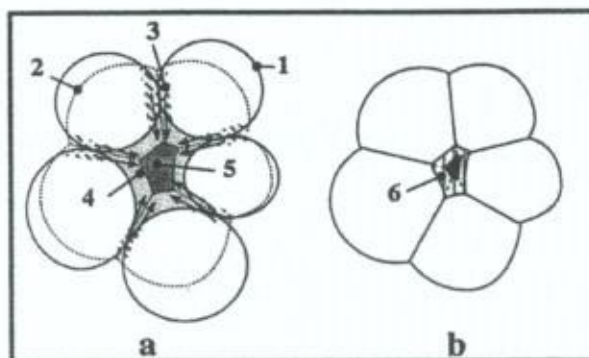


Figure 63: Simplified sketch illustrating (a) the assumed process of porosity reduction in a compressed frazil ice crystals aggregate, and (b) the further consolidation by freezing of the diluted interstitial water. The latter process will result in salt diffusion towards the bulk of the reservoir as long as the porosity threshold (5%) is not attained. The whole process prevents the development of intra-crystalline sub-structures. Numeral refer to 1, crystal before compaction; 2, crystal after compaction; 3, meltwater from pressure-melting; 4, interstitial water space before compaction; 5, interstitial water space after compaction; 6, refrozen interstitial meltwater.



**Paper 4**

**Stratigraphy, Stable Isotopes and Salinity in Multi-year Sea Ice from the Rift Area,  
South George VI Ice Shelf, Antarctic Peninsula**

**Authors**

**J.-L. Tison, E.M. Morris, R. Souchez, J. Jouzel**

**Journal**

**Journal of Glaciology, Vol. 37, n° 127**

**Year**

**1991**



*Journal of Glaciology*, Vol. 37, No. 127, 1991

## Stratigraphy, stable isotopes and salinity in multi-year sea ice from the rift area, south George VI Ice Shelf, Antarctic Peninsula

J.-L. TISON,

*Faculté des Sciences — C.P. 160, Université Libre de Bruxelles,  
50 avenue Franklin Roosevelt, B-1050 Bruxelles, Belgium*

E. M. MORRIS,

*British Antarctic Survey, Natural Environment Research Council, Cambridge CB3 0ET, England*

R. SOUCHEZ,

*Faculté des Sciences — C.P. 160, Université Libre de Bruxelles,  
50 avenue Franklin Roosevelt, B-1050 Bruxelles, Belgium*

J. JOUZEL

*Laboratoire de Géochimie Isotopique LODYC/DPC, Centre d'Etudes Nucléaires de Saclay,  
F-91191 Gif-sur-Yvette, France*

**ABSTRACT.** Results from a detailed profile in a 5.54 m multi-year sea-ice core from the rift area in the southern part of George VI Ice Shelf are presented. Stratigraphy, stable isotopes and Na content are used to investigate the growth processes of the ice cover and to relate them to melting processes at the bottom of the ice shelf.

The thickest multi-year sea ice in the sampling area appears to be second-year sea ice that has survived one melt season. Combined salinity/stable-isotope analyses show large-scale sympathetic fluctuations that can be related to the origin of the parent water. Winter accretion represents half of the core length and mainly consists of frazil ice of normal sea-water origin. However, five major dilution events of sea water, with fresh-water input from the melting base of the ice shelf reaching 20% on two occasions, punctuate this winter accretion. Two of them correspond to platelet-ice production, which is often related to the freezing of ascending supercooled water from the bottom of the ice shelf.

Brackish ice occurs between 450 and 530 cm in the core. It is demonstrated that this results from the freezing of brackish water (Jeffries and others, 1989) formed by mixing of normal sea water with melted basal shelf ice, with dilution percentages of maximum 80% fresh water.

## INTRODUCTION

Stratigraphy and salinity profiles in multi-year sea ice have been measured by several authors in the last decade, both in the Arctic (mainly the northern Ellesmere Island area, Fram Strait and the Beaufort Sea; Schwarzacher, 1959; Cherepanov, 1966; Weeks and Ackley, 1986; Gow and others, 1987b; Meese, 1989) and the Antarctic (mainly in the McMurdo Sound area and in the Weddell Sea; Weeks and Ackley, 1986; Gow and others, 1987a; Lange and others, 1989). However, these studies were mainly focused on drifting pack ice, the properties and

formation mechanisms of which are often quite different from land-fast sea ice.

Combined salinity/stable-isotope analyses are less extensive in the literature but have also been undertaken in both polar regions. One major advantage of the method is that it allows the discrimination of different parent-water sources for the ice growth, as has been clearly demonstrated by previous authors (Friedman and others, 1961; Lyons and others, 1971; Gow and Epstein, 1972). Recently, a study by Jeffries and others (1989) has provided the first attempt to use the stable-isotope ratio  $^{18}\text{O}/^{16}\text{O}$  as a tracer to detect fresh, brackish and sea-



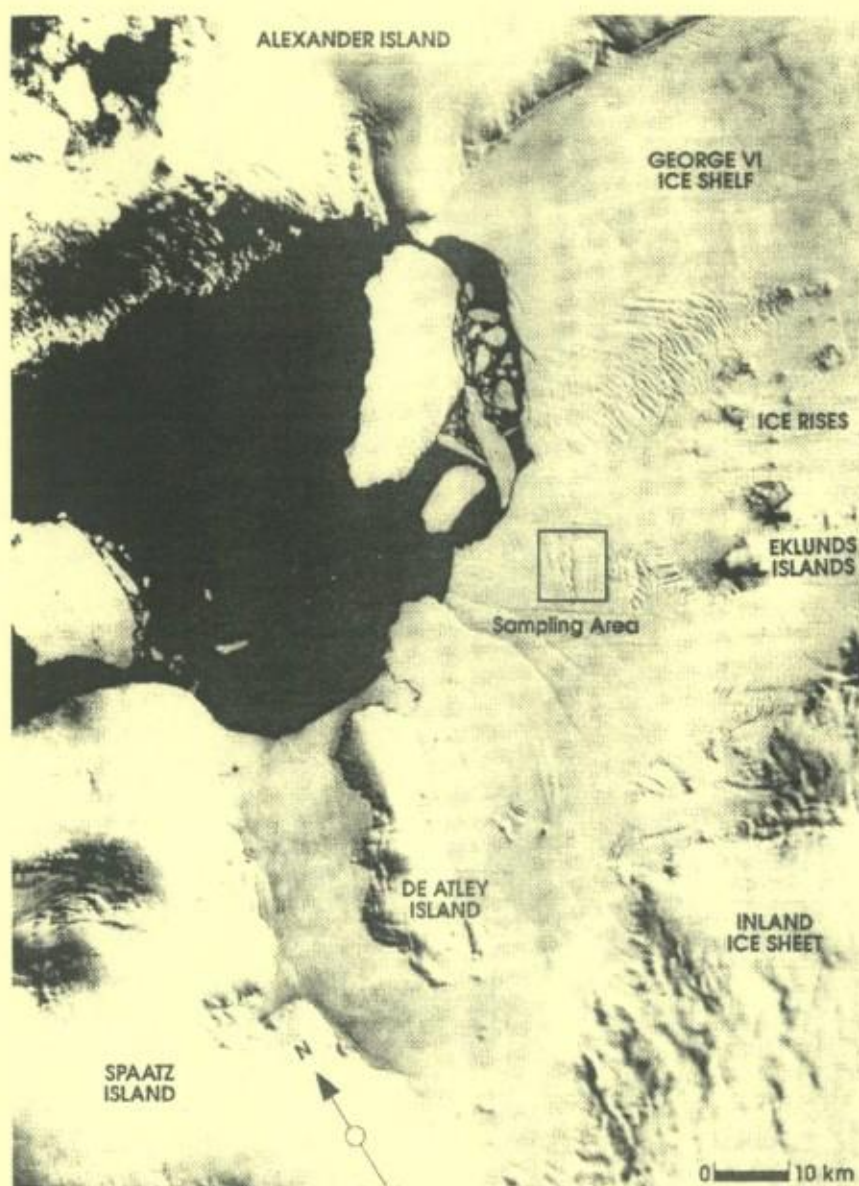


Fig. 1. Landsat image of southern George VI Ice Shelf (9 January 1973).

water origins in multi-year land-fast sea ice from the Arctic (north Ellesmere Island, Canadian Arctic). Brackish ice was found there in significant amounts.

This paper gives the results of a detailed textural, isotopic and chemical analysis performed on multi-year land-fast sea ice from the Antarctic Peninsula. The properties of the ice samples from the large rifts affecting the southern part of George VI Ice Shelf are related to the melting processes at the surface and at the bottom of the ice shelf.

#### SAMPLING SITE AND ANALYTICAL PROCEDURE

Ten sea-ice cores and two surface ice-shelf cores were retrieved from the major rift closest to the southern active border of George VI Ice Shelf (Fig. 1) as part of a joint

Belgian/British project in the 1987–88 British Antarctic Survey field programme.

Two major sets of large surface waves affect the George VI Ice Shelf surface where it thins in the southwestern part and where the main outlet flow of the ice shelf from the northeast meets the local southeasterly flow from the Plateau. One of these wave sets happens to be roughly parallel to the actively calving ice-shelf edge and so the troughs are preferred sites for the opening of major rifts where sea water reaches the surface. During the summer, open-water areas are located where troughs from each wave system meet. The remaining bottom surface of the rift is covered with sea ice of variable thickness (1–5.5 m). Away from the transverse depression, the rift borders turn into sharp cliffs about 20 m high. First-year sea ice started to cover the open water close to the sampling site at the end of February 1988.



Tison and others: Stratigraphy, etc., in rift area of George VI Ice Shelf

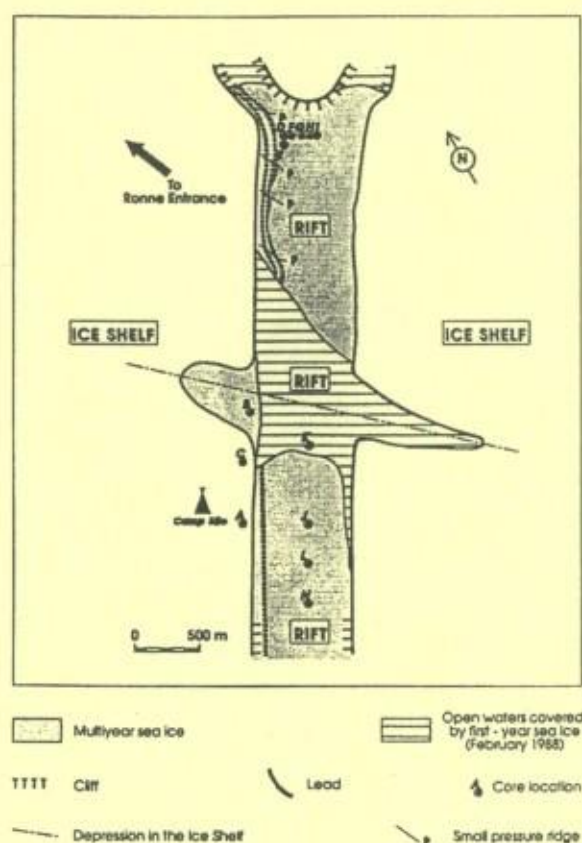


Fig. 2. Sketch showing the location of the cores in the sampling area.

Two different sets of sea-ice cores were retrieved in the sampling area (Fig. 2). One set was collected along a longitudinal profile south of the open water where the sea-ice thicknesses varied from 0.97 to 2.57 m (cores J to N) and the other set along a transverse profile a few kilometres to the north, where ice thicknesses fluctuated between 3.49 and 5.54 m (cores F to I). In addition, one core was sampled in the multi-year sea ice from the transverse depression (B) and another in the freshly formed first-year sea ice (K). Finally, the surface ice shelf was sampled in two different locations (cores A and C). As the main focus was to study multi-year sea ice, the thickest core (H) has been selected for detailed analyses.

The cores were sampled with a PICO drill, transferred to plastic bags and stored below  $-20^{\circ}\text{C}$  in a small "sledge-fitting" freezer until transport by aircraft to Rothera base. At Rothera and aboard RRS Bransfield on the journey to the U.K., the cores were again stored in freezers at  $-20^{\circ}\text{C}$ . The following analytical techniques were performed in the cold laboratory ( $-25^{\circ}\text{C}$ ) in Brussels:

**Ice texture:** vertical thin sections were taken along the whole profile to estimate the proportion of the different sea-ice crystal types and to guide the isotopic sampling.

**Sodium profile:** for each individual part of the core, the entire outside part of the cylindrical core sample was

trimmed off with a band saw to avoid contamination which may have occurred during sampling in the field and during transport. A 1 cm thick vertical slice was then cut through samples of 0.5 cm width using standard methods to reduce contamination to the noise level of the Perkin-Elmer atomic absorption spectrophotometry. A total of 1120 samples, regularly spaced throughout the core, have been measured for their Na content. Sodium will be used here as a "proxy" for the global salinity, bearing in mind that the ratio Na/global salinity is 0.3074 in the oceans and is independent of the salinity level for a large range of salinities (Riley and Skirrow, 1965), and that the same ratio is valid for sea ice as indicated by the dilution curves and statistical analyses performed by Meese (1989) on sea-ice samples from the Beaufort Sea.

**Isotopic profiles:** a second 1 cm thick vertical slice of each individual part of the core was sampled in selected spots for co-isotopic analysis of deuterium and oxygen-18 (120 samples). The small amounts of ice necessary for the mass-spectrometer measurements (0.3 ml) were collected using a microtome, allowing precise location of the samples and detailed profiling where required. The mass-spectrometer analyses were performed at the Laboratoire de Géochimie Isotopique, Centre d'Etudes Nucléaires de Saclay, France.

HDO concentrations will be given hereafter in  $\delta$  units calculated with respect to VSMOW (Vienna Standard Mean Ocean Water) expressed in parts per thousand (ppt), e.g.

$$\delta D = 1000 \left[ \frac{R_{D \text{ sample}} - R_{D \text{ VSMOW}}}{R_{D \text{ VSMOW}}} \right]$$

where  $R_{D \text{ sample}}$  and  $R_{D \text{ VSMOW}}$  are the isotopic ratios of the sample and of the VSMOW, respectively. The accuracy of the measurements is  $\pm 0.5\text{‰}$  in  $\delta D$  and  $\pm 1.0\text{‰}$  in  $\delta^{18}\text{O}$ .

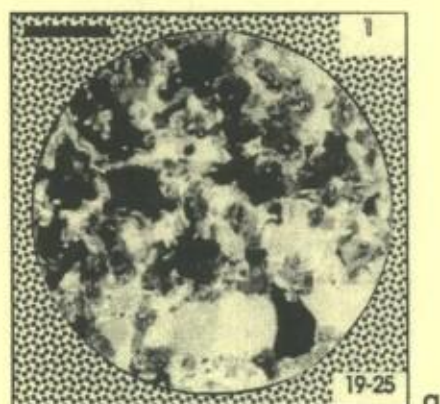
## RESULTS AND DISCUSSION

### General features of the core

Figures 3 and 4 summarize the textural, isotopic and chemical characteristics of the core. An example of the different types of ice observed in the core, together with a brief description of their characteristics is shown in Figure 3. Figure 4 presents the combined sodium/ $\delta^{18}\text{O}$  profile with depth. The symbols used for the different types of ice in this figure are defined in Figure 3. Na values have been smoothed with a running mean on 11 values to dampen high-frequency fluctuations and obtain a resolution similar to that of the  $\delta^{18}\text{O}$  values. Two major observations can be made:

- The core consists mainly of granular ice, which is essentially frazil ice, as will be discussed below. If we discard 100 cm of porous granular ice at the top, which is certainly, as will be shown later, not the result of water freezing, granular ice occurs in 74% of the core, columnar ice in 19.4% and needle-like ice (platelet ice as described by Lange and others (1989)) in 6.6%.

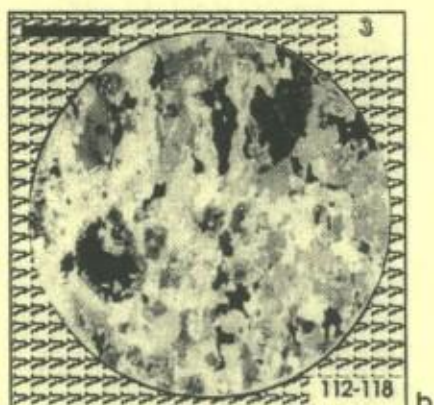




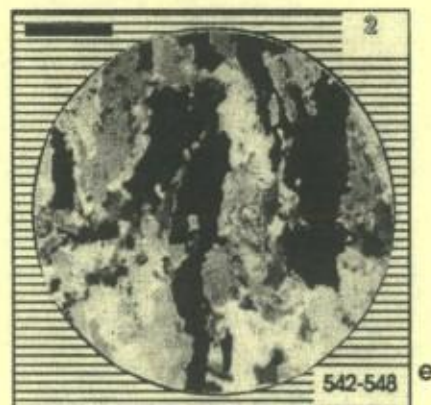
**Texture** : equigranular and porous  
**Crystals** : polygonal with sharp contours  
**Elongation** : none



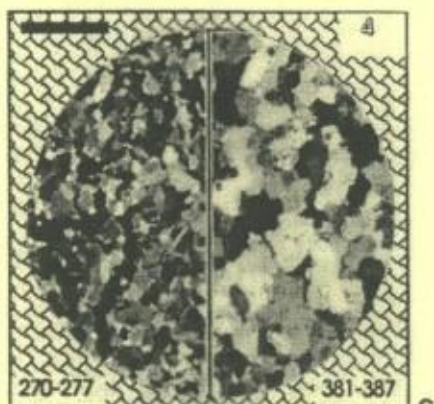
**Texture** : contact between platelets  
 and an equigranular matrix  
**Crystals** : needle-like  
**Elongation** : oblique



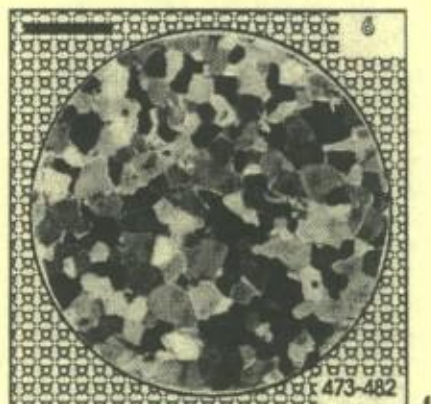
**Texture** : columnar  
**Crystals** : small elongated with smooth  
 contours  
**Elongation** : vertical



**Texture** : columnar  
**Crystals** : large with smooth contours  
**Elongation** : vertical to slightly oblique



**Texture** : equigranular  
**Crystals** : small or large with smooth  
 contours  
**Elongation** : none



**Texture** : equigranular  
**Crystals** : large polygonal with sharp  
 contours  
**Elongation** : none

Fig. 3. Textural characteristics of the main ice types in core H. The thin sections were prepared in the vertical plane. The symbols in the background and the numbers in the right upper corner are those used in Figure 4. The black scale is 1 cm long. The numbers in the lower corners give the location (in cm) of the sections in the core.



*Tison and others: Stratigraphy, etc., in rift area of George VI Ice Shelf*

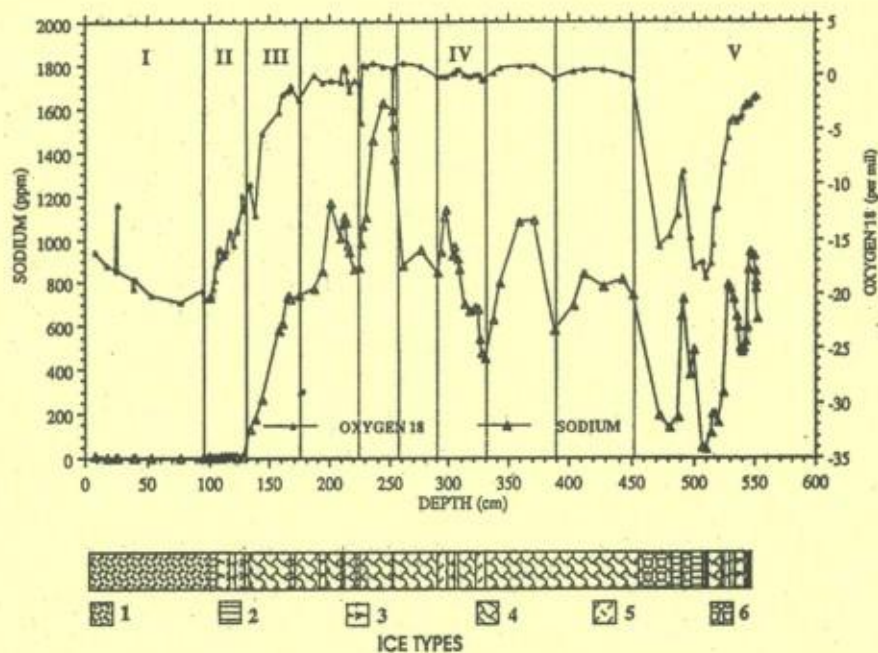


Fig. 4. Textural, isotopic and chemical characteristics of core H.

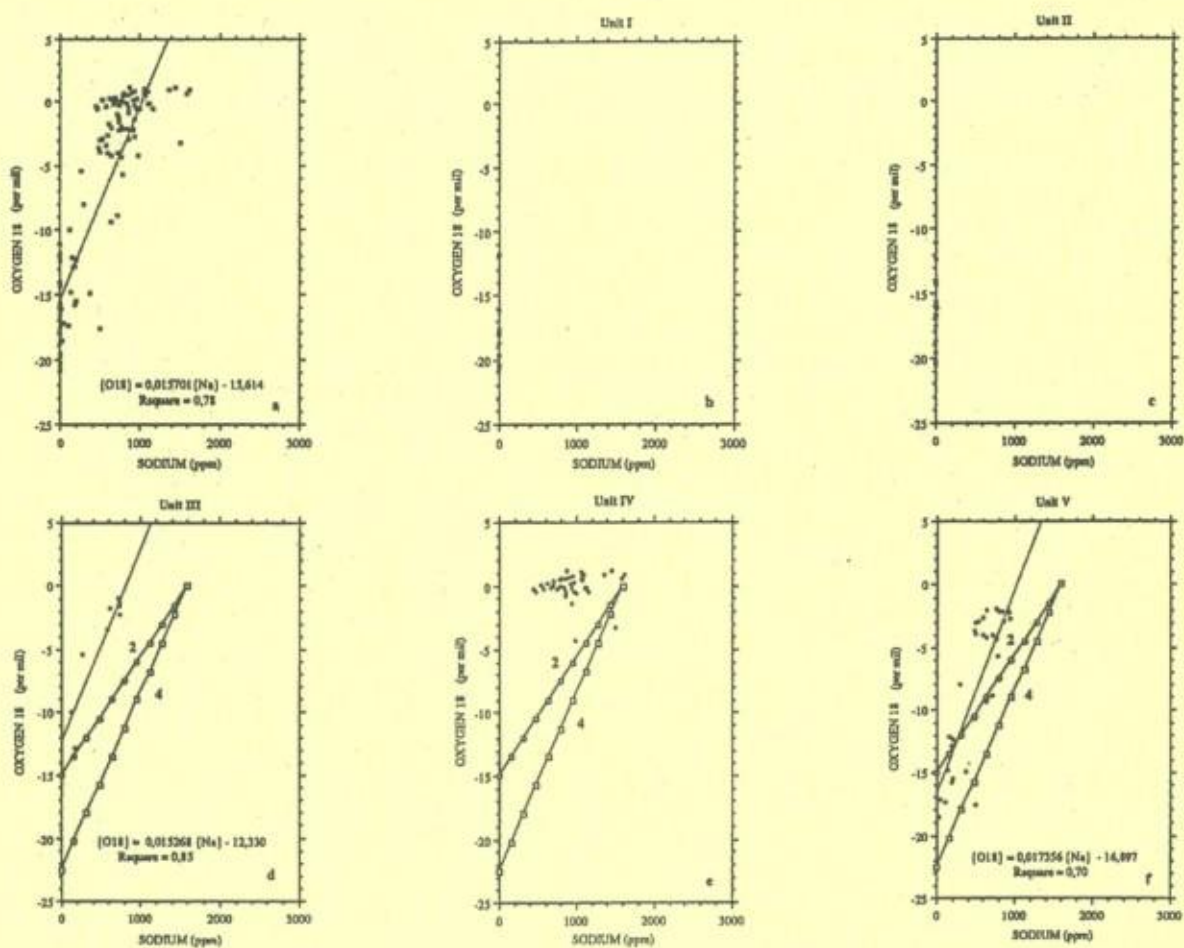


Fig. 5.  $\delta^{18}\text{O}/\text{Na}$  diagrams for the samples from core H. The dotted line shows the linear regression, and lines 2 and 4 correspond to those defined in Figure 8.



*Journal of Glaciology*

- b. The core presents a wide range of salinity and isotopic values. Na ranges from 0.00019 to 1.6‰ (e.g. global salinity ranging from 0.00062 to 5.2‰),  $\delta D$  from -162.5 to 8.2‰, and  $\delta^{18}O$  from -20.8 to 1.15‰. These ranges are comparable to those observed by Jeffries and others (1989, table II) for salinity and  $\delta^{18}O$ , in land-fast multi-year sea ice from the Arctic, although the variability in each individual core tends to be less important in their study.

### Growth processes of the multi-year sea-ice cover

#### *Dominance of parent-water effects*

A careful examination of Figure 4 reveals a fair positive correlation between the salinity and isotope profiles which is expressed by a regression coefficient of 0.78 in the  $\delta^{18}O/Na$  diagram of Figure 5a. This value is probably a low estimate of the strength of the correlation for two main reasons: (1) the diagram includes the samples from the top 130 cm of the core, which forms a special unit where the salinities are negligible and result from different genetic processes, and (2) the dispersion of the salinities for the samples displaying high isotopic values is probably due to the combined effect of a slight shift between isotopic and chemical values related to the sampling techniques, and of a higher sensitivity of the salinity signal to the inclusions of sea-water brines between frazil-ice grains, as will be discussed later.

The behaviour of  $\delta^{18}O$  and  $\delta D$  is very similar, as shown by the excellent linear regression of Figure 6a.

The two main factors which can influence the isotopic

and chemical signals during a water/ice phase change in an open semi-infinite reservoir (e.g. the formation of sea ice) are: (i) the characteristics of the parent water (a "meteoric ice-sea water" mixture confined to the surface layer, in this case), and (ii) the rate of freezing. Two major sources must be considered for the fresh-water input to sea water at the sampling site: either melting of desalinated sea ice formed at a previous stage (low salinity, high  $\delta$  values) or melting of snow and shelf ice (low salinity, low  $\delta$  values). In the first case, progressive dilution of sea water will produce a parent water showing decreased salinities and slightly increased  $\delta$  values, since sea ice is enriched in heavy isotopes with regard to sea water, and since no fractionation occurs during melting (Friedman and others, 1964; Moser and Stichler, 1980). During growth of new sea ice from this diluted parent water, a reduction in the growth rate will further enhance salt rejection from the ice and incorporation of heavy isotopes into the ice. Salinity and isotopic profiles fluctuating in opposite ways will thus be the signature of such a process. A decreasing freezing rate during growth of sea ice from undiluted sea water will give similar results, but the salinity drop will be less important. In the second case, the parent water will show decreasing salinities and decreasing  $\delta$  values with increasing dilution. The freezing-rate effect will, in this case, enhance salt rejection from the new sea ice and impede the decrease of  $\delta$  values. In the latter case, the maximum possible positive shifts, occurring at very low freezing rates, are 3‰ in  $\delta^{18}O$  and 20.8‰ in  $\delta D$ . Thus, for dilution events higher than 10% (and this is a worst case), this process will result in salinity and isotopic profiles in sea ice fluctuating

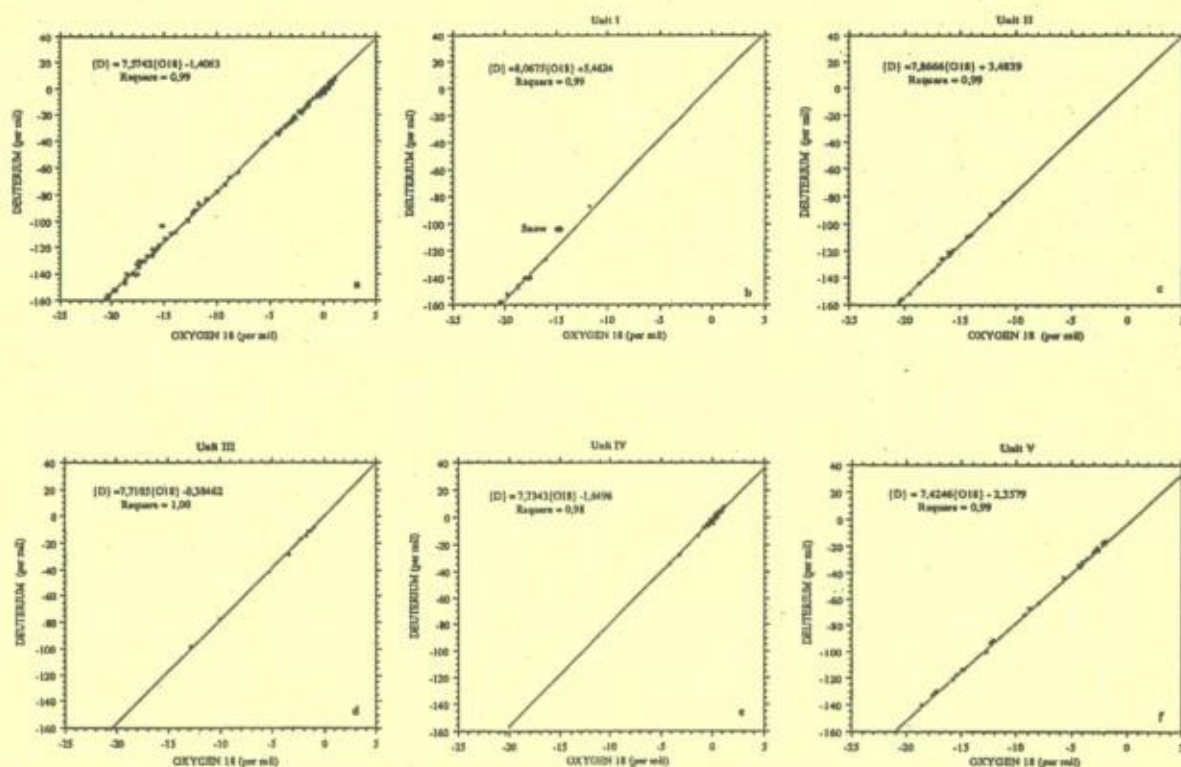


Fig. 6.  $\delta D$ - $\delta^{18}O$  diagrams for the samples from core H.



*Tison and others: Stratigraphy, etc., in rift area of George VI Ice Shelf*

in the same way. The large-scale strong positive correlation between the two curves in our core thus suggests that there were major fluctuations in the composition of the parent water during the sea-ice growth, and that this parent water results from dilution of sea water by melt from either snow or surface/basal shelf ice.

The dominance of parent-water effects over freezing-rate effects can be deduced from examination of the  $\delta D/\delta^{18}O$  diagram in Figure 6a, where all the samples lie on a line with a slope of 7.6 (correlation coefficient of 0.999) and  $\delta$  ranges of 170‰ in deuterium and 23‰ in oxygen-18. If we plot, on such a diagram, all the possible samples resulting from mixing of pure sea water (VSMOW) with glacial or snow meltwaters from the local environment, the points will lie on a straight line, the slope of which will be slightly lower than the value of 8.0 characteristic of the Meteoric Water Line (MWL). Using the seasonal range of co-isotopic values of the snowfalls in the rift area, typical slopes between 7.5 and 7.9 would be expected. If freezing effects are dominant, the samples could also lie on a straight line, provided that the parent water remained unchanged while the freezing rate changed significantly. The "freezing slope" would correspond to the differential fractionation during the water/ice phase changes (Jouzel and Souchez, 1982; Souchez and Jouzel, 1984). However, a much shorter range in the isotopic composition of the ice would be obtained in this case. Thus, the slope of 7.6, and the high  $\delta$  ranges observed in Figure 6a, must mainly reflect the presence of a parent water with an isotopic composition evolving through time because of mixing between normal sea water and fresh meltwaters.

The marked parallelism between the salinity and isotopic curves is also an indication that flushing out of the brine by downward percolation of surface meltwaters has been very limited, because of the absence of summer melt at the top surface. In addition, the limited amount of columnar ice, which, when present, is small-grained and lacks a brine-layer/ice-plate sub-structure, must strongly inhibit any brine-drainage process. Small-scale negative correlations between Na and  $\delta D$  have been observed in congelation ice layers from the first half of the core, possibly indicating fluctuations in the freezing rate.

#### Origin of the different units

Five different units can be distinguished in the core, each corresponding to a distinct process of formation. The

proposed limits between the different units are marked in Figure 4 by the vertical straight lines associated with the position of a sample. To ease the comparison with data previously mentioned in the literature, we choose to use  $\delta^{18}O$  values in the discussion when only one isotope is considered.

Unit I (0–98 cm; Figs 5b and 6b) resembles the surface layers of the ice shelf (Fig. 3a). It is a low-density porous medium characterized by small polygonal crystals with many voids between them and it shows two localized layers of recrystallization (type 1). The salinity is negligible (0.19–4.29 ppm) and the  $\delta^{18}O$  values are low (–11.8 to –20.8‰). This unit most probably corresponds to the snow accumulation during part of the year that followed the sea-ice-cover formation (from mid-winter 1987 to the end of the 1987–88 summer, when sampling occurred). The insignificant proportion of ice in the unit and the preservation of the high porosity of the medium is further evidence of the restricted surface melting in the area during the summer. It should be noted that the slope of the regression line on the  $\delta D/\delta^{18}O$  diagram of Figure 6b corresponds to the MWL (8.07).

Unit II (98–130 cm; Figs 5c and 6c) still displays a very low salinity (2.01–7.83 ppm Na) whereas the isotopic values steadily increase with depth from –20 to –10‰. Small-grained columnar ice is present (the contorted fibrous-like crystals of Figure 3b) probably indicating congelation effects. However, these congelation effects must be highly localized in the profile since the slope of 7.9 (correlation coefficient of 0.998) shown in the  $\delta D/\delta^{18}O$  diagram of Figure 6c is too high to be a freezing slope related to the decreasing freezing rate in a semi-infinite water medium with a constant isotopic value and a low salinity. The increasing isotopic values in the ice cannot be explained by an increasing share of normal sea water in the parent water, given the negligible salinities observed. Therefore, the most likely hypothesis is that this unit formed prior to unit I, and resulted from snow accumulation during the period that immediately followed the initial formation of the sea-ice cover (end of summer 1986–87 to mid-winter 1987).

The C-shaped profile of the isotopic values from these two upper units can therefore be considered as covering the net annual snow accumulation from summer to summer, between 1.00 and 1.30 m year<sup>-1</sup>, with  $\delta^{18}O$  values fluctuating between –11 and –20.8‰. These values correspond reasonably well to those observed by Potter and others (1984) at Monteverdi Peninsula, not far from

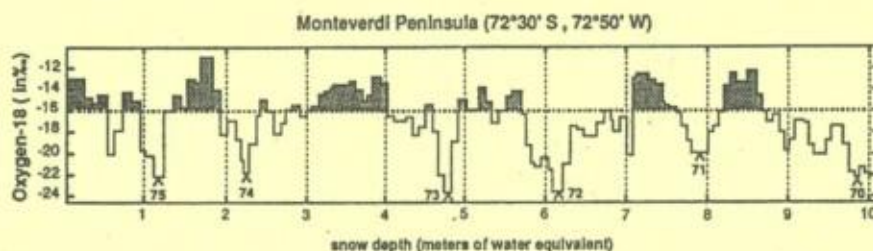


Fig. 7. Oxygen-18 profile in a 10 m core from Monteverdi Peninsula (data from J. G. Paren, British Antarctic Survey). The arrows mark the years and the horizontal dashed line is the mean value in  $\delta^{18}O$ .



*Journal of Glaciology*

the rift area, in a 10 m ice core (Fig. 7; data from J. Paren (personal communication)) with a mean annual accumulation of  $0.95 \text{ m year}^{-1}$  and a range of  $-12$  to  $-22\text{‰}$  in  $\delta^{18}\text{O}$ . The preservation of the whole year's accumulation cycle in our core gives weight to the assertion that summer melting is very limited in the area.

A sharp transition from a  $\delta^{18}\text{O}$  value of  $-13\text{‰}$  to a value of  $0\text{‰}$  marks the beginning of unit III (130–175 cm; Figs 5d and 6d). The linear regressions for  $\delta\text{D}/\delta^{18}\text{O}$  (slope of 7.7 with  $r^2 = 1.0$ ) and  $\delta^{18}\text{O}/\text{Na}$  ( $r^2 = 0.85$ ) clearly indicate the dominance of parent-water effects over freezing-rate effects.

Three main sources of fresh water to dilute the normal sea water can be proposed:

- Melting of first-year sea ice from the previous year.
- Melting of snow falling on the surface of the ice shelf and in the open sea water during the summer.
- Melting of bottom shelf ice.

Extensive melting of first-year sea ice from the previous year is highly improbable since most of the rift is covered with thick multi-year ice, with the exception of the restricted areas where depressions cross and open sea water forms during the summer. Also, mixing of melted sea ice with sea water would result in salinity and isotopic profiles fluctuating opposite ways in the new sea ice formed, as discussed above.

Surface melt on the ice shelf during the summer is a possible source of fresh water. However, as discussed previously and as attested by summer aerial photographs, by annual mean temperatures estimated on Monteverdi Peninsula or Spatz Island (Peel and Clausen, 1982) and by British Antarctic Survey traveling reports, surface melting is probably much more limited here than in the northern part of the ice shelf (between  $70^{\circ}30'$  and  $72^{\circ}\text{S}$ ; Potter and others, 1984). Nevertheless, if the hypothesis proposed for the formation of unit II is valid, partial dilution of surface sea water by snow falling in open waters should be considered. Potter and others (1984) calculated a mean  $\delta^{18}\text{O}$  value of  $-15.0 \pm 0.9\text{‰}$  for ice-shelf accumulation in the southern part of George VI Sound. This corresponds fairly well with the values of  $-15.10$  and  $-15.20\text{‰}$  measured in fresh snow from two different precipitation events on the sampling site at the end of the summer (March 1988). Surface melting will only occur during the summer season and will mainly affect the more positive values of the annual accumulation cycle, as shown by the flatness of the summer peaks (above the mean) in the isotopic records of Figure 7. The meltwater that will eventually reach the sea-ice/sea-water interface will thus display isotopic values ranging between  $-12$  and  $-16\text{‰}$  in  $\delta^{18}\text{O}$ . A value of  $-15\text{‰}$  will therefore be considered as typical of the melt either from the accumulation occurring at the surface of the ice shelf or from the snow falling in the open waters in the area.

The isotopic value of the melt from the base of the ice shelf is much more difficult to estimate. Potter and others (1984) used a mean  $\delta^{18}\text{O}$  value of  $-22.5 \pm 0.4\text{‰}$  for the ice flux into the southern part of the ice shelf from the inland ice sheet, estimated from an equilibrium mass and isotope balance partly using the temperature/ $\delta^{18}\text{O}$

relationship established by Peel and Clausen (1982) for the Antarctic Peninsula. We shall assume that this value can be used as the average  $\delta^{18}\text{O}$  for ice at the base of the ice shelf.

Using the salinity value of  $34.72\text{‰}$  ( $10.67\text{‰}$  in Na) and the  $\delta^{18}\text{O}$  value of  $+0.16\text{‰}$  proposed by Potter and others (1984) for Warm Deep Water (WDW), the two mixing lines respectively of surface and basal meltwaters with WDW can be calculated. In both cases, we can discriminate between fresh ( $<0.5\text{‰}$  global salinity), brackish ( $0.5\text{--}17\text{‰}$ ) and sea water ( $>17\text{‰}$ ) as proposed by Jeffries and others (1989).

Reconstruction of the Na/ $\delta^{18}\text{O}$  profile in the ice formed by freezing of these waters is complicated by non-equilibrium processes connected with fluctuations of the growth rates and by possible inclusion of liquid in the growing ice (Souchez and Jouzel, 1984; Souchez and others, 1987, 1988). However, by using a method similar to that of Jeffries and others (1989), a broad envelope of possible values can be obtained by applying minimum and maximum apparent fractionation coefficients for Na and  $\delta^{18}\text{O}$ . For  $\delta^{18}\text{O}$ , extremely low freezing rates will allow the maximum equilibrium fractionation to occur with a positive shift of  $3\text{‰}$  ( $\alpha = 1000 + \delta_i/1000 + \delta_o = 1.003$ , where  $\delta_i$  and  $\delta_o$  are the  $\delta$  values for ice and water respectively (O'Neil, 1968)), and fast freezing will not yield any apparent fractionation. The effect of sea-water inclusions on the isotopic signal of sea ice can be considered as negligible, as shown by Tison and Haren (1989). Na-incorporation factors ( $S_i/S_o$ , where  $S_i$  and  $S_o$  are the salinity for ice and water, respectively) as low as 0.04–0.05 have been observed at the bottom of first-year sea ice by Souchez and others (1988) and a maximum value of about 0.15, as observed in our core, should cover most of the observations quoted in the literature. This wide range of salinity-fractionation factors is also thought to cover any alteration of the signal by sea-water inclusions in the ice.

Figure 8 shows the four mixing lines obtained in the ice by applying the extreme values of the fractionation coefficients in Na ( $S_i/S_o$ ) and in oxygen-18 ( $\alpha$ ) to the two water-mixing lines calculated above. The sample values are displayed in the background. The percentage of WDW varies from 100 to 0% along each mixing line. Curves 1 and 2 correspond to dilution of normal sea water by meltwaters from the surface of the ice shelf and curves 3 and 4 to dilution by meltwaters from the base of the ice shelf. Only curves 2 and 4 have been drawn on Figure 5d, e and f, since curves 1 and 3 are very close to the ordinate axis and are therefore not relevant in distinguishing the various parent-water sources.

All the points from unit III lie above the two mixing lines in Figure 5d. This implies that these ice samples could either have resulted from the freezing of sea water diluted by surface meltwaters (with fresh-water proportions ranging between 10 and 90%) and/or from the freezing of sea water diluted by meltwaters from the base of the ice shelf (between 10 and 50% of fresh water).

Unit IV (175–452 cm; Figs 5e and 6e) is the thickest unit in the core. It is characterized by the stabilization of Na and  $\delta^{18}\text{O}$  around mean values of respectively  $0.9\text{‰}$  (900 ppm) and  $0\text{‰}$ . However, it is clear in Figure 4 that five major large-scale sympathetic fluctuations of



Tison and others: Stratigraphy, etc., in rift area of George VI Ice Shelf

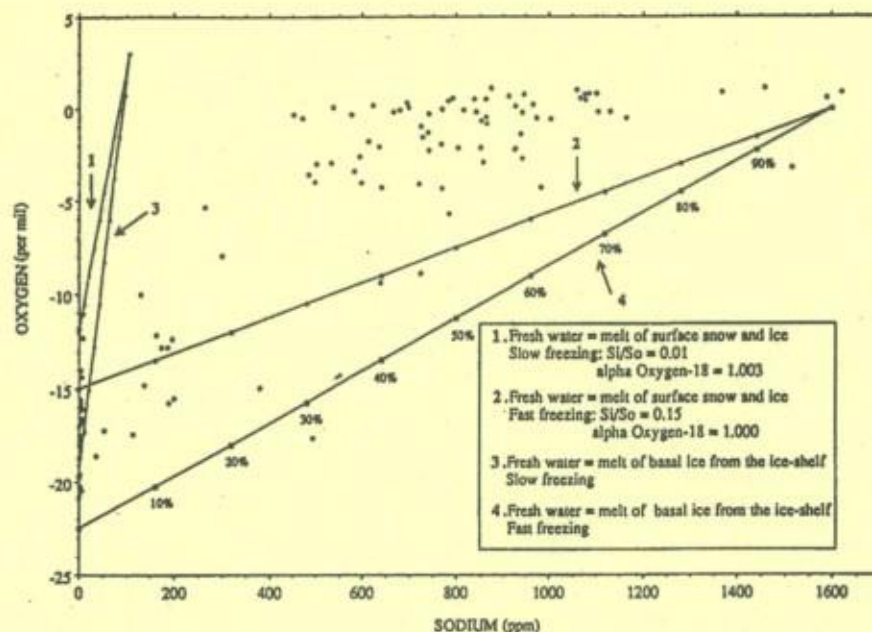


Fig. 8. Mixing lines for ice formed by freezing of sea water diluted by fresh water from surface or basal melting of the ice shelf and for extreme values of the fractionation coefficients. The percentage represents the proportion of normal sea water in the mix.

Na and  $\delta^{18}\text{O}$  characterize the unit, with minimum values at depths of 223, 258, 290, 330 and 390 cm (dashed lines in Figure 4). It should be noted that this sympathetic response between Na and  $\delta^{18}\text{O}$  does not show up as a good correlation in the  $\delta^{18}\text{O}/\text{Na}$  diagram of Figure 5e. This is probably the expression of a different sensitivity of the chemical and isotopic signals to the liquid water inclusions during accretion of individual frazil-ice crystals at the bottom of the pre-existing ice cover. Since at least 85% of the salts are rejected from the sea-ice crystals as they form, slight fluctuations in the amount of parent water entrapped between the crystals as they accumulate at the base of the ice cover may cause important variations in the measured salinity in the core. This effect is negligible for the isotopic signal (Tison and Haren, 1989), since most of the signal results from the crystal itself. Thus, at two different locations in the core, similar changes in the isotopic signal will correspond to chemical changes of the same sign but of different intensity.

Most of the samples in unit IV could result from the freezing of sea water diluted by fresh water from each of the two possible sources, the proportion of fresh-water input being a few per cent (maximum 20–30% in two-point samples at depths of 223 and 258 cm, both corresponding to columnar ice; Fig. 4). However, two arguments indicate a sub-ice-shelf origin. First, units I and II correspond to the snow accumulation of a whole year with limited melting during the summer and unit III results from the freezing of normal sea water which was less and less diluted by fresh water in the course of time. This last unit was therefore growing downward at the same time that unit II was piling up, at the beginning of the winter following the initial sea-ice-cover

formation. This implies that unit IV formed during the winter, when any surface melting is precluded. Secondly, one of the two stronger dilution peaks is located below the two mixing lines (Fig. 5e) and therefore could only be produced by fresh water with a  $\delta^{18}\text{O}$  value lower than  $-22.5\text{‰}$ . This could only be provided by melting at the base of the ice shelf.

Although dilution events are not always associated with textural differences (see, for example, the event at 390 cm), it should be noted that the only occurrence of platelet ice (Fig. 3d) is located around two of the main dilution peaks (at 290 and 330 cm). Platelet ice is a special type of frazil ice usually associated with adiabatic expansion of sea water as it ascends from beneath ice shelves (see, for example, Robin, 1979; Lange and others, 1989). If dilution occurs at the bottom of the ice shelf, it is therefore not surprising to trace it in the chemistry of the platelet ice in the core.

At 450 cm depth, the isotopic and chemical values drop sharply (from 741 to 190 ppm in Na and from  $-0.25$  to  $-15.75\text{‰}$  in  $\delta^{18}\text{O}$ ); and a fifth unit of alternate columnar (Fig. 3e) and granular ice (Fig. 3f) occurs (unit V (452–553 cm; Figs 5f and 6f)) partly showing the characteristics of ice resulting from the freezing of brackish water. About one-third of the samples from this unit can only be formed by freezing of waters resulting from the mixing of normal sea water with meltwaters from the base of the ice shelf, as indicated by Figure 5f. Dilution percentages as high as 80% fresh water/10% sea water can be observed. Contacts between individual grains are sharper and better defined than in the more saline units above (Fig. 3f). The higher dilutions correspond to the frazil-ice layers that must therefore have been formed at depth, not far from the production zone, thus freezing-



*Journal of Glaciology*

in the chemical and isotopic signature of the fresh water before significant mixing with the normal sea water occurred. However, the presence of considerable amounts of columnar ice in this unit seems to indicate that it partly forms by direct freezing of the brackish water layer at the bottom of the ice cover (congelation ice). The absence of brine-layer/ice-plate sub-structure in this columnar ice (Fig. 3e) might be a trademark of brackish congelation ice.

Isotopic and chemical profiles of sea water, down to 15 m (collected through boreholes G and I (Fig. 2)), confirm the sub-shelf origin for the fresh water. The water samples were taken just after coring, while a considerable number of equigranular small frazil crystals were regularly floating up to the open-water surface of the borehole. These frazil-ice crystals were sampled separately and yielded isotopic values of  $-4.55$  to  $-5.90\text{‰}$  ( $\delta^{18}\text{O}$ ) and  $-33$  to  $-46\text{‰}$  ( $\delta\text{D}$ ), at sites G and I respectively. Under the ice cover, the isotopic and chemical values of the sea water are around 8000–8500 ppm of sodium,  $-1.1$  to  $-1.8\text{‰}$  ( $\delta^{18}\text{O}$ ) and  $-8$  to  $-13\text{‰}$  ( $\delta\text{D}$ ). These isotopic values are too high to be responsible for those observed in the frazil ice at the extreme base of the core ( $-2\text{‰}$  in  $\delta^{18}\text{O}$  and  $-19\text{‰}$  in  $\delta\text{D}$ ), whatever the freezing rate. Similarly, the individual frazil-ice crystals accumulating at the surface need a parent water with isotopic values fluctuating between  $-66$  and  $-33\text{‰}$  in  $\delta\text{D}$  and  $-9$  to  $-4\text{‰}$  in  $\delta^{18}\text{O}$ . Such water was not observed under the sea-ice cover and must result from the mixing of normal sea water with meltwaters from the base of the ice shelf. The top of unit V therefore marks an increasing production of meltwater at the base of the ice shelf, probably at the beginning of the austral summer 1987–88.

## CONCLUSION

The major rifts developing in the southern part of George VI Sound, where the ice shelf calves into huge tabular icebergs, are ideal traps for the water masses ascending in front of the ice shelf. These contribute to the accretion of sea ice at the open surface between the sides of the rift. Combined salinity and isotopic profiles of this sea ice allow the origin of the parent water to be traced. Results from a detailed profile of a 5.54 m thick ice core sampled in the area show that it is probably second-year sea ice that has survived one melt season (Weeks and Ackley, 1986). Half of the core consists of sea ice, following the Jeffries and others (1989) terminology, formed in the winter. Although, during this period, the parent water is close to normal sea water, the Na and  $\delta^{18}\text{O}$  curves show a few sympathetic large-scale fluctuations indicating dilution events reaching 20% of fresh-water input that might reflect small variations in the basal melting of the ice shelf. A sharp transition from sea ice to brackish ice (450 cm depth), that must result from mixing with meltwater from basal shelf ice, indicates the importance of this process during the summer period, with maximum dilution coefficients up to 80% of fresh water. Winter accretion consists almost exclusively of frazil-ice production, while summer accretion alternates between frazil ice formed at depth close to the fresh-water-input location (low-salinity and low-isotopic signal) and congelation ice formed by direct progression of a freezing front under

the sea-ice cover into a less-diluted parent water. Further work on the multi-year sea ice formed in the rift area will aim to produce a semi-quantitative estimate of the fresh-water output from the base of George VI Ice Shelf at its southern ice front.

## ACKNOWLEDGEMENTS

The British Antarctic Survey is gratefully acknowledged for having supported the field work in the Antarctic Peninsula. Special thanks are due to J. Hall for his efficiency in organizing field operations and J. Pailthorpe for his help in collecting the samples. J.-L.T. is a "Chercheur Qualifié" with the Belgian National Scientific Research Foundation (F.N.R.S.). This paper is a contribution to the Belgian scientific programme in Antarctica.

## REFERENCES

- Cherepanov, N. V. 1966. Structure of sea ice of great thickness. Ottawa, Defense Research Establishment. (T448R.)
- Friedman, I., B. Schoen and J. Harris. 1961. The deuterium concentration in Arctic sea ice. *J. Geophys. Res.*, 66(6), 1861–1864.
- Friedman, I., A. C. Redfield, B. Schoen and J. Harris. 1964. The variation of the deuterium content of natural waters in the hydrological cycle. *Rev. Geophys.*, 2, 177–189.
- Gow, A. J. and S. Epstein. 1972. On the use of stable isotopes to trace the origins of ice in a floating ice tongue. *J. Geophys. Res.*, 77(33), 6552–6557.
- Gow, A. J., S. F. Ackley, K. R. Buck and K. M. Golden. 1987a. Physical and structural characteristics of Weddell Sea pack ice. *CRREL Rep.* 87-14.
- Gow, A. J., W. B. Tucker, III and W. F. Weeks. 1987b. Physical properties of summer sea ice in the Fram Strait, June–July 1984. *CRREL Rep.* 87-16.
- Jeffries, M. O., H. R. Krouse, W. M. Sackinger and H. V. Serson. 1989. Stable-isotope ( $^{18}\text{O}/^{16}\text{O}$ ) tracing of fresh, brackish and sea ice in multi-year land-fast sea ice, Ellesmere Island, Canada. *J. Glaciol.*, 35(119), 9–16.
- Jouzel, J. and R. A. Souchez. 1982. Melting–refreezing at the glacier sole and the isotopic composition of the ice. *J. Glaciol.*, 28(98), 35–42.
- Lange, M. A., S. F. Ackley, P. Wadhams, G. S. Dieckman and H. Eicken. 1989. Development of sea ice in the Weddell Sea. *Ann. Glaciol.*, 12, 92–96.
- Lyons, J. B., S. M. Savin and A. J. Tamburi. 1971. Basement ice, Ward Hunt Ice Shelf, Ellesmere Island, Canada. *J. Glaciol.*, 10(58), 93–100.
- Meese, D. A. 1989. The chemical and structural properties of sea ice in the southern Beaufort Sea. *CRREL Rep.* 89-25.
- Moser, H. and W. Stichler. 1980. Environmental isotopes in ice and snow. In Fritz, P. and J. C. Fontes, eds. *Handbook of environmental isotope geochemistry*. Vol. 1. New York, Elsevier, 141–178.
- O'Neil, J. R. 1968. Hydrogen and oxygen isotope fractionation between ice and water. *J. Phys. Chem.*, 72(10), 3683–3684.
- Peel, D. A. and H. B. Clausen. 1982. Oxygen-isotope



*Tison and others: Stratigraphy, etc., in rift area of George VI Ice Shelf*

- and total beta-radioactivity measurements on 10 m ice cores from the Antarctic Peninsula. *J. Glaciol.*, 28(98), 43-55.
- Potter, J. R., J. G. Paren and J. Loynes. 1984. Glaciological and oceanographic calculations of the mass balance and oxygen isotope ratio of a melting ice shelf. *J. Glaciol.*, 30(105), 161-170.
- Riley, J. P. and G. Skirrow. 1965. *Chemical oceanography*. New York, Academic Press.
- Robin, G. de Q. 1979. Formation, flow, and disintegration of ice shelves. *J. Glaciol.*, 24(90), 259-271.
- Schwarzacher, W. 1959. Pack-ice studies in the Arctic Ocean. *J. Geophys. Res.*, 64(12), 2357-2367.
- Souchez, R. and J. Jouzel. 1984. On the isotopic composition in  $\delta D$  and  $\delta^{18}O$  of water and ice during freezing. *J. Glaciol.*, 30(106), 369-372.
- Souchez, R., J.-L. Tison and J. Jouzel. 1987. Freezing rate determination by the isotopic composition of the ice. *Geophys. Res. Lett.*, 14(6), 599-602.
- Souchez, R., J.-L. Tison and J. Jouzel. 1988. Deuterium concentration and growth rate of Antarctic first-year sea ice. *Geophys. Res. Lett.*, 15(12), 1385-1388.
- Tison, J.-L. and J. Haren. 1989. Isotopic, chemical and crystallographic characteristics of first-year sea ice from Breid Bay (Princess Ragnhild Coast — Antarctica). *Antarct. Sci.*, 1(3), 261-268.
- Weeks, W. F. and S. Ackley. 1986. The growth, structure, and properties of sea ice. In Untersteiner, N., ed. *The geophysics of sea ice*. New York, Plenum Press, 9-164. (Nato ASI Series, Series B, Physics, 146.)

The accuracy of the references in the text and in this list is the responsibility of the authors, to whom queries should be addressed.

MS received 12 November 1990 and in revised form 24 May 1991



## **Paper 5**

**Ice Composition Evidence of Marine Ice Transfer along the Bottom of a Small  
Antarctic Ice Shelf**

## **Authors**

**R. Souchez, M. Meneghel, J.-L. Tison, R. Lorrain, D. Ronveaux, C. Baroni, A. Lozej, I.  
Tabacco, J. Jouzel**

## **Journal**

**Geophysical Research Letters, Vol. 18, n°5**

## **Year**

**1991**



GEOPHYSICAL RESEARCH LETTERS, VOL. 18, NO. 5, PAGES 849-852, MAY 1991

## ICE COMPOSITION EVIDENCE OF MARINE ICE TRANSFER ALONG THE BOTTOM OF A SMALL ANTARCTIC ICE SHELF

R. Souchez, M. Meneghel, J.-L. Tison, R. Lorrain, D. Ronveaux, C. Baroni, A. Lozej, I. Tabacco and J. Jouzel

**Abstract.** The existence of marine ice transfer along the underside of the Hell's Gate Ice Shelf (Victoria Land), is indicated by an isotopic and chemical study of ice cores. Because of top surface ablation, the marine ice formed at the ice shelf-ocean interface, ultimately appears at shelf surface. A succession of congelation, platelet and frazil ice is shown to occur. The combined study of stable isotope composition and of the sodium content of these different ice types proves to be a valuable tool for specifying the ice shelf-ocean interactions in this area. Two different freezing zones separated by a melting zone exist; the parent water for the frazil ice is meltwater from congelation ice which appears in the upstream zone.

## Introduction

Thermodynamic processes occurring at the base of an ice shelf are determined by the temperature of both ice and sea water near the interface and the direction and velocity of the ocean currents (Doake, 1976). Jacobs et al. (1979) proposed two modes for circulation near the ice front. A deep circulation beneath the ice shelf is driven by dense, saline water formed as a result of freezing at the sea surface. Water descends at the ice shelf front, because of its density increase due to salt rejection during sea ice formation in a polynya for example. The temperature of this water is the surface freezing point. After descending, this water has sensible heat available to cause melting of ice at depth, since increased pressure lowers the freezing point, a process related to the ice pump mechanism defined by Lewis and Perkin (1986). Another mode of circulation proposed by Jacobs et al. (1979) takes place at shallower depths and involves intrusions of warmer water from beyond the continental shelf break. This warm water flows beneath the ice shelf and undergoes cooling, dilution and lateral mixing. Now, in these two modes, melting of ice at depth can produce supercooled water since meltwater raises because of its lower density, and supercooling with respect to the in situ freezing point occurs since the pressure is reduced. Jenkins and Doake (1991) indicate that this potentially supercooled water can thus produce marine ice and that this process accounts for the majority of basal ice accumulation observed beneath the Ronne Ice Shelf. The present study will concentrate on these marine ice formation processes.

Most Antarctic ice shelves are accumulating snow on their surfaces. As a consequence, bottom ice layers cannot be reached unless expensive drilling programs are undertaken, such as the Ross Ice Shelf Drilling Program for example. In a few instances, mostly as a result of the action of katabatic winds, the surface of the ice shelf is snow-free and is losing ice by sublimation or melting. In such situations where sur-

face ablation is important, an upward vertical velocity component exists and ice initially at depth is transferred along an inclined surface towards the ice-atmosphere interface. Bottom ice layers previously at depth now constitute surface layers and the seaward edge of such an ice shelf can be composed exclusively of marine ice accreted at the bottom. In such a case, a longitudinal line of shallow ice core drillings can advantageously replace a single vertical profile through the ice.

## Sampling procedure and sample analyses

Twenty five ice cores, 1 to 1.5 m long, were retrieved from the Hell's Gate Ice Shelf, a part of Nansen Ice Sheet, and transferred frozen to Brussels. The first 50 cm of each ice core was discarded to avoid contamination problems. Isotopic analyses were performed in the Nuclear Research Center of Saclay in France. HDO and  $H_2^{18}O$  concentration will be denoted hereafter in  $\delta$  units versus V.S.M.O.W. (Vienna Standard Mean Ocean Water) expressed in per mil. Accuracy of  $\delta D$  measurements is 0.5‰ and of  $\delta^{18}O$  measurements 0.1‰. Sea ice samples containing more than 150 ppm Na were distilled under vacuum prior to isotopic analysis, by a procedure tested to avoid isotopic changes during the process. The Na content of the ice samples was determined by atomic absorption spectrophotometry with a Varian-SpectraAA 300 spectrometer, using standard procedures. Crystallographic investigations were made on vertical thin sections of the ice cores cut at  $-25^\circ C$  in a cold room in Brussels. In selected cases, the distribution of c-axes of the ice crystals was determined to substantiate the origin of the ice layer under consideration.

## The Hell's Gate Ice Shelf

This Antarctic ice shelf is located near Terra Nova Bay in the coastal zone of the Transantarctic Mountains (lat.  $\pm 74^\circ 50'S$ , long.  $\pm 163^\circ 50'E$ ). It is nourished by different affluents of the Priestley outlet glacier. A small rock outcrop, called Vegetation Island, acts as a pinning point for the ice shelf. Very strong katabatic winds from the polar plateau are frequent in this area; hence the name of this ice shelf and the existence of a polynya along its edge. The Hell's Gate Ice Shelf consists of three different sectors separated by ridges of debris cones. Only the western and central sectors will be considered here (Figure 1). They are separated from each other by a major shear zone including two ridges of debris cones containing rock fragments, shells and worm tubes incorporated into the ice by bottom freezing of sea water at the level of Vegetation Island. Baroni (1988) gave an uncalibrated  $^{14}C$  age of  $2495 \pm 160$  years BP (Gx-14084) for the oldest shells appearing at the surface of the ice shelf as a result of ablation which has been estimated to be about 10 cm per year. Marine ice is known to occur at the outer edge of the ice shelf

Copyright 1991 by the American Geophysical Union.

Paper number 91GL01077

0094-8534/91/91GL-01077\$3.00



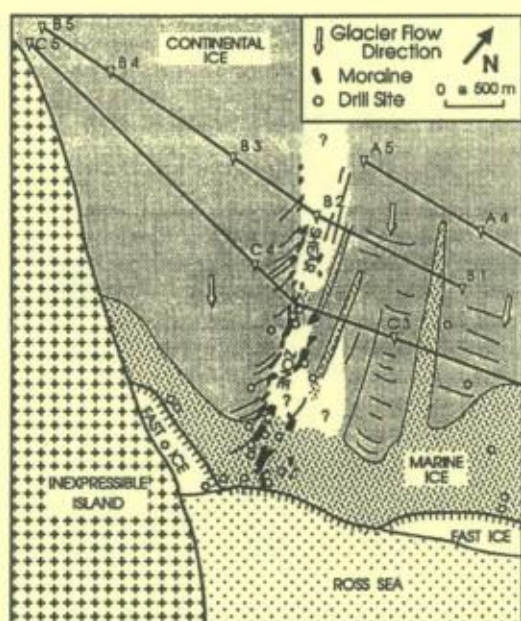


Fig.1 : The Hell's Gate Ice Shelf. Radio-echo-sounding lines are indicated.

and replaces progressively and completely glacier ice in that region. Such a situation indicated by a  $\delta^{18}\text{O}$  shift from largely negative to positive values (Baroni et al, in press) is very similar to the one described in 1972 by Gow and Epstein for the Koettlitz Ice Tongue in McMurdo Sound, Antarctica.

Radio-echo sounding of the Hell's Gate Ice Shelf shows a striking contrast between the western and central sectors. In the western sector, a principal reflector supposed to be, because of its strength, the interface between floating ice and sea water, can easily be identified but a complete disappearance of this reflector occurs at the level of the shear zone where the dip of the ice layers is subvertical. In this sector the ice shelf has an estimated thickness of about 60m and a relatively flat interface with sea water except an irregularity close to Inexpressible Island where it is deforming. With an ice surface at about 9m a.s.l., this is not far from hydrostatic equilibrium. By contrast, the central sector of the ice shelf displays an undulating interface at a depth between 25m and 50m, though it is occasionally shallower than 20m. This reflector is characterized by an energy contrast markedly lower than that found in the western part. The difference in reflecting energy with the western sector could be due to a change in the physical characteristics of the ice, the electromagnetic energy being absorbed because of the conductivity of a lower ice unit. The detection of the ice-water interface is thereby inhibited.

The contact zone between glacial and marine ice at the surface of the ice shelf is clearly seen on Spot imagery because of contrasting signatures of these two ice types. No debris is found at that limit. This seems to indicate that sea water freezing does not occur at the grounding line in contrast with the situation around Vegetation Island. For ice flowing into the western and central sectors of the Hell's Gate Ice Shelf, the grounding line is much farther northwest than Vegetation Island so that different interface conditions can prevail.

#### Ice types of the Hell's Gate Ice Shelf

Glacier ice, originating as snow of continental origin, can easily be distinguished in thin section by its structure consisting in polyhedral crystals (size : 1 to 2 cm) containing numerous air bubbles. Its Na content is very low, less than 0.001 ppt (part per thousand). Its isotopic composition is characterized by a low content in heavy stable isotopes, the  $\delta\text{D}$  values ranging between -160‰ and -245‰, the  $\delta^{18}\text{O}$  values between -23‰ and -31‰. The relationship between the two sets of values is  $\delta\text{D} = 8.13 \delta^{18}\text{O} + 6.5$  (correlation coefficient of 0.992), which can be considered as the result of a precipitation effect. The large altitudinal range of the source areas is sufficient to explain the large range of  $\delta$  values observed.

Marine ice which is substantially bubble-free by comparison with glacier ice, can be subdivided in the ice cores into columnar, granular and platelet ice.

Columnar ice consists of columnar crystals (length >2cm) with cell structure and brine layers. In the thin sections examined, the elongated crystals are only roughly parallel to each other indicating that undershelf currents were able to disturb the alignment and that pockets of sea water could be incorporated into the layer during growth and subsequently frozen. This columnar ice is thought to be congelation ice due to the progression of a freezing front in sea water. Its Na content is between 0.5 and 0.8 ppt. The isotopic composition of the samples analysed is indicated in Figure 2. The positive values imply freezing of sea water close to V.S.M.O.W.

Granular ice is composed of small rectangular crystals (length <1cm), more or less aligned horizontally. It is thought to be frazil ice generated in the sea water itself as a consequence of a double diffusion mechanism, heat diffusivity being one order of magnitude higher than salt diffusion (Weeks and Ackley, 1986). It has a Na content lower than 0.15 ppt. There is even a low salinity population with a Na content less than 0.025 ppt. This population is represented in the central sector of the ice shelf where it constitutes the main portion of the marine ice appearing at the surface. The isotopic

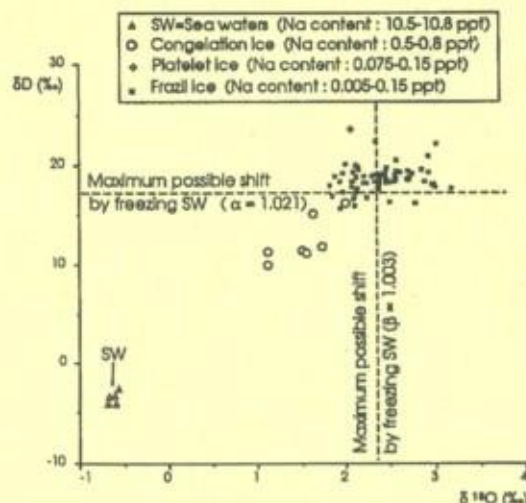


Fig.2 :  $\delta\text{D}$ - $\delta^{18}\text{O}$  diagram for sea waters and marine ice types of the Hell's Gate Ice Shelf.



composition of frazil ice is more positive than that of congelation ice, both in  $\delta D$  and  $\delta^{18}O$ . Frazil ice thus originated from sea water and not from glacial ice meltwater.

Platelet ice is characterized, as described by Lange (1988) by large elongated grains (length >2cm), sometimes acicular, pointing in different directions and often interspersed with regions of small grains. There is also a near absence of any substructure within the large grains, although in our thin sections brine pockets are sometimes seen, indicating probably a contribution of disaggregated columnar ice in the formation of the platelet ice. Platelet ice is considered as a variety of frazil ice, also generated within the water column. Platelet ice growth is very often associated with supercooling of water under an ice shelf (Lange et al., 1989). The Na content of the platelet ice samples is intermediate between that of congelation and frazil ice: from 0.075 to 0.15 ppt. Its isotopic composition is not significantly different from that of frazil ice.

#### Evidence for marine ice transfer along the bottom of the ice shelf

Sea water was sampled near the edge of the Hell's Gate Ice Shelf between 0 and 200 m depth.  $\delta^{18}O$  values of these waters are close to ISW (Jacobs et al., 1985).

Sea water samples, congelation, platelet and frazil ice samples are aligned, on a  $\delta D$ - $\delta^{18}O$  diagram (Figure 2), on a slope of 6.6 (correlation coefficient of 0.93). This slope can be considered as a freezing slope. Indeed, the freezing slope on which ice samples due to water freezing are aligned on a  $\delta D$ - $\delta^{18}O$  diagram can be calculated using the equation

$$S = \frac{(\alpha - 1)}{(\beta - 1)} \times \frac{(1000 + \delta_i D)}{(1000 + \delta_i^{18}O)} \quad (\text{Souchez and Jouzel, 1984})$$

where  $\alpha$  and  $\beta$  are the respective equilibrium fractionation coefficients for deuterium and oxygen 18 (taken usually as  $\alpha = 1.0208$  and  $\beta = 1.003$ ),  $\delta_i D$  and  $\delta_i^{18}O$  are the respective  $\delta$  values for the initial water at the beginning of freezing. Taking  $\delta_i D = -4\text{‰}$  and  $\delta_i^{18}O = -0.6\text{‰}$  (mean values of sea water at ice shelf's edge), the calculated slope is 6.9, which is fairly close to the measured value. The difference between the  $\delta$  values of most of frazil ice samples and sea water samples is higher than the maximum possible shift which can be obtained by a single freezing event, thus precluding this sea water as the parent water for frazil ice. This would still be true if a 2‰ higher  $\alpha$  value is considered, a possibility that might exist for deuterium but only for sea water of high salinity (Beck and Munnich, 1988).

The parent water for frazil ice must be a water of relatively low salinity compared with sea water. Indeed, water salinity of the parent water can be calculated if the frazil ice salinity and the distribution coefficient are known. Antarctic sea ice salinities given in the literature (Gow et al., 1987; Lange, 1988) usually range between 3 and 6 ppt for frazil ice, with very low values at 2 ppt or very high values around 15 ppt in freshly consolidated pancake ice (Eicken and Lange, 1989). Since this sea ice was formed from antarctic surface sea water, deduced distribution coefficients (sea ice salinity/sea water salinity) will range between 0.09 and 0.17 with extreme values of 0.06 and 0.44. It can be assumed that

the ratio Na/salinity is 0.3074 in the ocean and independent of the salinity level for a large range of salinities (Riley and Skirrow, 1965) and that the same ratio is valid for sea ice (Meese, 1989). Using a Na content typical of the low salinity frazil population (0.025 ppt), a maximum salinity of less than 1.35 ppt is obtained for the parent water of the frazil ice sampled at Hell's Gate.

Can water of such a low salinity be surface meltwater from marine ice percolating through tide cracks to the underside of the ice shelf, such as Gow and Epstein (1972) considered for the Koettlitz Glacier Tongue near the Dailey Islands, McMurdo Sound, Antarctica? Meltwater ponds effectively exist at the surface of the Hell's Gate Ice Shelf near its front. Several arguments can however be given which tend to indicate that this possibility is excluded here. First, not a single open crevasse has been encountered at the surface of the ice shelf where meltwater ponds are present and no islands with their attendant tide cracks exist in the ablation zone. Second, the zone of low salinity frazil ice appearing at the ice shelf surface is quite extensive and not restricted to the proximity of an eventual break-through percolation system. The zone of frazil ice at the shelf surface is in fact more extensive upstream than the zone where meltwater ponds are developed. Finally, there is no upper layer of water with low salinity in front of the ice shelf. Measurements in the top 0-200 m show that the Na content of sea water fluctuates between 10.5 and 10.8 ppt.

Thus, as shown by  $\delta$  values as well as salinity measurements, only meltwater of marine ice from the bottom of the ice shelf can serve as the source of frazil ice. Such water originates from congelation ice, the melting of which occurs without isotopic or chemical fractionation (Friedman et al., 1964; Moser and Stichler, 1980).

The decrease in salinity and the increase in  $\delta$  values from congelation to platelet and frazil ice, and the development of frazil ice downstream from congelation and platelet ice (Figure 3), indicate marine ice transfer along the bottom of the ice shelf. The meltwater produced by the melting of congelation ice is less dense than surrounding water because, at temperatures close to the freezing point, the density of sea water is primarily a function of salinity (Dietrich et al., 1980). As developed by Jenkins and Doake (1991), turbulent entrainment can provide a mechanism which supplies the heat required to warm the ascending current and sustain basal melting further downstream. This process becomes less efficient as the water reaches shallower depths, since the temperature contrast decreases. Then, supercooling, frazil ice formation and basal accretion will result. The development of frazil ice within the water column as a result of supercooling seems sufficiently efficient to prevent the

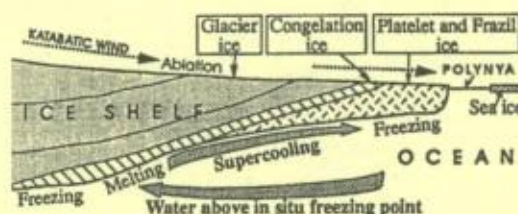


Fig.3 : Sketch indicating ice shelf-ocean interactions along the seaward part of the Hell's Gate Ice Shelf.



piling up of low salinity excess meltwater at the sea surface. Since this process not only operates in a downstream direction but also between the western sector and central sector of the ice shelf, an uneven lower surface of the ice in the latter region is likely to exist. This could be the result of the channelling of supercooled water and of the irregular production of frazil ice nucleated in the water column.

### Conclusion

We conclude that a study of the chemical and isotopic composition of the ice from an ice shelf is able to specify thermodynamic processes taking place at the base.

In the case of the Hell's Gate Ice Shelf, two freezing zones separated from each other by a melting zone have been shown to occur beneath its seaward margin. Frazil ice is formed by freezing of low salinity water which results from partial melting of congelation ice.

Since it is known that marine ice has accumulated in this ice shelf for the past 2500 years, a complete drilling would enable us to identify periods of shifting basal situations. Such corings could yield records of considerable palaeoclimatic significance.

**Acknowledgements.** This paper is a contribution to the "Programma Nazionale di Ricerche in Antartide (PNRA) and to the Belgian Antarctic Program (Science Policy Office). The first author thanks the Italian PNRA for the invitation to work at Terra Nova Bay in 1989-1990. Financial support of the ice analyses has been provided by the Geological Survey of Belgium under its global change program. J.-L. Tison benefits from a research contract of the Belgian Science Foundation.

### References

- Baroni, C., The Hell's Gate and Backstairs Passage ice shelves (Victoria Land, Antarctica), *Mem. Soc. Geol. It.*, **34**, 103-128, 1988.
- Baroni, C., Stenni, B., and Iacumin, P., Oxygen isotopic composition of ice samples from the Hell's Gate and Backstairs Passage ice shelves (Victoria Land, Antarctica): evidence for bottom freezing, *Mem. Soc. Geol. It.*, in press.
- Beck, N., and Munnich, K.O., Freezing of water: isotopic fractionation, *Chem. Geol.*, **70**, 168, 1988.
- Dietrich, G., Kalle, K., Krauss, W., and Siedler, G. (Eds.), *General oceanography*, 2nd ed., John Wiley, New York, 1980.
- Doake, C.S.M., Thermodynamics of the interaction between ice shelves and the sea, *Polar Record*, **18**, 37-41, 1976.
- Eicken, H., and Lange, M.A., Development and properties of sea ice in the coastal regime of the southeastern Weddell Sea, *J. Geophys. Res.*, **94**, 8193-8206, 1989.
- Friedman, I., Redfield, A.C., Schoen, B., and Harris, J., The variation of the deuterium content of natural waters in the hydrologic cycle, *Rev. Geophys.*, **2**, 177-189, 1964.
- Gow, A.L., and Epstein, S., On the use of stable isotopes to trace the origins of ice in a floating ice tongue, *J. Geophys. Res.*, **77**, 6552-6547, 1972.
- Gow, A.L., Ackley, S.F., Buck, K.R., and Golden, K.M., Physical and structural characteristics of Weddell Sea pack ice, *CRREL Report*, **87-4**, 70 pp., 1987.
- Jacobs, S.S., Gordon, A.L., and Ardal, J.L., Circulation and melting beneath the Ross Ice Shelf, *Science*, **203**, 439-443, 1979.
- Jacobs, S.S., Fairbanks, R.G., and Horibe, Y., Origin and evolution of water masses near the Antarctic continental margin: evidence from  $H_2^{18}O/H_2^{16}O$  ratios in seawater, *Oceanology of the Antarctic Continental Shelf*, *Antarct. Res. Ser.* AGU, Washington, D.C. **43**, 59-85, 1985.
- Jenkins, A., and Doake, C.S.M., Ice-ocean interaction on Ronne Ice Shelf, Antarctica, *J. Geophys. Res.*, **96**, 791-813, 1991.
- Lange, M.A., Basic properties of antarctic sea ice as revealed by textural analysis of ice cores, *Ann. Glaciol.*, **10**, 95-101, 1988.
- Lange, M.A., Ackley, S.F., and Wadhams, P., Development of sea ice in the Weddell Sea, *Ann. Glaciol.*, **12**, 92-96, 1989.
- Lewis, E.L., and Perkin, R.G., Ice pumps and their rates, *J. Geophys. Res.*, **91**, 11,756-11,762, 1986.
- Meese, D.A., The chemical and structural properties of sea ice in the Southern Beaufort Sea, *CRREL Rep.*, **89-25**, 134pp., 1989.
- Moser, H., and Stichler, W., Environmental isotopes in ice and snow, in *Handbook of environmental isotope geochemistry*, **1**, edited by Fritz, P., and Fontes, J.C., pp. 141-178, Elsevier, New York, 1980.
- Riley, J.P., and Skirrow, G., *Chemical Oceanography*, Academic Press, New York, 1965.
- Souchez, R., and Jouzel, J., On the isotopic composition in  $\delta D$  and  $\delta^{18}O$  of water and ice during freezing, *J. Glaciol.*, **30**, 369-372, 1984.
- Souchez, R., Tison, J.-L., and Jouzel, J., Freezing rate determination by the isotopic composition of the ice, *Geophys. Res. Lett.*, **14**, 599-602, 1987.
- Weeks, W.F., and Ackley, S.F., The growth, structure and properties of sea ice, in *The geophysics of sea ice*, edited by N. Untersteiner, pp. 9-164, Nato Asi Series, Plenum Press, New York, 1986.
- R. Lorrain, D. Ronveaux, R. Souchez and J.-L. Tison, University of Brussels, Faculty of Sciences - CP160, av. Roosevelt, 50, 1050 - Brussels, Belgium.
- M. Meneghel, University of Padova, Dept. of Geography, via del Santo, 26, 35123 - Padova, Italy.
- C. Baroni, Natural Science Museum of Brescia, via Ozanin, 4, 25100 - Brescia, Italy.
- A. Lozej and I. Tabacco, University of Milano, Dept. of Earth Sciences, via Cigognara, 7, 20100 - Milano, Italy.
- J. Jouzel, Centre d'Etudes Nucléaires de Saclay, F-91191, Gif-sur-Yvette - Cedex, France.

(Received: January 22, 1991)

Revised: March 19, 1991

Accepted: March 20, 1991



**Paper 6**

**Low Salinity Frazil Ice Generation at the Base of a Small Antarctic Ice Shelf**

**Authors**

**J.-L. Tison, D. Ronveaux, R. Lorrain**

**Journal**

**Antarctic Science, Vol. 5, n°3**

**Year**

**1993**



*Antarctic Science* 5 (3): 309–322 (1993)

## Low salinity frazil ice generation at the base of a small Antarctic ice shelf

J.-L. TISON, D. RONVEAUX<sup>1</sup> and R.D. LORRAIN

Département des Sciences de la Terre et de l'Environnement, CP160/03,  
Université Libre de Bruxelles, 50 Av. Franklin Roosevelt, B-1050 Bruxelles, Belgium

<sup>1</sup>Present address: Department of Geography, Villanova  
University, St. Augustine Liberal Arts Center, Villanova, PA 19085, USA

**Abstract:** Chemical, isotopic and crystallographic characteristics of marine ice formed at the base of the Hells Gate Ice Shelf, Terra Nova Bay, allow a better understanding of the dynamics of marine ice accretion under small ice shelves. The observed properties of the different types of frazil ice found in the area immediately behind the ice shelf front, result from a progressive evolution of the individual frazil ice crystals initially accreted at the base of the ice-shelf. Basal melting caused by the descending plumes of water masses at a temperature above their local freezing point, initiates partial melting of the frazil ice crystals. This dilutes the interstitial water and initiates chemical sorting effects as diffusion proceeds from the normal sea water in the free water column to the diluted interstitial water in the loose frazil layer. Different environmental conditions will result in contrasting properties. Where the subglacial interface is sculptured with domes or inverted channels, it will favour the accumulation of thick units of frazil ice, in a calm environment, that will be further protected from convection mixing over long time periods. This will result in the formation of orbicular frazil showing c-axes at random, strong dilution and important sorting effects. On the contrary, where no channel or dome exist, or where those are already filled with frazil, rectangular or wave-like banded frazil will form with properties showing interfacial streaming effects induced by water currents. Strong c-axes concentration at a single maximum, less dilution and weaker chemical sorting effects are then observed. These findings provide a tentative explanation for the apparent contradiction between the very low salinity levels detected in marine ice at the base of ice shelves and the comparatively minor salinity fluctuations in sea water profiles near ice shelves.

**Key words:** Hells Gate Ice Shelf, ice-ocean interface, frazil ice, cationic content, isotopic characteristics, ice crystallography

Received 1 September 1992, accepted 26 January 1993

### Introduction

Recent studies of marine ice (continental ice/ocean interface) from the base of Antarctic ice shelves, have indicated very low salinity levels compared to sea ice (atmosphere/ocean interface): for example at the Filchner-Ronne Ice Shelf (Oerter *et al.* 1991) and Hells Gate Ice Shelf (Souchez *et al.* 1991). In the latter paper, it has been shown on isotopic and chemical grounds that frazil ice forming under the seaward part of the Hells Gate Ice Shelf (HGIS) is produced by the freezing of meltwater from marine ice located upstream. This frazil ice has a very low salinity, probably resulting from the freezing of water with salinity levels of an order of magnitude less than undiluted sea water. However, such low salinities have never been detected by large scale oceanographic measurements. We need a better understanding of the processes occurring at the ice-ocean interface, from the production of the parent water to the solidification of the frazil ice. This paper describes detailed isotopic and chemical characteristics of the different frazil ice types accreted at the base of the HGIS and suggests mechanisms to account for the low salinity of this frazil ice.

### Site description

The Hells Gate Ice Shelf is a part of the Nansen Ice Sheet reaching the sea in Terra Nova Bay near Cape Russell (Fig. 1). It extends from north to south for 16.6 km with a maximum width of 9.8 km between 74° 44'/74° 53'S and 163° 36'/163° 57' E. It is composed of three main sections (western, central, eastern) separated by two medial moraines stretching from north to south. Echo sounding profiles, performed about 1.5 km inland from the ice front, showed a maximum ice shelf thickness between 60 and 70 m (Souchez *et al.* 1991). Between the western and central parts (the eastern part will not be considered here) there is a major shear zone characterized by two ridges of debris cones containing rock fragments, shells and worm tubes. As pointed out by Baroni (1988), the debris was incorporated into the ice by bottom freezing of sea water around Vegetation Island. This small rock outcrop acts as a pinning point of the ice shelf and is situated near its upstream boundary (slightly to the north of the upper limit of Fig. 1). Baroni (1988) gave an uncalibrated <sup>14</sup>C age of 2495 ± 160 years BP (GX-14084) for the older shells reaching the surface of the HGIS. This allowed him



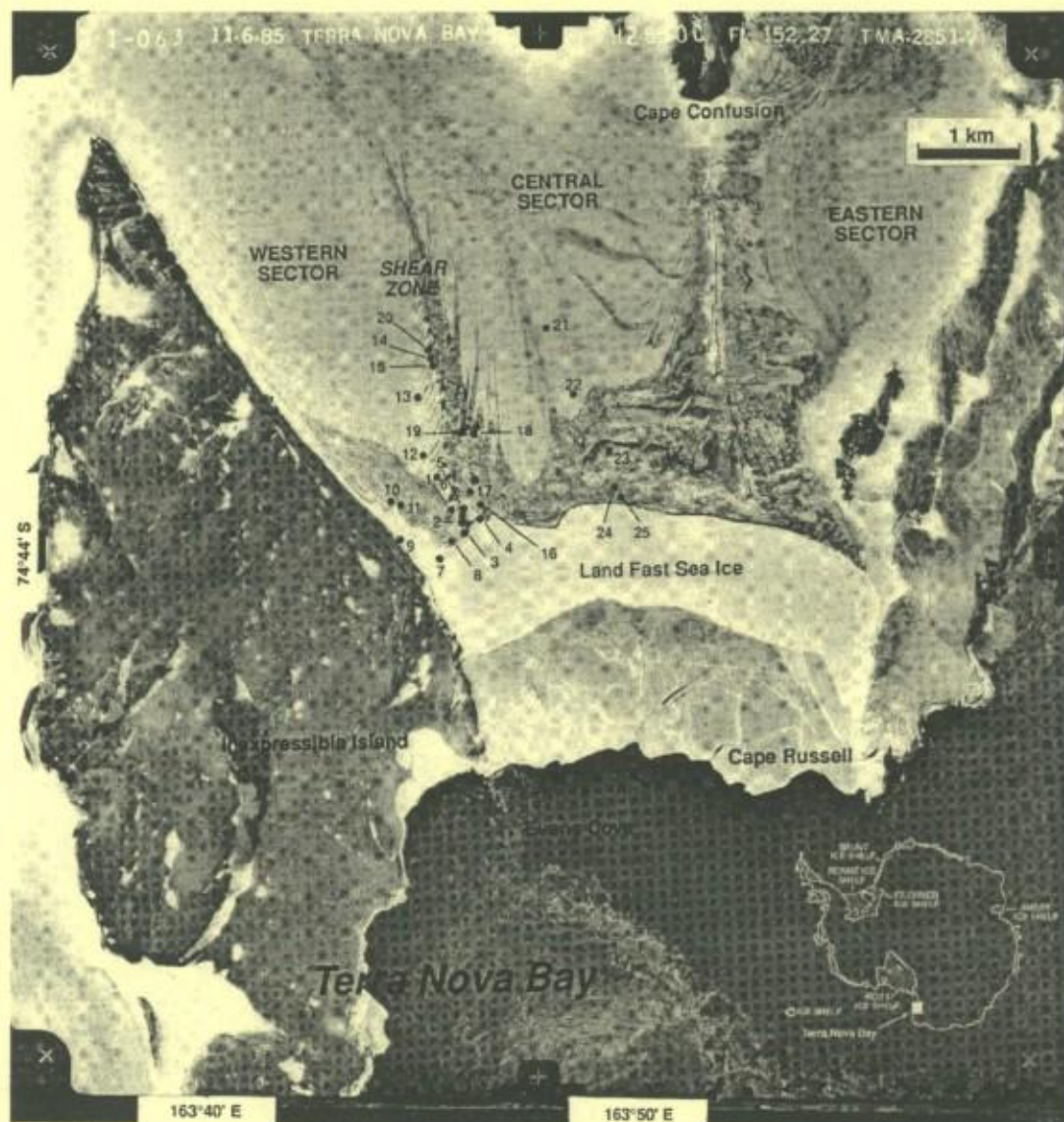


Fig. 1. Vertical aerial photograph of the area of Hells Gate Ice Shelf examined in the present study. The dots show the location of the ice cores analysed (Photo 1-063 11-6-85 Terra Nova Bay H2 8000 FL 152-27 TMA 2851-V).

to propose an ablation rate of about  $10 \text{ cm y}^{-1}$  due to very strong and frequent katabatic winds blowing across the ice from the polar plateau. As a result of this ablation, marine ice progressively replaces glacier ice downstream of Vegetation Island as confirmed by a  $\delta^{18}\text{O}$  shift from strongly negative to positive values (Baroni *et al.* 1991, Souchez *et al.* 1991). The boundary between continental and marine ice also appears clearly at the surface of HGIS (see Fig. 1) because of their respective clear-cut tones in the photograph, i.e., light-grey for continental ice and dark-grey for marine ice.

Two Italian oceanographic expeditions (1987–1988 and 1990) collected temperature and salinity data in the Terra Nova Bay area (Boldrin & Stocchino 1990). These data show the water of the Bay mostly consists of High Salinity Shelf Water

overlain by Antarctic Surface Water. The latter layer, less than 100 m deep, is generally warmer, fresher and more variable with respect to thermal and compositional properties. During the brief summer, this water will interact with the front and underside of HGIS, with temperatures reaching  $-0.5^\circ\text{C}$  between 20 and 50 m depth.

#### Sampling procedure and analytical treatment

As described above, marine ice initially accreted at the base of the HGIS now appears at its surface. This transfer occurred along an inclined surface due to an upward vertical velocity component derived from the surface ablation caused by the katabatic winds. To examine this situation a series of shallow



## FRAZIL ICE GENERATION

311

ice cores, distributed along two longitudinal lines (in the western and central sectors respectively), from the continental ice limit to the ice shelf edge, was taken in place of a complete vertical drilling to the bottom at a single location. Besides the fact that it is obviously easier to handle logistically, this sampling technique allows a better perception of the "cross-stream" spatial variability without losing the main spatio-temporal variability obtainable by drilling to the bottom at a given location (at least in the peculiar flow regime described above and if the samples are adequately chosen). However, it does not provide informations on the vertical variability of physical parameters such as the ice temperature, through the entire ice shelf thickness.

Twenty five ice cores, 1–1.5 m long, were retrieved from the HGIS (Fig. 1) with a CRREL 3 in. ice auger, transferred to plastic bags and stored below  $-20^{\circ}\text{C}$  until they were used in Brussels. The upper 50 cm of each ice core was discarded in order to avoid surficial effects. Vertical thin sections were made along the total length of each core to observe the different ice textures and to guide the isotopic sampling. After removing 0.5 cm of the outside surface of each ice core, a 1 cm thick vertical slice was cut with a clean band saw (tested as not contaminated by the major cations of interest) from along the entire length of each core, and each vertical slice was then subdivided into horizontal pieces at 0.5 cm intervals. These were allowed to melt in polyethylene tubes and were analysed for Na, K, Mg and Ca with a Varian-SpectraAA 300 atomic absorption spectrophotometer. Samples also were taken from the ice cores for co-isotopic analyses of deuterium ( $\delta\text{D}$ ) and oxygen-18 ( $\delta^{18}\text{O}$ ). The sampling spots were selected after a careful examination of the thin sections between crossed polarizers and on the basis of the concentrations of dissolved solutes obtained by the chemical analyses. Collecting the small amounts of ice needed for the mass spectrometer measurements (0.3 ml) was facilitated by use of a microtome. Where the Na content of the ice was above 150 ppm, the samples were distilled under vacuum prior to isotopic analysis by a procedure proven to conserve the isotopic signal. Thirty samples of artificial sea water, produced by adding salt to distilled water of known isotopic composition, were run through the distillation apparatus, and the isotopic composition of the distillate was found to be identical in the limits of the precision of the mass-spectrometer measurements to the initial value. The measurements were performed at the Nuclear Research Center of Saclay (France). HDO and  $\text{H}_2^{18}\text{O}$  concentrations are given in  $\delta$  units versus V.S.M.O.W. (Vienna Standard Mean Ocean Water) expressed in per mil. The accuracy of the measurements is  $\pm 0.5\text{‰}$  in  $\delta\text{D}$  and  $\pm 0.1\text{‰}$  in  $\delta^{18}\text{O}$ .

## Results and discussion

### Frazil ice characteristics

Fig. 2 summarizes the overall characteristics of the various marine ice types from HGIS. Most of the data used for making Fig. 2 are listed in Ronveaux (1992). Continental ice from

inland and fast sea ice from the front of the ice shelf are also briefly described for comparison. All marine ice samples from the 25 cores fall into four major textural categories, with contrasted frequencies of occurrence: columnar ice represents 2.5% of the total length of marine ice, 4.8% is platelet ice, 49.4% is orbicular granular ice, and 43.3% banded granular ice.

Columnar ice (a texture typical of congelation ice formed by the progression of a freezing front in a liquid water reservoir) and platelet ice are easily recognized by distinctive differences in their textural characteristics (Weeks & Ackley 1986, Lange 1988). They are a minor component of the Hells Gate Ice Shelf's environment. These two ice types, as underlined by Souchez *et al.* (1991), are intimately associated and spatially located at the boundary of the continental glacier ice (core 6 on Fig. 1). The same authors presented the isotopic values of marine ice from HGIS on a  $\delta\text{D}/\delta^{18}\text{O}$  diagram (their fig. 2) where congelation ice is situated in an intermediate position between sea water samples from the front of the ice-shelf (20–200 m depth) and frazil ice samples. Platelet ice does not differ significantly from the other frazil ice types in this environment. This is illustrated by the isotopic ranges given in Fig. 2. Both ice types show mean salinity values just below  $1.5\text{‰}$ , comparable to the lower values observed at the base of a first-year sea ice cover in Breid Bay (Tison & Haren 1989) and slightly lower than the minimum values (Gow *et al.* 1987) in the Weddell Sea ice floes. Low salinity values are to be expected when marine congelation ice forms under a thick continental ice cover at very slow freezing rates, and with a maximum salt rejection by the growing ice. The three last lines of Fig. 2 give the value of the K/Mg ratio (K and Mg being expressed in  $\text{meq l}^{-1}$  for charge and weight compatibility). This ratio has been chosen since it is unlikely to be affected by salt precipitation in the HGIS environment. Indeed, Richardson (1976), in his study of the phase relations in sea ice as a function of temperature, indicates that  $\text{CaCO}_3 \cdot 6\text{H}_2\text{O}$  is the first salt to precipitate from sea water at a temperature close to the freezing point and that  $\text{Na}_2\text{SO}_4 \cdot 10\text{H}_2\text{O}$  and  $\text{CaSO}_4 \cdot 2\text{H}_2\text{O}$  soon follow, at temperatures of  $-8^{\circ}\text{C}$  and  $-10^{\circ}\text{C}$  respectively. Marine ice subjected to such a range of temperatures, as is probably the case for the HGIS when it is progressively brought up to the surface by ablation, is likely to show a greater variability in the ratios of elements forming salts under freezing conditions. Following Richardson (1976), concentrations in K and Mg ions in sea water at sub-freezing temperatures, under quasi-equilibrium conditions, do not change until the temperature falls to  $-34^{\circ}\text{C}$ . This is confirmed by the observations of Cragin *et al.* (1986) in brine layers infiltrating the McMurdo Ice Shelf and progressively submitted to lower temperatures where, for Na/Mg as well as for Na/K, there is a good agreement between these ratios in sea water and in the ice samples. However, Meese (1989, 1990) showed from dilution curves for sea ice from southern Beaufort Sea that Mg is slightly enriched (1–2%) with regards to sea water and K slightly depleted (1–2%). These slight fluctuations, attributed to precipitation of Mg and to differential mobility (with regard to Cl) of K, will possibly explain a slight decrease in the K/Mg ratio. This ratio in



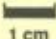




ICE TYPES	GLACIER ICE	FAST ICE		CONGELATION ▲	PLATELET △
		CONGE- LATION ●	FRAZIL ○		
CORE # (Fig. 1)	5,12,13,21,22,6 Top	7,9	7,9	6-Middle	6-Bottom
CRYSTAL SIZE	1-2 cm	l = 2-3 cm w = 0.5-1 cm	0.2-0.5 cm	l = 4-5 cm w = 1.5-2 cm	l = 2-4 cm w = 0.5-1 cm
TEXTURE 					
ICE FABRIC (vertical plane)	1 strong maximum near the shear zone (core 5) to small girdle or weaker maximum away from the shear zone (12, 21, 22)	—	—	—	—
IN- CLU- SION- S	Bubbles	YES : mainly spherical (0.5 mm in diameter), sometimes tubular according to flow. Intracrystalline and at grain boundaries.	YES : associated with brines inclusions	YES	YES : associated with brines inclusions
	Particulate matter	NO	NO	NO	NO
ISOTO- PES	# of samples	8	3	4	3
	$\delta D$ (‰) max min	-150.9 -245.0	11.6 11.0	16.0 9.8	23.3 16.1
	$\delta^{18}O$ (‰) max min	-19.76 -31.71	1.74 1.14	2.02 1.14	2.51 2.08
	# of samples mean salinity (‰)	—	11 1.33	19 1.19	27 1.35
	Na (ppm) max min mean	—	508.50 273.50 407.99	523.00 202.10 366.69	589.50 197.60 415.94
CHE- MIS- TRY	K (ppm) max min mean	—	17.32 8.78 12.91	14.72 8.41 11.63	24.08 6.77 17.95
	Ca (ppm) max min mean	—	15.95 6.74 11.24	16.29 6.02 11.38	21.76 8.15 17.09
	Mg (ppm) max min mean	—	52.10 25.55 37.85	45.65 22.60 34.32	70.80 18.60 51.32
	$\Sigma 4$ (meq l <sup>-1</sup> ) max min mean	—	27.64 14.56 21.75	27.41 11.66 19.64	30.77 14.87 26.16
	K/Mg max min mean	—	0.109 0.102 0.106	0.116 0.100 0.106	0.130 0.099 0.110
					0.111 0.089 0.099

Fig. 2. Textural, ice fabric, isotopic and chemical characteristics of the different ice types studied. The symbols representing the different ice types in the top row of the figure are also used in Fig. 3.  $\Sigma 4$  is used for the sum of the four cations in meq l<sup>-1</sup> ( $\Sigma 4 = [Na] + [K] + [Ca] + [Mg]$ ).



## FRAZIL ICE GENERATION

313







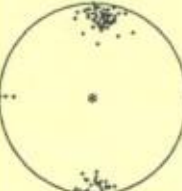
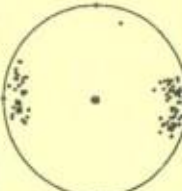
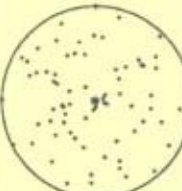
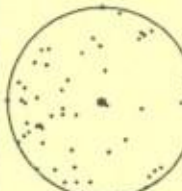
MARINE ICE				
FRAZIL BANDED ■ RECTANGULAR	FRAZIL BANDED □ WAVE-LIKE	FRAZIL ORBICULAR ● FINE	FRAZIL ORBICULAR ○ MEDIUM	FRAZIL ORBICULAR + COARSE
Part of : 2,3,24,25	Part of : 1,2,3,16,17,25	4 + Part of : 24	18 + Part of : 24	23 + Part of : 1,2,3,16,17,24,25
l = 0.2-0.4 cm w = 0.05-0.2 cm	l = 0.1-0.4 cm w = 0.05-0.1 cm	0.1-0.2 cm	0.2-0.7 cm	0.7-2 cm
				
				
CORE 2	CORE 24	CORE 4	CORE 18	CORE 23
NO	YES : few	NO	NO	NO
NO	NO	YES FOR CORE 4 : - sponge tests - echinoderm spicules - crustaceous faeces showing peritrophic membrane	YES FOR CORE 18 : ctr core 4 + worm tubes fragments	NO
23 19.9 16.7  2.76 1.86	25 22.1 15.0  3.02 1.64	13 24.5 16.0  3.26 1.82	10 21.9 15.5  3.19 1.90	7 24.3 15.7  2.92 2.12
176 0.19 235.80 7.34 57.13 9.33 0.17 2.24 4.34 0.15 1.70 19.52 0.24 6.29 9.68 0.36 2.79 0.289 0.056 0.119	173 0.36 801.00 17.50 109.79 26.64 0.60 3.85 21.21 0.58 2.66 72.10 1.07 10.79 36.35 0.91 4.20 0.256 0.046 0.114	95 0.03 35.42 5.35 10.69 1.20 0.17 0.34 1.50 0.06 0.51 4.38 0.27 0.86 1.80 0.11 0.54 0.259 0.063 0.162	136 0.03 52.85 2.76 8.81 3.61 0.05 0.34 2.48 0.01 0.41 8.68 0.03 0.74 3.22 0.13 0.49 0.628 0.064 0.316	163 0.14 229.50 1.74 41.65 5.39 0.10 1.60 6.77 0.01 1.41 15.84 0.03 4.93 11.19 0.09 2.36 1.287 0.058 0.324

Fig. 2.



congelation ice (0.110) and platelet ice (0.099) from HGIS is close to the one in standard sea water (0.096), thereby confirming the absence of significant fractionation with regard to sea water for these ice types. This is also the case for the congelation (0.106) and frazil ice (0.106) in fast ice formed in front of the ice shelf. The contrast between orbicular and banded granular ice (Fig. 2) is based on textural characteristics following the terminology proposed respectively by Lange (1990) and Gow *et al.* (1987) (Appendix 1). According to previous studies (Weeks & Ackley 1986, Gow *et al.* 1987) a granular ice texture may either result from the transformation of the snow cover at the sea-ice surface, or from the accretion of loose ice crystals initially formed in the water column by various processes and subsequently floating up to aggregate at the ocean-atmosphere interface or under a pre-existing ice-water interface. Since the first genetic process is precluded, for obvious reasons in the case of marine ice, we will use in the following the genetic term of frazil ice for the granular ice at HGIS. Orbicular frazil consists of crystals, roughly isometric and convex, with rounded grain boundaries. It occurs in three major size classes at HGIS (fine = 0.1–0.2 cm, medium = 0.2–0.7 cm and coarse = 0.7–2 cm). Banded frazil shows small rectangular crystals 0.2–0.4 cm in length and 0.05–0.2 cm in width, more or less aligned parallel to the local ice-water interface. Under crossed polarizers, some samples display a "wave-like" texture underlined by areas of uniform colours indicating a strong c-axes concentration in a single maximum. Occasionally, the crystals are arranged in a vortex fashion (the alignment parallel to the ice-water interface is locally disturbed by crystals organized in a circular arrangement). Generally, the textural contrast between orbicular and banded frazil ice is reinforced by the ice-fabric, the dirt content, and the major ions chemistry. The peculiar case of the fine orbicular frazil (e.g. core 4) will be discussed later. Banded frazil shows strong c-axes concentrations while in orbicular frazil c-axes are random. Particulate matter, mainly organic, only occurs in the orbicular frazil, and the mean chemical content in major cations of this ice type is lower than for the banded frazil. Finally, while the K/Mg ratio in both the banded and the orbicular frazil show evidence of chemical sorting effects, these obviously are stronger in the latter ice type.

#### *Evidence for dilution at the ice-ocean interface*

In interpreting the chemical and isotopic results from frazil ice, one must keep in mind that they are in fact the integration of a sequence of three processes:

- 1) formation of individual ice crystals in the water column under favourable temperature/salinity conditions
- 2) accretion of loose frazil crystals at the base of the ice shelf
- 3) consolidation of the accreted loose frazil to form a solid body of ice, under a temperature gradient.

During these three processes, the isotopic and chemical signals will be more or less affected, depending on variables such as the

characteristics of the parent water for the individual frazil ice crystals, the growth rate of the individual crystals, the characteristics of the host waters where the ice crystals accrete, the porosity of the loose frazil (porosity is used here in the meaning of White (1991), i.e., the % of water present in a volume of saturated frazil ice), the freezing rate of the accreted loose frazil and the possible post- or syn-genetic desalination. Uncertainties on the values of these parameters make it difficult to infer the characteristics of the parent and host waters from the observed chemical and isotopic signals of the consolidated frazil ice. However, hypotheses can be suggested for some of these parameters:

- a) Desalination processes in sea ice have been extensively described by several authors (Weeks & Ackley 1986, Cox & Weeks 1986, Cox & Weeks 1988). Formulations have been proposed to estimate desalination rates through either of the three major mechanisms involved: brine pocket migration, brine expulsion and brine drainage. Since these equations require the knowledge of parameters such as the temperature profile along the ice shelf thickness or the brine volume and salinity in the marine ice, the quantification of similar processes was not possible at HGIS. However, such an attempt has recently been made for the marine ice observed at the base of the Filchner-Ronne Ice Shelf where these data were available (Eicken *et al.*, personal communication 1992), and it can be shown by these authors that the calculated desalination rates are several orders of magnitude too low to explain the salinity values of the marine ice they observed. Although the Filchner-Ronne Ice Shelf is considerably thicker than HGIS at the B13 sampling site (239 m; Oerter *et al.* 1992), these results seem to indicate that the active desalination processes described in sea ice must be of minor importance for marine ice several tens of meters thick. Furthermore, the tight packing of the ice crystals in frazil ice from HGIS (thin sections of Fig. 2) and the lack of any visible gaseous or liquid inclusions (brine layers, brine pockets) or of cracking disruption, do not support the existence of an efficient process of brine pocket migration or brine expulsion. A process similar to brine drainage must however probably occur during the consolidation phase of the accreted loose frazil. The rejection of salts as frazil consolidates in the upper layers will produce denser interstitial waters, possibly initiating a convective process that will bring the low salinity water from the basal layers (where it originates) to the interior parts where ice growth takes place.
- b) A narrow range of values for the porosity of a loose frazil ice mixture at or near the water surface can be obtained from various sources. Laboratory investigations on freshwater frazil ice (White 1991, Andersson & Daly 1992), where porosities were calculated from the measured weight of a known volume of saturated frazil ice for 20 samples measuring 0.3 dm<sup>3</sup>, gave average values of 67±13% (Andersson & Daly 1992). Similar measurements in natural frazil ice



## FRAZIL ICE GENERATION

315

ranged between 43% and 48% and were close to those deduced from borehole dilution tests ( $43.6 \pm 3.2\%$ ; White 1991). Salinity can also be used as an indirect method to determine frazil ice porosity. For the simple experiments described in the next section, individual dry distilled ice crystals of various sizes were poured into an experimental reservoir of natural sea water until saturation was achieved. Since the individual ice crystals can be considered as pure ice, the ratio between the salinity of the sea water and the salinity of the mixture provides an estimate of the porosity of the latter. Porosity values between 43% (fine submillimetre sized crystals) and 52% (coarse centimetre sized crystals) were obtained. A similar approach can be used with natural samples: freshly formed pancake ice from the Weddell Sea studied by Eicken & Lange (1989) show maximum salinities of about  $15\text{‰}$  which, if compared to a normal sea water salinity of  $34.8\text{‰}$ , gives a minimum porosity of 43.1%. However, some buoyancy pressure related effect should be considered in the case of frazil occurring under the ice shelf at some depth, the upper layers being mechanically "squeezed" by the lower layers. Since this effect is difficult to quantify, especially if the total thickness of frazil ice accreted is not known, a value of 40% porosity will be used, bearing in mind that this value might eventually prove to be an overestimate.

- c) The freezing rate of the accreted loose frazil must be quite similar to that of congelation ice formed under comparable ice shelf thicknesses. Since it is very slow, isotopic and chemical fractionation in the freezing host water must occur very close to equilibrium. The equilibrium fractionation coefficients for  $\delta D$  and  $\delta^{18}O$  are well documented, and usually taken as  $\alpha = 1.0208$  and  $\beta = 1.003$  respectively, although the possibility of a  $2\text{‰}$  higher  $\alpha$  value might exist for platelet ice formed in high salinity sea water (Beck & Munnich 1988). Values for the effective chemical distribution coefficient ( $k_{\text{eff}}$  = concentration in the ice/concentration in the liquid away from the interface) are found in the Antarctic literature on sea ice (Gow *et al.* 1987, Souchez *et al.* 1988, Lange 1988). The lowest one ( $k_{\text{eff}} = 0.04$ ) was observed (Souchez *et al.* 1988) in congelation ice at the bottom of a first year sea ice cover in Breid Bay (Princess Ragnhild Coast) and can thus be considered as the closest value to the thermodynamic equilibrium coefficient. Using the mean salinity of our congelation ice at the base of HGIS ( $S_{\text{ice}} = 1.35\text{‰}$ ), an effective distribution coefficient of 0.04 can be calculated. However, as discussed below, it should be noted that these values of  $k$  are only valid for congelation ice formed in undiluted sea water since, as indicated by Gross (1968), the value of  $k_0$  (equilibrium distribution coefficient) can differ strongly from dilute solution to sea water due to different interface morphologies.
- d) The freezing rate of individual frazil ice crystals is much more difficult to estimate. Indeed, the validity of isotopic equilibrium fractionation for stable isotopes of oxygen and

hydrogen is probably strongly dependent on the degree of supercooling. To our knowledge, no experimental or field data are available on this subject for frazil formed by double diffusion or supercooling due to adiabatic upward movement of sea water. However, the situation is different for the major cations since individual crystals growing from a liquid reservoir are believed to be made of pure ice, impurities being concentrated at grain boundaries (Souchez & Lorrain 1991). Thus, one may consider that the chemical signal in the resulting unconsolidated frazil ice is independent of the chemical characteristics of the parent water in which the individual crystals originate, and exclusively reflects the characteristics of the host water where the crystals accrete.

Using a porosity of 40%, an equilibrium chemical distribution coefficient ( $k_0$ ) of 0.04, and the observed frazil ice salinities of Hells Gate, it is possible to reconstruct the salinity of the host water by studying the salinity of the different frazil ice types [ $S_{\text{HOST WATER}} = S_{\text{FRAZIL ICE}} / (k_{\text{eff}} \times \text{porosity})$ ]. This salinity increases from  $1.9\text{‰}$  for the host water derived from the mean salinity of fine and medium orbicular frazil ice to  $8.8\text{‰}$  for the coarse orbicular,  $12\text{‰}$  for the banded rectangular and  $22.5\text{‰}$  for the banded wave-like frazil. Such salinities have never been observed in large scale oceanographic salinity measurements below or in front of ice-shelves in the Terra Nova Bay (Boldrin & Stocchino 1990). Thermodynamic considerations suggest that the salinity values for the interstitial water in the loose orbicular frazil are already underestimated. Indeed, if, following Doake (1976), we consider the phase diagram relating temperature to salt concentration of a system consisting of salt, water and ice, and if we also consider that the system is allowed to reach equilibrium, a salinity of  $1.9\text{‰}$  for the solution in contact with the ice is only possible for water temperatures of the order of  $-0.1^\circ\text{C}$ . As indicated before, the maximum water temperatures observed in front of the ice shelf, at depths compatible with its base, are  $-0.5^\circ\text{C}$ . In the phase diagram, such a temperature value corresponds to a salinity of about  $9\text{‰}$  on the liquidus. Reducing drastically the porosity of the loose frazil to half its value, to emphasize the potential squeezing effect at depth, would still underestimate by 50% the minimum possible salinity for the host water of the fine and medium grained orbicular frazil. On the other hand, to obtain a salinity of  $9\text{‰}$  for this host water, using a porosity of 40%, one must use a  $k_0$  value of 0.008 in the calculations. This lower value of  $k_0$  is comparable to the one obtained by Gross *et al.* (1977) in experiments to determine solute distribution at the ice-water phase boundary. Indeed, a  $k_{\text{eff}}$  of 0.004 was observed in a monosaline solution of NaCl with a concentration of about  $10\text{‰}$  ( $1.8 \cdot 10^{-1}\text{M}$ ). The underestimation of the host water salinity for the orbicular frazil is thus most probably due to the combination of two factors: a possible lower porosity due to frazil ice compaction (at least in its higher levels) and the dependency of the  $k_0$  value on the global salinity of the freezing solution. Chemical sorting effects, that cannot be



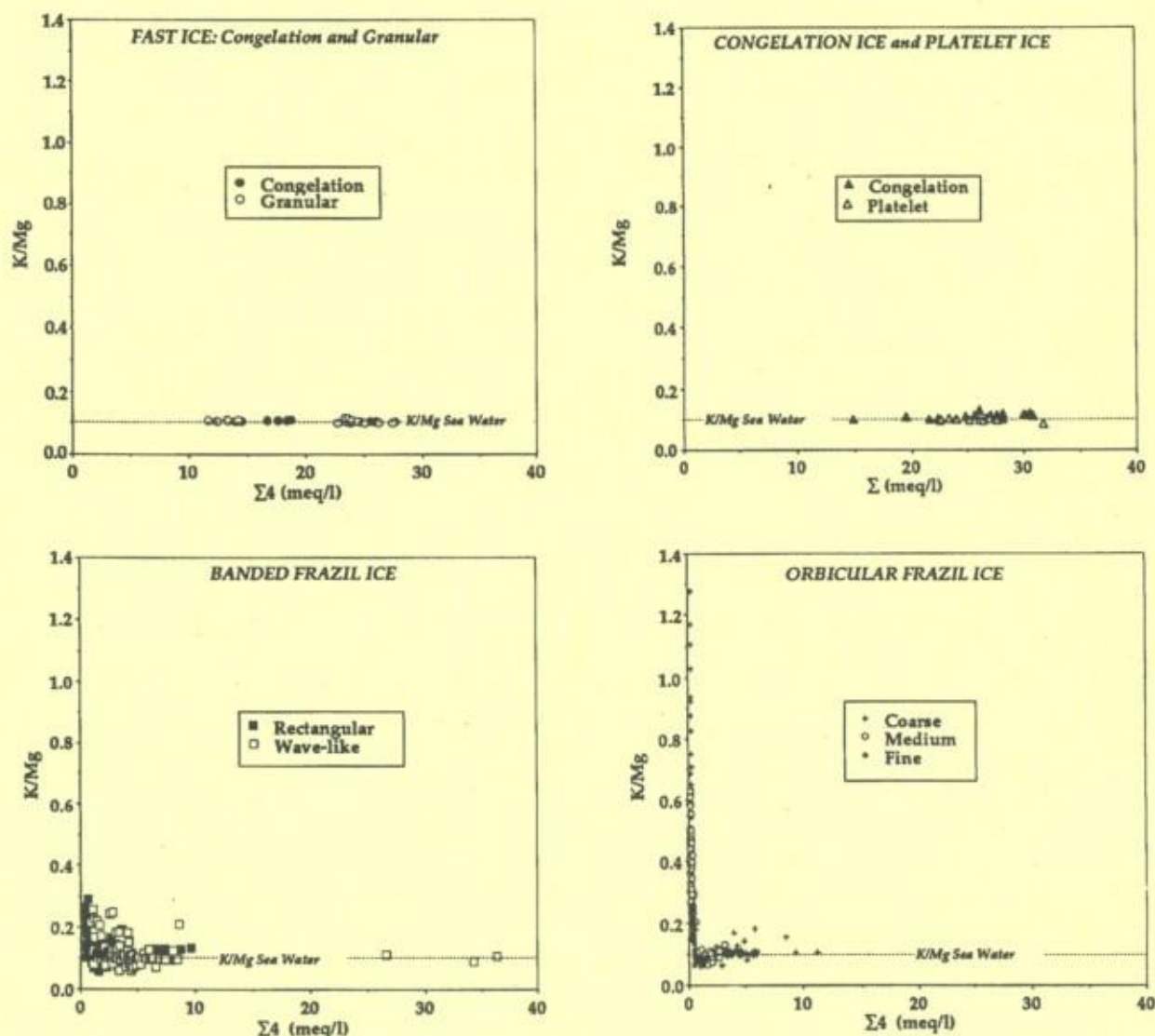


Fig. 3. Relationship between the K/Mg ratio (calculated in  $\text{meq l}^{-1}$ ) and the sum of the four cations in  $\text{meq l}^{-1}$  ( $\Sigma 4 = [\text{Na}] + [\text{K}] + [\text{Ca}] + [\text{Mg}]$ ) for different ice types from Hells Gate Ice Shelf.

explained by simple mechanical means, favour the latter process.

The scientific rationale used to determine the host water properties from the chemical signal cannot be followed using the isotopic characteristics of frazil ice since, with a porosity of 40%, the observed values will be a combination of fractionation processes both during the genesis of individual crystal (poorly known) and during the consolidation of the loose matrix. A considerable amount of frazil samples show isotopic values which are higher than the one obtained by applying the maximum possible fractionation shift of  $3\text{‰}$  (Souchez *et al.* 1991) in  $\delta^{18}\text{O}$  to the local parent sea water value of  $-0.6\text{‰}$ . Indeed, as seen in Fig. 2, the maximum values in  $\delta^{18}\text{O}$  for all frazil ice types are higher than  $2.4\text{‰}$ . This implies that, at least for the samples showing values higher than  $2.4\text{‰}$ , dilution by marine ice melt

water, with an isotopic signal more positive than normal sea water, has occurred. Moreover, even for the samples with a  $\delta^{18}\text{O}$  lower than  $2.4\text{‰}$ , dilution by melt water from marine ice must be the more frequent case. The large dilution factors of sea water by meltwater, deduced from the salinity data discussed above, preclude glacier ice as a source since the very negative  $\delta^{18}\text{O}$  values of the latter would result in much lower  $\delta^{18}\text{O}$  values in frazil ice than those observed (see Fig. 2).

#### Behaviour of the K/Mg ratio

The apparent contradiction between the chemical characteristics of frazil ice and the results of large scale oceanographic profiles suggests that syn- or post-genetic processes affect the characteristics of the frazil ice. The



## 317

Figure 1 is a line graph showing the K/Mg ratio versus depth (cm) for two cores, core 18 and core 23, from the Great Salt Lake. The y-axis represents depth below the top 50 cm, ranging from 0 to 40 cm. The x-axis represents the K/Mg ratio, ranging from 0.0 to 1.2. Core 18 is represented by open circles and core 23 by solid circles. A vertical dashed line at approximately 0.15 K/Mg is labeled 'sea water'. Both cores show a general increase in K/Mg ratio with depth, with core 23 generally having higher K/Mg values than core 18 in the upper 20 cm.

[illegible]



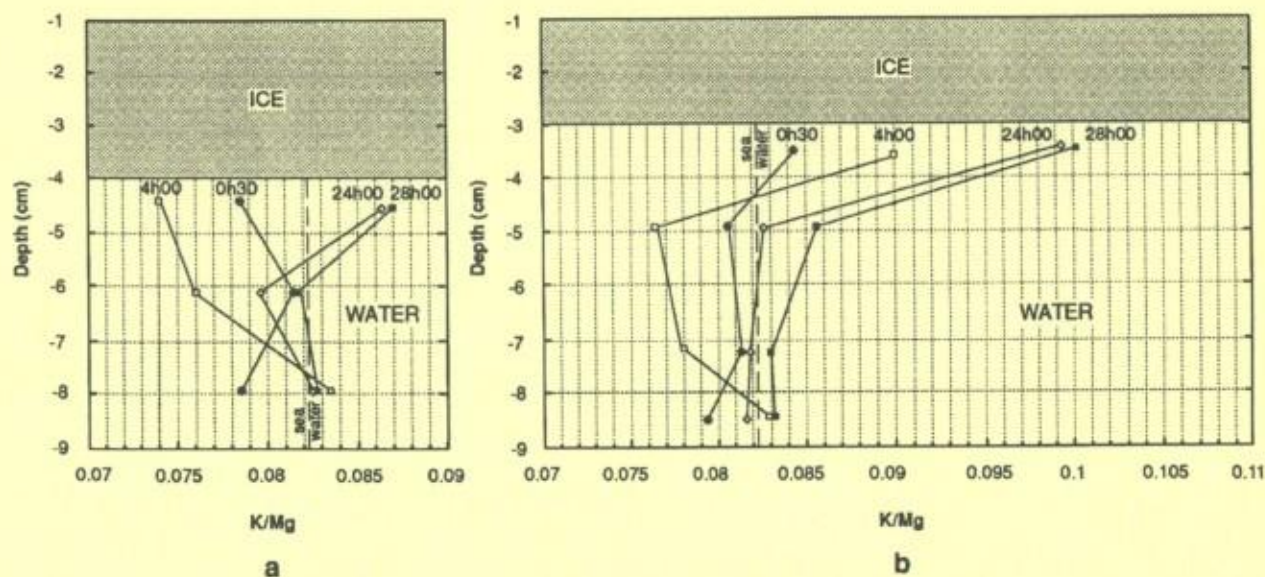


Fig. 5. Evolution of the K/Mg ratio with depth during the experiment of the melting fresh water "iceberg" floating on sea water (see text for explanation): a. profile out of the inverted channel; b. profile in and just below the inverted channel.

a porous glass diaphragm and after three days K/Mg ratio could attain more than 200% of its original value in sea water. It is worth noting that, outside the channel in the experiment shown in Fig. 5a, there is an initial lowering of the K/Mg ratio as diffusion occurs from the flat interface area to the inverted channel. Later on, diffusion from the bottom of the reservoir increases the K/Mg ratio close to the flat interface above the standard sea water value.

**Freezing of a loose frazil ice matrix.** Another set of four experiments were performed, in the same cold room, where individual freshwater ice crystals were poured to saturation into a sea water reservoir at negative temperature. The mixture was then frozen from top to bottom, using a metallic plate cooled with the aid of an ethanol temperature bath. The results of two of these experiments are shown in Fig. 6a & b, respectively, for fine grained (submillimeter sized crystals—porosity 43%) and coarse grained (centimetre sized crystals—porosity 51.6%) artificial frazil. In both experiments, ice crystals, sea water and the cold room were at  $-1^{\circ}\text{C}$ . Global salinities and K/Mg ratios are shown in each diagram. Freezing rates varied between  $2.8 \cdot 10^{-6} \text{ m sec}^{-1}$  and  $0.5 \cdot 10^{-6} \text{ m sec}^{-1}$  for the fine grained experiment and between  $4.2 \cdot 10^{-6} \text{ m sec}^{-1}$  and  $0.7 \cdot 10^{-6} \text{ m sec}^{-1}$  for the coarse grained. Both experiments give similar results. Three zones are clearly seen along the vertical (I=0–1  $10^{-2} \text{ m}$ ; II=1–5 or 6  $10^{-2} \text{ m}$ ; III=below 5 or 6  $10^{-2} \text{ m}$ ). In the top 1 cm, salinity abruptly decreases from values a few ‰ lower than the initial sea water to values between 5‰ and 8‰, depending on the grain size. This is probably the expression of the extremely rapid freezing rate allowing poor cationic expulsion from the solidifying loose ice matrix. The K/Mg ratio falls from values

nearly 50% higher than its value in sea water to values slightly lower than those in sea water. The probable explanation for this is the existence of a melting stage when the ice crystals were poured into the sea water, which was about  $0.9^{\circ}\text{C}$  above its freezing point. This would have resulted in selective diffusion of K and Mg from the main part of the reservoir to the top, where less dense water accumulates. Between 1 and 6 cm, salinity stabilizes around 9.5‰ in the fine grained matrix and 6‰ in the coarse grained. It can be seen in Fig. 6a & b that, for freezing rates lower than  $2.810^{-6} \text{ m sec}^{-1}$ , the K/Mg ratio drops slightly below the one of the host sea water. Since the cold wave did not reach depths greater than 6 cm at the end of the experiment, the matrix was still rather loose and, therefore, the K/Mg ratio returns to its initial value at the bottom of the reservoir. These experiments have shown that selective diffusion from normal sea water to fresh meltwater produced at the interface will favour an increase of the K/Mg ratio near this interface. Diluted waters may converge in inverted depressions at the ice-ocean interface. In the case where such irregularities affect the interface, flat undisturbed areas could temporarily show K/Mg ratios lower than standard sea water, providing an alternative explanation to the precipitation sorting effect discussed earlier. Experimental observations in a closed system, and after periods of a few days, indicate a maximum increase of the ratio of about 200%. On the contrary, freezing of a loose matrix of individual ice crystals in sea water will not favour the increase of the K/Mg ratio and will even lower it slightly for freezing rates below  $2 \cdot 10^{-6} \text{ m sec}^{-1}$ . This probably reflects the progressively overwhelming effect of the faster diffusion of K, from the enriched boundary layer at the interface to the bulk reservoir, as the freezing rate decreases.



## FRAZIL ICE GENERATION

319

*"Orbicular" versus "banded" frazil*

Careful examination of Fig. 2 demonstrates the obvious textural contrast between orbicular frazil and banded frazil accompanied by a contrast of the ice fabric, debris content and chemistry. It is therefore tempting to see if these characteristics signal different generation and evolution processes.

Banded frazil ice show strong c-axes concentrations at a maximum perpendicular to the crystal elongation, which is subhorizontal in the core. This suggests crystal growth in interface flowing conditions where differential shear favours rotation of the crystals parallel to the local ice-ocean interface. Local vortex structures in the wave-like frazil also suggest a transition from laminar to turbulent flow on some occasions. On isotopic grounds, the host water where the frazil accretes must result from partial dilution of normal sea water by marine ice melt. Souchez *et al.* (1991) show that the percolation of surface meltwater through tide cracks to the underside of the ice shelf (a mechanism invoked by Gow & Epstein (1972) for the Koettlitz Glacier Tongue in McMurdo Sound) is precluded for HGIS, and they suggest that the source in this case is the melting of congelation ice formed upstream of the zone of influence of descending "warm" (above local freezing point) waters. However, another possibility, compatible with the isotopic results, is that the "source" marine ice for the melt could have been frazil that was also formed upstream of the zone of influence of these warm water plumes. As congelation or frazil ice accumulated at the base of the ice shelf and made its way downstream it would possibly come into contact with sea water above its local freezing point (Souchez *et al.* 1991). Given the order of magnitude of difference between heat and salt diffusion, meltwater from either congelation or frazil ice itself will form and find its way downstream through (or with) the loose frazil ice matrix, progressively diluting the interstitial sea water. The salinity contrast with the normal sea water at the frazil/ocean interface will set up differential diffusion of K and Mg, raising the K/Mg ratio of this interstitial water. This transformation process of a pre-existing loose frazil layer will result in considerable inhibition of the mixing by convection between the fresh interstitial water and the normal sea water below, thus allowing the selective diffusion process to occur on a larger time scale. It would also make it easier to understand why no low salinity values were observed by the oceanographers in the free water column. Furthermore, when comparing banded rectangular to banded wave-like frazil, the latter shows stronger c-axis concentration, higher salinities, a lower K/Mg ratio and limited occurrence of vortices. All these observations converge to demonstrate enhanced interface flow conditions resulting in stronger mixing between the loose frazil and the underlying free ocean water. The c-axes pattern in medium and coarse orbicular frazil is strikingly different from the one of the banded frazil (Fig. 2). The obvious lack of preferential orientation in orbicular frazil suggests an accretion process in calm conditions with no effect of any interfacial flow or/and an increasing effect of recrystallization after deposition, as one would infer from the larger size of the

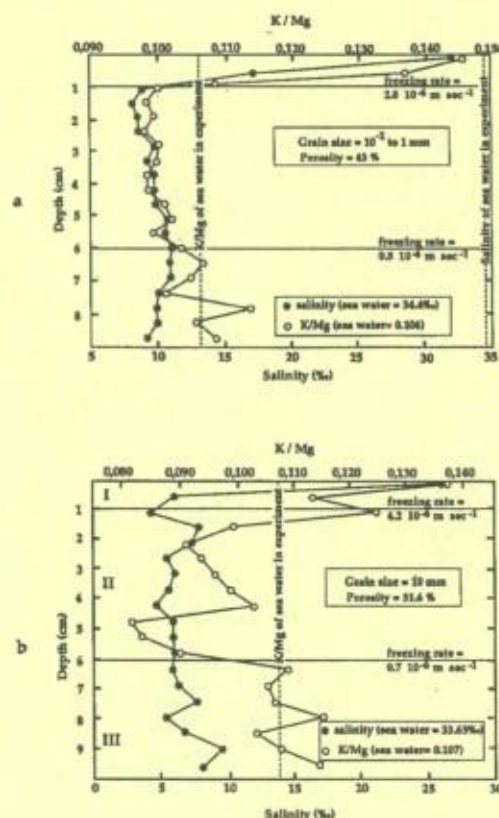


Fig. 6. Evolution of salinity and K/Mg ratio with depth during a typical experiment of freezing loose artificial frazil from top to bottom (see text for explanation): a. fine-grained frazil b. coarse-grained frazil.

crystals in these frazil ice types compared to other ice types. The case of the fine orbicular frazil in core 4, shown in thin section and ice fabric in Fig. 2, is peculiar. It is, in fact, an intermediate case between the banded and orbicular type, since, at the bottom of the core the small crystals tend to show a slight elongation along the vertical. It also shows a strong concentration of c-axes as the banded frazil does, but rotated by nearly 90°. The spatial location of core 4 easily explains these features. It is at the fringe of the shear zone where the western and central sector meet. There, ice layers are brought into a sub-vertical position, and initially horizontal layering can be rotated close to the vertical. When the orbicular frazil a few cm thick occurs sandwiched between two banded frazil layers, the chemical characteristics of the two types of frazil are similar, thereby indicating that these are the expression of the host water, while the texture reflects different interfacial flow conditions. On the other hand, when the orbicular frazil occurs as medium to coarse grained in thicker homogeneous sequences it shows minimum salinity values and maximum K/Mg ratios. Orbicular frazil is also the only kind of frazil ice from the HGIS that eventually contains particulate matter inclusions. These mainly consist of sponge tests and crustacean faeces, sometimes showing



peritrophic membrane, and occasionally echinoderm spicules and worm tubes fragments (G. Houvenaghel, personal communication, 1992). One out of 15 samples also contained two diatom fragments. The dominance of fragments of benthic origin indicates the proximity of the sea floor for the waters where the frazil ice formed. It also confirms the efficiency of the scavenging effect of rising frazil ice crystals on suspended matter, as was experimentally demonstrated by Reimnitz *et al.* (1990). Particulate matter in orbicular frazil ice has also been observed in larger ice-shelves such as the Filchner-Ronne (Oerter *et al.* 1992) and the Amery ice samples (provided by N.W. Young), especially close to the interface between continental and marine ice. The shifts in the K/Mg ratio observed in medium and coarse grained orbicular frazil are much higher than those observed experimentally in closed systems. This calls for an open system process, where successive melting events can occur in a strongly individualized frazil ice body. The subglacial topography of the ice shelf provides sheltered inverted depressions where frazil ice will accumulate and remain protected from mixing with ocean waters for a longer period of time. Radio-echo sounding and aerial photographs both show evidence of such channels or domes, possibly filled with marine ice at HGIS. The central sector of the ice shelf exhibits a transversely undulating interface at a depth between 25 and 50 m, though it is occasionally more shallow than 20 m (Souchez *et al.* 1991). This reflector is characterized by an energy contrast markedly lower than that found in the western part. Detection of the ice-water interface is thereby inhibited. Nevertheless, if the contrast is one between continental and marine ice, this undulating interface must represent a "fossil" ice-water interface. In Fig. 1, where marine ice is clearly identified by its dark tone, it is clear that lenses of marine ice penetrate into the glacier ice. These can be considered as the surface expression of the discontinuity observed in radio echo-sounding profiles. Several processes can be held responsible for the genesis of the inverted channels or domes at the base of the ice shelf: groove-type scarring at the grounding line (Musil 1989), merging of different floating ice streams with different discharges, folding where a minor ice stream is buttressed by a major one etc. Thanks to the sheltering role of these inverted channels and domes, and because of the strong mechanical damping effect of the significant thickness of loose frazil ice that accumulate into them, successive inputs of warm ocean water at the frazil/open ocean water interface will

repeat the melting events. Enhanced dilution and migration of low salinity waters in the highest parts of the inverted depressions will increase the shifts in the K/Mg ratio. In some cases (Fig. 4, core 23), the profile of the K/Mg ratio shows decreasing values with depth, suggesting that the chemical sorting is stronger in older frazil, further away from the ice-ocean interface. Table II compares the proportion (%) of the different ice types in the cores sampled on a longitudinal transect in the central sector, where the situation is tectonically less disturbed (cores 21–25). It is clear that orbicular frazil is more typical of the upstream zone of marine ice while the banded frazil is dominant closer to the ice-shelf front. In the western sector, where the sequence is complicated by shearing and folding, there is evidence that the orbicular frazil was formed further upstream (closer to the grounding line or to the pinning point of Vegetation Island), since it is rich in benthic particulate matter, while banded frazil is devoid of any solid inclusions. This spatial distribution pattern is another favorable factor, increasing the period for diffusion processes in the case of the orbicular frazil. Finally, the results of the melting experiments provide a possible explanation for the minor population of frazil ice showing K/Mg ratios lower than 0.099 (Fig. 3c & d) that could represent the freezing-in of loose frazil layers close to the free water interface being submitted to preferential K/Mg depletion.

### Conclusions

Comparison of the textural, isotopic and chemical characteristics of frazil ice at the base of HGIS provide us with new insights in the dynamics of marine ice accretion under small ice shelves.

Medium- to coarse-grained orbicular frazil accretes upstream in a relatively calm environment and eventually piles up as thick units in inverted channels or domes where the subglacial topography is favourable. As these frazil ice bodies or congelation ice, formed via conduction of heat through the ice shelf, enter the zone of influence of warm oceanic waters, they are subjected to melting. This produces isotopically heavy waters that progressively dilute the interstitial sea water of the loose frazil, initiating chemical differentiation that is preserved in the frazil matrix. These diluted waters will converge in the highest parts of the inverted depressions, where they are further protected from mixing by mechanical convection. Farther downstream, where the ice shelf is thinning under the effect of katabatic winds, the remaining ice will recrystallize resulting in the final crystal sizes and fabrics of medium and coarse grained solid frazil. In places where no channel or dome exists, or where those are already filled with frazil, the effect of interfacial streaming will increase where water currents exist. Individual frazil crystals will align more or less parallel to the ice/ocean interface showing strong c-axes fabrics with a single maximum. In places non-laminar flow will create vortices that will be frozen-in later on. In this type of frazil the chemical sorting is "single-step" and total salinity is higher, though less than in typical congelation or frazil in fast ice. It is not clear yet if the individual frazil ice crystals are generated by a double-diffusion process in a small

Table II. Proportion of the different ice types in the five cores of the longitudinal transect in the central sector of HGIS.

Ice core	Glacier ice	Ice types			Banded frazil	
		Fine	Orbicular frazil Medium	Coarse	Rectangular	Wave-like
21	100%	-	-	-	-	-
22	100%	-	-	-	-	-
23	-	-	-	100%	-	-
24	-	25%	11.5%	7.7%	53.9%	1.9%
25	-	-	-	5.1%	91%	3.9%



## FRAZIL ICE GENERATION

321

scale diluted layer at the ice-sea water interface, or as the result of supercooling in the rising water column. Further investigations on the isotopic fractionation in individual frazil ice crystals should allow a better understanding of the first step in the build-up sequence of marine ice at the base of this ice-shelf.

## Acknowledgements

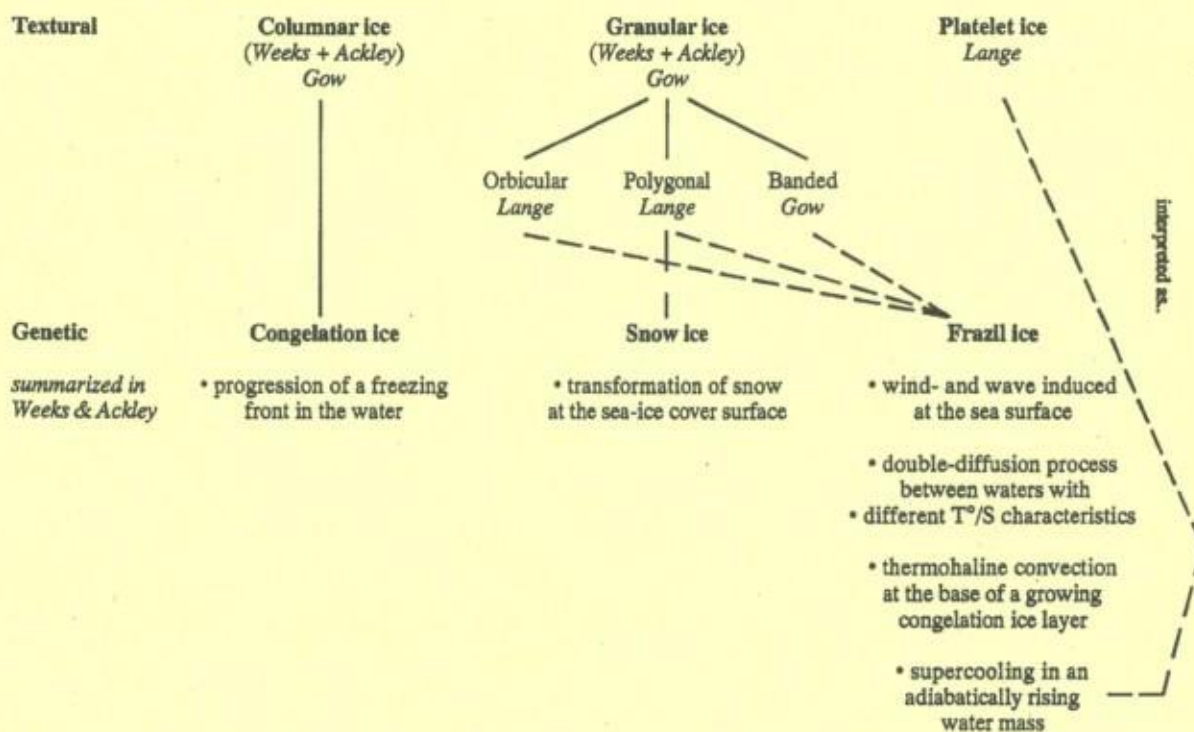
This paper is a contribution to the Belgian Antarctic Programme (Science Policy Office). The authors thank Prof. R. Souchez and Dr M. Meneghel for the ice core sampling funded by the "Programma Nazionale di Ricerca in Antartide". The Geological Survey of Belgium is gratefully acknowledged for its financial support of the ice analyses under its global change programme. The authors are especially indebted to Dr A.J. Gow and Prof. R. Souchez for their critical comments on an earlier draft and to Drs S. Ackley, I. Allison and H. Oerter for their constructive comments as referees of the manuscript. Thanks are also due to Dr J. Jouzel who made the isotopic analyses possible. J.-L. Tison is Research Associate at the Belgian Science Foundation (FNRS).

## References

- ANDERSSON, A. & DALY, S.F. (1992). Laboratory investigation of trash rack blockage by frazil ice. *CRREL Report*, 92-16, 11 pp.
- BARONI, C. 1988. The Hells Gate and Backstairs Passage ice shelves (Victoria Land, Antarctica). *Memorie della Societa Geologica Italiana*, 34, 103-128.
- BARONI, C., STENNI, B. & LACUMIN, P. 1991. Oxygen isotopic composition of ice samples from the Hells Gate and Backstairs Passage ice shelves (Victoria Land, Antarctica): Evidence of bottom freezing. *Memorie della Societa Geologica Italiana*, 46, 45-48.
- BIN-YAAKOV, S. 1972. Diffusion of sea water ions - I. Diffusion of sea water into a dilute solution. *Geochimica et Cosmochimica Acta*, 36, 1395-1406.
- BOLDWIN, A. & STOCCHINO, C. 1990. On the hydrological characteristics of Terra Nova Bay. In *Oceanographic Campaign 1987-88 Data Report*, Genova: University of Genova, 11-57.
- BECK, N. & MUNNICH, K.O. 1988. Freezing of water: isotopic fractionation. *Chemical Geology*, 70, 168.
- CRAGIN, J.H., GOW, A.J. & KOVACS, A. 1986. Chemical fractionation of brine in the McMurdo Ice Shelf, Antarctica. *Journal of Glaciology*, 32, 307-313.
- DOAKE, C.S.M. 1976. Thermodynamics of the interaction between ice shelves and the sea. *Polar Record*, 18, 112, 37-41.
- EICKEN, H. & LANGE, M.A. 1989. Development and properties of sea ice in the coastal regime of the southeastern Weddell Sea. *Journal of Geophysical Research*, 94, (C6), 8193-8206.
- GOW, A.J. & EPSTEIN, S. 1972. On the use of stable isotopes to trace the origins of ice in a floating ice tongue. *Journal of Geophysical Research*, 77, 6552-6557.
- GOW, A.J., ACKLEY, S.F., BUCK, K.R. & GOLDEN, K.M. 1987. Physical and structural characteristics of Weddell Sea pack ice. *CRREL Report*, 87-14, 70 pp.
- GROSS, G.W. 1968. Some effects of trace inorganics on the ice/water system: ch. 3. In GOULD, R.F., ed., *Trace inorganics in water*. Advances in Chemistry Series No. 73, Washington D.C.: American Chemical Society, 396 pp.
- GROSS, G.W., WONG, P.M. & HUMER, K. 1977. Concentration dependent solute redistribution at the ice-water phase boundary. III. Spontaneous convection, chloride solutions. *Journal of Chemical Physics*, 67, 5264-5274.
- LANGE, M.A. 1988. Basic properties of Antarctic sea ice as revealed by textural analysis of ice cores. *Annals of Glaciology*, 10, 95-101.
- LANGE, M.A. 1990. Development and physical properties of sea ice in the Weddell Sea, Antarctica. In ACKLEY, S.F. & WEEKS, W.F. eds., *Sea ice properties and processes*. *CRREL Monograph*, 90-1, 22-40.
- MEISE, D.A. 1989. The chemical and structural properties of sea ice in the Southern Beaufort Sea. *CRREL Report*, 89-25, 134 pp.
- MEISE, D.A. 1990. The chemical and structural properties of sea ice in the Southern Beaufort Sea. In ACKLEY, S.F. & WEEKS, W.F. eds., *Sea ice properties and processes*. *CRREL Monograph*, 90-1, 32-34.
- MUSIL, G.J. 1989. On the underside scarring of floating ice sheets. *Annals of Glaciology*, 12, 118-123.
- OERTER, H., KIPSTHUL, J., DIETMANN, J., MILLER, H., WAGENBACH, D., MINIKIN, A. & GRAF, W. 1992. Evidence for basal marine ice in the Filchner-Ronne ice shelf. *Nature*, 358, 399-401.
- REIMNITZ, E., KEMPEN, B.W., WEBER, W.S., CLAYTON, J.R. & PAYNE, J.R. 1990. Suspended-matter scavenging by rising frazil ice as observed in tank experiments. In ACKLEY, S.F. & WEEKS, W.F. eds., *Sea ice properties and processes*. *CRREL Monograph*, 90-1, 97-100.
- RICHARDSON, C. 1976. Phase relationships in sea ice as a function of temperature. *Journal of Glaciology*, 17, 507-519.
- RONVEAUX, D. 1992. *The dynamics of a small Antarctic ice shelf as indicated by an ice composition study*. Ph.D dissertation, Université Libre de Bruxelles, 391 pp. [Unpublished.]
- SOUCHÉZ, R., TISON, J.-L. & JOUZEL, J. 1988. Deuterium concentration and growth rate of Antarctic first-year sea ice. *Geophysical Research Letters*, 15, 1385-1388.
- SOUCHÉZ, R. & LORRAIN, R.D. 1991. *Ice composition and glacier dynamics*. Heidelberg: Springer-Verlag, 200 pp.
- SOUCHÉZ, R., MENEGHEL, M., TISON, J.-L., LORRAIN, R., RONVEAUX, D., BARONI, C., LOZE, A., TABACCO, I. & JOUZEL, J. 1991. Ice composition evidence of marine ice transfer along the bottom of a small Antarctic ice shelf. *Geophysical Research Letters*, 18, 849-852.
- TISON, J.-L. & HAREN, J. 1989. Isotopic, chemical and crystallographic characteristics of first-year sea ice from Breid Bay (Princess Ragnhild Coast - Antarctica). *Antarctic Science*, 1, 261-268.
- WEEKS, W.F. & ACKLEY, S.F. 1986. The growth, structure and properties of sea ice. In UNTERSTEINER, N. ed. *The Geophysics of Sea Ice*. Nato ASI Series, Series B, No. 146. New York: Plenum Press, 9-164.
- WIRTH, K.D. 1991. Determining the intrinsic permeability of frazil ice - Part 1. Laboratory investigations. *CRREL Report*, 91-23, 15 pp.



Appendix I. Simplified organigram for sea ice terminology.





**Paper 7**

**Investigating Processes of Marine Ice Formation in a Floating Ice Tongue by a High-Resolution Isotopic Study**

**Authors**

**R. Souchez, J.-L. Tison, R. Lorrain, C. Fléhoc, M. Stiévenard, J. Jouzel, V. Maggi**

**Journal**

**Journal of Geophysical Research, Vol. 100, n°C4**

**Year**

**1995**



## Investigating processes of marine ice formation in a floating ice tongue by a high-resolution isotopic study

R. Souchez, J.-L. Tison, and R. Lorrain

Département des Sciences de la Terre et de l'Environnement, Université de Bruxelles, Brussels

C. Fléhoc, M. Stiévenard, and J. Jouzel

Laboratoire de Modélisation du Climat et de l'Environnement, CEA/DSM, Gif-sur-Yvette, France

V. Maggi

Dipartimento di Scienze della Terra, Università di Milano, Milan, Italy

**Abstract.** A better knowledge of boundary conditions near a grounding line is critical for understanding the behavior of ice shelves and floating glaciers. We show here that significant information can be gained from a high-resolution isotopic and textural study of marine ice accreted at the bottom of a floating glacier near its grounding line. Two different types of marine ice have been found. Type 1 is bubble- and debris-free ice with properties which, we believe, can be explained by intrusion of brackish water in open basal fissures. Closing of the fissures by progression of a freezing front from the sides is precluded, and filling by frazil ice is favored. Type 2 is made of thin, clear ice and debris layers which are thought to have formed when a subglacial water-filled sediment enters into contact with seawater and is subjected to freezing under a double-diffusion process. The paper also stresses that in a  $\delta D$ - $\delta^{18}O$  diagram the alignment of marine ice samples on a mixing line does not necessarily imply a mixture of continental water and seawater in varying proportions.

### Introduction

Thermodynamic processes occurring at the base of an ice shelf control basal melting or accretion of marine ice. These thermodynamic processes are determined by the temperature of both ice and seawater near the interface and by the speed of the ocean currents.

Small Antarctic ice shelves or ice tongues, with an ice thickness at their front of approximately 100 m or less, are likely to react more rapidly than thicker shelves to a temperature change because their base can be affected by a temperature increase of oceanic waters. One critical area for the stability of the whole floating glacier is the grounding line.

It is generally assumed that if the melting point is reached at the glacier base in the coastal region, subglacial meltwater loaded with sediments discharges into the sea at the grounding line. Zotikov [1986] has pointed out that if this subglacial meltwater reaches the sea, a layer of relatively fresh water will exist above normal seawater beneath the ice shelf. Since the freezing point of fresh water is higher than the freezing point of seawater, bottom freezing will probably occur and be responsible for a thickening of the ice shelf at or near the grounding line. However, the only drilling made today of an ice shelf through its entire thickness (ice core J9 on the Ross Ice Shelf) showed no evidence of fresh water in accretion, but rather, adfreezing of sea ice [Zotikov *et al.*, 1980]. J9 is located along a flow line that connects with an ice stream. Accordingly, any fresh water flowing beneath the ice stream

at the grounding line could potentially accrete as freshwater ice to the base of the Ross Ice Shelf. This, in fact, is not observed in the J9 core.

In order to preserve a body of relatively fresh water, the water column must be relatively calm and not influenced by tidal mixing which MacAyeal [1984] thinks should be efficient near a grounding line. The presence of an inverted topography such as crevasses, domes, or channels at the ice-ocean contact [Orheim, 1986; Hellmer and Jacobs, 1992; Tison *et al.*, 1993] is a way to achieve this sheltering effect.

Marine ice of substantial thickness has been found at the base of some ice shelves [Oerter *et al.*, 1992] and ice tongues [Gow and Epstein, 1972] or at coastal ice margins under an ice cap [Goodwin, 1993]. In order to better understand phase changes at the ice shelf-ocean interface, different modes of water circulation have been described and various models of ice shelf-ocean interactions have been proposed in the literature [Jacobs *et al.*, 1979; Lewis and Perkin, 1986; Jenkins and Doake, 1991; Nicholls *et al.*, 1991; Hellmer and Jacobs, 1992].

An insight into the problem of determining the conditions necessary for freezing at the ice shelf-ocean interface can be gained by studying the isotopic properties of the marine ice, both in  $\delta D$  and  $\delta^{18}O$ . With this last perspective in mind a field program was conducted in Terra Nova Bay area within the 1989-1990 Italian Antarctic Program in order to study outcropping sites of marine ice which has been accreted at the base of ice shelves or ice tongues. Two such sites have been sampled, one at Hell's Gate Ice Shelf in the south of Terra Nova Bay [Souchez *et al.*, 1991] and the other at the Campbell Glacier Tongue in the north. The ice cores collected at these sites were kept frozen at  $-25^{\circ}C$ , transferred

Copyright 1995 by the American Geophysical Union.

Paper number 95JC00142.  
0148-0227/95/95JC-00142\$05.00



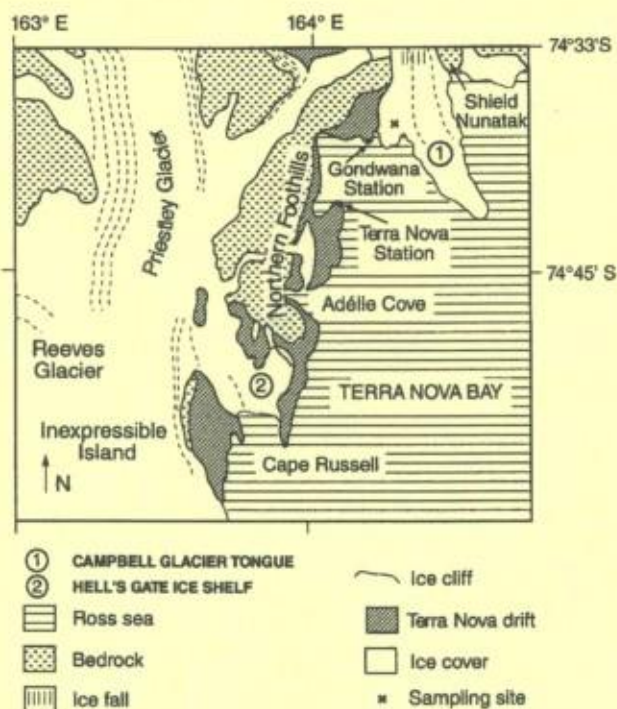


Figure 1. Location map of the Terra Nova Bay area.

to Brussels, and studied for their crystallographic and isotopic properties. The isotopic analyses were done at the Centre d'Etudes Nucléaires de Saclay in France with an accuracy of 0.5‰ for  $\delta D$  and of 0.1‰ for  $\delta^{18}O$  on 2-mL samples.

### Site Description

The Terra Nova Bay area is located in northern Victoria Land, along the western margin of the Ross Sea. It extends from Cape Washington in the north to the Drygalski Ice Tongue in the south.

Campbell Glacier has its accumulation zone in the Transantarctic Mountains; it flows in a NNW-SSE depression carved into the Precambrian and Paleozoic basement rocks [Carmignani *et al.*, 1987]. Being deviated by Mount Melbourne which is a Cenozoic volcano, it acquires a more or less north-south direction and shows a steeper gradient. The presence of small rock outcrops at this level indicates that the base of the glacier is above sea level. Then, Campbell Glacier reaches the sea, where it terminates as a protruding glacier tongue (Figure 1).

The grounding line, usually defined as a line across the glacier where it first goes afloat, is thought to be located just south of the zone with the steeper gradient [Frezzotti, 1993]. Radio echo sounding fails to detect it. The reflector is characterized by a weak energy contrast. This could be due to a change in the physical characteristics of the ice, the electromagnetic energy being absorbed because of the conductivity of a lower ice unit. Precise radio echo sounding is moreover difficult to perform in this crevassed area. Although the precise depth of the grounding line is not known, an approximate value can be given. A bathymetric survey in front of the ice tongue [Angrisano, 1989] gives a depth of about 160 m for the sea bottom. Overdeepening under the

Campbell Glacier Tongue is a possibility, but the grounding line depth should be around this value. The sampling site is about 3 km downglacier from the presumed position of the grounding line.

In the present paper an extended definition of the grounding line is considered. In such a definition a grounding line is the limit between grounded ice and floating ice, either if the glacier goes afloat or becomes grounded again, as, for example, in the case of a pinning point.

Strong katabatic winds from the polar plateau characterize both the Reeves and Priestley glacial troughs, hence the name Hell's Gate Ice Shelf. As a result, extensive blue ice areas are developed at the surface of these glaciers, and extensive ice-free areas such as the southern part of the northern foothills and Inexpressible Island exist nearby. Because of the action of these katabatic winds, the surface of the Hell's Gate Ice Shelf is snow free and is losing ice, mostly by sublimation. Since top surface ablation is prevalent, an upward vertical velocity component exists and ice initially at depth is transferred along an inclined surface toward the ice-atmosphere interface in the downglacier part of the ice shelf. The marine ice formed at the ice shelf-ocean interface ultimately appears at the surface. The Hell's Gate Ice Shelf has been studied by Baroni [1988], Baroni *et al.* [1991], Souchez *et al.* [1991], and Tison *et al.* [1993]. In the Souchez *et al.* and Tison *et al.* papers, ice composition studies have shown that marine ice transfer occurs along the bottom of this ice shelf and that the frazil ice accreted at its base reflects contrasting depositional environments.

By contrast, the role of katabatic winds in the Campbell Glacier trough is much reduced. The winds are relatively weak so that the entire glacier is accumulating snow on its surface, and, even at the terminus of the floating tongue, a substantial part of the ice cliff is made of ice derived from snow deposited on the tongue. As a result, there is no upward movement of ice, and therefore marine ice, if present at the bottom, is not likely to outcrop at the terminus of the floating tongue. However, the southwestern part of the ice tongue near Gondwana Station has impinged on bedrock promontories or protuberances. Consequently, basal ice containing debris layers is visible and can be sampled. At the sampling site (Figure 1) a stacked sequence, a few meters thick, dipping 60° toward the center of the glacier tongue shows two distinctive types of ice interbedded with bubbly glacier ice. A first type, located in the upper part of the basal sequence, consists of bands of bubble-free ice with a thickness of the order of a few centimeters. The second type, located in the lower part of the basal sequence, shows bands of thin, clear, ice layers and layers of fine debris sometimes appearing folded with a few occasional pebbles. The proportion of bubbly glacier ice layers is much lower in this case. Debris consists mainly of quartz grains with rounded shapes and smooth edges (60%), volcanic glasses with elongated bubbles (30%), and lithic fragments. A few sponge spicules and shell fragments are also present. The heavy minerals mainly consist of pyroxenes (80%), indicating a major volcanic component and a few olivine, garnet, and epidote minerals. The scanning electron microscope (X ray energy dispersion probe) analysis of the volcanic glass gives a dispersion in a  $SiO_2$  versus alkali diagram similar to that of rocks from the nearby Shield Nunatak complex [Worner *et al.*, 1989], thus suggesting a local origin.



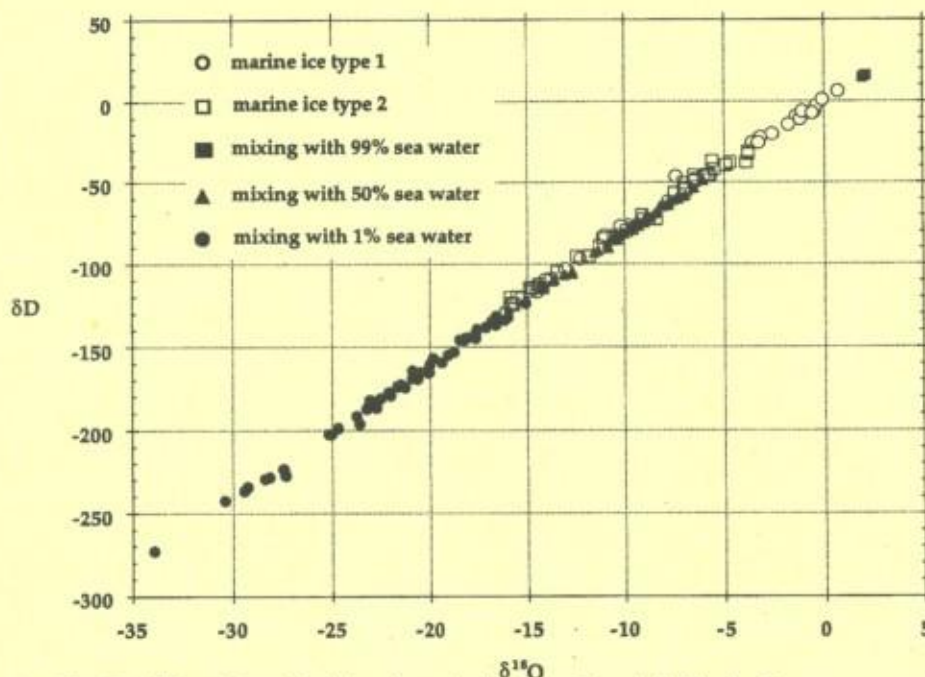


Figure 2. The  $\delta D$ - $\delta^{18}O$  relationship in basal marine ice from Campbell Glacier Tongue compared with a mixing computer simulation (see text).

### The $\delta D$ - $\delta^{18}O$ Characteristics of Basal Ice

An insight into the problem of the formation of these two ice types can be gained by a combined isotopic study of the ice, both in  $\delta D$  and  $\delta^{18}O$ . Indeed, if only a single isotopic ratio is considered, the effects of freezing, isotopic exchange with clay minerals, or mixing cannot be distinguished.

Bubbly glacier ice derived from snow of coastal origin and snow fallen in the Terra Nova Bay area have  $\delta D$  values more negative than  $-130\text{‰}$  and  $\delta^{18}O$  values more negative than  $-17\text{‰}$ . Together with bubbly glacier ice from the continental interior with lower  $\delta$  values, they are aligned, in a  $\delta D$ - $\delta^{18}O$  diagram, on a precipitation line with the equation  $\delta D = 7.92 \delta^{18}O + 2.76$ ; correlation coefficient  $r = 0.997$  ( $n = 41$  samples).

Basal ice with an isotopic composition less negative than  $-130\text{‰}$  in  $\delta D$  and  $-17\text{‰}$  in  $\delta^{18}O$  cannot be considered as unmodified glacier ice. Basal ice samples have been plotted as open symbols on Figure 2. They fit quite well a straight line with equation  $\delta D = 7.86 \delta^{18}O + 0.29$ ;  $r = 0.998$  ( $n = 71$  samples). The large range of isotopic values reaching values close to those obtained by freezing normal seawater and the slope of the line preclude a simple freezing process. Indeed, if Jouzel and Souchez [1982, equation (1)] is used to compute the  $\delta$  range between 1 and 99% freezing of a closed water reservoir, the range obtained is much less than the observed one. For an open reservoir the range in  $\delta$  values in the ice would be even smaller. Enrichment by isotopic exchange with clay minerals is able to produce important isotopic shifts but on a much lower slope [Souchez et al., 1990] and is therefore also precluded in this case.

A simulation has been conducted in order to test if this alignment of data of basal ice from the Campbell Glacier Tongue could correspond to a mixing line. The local seawater has been sampled at 30 m depth; its  $\delta D$  value is  $-3.23\text{‰}$ , and its  $\delta^{18}O$  value is  $-0.69\text{‰}$ . In the simulation (solid

symbols in Figure 2) this local seawater is mixed in varying proportions with the melt of each glacier ice sample collected in the area. It is assumed that no fractionation occurs during melting of ice. Three mixing ratios have been used as follows: 99% seawater (solid squares), 50% seawater (solid triangles), and 1% seawater (solid circles). The  $\delta$  values of the ice resulting from freezing of the mixtures have been calculated for deuterium and for oxygen 18, using the equation  $\delta_s = \alpha (1000 + \delta_w) - 1000$  where  $\alpha$  is the equilibrium fractionation coefficient and  $\delta_w$  is the  $\delta$  value of the mixed water. The equilibrium fractionation coefficient for deuterium is taken as 1.0208 [Arnason, 1969], and for oxygen 18, as 1.003 [O'Neil, 1968]. The points representing these various computations have a distribution which is very close to the points representing the samples of basal ice. Therefore the straight line on which the basal ice samples are aligned can be considered as a mixing line and, consequently, the basal ice samples as marine ice. Let us note here that if a 2% higher equilibrium fractionation coefficient for deuterium is considered for seawater, a possibility that might exist [Beck and Munnich, 1988], the fit would be even better. As discussed below, the presence of a mixing line does not, however, necessarily imply a mixture of continental water and seawater in varying proportions beneath the floating glacier.

### Texture-Isotope Relationships in the Marine Ice

Common features to all marine ice samples in this study can be deduced from a careful examination of Figure 3. Clear ice layers always display the less negative  $\delta$  values, and a gradual change to values typical of glacier ice occurs as one proceeds toward the boundaries of these layers. Very often, transitional  $\delta$  values occur within a single crystal layer which is bubble free in its inner part and contains bubbles in its



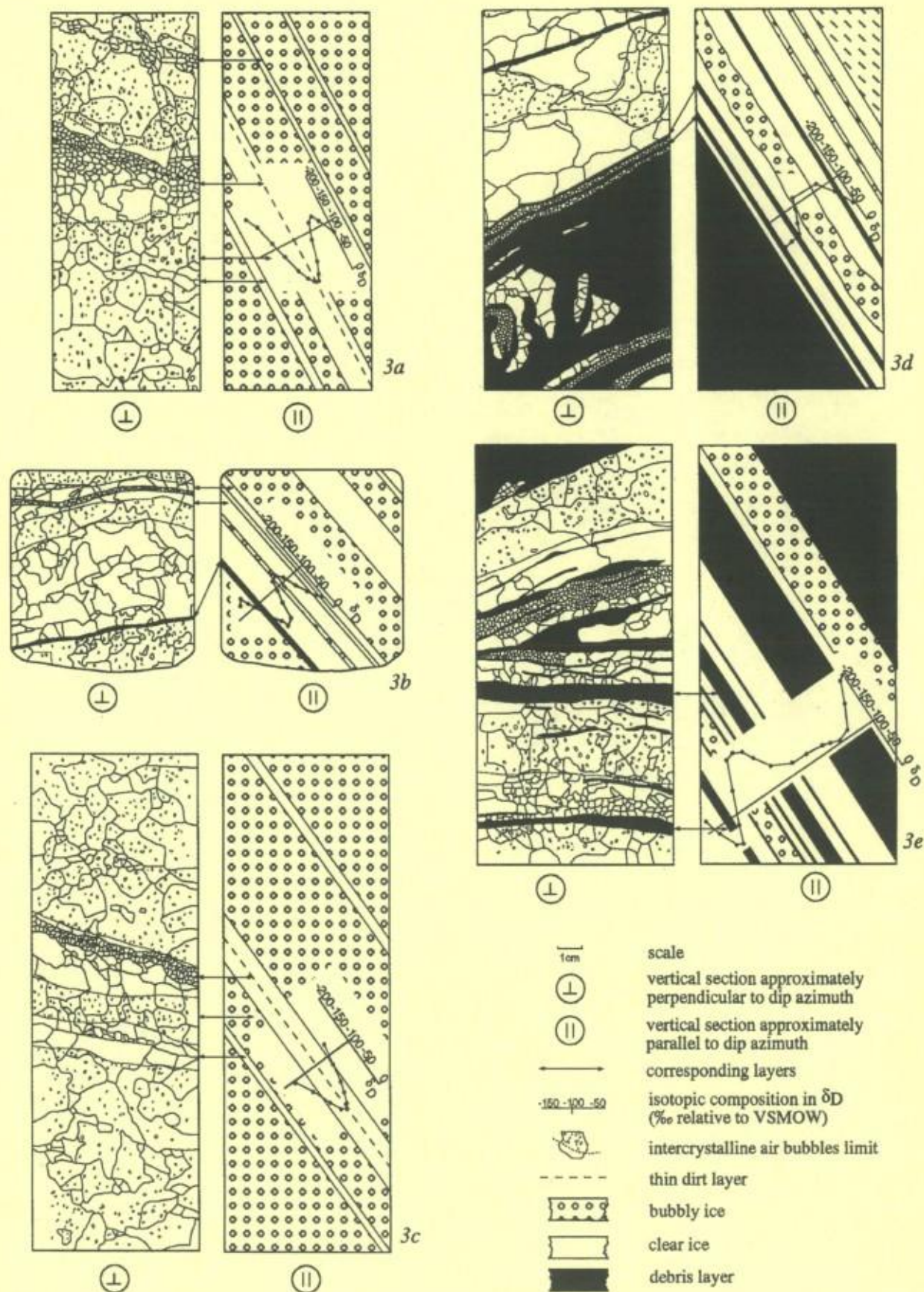


**Figure 3.** Detailed textural properties and  $\delta D$  profiles in selected ice cores from the (a)–(c) upper part, type 1, and (d)–(e) lower part, type 2, of the basal ice of Campbell Glacier Tongue.



outer part (Figure 3). The crystal size in this layer is similar to the one for unmodified glacier ice. Major differences, however, exist between the marine ice in the upper part of the basal sequence (type 1) and that occurring in the lower part (type 2).

In the upper part the center of the clear ice layers consists of very small crystals (sometimes with a thin line of tiny particles) where the maximum  $\delta D$  values vary between  $-30\text{‰}$  and  $+6\text{‰}$ , thus approaching values observed in frozen seawater (Figures 3a–3c). They form the group of marine ice samples in the top right corner of Figure 2. As developed below, these characteristics can be understood if intrusion of brackish water has taken place in fissures freshly open at the base of the floating glacier, with subsequent ice formation.

The area at the bottom of a floating glacier or ice shelf close to the grounding line is a favorable site for the formation and opening of basal crevasses. Bottom crevasses have been recorded by Orheim [1986] on the Riiser-Larsenisen by radio echo sounding. Hellmer and Jacobs [1992] indicate that bottom crevasses are common near grounding lines where tidal bending occurs. They also explain the filling of bottom crevasses with marine ice by an ice pump mechanism driven by the pressure dependence of the freezing point. This ice pump mechanism could readily fill a 200-m-high crevasse with marine ice, a probable reason for the rapid disappearance of bottom crevasses. Jezek and Bentley [1983] believe that most bottom crevasse fields are associated with rapid grounding or ungrounding of ice. The crevasses reported by all these authors have dimensions of meters. The type 1 marine ice inclusions studied in this paper are only centimeters wide. Possibly, these fissures could exist in the same situations but remain undetected by radio echo sounding. They might have formed at a larger scale and subsequently been subjected to strain thinning.

Strain thinning could explain the presence of very small crystals in the center of the fissure as a consequence of grain fracturation. However, the  $\delta$  values in the center of the fissure are so weakly negative that an overwhelming contribution of seawater is required. If present, the grain fracturation must thus have occurred after the formation of marine ice in the fissure.

This raises the possibility that larger crystals might have originally filled the fissure. Such large crystals could have been congelation ice due to ice growth from the sides of the fissure. Migration of a freezing front from the sides of the fissure toward its center as a consequence of the heat sink provided by the cold ice surrounding the crack must thus be investigated. There is no indication, in the large crystals present in the fissure, of the occurrence of brine layers which are a diagnostic feature for congelation ice. On the other hand, geometric selection of crystals during growth in the liquid phase cannot be detected in the thin sections examined. More importantly the isotopic distribution of  $\delta$  values in the fissure is a strong argument against such a process. Indeed, if a freezing front is progressing into water, the first ice formed (in this case, the ice closest to the sides of the fissure) will have the less negative  $\delta$  values since the maximum enrichment of heavy isotopes in the ice compared to the initial water is produced there. With the development of freezing the residual water becomes impoverished in heavy isotopes [Souchez and Jouzel, 1984]. The successive frozen layers will thus be more and more negative. Such an isotopic

distribution is not present; a reverse distribution is displayed with less negative  $\delta$  values in the center of the fissure and more negative  $\delta$  values toward the sides.

Frazil ice formation processes yield other ways to produce ice crystals from brackish water [Weeks and Ackley, 1986]. Frazil ice can be produced by turbulence, but such a process is not likely to occur here in the confined space of the fissure. Frazil ice can also be produced by a mechanism of double diffusion (heat and salt) involving the existence of two water masses with contrasted temperatures and salinities, both at their pressure melting point. Clearly, this is not possible here. Finally, frazil ice crystals could be formed in adiabatically raising water as a consequence of the pressure dependence of the freezing point. Although we cannot prove that this process is effective here, we consider that the filling of the fissure by frazil ice is the best explanation with the information at hand.

The frazil ice crystals were perhaps originally bigger and their size reduced by grain fracturation. Figure 4a is a sketch illustrating the processes involved. Recrystallization must have occurred as indicated by the presence of ice crystals which are bubble free in their inner part and bubbly in their outer part at the glacier ice–frazil ice contact. Diffusion of isotopes along the pathway represented by water films at the ice crystal limits during recrystallization must certainly be taken into account. It probably explains the gradual decrease in  $\delta$  values from the center of the fissure toward the sides in this type of marine ice. Clearly, in this case the alignment of the samples on a mixing line does not reflect the mixing of two water masses.

In the lower part of the basal sequence the type 2 marine ice with thin clear ice and debris layers (Figures 3d and 3e) exhibit a range in  $\delta D$  values of  $-110\text{‰}$  to  $-30\text{‰}$ , indicating a greater influence of continental meltwater. These characteristics can be explained if a water-filled sediment at the glacier-ocean-rock contact is subjected to freezing because of the difference in freezing points between continental meltwater and seawater. In this process, thermal diffusivity being higher than salt diffusion, the water-filled sediment loses heat more rapidly than it gains salt. Moreover, heat can diffuse through both liquid and solid fractions, but salt can only through the liquid. The water within the sediment will have an isotopic composition dependent on the variable contribution of continental meltwater versus seawater. This is reflected in the shift in  $\delta$  values of type 2 marine ice on the mixing line. Diffusion effects must also be considered for the transitional  $\delta$  values between adjacent layers.

The presence of these thin clear ice layers between the debris layers with such a specific isotopic signature requires basal freezing. If basal freezing is to occur, the seawater must itself be at the freezing point which is not the case for surface waters reaching the bottom of ice shelves [Lewis and Perkin, 1986]. This implies melting and the removal of basal ice in other regions. Although we have no measurements of water temperatures and salinities near the grounding line, the complexity of this contact zone in three dimensions makes the process plausible. In the case of type 2 marine ice at Campbell Glacier, it is clear that it forms where the glacier runs aground farther downstream at shallower depths. Figure 4b is a sketch showing the processes involved. Mechanical incorporation of the ice and debris layers into the ice shelf is certainly a possibility at this location. An investigation of the marine ice properties, like the one conducted in



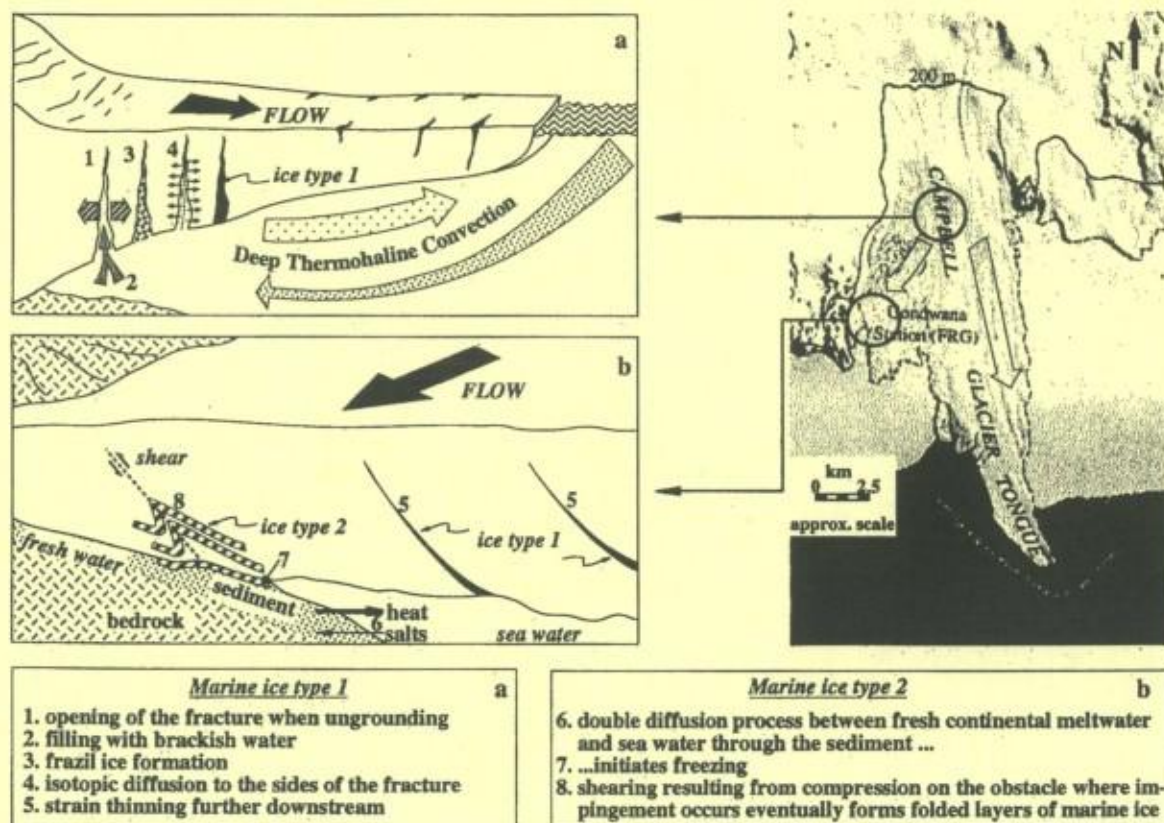


Figure 4. Sketches illustrating the processes involved in the formation of (a) type 1 marine ice and (b) type 2 marine ice. The scale of the features is enlarged for clarity.

this study, is able to give some clues to the formation processes but gives no indication of the transfer mechanisms. As shown in Figures 3d and 3e, small-scale folding can be invoked to explain the multiple-layered structure.

It is not known if the continental meltwater component has been produced at the glacier bed by melting due to geothermal and frictional heat or if it has been able to find its way to the bed from the surface. The geothermal heat flux does not seem to be abnormally high: geothermal anomalies have only been found in the top part of the Mount Melbourne volcanic edifice but not in the lower Campbell Glacier area [Rossi, 1991].

As the ice was raised to the surface when it impinged on bedrock promontories or protuberances, the possibility that pressure melting and regelation occurred should be discussed. Although it is not possible to prove that this process has not taken place, the type of debris included in the ice makes it unlikely as the initial accretion mechanism. It could have occurred as a postdepositional process. However, it has been shown earlier [Souchez et al., 1988] that pressure melting and regelation does not significantly modify the isotopic properties of the ice submitted to this process.

The presence of shell fragments and sponge spicules in the debris layers raises the possibility that the debris originated from the Terra Nova drift which mantles the eastern flank of the northern foothills in the coastal region from Cape Russell in the south to the Campbell Glacier Tongue farther north [Orombelli et al., 1990]. Shell fragments and worm tubes of mixed ages are common in Terra Nova drift but not sponge spicules. Near Adelie Cove (see Figure 1), this drift is

commonly ice cored and hummocky. The ice cores are made of bubbly glacier ice with  $\delta^{18}\text{O}$  values reaching  $-35\text{‰}$  and bands of bubble-free ice reaching  $\delta^{18}\text{O}$  values of  $+2\text{‰}$ . Such highly different values of  $\delta^{18}\text{O}$  characterize samples collected in a vertical sequence of a few decimeters in the same ice core. The similarity with type 1 marine ice might indicate the presence of a former grounding line at proximity. In this hypothesis the buried ice could have been partially formed near a fossil grounding line of a late Wisconsin Campbell Glacier advancing onto the Ross Sea continental shelf. It is now above sea level because of isostatic rebound. The type 2 marine ice consisting of debris and clear ice layers with its specific isotopic signature has never been found in the ice cores from Terra Nova drift. It is thus quite unlikely that reworking of Terra Nova drift could explain the layered structure of type 2 marine ice at Campbell Glacier Tongue.

With the extended definition of the grounding line in mind, one can thus consider that the two types of marine ice here studied were formed near a grounding line. Type 1 was probably formed closer to the center line of the glacier tongue than type 2. Their superposition (type 1 over type 2) results from impingement on bedrock protuberances. Unfortunately, ice fabrics of the marine ice types do not give additional information on their formation processes. Indeed, on a Schmidt diagram, ice crystal  $c$  axes form a small girdle indicative of horizontal compression against an obstacle. The ice fabrics thus reflect the impingement on bedrock protuberances, and no remnant of the original fabric is preserved.



## Conclusions

A combined isotopic study, both in  $\delta D$  and  $\delta^{18}O$ , is a powerful tool for understanding the mechanisms involved in marine ice formation. Two types of marine ice accreted at the base of a floating glacier near its grounding line have been distinguished. In both cases the ice samples are aligned in a  $\delta D$ - $\delta^{18}O$  diagram on a mixing line.

Freezing of brackish water in basal open fissures conducive to frazil ice production and consolidation followed by isotopic diffusion along grain boundaries is identified as the most plausible mechanism for formation of type 1 marine ice. Freezing of a water-filled sediment at the ice-ocean-bedrock contact as a consequence of double-diffusion effects is considered as the most likely process for formation of type 2 marine ice.

**Acknowledgments.** The "Programma Nazionale di Ricerche in Antartide" (PNRA) is gratefully acknowledged for having supported the field work of the first author at Terra Nova Bay in 1989-1990. This paper is a contribution to the Belgian Antarctic Programme (Science Policy Office). J.-L. Tison is research associate at the National Fund for Scientific Research (Belgium).

## References

- Angricano, G., *Carta batimetrica Mare di Ross-Baia Terra Nova*, Istituto Idrografico della Marina, Genoa, Italy, 1989.
- Arnason, B., Equilibrium constant for the fractionation of deuterium between ice and water, *J. Phys. Chem.*, **73**, 3491-3494, 1969.
- Baroni, C., The Hell's Gate and Backstairs Passage ice shelves (Victoria Land, Antarctica), *Mem. Soc. Geol. Ital.*, **34**, 103-128, 1988.
- Baroni, C., B. Stenni, and P. Iacumin, Oxygen isotopic composition of ice samples from the Hell's Gate and Backstairs Passage ice shelves (Victoria Land, Antarctica): Evidence for bottom freezing, *Mem. Soc. Geol. Ital.*, **46**, 45-48, 1991.
- Beck, N., and K. O. Munnich, Freezing of water: Isotopic fractionation, *Chem. Geol.*, **70**, 168, 1988.
- Carmignani, L., C. Ghezzi, G. Gosso, B. Lombardo, M. Meccheri, A. Montrasio, P. C. Pertusati, and F. Salvini, Geological map of the area between David and Mariner glaciers, Victoria Land, Antarctica, *Mem. Soc. Geol. Ital.*, **33**, suppl., 1987.
- Frezzotti, M., Glaciological study in Terra Nova Bay, Antarctica, inferred from remote sensing analysis, *Ann. Glaciol.*, **17**, 63-71, 1993.
- Goodwin, I. D., Basal ice accretion and debris entrainment within the coastal ice margin, Law Dome, Antarctica, *J. Glaciol.*, **39**(131), 157-166, 1993.
- Gow, A. J., and S. Epstein, On the use of stable isotopes to trace the origins of ice in a floating ice tongue, *J. Geophys. Res.*, **77**, 6552-6557, 1972.
- Hellmer, H. H., and S. S. Jacobs, Ocean interactions with the base of Amery Ice Shelf, Antarctica, *J. Geophys. Res.*, **97**, 20,305-20,317, 1992.
- Jacobs, S. S., A. L. Gordon, and J. L. Ardal, Circulation and melting beneath the Ross Ice Shelf, *Science*, **203**, 439-443, 1979.
- Jenkins, A., and C. S. M. Doake, Ice-ocean interaction on Ronne Ice Shelf, Antarctica, *J. Geophys. Res.*, **96**, 791-813, 1991.
- Jezek, K. C., and C. R. Bentley, Field studies of bottom crevasses in the Ross Ice Shelf, Antarctica, *J. Glaciol.*, **29**(101), 118-126, 1983.
- Jouzel, J., and R. Souchez, Melting-refreezing at the glacier sole and the isotopic composition of the ice, *J. Glaciol.*, **28**(98), 35-42, 1982.
- Lewis, E. L., and R. G. Perkin, Ice pumps and their rates, *J. Geophys. Res.*, **91**, 11,756-11,762, 1986.
- MacAyeal, D. R., Thermohaline circulation below the Ross Ice Shelf: A consequence of tidally induced vertical mixing and basal melting, *J. Geophys. Res.*, **89**, 597-606, 1984.
- Nicholls, K. W., K. Makinson, and A. V. Robinson, Ocean circulation beneath the Ronne ice shelf, *Nature*, **354**, 221-223, 1991.
- Oerter, H., J. Kipfstuhl, J. Determann, H. Miller, D. Wagenbach, A. Minikin, and W. Graf, Ice-core evidence for basal marine shelf ice in the Filchner-Ronne Ice Shelf, *Nature*, **358**, 399-401, 1992.
- O'Neil, J. R., Hydrogen and oxygen isotope fractionation between ice and water, *J. Phys. Chem.*, **72**, 3683-3684, 1968.
- Orheim, O., Glaciological research on Riiser-Larsenisen and nearby ice-shelves in Antarctica, *Skr. Nor. Polarinst.*, **187**, 5-22, 1986.
- Orombelli, G., C. Baroni, and G. H. Denton, Late Cenozoic glacial history of the Terra Nova Bay region, Northern Victoria Land, Antarctica, *Geogr. Fis. Din. Quat.*, **13**, 139-163, 1990.
- Rossi, A., Preliminary survey of the underground thermal regime in the area around Terra Nova Bay, Victoria Land, Antarctica, *Mem. Soc. Geol. Ital.*, **46**, 457-461, 1991.
- Souchez, R., and J. Jouzel, On the isotopic composition in  $\delta D$  and  $\delta^{18}O$  of water and ice during freezing, *J. Glaciol.*, **30**(106), 369-372, 1984.
- Souchez, R., R. Lorrain, J.-L. Tison, and J. Jouzel, Co-isotopic signature of two mechanisms of basal-ice formation in Arctic outlet glaciers, *Ann. Glaciol.*, **10**, 163-166, 1988.
- Souchez, R., M. Lemmens, R. Lorrain, J.-L. Tison, J. Jouzel, and D. Sugden, Influence of hydroxyl-bearing minerals on the isotopic composition of ice from the basal zone of an ice sheet, *Nature*, **345**, 244-246, 1990.
- Souchez, R., M. Meneghel, J.-L. Tison, R. Lorrain, D. Ronveaux, C. Baroni, A. Lozej, I. Tabacco, and J. Jouzel, Ice composition evidence of marine ice transfer along the bottom of a small Antarctic ice shelf, *Geophys. Res. Lett.*, **18**, 849-852, 1991.
- Tison, J.-L., D. Ronveaux, and R. D. Lorrain, Low salinity frazil ice generation at the base of a small Antarctic ice shelf, *Antarc. Sci.*, **5**, 309-322, 1993.
- Weeks, W. F., and S. F. Ackley, The growth, structure, and properties of sea ice, in *The Geophysics of Sea Ice*, NATO ASI Ser., Ser. B, vol. 146, edited by N. Untersteiner, pp. 9-164, Plenum, New York, 1986.
- Worner, G., L. Viereck, J. Hertogen, and H. Niephaus, The Mount Melbourne volcanic field (Victoria Land, Antarctica), II, Geochemistry and magma genesis, *Geol. Jahrb. Reihe E*, **38**, 395-433, 1989.
- Zotikov, I. A., *The Thermophysics of Glaciers*, 275 pp., D. Reidel, Norwell, Mass., 1986.
- Zotikov, I. A., V. S. Zagorodnov, and J. V. Raikovsky, Core drilling through the Ross Ice Shelf (Antarctica) confirmed basal freezing, *Science*, **207**, 1463-1465, 1980.
- C. Fléhoc, J. Jouzel, and M. Stiévenard, Laboratoire de Modélisation du Climat et de l'Environnement, CEA/DSM, Bâtiment 709, Orme des Mérisiers, CE Saclay, F-91191 Gif-sur-Yvette, France.
- R. Lorrain, R. Souchez, and J.-L. Tison, Département des Sciences de la Terre et de l'Environnement, CP 160/03, Université de Bruxelles, 50 Avenue F. D. Roosevelt, B-1050 Brussels, Belgium.
- V. Maggi, Dipartimento di Scienze della Terra, Università di Milano, 34 Via Mangiagalli, I-20133 Milano, Italy.

(Received April 2, 1993; revised July 6, 1994; accepted December 14, 1994.)



## **Paper 8**

**Preliminary Results from 60 Shallow Cores and from one 45-m Deep Marine Ice  
Core at Hells Gate Ice Shelf (Victoria Land, Antarctica)**

## **Authors**

**R. Lorrain, J.-L. Tison, A. Bondesan, D. Ronveaux, M. Meneghel**

## **Journal**

**Terra Antarctica Reports, Vol. 1**

## **Year**

**1997**





*Terra Antartica Reports*  
1997, 1, 19 - 24

## **Preliminary Results from 60 Shallow Cores and from one 45-m Deep Marine Ice Core at Hells Gate Ice Shelf (Victoria Land, Antarctica)**

R. LORRAIN<sup>1</sup>, J.-L. TISON<sup>1</sup>, A. BONDESAN<sup>2</sup>, D. RONVEAUX<sup>3</sup>,  
M. MENEGHEL<sup>2</sup>

<sup>1</sup>Département des Sciences de la Terre et de l'Environnement, Université Libre de Bruxelles 50, Av. F.D. Roosevelt, 1050 Bruxelles - Belgium

<sup>2</sup>Dipartimento di Geografia, Università di Padova, Via del Santo 26, 35213 Padova - Italy

<sup>3</sup>Department of Geography, Villanova University, St. Augustine Liberal Arts Center, Villanova, PA 19085 - USA

### **INTRODUCTION**

Marine ice accretion at the bottom of ice shelves is a process of major interest in the context of ice sheet stability under climatic changes. Ice shelves and the ice streams they collect are the pathways through which ice sheets discharge into the ocean. However, mass balance of ice shelves at the ice-ocean interface is still poorly known, mainly because of poor accessibility. Studies of a few deep ice cores through antarctic ice shelves (Morgan, 1972; Engelhart and Determann, 1987; Oerter et al. 1992; Eicken et al., 1994; Oerter et al., 1994), have confirmed the occurrence of thick marine ice layers under meteoric ice, showing very low salinity levels with regard to sea ice (as low as 0.026‰). In these cores, marine ice occurs as isometric crystals with rounded grain boundaries and weak c-axis fabrics (orbicular frazil - Morgan, 1972; Wakahama, 1974; Oerter et al., 1994).

Hells Gate Ice Shelf (HGIS - Fig.1), a small ice shelf located in Terra Nova Bay (lat. 74°50'S, long. 163°50'E), provides a unique opportunity to study marine ice properties in shallow cores, since strong ablation due to katabatic winds progressively brings marine ice to the ice shelf surface.

Stable isotope studies at Hells Gate Ice Shelf (Souchez et al. 1991; Tison et al. 1993) have shown that marine ice transfer must occur in a downstream direction, whereas textural and chemical analyses revealed two main contrasted types of marine ice related to specific environments and depositional processes (Fig. 2). In addition to the common orbicular frazil (Fig. 2a) with very low salinity, strong chemical fractionation and weak fabrics, banded (rectangular or wave like) frazil was observed (Fig. 2b) in considerable amounts, with slightly higher mean salinities, less chemical fractionation and single maximum fabrics. Statistical counting in 5 shallow cores on a longitudinal transect suggested that there might be a higher proportion of banded rectangular frazil closer to the ice shelf front.

### **NEW ICE CORES LOCATION AND MEASUREMENTS PERFORMED**

During the IX Italian Antarctic Expedition (1993-1994) extended shallow core sampling was performed. Sixty "2-meter" cores were retrieved from different places where isolated marine ice outcrops were clearly apparent and at the nodes of a grid centered on the continental ice/marine



R. Lorrain et al.

ice limit in the central sector (Fig. 1). The nodes of the grid were at 250 m intervals along the E-W direction and 200 m intervals along the N-S direction. An additional 10 shallow cores were distributed along the clear limit between continental and marine ice to study the transition from one to the other in more detail. At the bottom of each of these shallow cores, thin sections were made and studied in the laboratory of Terra Nova Station, in order to determine the different ice types on textural grounds.

In addition, eleven 10-meter cores and one 45-meter core (Y) were drilled to study the vertical transformation processes of marine ice. Only the preliminary results from core Y (a few meters from core 17 in Fig. 1) will be described here. Vertical thin sections about 9cm long were made along the total length of this core to observe the different ice textures. Two vertical 1cm thick slices were cut with a clean band saw and, corresponding to each thin section, a piece of ice was taken from each slice for salinity and major cations measurements. The salinity was measured by electrical conductivity and major cations by atomic absorption spectrophotometry. Precision on salinity is  $\pm 0.01\text{‰}$  and on major cations  $\pm 0.05\text{ppm}$ .

### SPATIAL DIFFERENTIATION OF MARINE ICE

Detailed study of marine ice at HGIS reveals different styles of outcrops (see Roman numbers on Fig. 1). Systems I and II appear to result from marine ice accretion into inverted depressions corresponding to limits between individual flows, eventually reworked later by glacier dynamics.



Fig. 1 - Location map of 1993-1994 ice coring sites at Hells Gate Ice Shelf. The different marine ice systems (dark grey areas) are also indicated (see text for further explanation).



## Preliminary Results from Shallow Cores and Deep Marine Ice Cores at Hells Gate Ice Shelf

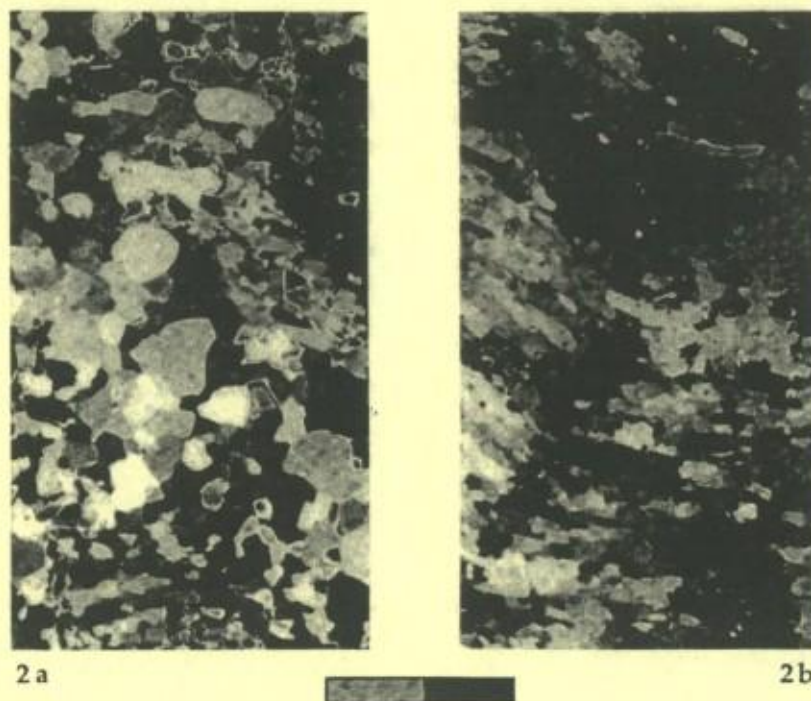


Fig. 2 - Typical examples of orbicular (2a) and rectangular (2b) frazil forming the marine ice of core Y. The scale bar is 2 cm long.

System III results from massive accretion closer to the ice shelf front. Systems IV, V, and VI consist of narrow marine ice injections into continental ice, running sub-parallel to local rocky outcrops (Vegetation Island, Inexpressible Island or the Eastern Moraine).

Results from the textural analyses of the shallow cores clearly demonstrate spatial differentiation of the main marine ice types, in close connection with the different marine ice outcropping systems (Fig. 3). Although dynamic factors might slightly complicate the overall picture, orbicular marine ice is stratigraphically located above banded marine ice, which results in most of the banded facies outcropping either closer to the ice shelf front or, if further upstream, at the limit of major glacier fluxes. Columnar ice, another minor marine ice type in this environment, occurs only in a few places, at the contact between continental ice and marine ice. Because of textural similarities with the columnar facies in sea ice, it is thought to result from slow freezing at the ice-ocean interface through heat conduction across the ice shelf

## CHEMICAL PROPERTIES OF CORE Y

As foreseen from the results presented in the previous section, most of the 45-meter deep core Y is made of banded rectangular consolidated frazil. Orbicular frazil is also present, but restricted to limited quantities in the topmost 6 meters of the core. It is worth comparing the conductivity profile (equivalent to salinity) to the one measured in selected deep cores on larger ice shelves (Fig. 4). The profiles from Amery Ice Shelf (AIS - Morgan, 1972) and Filchner-Ronne Ice Shelves (FRIS/B13-B15, Oerter et al., 1994) typically show conductivities between 50 and 400  $\mu\text{S}/\text{cm}$  (0.03 to 0.24‰ salinities) in the marine ice, globally decreasing and then eventually stabilizing with increasing depth.



## Preliminary Results from Shallow Cores and Deep Marine Ice Cores at Hells Gate Ice Shelf

The topmost values in core Y (100 - 300  $\mu\text{S}/\text{cm}$ ), where the orbicular marine ice is found, are in good agreement with the bottom values of cores B13 and B15 from FRIS (50 - 100  $\mu\text{S}/\text{cm}$ ) and with those of AIS core G1 (200 - 100  $\mu\text{S}/\text{cm}$ ). However, as one enters the monotonous banded rectangular facies, the conductivity is globally increasing with depth, from 500  $\mu\text{S}/\text{cm}$  (0.25‰) to 5000  $\mu\text{S}/\text{cm}$  (2 - 3‰), getting close to values commonly found in sea ice.

The profile is also step-like (using data smoothing techniques), with a major increase at about 32 meters deep. This level precisely corresponds to the moment where water first invaded the borehole during drilling. The conductivity of this water, measured in the field (C. Barbante, personal communication), appeared to be more than twice the value of sea water, probably reflecting brine concentration during frazil ice consolidation. Regular rising of the water level in the borehole during the next 24 hours, up to a depth of 11 meters (equivalent to the height of the cliff in front of the ice shelf), is an indicator of large-scale porosity of the ice shelf in its lower part.

In previous studies at HGIS (Tison et al., 1993), the K/Mg ratio was also chosen as a potential tracer of chemical fractionation processes during marine ice buildup. This ratio is of peculiar interest since it is one of the least likely affected by salt precipitation in the brines at typical antarctic temperatures. It therefore reflects possible chemical fractionation during formation and consolidation of the frazil leading to marine ice. Figure 5 shows the K/Mg profile with depth in core Y, together with a plot of K/Mg against the sum of the four major cations ( $\Sigma 4$ ).

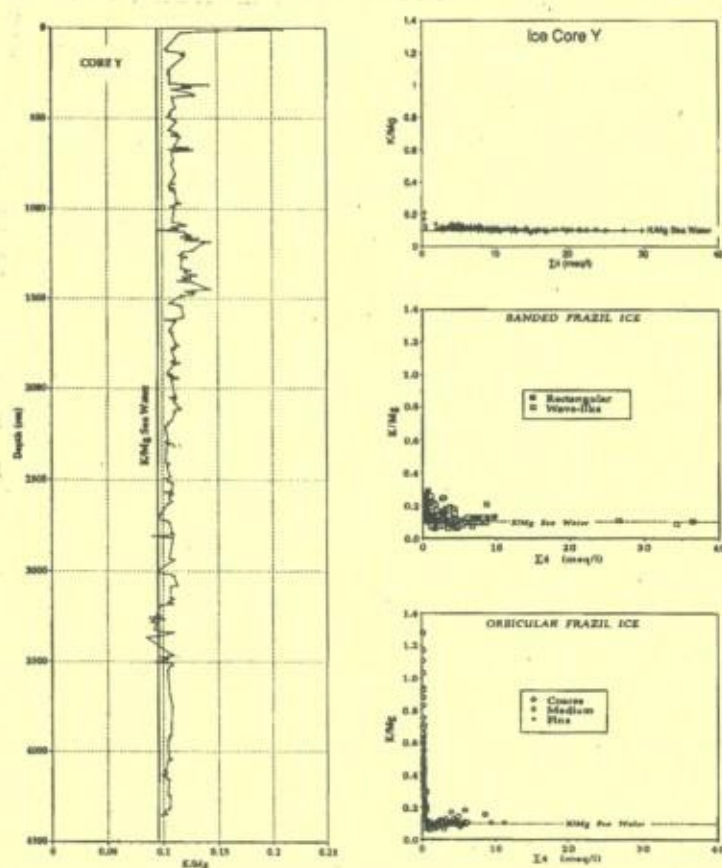


Fig. 5 - K/Mg profile versus depth at core Y (left); K/Mg versus  $\Sigma 4$  (sum of four major cations) plot for core Y (top right) as compared to similar graphs for the two types of marine ice sampled in 1989-1990 (bottom right - from Tison et al., 1993).



R. Lorrain et al.

The latter is compared to equivalent data from the 1989 -1990 expedition for the two main marine ice types.

As expected, core Y behaves typically as banded frazil ice with limited chemical fractionation, in contrast with the few occurrences of orbicular frazil at the top of the core. A slight (but systematic) fractionation however exists above 32 meters depth, compatible with a "single step" diffusion process from the free ocean water to the slightly diluted interstitial host water in the loose frazil (Tison et al., 1993).

### FOCUSING ON MARINE ICE TRANSFER PROCESSES

The new data discussed in the previous section clearly confirm and demonstrate the strong contrast that exists between orbicular and banded marine ice at HGIS. Since the orbicular frazil appears to be the dominant component of marine ice in all deep ice cores, it most likely results from the now classic "Deep Thermohaline Circulation" (see for example Nicholls et al., 1991 - Fig. 4) where it forms by super cooling in the "Ice Shelf Water" rising "limb" of the circulation cell. It is therefore necessary to look for another plausible mechanism to explain the formation of the banded frazil outcropping closer to the ice shelf front, but also observed to pile up in a thick 2-3 meters layer of loose crystals under the sea ice that fringes the ice shelf.

Preliminary results from stable isotope measurements in the marine ice, together with the peculiar properties of the ocean water in front of the ice shelf (see Tison et al., 1995 - this volume) suggest that a secondary circulation cell might exist closer to the front, sustaining the marine ice transfer in a downstream direction at the ice-ocean interface.

### ACKNOWLEDGEMENTS

The authors are greatly indebted to the "Programma Nazionale di Ricerche in Antartide" (PNRA) and to the logistic team of Terra Nova Bay for unconditional and efficient support in the field. This paper is a contribution to the Belgian Antarctic Program (SSTC) - Science Policy Office. J.-L. Tison is Research Associate at the Belgian National Fund for Scientific Research (F.N.R.S.).

### REFERENCES

- Eicken H., Oerter H., Miller H., Graf W. & Kipfstuhl J., 1994. Textural characteristics and impurity content of meteoric and marine ice in the Ronne Ice Shelf, Antarctica. *J. Glaciol.*, **40** (135), 386-398.
- Engelhart H. & Determann J., 1987. Borehole evidence for a thick layer of basal ice in the central Ronne Ice Shelf. *Nature*, **327**, 318-319.
- Morgan V.I., 1972. Oxygen Isotope Evidence for Bottom Freezing on the Amery Ice Shelf. *Nature*, **238**, 393-394.
- Nicholls K.W., Makinson K. & Robinson A.V., 1991. Ocean circulation beneath the Ronne Ice Shelf. *Nature*, **354**, 221-223.
- Oerter H., Eicken H., Kipfstuhl J., Miller H. & Graf W., 1994. Comparison between ice core B13 and B15. Filchner-Ronne Ice Shelf Programme (FRISP) - Report n°7 (1994) - AWI - Bremerhaven, 29-36.
- Oerter H., Kipfstuhl J., Determann J., Miller H., Wagenbach H., Minikin A. & Graf W., 1992. Evidence for basal marine ice in the Filchner-Ronne Ice Shelf. *Nature*, **358**, 399-401.
- Souchez R., Meneghel M., Tison J.-L., Lorrain R., Ronveaux D., Baroni C., Lozej A., Tabacco I. & Jouzel J., 1991. Ice composition evidence of marine ice transfer along the bottom of a small Antarctic ice shelf. *Geophys. Res. Lett.*, **18**, 849-852.
- Tison J.-L., Ronveaux D. & Lorrain R., 1993. Low salinity frazil ice generation at the base of a small antarctic ice shelf. *Antarctic Science*, **5** (3), 309-322.
- Tison J.-L., Barbante C., Bondesan A., Lorrain R. & Capra A., 1995. Ice shelf/ocean interactions at the front of Hells Gate Ice Shelf (Terra Nova Bay - Antarctica). This volume.
- Wakahama G., 1974. Structures and textures of the Amery Ice Shelf, Wilkes Ice Cap and Cape Folger, Antarctica. In *Physical and chemical studies of ice from glaciers and ice sheets*. Tokyo, Japanese Science Foundation, 99-108. [In Japanese]



**Paper 9**

**Ice Shelf/Ocean Interactions at the Front of Hells Gate Ice Shelf  
(Terra Nova Bay – Antarctica)**

**Authors**

**J.-L. Tison, C. Barbante, A. Bondesan, R. Lorrain, A. Capra**

**Journal**

**Terra Antarctica Reports, Vol. 1**

**Year**

**1997 (b)**





*Terra Antartica Reports*  
1997, 1, 29 - 32

## **Ice Shelf/Ocean Interactions at The Front of Hells Gate Ice Shelf (Terra Nova Bay - Antarctica)**

J.-L. TISON<sup>1</sup>, C. BARBANTE<sup>2</sup>, A. BONDESAN<sup>3</sup>, R. LORRAIN<sup>1</sup>, A. CAPRA<sup>4</sup>

<sup>1</sup>Département des Sciences de la Terre et de l'Environnement  
Université Libre de Bruxelles; 50, Av. F.D. Roosevelt, 1050 Bruxelles - Belgium

<sup>2</sup>Dipartimento Scienze Ambientali, Università di Venezia, Calle Larga S. Marta,  
2137 - 30123 Venezia - Italia

<sup>3</sup>Dipartimento di Geografia, Università di Padova, Via del Santo 26,  
35123 Padova - Italia

<sup>4</sup>Ist. Topografia, Geodesia e Geofisica Mineraria, Viale Risorgimento 2,  
40136 Bologna - Italia

### **INTRODUCTION**

Ice shelves and ice streams are an essential key to the stability of ice sheets under climatic changes. Ice streams are high velocity components draining about 90% of inland ice from the Antarctic. Ice shelves play a buttressing role on the ice streams outflow through the backstress they exert from spreading and shear on ice rises and bedrock sides.

Mass balance of ice shelves at the ice-ocean interface is still a variable difficult to appraise, partly because of poor accessibility. A major unknown is the process of stabilisation of the ice shelf by marine ice (ice formed in the water column below the ice shelf) accretion at the bottom; considerable amounts are observed in place where they are not always predicted by the models (Hellmer & Jacobs, 1992). Hells Gate Ice Shelf (HGIS - Fig. 1), a small antarctic ice shelf located in Terra Nova Bay (lat. 74°50'S, long. 163°50'E), provides a unique opportunity for studying marine ice properties, since strong ablation due to katabatic winds progressively brings marine ice to the ice shelf surface, where it extensively crops out near the front. Previous work at Hells Gate Ice Shelf (Souchez et al., 1991 ; Tison et al., 1993) has shown that contrasted types of marine ice reveal different environments and depositional processes. Orbicular and rectangular frazil (see Figs. 2a and 2b in Lorrain et al., 1995 - this volume) are the two major marine ice types observed at HGIS. The first one is frequently described in deep ice cores reaching marine ice on Filchner-Ronne and Amery Ice Shelves (Oerter et al., 1992; 1994). Rectangular frazil has not been described elsewhere in the literature and appears to form closer to the margin (Lorrain et al., 1995 - this volume).

The aim of this work is to investigate the properties of the water column in front of the ice shelf in order to gain insight in the ongoing processes of marine ice formation.

### **PHYSICAL SETTING, SAMPLING PROCEDURE AND DATA PROCESSING**

During the IX Italian Antarctic expedition (1993 - 1994) 19 CTD (Conductivity-Temperature-Depth) multiparametric ocean water profiles were performed on three East-West transects across Evans Cove, at the front of the Hells Gate Ice Shelf (Fig. 1).



J. L. Tison et al.

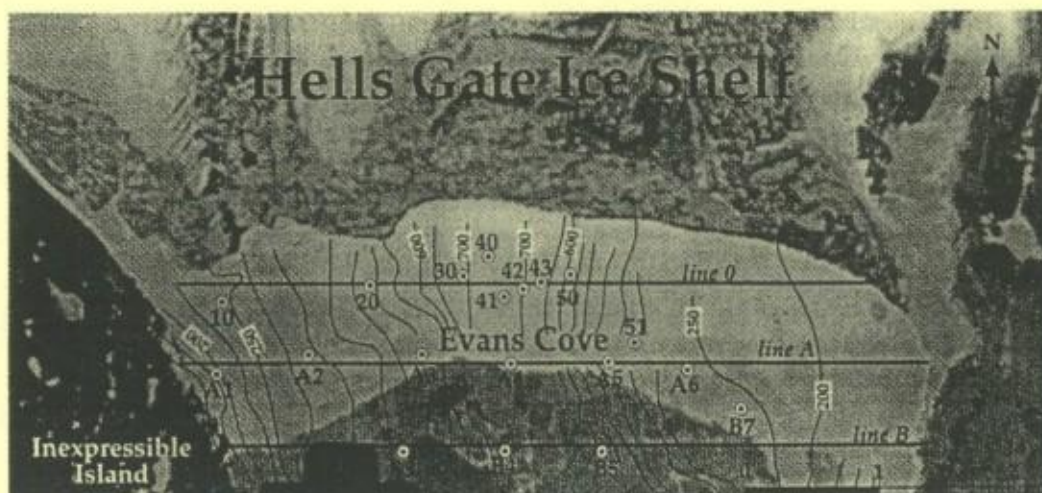


Fig. 1 - Water sampling stations in front of Hells Gate Ice Shelf. Bathymetry is from Stocchino (1991), and background is from Photo 1-063 11-6-85 Terra Nova Bay H2 8000 FL 152-27 TMA 2851-V.

The first transect closely followed the limit of the annual sea ice (January 1994) and the two others were approximately located respectively 0.5 and 1.5 km seaward (Fig. 1).

The profiles were performed from the ship *Malippo* and the stations located using the GPS equipment aboard (about 100 meters accuracy, including the most relevant component as systematic error). The depth of the profiles ranged between 180m and 600m depending on the depth of the sea floor, as estimated from the bathymetric map of "Mare di Ross - Baia Terra Nova" (Stocchino, 1991) and controlled by the echoradar of the ship. Additionally, 30 water samples were collected on the three central profiles at depths between 0 and 140m for future stable isotopes analyses, both in oxygen and deuterium, and to help in calibrating the CTD probe measurements. The rough data collected by the probe are : pressure ( $\pm 0.01$  dbars), *in-situ* temperature ( $\pm 0.02^\circ\text{C}$ ) and conductivity ( $\pm 0.01$  mS/cm). The data were processed using UNESCO recommendations of 1981 and include : practical salinity ( $\pm 0.01\text{‰}$ ), density from the equation of state of sea water ( $\pm 0.1$  in  $\sigma_t$  units) and temperature above freezing point (corrected for salinity and pressure following Fujino et al., 1974).

### PRELIMINARY RESULTS

Results are summarized here from one of the stations of line 0 (station 40 - Fig. 1). Since this line closely follows the residual cover of first-year sea ice, it probably gives the best proxy of the characteristics of water masses below the ice shelf. Figure 2 gives the various profiles at station 40 as a function of pressure in decibars, which, in first approximation, corresponds to depth in meters.

As a whole, six (four major and two minor) units can be distinguished in the water column at HGIS :

- Unit A (0-20m): shows stable temperature and salinity in a warm and diluted surface water, far above the pressure melting point (pmp). It is covered by a few meters of slightly fresher and colder water probably due to sea ice melting
- Unit B (20-37m): displays a strong thermocline, where temperature drops by about  $1.6^\circ\text{C}$  and where salinity drops about  $0.1\text{‰}$  and then rises again. A strong pycnocline results in the lower 7 meters of this unit where temperature still drops and salinity rises again



## Ice Shelf/Ocean Interactions at the Front of Hells Gate Ice Shelf

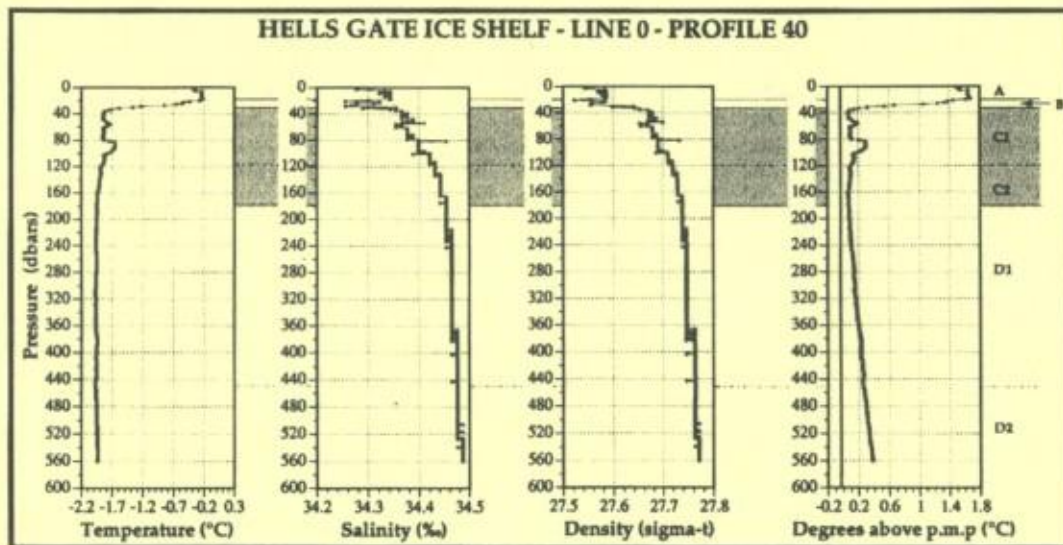


Fig. 2 - Water column characteristics at station 40 - line 0. The sampling site is the closest to the Ice Shelf front. Shaded area underlines unit C, which is typical of the HGIS oceanographic environment (see text).

- Unit C (37-180m): is a unit of intermediate density (shaded in Fig. 2) that can be subdivided in an upper layer (C1, 37-120m) showing a fair salinity gradient ( $0.09\text{‰ } 10^{-1} \text{ m}$ ) and large scale temperature fluctuations of about  $0.3^{\circ}\text{C}$  above the *in-situ* pmp; and a lower layer (C2, 120-180 m) with a decreasing salinity gradient ( $0.05\text{‰ } 10^{-1} \text{ m}$ ) and slowly decreasing temperatures resulting in *in-situ* pmp values
- Unit D (180-560m): is characterized by a small positive salinity gradient. In the upper layer D1 (180-450m) the temperature is stable and thus slowly rises above the *in-situ* pmp. From 450m downwards, the temperature starts to increase, enhancing the departure from *in-situ* pmp

Whilst unit A can be shown to correspond to Antarctic Surface Waters and unit D to Ice Shelf Waters and transition to High Salinity Shelf Waters, as described in the literature (see, for example, Jacobs et al., 1979; Foldvik et al., 1985; Nicholls et al., 1991), unit C appears to be a typical feature of the HGIS oceanographic environment. It calls for an output of relatively fresher water from the ice-shelf-ocean interface, close to the ice shelf margin. This could result from either:

- a) inflow of a warm core from the open sea and melting at the ice-ocean interface, as is the case for the eastern Mc. Murdo Ice Shelf (Jacobs et al., 1979)
- b) production of surface meltwaters that join the ice-ocean interface through crevasses and fissures, as is the case for the Koettlitz Ice Tongue (Gow & Epstein, 1972)
- c) basal melting caused by warm water being introduced from the open sea surface by tidal action (Nicholls et al., 1991)

Three-dimensional combination of all CTD profiles, together with stable isotope measurements, can be used to determine which of these sources applies. This will be the subject of an extended paper now in preparation.

This work also allows us to suggest some refinements to the classical scheme of the deep thermohaline convection theory (Nicholls et al., 1991). In addition to the main and secondary convection cells, a third one is shown to exist close to the ice shelf front. It produces cold and fresh water at the *in-situ* pmp, which are readily entrained to the open sea by the underlying flow of colder and more saline Ice Shelf Waters also at *in-situ* pmp. These conditions should be favourable to the production of double diffusion frazil ice between the two water masses, and it is



J. L. Tison et al.

tempting to see the rectangular frazil ice outcropping close to HGIS margin (see Lorrain et al., 1995 - this volume) as the result of this process. Sudden release of latent heat, as the frazil actively forms close to the margin, could explain the large scale temperature fluctuations of unit C1. Further developments should help in supporting this working hypothesis.

#### ACKNOWLEDGEMENTS

The authors are greatly indebted to the Italian *Programma Nazionale di Ricerche in Antartide* (PNRA) and to the logistic team of Terra Nova Bay for unconditional and efficient support in the field. This paper is a contribution to the Belgian Antarctic Program (SSTC - Science Policy Office). The authors also wish to thank Prof. Stocchino who kindly provided Malippo's availability for the CTD profilings. J.-L. Tison is Research Associate at the Belgian National Fund for Scientific Research (F.N.R.S.).

#### REFERENCES

- Foldvik A., Gammelsrod T., Slotsvik N. & Torresen T., 1985. Oceanographic conditions on the Weddell Sea Shelf during the German Antarctic Expedition 1979-1980. *Polar Res.*, 3, 209-226.
- Fujino K., Lewis E.L. & Perkin R.G., 1974. The freezing point of sea water at pressures up to 100 bars. *J. Geophys. Res.*, 79 (12), 1792-1797.
- Gow A.J. & Epstein S., 1972. On the use of stable isotopes to trace the origins of ice in a floating ice tongue. *J. Geophys. Res.*, 77, 6552-6557.
- Hellmer H.H. & Jacobs S.S., 1992. Ocean interactions with the base of the Amery Ice Shelf, Antarctica. *J. Geophys. Res.*, 97 (20), 305-320.
- Jacobs S.S., Gordon A.L. & Ardai Jr. J.-L., 1979. Circulation and melting beneath the Ross Ice Shelf. *Science*, 203, 441-443.
- Lorrain R., Tison J.-L., Bondesan A., Ronveaux D. and Meneghel M., 1995. Preliminary results from 60 shallow cores and from one 45-m deep marine ice core at Hells Gate Ice Shelf, Victoria Land - Antarctica. This volume.
- Nicholls K.W., Makinson K. & Robinson A.V., 1991. Ocean circulation beneath the Ronne Ice Shelf. *Nature*, 354, 221-223.
- Oerter H., Eicken, H., Kipfstuhl J., Miller, H. and Graf, W., 1994. Comparison between ice core B13 and B15. Filchner-Ronne Ice Shelf Programme (FRISP) - Report n°7 (1994) - AWI - Bremerhaven, pp. 29-36.
- Oerter H., Kipfstuhl J., Determann J., Miller H., Wagenbach H., Minikin A. & Graf W., 1992. Evidence for basal marine ice in the Filchner-Ronne Ice Shelf. *Nature*, 358, 399-401.
- Souchez R., Meneghel M., Tison J.-L., Lorrain R., Ronveaux D., Baroni C., Lozej A., Tabacco I. & Jouzel J., 1991. Ice composition evidence of marine ice transfer along the bottom of a small Antarctic ice shelf. *Geophys. Res. Lett.*, 18, 849-852.
- Stocchino C. 1991. Mare di Ross - Baia Terra Nova - Carta Batimetrica - 1:50000. Istituto Idrografico della Marina, 2a Edizione - Genova, Febbraio 1991.
- Tison J.-L., Ronveaux D. & Lorrain R., 1993. Low salinity frazil ice generation at the base of a small antarctic ice shelf. *Antarctic Science*, 5 (3), 309-322.



**Paper 10**

**Linking Landfast Sea Ice Variability to Marine Ice Accretion at Hells Gate Ice Shelf,  
Ross Sea**

**Authors**

**J.-L. Tison, R.D. Lorrain, A. Bouzette, M. Dini, A. Bondesan, M. Stiévenard**

**Journal**

***In Antarctic Sea Ice Physical Processes, Interactions and Variability*  
Antarctic Research Series, Volume 74  
AGU Publication**

**Year**

**1998**



ANTARCTIC SEA ICE: PHYSICAL PROCESSES, INTERACTIONS AND VARIABILITY  
ANTARCTIC RESEARCH SERIES, VOLUME 74, PAGES 375-407LINKING LANDFAST SEA ICE VARIABILITY TO MARINE ICE ACCRETION  
AT HELLS GATE ICE SHELF, ROSS SEA.J.-L. Tison<sup>1</sup>, R.D. Lorrain<sup>1</sup> and A. Bouzette<sup>1</sup>, M. Dini<sup>2</sup>, A. Bondesan<sup>3</sup>, and M. Stiévenard<sup>4</sup>

Eleven first-year sea ice cores collected in the vicinity of Hells Gate Ice Shelf (Terra Nova Bay, Ross Sea) are analyzed for their textures, ice fabrics, salinities, chemical composition and oxygen-18 values. These are compared to a new data set of four 10-45 m long marine ice cores drilled close to the ice shelf front. During most of the winter, granular frazil ice accretion prevails at the bottom of the landfast first-year sea ice cover in front of Hells Gate Ice Shelf, eventually in alternation with a draped facies. At the end of the winter, platelet ice is more commonly found. These facies are thought to result from frazil ice production in the Ice Shelf Water outflow associated with a Deep Thermohaline Circulation (DTC) in which High Salinity Shelf Water (HSSW) formed in the Terra Nova Bay Polynya descends beneath the Nansen Ice Shelf. Bottom accretion at the base of the landfast first-year sea ice still occurs during the summer as a banded rectangular facies. It can form up to 54% of the ice core thickness. The seasonality of this banded facies accretion at the bottom of the landfast sea ice, the dominance of the banded marine ice facies closer to the ice shelf front and the chemical trends in the granular marine ice facies suggest that a link must exist between the banded facies' genesis and the tidal pumping of warm surface waters below the ice shelf during the summer.

## INTRODUCTION

Ice shelves and ice streams are an essential key to the stability of ice sheets under climatic changes. Ice shelves play a buttressing role on the ice streams' outflow, through their restricted flow over ice rises and rumples as well as due to lateral boundaries. A major issue in this regard is the process of ice shelf stabilization through increased thickness resulting from

marine ice accretion at the bottom (ice crystals formed in the water column below the ice shelf). Considerable amounts of marine ice are sometimes observed where they are not predicted to occur in such quantities by 2-D models applied along longitudinal profiles of the ice shelf/sub-ice shelf cavity system [Hellmer and Jacobs, 1992].

The mass balance of ice shelves at the ice-ocean interface is, however, a variable still difficult to appraise, partly because of poor accessibility. Firstly, only a few deep ice cores drilled through the entire ice shelf thickness (or nearly so) are available at present in the Antarctic [Eicken *et al.*, 1994; Morgan, 1972; Oerter *et al.*, 1994; Oerter *et al.*, 1992; Ragle *et al.*, 1960; Zotikov *et al.*, 1980]. Secondly, specific climatic conditions, namely strong katabatic wind regimes inducing sustained surface ablation, sometimes allow marine ice to outcrop at the surface of smaller antarctic

<sup>1</sup>Département des Sciences de la Terre et de l'Environnement, Université de Bruxelles, Brussels, Belgium

<sup>2</sup>Laboratorio di Geochimica Isotopica, Università di Trieste, Trieste, Italy

<sup>3</sup>Dipartimento di Geografia "G. Morandini", Università di Padova, Padova, Italy

<sup>4</sup>Laboratoire de Modélisation du Climat et de l'Environnement, Gif sur Yvette, France



ice shelves and ice tongues providing sampling opportunities at minimal cost [Gow and Epstein, 1972; Souchez *et al.*, 1991; Tison *et al.*, 1993]. A third approach consists of the study of landfast sea ice forming at the front of ice shelves or in the large rifts that often dissect the ice shelf (ice tongue) area close to the front [Jeffries *et al.*, 1993; Kipfstuhl, 1991; Tison *et al.*, 1991]. These landfast sea ice cores show specific facies rarely described in drifting pack ice.

The purpose of this paper is to: (1) present a new data set on 10–45 m long marine ice cores from Hells Gate Ice Shelf (HGIS), that will be shown to change, at least to some extent, the perspectives obtained from previous work; (2) present two data sets on first-year landfast sea ice at HGIS and discuss the processes leading to the build-up of the landfast ice cover; (3) relate the spatial and temporal variability of the landfast first-year sea ice facies to the one observed in the marine ice cores on a larger time scale (typically several hundreds of years); and (4) suggest paths for future investigations of ice-ocean interactions in the area.

### CURRENT SEA ICE/MARINE ICE FACIES NOMENCLATURE

At this stage, we feel it is useful to support our data with a summary of the present-day knowledge of the sea ice textural facies and associated genetic processes. The purpose of this section is primarily to unambiguously illustrate the terminology used in the following sections. It has often been a matter of debate in which circumstances should textural or genetic terminology be used, and many authors use both indiscriminately. Also, the same terminology is used for different facies by different authors and vice-versa. For example, as discussed below, there is a strong discrepancy between the textural term of "platelet ice" introduced by Lange [1988] and the actual texture of the ice described, where all crystals appear acicular (needle-like) both in horizontal and vertical thin sections. Finally, some textural genetic equivalencies are still controversial or poorly known. Therefore, the contents of Plate 1 and Table 1 should by no means be considered as an exhaustive classification of sea ice facies, a subject far beyond the scope of the present work. Marine ice studies are fairly recent and, therefore, no attempt has been made until now to develop a proper nomenclature. Initially, textural facies in marine ice cores should not significantly differ from those observed in sea ice given the similarity of environments. Furthermore, as shown later in the paper, ice facies described in marine ice are also showing up in

landfast sea ice cores. For these reasons, Plate 1 groups the main sea- and marine-ice textural facies under the same nomenclature. It should, however, be kept in mind that the marine ice accreted at the bottom of large ice shelves undergoes large post-depositional cumulative strains with time that can lead to considerable alterations of the original texture. Similarly, the impact of shearing on the ice shelf margins and/or converging flow in smaller ice shelves (as is the case for HGIS) can also partially alter the textures in the marine ice, producing typical facies that should not be expected in sea ice (even if it is deformed at a later stage).

In Plate 1, we have selected small illustrative samples that we believe best reflect the descriptive terms. Text in blue relates to the main "classical" marine or sea ice types from the literature. Text in red refers to more recent discoveries in landfast sea ice or marine ice, mainly in the Ross Sea area. Table 1 summarizes, in a few simple words, possible textural-genetic connections. Both Plate 1 and Table 1 were compiled from multiple references in the literature [Dieckmann *et al.*, 1986; Eicken and Lange, 1989; Eicken *et al.*, 1994; Gow *et al.*, 1987; Jeffries *et al.*, 1993; Kipfstuhl, 1991; Lange, 1988; Lange, 1990; Lorrain *et al.*, 1997; Oerter *et al.*, 1992; Tison *et al.*, 1993; Weeks and Ackley, 1986]. In this paper we will use the "facies" terminology *sensu lato*, that is, to describe various textural arrangements, without any implication of their genesis.

*Columnar ice*, made of large, vertically elongated crystals with intracrystalline substructures is unanimously recognized as the unequivocal signature of *congelation* ice resulting from direct freezing of sea water, at the bottom of an ice floe, for example. It is also generally agreed that the term *granular* applies to any sea (marine ice) texture with equigranular crystals. When it is polygonal (sharp linear crystal contours) with no interlocking grains and often quite porous, it is the signature of *snow ice*, a facies inherited from sea water infiltration of the surface snow layer of the sea ice cover. Another granular facies closely related to the snow cover, but less frequently encountered, and described but not illustrated here, is *superimposed ice* [see, for example, Kawamura *et al.*, 1997]. When granular ice is polygonal, but clearly shows interlocking morphology of grain boundaries and eventually subgrains and polygonization features, it points to a considerable retexturing of the initial crystals through recrystallization under stress.

*Frazil ice* is a general genetic term for individual ice crystals formed in the water column. Although, following the WMO nomenclature [WMO, 1985], individ-



Table 1. Textural-Genetic Equivalences for Sea Ice and Marine Ice

Textural Facies	Sub-facies	Genetic term	Process
Columnar		<i>Congelation sea ice</i>	Direct freezing of sea water
Granular	Polygonal (not interlocking, voids)	<i>Snow ice</i>	Infiltration of sea water in the surface snow-cover
	Polygonal (interlocking, medium to coarse)	<i>Frazil ice</i>	Modified by dynamical recrystallization (cumulative strain during ice shelf spreading)
	Orbicular	<i>Frazil ice</i>	Individual ice crystals forming in the water column: <ul style="list-style-type: none"> <li>• wind- and wave-induced (surface layer-max:50 cm)</li> <li>• double diffusion between two water masses</li> <li>• thermohaline convection at the base of a growing congelation layer</li> <li>• adiabatic supercooling in rising water masses</li> </ul>
Platelet		<i>Frazil ice</i>	Adiabatic supercooling in rising water masses, and passive transport to the front of ice shelves
Draped		<i>Mixed Platelet/ Congelation</i>	
String-lined		<i>Frazil ice</i>	Modified by dynamical recrystallization under compressive stress
Banded	Rectangular	<i>Frazil ice</i>	Adiabatic supercooling in rising water masses
	Wave-like		

ual crystals are described as "fine spicules or plates of ice, suspended in water", it can result in more diverse textural facies both in sea ice and marine ice. It commonly occurs in sea ice as a *granular orbicular* texture, with rounded crystal boundaries both in vertical and horizontal thin sections. Weeks and Ackley [1986] gave a clear synthesis of the four major processes that contribute to frazil ice production in the polar oceans (see Table 1). The *wind- and wave-induced* process concerns sea ice exclusively. *Thermohaline convection at the base of a growing congelation ice layer* applies whenever congelation ice forms, that is both below sea ice and, at least theoretically, at the bottom of ice shelves.

*Double-diffusion between two water masses* occurs wherever a salinity gradient exists between water masses both at their pressure melting point. Finally, *adiabatic supercooling in rising water masses* requires the large thicknesses of ice shelves (marine ice), although it can eventually feed the landfast sea ice cover with individual frazil ice crystals.

Of particular interest is the *platelet facies*. Since it has generally only been observed close to ice shelf fronts it has been attributed to unrestrained frazil ice nucleation and growth resulting from adiabatic supercooling in ascending Ice Shelf Water as part of the Deep Thermohaline Convection (DTC) [e.g., Eicken



and Lange, 1989; Kipfstuhl, 1991]. Nucleation and growth of plate-like frazil ice crystals directly to the bottom of an existing ice sheet from an adiabatically supercooled water mass has also been invoked [Eicken and Lange, 1989; Gow *et al.*, this volume]. Some authors [Eicken *et al.*, 1994] suggest that the platelet facies is the original texture of all marine ice formed in the DTC under large ice shelves, and that it is eventually later reduced in size and shape under deviatoric buoyancy stress, as thick layers of loose platelets accrete at the bottom. Platelet facies are indeed only observed in very small amounts and in particular occurrences in marine ice cores [Tison *et al.*, 1993]. Some debris-free granular marine ice facies observed at HGIS are, however, so fine grained that, in that case, a process of fragmentation under the deviatoric buoyancy stress is hard to envisage. Furthermore, these fine grained facies also occur as irregular pockets surrounded by populations with larger crystal sizes, and these structures are more easily explained in terms of heterogeneity of the loose frazil as it consolidates, rather than in terms of homogeneous large scale post-depositional deformation structures. Bombosch and Jenkins [1995] suggest, by modeling frazil ice production in Ice Shelf Water, that the platelet ice facies could be associated with the evolution of ice crystals passively entrained in Ice Shelf Water as it levels off and exits at some depth in front of the ice shelf.

Recent work has demonstrated that what is commonly named as the platelet facies shows in fact a considerable variability. Lange [1988], who initially introduced the terminology, describes this facies as predominantly made of "elongated grains" (spicules) both in vertical [Lange, 1988: Figure 5a] and horizontal [Lange, 1988: Figure 5b] thin sections. The author mentions that platelet ice is, however, often interspersed with regions of smaller equigranular grains. Further observations [Jeffries and Weeks, 1993; Jeffries *et al.*, 1993] pointed to the fact that the platelet facies generally occurs as a *mixed platelet/congelation facies* with a wide range of proportions between the two components. Figure 1b illustrates an example of the platelet ice facies comprised almost entirely of platelet crystals. Figure 1a shows an example where individual platelet crystals are less abundant. In that case, they are eventually less angular and show wavy uneven edges. This we call the *draped facies* following Jeffries *et al.* [1993] who pointed out the draped appearance of the platelet crystals. Other mixed facies like the mixed columnar/granular facies were also extensively described in the Weddell Sea [e.g. Eicken and Lange, 1989].

When granular orbicular marine ice is submitted to strong compressive stresses (for example between two coalescent continental floating ice flows) it develops fold structures underlined by rectangular crystals arranged in individual curved alignments. This particular facies was recently described by Tison *et al.* [1997] and called *string-lined facies*. It is not known presently if it could develop in strongly deformed pressure ridges of landfast sea ice.

Finally, as discussed further in this paper, a new marine ice facies was discovered in the frontal area of Hells Gate Ice Shelf. Typically it is composed of stacks of rectangular crystals of various sizes in vertical thin section, the limits of which are commonly underlined by trains of brine inclusions [Lorrain *et al.*, 1997; Tison *et al.*, 1993]. This facies was named "banded facies" and shows strong similarities with the bottom layer of some of the southernmost sea ice cores (52 and 54) described by Gow *et al.* [1987] in the Weddell Sea. These authors describe it as "wafer-like" crystals [Gow *et al.*, 1987: Figure 14 (left) and Figure 25] and note that "the crystals are so loosely bonded at the very bottom that it was often difficult to obtain competent core when drilling floes containing this kind of ice". Ice fabrics in these layers exhibited vertical c-axes and the authors suggested that this type of ice might represent underwater ice as described by Russian observers at Antarctic coastal locations [e.g., Serikov, 1963]. We will see later that this facies is also found in the landfast sea ice accreting in front of HGIS. It should be noted (see Plate 1 and Figure 1) that the banded facies strongly differs from the other frazil ice facies associated with adiabatic supercooling in DTC, i.e., platelet and draped facies. It shows no interstitial congelation ice, and the crystals appear rectangular in vertical thin sections, and platy (with shaded extinctions) in horizontal thin sections (see also Plate 3 and Figures 11 and 13). Furthermore, c-axes are strongly concentrated in a single maximum roughly perpendicular to the plates instead of the random arrangement found in the platelet facies. As a matter of fact, this facies would probably better deserve the "platelet" denomination than the platelet facies which would, in turn, be better described as an "acicular facies" or "mixed acicular-congelation facies".

#### CURRENT STATE OF KNOWLEDGE OF SEA ICE VARIABILITY IN THE ROSS SEA

Recent work by Jeffries and Weeks [1991a; 1991b; 1993], Jeffries *et al.* [1993] and Jeffries and Adolphs [1997], has concentrated on sea ice properties in



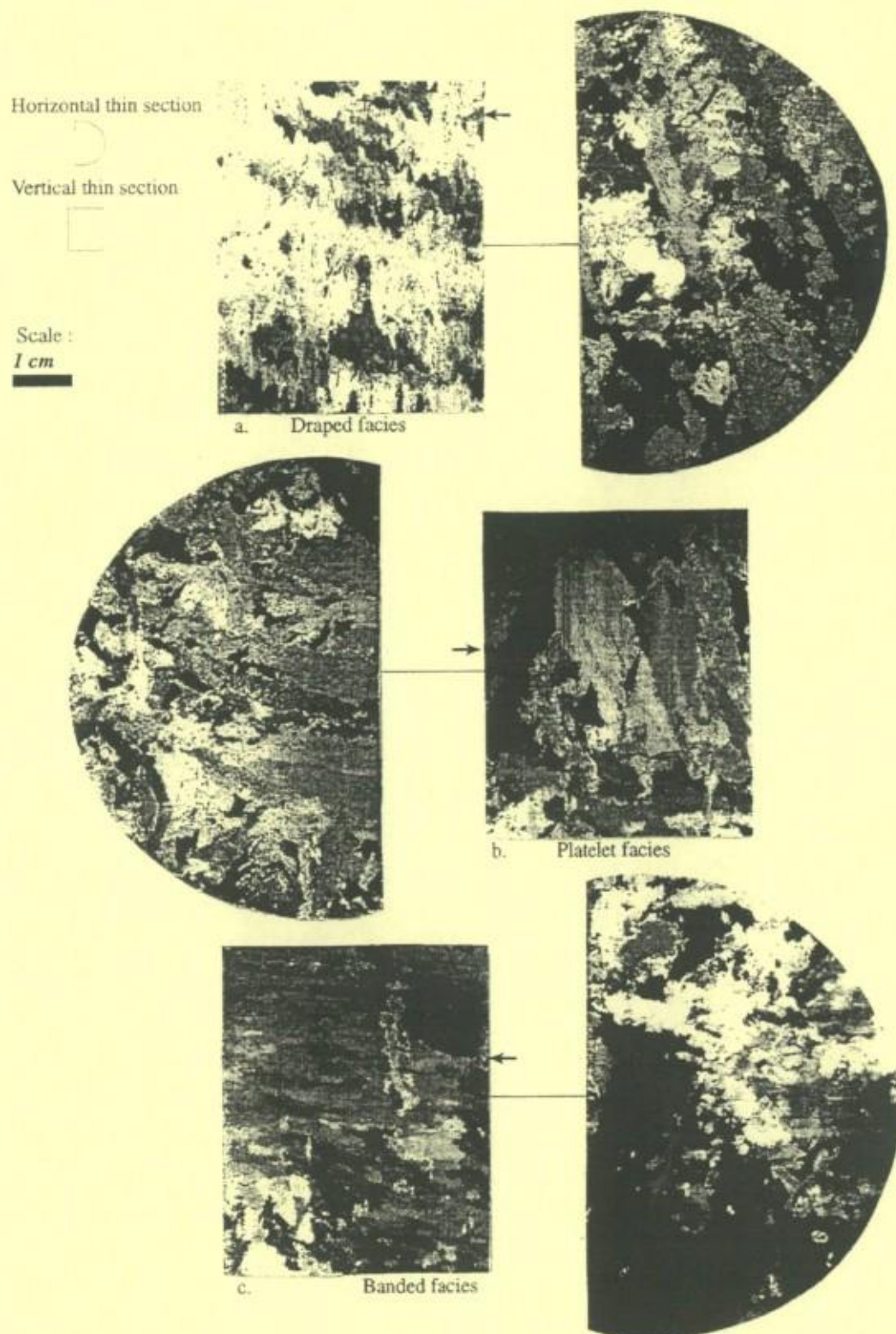


Fig. 1 : Comparison of the draped (a), platelet (b) and banded (c) facies in horizontal and vertical thin sections. The arrow on the vertical thin sections shows the location of the horizontal thin sections. All samples are from the landfast sea ice data sets at HGIS (a = core SA, depth : 212 cm; b = core SA, depth : 221 cm; c = core SE, depth : 175 cm).



McMurdo Sound and the western Ross Sea. *Jeffries and Weeks* [1993] sampled the sea ice cover in a transect from the Balleny Islands (62.50° S, 158.8° E) to McMurdo Station, via Cape Adare, Terra Nova Bay and Franklin Island (their Figure 1). Eighteen ice cores between 0.53 and 1.56 m long were sampled and analysed for their textural facies. Most of these cores were obtained quite far from the coast. Their texture is dominated by columnar (congelation) ice (22 to 100%) and frazil ice (5 to 74.4%). The latter is thought to have originated from a "pancake cycle" similar to the one described by *Wadhams et al.* [1987] and *Lange et al.* [1989] in the Weddell Sea. Attention should be drawn, however, to cores RS14 to RS16, that were retrieved from the South side of Drygalski Ice Tongue, i.e. close to a coastal floating ice body. Indeed, one of them (RS15) is the only one displaying platelet ice, and this in considerable amounts (64%). The authors drew attention on the fact that ISW was detected near the ice tongue and that the high proportion of platelet ice observed in the core might reflect adiabatic supercooling in this low density water outflow. On the other hand, core RS16 shows the highest percentage of frazil ice (88.5%), of which it is exclusively formed, if we discard "deformed ice" facies. Most recently, *Jeffries and Adolphs* [1997] have confirmed the strong contrast between pack ice and landfast sea ice characteristics in the Ross Sea, on an even wider scale. The pack ice floes they described were primarily built through dynamic processes and showed generally lesser thickness than the landfast ice for which thermodynamic processes are dominant.

Of even greater interest for studies of ice-ocean interactions under ice shelves is the investigation of landfast sea ice in McMurdo Sound (see detailed synthesis in *Gow et al.* [this volume]). *Jeffries et al.* [1993] describe sixteen sea ice cores between 1.26 and 2.34 m long sampled in the area. A typical structure of all these cores (illustrated in their Figure 6) consists of an upper congelation ice layer and lower layers of mixed congelation/platelet or platelet ice. Overall, the fast ice comprised 62.1% congelation ice, 28.3% platelet ice and 9.3% congelation/platelet ice. However the proportion of platelet ice might be underestimated due to bottom melting earlier in the summer. Apart from two exceptions, the basal layer of each core was platelet ice. However, the authors stressed clearly that the distinction between platelet and mixed platelet/congelation ice was quite arbitrary, since the platelet facies always showed interstitial congelation ice. The limit was arbitrarily taken at 50% between the "mixed" and the "pure"

platelet facies. *Jeffries et al.* [1993] and *Jeffries and Weeks* [1993] also showed that fabric diagrams from platelet and platelet/congelation facies are bi-modal: c-axes concentrated in the equatorial circle on a Schmidt net correspond to congelation ice crystals whilst most of the platelet crystals from the same sample show a random distribution. It is also worth noting that a wide variety of platelet ice textures was observed in McMurdo Sound. The same authors mention that "...many of the platelets were less angular, more equidimensional and had wavy, uneven edges... densely packed accumulations of these wavy-edged platelets gave the ice a distinctive appearance resembling a draped fabric". Comparison of the percentage of each core containing platelet ice with contour lines of surface supercooling measured in 1982 by *Lewis and Perkins* [1986] supports the idea that the platelet ice originated by adiabatic supercooling of the Ice Shelf Water formed below the Ross Ice Shelf.

Finally, *Jeffries et al.* [1993] used the mean plate width in the congelation crystal sub-structure to compare growth rates of congelation ice at the top of the cores and of interstitial congelation ice in the mixed platelet/congelation facies. Surprisingly, they noticed no significant trend of decreasing growth rate with depth, as would be expected in a process where freezing is mainly controlled by heat conduction through the existing sea ice cover. This particular phenomenon was seen as the expression of a lower heat flux at the platelet-rich growth interface (where only interstitial water has to be frozen and is guaranteed to be at, or even below, the freezing point) than at the base of the unconsolidated platelet crystal layer.

The most recent description of McMurdo Sound landfast sea ice (based on a data set sampled in October-November 1980) by *Gow et al.* [this volume] generally supports the material published earlier. It shows in greater detail the relationship between the circulation patterns of near-surface currents and the strength of the ice fabric in the columnar-congelation ice. It also suggests from field and textural observations that the dominant mechanism of platelet ice accretion is nucleation and growth of plate-like frazil ice crystals directly to the bottom of the existing ice sheet.

#### HELLS GATE ICE SHELF : MORPHOLOGY, ICE DYNAMICS AND MASS BALANCE

Hells Gate Ice Shelf (Figure 2) is a small antarctic ice shelf located in Terra Nova Bay (Victoria Land, lat. 74°50'S, long. 163°50'E). It is derived from the larger



## Nomenclature of main SEA/MARINE ICE facies

- **COLUMNAR**  
(vertically strongly elongated crystals; intracrystalline sub-structures)

1 cm



- **GRANULAR**  
(equigranular crystals)

- **POLYGONAL**

- Not interlocking



- Interlocking (Medium)



- Interlocking (Large)



- **ORBICULAR**

- Medium



- **PLATELET**  
(elongated acicular crystals)



- **DRAPED**  
(draped texture)



- **STRING-LINED**



- **BANDED**

- **RECTANGULAR**

- Small

- Large



- **WAVE-LIKE**



Plate 1 : Nomenclature for the main sea ice and marine ice facies discussed in this paper. The thin sections are in the vertical plane and the scale is valid for all pictures (see text for details).



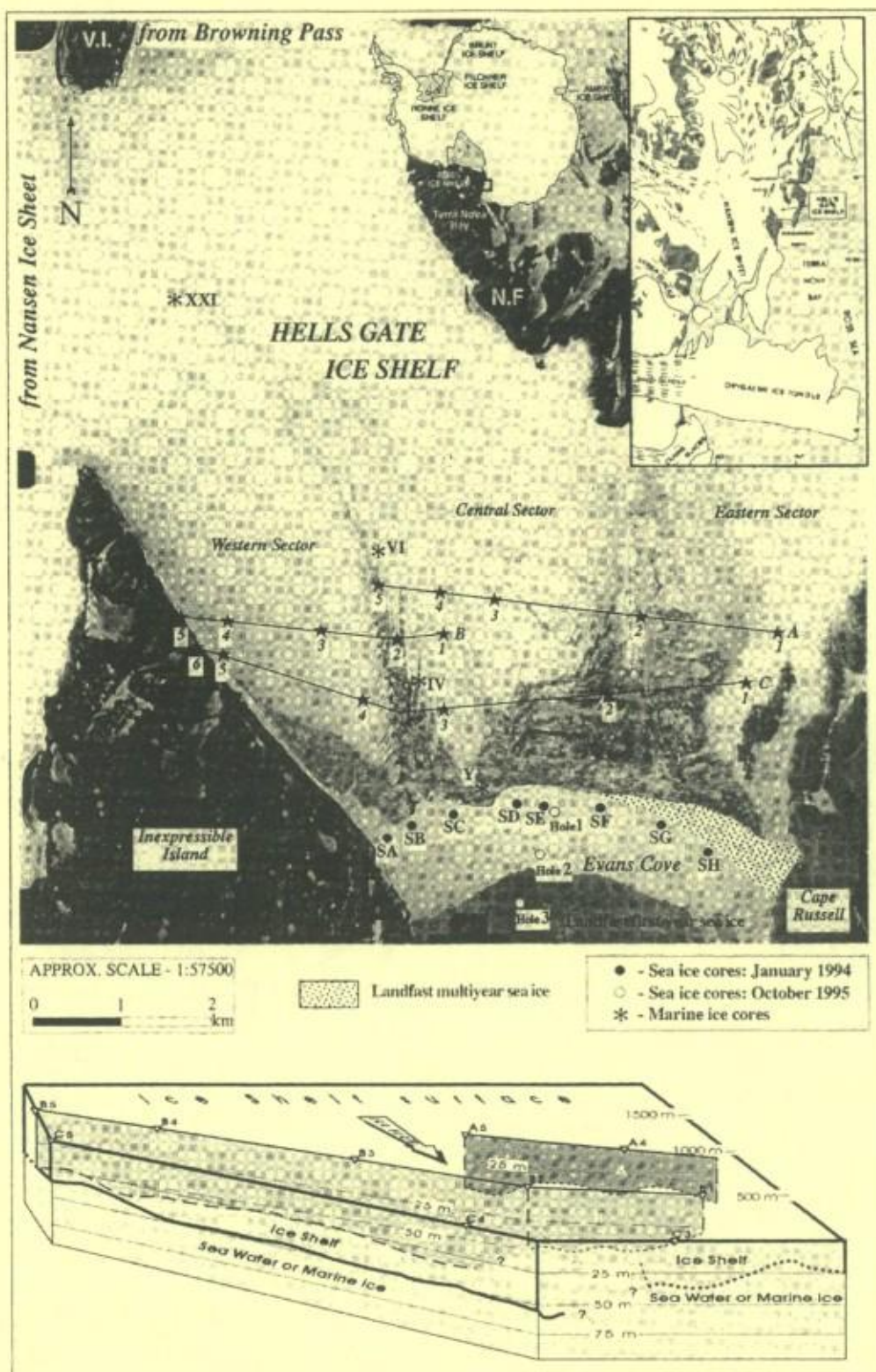


Fig. 2 : Location and main features of Hells Gate Ice Shelf showing the position of marine and sea ice cores and of the echosounding profiles from 1991 (top). The bottom drawing is a 3-D sketch of ice shelf thicknesses deduced from the 1991 echosoundings. Aerial photograph in the background is : Terra Nova Bay - 11.06.1985 - FL 152.27 - TMA-2851-V. V.I. = Vegetation Island; N.F. = Northern Foothills.



Nansen Ice Shelf (NIS) and reaches the sea near Cape Russell. HGIS extends from North to South for 16.6 km with a maximum width of 9.8 km. It is composed of three main sectors (western, central, eastern) separated by two medial moraines stretching roughly North-South.

Early radio-echo sounding (RES) profiles [Souchez *et al.*, 1991] obtained about 1.5 km inland from the ice front (Figure 2, bottom), showed a maximum ice shelf thickness of 70 m in the western sector reducing to only 20 m in some areas of the central sector. Furthermore, the interface picked-up by the RES was typically undulating in the central sector (A5-A3, B2-B1, C4-C3 in Figure 2 bottom), in phase with a clear-cut surface boundary between clear ice upstream and dark ice downstream. These data must, however, be treated carefully since, in several instances (especially in the central sector), the return signals were quite weak. It is, therefore, not known, in these cases, if the depth obtained corresponds to the ice-ocean interface, or to the continental meteoric ice-marine ice interface. Several arguments favor the latter hypothesis. First, seismic investigations [F. Merlanti, personal communication, May 1997] performed in the same area systematically provide higher ice thicknesses (22% higher in the western sector, 33% to 55% higher in the central sector). Secondly, isotopical ( $\delta^{18}\text{O}$ ,  $\delta\text{D}$ ) and crystallographic investigations of the surface clear-cut boundary indicate that it delimits continental meteoric ice (light gray, upstream) from marine ice (dark gray, downstream) [Lorrain *et al.*, 1997; Tison *et al.*, 1993]. Finally, core Y (Figure 2, top), obtained downstream of line C within a few tens of meters of the ice front, reached a depth of 44 m, clearly in contradiction of the RES data from C3-C2. For the same reasons, more recent RES data from further upstream are somewhat discordant [Tison *et al.*, 1997 and A. Lozej, personal communication]. However, measurements agree on a thickness of about 150 m some 6 kilometers inland from the front. A maximum value of 250 m has been measured nearly 10 kilometers from the front, in the central part of the flow between Vegetation Island and the Northern Foothills (Figure 2).

The specific lay-out of the meteoric ice/marine ice boundary near the front, the shape of the marine ice outcrops visible upstream in the eastern part of the central sector, the large scale foliation patterns and the RES return from the central sector all suggest that the ice shelf results from the coalescence of several individual ice flows of different sizes, marine ice accreting in the upstream area (near the grounding area or around a pinning point) acting as a "welding unit" between these various ice flows. This is a situation similar to the one

detected, at a much larger scale, beneath the Ronne Ice Shelf by Corr *et al.* [1995]. Comparing RES data to precise GPS determination of ice thickness at Ronne Ice Shelf revealed large discrepancies due to considerable lateral accumulation of marine ice between the Rutford and Evans Ice Streams. These accumulations could only have formed as the two ice streams were ungrounding and joining together, upstream of the measured profiles.

Large scale morphological patterns (e.g. twin alignments of morainic dirt cones), marine ice outcropping patterns and ice foliation patterns also suggest a complex dynamical behavior of converging flow in the Hells Gate Ice Shelf. Side effects considerably affect the flow patterns in some areas [Tison *et al.*, 1997]. An oblique component of the flow in the western sector brings the ice in compression against the central sector, and results in shearing of part of the marine ice initially accreted between the two flows (Figure 3a). This results in the typical outcropping and foliation patterns of Figure 3b. At a smaller scale, this compressive regime affects the crystal structures both in the granular and banded facies (Figure 3c). The granular facies develops a preferential curved alignment of rectangular crystals ("string-lined" facies) and the initially rectangular crystals of the banded facies are re-arranged in folded structures. Similar features were successfully modeled and experimentally produced by Wilson *et al.* [1986] and Wilson and Zhang [1994]. More generally, the granular facies is frequently polygonal with interlocking crystal boundaries, a sign of crystal evolution under considerable cumulative strains (see section 2).

Horizontal surface velocities were estimated using two independent techniques by Baroni [1990], Baroni *et al.* [1991a], Baroni *et al.* [1991b], and Frezzotti [1993]. The western medial moraine is associated with marine ice forming at the southern tip of Vegetation Island (V.I. in Figure 2), where the flows from NIS and from Browning Pass meet. This moraine is composed of twin dirt cones that contain shells, worm tubes (serpulids) and sponges spicules, some in "living" position. Hypothesizing that these biogenic materials were incorporated into the marine ice at the ice-bedrock interface around Vegetation Island, dating of the shells [Baroni, 1990] provided estimates of surface velocities varying between 10.4 and 17.4  $\text{m a}^{-1}$ . Similarly, on the eastern moraine, velocities of 3 to 3.7  $\text{m a}^{-1}$  were obtained. These values are in good agreement with those calculated from comparison of aerial photographs taken in 1956 and 1985 giving 2.9 to 3.8  $\text{m a}^{-1}$  and 8.8 to 11.9  $\text{m a}^{-1}$  for the eastern and western sectors respectively.

Marine ice accretion rates are difficult to assess



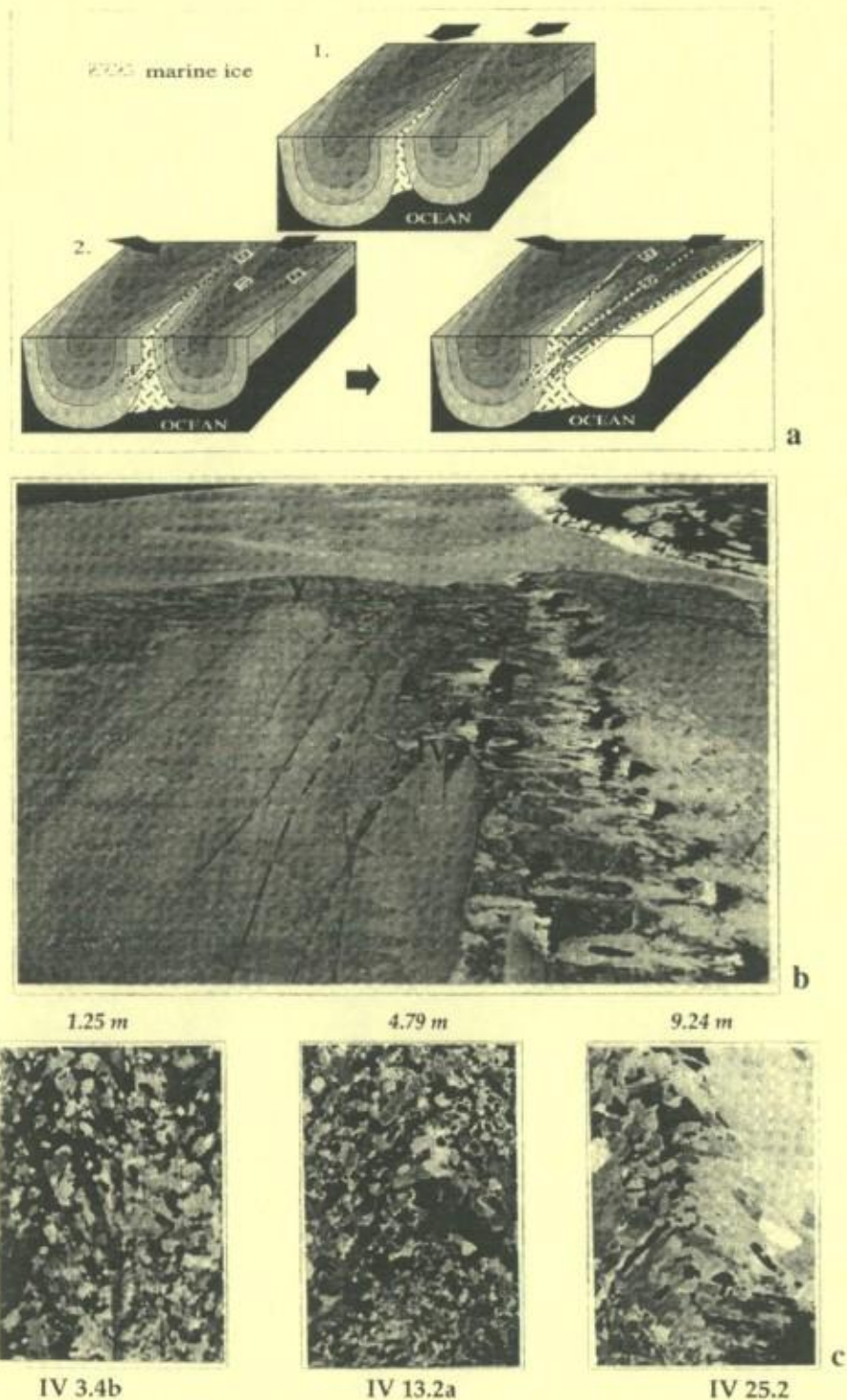


Fig. 3 : Deformational structures at Hells Gate Ice Shelf (see text for details): a) Diagram illustrating the process of shearing of marine ice at the junction of two individual ice flows with different flow directions (2); b) Oblique aerial photograph of the western-central sector of HGIS, close to the ice shelf front, showing the location of ice cores IV and Y. Note the similarity of patterns with diagram a; c) Three examples of folds and crystals bending in the orbicular and banded marine ice facies of core IV. Thin sections are shown at scale 1:1 in the vertical plane. Mean depths are shown on top and sample codes below.



from mass balance calculations, since these require surface strain rates measurements that are not available at present for HGIS. A crude estimate can, however, be made on the basis of shell dating and thickness estimates near the front. Baroni [1990] obtained a range of 0.122 to 0.250 m a<sup>-1</sup>, depending on the method used to correct the <sup>14</sup>C ages BP. These values are, however, minimum estimates, since the shells might have been brought to the surface further upstream in the ablation area, where thicknesses are higher. Another calculation can be made considering the surface velocity range obtained from aerial photographs for the western moraine, and the (minimum) seismic ice thickness of 126 m [F. Merlanti, personal communication, May 1997] measured at the location of marine ice core XXI. As clearly seen on Figure 2, this ice core is located on the most upstream outcrops of the marine ice body that formed at the southern tip of Vegetation Island. A somewhat higher range of 0.43 to 0.58 m a<sup>-1</sup> is obtained. These marine ice accretion rates are also higher than the surface ablation rates of 0.17 to 0.28 m a<sup>-1</sup> calculated by Baroni [1990] from dirt cone build-up rates or 0.20 to 0.30 m a<sup>-1</sup> estimated from bamboo poles ablation measurements [A. Bondesan, personal communication, June 1996]. The marine ice accretion rates estimated here are of the same order of magnitude as those modelled by Jenkins and Bombosch [1995] at Filchner-Ronne Ice Shelf for different frazil crystal sizes (about 0.5 m a<sup>-1</sup> mean value), although these were occurring much further away from the grounding line in their case of a much larger ice shelf with expected much lower thickness gradients [Paterson, 1994: Figure 12.3]. Furthermore, the estimates given here at the location of ice core XXI should still be considered as minimum values, since accretion is thought to occur in the inverted depression associated with the merging of the two ice flows at the southern tip of Vegetation Island, as discussed above.

Finally, it is worth comparing marine ice accretion rates to an estimate of direct accretion rates from heat conduction through the ice shelf at the location of ice core XXI. Using a thickness of 126 m and a mean air temperature of -18°C [Ronveaux, 1992: Table 4] gives a value of 0.029 m a<sup>-1</sup> for direct freezing of sea water at the interface. Therefore, marine ice accretion rates are an order of magnitude higher than for direct congelation of sea water at the bottom of 126 m of ice. It is only for marine ice accretion under less than 20 m of solid ice that the consolidation rate of the loose frazil will "keep pace" with the accretion rate, considering a porosity of 40%. A considerable delay will therefore exist between

the accretion time and the consolidation time, especially for the lower units of the loose frazil ice accretion. This is of crucial importance, as will be discussed later.

## MARINE ICE RECORDS AT HELLS GATE ICE SHELF

### Previous Work

Taking advantage of specific climatic conditions that allow marine ice to outcrop at the surface of Hells Gate Ice Shelf, Souchez *et al.* [1991] and Tison *et al.* [1993] used shallow depth (2 m) surface ice cores on two longitudinal profiles (along flow lines) to study marine ice properties within a few kilometers of the ice shelf front. The latter authors have shown that two main types of marine ice exist at Hells Gate Ice Shelf, with contrasting textural and chemical properties revealing specific environments and depositional processes.

The first type is a granular facies, similar to the one described in other deeper marine ice cores with thicknesses ranging from 45 to 170 m (Amery Ice Shelf - [N. Young, personal communication, March 1995] and Filchner-Ronne Ice Shelf [Eicken *et al.*, 1994; Oerter *et al.*, 1994; Oerter *et al.*, 1992]). At Filchner-Ronne, crystals were equigranular in dimensions but showed a regular increase in size down the profile that was explained in part by the thermal history of this layer [Eicken *et al.*, 1994; Oerter *et al.*, 1994; Oerter *et al.*, 1992]. Conductivities (salinities) were very low (down to <0.03‰ salinity, i.e., up to 2 orders of magnitude lower than those measured in sea ice), decreasing downwards along the profile and eventually stabilizing in the lower part of the core. Stable isotopes were reckoned as fairly constant and reflecting equilibrium fractionation during freezing from sea water (slightly positive  $\delta^{18}\text{O}$  values) both at Amery and Filchner-Ronne Ice Shelves. Sediment layers (aggregates of silt and clay-sized minerals and biogenic material) were found within the marine ice at Filchner Ronne Ice Shelf, close to the transition from meteoric ice.

In addition to the granular facies (not only showing very low salinities, but also strong chemical fractionation and random ice fabrics at HGIS), another facies, called "banded facies" (Plate 1 and Figure 1c), was observed in considerable amounts, with higher mean salinities, less chemical fractionation and strong single maximum fabrics. Statistical counting on a longitudinal profile suggested that there might be an increasing proportion of the banded facies as one gets closer to the ice shelf front. This was later confirmed by a systematic



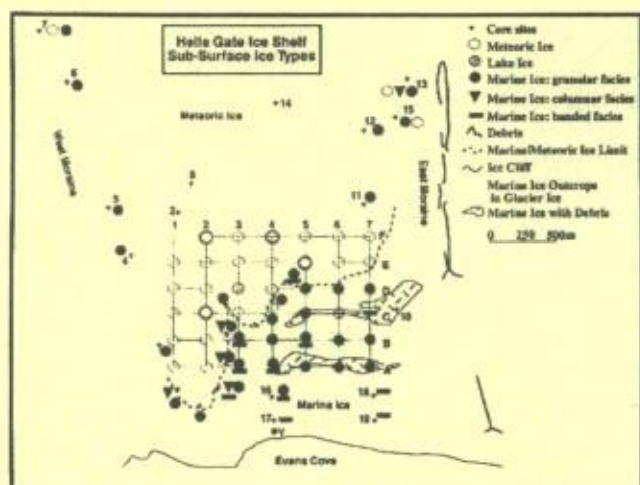


Fig. 4 : Sub-surface (2m depth) ice types at Hells Gate Ice Shelf (after [Lorrain *et al.*, 1997]).

grid survey of 60 shallow cores (Figure 4 and Lorrain *et al.* [1997]). From these data, together with observed shifts in isotopic compositions ( $\delta^{18}\text{O}$ - $\delta\text{D}$ ) of marine ice samples larger than the maximum possible equilibrium fractionation from sea water values, we conclude that active transfer of marine ice was occurring in a downstream direction at the bottom of Hells Gate Ice Shelf [Souchez *et al.*, 1991].

Of particular concern are the very low salinities observed in the granular marine ice facies. Authors agree on the fact that such levels can be produced neither by a simple process of equilibrium freezing (at very low rate) of loose frazil ice crystals in a matrix of sea water, nor by desalination processes at a later stage [Eicken *et al.*, 1994; Tison *et al.*, 1993]. Kipfstuhl *et al.* [1992] and Eicken *et al.* [1994] favor a process by which mechanical compaction of centimeter-sized platelet ice crystals results in reduction of crystal size, reduction of porosity and consolidation under the deviatoric buoyancy stress, with no significant in-situ ice growth. Tison *et al.* [1993] propose another explanation that links the low salinities of the consolidated granular facies to dilution processes of the "host" water in which accretion of the loose frazil ice crystals occurs. Dilution results from melting at the base of the ice shelf, and irregularities at the ice shelf/ocean interface favor "trapping" and relative isolation of both the loose crystals and the water of reduced density. This process allows for chemical fractionation under differential diffusion processes between the "host" water of the loose frazil and the ocean water below the interface. The whole mechanism, however, requires having both melting and frazil ice accretion occurring in areas nearby. One way to deal with this ap-

parent contradiction is to consider areas near the grounding line where melting by HSSW inflows in the DTC can occur and where large lateral irregularities must exist because of merging of individual ice flows (see discussion of RES in previous section). These would hold particularly for larger and thicker ice shelves like the Filchner-Ronne, but obviously not for HGIS where maximum ice thicknesses of 250 m are observed upstream of the southern tip of Vegetation Island. The heat source for melting was therefore left unresolved in previous marine ice studies at HGIS.

#### Location and Sampling of a New Data Set

During the IXth Italian Antarctic Expedition (1993-1994) about 60 shallow (2 m) to medium depth (10-45 m) ice cores were sampled at Hells Gate Ice Shelf, downstream of Vegetation Island, a local pinning point (Figures 2 and 4). We will concentrate here on a set of four cores (XXI, VI, IV, Y), drilled on the eastern flank of the western dirt cones moraine and aligned parallel to the flow lines, as deduced from the horizontal surface velocity field [Frezzotti, 1993].

The cores were retrieved using a modified version of the CRREL Rand Auger [Rand and Mellor, 1985], transferred into polyethylene bags, stored at  $-25^{\circ}\text{C}$  at Terra Nova Station and shipped to Brussels at the same temperature for further processing. Vertical thin sections were cut along the total length of each core to allow observation of the different ice textures and to guide the isotopic sampling. The thin-sections were prepared using standard microtoming techniques and photographed between crossed polarizing filters. It should be noted, in this regard, that the subvertical striae visible in some of the thin sections illustrated in this paper are artefacts of the microtoming procedure. After reducing the diameter of each core by 5 mm to eliminate surface contamination, two samples, each with dimensions of  $1 \times 2 \times 7.5$  cm, were collected at depths corresponding to the top of each thin section, i.e., with a mean sample spacing of about 0.1 m. Non-contaminating polyethylene gloves were always used for handling, and cutting was performed with a clean band-saw previously tested as non-contaminating for the major ions of interest. The twin samples were then allowed to melt in polyethylene tubes, before their conductivity was measured using a Taccussel CD 810 conductimeter in a  $25 \pm 0.01^{\circ}\text{C}$  thermostatically-controlled bath. Salinities were deduced using calibration curves based on high precision ( $\pm 10^{-3} \text{‰}$ ) IAPSO salinity standards provided by Ocean Scientific International. The overall precision of the method is  $\pm$



0.05‰. The other sample collected at the same depth was analyzed for Na, K, Ca and Mg with a Varian SpectrAA 300 atomic absorption spectrophotometer.

Samples were also collected in selected locations for co-isotopic analyses of deuterium ( $\delta D$ ) and oxygen-18 ( $\delta^{18}O$ ). Samples with a volume of 5 ml were collected with the band-saw, and those with a salinity above 0.5‰ were distilled under vacuum prior to the isotopic analyses by a procedure proven to conserve the isotopic signal [Tison *et al.*, 1993]. The measurements were performed at the Nuclear Research Center of Saclay (France). HDO and  $H_2^{18}O$  concentrations are given in  $\delta$ -units versus V.S.M.O.W. (Vienna Standard Mean Ocean Water) expressed in per mil. The accuracy of the measurement is  $\pm 0.5\text{‰}$  in  $\delta D$  and  $\pm 0.1\text{‰}$  in  $\delta^{18}O$ .

### Results and Discussion

Plate 2 shows selected pictures of the textural characteristics of the studied ice cores. Cores XXI, VI and IV are each 10 m long and core Y is 45 m long. The pictures are full scale vertical thin sections photographed between crossed polarizers. Depths are given at the appropriate level on the right side of the pictures. The four cores were drilled on a longitudinal profile in the marine ice outcropping between the western and the central sectors (Figure 2 top). Given that the marine ice thickness is already 126 m at the location of core XXI, that the mean ablation rate is estimated to be between 0.20 and 0.30  $m\ a^{-1}$  and that the surface velocities are between 9 and 12  $m\ a^{-1}$  the cores are thought to adequately approximate what would be recorded with depth in a single ice core, close to the ice shelf front, supposing it had not been subjected to surface sublimation. Indeed, using the most conservative estimates for surface velocity (9  $m\ a^{-1}$ ) and for ablation rate (0.20  $m\ a^{-1}$ ) one can calculate that the amount of marine ice ablation between two successive core locations is 3 to 8 times higher than the core length at the most upstream site of each pair. Resulting profiles are therefore plotted on top of each other in Figures 5 and 6. It should be stressed, however, that this does not necessarily mean that the ice in core IV is younger than in core XXI, since this obviously depends on factors like the balance between horizontal velocities, surface ablation rates, marine ice accretion rates (of which we only have minimum estimates) and longitudinal extension of the marine ice depositional areas. Also, the dynamical characteristics of HGIS flow described above are likely to affect the original stratigraphy of the

marine ice deposits to a certain extent, and this will have to be taken into account in the discussion below.

Figure 5 gives the smoothed salinity profile. Figure 6 shows the K/Mg ratio at the same resolution and with the same smoothing interval as for salinity. This K/Mg ratio was chosen since it is unlikely to be affected by salt precipitation at temperatures encountered in the HGIS environment, or by subsequent long-term storage in freezers. Indeed, Richardson [1976], in his study of the phase relations in sea ice as a function of temperature, indicates that  $CaCO_3 \cdot 6H_2O$  is the first salt to precipitate from sea water at a temperature close to the freezing point and that  $Na_2SO_4 \cdot 10H_2O$  and  $CaSO_4 \cdot 2H_2O$  soon follow, at temperatures of  $-8^\circ C$  and  $-10^\circ C$  respectively. Following the same author, concentrations in K and Mg ions in sea ice at sub-freezing temperatures under quasi-equilibrium conditions do not change until the temperature falls below  $-34^\circ C$ .

Figure 7 shows the same data sets in K/Mg-salinity correlation graphs for each of the cores, compared to the range of sea water values of the K/Mg ratio (0.087–0.096) compiled from various authors [Addison, 1977; Goldberg, 1957; Wilson, 1975]. This reference level is also shown on Figure 6.

As mentioned before, selected samples were collected for co-isotopic measurements in  $\delta D$ – $\delta^{18}O$ . A commonly used representation for these data is a  $\delta D$ – $\delta^{18}O$  diagram (Figure 8), where samples of natural waters from large unconfined reservoirs would lie on a Meteoric Water Line of equation  $\delta D = 8\delta^{18}O + 10$  [Dansgaard *et al.*, 1973]. For the purpose of the discussion below, samples have been grouped in the two main marine ice textural facies.

Textural results from the studied cores (Plate 2) confirm the observations from previous work at HGIS. The two upstream cores (XXI and VI) show a granular facies exclusively, whilst core Y consists of 97% banded facies. The remaining 3% consists of granular ice, confined to discrete layers or pockets in the first 10 m of the core. Core IV, located about half-way between VI and Y (Figure 2), is of particular interest. Down to 5.35 m it shows a typical fine grained granular texture. It is also quite rich in fine insoluble particles (up to 0.8% debris in weight, excluding surface samples), as opposed to the other cores where virtually no debris was found. This is what would be expected for marine ice accreted close to a rock interface where suspension of mineral particles in the water can occur under tidal agitation. Below 6 m, core IV is exclusively banded, with the exception of the bottom 50 mm which consist of granular ice. Between 5.35 and 6 m, mixed



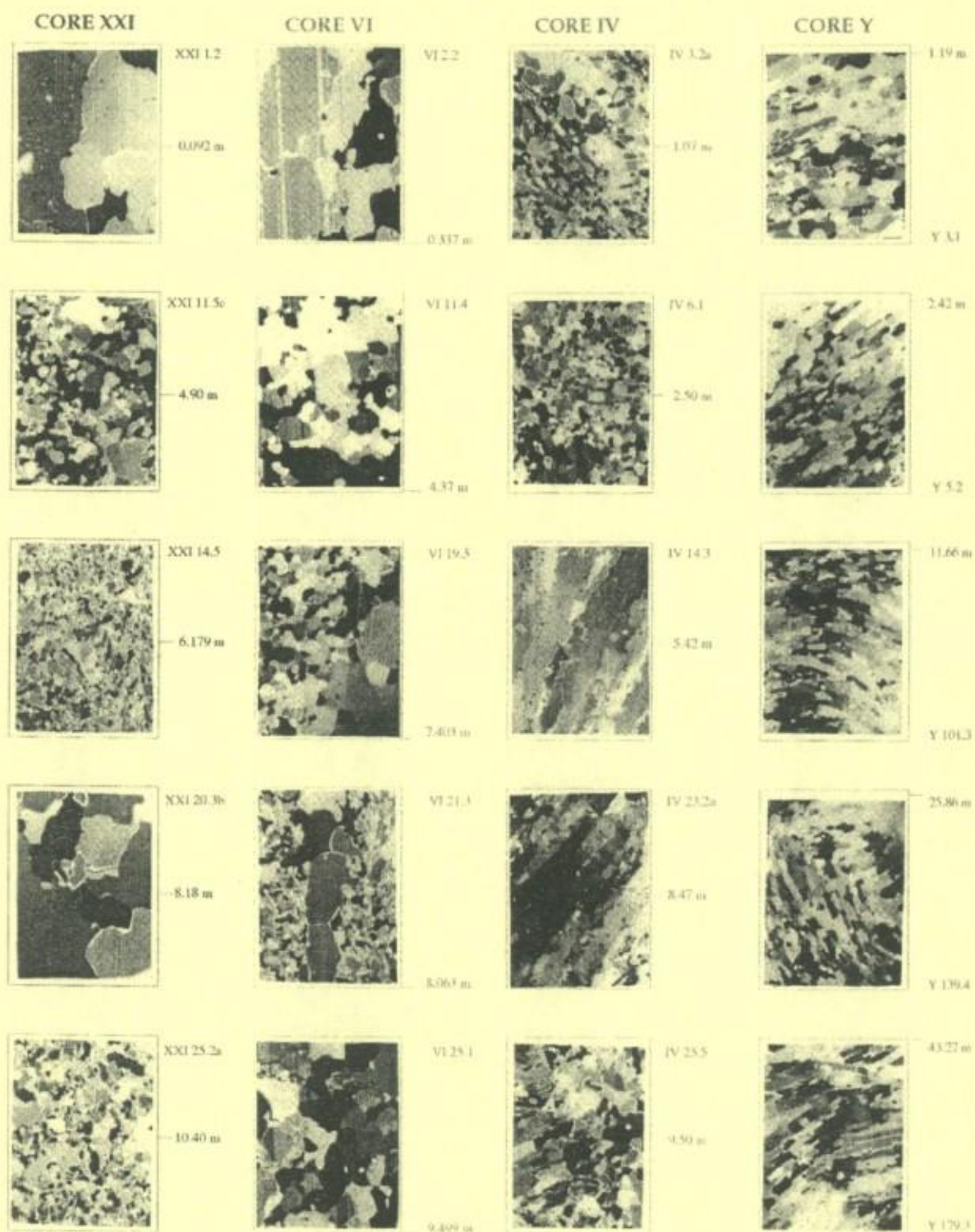
SCALE FOR ALL PHOTOGRAPHS :  = 1cm

Plate 2 : Selected typical textural characteristics of the four marine ice cores, shown in vertical thin sections between crossed polarizers. The scale shown at the top is valid for all photographs. Depths in meters are indicated to the right. Selection has been made to give a complete overview of textural variability inside the cores, rather than a true representation of the frequency of occurrence of the different facies.



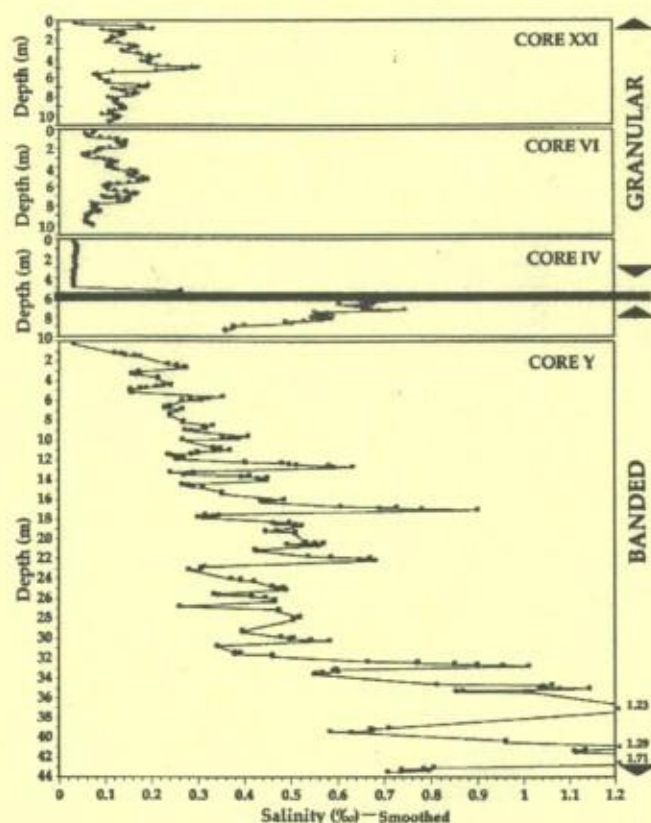


Fig. 5: Smoothed salinity profiles in the four marine ice cores. The smoothing interval is 0.40 m. The shaded area shows the transition zone of mixed congelation-platelet ice facies in core IV (see text for details).

congelation-platelet ice texture is observed, a facies only described once in the marine ice literature [Souchez *et al.*, 1991], at the limit of meteoric and granular marine ice at HGIS. This spatial layout supports the assumption made above that the vertical juxtaposition of the four cores illustrates the large scale (kilometre) distribution of the textural facies in a vertical plane oriented parallel to the mean flow line. The assumption, however, probably does not hold at the smaller metre to centimetre scales, owing to the specific geometry of Hells Gate Ice Shelf. The sharp textural contrast occurring at 5.35 m and the re-occurrence of the granular facies at the bottom of core IV could, therefore, be the signature of shearing of a lower stratigraphic unit higher up in the core. The tilting of the crystals might be a further argument in this respect.

The occurrence of medium to small-scale disturbances in the individual cores' stratigraphy are quite likely to affect equally the distribution of their chemical characteristics, as suggested by the sharp salinity gradient in core IV between 5 and 6 m depth (Figure 5) and

by the strong "noise" of unsmoothed salinity profiles. It would, therefore, be hazardous to discriminate between genuine and post-tectonic events in the fluctuation of salinity and K/Mg in each individual core of Figures 5 and 6, and we will only focus on general trends and mean values for each core and from core to core. Furthermore, besides dynamical disturbances, we have to keep in mind two other possible sources of alteration of the signals: surface modifications during the summer melt season, and interactions with the solid impurity content. The first process could be responsible for desalination of the top meter of the cores, as seems to be the case for all cores in Figure 5. It could also increase the K/Mg ratio through surface input of impurities of continental origin, since, as demonstrated by Casella *et al.* [in press] for snow accumulation in the Terra Nova Bay area (McCarthy Ridge and Styx Glacier), potassium is mainly of continental origin, whilst magnesium is mainly oceanic.

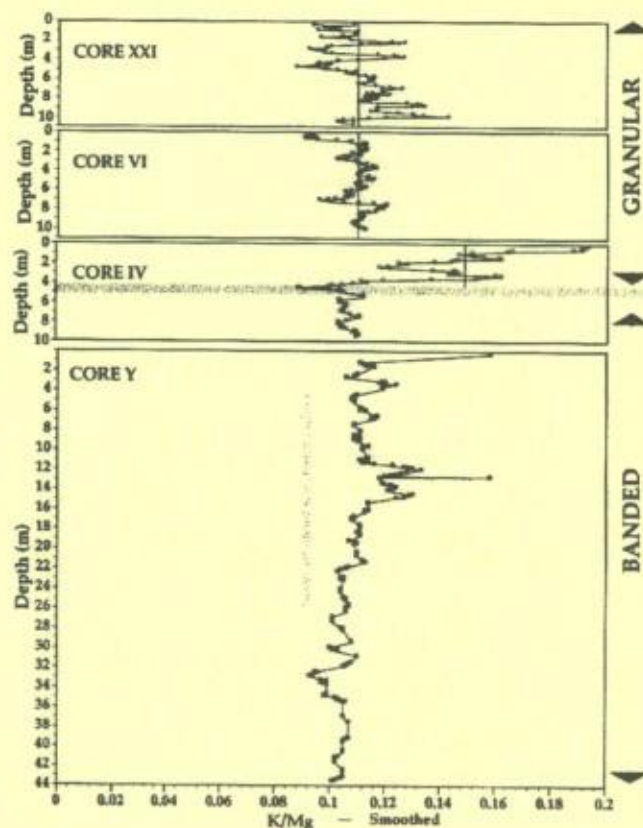


Fig. 6: Smoothed K/Mg profiles (ratios calculated from concentrations expressed in meq/l units) in the four marine ice cores. The smoothing interval is 0.40 m. The dark shaded area shows the transition zone of mixed congelation-platelet ice facies in core IV (see text for details). The K/Mg range in sea water is also indicated in light gray (see text for details).



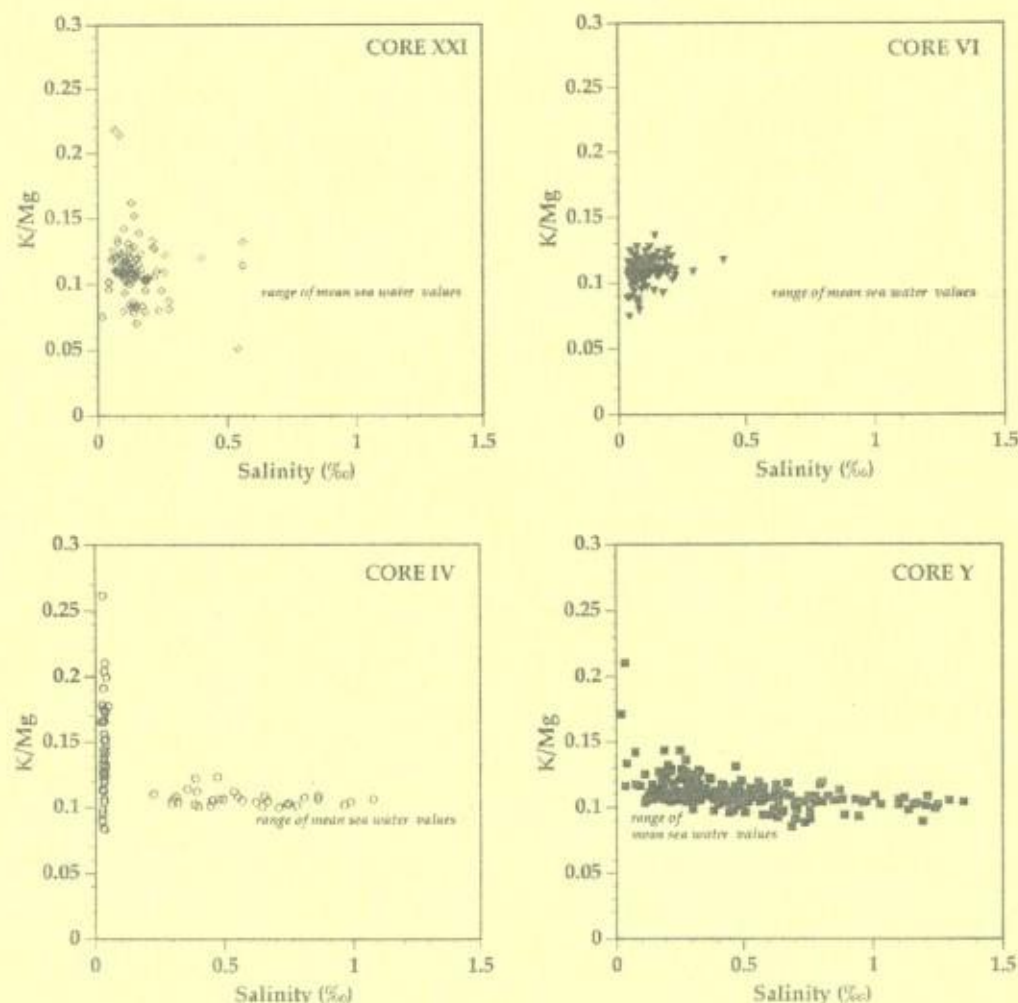


Fig. 7 : K/Mg-Salinity relationship in the four marine ice cores. Same conventions as in Figures 5 and 6.

Interactions with solid inclusions could also modify the chemical content of the ice samples through simple dissolution or, more likely, desorption effects from the surface of silt to clay-sized particles. This latter process, particularly, was shown to increase the alkali concentration with respect to that of the alkaline-earths in the solution, even after relatively short (minutes) contact times and for small amounts of particles [Souchez *et al.*, 1978]. This would, then, provide an artificial means of increasing the K/Mg in marine ice samples loaded with fine-grained solid impurities. Careful examination of the bottom of the sample tubes used for the chemical analyses performed on core IV revealed a thin deposit of insoluble residues. These were filtered, weighed with a precision balance ( $\pm 0.1$  mg) and expressed as debris/ice concentrations in weight percent. The results are plotted as a function of the K/Mg ratio in Figure 9. Except for three surface samples, all concentrations are

low (below 0.8% in weight), and there is no significant correlation ( $r^2 = 0.07$ ) between the two data sets. Contamination by the solid impurity content is, therefore, in this case, not likely to alter the conclusions of our study.

The salinity trend (Figure 5) in the granular facies corresponds to a decrease in a downstream direction, from maximum values of 0.3‰ in core XXI to values less than 0.03‰ in core IV. Both the trend and the minimum values are consistent with the observations in other deeper marine ice cores at Filchner Ronne Ice Shelf and Amery Ice Shelf [Eicken *et al.*, 1994; Morgan, 1972; Oerter *et al.*, 1992]. There is a sharp increase of the salinity when entering the mixed platelet-congelation horizon in core IV, with values of up to 1.1‰. In the banded facies of core Y, salinities are noticeably higher and universally increase with depth, especially below 32 m, where water was first



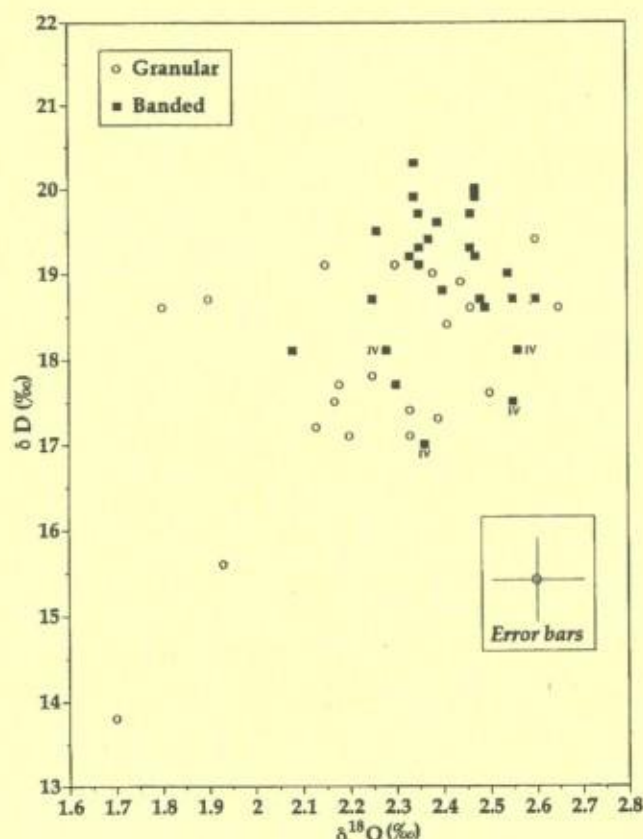


Fig. 8:  $\delta D - \delta^{18}O$  (‰) relationship for the two main marine ice facies.

observed to invade the drill hole. The water level rose slowly in the hole in the next 24 hours, and stabilized at 11 m depth, which is equivalent to the ice-shelf freeboard in front of the drill site. Conductivity measurements on two water samples taken in the hole at the beginning and at the end of the process were equivalent to respectively 3 and 0.9 times the conductivity of normal sea water. This indicates that the bottom part of the banded facies is still thoroughly permeable to sea water and that the "in-situ" interstitial water in these layers is considerably enriched by the brine exclusion process resulting from the consolidation of the upper levels. This supports the idea that, in this case, freezing is actively taking place in the consolidation process.

In previous work (Tison et al., 1993), the K/Mg ratio of marine ice samples was shown to be a good indicator of active chemical fractionation below the ice shelf. In particular, K/Mg - salinity relationships clearly showed a transition from saltier samples, with K/Mg ratios close to the sea water value, to low salinity samples with much higher K/Mg ratios. Simple experiments, where fresh-water ice blocks were melted in a sea water

reservoir above its freezing point [Tison et al., 1993: their Table 1 and Figure 5], were shown to result in a 30% reduction of the salinity and a 125% increase of the K/Mg ratio in the interface water layer.

This process, reflecting a selective diffusion mechanism from undiluted to diluted sea water had previously been demonstrated by Ben-Yaakov [1972] and shown to lead to an increase of K/Mg of up to 200% of its original value in sea water. Repeating the experiment described above with a gauge incising the bottom of the melting ice block, showed increased differences, thereby indicating accumulation of waters of least density in inverted depressions below the ice [Tison et al., 1993]. It was then proposed that melting below an ice shelf would enhance dilution of the interstitial host water within the loose frazil accumulating underneath. It would also enhance chemical fractionation between sea water and this interstitial water, resulting in the original chemical signature of the granular facies.

Data presented in Figure 7 confirm this behavior. Core IV is especially illustrative, showing two distinct groups of samples: the low salinity-high K/Mg in the topmost granular facies, and the high salinity-low K/Mg in the lowermost banded facies and the transition zone. The granular facies of cores XXI and VI show a similar pattern of a dense cloud of samples with rather low salinities and moderate fractionation. The banded facies of core Y stretches between a similar cloud (although slightly more saline) and numerous saltier samples with sea water K/Mg values. The few low-salinity / high K/Mg samples in core Y can be shown to correspond to the discrete layers of granular crystals in the upper part of the core, and are thus not representative of the banded facies.

The new data set, however, differs in two major respects from the results described in Tison et al. [1993], suggesting that some of their conclusions have to be reconsidered. The maximum K/Mg value of 0.26 observed here is of the same magnitude as the maximum shift observed by Ben-Yaakov [1972] after three days of diffusion experiments. Tison et al. [1993], however, quote K/Mg values as high as 1.26 in coarse granular frazil from shallow (2 m) cores, and, therefore, call for repeated melting events at the ice-ocean interface to account for this cumulative fractionation. The fact that such very high values were only observed close to the surface, and did not occur in any of the deeper cores described in this paper, suggests possible surface contamination processes, even though the first 0.5 m of the cores were systematically discarded in Tison et al. [1993]. It is worth noting that, in these surface cores, the highest values were observed in the coarser textural



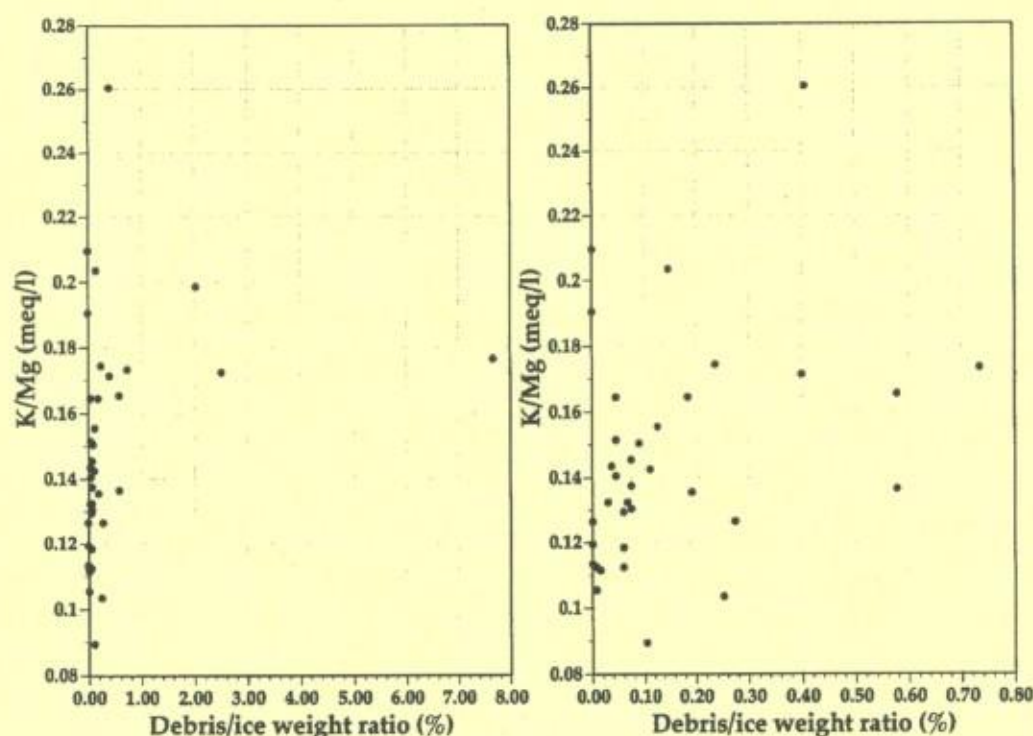


Fig. 9: K/Mg ratio as a function of the debris/ice weight ratio for samples of the granular facies in core IV. K/Mg ratios are calculated from concentrations expressed in meq/l units.

horizons where recrystallization processes during the summer season were probably the strongest. Along the same line, the observations by these authors of decreasing K/Mg values with depth, suggesting a stronger chemical sorting in the older frazil (further away from the ice-ocean interface on the same vertical), is probably only mirroring a decreasing effect of alteration in the surface layers.

On the contrary, the behavior of the K/Mg ratio in Figure 6 seems to indicate a stronger chemical fractionation with depth in the granular facies. This is clear if one compares the mean values of cores XXI and VI to the mean value of core IV. On the other hand, although cores XXI and VI show the same mean values (due to homogenizing dynamical effects) there is a trend towards larger K/Mg ratios with depth.

*Souchez et al.* [1991] have shown, on co-isotopic grounds, that marine ice transfer occurs at the bottom of HGIS. Now that the spatial distribution of the two main marine ice facies is clearly demonstrated, and that core IV suggests an episode of direct freezing under heat conduction through the ice shelf (mixed platelet-congelation transition) occurring between the successive accumulation of these two facies, it is tempting to see the banded facies as forming in a water partially diluted by

the melting of the granular facies. Could this process be traced by the co-isotopic signature of the two facies? This is a difficult task to achieve, if one keeps in mind all the cumulative steps involved in the build up of a consolidated marine ice layer. The final isotopic signature will depend on a number of factors: the signal of the "parent water" for individual frazil ice crystals, the apparent fractionation coefficient, the signal of the "host water" where individual frazil ice crystals accumulate, the porosity of the loose frazil (proportion of water to ice) and the efficiency of fractionation during the consolidation process by freezing of the "host water". The slight increase of the isotopic signal in the water resulting from mixing of the granular ice meltwater with sea water, that will eventually form the parent water for individual crystals of the banded facies, could easily become lost in this multiple step process. Nevertheless, Figure 8 plots the  $\delta D$ - $\delta^{18}O$  relationship for samples from the two facies in cores XXI, IV and Y. Although, as foreseen, all the samples lie in the area of a few error bars, the pattern suggests that samples from the banded facies are slightly enriched with regards to those from the granular facies, especially if one does not consider the four samples from the banded facies occurring just below the transition zone in core IV.



New insights from the data set on deeper marine ice cores at HGIS can be summarized as follows. The existence of two main facies of marine ice has been confirmed. Besides the widespread granular facies described in all other marine ice cores, a banded facies is dominant closer to the ice shelf front. In places where both facies are present on top of each other, a transition zone exists showing a mixed platelet-congelation facies indicating an episode of direct freezing of sea water at the interface driven by heat conduction through the ice shelf. The granular facies is characterized by low salinities and moderate to high chemical fractionation. The trend is to a decrease in salinity and increase in fractionation downstream on the profile (i.e., as one gets closer to the ice shelf front), suggesting that the heat source requested for melting and dilution processes, hypothesized by Tison *et al.* [1993], is to be found in the frontal area of HGIS. A potential candidate for this is the tidal pumping in summer of warmer water of the coastal currents, described by Jacobs *et al.* [1992] as "circulation mode-3". This circulation-mode affects shallow ice shelf bases and walls within 100 km of the ice front and leads to high melting rates, involving about 35% of the total annual net loss of Antarctic ice shelves [Jacobs *et al.*, 1992].

#### LANDFAST FIRST-YEAR SEA ICE RECORDS AT HELLS GATE ICE SHELF

In this section we focus on the information that can be gained from the study of the short-term depositional pattern in landfast first-year sea ice in front of HGIS and discuss how these can shed some light on the genesis of the banded marine ice facies in the context of ice-ocean interaction processes.

##### The Data Set

In the course of January 1994, during the IX<sup>th</sup> Italian Antarctic Expedition, eight landfast first-year sea ice cores were collected. The cores were equally distributed on a west-east transect of Evans Cove (Figure 2) roughly following the limit of the remaining sea ice at the time, within a distance of 50-150 m from the ice shelf front (to the West) or from the multiyear landfast sea ice (to the East). For the western cores (SA to SC), no significant amount of loose ice crystals was found in the drill holes and the bottom of the cores was quite solid. In contrast, in cores SD to SH, a thick layer of about 3-4 m (rough estimate from the sea ice cover freeboard measured in the hole, supposing a porosity of

about 50% i.e., a density of 0.45 for the loose frazil) of loose frazil ice crystals was found at the bottom of the solid sea ice cover. These frazil ice crystals were rather small and plate-like, up to 10 mm in diameter and about 1 mm thick and typically of rectangular shape.

To complement the textural results from 1994, three additional first-year sea ice cores were sampled at the end of the winter period (October 1995) during the XI<sup>th</sup> Italian Antarctic Expedition. These were located roughly on a North-South transect respectively 200m, 700m and 1500m from the ice shelf front in its central part (Figure 2: Holes 1, 2, 3). Again, large amounts of loose frazil crystals were accumulating at the bottom of the ice cover. These were much larger than those observed in the summer, commonly reaching 80 to 100 mm in diameter and a thickness of about 2 mm. Individual frazil ice crystals were often welded together in "packs" of up to 10 units.

##### Sampling Procedure and Analytical Treatment

The sea ice cores were sampled and processed as described before for marine ice as far as crystallographic investigations and salinity measurements are concerned. Using textural profiles in conjunction with salinity profiles from all ice cores, a total of 70 samples were selected for  $\delta^{18}\text{O}$  measurements. The isotopic measurements were performed at the University of Trieste using a Finnigan Delta-S mass spectrometer. Precision of the measurement is  $\pm 0.08\text{‰}$ . In selected cores, c-axis measurements were performed using a four-axis universal stage and standard procedures developed by Langway [1958]. The data were plotted on the lower hemisphere of a Schmidt (equal-area) net.

##### Results

**Textures and fabrics in the October 1995 profiles (end of winter).** Figure 10 summarizes the textural data of the three cores sampled at the end of the winter on the North-South transect. In this and the following figures and descriptions, a depth scale in centimeters will be used, in accordance with the scale of the textural and chemical variability. All the cores show the same major characteristics. First of all, no congelation ice is found in the cores, unlike the top of the sea ice cores from McMurdo Sound [Jeffries *et al.*, 1993; Gow *et al.*, this volume]. Most of the winter accretion consists of granular frazil, with some limited occurrences of the draped (mixed congelation/platelet) facies. Platelet accretion is also present, but limited to the end of the



## ANTARCTIC SEA ICE: PHYSICAL PROCESSES, INTERACTIONS AND VARIABILITY

## North - South Transect - October 1995

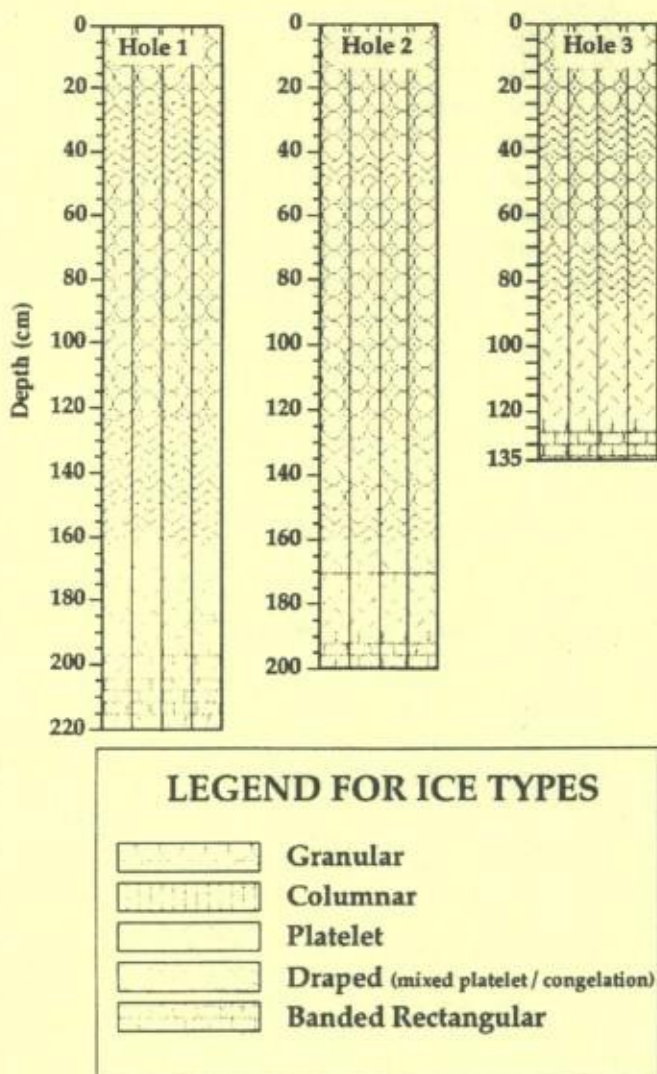


Fig. 10 : Textural profiles from the October 1995 (north-south transect) data set. See Plate 1 for thin sections illustrations of the ice types.

winter season in all cores. However, platelet ice does not form the very bottom of the core, where small amounts (max. 20 cm) of the banded rectangular facies occur.

Plate 3 and Figure 11 illustrate in more detail the textural and crystallographic characteristics of the cores at "Hole 1" and "Hole 2". Of major interest is the contrast between the granular facies forming the surface layer and the one occurring further below at 50-125 cm depth. The first is orbicular, richer in air/brine inclusions, shows heterogeneous colors between crossed polarizers and a fabric close to random. The latter has fewer bubble inclusions and these are of larger size.

Crystals are also slightly elongated in the vertical plane (see also Figure 13). Both in vertical and horizontal thin sections, the color is quite uniform, indicating a strongly oriented pattern, as confirmed by the c-axes clustering. Even more significant is the type of clustering, which is close to a strong maximum in the vertical plane, an unusual feature in sea ice.

Platelet ice and draped mixed congelation/platelet facies show essentially random fabrics in accordance with those measured by Jeffries *et al.* [1993] and Jeffries and Weeks [1993], although we did not perform separate plotting of platelet and congelation crystals to show the bimodal nature of this arrangement. Finally, the bottom, banded rectangular facies shows strongly aligned vertical c-axes.

**Textures in the January 1994 profiles (mid-summer).** Textural profiles from mid-summer 1994 (Figure 12) exhibit, in their top sections, similar features to those observed two years later (October 1995), with the exception that more draped facies events occurred during the course of the winter. There is, however, for the bottom part of the cores, a strong contrast both in time (as compared to the October 1995 cores) and space (comparing western SA-SB-SC and eastern SD-SE-SF-SG-SH cores). Platelet accretion marks the end of the winter season in the western cores. As in the McMurdo Sound samples, the relative thickness of this bottom platelet layer might be underestimated, given possible ablation in the course of the summer. In contrast to the other sites, virtually no platelet facies are observed in core SD to SH, either because it never formed, or because it melted away before accretion of the banded rectangular facies.

Probably the most striking feature of this West-East mid-summer transect is the well developed (up to 1.40 m consolidated) banded rectangular facies at the base of the eastern (SD to SH) cores. This layer is neither present (or barely so) at the same location at the end of the winter season (compare "Hole 1" in Figure 10 to "SE" in Figure 12), nor at the same moment in the western sector of Evans Cove.

As an example, Figure 13 illustrates the typical textural contrast between the granular frazil ice occurring between 75 and 85 cm depth and the banded rectangular facies accreted at the bottom in core SE. The former shows appreciable elongation in the vertical plane resulting in U-shaped crystals and uniform tints in horizontal thin section, indicating near-vertical c-axes clustering. The latter displays obvious strongly elongated rectangular shapes with intracrystalline brine inclusions in vertical thin sections, and appears as large flattened



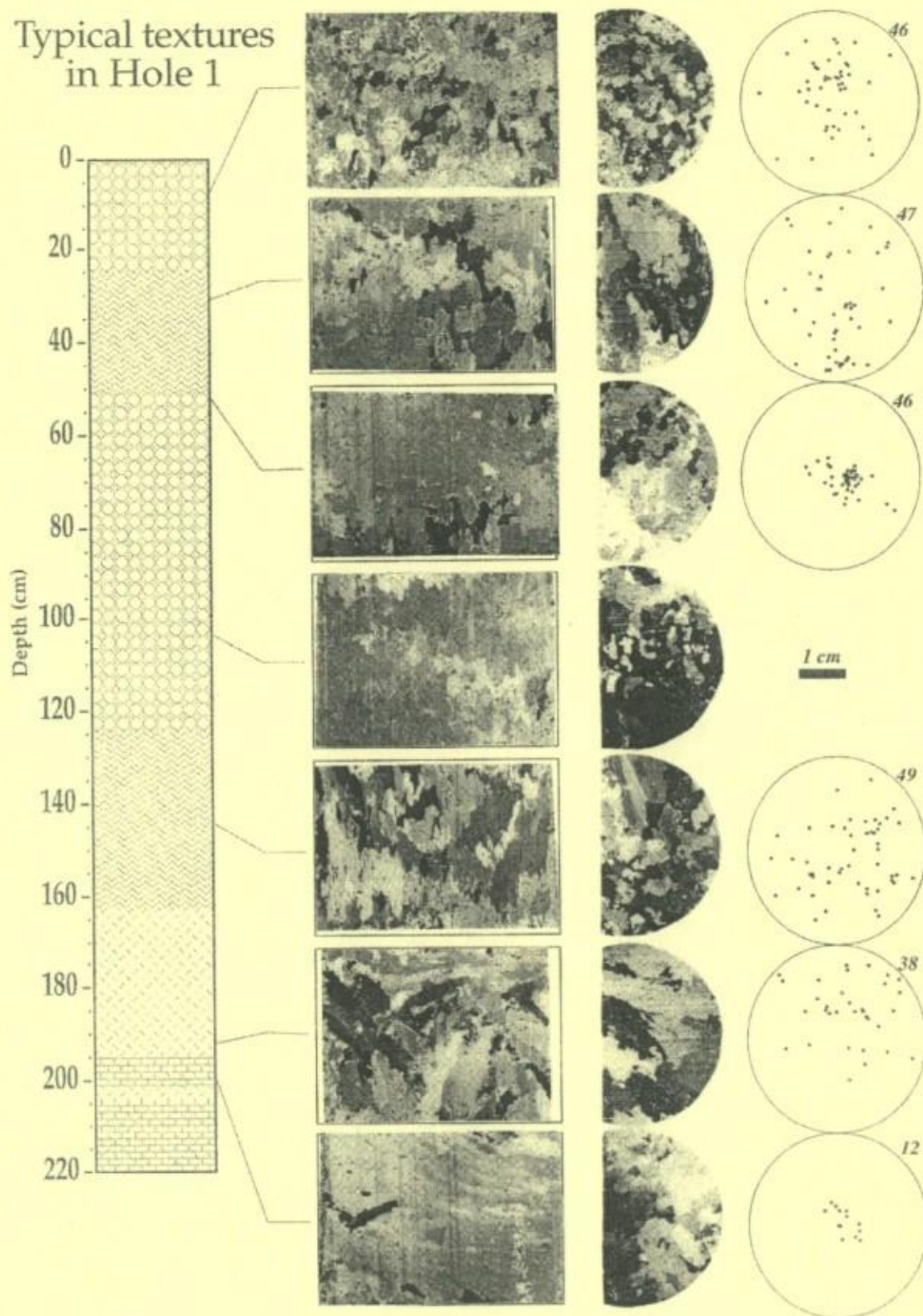


Plate 3 : Textures and fabrics in Hole 1 (October 1995). Rectangular photographs are vertical thin sections and circular photographs show horizontal thin sections at equivalent depths. The scale is valid for all pictures. C-axes are shown in the horizontal plane and plotted in the lower hemisphere of a Schmidt net and the number of c-axes measured is specified. Legend of ice types as in Figure 10.



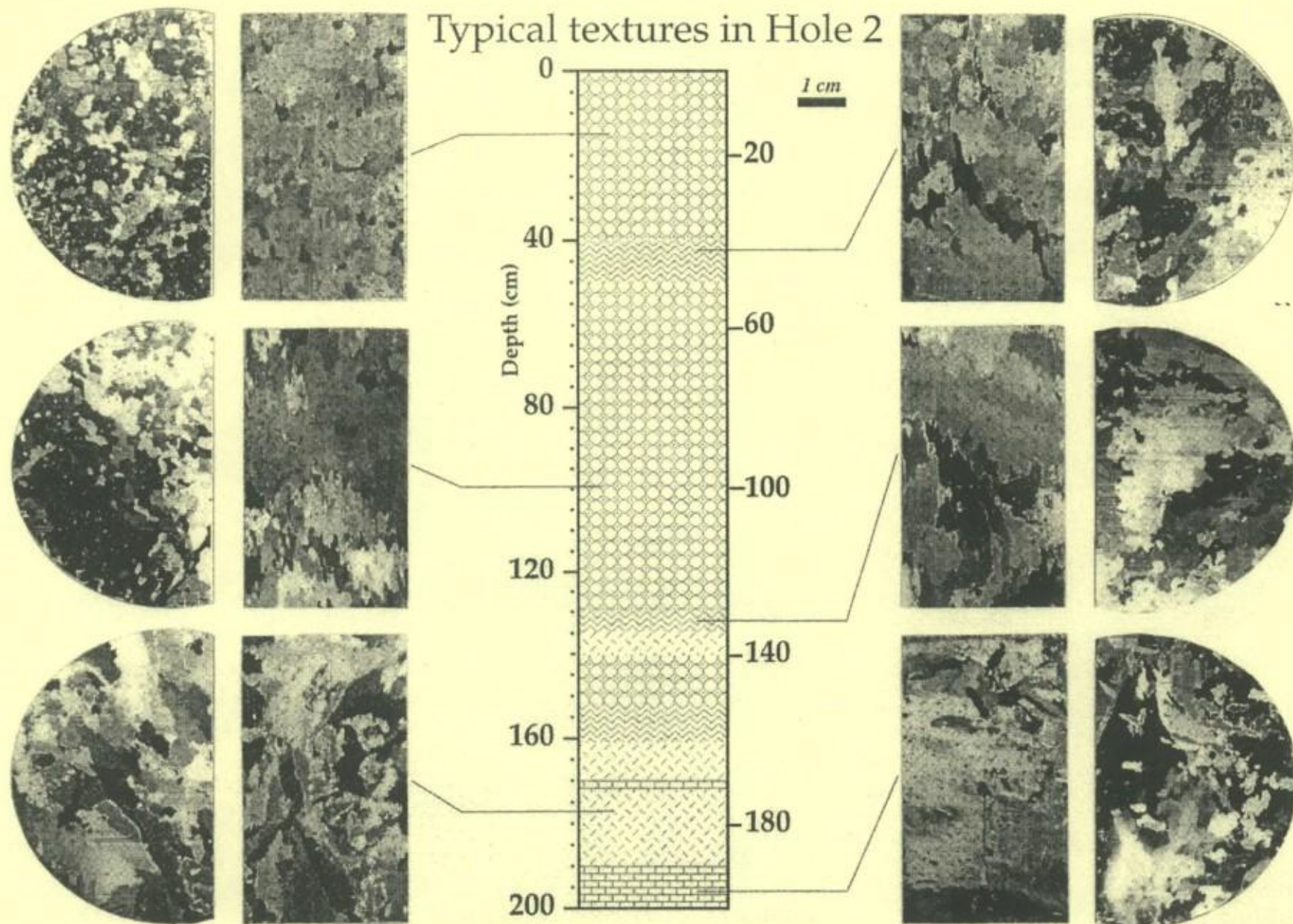


Fig. 11 : Textures in Hole 2 (October 1995). Conventions as in Plate 3.



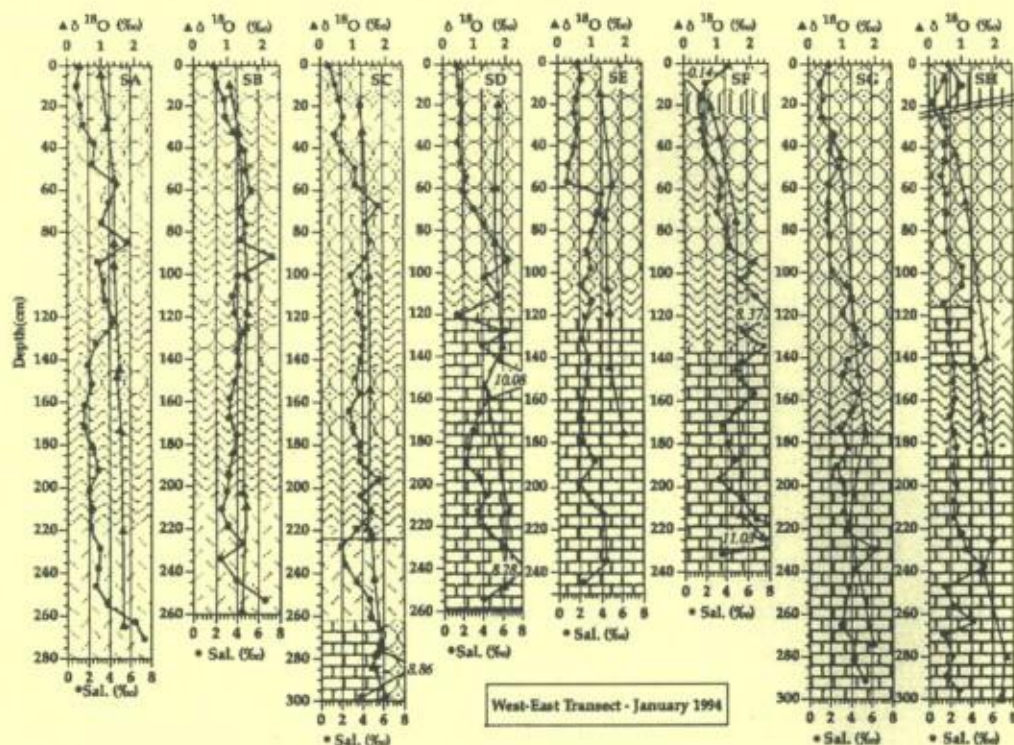


Fig. 12 : Textural, salinity and  $\delta^{18}\text{O}$  profiles from the January 1994 data set. See Plate 1 for thin sections illustrations of the ice types. The sloping lines in the top part of core SH refer to deformational structures. Legend of ice types as in Figure 10.

crystals displaying near vertical c-axes orientations in horizontal thin sections.

**Salinity and  $\delta^{18}\text{O}$  profiles in the 1994 data set.** Figure 12 displays all the salinity and  $\delta^{18}\text{O}$  results in the landfast sea ice cores from the January 1994 (mid-summer) data set. Figures 14a and 14b are enlarged graphs for selected stations, to ease the comparison between western (SA-SB - Figure 14a) and eastern (SE-SF - Figure 14b) cores. In the top 40-90 centimeters salinity rises from 1-2‰ to 4-8‰, whilst  $\delta^{18}\text{O}$  steadily increases from a minimum of -0.14‰ to about +1.5‰. Further down (40-90cm to 120-140cm), salinity fluctuates in the 4-8‰ range, whilst  $\delta^{18}\text{O}$  stabilizes. In this unit, there is no obvious correlation between textural (granular vs. mixed platelet/congelation) and compositional properties. In most of the lower half of the cores, salinity steadily decreases whilst  $\delta^{18}\text{O}$  remains quite constant in cores that do not show a banded facies accreted at the bottom (SA and SB). In all other cores with a banded facies at the bottom, the  $\delta^{18}\text{O}$  signal rises slightly. Finally, a general salinity increase is observed in the bottom 40-60 centimeters of most cores, although it is not so clear-cut in those cores consisting of banded rectangular ice (SC, SE, SG and SH).

## Discussion

Previous work on marine ice has already underlined the potential difficulties in interpreting salinity-stable isotope data in consolidated frazil ice (see for example *Tison et al.* [1993], *Eicken et al.* [1994] and discussion in previous sections). In congelation sea ice, resulting from direct freezing of the ocean water reservoir at the base of an existing sea ice cover, salinity and  $\delta^{18}\text{O}$  essentially depend on two factors : the signal of the "parent" ocean water and the freezing rate. If one assumes constant parent water properties and limited desalination processes, the profiles will essentially reflect fluctuations of the freezing rate with depth. A decreasing freezing rate will enhance expulsion of brines (lowering bulk ice salinity) and increase isotopic fractionation (increasing ice  $\delta$ -values) as one approaches equilibrium. Numerous studies of salinity profiles in first-year congelation sea ice (see, for example, *Nakawo and Sinha* [1981] and synthesis in *Weeks and Ackley* [1986]) display a typical c-shaped profile that has been satisfactorily modeled, combining initial salt entrapment with subsequent drainage processes [*Cox and Weeks*, 1988]. Apart from the relatively enriched top (frazil and brine-



## ANTARCTIC SEA ICE: PHYSICAL PROCESSES, INTERACTIONS AND VARIABILITY

## Typical textures in core SE

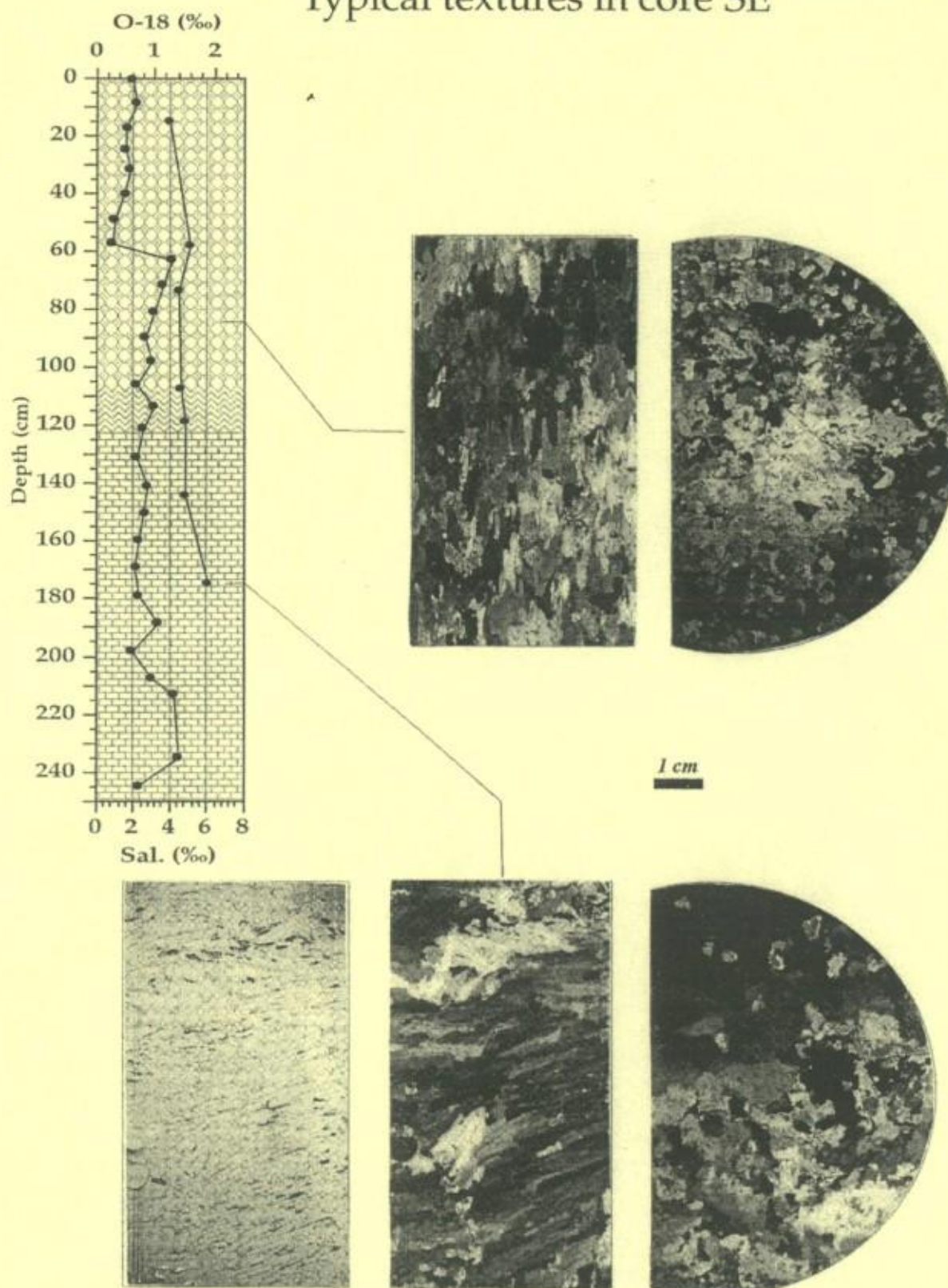


Fig. 13 : Ice core structure/stratigraphy and ice textures in core SE (January 1994). Same conventions as for Plate 3. The bottom left photograph is taken in transmitted light.



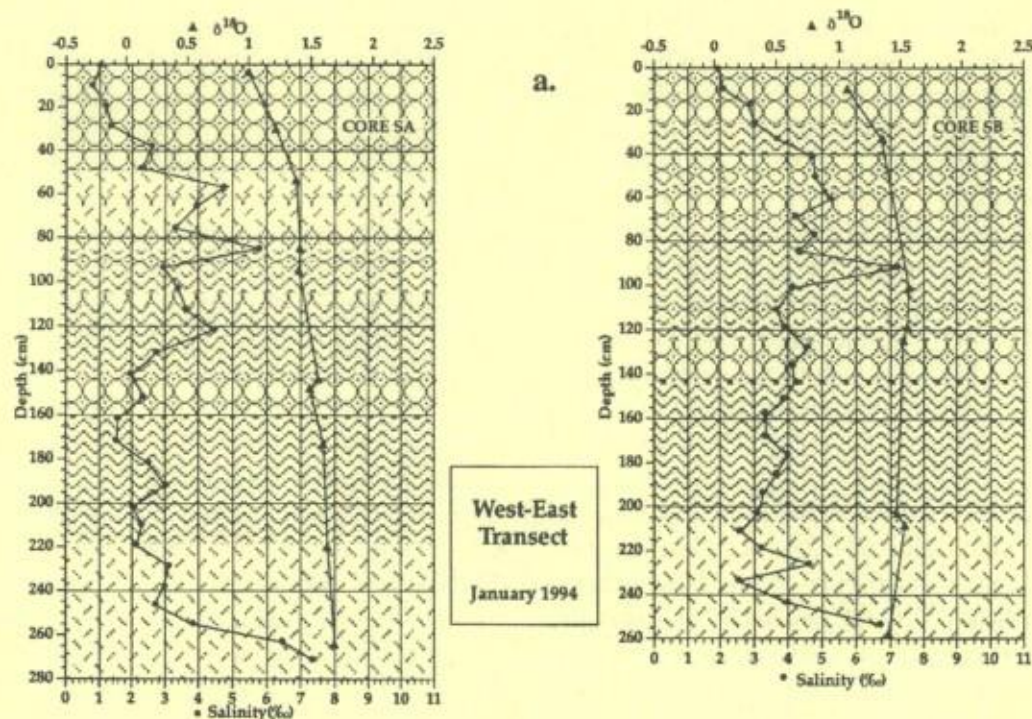


Fig. 14a : Enlarged structure/stratigraphy/texture diagrams and salinity and  $\delta^{18}\text{O}$  profiles for cores SA-SB. Legend of ice types as in Figure 10.

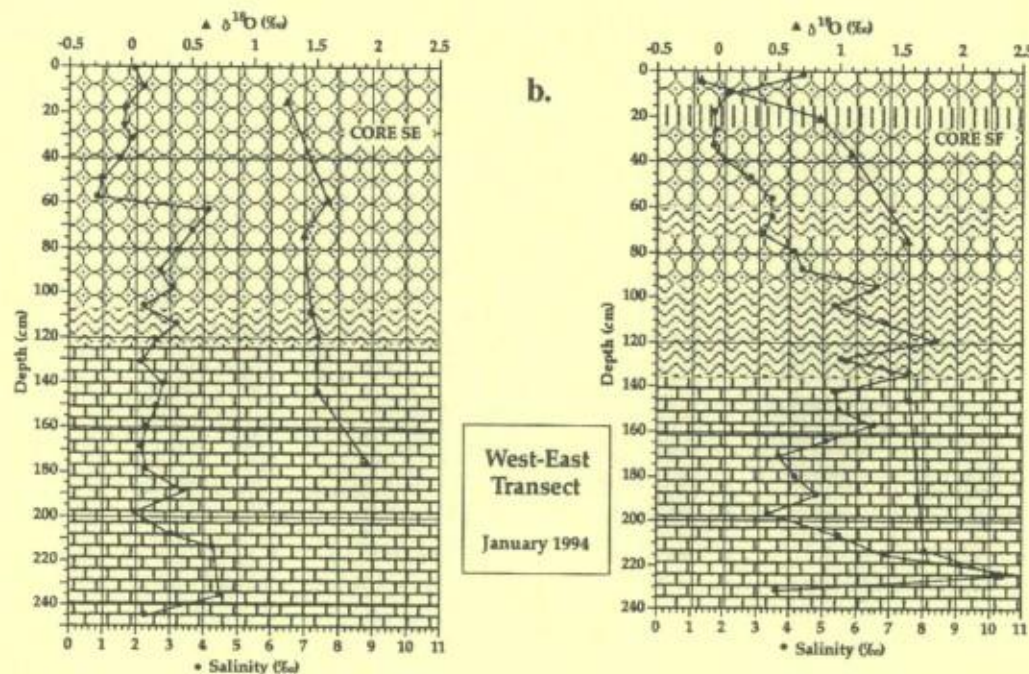


Fig. 14b : Enlarged structure/stratigraphy/texture diagrams and salinity and  $\delta^{18}\text{O}$  profiles for cores SE-SF. Legend of ice types as in Figure 10.



rich snow ice, rapid congelation growth rates in the top 0.10 m, expulsion of brine onto the surface following freezing) and bottom (capillary retention of brine in the highly permeable skeletal layer [Gow *et al.*, 1990]), the profile will reflect the dependence of the freezing rate on the balance between the trend of the ambient air temperature and the insulating effect of the ice. This is clearly seen, for example, in a detailed case study of a freezing lead in the Arctic by Gow *et al.* [1990: Figures. 2, 4a and 4c]. When desalination processes are important, as in arctic multiyear sea ice, for example, this initial freezing effect can be completely altered and the c-shaped profile turned into a monotonically increasing salinity with depth (e.g., Figure 65 in Weeks and Ackley [1986]).

These relatively simple patterns are not valid for frazil/platelet/mixed sea ice, unless one develops a set of hypotheses on the variables in play (see discussion in Eicken [this volume]). Indeed, one has to remember that the formation process is threefold: formation of individual ice crystals in a "parent" water, accretion of the loose ice crystals in a "host" water and, finally, consolidation by freezing of the interstitial "host water". In such a process, the resulting isotopic signal will depend on many factors such as the signal of the parent water (with poorly known fractionation efficiency), the signal of the host water, the freezing rate of the host water, and the grain size and porosity of the loose frazil. The salinity will depend on the same factors, except perhaps the signal of the parent water, if one considers that frazil ice crystals are chemically pure.

It is difficult, with the two data sets at hand, to discriminate inter-annual from seasonal variability in the cores' facies. However, the contrast between eastern and western cores in January 1994, the strong textural similarity between cores SA, SB and SC and those from October 1995, and the occurrence of large amounts of loose frazil below the eastern side of the sea ice cover in mid-summer, suggest the dominance of seasonal effects on the main facies contrasts. Therefore, a comparison of various salinity,  $\delta^{18}\text{O}$  and textural profiles from different periods of the year and at two year intervals enables us to propose a typical sequence of first-year sea ice accretion in Evans Cove at the front of HGIS, keeping in mind the potential complications discussed above.

Consolidation of wind- and wave-induced frazil ice produced in surface sea water, showing dilution effects by continental meltwaters (lower salinity, lower  $\delta^{18}\text{O}$ ), forms the initial sea ice cover. The crystallographic and textural contrasts between the granular facies forming

the surface layer and the one occurring further below suggest different origins. The richness in air/brine inclusions and the random c-axes fabric in the surface layer are consistent with a wind- and wave-induced frazil ice forming at the beginning of the winter, in highly agitated waters subject to strong katabatic winds. The prevailing north west origin of these winds (see records at Automatic Weather Station Manuela: Figure 37 in Ronveaux [1992]) however prevents fully efficient export of the new frazil ice crystals formed in Evans Cove towards the Terra Nova Bay Polynya. Consolidation of the initial cover can thus occur. The salinity and  $\delta^{18}\text{O}$  signatures in this 40-90cm thick surface layer reflect a dominant influence of the host water signal, since both variables increase with depth. This is compatible with the surface water conditions close to the ice shelf at the end of the summer. This water is likely to be slightly diluted and depleted in heavy isotopes from contribution of melted meteoric ice that is seen to accumulate in numerous ponds at the surface of HGIS. This meltwater is subsequently drained by supraglacial streams joining in a waterfall at the ice shelf front. A dominant influence of the freezing rate would, in contrast, decrease salinity and increase  $\delta^{18}\text{O}$  with depth. The salinity increase with depth could eventually reflect a post-genetic desalination process. However, in that case, the isotopic signal should not be significantly altered, since there is no fractionation on ice melting [Friedman *et al.*, 1964; Moser and Stichler, 1980]. The salinity anomalies in the first 20cm of cores SF and SH are probably associated with deformational processes (rafting), as also suggested by the occurrence of oblique textural discontinuities that were an obvious exception in the very top part of these cores. Finally, it should be stressed that the thickness of this surfacial layer might be underestimated, given the strong surface sublimation that probably dominates because of the steady katabatic winds that prevail in the area (see previous discussion).

In more than half of the cores, the surface layer is underlain by a platelet or a draped facies. Then, the lower granular facies develops, eventually in alternation with the draped facies. This granular facies shows a slight elongation of the crystals in the vertical plane, denoting partial influence of a downward congelation process. However, instead of the usual concentration of c-axes in the horizontal plane typical of congelation sea ice, it displays a strong clustering along the vertical. This suggests that most of the winter accretion in front of HGIS consists of small individual discs of frazil ice crystals (with c-axes perpendicular to the disc), gently settling upward at the base of the existing sea ice cover



in a calm environment, allowing orderly packing. Sweeping of wind- and wave- induced frazil ice crystals formed in the polynya down to a maximum 1.70 m underneath the already existing fast ice cover in Evans Cove is improbable because of the steady south-eastward blowing katabatic winds. These are constantly "skimming" away the thin surficial buoyant layer of newly formed frazil. Moreover, the thickness of this facies tends to increase towards the ice shelf front in the 1995 cores (Figure 10). Dynamical thickening through rafting is equally precluded given the maximum depth observed for this facies and the absence of typical signatures of the process (see, for example, *Eicken* [this volume] and discussion above). Also (see processes in Table 1), (1) wind- and wave- induced frazil would build a facies similar to the surface layer described above, (2) no congelation ice layer is present to sustain small scale thermohaline convection and (3) there is no obvious source for diluted waters in the environment to induce double-diffusion processes. The most plausible source for these frazil ice crystals is, therefore, active supercooling in the Deep Ice Shelf Water adiabatically rising below HGIS during the winter. As shown in the next section, the structure of the water column in front of HGIS confirms the presence of large amounts of Deep Ice Shelf Water (DISW). Further consolidation of the host water leads to elongation of the crystals, which, however, retain their original crystallographic signature. In the top part of this second unit, salinity fluctuates around a mean value and  $\delta^{18}\text{O}$  stabilizes. This probably reflects the combination of Ice Shelf Water characteristics for the "parent" water of the loose frazil and the onset of constant more saline winter "host" water characteristics. Further down, in the lower half of the winter accretion of cores SA and SB (120-220cm), salinity steadily decreases and  $\delta^{18}\text{O}$  remains quite constant. This could either reflect a progressive reduction of the freezing rate or a progressive change in the host water characteristics towards dilution. In the first case, the rise of the isotopic signal in the freezing interstitial water could be "masked" by the background (up to 60%) signal of the loose individual crystals. This however would be in contradiction to the "a<sub>0</sub>" (plate width in individual congelation ice crystals) measurements of *Jeffries et al.* [1993] in interstitial congelation ice from the lower layers of the McMurdo Sound sea ice cover, which indicate no decrease of the freezing rate with depth. The other alternative, although rather improbable in the middle of the winter, would be the scenario of a rising  $\delta^{18}\text{O}$  in a diluted host water as suggested for the bottom part of cores SD to SH discussed below.

The end of the winter season is dominated by platelet accretion (Hole 1 to 3 and SA to SC). This facies is nearly absent in the eastern cores, where the winter accretion is thinner. It is not clear, however, if the lack of platelet ice in the eastern cores results from a lower accretion of platelet ice compared to the western zone, or increased bottom melting in the beginning of the summer season.

Bottom accretion still occurs during the summer as a banded rectangular facies. This facies does not exist in front of the western sector (west of the western medial moraine) and forms between 44% and 54% of all consolidated ice cores in front of the central and eastern sector. There also, a thick layer (several meters) of unconsolidated loose rectangular frazil ice crystals exists at the base of the sea ice cover from the end of the winter through most of the summer. This banded rectangular facies is thus actively building preferentially in the eastern sector in the first half of the summer. The  $\delta^{18}\text{O}$  signal increases slightly as the banded facies starts to build up. This last observation is consistent with the suggestion made in the previous section that warm surface water is forced under HGIS by tidal action and partially melts marine ice accreted at the bottom. The meltwater produced is likely to increase the  $\delta$ -value of the resultant sub-ice shelf top water layer, since marine ice has a slightly positive signature. This water mass will be the host water (and possibly the parent water, if further growth or new crystal growth is allowed by adiabatic supercooling) for the loose crystals that will form the banded rectangular facies in the landfast sea ice, resulting in the higher  $\delta^{18}\text{O}$  values observed.

Another way to visualize this process is to plot the granular frazil from winter accretion in the sea ice and the banded rectangular frazil from summer accretion, on a salinity- $\delta^{18}\text{O}$  diagram (Figure 15). The banded rectangular frazil is clearly shifted towards higher salinities and higher  $\delta^{18}\text{O}$  values. This trend is similar to the one observed for co-isotopic values in the marine ice cores (Figure 8). However,  $\delta^{18}\text{O}$  ranges in the sea ice are, in both facies, shifted towards less positive values. This can be clearly related to differences in freezing rates of the host water, which must be significantly higher below 1.50 m of first-year sea ice than below several tens of meters of shelf ice. Higher salinities in the banded rectangular facies probably result partly from grain sizes, shapes, and hence, porosity.

Finally, the sudden increase of salinity at the very base of nearly all profiles is typical of the bottom of sea ice that has not yet undergone the rapid desalination which often occurs in the first few weeks after initial



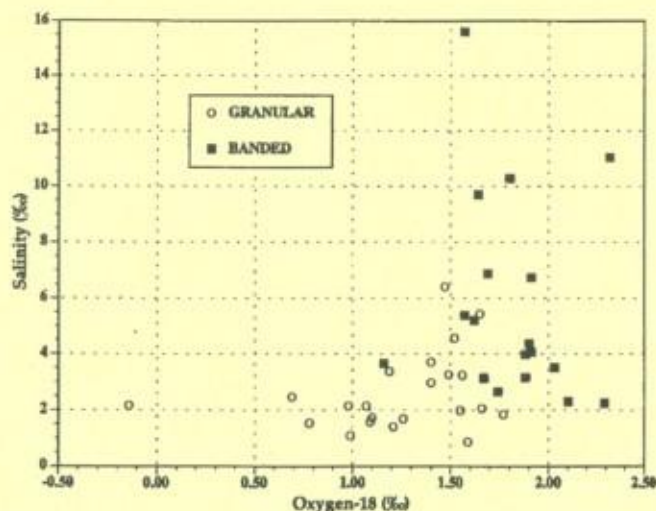


Fig. 15 :  $\delta^{18}\text{O}$  versus salinity for samples of the granular and banded rectangular facies.

freezing [Nakawo and Sinha, 1981]. In this case it could also result from higher porosity of the bottom layers. This situation is, however, less clear in those cores where the banded rectangular facies exists at the bottom, which probably reflects brine loss from the loosely consolidated bottom layer of these ice cores from the eastern part of Evans Cove during sampling.

#### LINKING MARINE ICE AND SEA ICE RECORDS IN AN ICE/OCEAN INTERACTION PERSPECTIVE

The granular marine ice facies observed at HGIS must result from adiabatic supercooling in Ice Shelf Water produced in a Deep Thermohaline Circulation (DTC), as it occurs beneath larger ice shelves [Jacobs *et al.*, 1992]. Adiabatic decompression in recently opened bottom crevasses at the grounding line could only account for the production of negligible amounts of granular ice. A rough calculation can be made hypothesizing that all the supercooling occurring within a sea water mass at local pressure melting point as it is adiabatically rising in a bottom crevasse is compensated by ice crystal growth. For example, a 400 m water column, with a "mean" adiabatic rise of 200 m, would result in the production of, at most, 1 m of loose frazil with a 50% porosity. The only oceanic profile presently available in Evans Cove [Fabiano *et al.*, 1991], shows Ice Shelf Water from 100 m deep to about 100 m above the sea floor, which consists of a narrow trough 700 m deep in the central part of Evans Cove, with depth increasing inland. The maximum thickness of HGIS as far as half

way to the northern tip of Vegetation Island is only 250 m, which implies a larger-scale circulation pattern in which HSSW produced elsewhere, e.g. in the Terra Nova Bay Polynya, can access the Nansen Ice Sheet grounding lines, perhaps beneath Reeves and Priestley Glaciers (Figure 2). Part of the Ice Shelf Water produced in those locations could recirculate along the eastern and western flanks of Vegetation Island, carrying with it loose frazil ice crystals formed by adiabatic supercooling. These crystals would accumulate in the depression formed at the southern tip of Vegetation Island, between the two merging flows as suggested previously.

Remnants of frazil ice crystals formed in this manner (hereafter DTC-granular facies) escape at the front of the ice shelf, where they accrete under the sea ice during the winter to form the granular facies with vertical c-axes fabrics. In all first-year sea ice cores that are thought to have retained the whole of the winter accretion (Hole 1, 2 and 3; SA, SB, SC), platelet ice bounds the lower limit of this winter accretion, while the upper limit (boundary with the initial wind- and wave- frazil ice accretion where it exists) consists of either the platelet (SA, SC) or the draped mixed congelation/platelet facies (Hole 1, 2 and 3). We postulate that these observations can be interpreted as the expression of variable intensities of the DTC. *Bombosch and Jenkins* [1995], show that the large size of crystals in the platelet facies reflects slower frazil ice crystal growth rates in the Ice Shelf Water as it levels off and eventually escapes at depth in front of the ice shelf. Transition from a small grained DTC-granular facies to a platelet or a draped facies in the landfast first-year sea ice could thus reflect variations in the degree of supercooling of the ISW where these crystals were formed. In early winter, enhanced freezing at the polynya surface is likely to increase HSSW production and speed up the DTC. At that time, the density contrast between ISW and HSSW should be moderate and supercooling weak. This would favor formation of the platelet facies or, probably more often, the draped mixed platelet-congelation facies, since congelation ice growth rates would still be competitive with the platelet crystal accretion rates beneath a thin sea ice cover.

In the mid-winter, the DTC may accelerate, resulting in higher density contrasts between ISW and HSSW and stronger supercooling producing the fine grained matrix of the DTC-granular sea ice facies. At the end of the winter, a slower DTC would again favor larger crystal growth. The heat sink through the sea ice cover is also reduced, along with the consolidation rate. The lat-



ter part of this proposed cycle would result in the platelet ice facies observed at the bottom of the winter accretion of the cores where summer melting at the base of the ice was less important. In addition, large scale fluctuations in the HSSW production related to katabatic wind activity during the winter could explain the alternations of the draped and the DTC-granular facies.

Several hypothesis can be formulated for the genesis of the banded marine and sea ice facies :

**Post-depositional deformation processes** leading to recrystallization of the original textures and fabrics. This is unlikely, as the banded facies are spatially confined to the frontal zone, and not developed in cores XXI and VI, where surface morphology and foliation show that the deformation is quite active. Also, discs or plates are seen to accrete in the water column below the sea ice cover and thin sections of these half frozen bottom deposits are identical to the banded facies observed at the base of the solid level sea ice cover above, where no evidence of deformation was found.

**Expression of a spatially changing environment** for the frazil ice crystals formed in the DTC, as the geometry of the base of the ice shelf switches from highly irregular (with transverse inverted depressions between individual flows close to the grounding line or around pinning points) towards a smoother interface closer to the front. In the first case, rapid lateral ascension of frazil crystals along steep slopes would favor the production of small crystals accreting in a random fashion at the base of the ice shelf. In the latter case, slower ascension further away from the initial production site would favor slower growth of larger crystals, accreting in an orderly fashion at the bottom of the ice shelf. The lower growth rates would result in higher isotopic values because of the higher fractionation efficiency. However, granular marine ice is observed up to several hundred meters downstream of the contact line between meteoric ice and marine ice (Figure 4). Moreover, if this hypothesis is correct, only the banded facies should be found in the first-year landfast sea ice in front of the ice shelf.

**Expression of a temporally changing environment.** The seasonal character of the banded facies accretion (summer only) suggests that it is linked to seasonal processes in the water column in front of or below the ice shelf. We have seen that the lower salinity and enhanced chemical fractionation in the granular marine ice consolidating closer to the ice shelf front suggest tidal forcing of warm surface waters below HGIS during the summer. These waters would favor partial

melting of the loose granular frazil and produce a water mass at local pressure melting point showing lower salinities and higher isotopic signatures. This water mass, perhaps mixed with water carrying DTC-granular frazil, would eventually exit at the front. The marine and sea ice banded facies, then represent either transformed granular frazil ice crystals initially formed in the DTC, or new crystals formed by adiabatic supercooling, or both.

### CONTRASTS WITH SEA ICE ACCRETION IN MCMURDO SOUND

The first-year sea ice cover at HGIS differs from the one observed in McMurdo Sound [Jeffries *et al.*, 1993; Gow *et al.*, this volume] in several aspects. Firstly, no thick (about 1 m) layer of congelation ice exists at the top of the cores in Evans Cove. Congelation ice occurs in limited amounts (10-15 cm) in only two cores (SF and SH), with both cores showing evidence of deformation in their top sections. Strong sublimation under katabatic winds could be responsible for ablation of a surficial congelation ice layer, but this is improbable for most of the cores, given the general occurrence of wind- and wave-induced frazil ice in the surficial layer. This contrasting situation simply reflects the calm conditions of landfast sea ice growth in McMurdo Sound in 1990, as suggested by Jeffries *et al.* [1993], as opposed to initial turbulent growth conditions occurring in Evans Cove.

Secondly, winter accretion is dominated more by the DTC-granular facies than by the congelation and platelet ice facies. This could be the expression of different geometries for HGIS and the Ross Ice Shelf (near McMurdo Sound). The length of HGIS is indeed quite small and, therefore, the granular frazil possibly "escapes" more easily from under the ice shelf, whilst it accretes much more upstream at the base of the Ross Ice Shelf. Platelet accretion is limited during the winter and more abundant at the end of the season at HGIS, but this is not necessarily in contradiction to the situation in McMurdo Sound. As a matter of fact, it is the case that the platelet observed at the base of all McMurdo ice cores accretes in the second half of the winter, and that congelation ice growth dominates in the beginning of the winter. Ice growth calculations based on freezing degree days indicate that platelet ice crystals begin to appear at the base of the existing columnar ice layer in McMurdo Sound at some time during the period July-September [Gow *et al.*, this volume; Veazey, 1994].

Finally, as underlined before, a thick layer of banded rectangular frazil accretes at the bottom of the



sea ice at HGIS during the summer, and it is not observed in McMurdo Sound. Since warm surface waters have been detected in the McMurdo Sound area (see, for example, *Jacobs et al.* [1989: Stations 1, 70, 71]), contrasts in ocean circulation patterns, size and geometry of the ice shelf, or unavailability of loose DTC-granular frazil close to the ice shelf front are amongst possible reasons for this discrepancy.

### CONCLUDING REMARKS

Our data set on landfast first-year sea ice from HGIS has confirmed that the variability of sea ice facies increases as one gets close to ice shelves. Besides the main columnar and granular facies associated respectively with congelation ice, wind- and wave-induced frazil ice or snow ice usually found in drifting sea ice (eventually as mixed facies), other facies develop that can be linked to ice-ocean interactions below ice shelves. The platelet ice facies, already shown before to be linked to the proximity of ice shelves, can turn into a draped mixed congelation-platelet facies depending on the balance between the accretion rate of the individual acicular platelet ice crystals, formed in the supercooled Ice Shelf Water under circulation mode-1, and the congelation freezing rate at the bottom of the existing sea ice cover. In addition, the Deep Thermohaline Convection can sustain winter accretion of a granular facies that differs from the surficial wind- and wave-induced facies by its much lower bubble content and its slightly vertically elongated crystals showing a strong vertical maximum of c-axes. Finally, bottom accretion still occurs during the summer as a banded facies which is thought to reflect interactions of the ice shelf base with a circulation mode-3 under HGIS.

Annual rhythmicity in landfast first-year sea ice records at HGIS, therefore allow us to investigate the variability within and between the two main ocean circulation modes below the ice shelf. Surprisingly, this rhythmicity is not recorded in the 45m-deep marine ice core Y close to the ice shelf front, where the banded facies forms more than 95% of the total core. A logical reason for this is the strong contrast in thermodynamical regimes between the bottom of the ice shelf and the base of the first-year sea ice cover. To be recorded, the seasonal variability of the frazil ice accretion needs to be "frozen-in". Obviously, the freezing rate at the bottom of an ice shelf is one to two order of magnitude less than the one at the base of a sea ice cover. Therefore, the winter accretion below the ice shelf and close to the front (where circulation mode-3 should be the most ac-

tive) is easily remobilized and melted away during the next summer. Marine ice cores, therefore, mainly record the main spatial differentiation of the two ocean circulation modes on time scales of hundreds of years. This, in turn, highlights the specific input of landfast first-year sea ice studies as a useful complement of coupled oceanographical-shelf ice research in the vicinity of floating ice bodies.

Hells Gate Ice Shelf is a small and narrow ice shelf subject to a strong katabatic wind regime. We have shown that these characteristics makes it easier to study marine ice properties at minimal cost but, at the same time, in a peculiar dynamical setting that enhances the complexity of data interpretation. This also raises the question as to the degree to which the findings discussed here can be applied to large floating ice bodies? First of all, HGIS shows geometries of granular marine ice accretion, between the individual ice flows forming the ice shelf, that are similar to those on the Ronne Ice Shelf [*Corr et al.*, 1995]. This stresses the importance of considering 3-D modelling of the DTC, since local transverse gradients of the ice shelf base might exist close to grounding lines and around pinning points, that are much steeper than the longitudinal gradient considered in 2-D modelling exercises [*Bombosch and Jenkins*, 1995; *Hellmer and Jacobs*, 1992; *Jenkins and Bombosch*, 1995]. Recent developments along these lines [*Grosfeld et al.*, 1997; *Williams et al.*, in press] stress the complexity of marine ice accumulation patterns below ice shelves. On the other hand, HGIS should really be considered as part of the larger Nansen Ice Sheet. Although this whole floating ice mass is still smaller than the Filchner-Ronne or the Amery ice shelves, it clearly shows evidence of a similar 3-D oceanic circulation in which Deep Thermohaline Convection, Ice Shelf Water production and marine ice accretion take place. Recent radio echo sounding profiles, detailed surface velocity and GPS thickness measurements at Nansen Ice Sheet demonstrate that large marine ice production rates are required in order to sustain a steady state profile [*M. Frezzotti*, personal communication, June 1996]. Extensive marine ice outcrops are clearly seen at the NIS surface and are currently under investigation by the authors. Finally, accretion of the banded marine ice facies in the frontal zone of HGIS (and at the bottom of the landfast sea ice) might also be considered as a peculiar process, essentially restricted to the study case. Indeed, no deep marine ice cores from the major antarctic ice shelves has ever shown this type of facies, and the frontal zone of ice shelves has always been considered as subject to a



strong basal melting regime (e.g. [Jacobs et al., 1992]). It should be noted, however, that none of the deep marine ice cores has been drilled within a few tens of kilometers of the margins of ice shelves and that recent 3-D modelling of ice-ocean interactions in sub-ice shelf cavities reproduce a fringe of net basal accretion near these ice shelf margins in a number of realistic scenarios [Grosfeld et al., 1997; Williams et al., in press]. The similarity between the banded facies and the "wafer-like" facies described by Gow et al. [1987] in the Weddell Sea also suggests that our observations in the Ross Sea might be valid for other ice shelf areas around Antarctica.

Oceanographic measurements at the ice shelf front are obviously a crucial "missing link" in this study. Future work should focus on coupled oceanographic and landfast sea ice studies both in summer and winter. The development of experimental procedures to better understand the controlling factors on the shape and size of frazil ice crystals, and to support interpretation of the observed landfast sea ice facies variability in the field are also essential.

**Acknowledgments.** This paper is a contribution to the Belgian Antarctic Program (SSTC-Science Policy Office). The authors are greatly indebted to the "Programma Nazionale di Ricerche in Antartide" (PNRA) and to the logistic team of Terra Nova Bay for unconditional and efficient support in the field. Thanks are also due to Dr. J. Jouzel and Prof. A. Longinelli for allowing use of the facilities in their respective Laboratories. M. Dini benefited from a research scholarship from the University of Trieste. J.-L. Tison is a Research Associate of the Belgian National Fund for Scientific Research (F.N.R.S.). The authors especially wish to thank H. Eicken, S. Jacobs and three anonymous referees for constructive and detailed comments on earlier versions of the manuscript. M. Naessens is acknowledged for analytical work on some of the sea ice cores.

## REFERENCES

- Addison, J.R., Impurity concentrations in sea ice., *J. Glaciol.*, 18(78), 117-127, 1977.
- Baroni, C., The Hells Gate and Backstairs Passage Ice Shelves, Victoria Land, Antarctica, *Mem. Soc. Geol. Ital.*, 43, 123-144, 1990.
- Baroni, C., M. Frezzotti, C. Giraudi, and G. Orombelli, Ice flow and surficial variation inferred from satellite image and aerial photograph analysis of Larsen Ice Tongue, Hells Gate and Nansen Ice Shelves (Victoria Land, Antarctica), *Mem. Soc. Geol. Ital.*, 46, 69-80, 1991a.
- Baroni, C., B. Stenni, and P. Iacumin, Oxygen isotopic composition of ice samples from the Hells Gate and Backstairs Passage ice shelves (Victoria Land, Antarctica): Evidence of bottom freezing, *Mem. Soc. Geol. Ital.*, 46, 45-48, 1991b.
- Ben-Yaakov, S., Diffusion of sea water ions - I. Diffusion of sea water into a dilute solution, *Geochim. Cosmochim. Acta*, 36, 1395-1406, 1972.
- Bombosch, A., and A. Jenkins, Modeling the formation and deposition of frazil ice beneath Filchner-Ronne Ice Shelf., *J. Geophys. Res.*, 100(C4), 6983-6992, 1995.
- Casella, F., R. Udisti, and G. Piccardi, The oceanic source contribution to the snow composition, as function of elevation, at two Antarctic coastal stations, *Terra Antarctica*, in press.
- Corr, H., M. Popple, and A. Robinson, Airborne radio echo investigations of a marine ice body. *Filchner-Ronne Ice Shelf Programme (FRISP) Report 8*, AWI - Bremerhaven, 14-17, 1995.
- Cox, G.P.N., and W.F. Weeks, Numerical simulations of the profile properties of undeformed first-year sea ice during the growth season, *J. Geophys. Res.*, 93(10), 12449-12460, 1988.
- Dansgaard, W., S.J. Johnsen, H.B. Clausen, and N. Gundestrup, Stable isotope glaciology, *Medd. Grøn.*, 197(2), 1-53, 1973.
- Dieckmann, G.S., G. Rohardt, H. Hellmer, and J. Kipfstuhl, The occurrence of ice platelets at 250m depth near the Filchner Ice Shelf and its significance for sea ice biology., *Deep-Sea Res.*, 33, 141-148, 1986.
- Eicken, H., Factors determining microstructure, salinity and stable-isotope composition of Antarctic sea ice: Deriving modes and rates of ice growth in the Weddell Sea, *Antarct. Res. Ser.*, this volume.
- Eicken, H., and M.A. Lange, Development and properties of sea ice in the coastal regime of the Southeastern Weddell Sea, *J. Geophys. Res.*, 94(C6), 8193-8206, 1989.
- Eicken, H., H. Oerter, H. Miller, W. Graf, and J. Kipfstuhl, Textural characteristics and impurity content of meteoric and marine ice in the Ronne Ice Shelf, Antarctica, *J. Glaciol.*, 40(135), 386-398, 1994.
- Fabiano, M., P. Povero, G. Catalano, and F. Benedetti, Hydrological data collected during the biological, chemical and geological sampling in Terra Nova Bay, *Nat. Sc. Com., Ocean. Camp. 1989-90, Data Rep.*, 35-71, 1991.
- Frezzotti, M., Glaciological study in Terra Nova Bay, Antarctica, inferred from remote sensing analysis, *Ann. Glaciol.*, 17, 63-71, 1993.
- Friedman, I., A.C. Redfield, B. Schoen, and J. Harris, The variation of the deuterium content of natural water in the hydrologic cycle, *Rev. Geophys.*, 2(1), 177-189, 1964.
- Goldberg, E.D., Biogeochemistry of trace elements., *Geol. Soc. Amer. Mem.*, 67, 345-358, 1957.
- Gow, A.J., S.F. Ackley, K.R. Buck, and K.M. Golden, Physical and structural characteristics of Weddell Sea pack ice, *CRREL Report*, 87-14, pp. 70, 1987.
- Gow, A.J., S.F. Ackley, J.W. Govoni, and W.F. Weeks, Physical and structural properties of land-fast sea ice in



## 406 ANTARCTIC SEA ICE: PHYSICAL PROCESSES, INTERACTIONS AND VARIABILITY

- McMurdo Sound, Antarctica, *Antarct. Res. Ser.*, this volume.
- Gow, A.J., and S. Epstein, On the use of stable isotopes to trace the origins of ice in a floating ice tongue, *J. Geophys. Res.*, 77, 6552-6557, 1972.
- Gow, A.J., D.A. Meese, D.K. Perovich, and W.B. Tucker III, The anatomy of a freezing lead, *J. Geophys. Res.*, 95(C10), 18221-18232, 1990.
- Grosfeld, K., R. Gerdes, and J. Determann, Thermohaline circulation and interaction between ice shelf cavities and the adjacent open ocean, *J. Geophys. Res.*, 102(C7), 15595-15610, 1997.
- Hellmer, H.H., and S.S. Jacobs, Ocean interactions with the base of the Amery Ice Shelf, Antarctica, *J. Geophys. Res.*, 97(20), 305-320, 1992.
- Jacobs, S.S., W.E. Haines, J.J.L. Ardai, and P.A. Mele, Ross Sea oceanographic data, 1983-1987, *Lamont-Doherty Geological Observatory of Columbia University, New York*, 1989.
- Jacobs, S.S., H.H. Helmer, C.S.M. Doake, A. Jenkins, and R.M. Frolich, Melting of ice shelves and the mass balance of Antarctica, *J. Glaciol.*, 38(130), 375-387, 1992.
- Jeffries, M.O., and W.F. Weeks, Fast-ice properties and structure in McMurdo Sound, *Antarct. J. U.S.*, 26(5), 94-95, 1991a.
- Jeffries, M.O., and W.F. Weeks, Summer pack-ice properties and structure in the western Ross Sea, *Antarct. J. U.S.*, 26(5), 95-97, 1991b.
- Jeffries, M.O., and W.F. Weeks, Structural characteristics and development of sea ice in the western Ross Sea, *Antarct. Sci.*, 5(1), 63-75, 1993.
- Jeffries, M.O., W.F. Weeks, R. Shaw, and K. Morris, Structural characteristics of congelation and platelet ice and their role in the development of Antarctic land-fast sea ice, *J. Glaciol.*, 39(132), 223-238, 1993.
- Jeffries, M.O., and U. Adolphs, Early winter ice and snow thickness distribution, ice structure and development of the western Ross Sea pack ice between the ice edge and the Ross Ice Shelf, *Antarct. Sci.*, 9(2), 188-200, 1997.
- Jenkins, A., and A. Bombosch, Modeling the effects of frazil ice crystals on the dynamics and thermodynamics of Ice Shelf Water plumes, *J. Geophys. Res.*, 100(C4), 6967-6981, 1995.
- Kawamura, T., K.I. Oshima, T. Takizawa, and S. Ushio, Physical, structural, and isotopic characteristics and growth processes of fast sea ice in Lützow-Holm Bay, Antarctica, *J. Geophys. Res.*, 102(C2), 3345-3355, 1997.
- Kipfstuhl, J., Zur entstehung von unterwassereis und das wachstum und die energiebilanz des meereises in der Akta Bucht, Antarktis. On the formation of underwater ice and the growth and energy budget of the sea ice in Atka Bay, Antarctica, *Ber. Polarforsch.*, 85, 1991.
- Kipfstuhl, J., G. Dieckmann, H. Oerter, H. Hellmer, and W. Graf, The origin of green icebergs in Antarctica, *J. Geophys. Res.*, 97(C12), 20319-20324, 1992.
- Lange, M.A., Basic properties of Antarctic sea ice as revealed by textural analysis of ice cores, *Ann. Glaciol.*, 10, 95-101, 1988.
- Lange, M.A., Development and physical properties of sea ice in the Weddell Sea, Antarctica, in *Sea Ice Properties and Processes, CRREL Monograph 90-1*, 22-40, 1990.
- Lange, M.A., S.F. Ackley, P. Wadhams, G.S. Dieckmann, and H. Eicken, Development of sea ice in the Weddell Sea, Antarctica, *Ann. Glaciol.*, 12, 92-96, 1989.
- Langway, C.C.J., Ice fabrics and the Universal stage, *CRREL Tech. Rep.* 62, pp. 16, 1958.
- Lewis, E.L., and R.G. Perkin, Ice pumps and their rates, *J. Geophys. Res.*, 91(10), 11.756-11.762, 1986.
- Lorrain, R., J.-L. Tison, A. Bondesan, D. Ronveaux, and M. Meneghel, Preliminary results from 60 shallow cores and from one 45-m deep marine ice core at Hells Gate Ice Shelf, Victoria Land, Antarctica, *Terra Antarctica Reports*, 1, 19-24, 1997.
- Morgan, V.I., Oxygen isotope evidence for bottom freezing on the Amery Ice Shelf, *Nature*, 238, 392-394, 1972.
- Moser, H., and W. Stichler, Environmental isotopes in ice and snow, in *Handbook of Environmental Isotope Geochemistry*, in *The terrestrial environment*, edited by P. Fritz, and J. Fontes, pp. 141-178, Elsevier, New York, 1980.
- Nakawo, M., and N. Sinha, Growth rate and salinity profiles of first-year sea ice in the high Arctic, *J. Glaciol.*, 27, 315-330, 1981.
- Oerter, H., H. Eicken, J. Kipfstuhl, H. Miller, and W. Graf, Comparison between ice core B13 and B15, *Filchner-Ronne Ice Shelf Programme (FRISP) Report 7*, AWI - Bremerhaven, 29-36, 1994.
- Oerter, H., J. Kipfstuhl, J. Determann, H. Miller, D. Wagenbach, A. Minikin, and W. Graf, Evidence for basal marine ice in the Filchner-Ronne Ice Shelf, *Nature*, 358, 399-401, 1992.
- Paterson, W.S.B., *The Physics of Glaciers*, 480 pp., Pergamon, Oxford, 1994.
- Ragle, R.H., B.L. Hansen, A. Gow, and R.W. Patenaude, Deep core drilling in the Ross Ice Shelf, Little America V, Antarctica, *CRREL Technical Report*, 70, pp. 10, 1960.
- Rand, J., and M. Mellor, Ice-coring augers for shallow depth sampling, *CRREL Rep.* 85-21, pp.22, 1985.
- Richardson, C., Phase relationships in sea ice as a function of temperature, *J. Glaciol.*, 17(77), 507-519, 1976.
- Ronveaux, D., The dynamics of a small antarctic ice shelf as indicated by an ice composition study, thèse thesis, Université Libre de Bruxelles, 1992.
- Serikov, M.I., Structure of Antarctic sea ice, *Information Bulletin of the Soviet Antarctic Expedition*, 4(5), 265-266, 1963.
- Souchez, R., M. Lemmens, R. Lorrain, and J.-L. Tison, Pressure-melting within a glacier indicated by the chemistry of regelation ice, *Nature*, 273, 454-456, 1978.
- Souchez, R., M. Meneghel, J.-L. Tison, R. Lorrain, D. Ronveaux, C. Baroni, A. Lozej, I. Tabacco, and J. Jouzel, Ice composition evidence of marine ice transfer along the



## TISON ET AL.: LANDFAST SEA ICE VARIABILITY AND MARINE ICE AT HELLS GATE ICE SHELF

407

- bottom of a small Antarctic ice shelf, *Geophys. Res. Lett.*, 18(5), 849-852, 1991.
- Tison, J.-L., A. Bondesan, G. Delisle, A. Lozej, F. Merlanti, and L. Janssens, A dynamical approach to explain ice structures and complex morainic genesis on a partially grounded ice shelf (Hells Gate Ice Shelf - Victoria Land, Antarctica), *Terra Antarctica Reports*, 1, 33-38, 1997.
- Tison, J.-L., E.M. Morris, R. Souchez, and J. Jouzel, Stratigraphy, stable isotopes and salinity in multi-year sea ice from the rift area, south George VI Ice Shelf, Antarctic Peninsula, *J. Glaciol.*, 37(127), 357-367, 1991.
- Tison, J.-L., D. Ronveaux, and R. Lorrain, Low salinity frazil ice generation at the base of a small antarctic ice shelf, *Antarct. Sci.*, 5(3), 309-322, 1993.
- Veazey, A.D., Development and variability of the structure and physical properties of landfast sea ice in McMurdo Sound, M.S. Thesis, University of Alaska Fairbanks, 1994.
- Wadhams, P., M.A. Lange, and S.F. Ackley, The ice thickness distribution across the Atlantic sector of the Antarctic Ocean in midwinter, *J. Geophys. Res.*, 92, 14535-14552, 1987.
- Weeks, W.F., and S.F. Ackley, The growth, structure and properties of sea ice, in *The geophysics of sea ice*, edited by N. Untersteiner, pp. 9-164, Martinus Nyhoff Publ., Dordrecht (Nato ASI Series B, Physics), 1986.
- Williams, M.J.M., R.C. Warner, and W.F. Budd, The effects of ocean warming on melting and ocean circulation under the Amery Ice Shelf, East Antarctica, *Ann. Glaciol.*, in press.
- Wilson, C.J.L., J.P. Burg, and J.C. Mitchell, The origin of kinks in polycrystalline ice, *Tectonophysics*, 127(1-2), 27-48, 1986.
- Wilson, C.J.L., and Y. Zhang, Comparison between experiment and computer modelling of plane strain simple shear ice deformation., *J. Glaciol.*, 40(134), 46-55, 1994.
- Wilson, T.R.S., Salinity and the major elements of sea water, edited by Riley and Skirrow, pp. 365-413, Academic Press, London, 1975.
- World Meteorological Organization, WMO *Sea Ice Nomenclature Terminology, Codes and Illustrated Glossary*, WMO/DMM/BMO 259-TP-145, Secretariat of the WMO, Genova, 1985.
- Zotikov, I.A., V.S. Zagorodnov, and J.V. Raikovsky, Core drilling through the Ross Ice Shelf (Antarctica) confirmed basal freezing, *Science*, 207(4438), 1463-1465, 1980.
- A. Bouzette, R. D. Lorrain and J.-L. Tison, Département des Sciences de la Terre et de l'Environnement, Laboratoire de Glaciologie, Faculté des Sciences (CP 160/03), Université Libre de Bruxelles, 50, av. F.D. Roosevelt, 1050 Bruxelles, Belgique.
- M. Dini, Laboratorio di Geochimica Isotopica, Dipartimento di Scienze della Terra, Università di Trieste, via E. Weiss, 6, 34127 Trieste, Italy.
- A. Bondesan, Dipartimento di Geografia G. Morandini, Università di Padova, via del Santo, 26, I-35123, Padova, Italy.
- M. Stiévenard, Laboratoire de Modélisation du Climat et de l'Environnement, CEA/DSM, Bâtiment 709, Orme des Merisiers, CE Saclay, F-91191, Gif-sur-Yvette, CEDEX France.

(Received June 23, 1997;

accepted August 22, 1997)



**Paper 11**

**Significant Marine Ice Accumulation in the Ablation Zone beneath  
an Antarctic Ice Shelf**

**Authors**

**A. Khazendar, J.-L. Tison, B. Stenni, M. Dini, A. Bondesan**

**Journal**

**Journal of Glaciology, Vol. 47, n° 158**

**Year**

**2001**



## Significant marine-ice accumulation in the ablation zone beneath an Antarctic ice shelf

A. KHAZENDAR,<sup>1</sup> J.-L. TISON,<sup>1</sup> B. STENNI,<sup>2</sup> M. DINI,<sup>2</sup> A. BONDESAN<sup>3</sup>

<sup>1</sup>Département des Sciences de la Terre et de l'Environnement, Faculté des Sciences, CP 160/03, Université Libre de Bruxelles, B-1050 Brussels, Belgium

<sup>2</sup>Laboratorio di Geochimica Isotopica, Università di Trieste, I-34127 Trieste, Italy

<sup>3</sup>Dipartimento di Geografia, Università di Padova, Via del Santo 26, I-35127 Padua, Italy

**ABSTRACT.** High-resolution crystallographic, salinity and isotopic analyses of a 45 m ice core reveal the presence of a thick layer of marine ice near the grounding line of the Nansen Ice Shelf, Antarctica. The anomalous formation of marine ice in a zone assumed to be the site of active basal melting leads us to propose the hypothesis of large basal crevasses as a favorable environment for important marine-ice accretion. This hitherto unexplored possibility is supported by the overall field configuration and by the discrepancy in some ice properties between this core and the marine-ice sections of previous drilling projects. These findings could have important implications for the general stability of ice shelves and their disintegration processes. The specific properties of this core reveal that marine ice is post-genetically deformed.

### FRAMEWORK

The three-decade-old quest to recover ice samples from the interface zone between an ice shelf and the ocean has led investigators down several paths. Work was first done on shallower and thus more accessible ice tongues. The objective of earlier efforts was to demonstrate that sea water must be directly freezing on to the base of ice tongues due to upward heat conduction through the ice, forming congelation ice. Gow and Epstein (1972) provided the first conclusive verification of this assumption. Their work was based on ice cores up to 13 m deep that had been drilled in the Koettlitz Ice Tongue, Antarctica. The same process, but on a much larger scale, was shown to take place beneath the Ross Ice Shelf (Zotikov and others, 1980) where the bottom-most 6 m of a 416 m ice core were composed of frozen sea water. The estimated average freezing rate at this location was inferred by Zotikov and others (1980) to be  $2 \text{ cm a}^{-1}$ , which was in good agreement with what Robin (1979) had already theoretically suggested for the Ross Ice Shelf.

Another access to interface ice was identified when Kipfstuhl and others (1992) and then Warren and others (1993) established the basal ice-shelf origin of green icebergs. The latter authors did not hypothesize on the formation mechanism of their green iceberg ice, but they did suggest the possibility that it had accreted at the base of the Amery Ice Shelf. This shelf was earlier the site of a 315 m deep coring project of which the preliminary results were presented by Morgan (1972). The lowermost 45 m of this core, known as G1, were composed of what Morgan (1972) at the time considered to be sea-water ice. However, the slow rate of this conduction-driven process made it inadequate to explain such thick accumulations of basal ice. Hence, a second mechanism was introduced when Robin (1979) linked for

the first time the formation of basal ice at G1 with water circulation patterns in the sub-ice-shelf cavity. The process was theoretically elaborated by Lewis and Perkin (1986) through their ice-pump model by which ice is melted at depth and deposited higher in the water column due to the freezing-point dependence on pressure. Later, Engelhardt and Determann (1987) explained how frazil-ice crystals would form in thermohaline circulation and subsequently accrete at the bottom of an ice shelf and consolidate. Modeling of melting and accretion processes at the ice-shelf/ocean interface has been further improved in recent years by several authors including Hellmer and Jacobs (1992), Determann and Gerdes (1994), Bombosch and Jenkins (1995) and Jenkins and Bombosch (1995).

The number of available marine-ice samples and cores still remains limited. This could be explained in part by the relatively recent interest in the subject. Then there are the difficulties associated with the two possible sources of basal marine-ice samples. Green icebergs are rarely found in Nature, for the reasons discussed by Warren and others (1993) and Grosfeld and others (1998). On the other hand, drilling for marine ice at the bottom of ice shelves is confronted with the obvious necessity of having to penetrate hundreds of meters of meteoric ice. Other than at G1, bottom-ice accretion has also been found to constitute the lower 62 m of the 215 m core drilled in the Filchner-Ronne Ice Shelf at site B13 (Oerter and others, 1992). Another 320 m core recovered further upstream from the same ice shelf at site B15 revealed the presence of a 167 m thick accretion layer at the bottom (Oerter and others, 1994). Layers of solid ice formed below meteoric ice at the bottom of ice shelves are now known by most authors as marine ice (Oerter and others, 1992) and we follow this terminology.

As part of the 1995–96 Belgo-Italian collaboration



program, a 45 m ice core was drilled out of the Nansen Ice Shelf (NIS), which is misleadingly identified as an ice sheet on official maps. The NIS core is comparable in length with the marine-ice sections of both the G1 and B13 cores. We present here the results of high-resolution multiparametric measurements showing that the properties of the entire core correspond to those of marine ice. We believe that this is the first time that a core of marine ice with a formation site so relatively near to the grounding line has been directly collected from the surface of an ice shelf. More importantly, the core's proximity to the grounding line and its specific ice properties prompt us to consider and propose in this work the accretion of marine ice in basal crevasses opening where meteoric ice goes afloat as an active and previously undocumented process.

## SETTING

The NIS is located in Victoria Land, East Antarctica (Fig. 1). Its grounding line (Fig. 2) is thought to run in a roughly south-north direction across Reeves Glacier, along the eastern side of Teall Nunatak (Frezzotti and others, 2000). The area of interest for this study is the branch of the Reeves Glacier flow which passes north of Teall Nunatak. In that section, surface velocities at the grounding line vary between  $< 50 \text{ m a}^{-1}$ , near Teall Nunatak, and  $100\text{--}150 \text{ m a}^{-1}$  further north, as illustrated in figure 6 of Frezzotti and others (2000). Radio-echo sounding data provided by the same authors show that ice thickness ranges from 120–150 m, in the highly crevassed area located about halfway through, to 660 m further north. In addition to crevasses, rifts have opened near the grounding line. Some contain "islands" of continental ice chunks that have been frozen in place by the surrounding sea/marine ice (Fig. 3). From that point the shelf flows out into Terra Nova Bay for about 35 km to the front and is about 25 km across between Tarn Flat and Inexpressible Island. These two bedrock features together with the Northern Foothills laterally constrain the flow. The core was taken at  $74^{\circ}50.9' \text{ S}$ ,  $162^{\circ}51.3' \text{ E}$ , as close as was logistically possible to the grounding line, about 7.5 km downstream from it. This position was chosen in ice outcrops shown to be of sea-water origin by preliminary tests. Typical ice-flow horizontal velocities in the vicinity of the core site were measured by Frezzotti (1992) to be about  $160 \text{ m a}^{-1}$ . In the same paper, the author estimates that the ice shelf covers an area of approximately  $1800 \text{ km}^2$ . Therefore, its area and average thickness make it a small to medium-sized ice shelf.

The phenomenon of lower strata of an ice shelf finding their way to the surface due to high ablation rates was first demonstrated by Gow and Epstein (1972). Souchez and others (1991) invoked such a process to explain the marine-ice nature of certain frontal sections of the Hells Gate Ice Shelf in the Terra Nova Bay area. Mass loss at the surface of an ice shelf could be induced by either melting and drainage or sublimation. The latter process is the one most likely to be prevalent in the NIS situation due to the intense and frequent katabatic wind activity. Wind velocity measurements are available from the weather station AWS 8931 (PAT) which is nearest to the core site, at  $74^{\circ}53' \text{ S}$ ,  $163^{\circ}00' \text{ E}$  (Fig. 1). For the years 1989 and 1990, 41.2% of the wind blew from the southwest, the direction of the Antarctic plateau, with wind speeds exceeding 28 knots ( $52 \text{ km h}^{-1}$ ) for  $> 39\%$  of the time (Baroni, 1996). This has undoubtedly contributed to enhanced surface

ablation rates in the area, estimated by Frezzotti and others (2000) to be between  $500 \pm 100$  and  $400 \pm 80 \text{ kg m}^{-2} \text{ a}^{-1}$  ( $56 \pm 11$  and  $44 \pm 9 \text{ cm a}^{-1}$ ).

## ANALYTICAL TREATMENT

Traditionally, the three principal parameters used to establish the marine-ice identity of a body of ice are crystallography, salinity and stable isotopes.

All work on the ice core was done in a cold room kept at  $-25^{\circ}\text{C}$ . Vertical thin sections 7–10 cm long were continuously prepared along the entire 45 m of core length. Sampling for salinity measurements was done at the same frequency by cutting, at positions corresponding to the top of each thin section, a volume of ice necessary to produce about 15 mL of meltwater. This high sampling frequency has never been attempted in previous Antarctic marine-ice-core studies and it insures a much enhanced insight into the variability with depth of the ice properties and a better chance of detecting any interceding layers of different properties/origin.

Thin sections were viewed and photographed between crossed polarizers and then their crystal sizes were calculated using the linear intercept method (Tison and others, 1994). Conductivity was measured with a Tacussel CD810 conductimeter used with probe XE110 (cell constant =  $2.01 \text{ cm}$ ). During the conductivity measurements, the temperature of the melted samples was stabilized at  $25.00^{\circ}\text{C}$  by submerging their containers in a thermal bath. Since the temperature was not allowed to deviate in either direction by  $> 0.09^{\circ}\text{C}$ , the biggest error source was the error in the conductivity of the standard KCl solution used for calibrating the cell. Therefore, we estimate the error in the conductivity readings to be around  $\pm 2.5\%$ .

Mass-spectrometry analysis of the oxygen isotope composition relative to Vienna Standard Mean Ocean Water (V-SMOW) was conducted on 99 samples chosen more or less regularly along the core length and guided in part by the salinity results. Measurement accuracy is  $\pm 0.05\%$ .

## EVIDENCE

The crystalline structure revealed by the thin sections is conspicuous by its complete lack of bubbles, which, for Antarctic ice, is a strong indication of its non-continental origin. Following the scheme outlined by Tison and others (1998) for the classification of marine-ice types, two sub-categories can be used to describe most of the facies exhibited by the NIS core crystals. Few thin sections are observed to exclusively contain one of the facies, and for the most part the two facies are observed together in different proportions.

A first facies, which is attributed a frazil-ice origin, is made of small equigranular crystals with rounded boundaries that could therefore be identified as "granular orbicular" (Fig. 4a). One of the mechanisms listed by Weeks and Ackley (1982) for the formation of frazil ice is the adiabatic drop in pressure of rising water as a result of deep thermohaline circulation processes described above. Cores B13 (Oerter and others, 1992) and B15 (Oerter and others, 1994) also exhibit a granular facies, but some of the crystals show polygonal interlocking structure. According to Eicken and others (1994), this is probably inherited from the specific



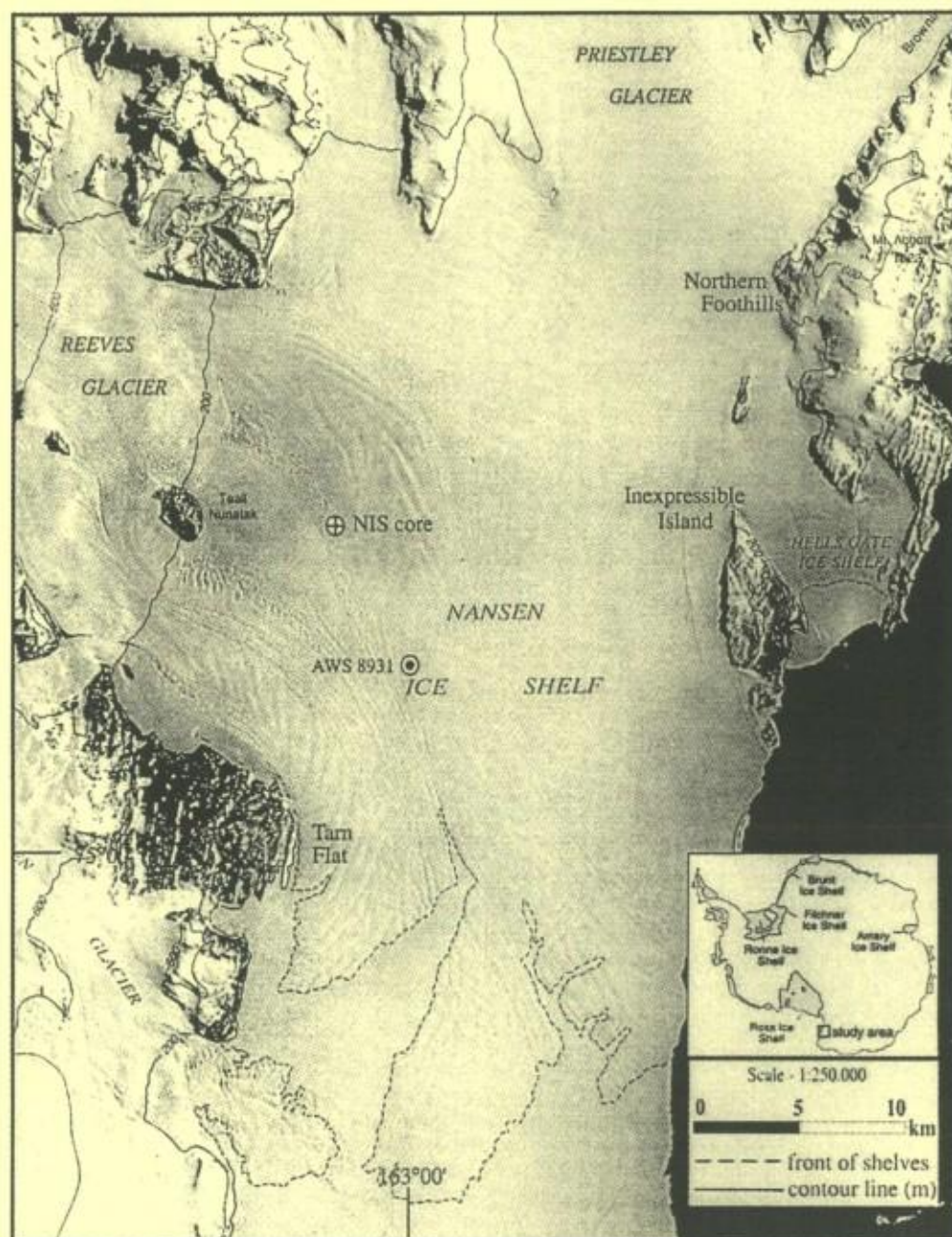


Fig. 1. Map of the NIS showing main surface features, the location of the drilling site and that of the meteorological station AWS 8931. Ice flows from the grounding line (located along the 200 m contour line around Teall Nunatak) to the front of the ice shelf indicated by the dashed line. The black area in the lower right corner of the picture is the open water of Terra Nova Bay. Background satellite image is taken from Borfecchia and Frezzotti (1991).

time/temperature (and perhaps deformation) growth history of the ice crystals as they accrete at the bottom of the ice shelf.

The second facies, which has not been reported for these other cores, is described by Tison and others (1998) as "string-lined" and presents a striking feature of the NIS core. Grains belonging to this latter category are noticeable for their elongation which shows a clear preference to occur in a vertical or near-vertical direction. Most of these crystals have a distinct rectangular aspect with an elongation factor of 2.5–6 and appear in thin sections throughout the core (Fig. 4b). This is in complete opposition to what has been

observed in the B13 core. Eicken and others (1994) describe how most grains in the top part of B13 are elongated in a horizontal direction and how this elongation tends to disappear with depth. The occurrence of the string-lined facies in the NIS core is often accompanied by clear small-scale folding that has a wavelength and an amplitude both of the order of 4 cm (Fig. 4c). Folding tends to be absent from the core segment at 17–27 m depth.

Crystal-size variation with depth is plotted in Figure 4d. The mean NIS core crystal breadth is 1.7 mm. If we were to use a rounded approximation, the corresponding average crystal cross-sectional area would be 2.7 mm<sup>2</sup>. This value is





Fig. 2. Aerial photograph showing the morphological features of the NIS near its grounding line at the foot of Reeves Glacier. Approximate location of the drilling site is marked by a star. The larger rocky structure in the top left corner is Teall Nunatak. Beyond it is Reeves Glacier flowing towards the viewer. Notice how the marine ice in the crescent-shaped outcrops occurs in a series that extends all the way from the grounding line. A more detailed photograph of the source area of these structures is shown in Figure 3. At the coring site, marine ice was at the same level as meteoric ice at the surface of the ice shelf.

distinctly lower than those reported for the marine-ice sections of the other cores. While crystal cross-sectional areas were not mentioned for G1, Oerter and others (1994) report values that vary mostly between 5 and 60 mm<sup>2</sup> for B13 and B15 crystals. Furthermore, with most NIS crystals having cross-sectional areas fluctuating between 1.1 and 3.8 mm<sup>2</sup>, they also exhibit a much more confined range than that of B13 and B15. NIS core crystal size shows a very weak tendency to increase with depth in the lower third of the core, as manifested by the smoothed (11-point running mean) profile of Figure 4d. The B13 core (Eicken and others, 1994), by contrast, shows a much clearer trend of increased crystal size with depth.

Both the quantitative values and the general qualitative behavior of the resulting conductivity profile with depth conform with those of marine ice. As can be seen from Figure 5a, most conductivity readings are clustered in the interval between 80  $\mu\text{S cm}^{-1}$  (0.035‰ salinity) and 300  $\mu\text{S cm}^{-1}$  (0.145‰). These values are considerably lower than typical sea-ice salinities which extend between 3‰ and 25‰ (Weeks and Ackley, 1982). Even congelation ice which is thought to have formed beneath the Ross Ice Shelf does not exhibit any salinities below 2‰ (Zotikov and others, 1980). On the other hand, the NIS conductivity results do overlap the ranges of 40–200  $\mu\text{S cm}^{-1}$  for B13 (Oerter and others, 1992) and 100–210  $\mu\text{S cm}^{-1}$  for G1 (Morgan, 1972). Furthermore, the general trend of decreasing salinity with increasing depth echoes what has been observed in the above-cited studies. This can be seen from the smoothed (11-point running mean) profile of Figure 5a. On the other hand, it should be noted that the NIS core, with a maximum measured conductivity of 390  $\mu\text{S cm}^{-1}$ , generally exhibits higher salinities than B13 and G1. The top 0.4 m of marine ice in the B15 core exhibit conductivity values as high as 390  $\mu\text{S cm}^{-1}$  (Oerter and others, 1994), but interaction with particle inclusions abundant in these layers could have occurred. Moreover, its conductivity profile rapidly drops back to a baseline value of around 40  $\mu\text{S cm}^{-1}$ , similar to that of B13 (Oerter and others,

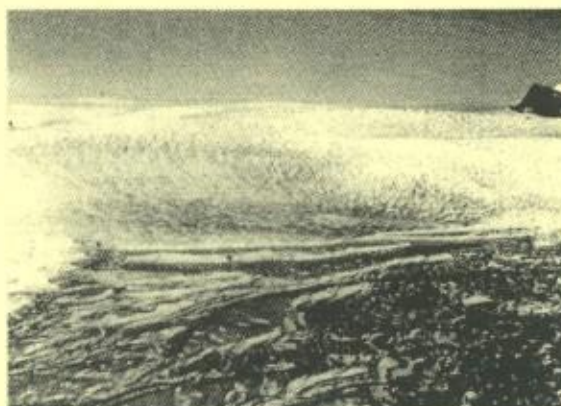


Fig. 3. Details of the fracture area at the origin of the flowline that passes through the location of the drilling site, 7.5 km downstream. The meteoric ice of Reeves Glacier (which is flowing towards the viewer) appears white in the upper half of the photograph, marine/sea ice is dark gray in the lower right area, and continental ice islands are visible as middle-gray flat surfaces delimited by white cliffs.

1994). The NIS core, by contrast, has a conductivity baseline value that falls from around 140  $\mu\text{S cm}^{-1}$  to 90  $\mu\text{S cm}^{-1}$  with increasing depth (Fig. 5a). However, significant deviations from the baseline of the salinity/conductivity signal occur as "bumps", each extending over a few meters of depth along the profile. Furthermore, the high resolution of sampling has revealed the presence of smaller-scale (decimeter) fluctuations in the salinity signal which exceed the measurement error. The amplitude of this variation clearly increases with higher salinity values. Fluctuations have also been observed in sea ice, where Weeks and Ackley (1982) have emphasized the fact that even in the most homogeneous-seeming ice there is a small-scale, apparently random variation in the salinity.

The oxygen isotope composition results presented in Figure 5b do not show any clearly discernible trend with depth, nor do they show substantial variability (standard deviation = 0.09‰). The  $\delta^{18}\text{O}$  values cover a range between +1.80‰ and +2.37‰, with a mean value of +2.12‰. This corresponds well with the slightly positive values reported for G1 by Morgan (1972), and the value of +2‰ for B13 measured by Oerter and others (1992). Such slightly positive  $\delta^{18}\text{O}$  values are consistent with fractionation of sea water.

For comparison,  $\delta^{18}\text{O}$  values for continental ice samples from Hells Gate Ice Shelf, which is part of the NIS, cover a range between -26‰ and -32‰ (Ronveaux, 1992).

Plotting corresponding values in a  $\delta^{18}\text{O}$ /conductivity diagram (Fig. 6) does not result in a significant correlation ( $r^2 = 0.07$ , 99 points).

## DISCUSSION

The evidence presented above strongly supports the idea that the NIS core is entirely composed of marine ice. This conclusion is reinforced by the comparison with B13, B15 and G1. It is excluded that this marine ice could have resulted from deep thermohaline circulation. Modeling work cited in the framework section predicts that melting prevails beneath an ice shelf near its grounding line. More specifically, Frezzotti and others (2000) calculated discharge fluxes across a flow channel located north of the crevassed



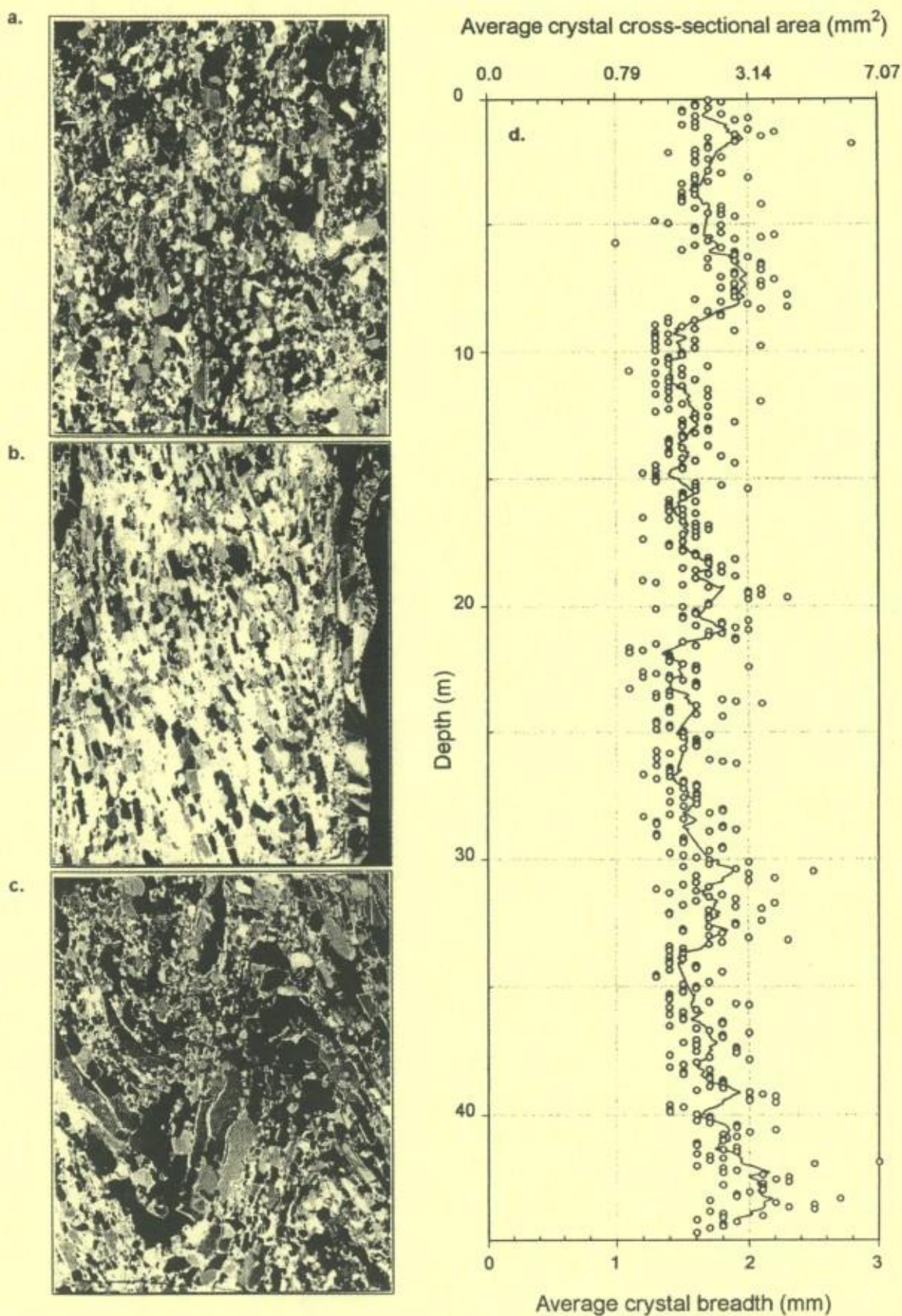
*Khazendar and others: Marine ice in ablation zone beneath Antarctic ice shelf*

Fig. 4. Crystallographic characteristics of the NIS core. Scale for photographs is shown on the bottom. (a) Granular/orbicular facies at 6.6 m depth; (b) string-lined facies at 16.6 m depth; (c) small-scale folding at 42.9 m depth; (d) profile of average crystal size with depth. Solid line in (d) is an 11-point running mean.



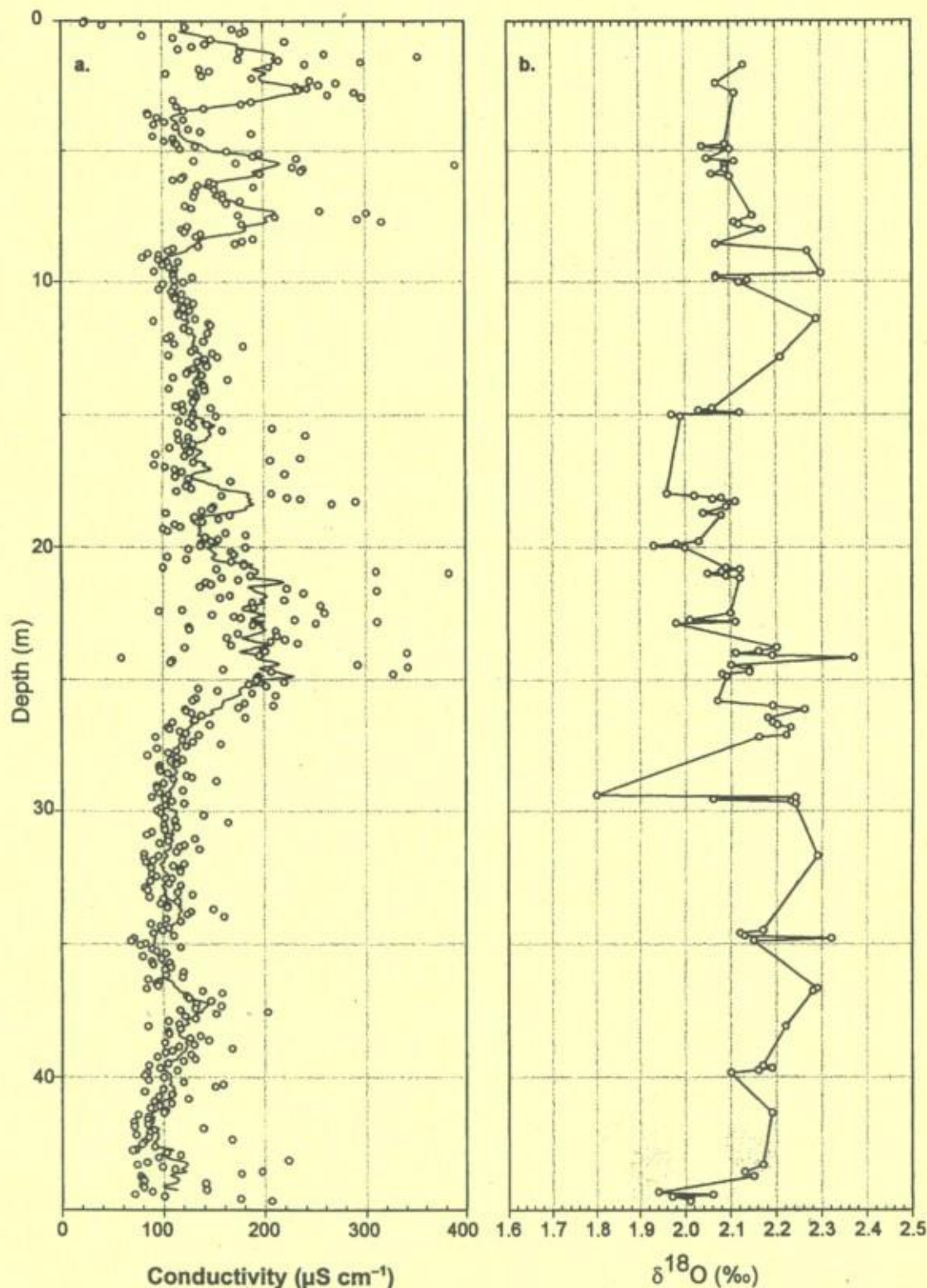


Fig. 5. Profiles of conductivity (a) and  $\delta^{18}\text{O}$  (b) for the NIS core. Solid line in (a) is an 11-point running mean through the data points.

area where the marine ice originated. They deduced a mean net melting rate of the order of  $0.26 \pm 0.90 \text{ m a}^{-1}$  between the NIS grounding line and 16 km down-flow, which well includes the core site. It is difficult to envisage marine ice accreting under such conditions. Furthermore, a very crude

calculation would show that even if marine ice were to form near the grounding line at 120–660 m depth, it would never have the time necessary to reach the surface, given the prevalent flow velocities and ablation rates. This last point implies to us that perhaps marine ice is being formed nearer



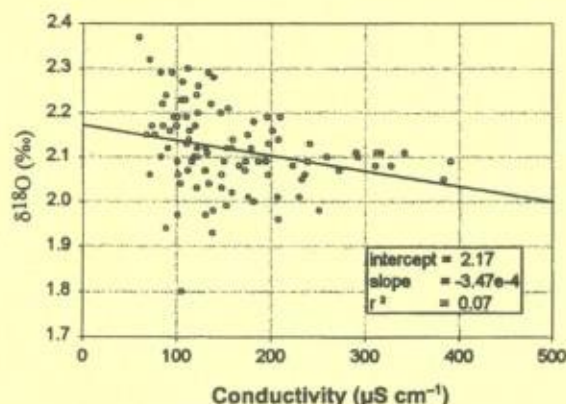


Fig. 6.  $\delta^{18}\text{O}$ /conductivity relation for 99 samples of the NIS core. Solid line represents linear regression through all points.

to the surface in some feature of the bottom topography of the ice shelf. Considering the geographical location near the grounding line of the study area which is cut by several rifts reaching all the way to the bottom of the ice shelf, and that the formation of such deep rifts often requires the presence of bottom crevasses reaching the surface, we regard basal crevasses as the most plausible explanation of our observations. Bottom crevasses are common features of Antarctic ice shelves. This has been demonstrated using radar sounding methods (e.g. Jezek and others, 1979). Shabtaie and Bentley (1982) describe how bottom crevasses vary widely in distribution and dimensions, with some reaching heights up to 250 m and bottom widths of 100 m. Still more interestingly, Jezek and Bentley (1983) observed that bottom crevasses in the Ross Ice Shelf generally disappear from the radar record within 100 km downstream from their point of formation. This could be taken as a strong indication of bottom crevasses being filled with ice. We therefore propose that a large basal crevasse near the grounding line would provide a sheltered setting permitting the formation of marine ice in the midst of the basal ablation zone at the grounding line. A volume of Ice Shelf Water, which should become buoyant as a result of ice-shelf melting, would enter and ascend the crevasse, thus becoming supercooled. The basal crevasse would eventually, in part at least, become filled with marine ice in a manner similar to that described above for the formation, accumulation and subsequent consolidation of frazil ice under ice shelves. A similar local ice pump, but at the front of an ice shelf, has been hypothesized by Grosfeld and others (1998) to account for the occurrence of marine ice at the bottom of green icebergs thought to have originated in the former Grand Chasm of the Filchner Ice Shelf.

A complementary mechanism that could contribute to ice formation in open rifts and basal crevasses is the possibility of ice directly forming on the walls, as a result of heat conduction into the ice shelf. Such accretion would be relatively small in the lower parts of the crevasse, where conditions are comparable to those at the interface between the bottom of an ice shelf and the water (Jacobs and others, 1979). In the higher parts, especially shortly after the crevasse had opened, water would be in contact with ice that could be as cold as  $-20^\circ\text{C}$ , so more significant direct accretion is certain to occur. However, it is possible that, with time, the presence of the crevasse itself would transform the thermal regime of the ice shelf surrounding it to one more similar to that at the ice-shelf/ocean interface, thus gradually reducing the magni-

tude of congelation. Furthermore, in view of the generally large widths of rifts considered, congelation ice at the walls should only form a minor fraction of the total ice in the rift. Finally, in the particular case of the NIS core, the absence of ice with columnar texture, which is a distinctive sign of direct-freezing origin, shows that none of the marine ice examined here formed directly at the walls of the crevasse.

Many of the underlined observed discrepancies between the NIS core and the marine-ice segments of the other cores considered actually support the hypothesis of a local ice pump being active in the suggested morphological configuration. This includes the relatively higher general salinity of the NIS core compared with BI3, BI5 and G1. In the situation we are proposing, higher salinity would be explained by the higher freezing rate of the interstitial water existing among the frazil crystals after their accumulation at the top of the water column and before their consolidation. In the case of a basal crevasse, the ambient water-frazil mixture would be nearer to the surface, thus resulting in a more rapidly advancing freezing front and hence less efficient rejection of salt upon freezing. As the freezing front descends further away from the surface, the freezing rate would be reduced, resulting in better salt rejection and the observed trend of decreasing conductivity/salinity with depth. The direct relationship between the freezing rate and initial salt entrapment in sea ice was addressed by Weeks and Lofgren (1967) and further developed by Weeks and Ackley (1982). On the other hand, work on stable-isotope fractionation in growing sea ice (Souchez and others, 1988; Eicken, 1998) showed an inverse relationship between the freezing rate and the  $\delta^{18}\text{O}$  or  $\delta\text{D}$  signal. The question might then be raised as to why the  $\delta^{18}\text{O}$  isotopic profile with depth (Fig. 5b) does not show a clear analogous influence by the freezing rate, nor does it show a clear inverse correlation with salinity (Fig. 6). This could be explained by the fact that frazil crystals themselves are almost completely desalinated, such that the salinity signal results only from the intergranular brine inclusions, while the isotopic signal reflects both contributions. Therefore, even if isotopic fractionation does occur in the brine inclusions due to the advancement of a freezing front, the resulting signal will be dominated by the overwhelming and unmodified contribution from the crystals. As for the isotopic signal of the crystals themselves, it is plausible that the temperature and pressure conditions necessary for the formation of frazil ice in the successive ascending water masses are regularly satisfied at a certain specific depth in the water column, thus producing frazil crystals with more or less the same isotopic enrichment, which would account for the rather weak variability of the NIS core isotopic signal. Eicken and others (1994), while noting the decreasing salinity with depth in the BI3 core, exclude the advancement of a freezing front as an explanation of the salinity profile on the basis of thermodynamic constraints (conductive heat fluxes in the central Ronne Ice Shelf of the order of  $0.1\text{ W m}^{-2}$ ) and of the "anomalously" low salt distribution coefficient ( $k_{\text{eff}} < 0.001$ ) that would be needed to explain the observed salinity. The authors suggest that consolidation under the deviatoric buoyancy stress associated with the tens of meters of crystals accumulating beneath would lead to densification and expulsion of brine through fragmentation and settling of individual platelet crystals. However, in a companion paper (Tison and others, in press) we argue that both compaction and heat conduc-



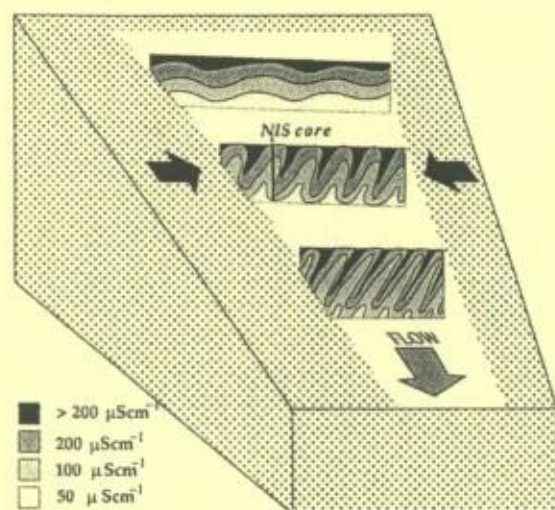


Fig. 7. Sketch of possible modification of the initial ice stratification due to lateral compression.

tion are probably needed to account for the chemical properties of marine ice. In the near-surface formation setting for marine ice being proposed in this paper, thermodynamic growth through the progressively slowing descent of a freezing front can certainly not be neglected.

Although initial salt entrapment and stable-isotope fractionation of the NIS marine ice have been determined by thermodynamic growth, subsequent reworking has clearly taken place, as attested by the salinity profile (Fig. 5a). It is the location of the core and its geomorphological context which provide at least two possible explanations for the presence of large-scale conductivity/salinity deviations from the baseline value: the first is related to the dynamically active core-site environment, which was described above to be a zone where different ice streams converge with different velocities and thickness, thus creating a situation where the ice is subjected to lateral compression. Such a stress configuration would fold the ice body and disturb the initial stratification as sketched in Figure 7 and as witnessed by the small-scale folding features in the core (Fig. 4c). The question remains why large-scale compression would only selectively affect the part of the core above 28 m and spare the lower part, as inferred from Figure 5a. The answer could be that large-scale folding has also occurred in the lower parts of the core but is not as visible because ice strata there are characterized by low salinity contrast. A second possible explanation is related to the core's location near the surface of the ice shelf, where its brine content could be affected by seasonal temperature changes. The resulting temperature gradients could produce brine-pocket migration (Hoekstra and others, 1965; Seidensticker, 1966), especially in the top few meters. The problem with this idea, however, is the slowness of the process (Weeks and Ackley, 1982; Eicken and others, 1994), associated with the fact that the seasonal temperature signal does not significantly affect the temperature profile below a certain depth (in continental ice, its amplitude would only be 5% of its surface value at 10.2 m (Paterson, 1994)).

A basal crevasse, with its vertical spatial extension, would also account for the appearance of marine-ice layers on the ice-shelf surface despite proximity to the grounding line. This would also imply a relatively young age for the

NIS core ice (on the order of 50 years) compared to the hundreds of years estimated for the Filchner–Ronne cores by Eicken and others (1994). This would give the NIS grains less time to recrystallize, thus resulting in their relatively smaller sizes. On the other hand, the abundance of the string-lined facies and their vertical orientation could be due to grain recrystallization under the influence of a stress field applied by the walls of the crevasse. The presence of such stresses could in part be inferred from the appearance of folding in the core and its direction that suggest at least a horizontal component for the acting force.

It is worth noting that the proposed local ice-pump accretion process for marine ice in basal crevasses near the grounding line could easily be extended to the case of rifts opening in ice shelves, especially in the vicinity of ice rises, ice islands, on the side of large embayments and in the frontal regions of Antarctic shelves. Similarly, the process could occur in the regions of thinner ice that form between two converging ice streams (Tison and others, 1998, especially their fig. 3). Strong evidence for such occurrence is provided by the recent work of Fricker and others (in press). The authors infer the presence of two main bands of marine ice beneath the Amery Ice Shelf; both are clearly associated with the convergence points of ice streams.

To conclude this discussion, we consider a possible alternative explanation for the properties observed in the NIS core, namely, that a body of marine ice, originally formed in a bottom crevasse upstream from the core location, is detached, tilted and lodged in another crevasse downstream with an angle relative to its initial position, as has been observed for continental ice chunks. However, such a process does not account for the general tendency of conductivity to decrease with depth, nor for the presence of vertically aligned crystals along the whole length of the core. Furthermore, ongoing work on another 45 m core, located 24.5 km downstream from the grounding line, reveals properties similar to those described in this work. That the results of such a peculiar alternative process are observed at two different sampling locations is highly improbable.

## CONCLUSIONS

We have demonstrated in this work that marine ice could be more readily recovered and studied by exploiting a combination of climatic (high surface ablation rates) and accretion locations (nearer to the surface in a basal crevasse or rift) for certain ice shelves. Recent ice–ocean modeling and fieldwork efforts are increasingly underlining the importance of marine-ice formation and accretion beneath Antarctic ice shelves. Improved comprehension of these processes is indispensable for accurate mass-balance estimations of ice shelves. We have shown that an important segment of the thickness of small to medium Antarctic shelves, at certain locations, could be formed of marine ice. These same shelves could be among the first to show signs of regional warming because of their smaller thermal inertia and proportionally more rapid reduction of contact surfaces with pinning points and embayment sides. The thermal properties of Antarctic ice shelves, and hence their heat exchange with the atmosphere and/or the ocean, could be modified if a larger proportion of their mass was composed of saline, bubble-free ice instead of fresh, bubbly continental ice. Most importantly perhaps, we have proposed a new possible setting for the formation of



marine ice in the vicinity of the grounding line, where basal melting would normally prevail. In this context, a modeling effort and the analysis of another core recovered from the same ice shelf are progressing. Basal crevasses and rifts are common features near the grounding lines of ice shelves and in their frontal zones as precursors for iceberg calving. Studies of the dynamic stability of Antarctic ice shelves and their fragmentation mechanisms would benefit from better insight into the interaction of shelf rifts and crevasses with the ocean. Hughes (1983) explored the important role that these fracture features play in the disintegration of ice shelves, while Stephenson and Zwally (1989) discussed the stabilizing effect that might result from the filling of rifts with ice. Recently, Rignot and MacAyeal (1998) and MacAyeal and others (1998) have demonstrated how the dynamic properties of what they call the "ice melange" in open rifts do play an important role in the calving process at the front and in the overall stability of an ice shelf. According to these authors, the melange is composed of multi-year sea ice, ice-shelf fragments and wind-blown snow. It is quite plausible that the dynamic properties of the material filling the rifts, and its response to temperature variation, would be different if the ice was mainly composed of a homogeneous body of marine ice resulting from a process such as the one described in this paper rather than the mixture described by the above authors.

Although Antarctic rifts and basal crevasses are common, their overall area probably does not exceed a small fraction of that of a big ice shelf. However, they could make a disproportionate contribution if they occur at the grounding line, which is a point of compulsory passage for continental ice on its way to the sea. There, fractures could be filled with marine ice and exported downstream before new fractures form at the same point again and the process is repeated. A hint of such a sequence of events can be seen in Figure 2. Furthermore, as indicated by Corr and others (1995), considerable amounts of marine ice form at the confluence of individual ice streams that join together to form ice shelves. Such zones of steep lateral slopes are akin to a basal crevasse configuration and thus conducive to productive local ice pumps.

Finally, we believe that the high-resolution measurements presented in this work improve our perception of the variability patterns of ice-core properties with depth. Ongoing work on the three-dimensional variability of these signals should allow us to distinguish between the contribution to ice properties of the initial processes of consolidation and freezing and their subsequent modification through dynamic processes. Such an approach could help in revealing the mechanisms that lead to the comparatively very low salinities encountered in marine ice, still a subject of strong debate.

## ACKNOWLEDGEMENTS

This paper is a contribution to the Belgian Antarctic Programme (Science Policy Office). The authors are greatly indebted to the "Programma Nazionale di Ricerche in Antartide" for their logistic support during the field campaign. The authors would also like to thank R. Souchez and R. Lorrain for informative discussions. The constructive criticism of the scientific editor, M. Lange, and two anonymous reviewers was much appreciated and helped improve the manuscript. J.-L. Tison is a Research Associate at the Belgian Science Foundation (FNRS).

## REFERENCES

- Baroni, C., ed. 1996. *Mount Melbourne Quadrangle (Victoria Land)*. Siena, Museo Nazionale dell'Antartide. Ministero dell'Università e della Ricerca Scientifica e Tecnologica. Programma Nazionale di Ricerche in Antartide. (Antarctic Geomorphological and Glaciological Series, scale 1:250,000).
- Bombosch, A. and A. Jenkins. 1995. Modeling the formation and deposition of frazil ice beneath Filchner-Ronne Ice Shelf. *J. Geophys. Res.*, **100**(C4), 6983-6992.
- Borfecchia, F. and M. Frezzotti. 1991. *Satellite image mosaic of the Terra Nova Bay area (Victoria Land, Antarctica)*. Rome, Ente per le Nuove Tecnologie, l'Energia e l'Ambiente.
- Corr, H., M. Poppe and A. Robinson. 1995. Airborne radio echo investigations of a marine ice body. In Oerter, H., ed. *Filchner-Ronne Ice Shelf Programme (FRISP). Report No. 9 (1995)*. Bremerhaven, Alfred Wegener Institute for Polar and Marine Research, 14-17.
- Determann, J. and R. Gerdes. 1994. Melting and freezing beneath ice shelves: implications from a three-dimensional ocean-circulation model. *Ann. Glaciol.*, **20**, 413-419.
- Eicken, H. 1998. Deriving modes and rates of ice growth in the Weddell Sea from microstructural, salinity and stable-isotope data. In Jeffries, M. O., ed. *Antarctic sea ice: physical processes, interactions and variability*. Washington, DC, American Geophysical Union, 89-122. (Antarctic Research Series 74).
- Eicken, H., H. Oerter, H. Miller, W. Graf and J. Kipfstuhl. 1994. Textural characteristics and impurity content of meteoric and marine ice in the Ronne Ice Shelf, Antarctica. *J. Glaciol.*, **40**(135), 386-398.
- Engelhardt, H. and J. Determann. 1987. Borehole evidence for a thick layer of basal ice in the central Ronne Ice Shelf. *Nature*, **327**(6120), 318-319.
- Frezzotti, M. 1992. Fluctuations of ice tongues and ice shelves derived from satellite images in Terra Nova Bay area, Victoria Land, Antarctica. In Yoshida, Y., K. Kaminuma and K. Shiraiishi, eds. *Recent progress in Antarctic earth sciences*. Tokyo, Terra Scientific Publishing Co., 733-739.
- Frezzotti, M., I.E. Tabacco and A. Zirizzotti. 2000. Ice discharge of eastern Dome C drainage area, Antarctica, determined from airborne radar survey and satellite image analysis. *J. Glaciol.*, **46**(153), 253-264.
- Fricker, H.A., S. Popov, I. Allison and N. Young. In press. Distribution of marine ice under the Amery Ice Shelf, East Antarctica. *Geophys. Res. Lett.*
- Gow, A.J. and S. Epstein. 1972. On the use of stable isotopes to trace the origins of ice in a floating ice tongue. *J. Geophys. Res.*, **77**(35), 6552-6557.
- Grosfeld, K., H. H. Hellmer, M. Jonas, H. Sandhager, M. Schulte and D. G. Vaughan. 1998. Marine ice beneath Filchner Ice Shelf: evidence from a multi-disciplinary approach. In Jacobs, S. S. and R. F. Weiss, eds. *Ocean, ice and atmosphere: interactions at the Antarctic continental margin*. Washington, DC, American Geophysical Union, 321-341. (Antarctic Research Series 75).
- Hellmer, H. H. and S. S. Jacobs. 1992. Ocean interactions with the base of Amery Ice Shelf, Antarctica. *J. Geophys. Res.*, **97**(C12), 20,305-20,317.
- Hoekstra, P., T. E. Osterkamp and W. F. Weeks. 1965. The migration of liquid inclusions in single ice crystals. *J. Geophys. Res.*, **70**(20), 5035-5041.
- Hughes, T. 1983. On the disintegration of ice shelves: the role of fracture. *J. Glaciol.*, **29**(101), 98-117.
- Jacobs, S. S., A. L. Gordon and J. L. Arda, Jr. 1979. Circulation and melting beneath the Ross Ice Shelf. *Science*, **203**(4379), 439-443.
- Jenkins, A. and A. Bombosch. 1995. Modeling the effects of frazil ice crystals on the dynamics and thermodynamics of ice shelf water plumes. *J. Geophys. Res.*, **100**(C4), 6967-6981.
- Jezeq, K. C. and C. R. Bentley. 1983. Field studies of bottom crevasses in the Ross Ice Shelf, Antarctica. *J. Glaciol.*, **29**(101), 118-126.
- Jezeq, K. C., C. R. Bentley and J. W. Clough. 1979. Electromagnetic sounding of bottom crevasses on the Ross Ice Shelf, Antarctica. *J. Glaciol.*, **24**(90), 321-330.
- Kipfstuhl, J., G. S. Diekmann, H. Oerter, H. Hellmer and W. Graf. 1992. The origin of green icebergs in Antarctica. *J. Geophys. Res.*, **97**(C12), 20,319-20,324.
- Lewis, E. L. and R. G. Perkin. 1986. Ice pumps and their rates. *J. Geophys. Res.*, **91**(C10), 11,756-11,762.
- MacAyeal, D. R., E. Rignot and C. L. Hulbe. 1998. Ice-shelf dynamics near the front of the Filchner-Ronne Ice Shelf, Antarctica, revealed by SAR interferometry: model/interferogram comparison. *J. Glaciol.*, **44**(147), 419-428.
- Morgan, V. I. 1972. Oxygen isotope evidence for bottom freezing on the Amery Ice Shelf. *Nature*, **238**(5364), 393-394.
- Oerter, H. and 6 others. 1992. Evidence for basal marine ice in the Filchner-Ronne Ice Shelf. *Nature*, **358**(6385), 399-401.
- Oerter, H., H. Eicken, J. Kipfstuhl, H. Miller and W. Graf. 1994. Comparison between ice core B13 and B15. In Oerter, H., comp. *Filchner-Ronne Ice Shelf Programme (FRISP). Report No. 7 (1994)*. Bremerhaven, Alfred Wegener Institute for Polar and Marine Research, 29-36.
- Paterson, W. S. B. 1994. *The physics of glaciers. Third edition*. Oxford, etc., Elsevier.
- Rignot, E. and D. R. MacAyeal. 1998. Ice-shelf dynamics near the front of the



- Filchner-Ronne Ice Shelf, Antarctica, revealed by SAR interferometry. *J. Glaciol.*, **44**(147), 405–418.
- Robin, G. de Q. 1979. Formation, flow and disintegration of ice shelves. *J. Glaciol.*, **24**(90), 259–271.
- Ronveaux, D. 1992. The dynamics of a small Antarctic ice shelf as indicated by an ice composition study. (Ph.D. thesis, Université Libre de Bruxelles.)
- Seidensticker, R. G. 1966. Comment on paper by P. Hockstra, T. E. Osterkamp and W. F. Weeks, "The migration of liquid inclusions in single ice crystals". *J. Geophys. Res.*, **71**(8), 2180–2181.
- Shabtaie, S. and C. R. Bentley. 1982. Tabular icebergs: implications from geophysical studies of ice shelves. *J. Glaciol.*, **28**(100), 413–430.
- Souchez, R., J.-L. Tison and J. Jouzel. 1988. Deuterium concentration and growth rate of Antarctic first-year sea ice. *Geophys. Res. Lett.*, **15**(12), 1385–1388.
- Souchez, R. and 7 others. 1991. Ice composition evidence of marine ice transfer along the bottom of a small Antarctic ice shelf. *Geophys. Res. Lett.*, **18**(5), 849–852.
- Stephenson, S. N. and H. J. Zwally. 1989. Ice-shelf topography and structure determined using satellite-radar altimetry and Landsat imagery. *Ann. Glaciol.*, **12**, 162–169.
- Tison, J.-L., T. Thorsteinsson, R. D. Lorrain and J. Kipfstuhl. 1994. Origin and development of textures and fabrics in basal ice at Summit, central Greenland. *Earth Planet. Sci. Lett.*, **125**, 421–437.
- Tison, J.-L., R. D. Lorrain, A. Bouzette, M. Dini, A. Bondesan and M. Stiévenard. 1998. Linking landfast sea ice variability to marine ice accretion at Hells Gate Ice Shelf, Ross Sea. In Jeffries, M. O., ed. *Antarctic sea ice: physical processes, interactions and variability*. Washington, DC, American Geophysical Union, 375–407. (Antarctic Research Series 74.)
- Tison, J.-L., A. Khazendar and E. Roulin. In press. A two-phase approach to the simulation of the combined isotope/salinity signal of marine ice. *J. Geophys. Res.*
- Warren, S. G., C. S. Roesler, V. I. Morgan, R. E. Brandt, I. D. Goodwin and I. Allison. 1993. Green icebergs formed by freezing of organic-rich seawater to the base of Antarctic ice shelves. *J. Geophys. Res.*, **98**(C4), 6921–6928. (Correction: **98**(C10), 18,309.)
- Weeks, W. F. and S. F. Ackley. 1982. The growth, structure and properties of sea ice. *CRREL Monogr.* 82-1.
- Weeks, W. F. and G. Lofgren. 1967. The effective solute distribution coefficient during the freezing of NaCl solutions. In Öura, H., ed. *Physics of snow and ice. Vol. 1, Part 1*. Sapporo, Hokkaido University. Institute of Low Temperature Science, 579–597.
- Zotikov, I. A., V. S. Zagorodnov and J. V. Raikovskiy. 1980. Core drilling through the Ross Ice Shelf (Antarctica) confirmed basal freezing. *Science*, **207**(4438), 1463–1465.

MS received 20 December 1999 and accepted in revised form 8 May 2001



**Paper 12**

**A two-phase Approach to the Simulation of the Combined Isotope/salinity Signal of  
Marine Ice**

**Authors**

**J.-L. Tison, A. Khazendar, E. Roulin**

**Journal**

**Journal of Geophysical Research, Vol. 106, n° C12**

**Year**

**2001**



## A two-phase approach to the simulation of the combined isotope/salinity signal of marine ice

J.-L. Tison and A. Khazendar<sup>1</sup>

Unité de Glaciologie, Université Libre de Bruxelles, Brussels, Belgium

E. Roulin

Royal Meteorological Institute, Brussels, Belgium

**Abstract.** A modified boundary layer box diffusion model is used to simulate the production of the combined oxygen isotope/salinity signal of a body of marine ice. The final signal is considered to be the result of fractionation and segregation processes occurring first upon the formation of frazil crystals in suspension and second during their accumulation and consolidation due to the advancement of a freezing front. The model results are compared to oxygen isotope and salinity values in a 45-m marine ice core from the Nansen Ice Shelf, Antarctica. Parameters more suitable to the modeling of marine ice (as opposed to sea ice) are introduced and conclusions are drawn on the origin of the impurity characteristics of marine ice, including the still unresolved question of its anomalously low salinity.

### 1. Introduction

Marine ice forms as individual frazil ice crystals in the ocean that subsequently accumulate and consolidate at the base of ice shelves. It has now become clear that it can contribute significantly to the mass balance of ice shelves, especially those of small to medium size. Marine ice accretion is one of the possible results of the complex ice-ocean interactions occurring at the periphery of ice sheets where they cross the grounding line and go afloat. Field observations in areas where specific climatic conditions allow direct observation of marine ice outcrops at the ice shelf surface indicated that junction areas between individual flows converging to form the ice shelf (near grounding zones or in the lee of pinning points) are preferred sites of accretion [Tison *et al.*, 1993, 1998]. This confirms indirect observations by Radio Echo Soundings (RES) and Global Positioning System (GPS) measurements from other much larger ice shelves [Corr *et al.*, 1995; Grosfeld *et al.*, 1998]. Grosfeld *et al.* [1998] suggest, from green iceberg observations in the Weddell Sea, that marine ice accumulation could also be significant in the rifts forming prior to iceberg calving near ice shelf fronts. This corroborates earlier observations on multiyear ice formed within rift areas south of the George VI Ice Shelf in the Antarctic Peninsula [Tison *et al.*, 1991]. Measurements and observations described by Khazendar *et al.* [2001] demonstrate the existence of significant marine ice accumulation in rifts and basal crevasses, close to the grounding line of the Nansen Ice Shelf (NIS, Terra Nova Bay, Antarctica), where basal melting from the Deep Thermohaline Circulation should normally prevail.

The occurrence of marine ice bodies in such a wide range of locations, most of it corresponding to weak points of ice shelves, suggests it might play a significant mechanical role, as a welding agent, contributing to ice shelf stability. The bulk salinity of marine ice (as low as 0.03‰) is an important factor in this regard. It is indeed an order of magnitude higher than that of meteoric ice, but 2 orders of magnitude lower than those observed in granular sea ice (a few ‰) which, with the exception of snow ice, also results from frazil ice formation and consolidation in seawater. These contrasts in impurity content are thought to be responsible for misleading detection of the ice/ocean interface through RES measurements [Robin *et al.*, 1983; Thyssen, 1988; Souchez *et al.*, 1991; Corr *et al.*, 1995; Grosfeld *et al.*, 1998] and should lead to different rheologies for these various ice types (as observed, for example, in impurity-rich continental ice [e.g., Hooke *et al.*, 1988]). Recent studies of ice shelf dynamics near the front of the Filchner-Ronne Ice Shelf, using Synthetic Aperture Radar (SAR) interferometry, are another example of the importance of developing a better understanding of the physico-chemical properties of marine ice [MacAyeal *et al.*, 1998; Rignot and MacAyeal, 1998]. Such ice, with its distinct thermomechanical attributes, could be the main component of the "melange" that these authors suggest is filling frontal rifts.

The reasons for such a stark contrast in bulk salinity between marine ice and granular sea ice are still a subject of debate in the literature. Eicken *et al.* [1994] have clearly demonstrated that none of the postgenetic desalination processes summarized by Weeks and Ackley [1986] is strong or fast enough to explain the relative purity of marine ice. The anomalous low salinity in the marine ice can thus only be explained by the low initial salinity of newly consolidated ice layers. There are, however, several differences between the genetic processes of sea ice and marine ice that have been used by different authors to provide an explanation. First, the latter is formed in an environment that is directly influenced by continental ice-ocean interactions and protected from the atmosphere. Furthermore, it is formed at much greater depths,

<sup>1</sup>Now at Institute of Theoretical Geophysics, Dept. of Applied Mathematics and Theoretical Physics, University of Cambridge, Cambridge, United Kingdom.



31,388

TISON ET AL.: ISOTOPE/SALINITY SIGNAL IN MARINE ICE

**Table 1.** Main Results From the 45-m Ice Core Retrieved From Nansen Ice Shelf (Victoria Land, East Antarctica)

	Crystal Size	Conductivity	Salinity	$\delta^{18}\text{O}$
	mm	$\mu\text{Scm}^{-1}$	‰	‰
Mean	1.66	138.00	0.06	2.12
Minimum	1.00	22.30	0.005	1.80
Maximum	3.00	390.00	0.19	2.37
$\sigma$	0.27	54.01	0.02	0.09

that is under considerably lower freezing and consolidation rates. As a result, a much larger thickness of loose frazil crystals could accumulate before consolidation takes place, which implies a possible stress build up from buoyancy or converging flow, thereby reducing the porosity (proportion of the water volume to the total volume of the ice/water mixture) of the loose frazil.

Stable-isotope signatures ( $\delta^{18}\text{O}$  or  $\delta\text{D}$ ) of marine ice have also been investigated by several authors [Morgan, 1972; Oerter *et al.*, 1992; Souchez *et al.*, 1991; Tison *et al.*, 1993, 1998]. They show a narrow range of values, which was generally interpreted as the expression, in the frazil ice crystal, of near-equilibrium fractionation from seawater, often slightly modified by glacial meltwater [Morgan, 1972; Oerter *et al.*, 1992]. However, even in such a narrow range of values, the variations were significant enough to be used to demonstrate the transfer of marine ice along the ice shelf flow line and to interpret seasonal variations in landfast sea ice forming in front of the Hells Gate Ice Shelf (Terra Nova Bay, Antarctica) [Souchez *et al.*, 1991; Tison *et al.*, 1993, 1998].

In this paper we develop a conceptual model of genesis and consolidation of marine ice, integrating several of the main variables at play in this complex process, to simulate and analyze the  $\delta^{18}\text{O}$ /salinity relationship observed in a 45-m deep marine ice core from the Nansen Ice Shelf (Terra Nova Bay, Ross Sea, Antarctica). The extent of agreement with measured values, together with the sensitivity of the model's response to each of the variable settings, are discussed.

## 2. The $\delta^{18}\text{O}$ /Salinity Relationship From Field Data

Table 1 summarizes the main results from the high-resolution crystallographic, salinity, and isotopic analyses of a 45-m ice core retrieved from the Nansen Ice Shelf (Victoria Land, East Antarctica) at coordinates  $74^{\circ}50.9\text{S}$  and  $162^{\circ}51.3\text{E}$ , some 27.5 km from the front and 7.7 km downstream of the grounding line (Figure 1). The ice shelf covers  $1800\text{ km}^2$  [Frezzotti, 1992], and its thickness at the grounding line reaches a maximum of 600 to 700 m [Frezzotti *et al.*, 2000]. It can therefore be considered as a small- to medium-sized ice shelf. The grounding area upstream of the core location is heavily crevassed, and rifts several hundreds meters wide have opened, containing "islands" of continental ice chunks that have been frozen in place by the surrounding sea/marine ice (Figure 1). A full description of the core location, environmental setting, analytical techniques, and data profiles is given by Khazendar *et al.*, [2001]. The overall field configuration and the differences in some properties between this core and the marine ice sections of previous drilling

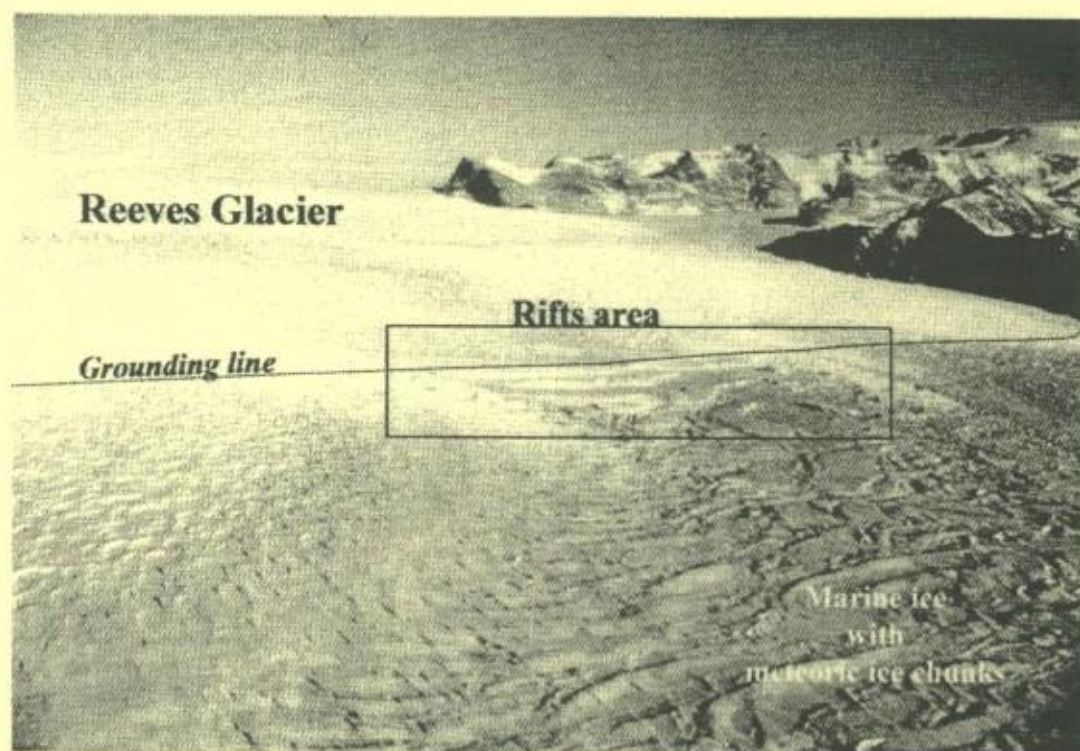


**Figure 1.** Oblique aerial photograph looking up the glacier showing the morphological features of the Nansen Ice Shelf (Terra Nova Bay, Antarctica) near its grounding line at the foot of the Reeves Glacier. The width of the photograph represents approximately 7.5 km on the surface. The framed area indicates the open rifts developing at the grounding line. The studied marine ice core was obtained further downstream.



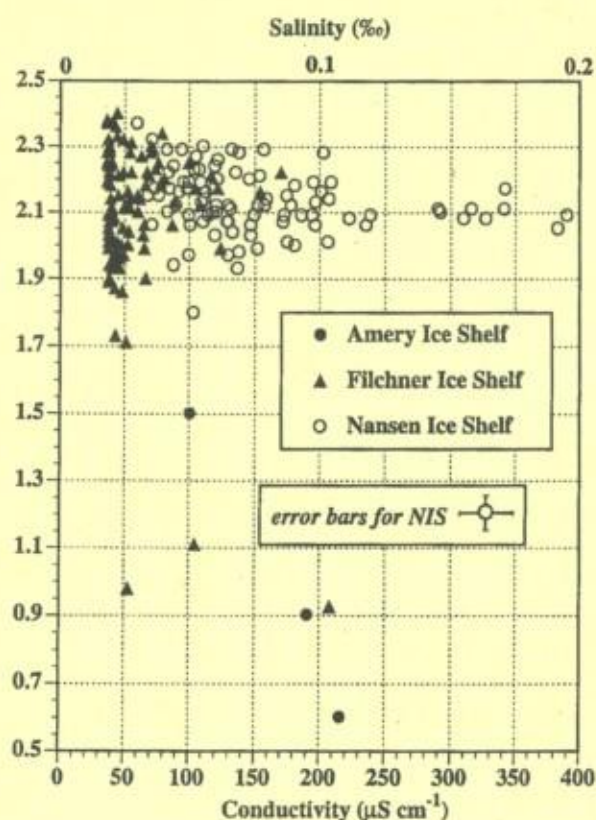


Figure 2. The  $\delta^{18}\text{O}$ /salinity relationship for 99 samples in the 45-m ice core from the Nansen Ice Shelf (dotted circles), Victoria Land, East Antarctica. Also plotted are the marine ice data from the B13 core (solid triangles, Filchner Ice Shelf, courtesy of H. Oerter and W. Graff, Alfred Wegener Institute) and the G1 core (black circles, Amery Ice Shelf, courtesy of V. Morgan, Australian Antarctic Division).

projects support the idea that this ice originates by the filling of basal crevasses or rifts occurring at the grounding line, thereby modifying the view of an exclusively melting regime in these zones of sub ice shelf cavities. In the present case, the surface coverage of the marine ice outcrop where the drilling has been performed (several tens to a hundred of meters in width) supports evolution from open rift filling.

Figure 2 shows the  $\delta^{18}\text{O}$ /salinity (conductivity) relationship for the 99 samples where both measurements were performed. The  $\delta^{18}\text{O}$  measurements were performed at the Laboratorio di Geochimica Isotopica di Trieste (Italy) with a Finnigan DeltaS mass spectrometer using the  $\text{H}_2\text{O}-\text{CO}_2$  equilibration technique. Accuracy of the  $\delta^{18}\text{O}$  measurements is  $\pm 0.05\text{‰}$ . The salinity values were obtained from conductivity measurements using a calibration curve based on 40 samples of known salinity (dilution of International Association for Physical Sciences of the Ocean seawater standards 10L-series to between 0.02 and 0.3‰). The prediction interval on the calibration curve, at a confidence level of 0.95, is  $\pm 0.01\text{‰}$ . Although the total range of values, both for  $\delta^{18}\text{O}$  and salinity, is narrow, it is still several times the error. As stated above, the salinity is 10 to 100 times lower than granular sea ice, and the positive  $\delta^{18}\text{O}$  values indicate ocean water freezing.

For the sake of comparison, marine ice data from drilling chips of the B13 ice core on the Filchner Ice Shelf (1 m

averaged [Oerter *et al.*, 1992]) and from the G1 ice core on the Amery Ice Shelf [Morgan, 1972] are plotted also in Figure 2. B13 samples and our data set have in common their  $\delta^{18}\text{O}$  range and a general trend of increasing  $\delta^{18}\text{O}$  variability with decreasing conductivity/salinity. However, our data set shows an offset of conductivity toward higher values. The three data points available for the Amery Ice Shelf (roughly located at the top, middle, and bottom of the marine ice section) show a concomitant decrease of the conductivity and increase of the  $\delta^{18}\text{O}$  with depth, interpreted by Morgan [1972] as the signature of a decreasing freezing rate with increasing ice thickness. It is our data set in Figure 2 that we aim to simulate in the marine ice formation model described below. We will then discuss the applicability of the modeled processes to the other marine ice cores, keeping in mind that these were sampled at greater depths and have a longer history (e.g., 400 to 500 years for B13) of consolidation and recrystallization [Eicken *et al.*, 1994].

### 3. Model Concept

In the following, by marine ice we strictly refer to ice that forms as a product of the accumulation of frazil crystals and the subsequent consolidation of the resulting crystal/seawater mixture. Such a definition excludes direct freezing at the underside of ice shelves such as at J9 ice core location on the Ross Ice Shelf [Zotikov *et al.*, 1980]. Predicting the salinity and isotopic composition of marine ice as defined here is complicated by the fact that these properties reflect the contribution of two main processes.

The first process, which we refer to as the “frazil ice phase”, consists of the formation of individual frazil ice crystals in the oceanic sub-ice shelf cavity, as a result of supercooling. The “parent” water of these crystals (ice shelf water – ISW) is a mixture of high salinity shelf water (HSSW) with glacial meltwater from the base of the ice shelf. As they are transported in the density-driven rising ISW plume, the crystals float upward due to their buoyancy and accumulate at the base of the ice shelf further downstream.

The second process, to which we refer to as the “consolidation phase”, is less well understood. As crystals rise under buoyancy and accumulate, they are surrounded by a water body that we call the “host” water. The proportion of water volume to the total volume of the ice/water mixture (“porosity”) varies depending on the local conditions. The porosity of loose frazil ice mixtures derived from laboratory experiments and field measurements, both for freshwater ice and sea ice, ranges between 40% and 67% [Andersson and Daly, 1992; Daly, 1984; White, 1991]. However, as suggested by Eicken *et al.* [1994], the deviatoric buoyancy stress exerted by the accumulation of tens of meters of loose frazil ice crystals could greatly increase the packing density. Similarly, the lateral compressive stresses induced by the converging flow of individual ice streams as they merge to form the ice shelf (or “reconstitute” it, around pinning points), as was observed at Hells Gate Ice Shelf [Tison *et al.*, 1997, 1998] and Nansen Ice Shelf [Khazendar *et al.*, 2001], can also quite significantly reduce the porosity of the marine ice that has already accumulated. Obviously, for accumulated ice crystals to be “squeezed” by lateral compression, its mechanical behavior should have developed solid-like characteristics so it is no longer merely an aggregate of loose crystals in



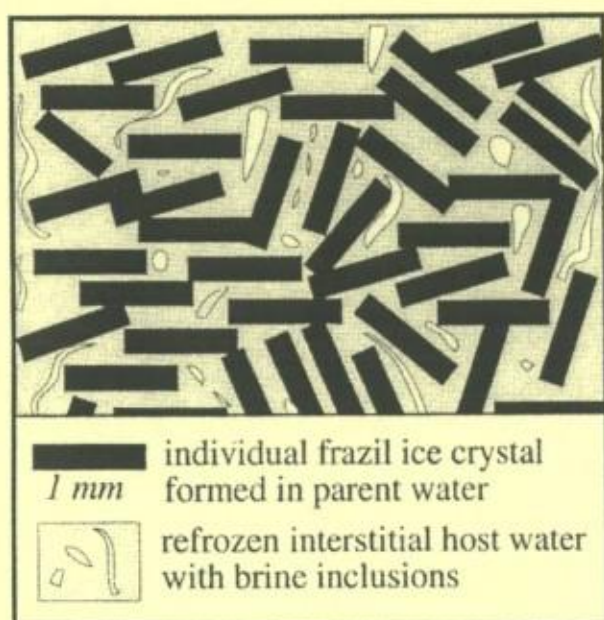


Figure 3. Sketch illustrating the model concept (see text for details).

suspension. Experiments by Martin and Kauffman [1981] demonstrate that this is indeed already the case for slush of 30 to 40% ice concentrations.

This packing process will contribute to the reduction of the bulk salinity (host water being expelled from the mixture) and is a first step in the consolidation process. Two major mechanisms could then be invoked to explain further consolidation of the marine ice body: (1) heat conduction across the ice shelf leading to the freezing of the interstitial water (either in a process of coarsening and joining of existing grains, or by the nucleation of new grains) and (2) local melt-regelation processes at contact points between grains in the compacting aggregate. The first mechanism has the potential to further reduce the impurity content of the ice by salt rejection and its subsequent diffusion toward the bulk seawater reservoir. The second mechanism will eventually alter the small-scale chemical properties of marine ice.

The discussion above shows a level of complexity difficult to simulate in the present state of knowledge. However, we believe that considerable insight can be gained into the processes at work by using a simplified approach where the final  $\delta^{18}\text{O}$ -salinity signal is modeled by combining the following two steps: (1) the formation of individual frazil crystals in the parent water and, (2) the freezing of interstitial host water (Figure 3). Different combinations of porosity and freezing rates could occur in nature. For example, a high freezing rate would be associated with high porosity at the top of the water column in an open rift where sufficient frazil discs had yet to accumulate and produce significant compaction. Lower in the water column, where accumulation is perhaps progressing faster than freezing, high compaction would produce a low-porosity slush subjected to a very slow freezing rate due to the insulating effect of overlying ice. The lateral stresses associated with converging ice streams or a closing rift would produce a situation where low porosity is combined with a large range of freezing rates depending on depth. We have taken this variety into account in our simulations by

considering each porosity level for a range of plausible freezing rates.

Before we discuss how the acquisition of the chemical properties is simulated in the model, we believe it is important to briefly summarize the current thinking on how chemical species are initially incorporated into the ice during freezing. As freezing progresses in a water reservoir, physico-chemical changes occur at the ice-water interface, which result in a differentiation of the chemical signals between ice and water. Depending on whether the chemical species under consideration is retained within microscopic inclusions in the host phase (e.g., sea-salt ions) or occurs as a true solid solution (e.g., water isotopes in ice) the differentiation process is called "segregation" or "fractionation", respectively. The proportion of heavy isotopes (or salts) incorporated from the liquid into the solid at the interface is constant for a given temperature. For the stable isotopes it is described by the equilibrium fractionation factor:

$$\alpha_{\text{eq}} = \frac{R_s}{R_l}, \quad (1)$$

where  $R_s$  and  $R_l$  are the isotopic ratios  $^{18}\text{O}/^{16}\text{O}$  (or D/H) in the solid and liquid phases at the interface, under thermodynamic equilibrium conditions. Comparing the isotopic compositions of different samples is done through the  $\delta$  scale, where the  $\delta$  value of a given sample is the relative difference between the  $R$  ratio in the sample and  $R$  ratio of a standard known as Vienna-standard mean ocean water (V-SMOW). Therefore

$$\delta^{18}\text{O} = \left( \frac{R_{\text{sample}}}{R_{\text{V-SMOW}}} - 1 \right) 1000 \text{‰} \quad (2)$$

For salinity, one similarly uses the equilibrium segregation factor:

$$k_{\text{eq}} = \frac{C_s}{C_l}, \quad (3)$$

where  $C_s$  and  $C_l$  are the impurity concentration in the solid and the liquid, respectively, at the interface.

As a result of this process, concentration on the liquid side of the interface differs from that of the bulk of the reservoir. Species transport therefore occurs, through molecular diffusion, convecto-diffusive fluxes and turbulent mixing in the melt. These processes are commonly integrated into a boundary layer concept, such that the concentration in the liquid takes on the reservoir value (in the case of a semi-infinite reservoir, e.g., for seawater) at a finite distance  $z_M$  from the interface. Within this boundary layer, transport occurs by diffusion processes only. Depending on the freezing rate, the gradient in the boundary layer will vary and therefore so will the concentration in the liquid at the interface. As a result,  $\alpha_{\text{eff}}$ , the effective (apparent) fractionation factor (or  $k_{\text{eff}}$ , the effective segregation factor) will differ from the equilibrium fractionation factor  $\alpha_{\text{eq}}$  ( $k_{\text{eq}}$ ) that would be observed either in the case of near-zero growth rate or during forced convection ( $z_M=0$ ).

For a given freezing rate, in the case of a semi-infinite reservoir, after a short "initial transient" the concentration in the ice remains constant since a steady state regime arises, where the flux of a given species into the ice is exactly compensated by the one at the base of the boundary layer. The effective fractionation factor for that steady state is given by



Burton et al. [1953]:

$$\alpha_{\text{eff}} = \frac{\alpha_{\text{eq}}}{\alpha_{\text{eq}} - (\alpha_{\text{eq}} - 1) e^{-\frac{z_M v}{D}}}, \quad (4)$$

where  $v$  is the growth rate and  $D$  is the diffusion coefficient. A similar relationship is valid for the effective segregation factor, with  $k_{\text{eff}}$  and  $k_{\text{eq}}$  instead of  $\alpha_{\text{eff}}$  and  $\alpha_{\text{eq}}$  in (4). The initial transient marks the transition from the equilibrium fractionation recorded in the initial ice increment toward the steady state value.

Souchez et al. [1987, 1988] used a box diffusion model to apply the boundary layer concept to isotopic fractionation in sea ice. In their approach the simulation of the stable-isotope distribution in the ice was performed in two steps: (1) freezing of an ice thickness during a time increment depending on the freezing rate, with associated fractionation, and (2) diffusion in the boundary layer and homogenization in the bulk of the reservoir during the appropriate time lapse. In nature, freezing and diffusion are simultaneous. Using an axis moving with the ice front, both processes can be described by the same partial differential equation:

$$\frac{\partial c}{\partial t} = D \frac{\partial^2 c}{\partial x^2} + V \frac{\partial c}{\partial x}, \quad (5)$$

(where  $c$  is the concentration,  $x$  is the space coordinate measured normal to the ice/water interface and  $V$  is the velocity of the ice front) applying the appropriate boundary conditions and using the equilibrium fractionation (1) or segregation (3) coefficients to calculate the concentrations on both sides of the interface. The model used here (see below) solves (5) numerically using the Crank-Nicolson method. At each time step, the solution of the resulting set of linear equations is obtained by Gaussian elimination using a simple algorithm for tridiagonal systems. These adjustments reduce the execution time considerably and improve the precision of the results.

## 4. Procedure and Results

### 4.1. Acquisition of the chemical properties in the frazil ice phase

It is reasonable to assume, in the case of marine or granular sea ice, that the salinity signal of single ice crystals is negligible [see, e.g., Eicken, 1998; Tison et al., 1993]. Therefore our main concern in this section will be to estimate the isotopic composition of individual frazil ice crystals forming in an ice shelf water plume, a task complicated by the scarcity of relevant field data. Kipfstuhl [1991] measured effective fractionation coefficients  $\epsilon_{\text{eff}}$  (between 2.2 and 2.3‰) close to the equilibrium value in large ice platelets found under coastal sea ice. Eicken [1998], using Burton's [1953] equation (4), infers that the frazil ice crystals are likely to exhibit  $\delta^{18}\text{O}$  values close to seawater composition, given the plausible growth velocities. However, to unequivocally associate an  $\epsilon_{\text{eff}}$  to given growth rate and  $z_M$  values using the boundary layer model in the case of a semi-infinite reservoir, one must be sure to be away from the influence of the initial transient, that is, that Burton's steady state equation (4) strictly applies. This condition is not likely to be fulfilled for single crystals, which

are only of the order of millimeters in size. Also, we have to be certain that the  $z_M$  values commonly used in the case of a growing ice front in a water reservoir apply to single crystals in suspension in a liquid phase. For these reasons, we have opted to calculate the isotopic signal of our single frazil ice crystals by using the model described in the previous section, with high resolution in the 0 to 1-mm range. In order to run the model we need to assess the values of the following inputs: isotopic value of the parent water, growth rate, boundary layer thickness, and equilibrium fractionation factor for  $\delta^{18}\text{O}$  ( $\alpha_{\text{eq}}$ ).

**4.1.1. Isotopic value of the parent water.** Individual frazil ice crystals form in the rising ISW branch of the sub-ice shelf oceanic circulation. Therefore we use a mean  $\delta^{18}\text{O}$  value of -0.61‰, based on ISW data obtained in the Ross Sea [Jacobs et al., 1985, Table 1, p. 62].

**4.1.2. Growth rate.** The question of the degree of supercooling required to produce frazil ice (at a certain growth rate) is closely linked to the not yet well-understood problem of initial nucleation. Noting that frazil production in rivers is associated with weak supercooling levels of 0.01° to 0.1°C, Martin [1981] concludes that heterogeneous, rather than spontaneous, frazil nucleation is most likely to occur in nature. Jenkins and Bombosch [1995] discuss possible seeding mechanisms for frazil production beneath ice shelves and suggest, for example, that zones of basal crevassing (which is the case of the NIS core location) would be favorable sources of seed crystals. Analysis and observations of water beneath an ice shelf suggest that supercooling is unlikely to exceed 0.05°C [Nicholls and Jenkins, 1993]. These investigations provide possible upper limits on the supercooling levels that could be used in the current simulations of the NIS ice. Therefore, having experimented with supercooling levels up to 0.05°C, the representative results corresponding to the two supercooling values of 0.007° and 0.018°C (associated, respectively, with freezing rates of  $10^{-6}$  and  $2.7 \times 10^{-6}$  m s $^{-1}$  [Hobbs, 1974, p. 584]) will be presented and discussed here. Furthermore, at such levels of supercooling, according to Hobbs [1974, p. 582] and Daly [1984], the resulting frazil would be plain disc crystals without protuberances or dendrites, thus corresponding best to the assumption adopted in these simulations of frazil crystals growing through the advancement of a stable planar interface.

**4.1.3. Boundary layer thickness.** In their discussion of the influence of the crystal size on the heat and salt transfer around a single frazil crystal, Jenkins and Bombosch [1995, pp. 6973-6974] follow the analysis of Daly [1984] and assume that crystal growth occurs preferentially along the  $a$  axes. This assumption implies that heat and mass transfer mainly take place at the edge of the discs. In that case, and since according to these authors the typical disc thickness (of the order of  $10^{-2}$  mm) is much smaller than the dissipation length scale in the plume, they suggest that, to a first approximation, the crystals can be treated as if they move with the fluid, and heat and salt (and also stable isotopic) transfer occur only by molecular diffusion. Since, following Daly [1984], the appropriate length scale for transfer at disc edges is the half thickness of the disc, we then use a  $z_M$  of  $5 \times 10^{-3}$  mm in the context of a boundary layer model, if, for example, we adhere to crystal thickness of  $10^{-2}$  mm. Sensitivity tests will, however, be performed for  $z_M$  values between 1 and  $5 \times 10^{-3}$  mm.

**4.1.4. Equilibrium fractionation factor for  $\delta^{18}\text{O}$  ( $\alpha_{\text{eq}}$ ).** This parameter has been derived from extrapolation of laboratory



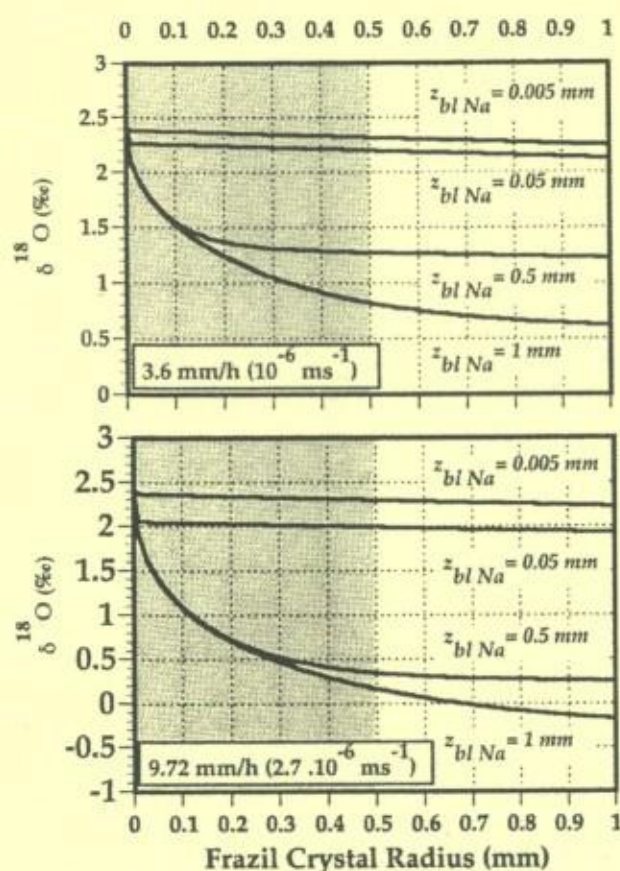


**Figure 4.** Plot of  $\delta^{18}\text{O}$  (‰) as a function of the radius (mm) of a single frazil crystal disc from model simulations for growth rates of  $2.7 \times 10^{-6}$  and  $10^{-6} \text{ m s}^{-1}$  and a range of boundary layer thickness ( $z_{bl}$ ) between 1 and  $5 \times 10^{-3} \text{ mm}$  ( $\alpha_{eq} = 1.003$ ). The shaded area represents a 0.5 mm frazil ice disc radius.

measurements of  $\alpha_{eff}$  to zero growth rates by three different authors. The most commonly used value ( $1.003 \pm 0.0001$ ) is also the oldest [O'Neil, 1968]. It is, however, very close to the  $1.00291 \pm 0.00003$  value determined more recently by Lehmann and Siegenthaler [1991]. Beck and Münich [1988] derived a slightly lower value of 1.00287.

Figure 4 shows the results of the model simulations for growth rates of  $2.7 \times 10^{-6}$  and  $10^{-6} \text{ m s}^{-1}$  and a range of  $z_{bl}$  values, between 1 and  $5 \times 10^{-3} \text{ mm}$  ( $\alpha_{eq} = 1.003$ ). Taking the minimum 1 mm crystal size from our field data (Table 1) as an indication of the size of accreting single frazil ice crystals, the shaded areas in Figure 4 represent the disc radius. Table 2 summarizes the bulk isotopic signal of a frazil ice disc 1 mm in diameter, as a function of freezing rate and boundary layer thickness, calculated from integration of the data in Figure 4, for a disc geometry. It is clear from Figure 4 and Table 2 that (1) the initial transient has to be considered in assessing the  $\delta^{18}\text{O}$  signal of the crystal, and (2) the role of the boundary layer thickness ( $z_{bl}$ ) is crucial. If we consider, following Jenkins and Bombosch [1995], a disc thickness of  $10^{-2} \text{ mm}$  ( $z_{bl} = 5 \times 10^{-3} \text{ mm}$ ), then the  $\delta^{18}\text{O}$  values are very close to equilibrium fractionation, for both freezing rates considered. If, on the other hand, we consider a shape ratio that is close to unity ( $z_{bl} = 0.5$  to  $1 \text{ mm}$ ), the effective fractionation is reduced by a factor of 2 to 4, depending on the freezing rate considered.

#### 4.2. Acquisition of the Chemical Properties in the Consolidation Phase

Based on the review of earlier papers [Burton et al., 1953; Cox and Weeks, 1975; Garandet et al., 1994; Nakawo and Sinha, 1981; Souchez et al., 1987, 1988], Eicken [1998] provides a thorough discussion of fractionation and segregation processes in sea ice. As stated above, models of chemical segregation were developed for the case of a solid solution with a planar liquid-solid interface [Burton et al., 1953]. But this is not the case for seawater freezing where a planar interface becomes unstable because constitutional supercooling takes place as salts are rejected from the growing ice. Instead, a cellular or dendritic interface with intracrystalline and intercrystalline brine layers develops [Eicken, 1998, Fig. 13; Weeks and Ackley, 1986]. However following previous studies on sea ice, Eicken [1998] suggests that the stagnant boundary layer diffusion model developed for a planar interface [Burton et al., 1953; Garandet et al., 1994] can also be used to adequately simulate both the  $\delta^{18}\text{O}$  fractionation and the initial salinity segregation during columnar-congelation sea ice growth (progression of a freezing front in a body of seawater).

In the case of granular sea ice (the closest textural equivalent to marine ice), there is an additional complication since, instead of resulting from the simple progression of a freezing front in a liquid reservoir, it forms as a result of individual crystals joining and coarsening in a liquid. Since the porosity of unconsolidated frazil in the absence of stress is higher than 50% (see above), Eicken [1998, section 8.1] surmises (assuming that negligible fractionation occurs during the growth of individual frazil ice crystals, see above) that the bulk isotopic signal of granular sea ice forming from frazil is actually generated during consolidation of the slush. The developments in the previous section suggest that it might not be the case for marine ice, where porosities can be much lower and where the higher isotopic fractionation characterizing the initial transient is likely to affect the bulk crystal's signature.

Since individual frazil ice crystals are, to a first reasonable approximation, devoid of salt inclusions, all the salinity signal of granular sea ice will come exclusively from the consolidation process of the interstitial host water. Considering that in the Weddell Sea data set presented by Eicken [1998] the characteristic patterns in the  $\delta^{18}\text{O}$  profile from columnar congelation ice are also displayed in cores consisting predominantly of granular ice, and that frazil embedded in congelation ice often does not exhibit any significant deviation from the adjacent layers, Eicken considers that the boundary layer concept should also be valid, at least to a first approximation, for granular sea ice. We will use this assumption for granular marine ice, and therefore calculate the

**Table 2.** Mean  $\delta^{18}\text{O}$  Values for Frazil Ice Discs 1 mm in Diameter, as a Function of Growth Rate and Boundary Layer Thickness<sup>a</sup>

$z_{bl}$ / Growth Rate	$10^{-6} \text{ m s}^{-1}$	$2.7 \times 10^{-6} \text{ m s}^{-1}$
0.005 mm	2.34	2.32
0.05 mm	2.22	2.01
0.5 mm	1.33	0.54
1 mm	1.04	0.46

<sup>a</sup> Values in ‰. The  $\delta^{18}\text{O}$  of parent water is taken as  $-0.6\text{‰}$ .



isotopic and salinity signature of the frozen interstitial host water using (4) and considering that we are dealing with a continuous freezing process in a semi-infinite reservoir, where the profile of the chemical species results from a succession of steady state values.

Table 3 summarizes the range of available values that we could use as inputs in (4). Most of these variables show a large range of values.

**4.2.1. Isotopic value of the host water.** Two main water masses are likely to act as host water for the individual frazil ice crystals accreting below the ice shelf; ice shelf water and high salinity shelf water. We will use mean values of respectively  $-0.61\text{‰}$  and  $-0.42\text{‰}$  given for the Ross Sea by *Jacobs et al.* [1985].

**4.2.2. Porosity.** As discussed above, the porosity of the unconsolidated marine ice will depend on the degree of compaction under the deviatoric buoyancy stress and lateral compression. It can thus vary greatly between 40 and 67% and 5%. This latter value is indeed a limiting value since, below it, it is generally considered that the brine inclusions are isolated from each other (see "law of fives" by *Cox and Weeks* [1975]) [*Golden et al.*, 1998; *Weeks and Ackley*, 1986]. Below that limit, freezing would thus occur in a closed system.

**4.2.3. Equilibrium segregation/fractionation coefficient (factor).** A large range (nearly 3 orders of magnitude) exists for the value of the equilibrium segregation coefficient (or factor). This results from the fact that the concept of "equilibrium" segregation, as used in the boundary layer model, is strictly valid only in the case of a planar interface. However, as the concentration in the liquid at the ice/water interface increases, salt inclusions will be located (1) in the crystal lattice, (2) at grain boundaries (intercrystalline brine inclusions), and (3) in intracrystalline brine inclusions between ice platelets resulting from the development of a non planar cellular or dendritic interface. This latter process results in the typical "skeletal layer" described in the bottommost layers of sea ice [*Weeks and Ackley*, 1986; *Eicken*, 1998, Fig. 13].

*Gross et al.* [1977] tested the concentration dependency of the equilibrium segregation factor for  $\text{Na}^{36}\text{Cl}$  solutions between  $10^{-6}$  and  $10^{-1}$  M ( $6 \times 10^{-4}$  to 6‰) in forced convection (Table 3). Although the growth rate for all experiments was about  $10^{-4}$  cm s $^{-1}$  (i.e., in the range of the high freezing rates of *Cox and Weeks* [1975]), forced convection ensured the non dependence of  $k_{\text{eff}}$  on the growth rate, that is,  $k_{\text{eff}} = k^*_{\text{eq}}$  (an asterisk denotes an experimentally derived value). For initial concentrations between  $10^{-6}$  and  $10^{-3}$  M, the experiments yielded a mean  $k^*_{\text{eq}}$  of  $2.78 \times 10^{-3}$ , with no detectable dependency on the concentration [*Gross et al.*, 1977, Fig. 10]. However, between  $10^{-2}$  and  $10^{-1}$  M (the upper range of the set of experiments), considerable changes occur, with  $k^*_{\text{eq}}$  increasing to  $4.7 \times 10^{-3}$ . *Gross et al.* [1977] attribute these changes to the effect of solubility limit being approached and the occurrence of "interface breakdown." Concentrations in the ice at that stage are of the order of 200  $\mu\text{M}$ , a value reasonably close, given the measurement errors in both cases, to the solubility limit of 300  $\mu\text{M}$  Cl $^{-}$  observed by *Moore et al.* [1994] on B13 samples. The increased value of  $k^*_{\text{eq}}$  observed by *Gross et al.* [1977] for bulk solution saltiness of a few ‰ likely corresponds to the transition from saturation of the crystal lattice to inclusions at crystal boundaries and, eventually, intracrystalline cells. *Lofgren and Weeks* [1969] recorded transition between planar and non planar interfaces

during freezing of 1‰ (unstirred) and 3‰ (stirred) NaCl solutions. More recently, *Nagashima and Furukawa* [1997] recorded transitions during the freezing of 3‰ NaCl solutions in a thin cell (unstirred). All these observations corroborate calculations from *Tiller* [1962] and *Weeks and Ackley* [1986], suggesting that a non planar interface with steep wall planar grooves will be stable for reservoir salinity of a few ‰, thus increasing the value of  $k^*_{\text{eq}}$ .

Because the interface is no longer planar, the value of  $k^*_{\text{eq}}$  will depend on the detailed morphology of the interface, itself a function of the interface water salinity ( $C_i$ ), that is, of the growth rate, all other things (bulk reservoir salinity, boundary layer thickness) being equal. This has been demonstrated experimentally by *Cox and Weeks* [1975] who determined "equilibrium" segregation factors for NaCl solutions at 34.7‰ salinity (Table 3) by extrapolating laboratory measurements of  $k_{\text{eff}}$  to zero-growth rate ( $k_{\text{eff}}$  thus equals  $k_{\text{eq}}$ ). For growth rates generally higher than those encountered in natural sea ice,  $k^*_{\text{eq}} = 0.26$  is obtained. For typical sea ice freezing rates, the experimental data produce  $k^*_{\text{eq}} = 0.17$ , to be compared to  $k^*_{\text{eq}} = 0.12$  extrapolated from field data by *Nakawo and Sinha* [1981]. Finally, for even lower growth rates,  $k^*_{\text{eq}}$  still decreases. We suggest that this dependency of the observed  $k^*_{\text{eq}}$  on the range of experimental velocities used is the expression of the impact of the growth rate dependent interface water salinity on the ice-water interface micromorphology.

Field observations from exceptionally thick sea ice (10 to 12 m [see *Cherepanov*, 1966]) and columnar/congelation ice forming at the bottom of the Ross Ice Shelf (site J9) at 416 m depth [*Zotikov et al.*, 1980], confirm this trend of decreasing  $k^*_{\text{eq}}$  with decreasing growth rate at similar reservoir salinity (Table 3). Indeed, applying *Burton's* [1953] equation (4) to the  $k_{\text{eff}}$  value of 0.071 observed at the bottom of 10 to 12-m-thick, old Arctic sea ice (with  $z_{\text{bl}} = 0.29$  cm,  $v = 1.5 \times 10^{-6}$  cm s $^{-1}$  and  $D = 6.9 \times 10^{-6}$  cm $^2$  s $^{-1}$ ) gives  $k_{\text{eq}} = 0.067$ . Similarly, using  $k_{\text{eff}} = 0.068$  and  $v = 5 \times 10^{-6}$  cm s $^{-1}$  for J9 gives  $k_{\text{eq}} = 0.0678$ . It should be noted, however, that these  $k_{\text{eq}}$  values could be underestimated since the observed  $k_{\text{eff}}$  values include possible desalination effects. However, the latter are probably limited, particularly in the case of J9, where flushing by meltwater is precluded and where fluctuations of the temperature gradient, an essential driving force for the other desalination processes, is much smaller than for sea ice.

The close agreement between  $k_{\text{eff}}$  and  $k_{\text{eq}}$  suggests that for such low growth rates,  $C_i \cong C_o$  (the bulk reservoir salinity)  $\cong 34.6\text{‰}$  (the mean seawater salinity used in the calculation above), which provides us with the lowest bulk  $k_{\text{eq}}$  value at this salinity level of a typical ocean water reservoir freezing with a non planar cellular interface.

**4.2.4. Boundary layer thickness.** Another parameter to consider is the choice of boundary layer values ( $z_{\text{bl}}$ ) for both species. In his approach for sea ice, *Eicken* [1998] derives a lower value for  $z_{\text{bl}}^{18\text{O}}$  (1.3 mm) than for  $z_{\text{bl}}^{\text{NaCl}}$  (2.9 mm). This is physically sound since oxygen isotopes are mainly incorporated at the tip of the ice lamellae whilst NaCl is mainly incorporated in the grooves of the skeletal layer which are more sheltered from mechanical convection in the reservoir. The layer where transport occurs by diffusion only is thus likely to be thicker in the NaCl case. This geometrical configuration is, however, only strictly valid for columnar sea ice.



**Table 3.** Literature Survey of the Parameter Values for Use in *Burton's* [1953] Equation (4)

Variable	Salinity Signal			Isotopic Signal		
	Values	Remarks	Sources	Values	Remarks	Sources
Host water	34.535‰	mean ISW from Ross Sea	<i>Jacobs et al.</i> , [1985]	-0.61‰	mean ISW from Ross Sea	<i>Jacobs et al.</i> , [1985]
	34.84‰	mean HSSW from Ross Sea	<i>Jacobs et al.</i> , [1985]	-0.42‰	mean HSSW from Ross Sea	<i>Jacobs et al.</i> , [1985]
Porosity	40 to 67%	frazil in rivers and experiments indirect from sea ice salinity	<i>Andersson and Daly</i> , [1992], <i>Eicken</i> , [1998], <i>Tison et al.</i> , [1993], <i>White</i> , [1991]	-	-	-
	below 40%	effect of deviatoric buoyancy stress effect of lateral compression	<i>Eicken et al.</i> , [1994], <i>Khazendar et al.</i> , [2001], <i>Tison et al.</i> , [1997, 1998]	-	-	-
"Equilibrium" segregation / fractionation coefficient (factor)	$k_{eq}^* = 0.26$	$^{22}\text{NaCl}$ experiments and high freezing rates	<i>Cox and Weeks</i> , [1975]	$\alpha_{eq} = 1.0030$		<i>O'Neil</i> , [1968]
	$k_{eq}^* = 0.17$	$^{22}\text{NaCl}$ experiments and natural sea ice freezing rates	<i>Cox and Weeks</i> , [1975]	$\alpha_{eq} = 1.00287$		<i>Beck and Münnich</i> , [1988]
	$k_{eq}^* = 0.12$	Arctic first year sea ice data set	<i>Nakawo and Sinha</i> , [1981]	$\alpha_{eq} = 1.00291$		<i>Lehmann and Siegenthaler</i> , [1991]
	$k_{eq}^* = 0.068$	congelation/columnar ice at the bottom of J9 ice core (Ross Ice Shelf, 416 m depth)	<i>Zotikov et al.</i> , [1980]			
	$k_{eq}^* = 0.067$	bottom of drifting Arctic Station SP6 (10 to 12 m thick)	<i>Cherepanov</i> , [1966]			
	$k_{eq}^* = 0.04$	Antarctic first year sea ice	<i>Souchez et al.</i> , [1988]			
	$k_{eq}^* = 0.0047$	forced convection experiments on medium salinity chloride solutions ( $10^{-1} M$ )	<i>Gross et al.</i> , [1977]	-	-	-
	$k_{eq}^* = 0.0028$	forced convection experiments on low salinity chloride solutions ( $10^{-6}$ to $10^{-2} M$ )	<i>Gross et al.</i> , [1977]			
Boundary layer thickness (cm)	$z_{bbl} = 0.29$	-	<i>Eicken</i> , [1998]	$z_{bl} \delta^{18}\text{O} = 0.13$		<i>Eicken</i> , [1998]
	$z_{bbl} = 0.09$	-	<i>Souchez et al.</i> , [1988]	$z_{bl} \delta^{18}\text{O} = 0.09$		<i>Souchez et al.</i> , [1988]
Diffusion coefficient ( $\text{m}^2 \text{s}^{-1}$ )	$D_{\text{NaCl}} = 6.9 \times 10^{-10}$	-	<i>Eicken</i> , [1998]	$D_{\delta^{18}\text{O}} = 1.2 \cdot 10^{-9}$		<i>Eicken</i> , [1998]
Freezing rate	variable	based on heat conduction across the ice shelf and modulated by the porosity	-	variable	based on heat conduction across the ice shelf and modulated by the porosity	-



### 4.3. Derivation of Bulk Chemical Properties and Sensitivity Tests

As stated above, we will use the approximation that the bulk signal we measure in the marine ice core results from the combination of the signal from a single frazil crystal with the signal in the frozen interstitial host water. The mixing ratio between the two signals will be the chosen porosity of the medium at the time of consolidation. Representative results of sensitivity tests of the model are shown in Figure 5. All graphs are designed along the same lines. Field data from the NIS core are shown as dotted open circles in the foreground. Each curve with a gray scale symbol represents the results of one simulation run for a given porosity (mixing ratio) of the medium. The gray scale of each symbol is based on the freezing rate scale from  $10^{-7}$  cm s $^{-1}$  (white) to  $10^{-3}$  cm s $^{-1}$  (black). Parameter settings are indicated on the top of each graph.

In Figures 5a to 5c we focus on the effect of the segregation factor for Na ( $k^*_{eqNa}$ );  $z_{bNa}$ ,  $z_{b\delta^{18}O}$ ,  $\alpha_{eq}$  (1.003), the  $\delta^{18}O$  value of individual frazil ice crystals ( $\delta^{18}O_{frazil}$ ) and of the host water are therefore kept constant. Eicken [1998] values for  $D_{Na}$ ,  $D_{\delta^{18}O}$ ,  $z_{bNa}$ , and  $z_{b\delta^{18}O}$  were chosen, and we selected a mean value of 2.22‰ for  $\delta^{18}O_{frazil}$ . This corresponds to the lowest growth rate and a  $z_M$  of 0.05 mm in Table 2. We thus favor at this stage a disc thickness-to-length ratio of 1/10 on the basis of visual observations [Arakawa and Higuchi, 1954; Weeks and Ackley, 1986, Fig. 8 and 9]. The host water was taken as the mean Ross Sea ISW value (Table 3). Figures 5d and 5e use  $\delta^{18}O_{frazil}$ , host water and  $\alpha_{eq}$  values as before, with a  $k^*_{eqNa}$  of 0.005, and test the sensitivity of the results to changes in boundary layer thickness for both Na and  $\delta^{18}O$ . In Figures 5f and 5g, the  $\delta^{18}O_{frazil}$  is varied to evaluate the consequence of choosing a fractionation factor closer to equilibrium (as would occur for thinner discs and/or smaller  $z_M$ ), or further away from equilibrium (as would occur for faster growth rates and/or larger  $z_M$ ). Finally, Figure 5h shows the impact of lowering the  $\delta^{18}O$  value of the host water to the mean HSSW value from the Ross Sea data.

## 5. Discussion

### 5.1. Model Simulation of the NIS Data Set

In a first attempt we used the set of parameters applied by Eicken [1998] for sea ice growth in the Weddell Sea (Figure 5a). There is obviously a total discrepancy between the distribution of the field data and the simulation results as far as salinity is concerned, even for the lowest porosity value of 5%. Simple compaction down to the connectivity threshold will thus not satisfactorily explain the observed salinity values, even at the lowest freezing rates. We then have to look for alternative paths (other than porosity) to decrease the simulated salinity of the bulk marine ice. As discussed previously [Tison et al., 1993], we are left with only two main options: either a considerable dilution of the host water, or the choice of a much lower "equilibrium" segregation factor for salts ( $k^*_{eq}$ ). Considering the data from Figure 5a, dilution factors between 2 (for the lowest porosity and at the lowest freezing rates) and 15 (for porosity of 50% and at the lowest freezing rates) are necessary to shift the simulation results close to the saltiest

records of the field data. Running the model choosing a host water dilution factor of 2 by glacial melt of meteoric origin ( $S = 17.26\text{‰}$  and  $\delta^{18}O = -10.31\text{‰}$ ) gives  $\{S; \delta^{18}O\}$  values ranging between  $\{0.863; 1.59\}$  at  $3.6 \times 10^{-4}$  cm s $^{-1}$  and  $\{0.115; 1.74\}$  at  $2.9 \times 10^{-6}$  cm s $^{-1}$  for a porosity of 5%. Although this indeed brings the salinity value to the level of the highest observed values for low freezing rates, it also decreases the isotopic signal below the lowest observed value. Clearly, as underlined by Tison et al. [1993], this dilution process is only conceivable if a peculiar environment exists that would protect the host water from mixing with seawater existing below the loose frazil ice accumulation, and if the melting ice that contributes to the dilution process already has a marine isotopic signature. Such a situation could, for example, exist in the case of loose marine ice accumulations in rifts or inverted depressions at the ice shelf's base, close to the ice shelf front, where melting resulting from tidal forcing of warm summer surface waters under the ice shelf is active [Tison et al., 1998].

In Figures 5b and 5c,  $k^*_{eqNa}$  has been reduced to 0.068 (the lowest observed value in natural columnar ice grown from seawater) and 0.005 (the equilibrium fractionation observed at "interface breakdown" for a 6‰ salinity in the Gross et al. [1977] experiments), respectively. Only in the latter case do the simulations cover the range of salinity observed in the NIS marine ice samples, for porosity lower than 60-70%. These results suggest that we must find the origin of the discrepancy in fractionation between slowly growing columnar ice (e.g., J9) and our marine ice in the morphology of the freezing interface that penetrates the unconsolidated frazil ice slush. Although we do not know the morphology of the freezing interface in the case of marine ice consolidation, we know that the segregation process is limited to intercrystalline brine inclusions, since no intracrystalline substructure is observed in any of the deep marine ice cores described in the literature. Therefore it is plausible that the processes at work require equilibrium fractionation values similar to the lowest one measured at saturation of crystal lattice and interface breakdown by Gross et al. [1977], when approximated by a boundary layer modeling concept.

Figure 6 proposes a schematic depiction of how processes that combine melting under compaction and refreezing under heat conduction might work. Starting at a stage where the aggregate of loose crystals begins to develop solid-like characteristics (approximately 30-40% porosity, see above) under lateral compression and deviatoric buoyancy stress, neighboring grains (solid line) will partially melt at contact points and feed fresh meltwater into the interstitial host water. This will (1) reduce the porosity (broken lines) and (2) lower the salinity and enrich the  $\delta^{18}O$  of the interstitial water. Subsequent freezing of the host water under heat conduction will enrich the ice phase in  $\delta^{18}O$ , impoverish the remaining liquid in  $\delta^{18}O$ , increase its salinity and drive salt and isotopic diffusion through the interconnected interstitial water network. The process is likely to continue until the 5% porosity threshold is reached and closed system freezing occurs. The resulting texture is in accordance with that observed, lacking the intracrystalline cellular inclusions, and salt impurities remain located at grain boundaries once the ice lattice is saturated.

Since no intracrystalline substructure is developed in marine ice, one might wonder if different boundary layer thicknesses



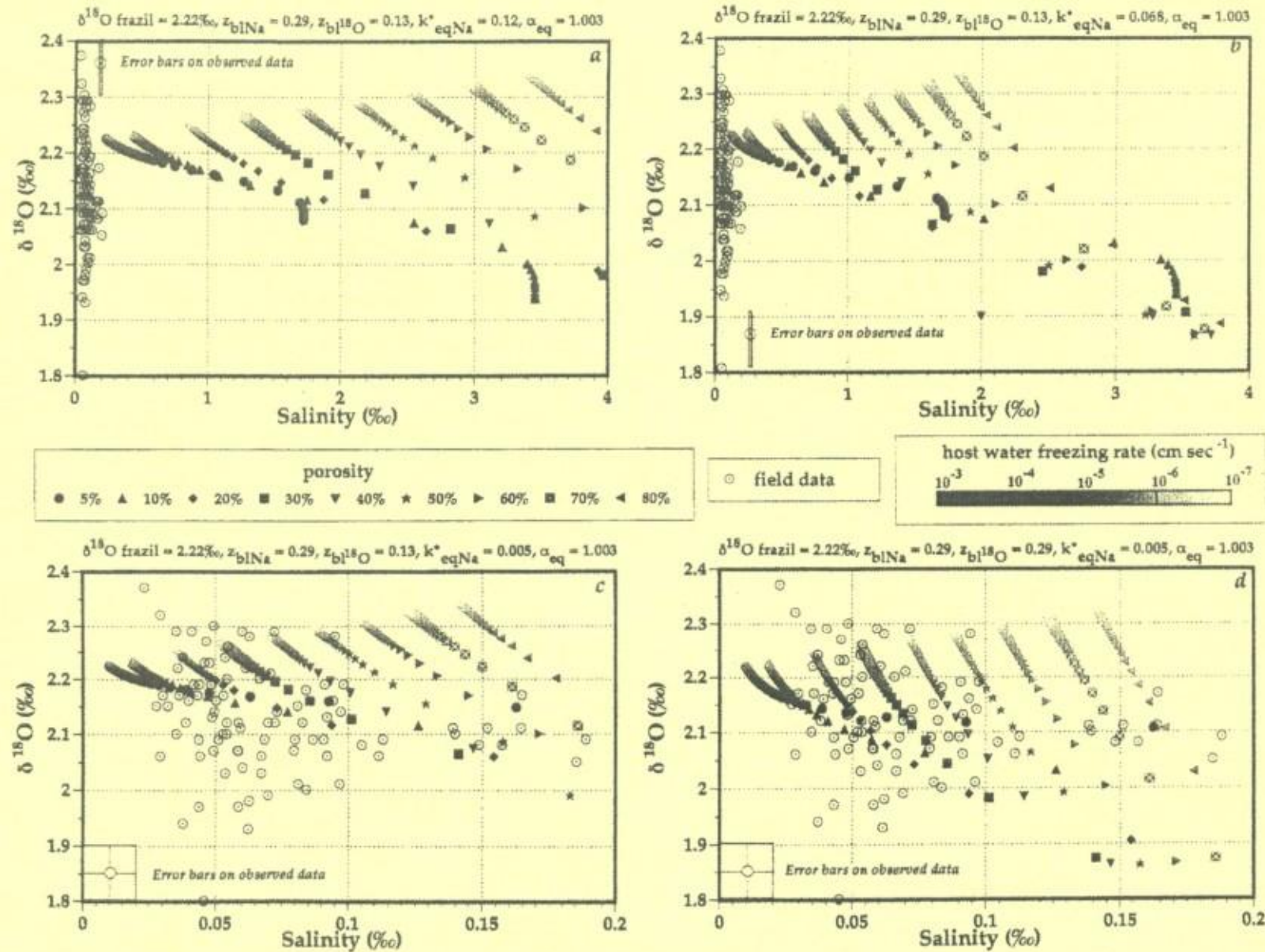


**Figure 5.** Results of the simulations for different sets of parameters, as described at the top of each graph. Field data are shown as dotted open circles. Each gray scale symbol represents the results of one simulation run for a given porosity of the medium. Porosity is defined as the proportion of water volume to the total volume of the ice/water mixture. The gray scale of each symbol is calibrated to the freezing rate. Figure 5a to d.



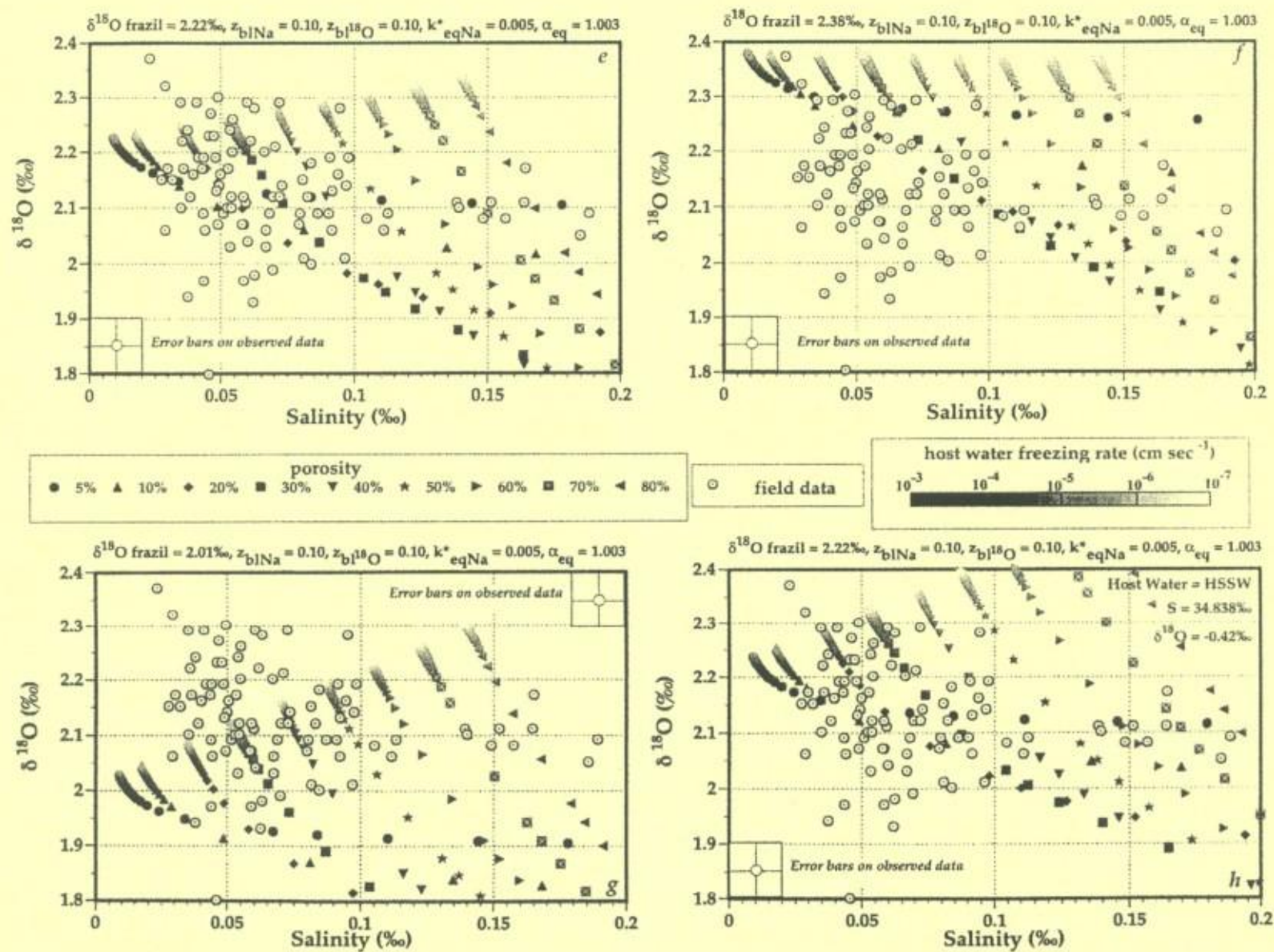
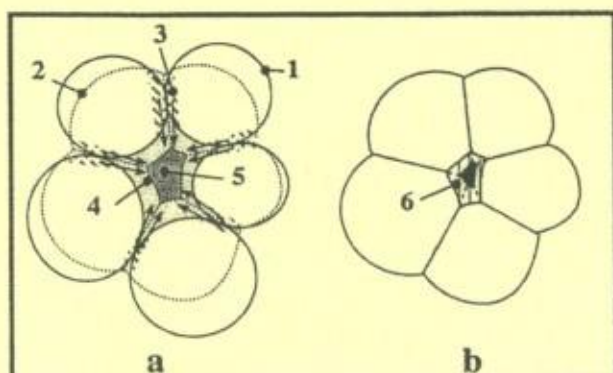


Figure 5. Continued





**Figure 6.** (a) Simplified sketch illustrating the assumed process of porosity reduction in a compressed frazil ice crystals aggregate, and (b) the further consolidation by freezing of the diluted interstitial water. The latter process will result in salt diffusion toward the bulk of the reservoir as long as the porosity threshold (5%) is not attained. The whole process prevents the development of intracrystalline substructures. Numerals refer to 1, crystal before compaction; 2, crystal after compaction; 3, meltwater from pressure-melting; 4, interstitial water space before compaction; 5, interstitial water space after compaction; 6, refrozen interstitial meltwater.

still apply to salinity and  $\delta^{18}\text{O}$ . Figure 5d is identical to Figure 5c, with the exception that the  $z_{\text{hNa}}$  and  $z_{\text{hO}}$  values are both set to 2.9 mm. Results from the model now better cover the range of the observed  $\delta^{18}\text{O}$  values, taking error bars into account. A major uncertainty nevertheless persists in the actual value of  $z_{\text{h}}$ . However, Figure 5e shows that changing the value of  $z_{\text{h}}$  to 1 mm does not alter the location of the simulation curves in the graph. The only change is that lower salinity and higher  $\delta^{18}\text{O}$  values are obtained for the same freezing rates and porosity.

Figures 5f to h have been designed to illustrate the sensitivity of the model results to changes in parent water and host water values. If the disc thickness of the individual ice crystals forming in the "frazil ice phase" is closer to the 0.01 mm chosen by Jenkins and Bombosch [1995] ( $z_{\text{h}} = 0.005$  mm) and/or if the growth rate is lower than the lower value of the range produced in their case study, the mean  $\delta^{18}\text{O}$  value of the frazil discs will be very close to the equilibrium (2.38‰). Figure 5f shows that, in that case, the highest isotopic values from the data set can be reproduced, at low porosity (5 to 10%). Inversely, if the growth rate equals the maximum predicted values from Jenkins and Bombosch [1995], then the lowest isotopic values from the data set are covered (Figure 5g). Choosing even higher supercooling levels (i.e., higher growth rates) would clearly further increase the discrepancy between the data and the simulations. Changing the host water values from ISW to HSSW ( $S = 34.838\text{‰}$  and  $\delta^{18}\text{O} = -0.42\text{‰}$ ) [Jacobs et al., 1985] in the consolidation phase only slightly alters the simulation results (Figure 5h).

Although small realistic changes in the isotopic signal of the individual frazil ice crystals allow coverage of the whole range of observed isotopic values, one should be careful not to consider this as the only option. Indeed, the model in its present state does not include melting-refreezing effects under stress. Closed system refreezing at low freezing rates and low porosity (i.e., in the low salinity range), in a process such as

that sketched in Figure 6, would increase the isotopic variability allowing both higher enrichment of the first refrozen layers and entrapment of depleted residual waters [see, e.g., Jouzel and Souchez, 1982; Souchez and Jouzel, 1984]. This is the trend observed for our data points in Figure 2.

## 5.2. Applicability of the Model to Other Marine Ice Cores

Now that the model has been used to simulate the NIS data set, with the appropriate parameter choice, we discuss its potential suitability for other marine ice cores. It could be asked whether the process of consolidation through heat conduction across the ice shelf is still valid for marine ice occurring at greater depths, as is the case for B13 in the central part of the Ronne Ice Shelf [Eicken et al., 1994]. To test this possibility, we have plotted in Figure 7 the results from a simple thermodynamic calculation applied to the B13 case. Based on the assumption that the heat conducted through the ice results in the freezing of the interstitial host water, an iterative calculation of the ice increment consolidated per unit time can be performed for various fixed porosity, starting with an initial thickness of 153 m (meteoric ice thickness at B13 [Oerter et al., 1992]). Plotting the total ice thickness at B13 (239 m [Oerter et al., 1992]) versus the estimated travel time from initiation of marine ice accretion to B13 (450 years [Oerter et al., 1992]) shows that consolidation through heat conduction is a plausible process (with a mean constant porosity slightly lower than 20%). That similar processes are at work is further supported by the similarities between the NIS and B13 data sets in Figure 2. The mean isotopic values for B13 and NIS are 2.01‰ and 2.12‰, respectively. This difference of 0.1‰ can be partially explained by the fact that ISW has been reported to be slightly more negative in the Weddell Sea ( $-0.66\text{‰}$  [Weiss et al., 1979] against  $-0.61\text{‰}$  in the Ross Sea; Table 3). Furthermore, the B13 data set shows the same pattern of isotopic dispersion at low salinity as is observed for the NIS

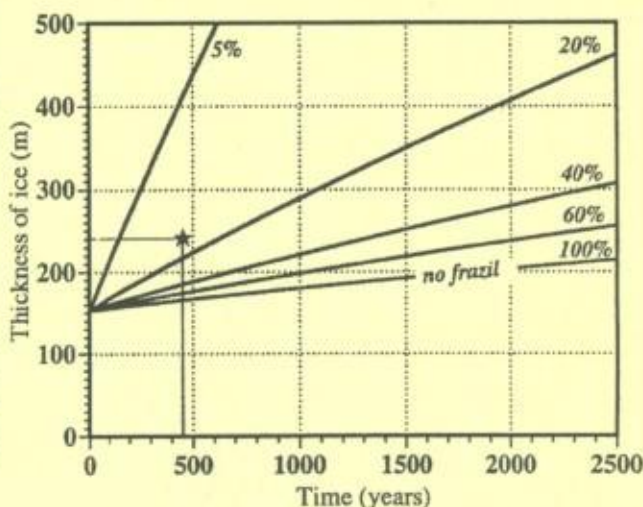


**Figure 7.** Cumulated consolidated ice thickness for various constant porosity values as a function of time in the case of the B13 ice core (Filchner Ice Shelf), calculated using a simple heat conduction model. Initial thickness is 153 m of meteoric ice, as observed at B13. Total ice thickness at B13 and estimated travel time from initiation of marine ice accretion to the B13 site [Oerter et al., 1992] are plotted as a star (see text).



case. Note that entrapment of depleted residual waters, as suggested in the processes described above, could also be responsible for the few outliers in the isotopic distribution of marine ice samples from B13. NIS samples that were consolidated closer to the surface, and therefore at higher freezing rates of the interstitial host water, accordingly show a salinity range shifted toward higher values. Finally, although it is difficult to rely on only three sample points, the isotope/salinity data from marine ice of the G1 Amery Ice Shelf core suggest that the growth rate is the primary control on both signals, but at different levels of parent and/or host waters.

## 6. Conclusions

Marine ice has now been shown to form in a wide range of locations, generally coincident with initially weaker (thinner) areas of ice shelves. These ice bodies, usually several tens of meters thick, act as a welding agent with its own peculiar chemical properties. The latter are likely to control the rheological behavior of marine ice and therefore its efficiency in stabilizing ice shelf flow. It is thus crucial to obtain some better insight into the processes that lead to its formation.

In this study, an attempt has been made to model for the first time the combined  $\delta^{18}\text{O}$ /salinity signal of marine ice and compare it to the measured properties of an actual body of marine ice. Isotopic fractionation during phase 1 of the process ("frazil ice phase") is adequately simulated using a boundary layer model with variable settings appropriate to growth of small size individual discs. No dedicated model is currently available for fractionation during the "consolidation phase" where individual crystals are thought to join and coarsen while immersed in the host water under the combined effect of buoyancy deviatoric stress, lateral compression and heat conduction through the ice shelf. As a first step we have tested the efficiency of a consolidation process solely driven by the freezing of the host water, using a boundary layer modeling approach in a semi-infinite reservoir. The simulations show the following:

1. Initial transient characteristics have to be considered while estimating the  $\delta^{18}\text{O}$  signature of the small individual crystals forming in the "frazil ice phase." For a realistic range of growth rates, the  $\delta^{18}\text{O}$  signature of these frazil ice crystals will indeed be higher compared to parent water when the initial transient is considered,

2. Applying a boundary layer model concept to the "consolidation phase," with the parameter values used for sea ice or columnar/congelation marine ice, cannot explain the observed  $\delta^{18}\text{O}$ /salinity relationship, even for porosity close to the permeability limit (5% [Cox and Weeks, 1975; Golden et al., 1998; Weeks and Ackley, 1986]),

3. In the framework of the boundary layer concept used as an approximation for the consolidation process, the simulations compare well with the measured properties only when using a segregation factor value of  $k_{eq}^* = 0.005$ . This value is an order of magnitude lower than the lowest observed value in columnar ice growing from seawater at equivalent depth. It reflects the fact that the actual process of consolidation does not allow the development of intracrystalline substructures, impurities being confined to intercrystalline location after saturation of the crystal lattice,

4. It is obviously unrealistic to cover the isotope/salinity signal of all the observed data points in a single simulation with decreasing growth rate and a constant set of parameters. Porosity and water characteristics are also susceptible to change in the course of the process. For example, the small group of samples with the highest salinity could have resulted from a consolidation process at low porosity and relatively high freezing rates as a result of closure under high lateral compressive stresses occurring relatively close to the surface. Choosing boundary layers of equivalent size and/or changing the isotopic signal of the individual frazil ice crystals (in accordance with the growth rates range in the water column) would account for the extremes in the  $\delta^{18}\text{O}$  distribution in the consolidated marine ice. However, closed system refreezing in the pores at low freezing rates and low porosity is an alternative explanation for the observed increased  $\delta^{18}\text{O}$  variability at low salinity,

5. Although spanning a different range of salinity, because of their different depth location, the NIS and B13 cores show nearly identical  $\delta^{18}\text{O}$  ranges and a similar trend to increased  $\delta^{18}\text{O}$  variability at low salinity. This suggests that the same processes are controlling the isotope/salinity signature of the marine ice at both locations. As a first approximation, we might consider that the  $\delta^{18}\text{O}$  signature is mainly controlled by the one of the individual frazil ice crystals. Dispersion occurs through dissociation of the host water freezing products at lower freezing rates and porosity. Salinity is mainly controlled by the freezing rate (and thus the freezing depth) of the host water and by the porosity reduction in the consolidating medium.

Obviously, the model described here is only a crude description of the real world situation. Processes such as coarsening and sintering of discs, which are known to occur in bodies of consolidating frazil [e.g., Martin and Kauffman, 1981], were not included. However, sensitivity tests have allowed us to define several important variable settings, different from those used in sea ice growth models, that will have to be considered in future more sophisticated models for marine ice formation. Experimental work and theoretical development on equilibrium fractionation processes in granular media (both in the genesis and consolidation phases) are also clearly needed to further assess the parameter choices made in this paper. On a broader scale, mechanical tests on marine ice samples are currently underway in order to characterize their rheological behavior.

## Notation

$\alpha_{eq}$	equilibrium fractionation factor (coefficient) for $^{18}\text{O}$ .
$\alpha_{eff}$	effective (apparent) fractionation factor (coefficient) for $^{18}\text{O}$ .
$\delta^{18}\text{O}_{frazil}$	$\delta^{18}\text{O}$ value of individual frazil ice crystal
$\epsilon$	$(\alpha - 1) \times 1000$ ‰.
$C_s$	impurity concentration in the solid at the ice-water interface.
$C_l$	impurity concentration in the liquid at the ice-water interface.
$C_0$	impurity concentration in the bulk reservoir.
$D$	diffusion coefficient



31,400

TISON ET AL.: ISOTOPE/SALINITY SIGNAL IN MARINE ICE

$k_{eq}$	equilibrium segregation factor (coefficient) for salt impurities; an asterisk denotes an experimentally derived value.
$k_{eff}$	effective (apparent) segregation factor (coefficient) for salt impurities.
$R_s$	isotopic ratio $^{18}\text{O}/^{16}\text{O}$ (or D/H) in the solid.
$R_l$	isotopic ratio $^{18}\text{O}/^{16}\text{O}$ (or D/H) in the liquid.
$R_{V-SMOW}$	isotopic ratio $^{18}\text{O}/^{16}\text{O}$ (or D/H) in Vienna standard mean ocean water.
$v$	growth rate.

**Acknowledgments.** This paper is a contribution to the Belgian Antarctic program (Science Policy Office). The authors would like to thank the Programma Nazionale di Ricerche in Antartide for their logistic support during the field campaign, and H. Oerter, W. Graff, and V. Morgan for providing data sets from other marine ice cores. M. Dini and B. Stenni kindly performed the  $\delta^{18}\text{O}$  measurements at the Laboratorio di Geochimica Isotopica in Trieste (Italy). Critical comments from the scientific editor, H. Eicken, and two anonymous referees greatly improved the quality of the manuscript. J.-L. Tison is Research Associate at the Belgian Science Foundation (FNRS).

## References

- Andersson, A., and S.F. Daly, Laboratory investigation of trash rack blockage by frazil ice, *CRREL Rep. 92-16*, 11 pp., Cold Reg. Res. and Eng. Lab., Hanover, N. H., 1992.
- Arakawa, K., and K. Higuchi, On the freezing process of aqueous solutions, *Low Temp. Sci.*, **A12**, 73-86, 1954.
- Beck, N., and K.O. Münnich, Freezing of water: Isotopic fractionation, *Chem. Geol.*, **70**, 168, 1988.
- Burton, J.A., R.C. Prim, and W.P. Slichter, The distribution of solute in crystals grown from the melt, I, Theoretical, *J. Chem. Phys.*, **21**, 1987-1991, 1953.
- Cherepanov, N.V., Structure of sea ice of great thickness, translated from Russian by E.R. Hope, *Dir. of Sci. Inf. Serv. - DRB Canada*, 1966.
- Corr, H., M. Popple, and A. Robinson, Airborne radio echo investigations of a marine ice body. Filchner-Ronne Ice Shelf Programme (FRISP), *Filchner Ronne Ice Shelf Programme Rep. 9*, edited by H. Oerter, pp. 14-17, Alfred Wegener Inst. for Polar and Mar. Res., Bremerhaven, Germany, 1995.
- Cox, G.F.N., and W.F. Weeks, Brine drainage and initial salt entrapment in sodium chloride ice, *CRREL Res. Rep. 345*, 85 pp., Cold Reg. Res. and Eng. Lab., Hanover, N. H., 1975.
- Daly, S.F., Frazil ice dynamics, *CRREL Monograph 84-1*, 44 pp., Cold Reg. Res. and Eng. Lab., Hanover, N. H., 1984.
- Eicken, H., Deriving modes and rates of ice growth in the Weddell Sea from microstructural, salinity and stable-isotope data, in *Antarctic Sea Ice: Physical Processes, Interactions and Variability*, Ant. Res. Ser., vol. 74, edited by M.O. Jeffries, pp. 89-122, AGU, Washington, D. C., 1998.
- Eicken, H., H. Oerter, H. Miller, W. Graf, and J. Kipfstuhl, Textural characteristics and impurity content of meteoric and marine ice in the Ronne Ice Shelf, Antarctica, *J. Glaciol.*, **40**, 386-398, 1994.
- Frezzotti, M., Fluctuations of ice tongues and ice shelves derived from satellite images in Terra Nova Bay area, Victoria Land, Antarctica, in *Recent Progress in Antarctic Earth Science*, edited by Y. Yoshida et al., pp. 733-739, Terra Sci., Tokyo, 1992.
- Frezzotti, M., I.E. Tabacco, and A. Zirizzotti, Ice discharge of eastern Dome C drainage area, Antarctica, inferred from airborne radar survey and satellite image analysis, *J. Glaciol.*, **46**, 253-264, 2000.
- Garand, J.P., J.J. Favier, and D. Camel, Segregation phenomena in crystal growth from the melt, in *Handbook for Crystal Growth*, edited by D.T.J. Hurle, pp. 659-707, Elsevier Sci., New York, 1994.
- Golden, K.M., S.F. Ackley, and V.L. Lytle, The percolation phase transition in sea ice, *Science*, **282**, 2238-2240, 1998.
- Grosfeld, K., H.H. Hellmer, M. Jonas, H. Sandhäger, M. Schulte, and D.G. Vaughan, Marine ice beneath Filchner Ice Shelf: Evidence from a multidisciplinary approach, in *Ocean, Ice and Atmosphere: Interactions at the Antarctic Continental Margin*, Antarctic Res. Ser., vol. 75, edited by S.S. Jacobs and R.F. Weiss, pp. 319-339, AGU, Washington D. C., 1998.
- Gross, G.W., P.M. Wong, and K. Humes, Concentration dependent solute redistribution at the ice-water phase boundary, III, Spontaneous convection, chloride solutions, *J. Chem. Phys.*, **67**(11), 5264-5274, 1977.
- Hobbs, P.V., *Ice Physics*, 837 pp., Clarendon, Oxford, England, 1974.
- Hooke, R.L.B., Gao, X.Q., Jacka, T.H., Souchez, R.A., Rheological contrast between Pleistocene and Holocene ice in Barnes Ice Cap, Baffin Island, N.W.T., Canada: a new interpretation, *J. of Glaciol.*, **34** (118), 364-365, 1988.
- Jacobs, S.S., R.G. Fairbanks, and Y. Horibe, Origin and evolution of water masses near the Antarctic and continental margin: Evidence from  $\text{H}_2^{18}\text{O}/\text{H}_2^{16}\text{O}$  ratios in sea water, in *Oceanology of the Antarctic Continental Shelf*, Antarctic Res. Ser., vol. 75, edited by S.S. Jacobs, pp. 59-85, AGU, Washington D.C., 1985.
- Jenkins, A., and A. Bombosch, Modeling the effects of frazil ice crystals on the dynamics and thermodynamics of Ice Shelf Water plumes, *J. Geophys. Res.*, **100**, 6967-6981, 1995.
- Jouzel, J., and R. Souchez, Melting and refreezing at the glacier sole and the isotopic composition of the ice, *J. Glaciol.*, **28**, 35-42, 1982.
- Khazendar, A., J.-L. Tison, B. Stenni, M. Dini, and A. Bondesan, Significant marine ice accumulation in the ablation zone beneath an Antarctic ice shelf, *J. Glaciol.*, in press, 2001.
- Kipfstuhl, J., Zur Entstehung von Unterwassereis und das Wachstum und die Energiebilanz des Meereises in der Akta Bucht, Antarktis (On the formation of underwater ice and the growth and energy budget of the sea ice in Atka Bay, Antarctica), *Ber. Polarforsch.*, **85**, 1991.
- Lehmann, M., and U. Siegenthaler, Equilibrium oxygen- and hydrogen-isotope fractionation between ice and water, *J. Glaciol.*, **37**, 23-26, 1991.
- Lofgren, G., and W.F. Weeks, Effect of growth parameters on substructure spacing in NaCl ice crystals, *J. Glaciol.*, **8**, 153-164, 1969.
- MacAyeal, D.R., E. Rignot, and C.L. Hulbe, Ice-shelf dynamics near the front of the Filchner-Ronne Ice Shelf, Antarctica, revealed by SAR interferometry: Model/interferogram comparison, *J. Glaciol.*, **44**, 419-428, 1998.
- Martin, S., Frazil ice in rivers and oceans, *Annu. Rev. Fluid Mech.*, **13**, 379-397, 1981.
- Martin, S., and P. Kauffman, A field and laboratory study of wave damping by grease ice, *J. Glaciol.*, **27**, 283-313, 1981.
- Moore, J.C., A.P. Reid, and J. Kipfstuhl, Microstructure and electrical properties of marine ice and its relationship to meteoric ice and sea ice, *J. Geophys. Res.*, **99**, 5171-5180, 1994.
- Morgan, V.L., Oxygen isotope evidence for bottom freezing on the Amery Ice Shelf, *Nature*, **238**, 392-394, 1972.
- Nagashima, K., and Y. Furukawa, Solute distribution in front of an ice/water interface during directional growth of ice crystals and its relationship to interfacial patterns, *J. Phys. Chem. B*, **101**, 6174-6176, 1997.
- Nakawo, M., and N. Sinha, Growth rate and salinity profiles of first-year sea ice in the high Arctic, *J. Glaciol.*, **27**, 315-330, 1981.
- Nicholls, K.W., and A. Jenkins, Temperature and salinity beneath Ronne Ice Shelf, Antarctica, *J. Geophys. Res.*, **98**, 22,553-22,568, 1993.
- Oerter, H., J. Kipfstuhl, J. Determann, H. Miller, D. Wagenbach, A. Minikin, and W. Graf, Evidence for basal marine ice in the Filchner-Ronne Ice Shelf, *Nature*, **358**, 399-401, 1992.
- O'Neil, J.R., Hydrogen and oxygen isotope fractionation between ice and water, *J. Phys. Chem.*, **72**, 3683-3684, 1968.
- Rignot, E., and D.D. MacAyeal, Ice shelf dynamics near the front of the Filchner Ronne Ice Shelf, Antarctica, revealed by SAR interferometry, *J. Glaciol.*, **44**, 405-418, 1998.
- Robin, G., de Q., C.S.M. Doake, H. Kohnen, R.D. Crabtree, S.R. Jordan, and D. Möller, Regime of the Filchner-Ronne ice shelves, Antarctica, *Nature*, **302**, 582-586, 1983.
- Souchez, R., and J. Jouzel, On the isotopic composition in  $\delta\text{D}$  and  $\delta^{18}\text{O}$  of water and ice during freezing, *J. Glaciol.*, **30**, 369-372, 1984.
- Souchez, R., J.-L. Tison, and J. Jouzel, Freezing rate determination



## TISON ET AL.: ISOTOPE/SALINITY SIGNAL IN MARINE ICE

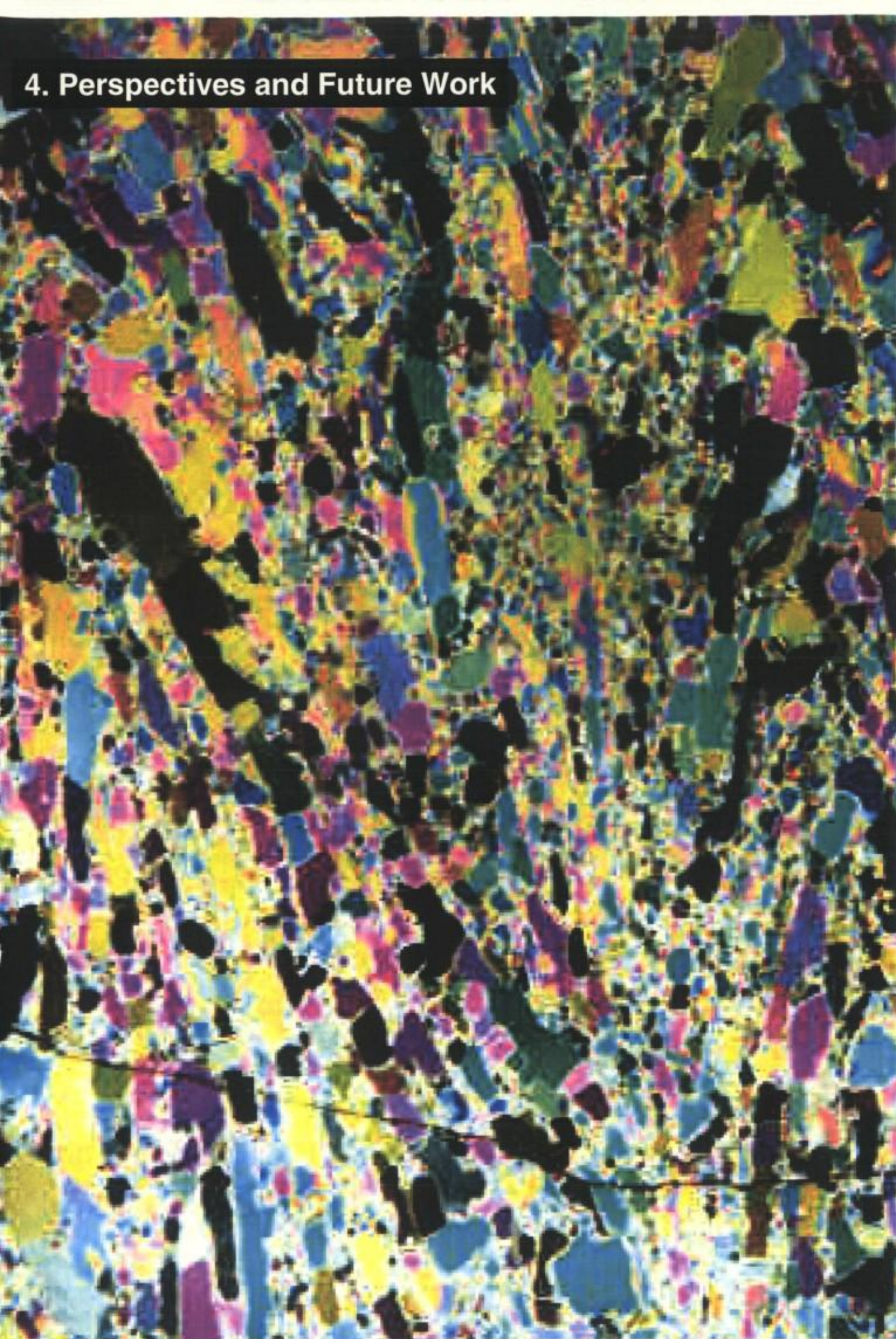
31,401

- by the isotopic composition of the ice, *Geophys. Res. Lett.*, **14**(6), 599-602, 1987.
- Souchez, R., J.-L. Tison, and J. Jouzel, Deuterium concentration and growth rate of Antarctic first-year sea ice, *Geophys. Res. Lett.*, **15**(12), 1385-1388, 1988.
- Souchez, R., M. Meneghel, J.-L. Tison, R. Lorrain, D. Ronveaux, C. Baroni, A. Lozej, I. Tabacco, and J. Jouzel, Ice composition evidence of marine ice transfer along the bottom of a small Antarctic ice shelf, *Geophys. Res. Lett.*, **18**(5), 849-852, 1991.
- Thyssen, F., Special aspects of the central parts of Filchner-Ronne Ice Shelf, Antarctica, *Ann. Glaciol.*, **11**, 173-179, 1988.
- Tiller, W.A., Effect of grain boundaries on solute partitioning during progressive solidification, *J. Appl. Phys.*, **33**(10), 3106-3107, 1962.
- Tison, J.-L., E.M. Morris, R. Souchez, and J. Jouzel, Stratigraphy, stable isotopes and salinity in multi-year sea ice from the rift area, south George VI Ice Shelf, Antarctic Peninsula, *J. Glaciol.*, **37**(127), 357-367, 1991.
- Tison, J.-L., D. Ronveaux, and R. Lorrain, Low salinity frazil ice generation at the base of a small Antarctic ice shelf, *Antarct. Sci.*, **5**(3), 309-322, 1993.
- Tison, J.-L., A. Bondesan, G. Delisle, A. Lozej, F. Merlanti, and L. Janssens, A dynamical approach to explain ice structures and complex morainic genesis on a partially grounded ice shelf (Hells Gate Ice Shelf - Victoria Land, Antarctica), *Terra Antart. Rep.*, **1**, 33-37, 1997.
- Tison, J.-L., R.D. Lorrain, A. Bouzette, M. Dini, A. Bondesan, and M. Stiévenard, Linking landfast sea ice variability to marine ice accretion at Hells Gate Ice Shelf, Ross Sea, in *Antarctic Sea Ice: Physical Processes, Interactions and Variability*, Antarct. Res. Ser., vol. 74, edited by M.O. Jeffries, pp. 375-407, AGU, Washington D.C., 1998.
- Weeks, W.F., and S.F. Ackley, The growth, structure and properties of sea ice, in *The Geophysics of Sea Ice*, edited by N. Untersteiner, pp. 9-164, Martinus Nijhoff, Zoetermeer, Netherlands, 1986.
- Weiss, R.F., H.G. Ostlund and H. Craig, Geochemical studies in the Weddell Sea, *Deep Sea Res.*, **26A**, 1093-1120, 1979.
- White, K.D., Determining the intrinsic permeability of frazil ice, 1, Laboratory investigations, CRREL Rep. 91-23, 15 pp., Cold Reg. Res. and Eng. Lab., Hanover, N. H., 1991.
- Zotikov, I.A., V.S. Zagorodnov, and J.V. Raikovsky, Core drilling through the Ross Ice Shelf (Antarctica) confirmed basal freezing, *Science*, **207**, 1463-1465, 1980.
- A. Khazendar and J.-L. Tison, Unité de Glaciologie, Science Faculty, Department of Earth Science and Environment, Université Libre de Bruxelles, CP 160/03, Avenue F.D. Roosevelt 50, B-1050 Brussels, Belgium. (jtison@ulb.ac.be)
- E. Roulin, Royal Meteorological Institute, Avenue Circulaire 3, B-1050 Brussels, Belgium

(Received January 3, 2000; revised March 8, 2001; accepted June 11, 2001.)



## 4. Perspectives and Future Work





## 4.1. Foreword

We have shown in the previous sections how marine ice can be widely distributed into ice shelves, and demonstrated the various processes involved in its genesis. Here we will discuss the potential contribution of those processes to the sensitivity of these key polar areas to the ongoing global climate warming, as well as to previous natural climatic changes. We will also show how working on the ice-ocean interactions processes under ice shelves enlarges our perception of the mechanisms occurring at other ice-water interfaces. Finally, we will enumerate a series of recommendations that we see as the milestones for future research in the area.

## 4.2. Implications for ice shelf mass-balance and stability in a global warming perspective

### 4.2.1. Dielectric properties of marine ice, radio-echo-soundings and ice shelf mass-balance

During the metamorphism of snow into ice or during the phase change from water to ice, most of the impurities will be expelled from the ice lattice. Some however, like  $\text{NH}_4^+$  or  $\text{Cl}^-$  (of peculiar interest in marine environments), have an ionic or atomic radius, which is very close to the one of Oxygen. For those components, substitution can therefore occur within the crystal lattice, introducing defects. As the impurity concentration increases, saturation of the lattice will be reached, and impurities in excess will be located at grain boundaries. It is interesting, in this regard, to see where marine ice stands in the range of natural ice bodies. Moore et al. (1994) studied the relationship between conductivity (absorption) and chlorinity (salinity) at  $-22^\circ\text{C}$  for samples of meteoric ice (crosses), marine ice (squares) and sea ice (other

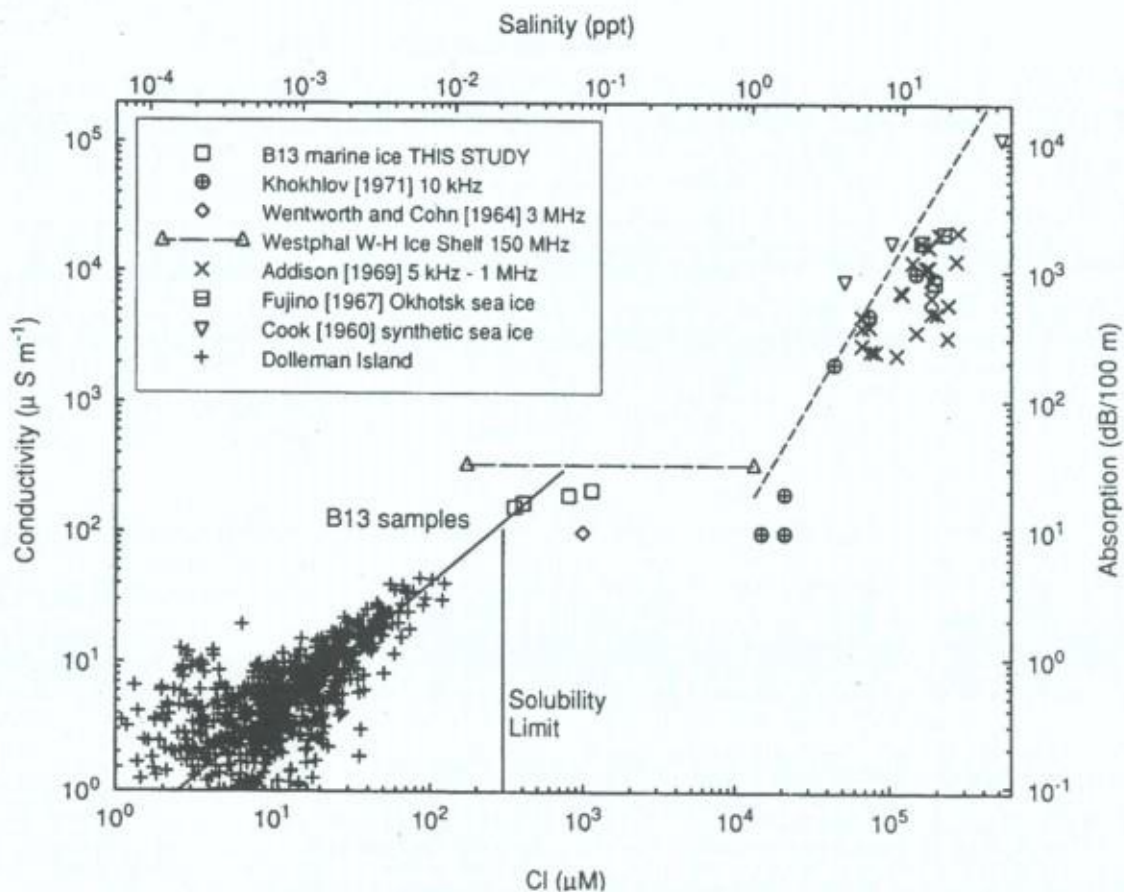


Figure 64: Logarithmic plot of conductivity (absorption) versus Cl concentration (salinity) at  $-22^\circ\text{C}$  for samples of meteoric ice, marine ice, and sea ice (Moore et al., 1994).



symbols), as shown in Figure 64. The same authors also used Scanning Electron Microscope (SEM) pictures to show that the solubility limit for chlorine in the ice lattice is of about 300  $\mu\text{M}$  (confirming earlier laboratory observations by Seidensticker (1972) and Gross et al. (1977) - 100-200  $\mu\text{M}$ ). Clearly from Figure 64, marine ice lies just above that limit, with a chlorinity concentration about 1 order of magnitude higher than meteoric ice and two order of magnitude less than sea ice, as we have already stated before. The important fact, is that marine ice therefore shows a much higher density of lattice defects than meteoric ice, that are of major importance in controlling the dielectric properties of the ice. Dielectric properties characterize the capacity of energy storage and dissipation of a non-metal (ice, in this case) when it is submitted to an electro-magnetic wave field (radio echo-soundings, for example). It has been shown (e.g. Hobbs, 1974), that imperfections in the crystal lattice (L and D defects) induce higher energy dissipation due to dipoles re-orientation under alternative currents (polarizing effect of the current), and this explains why the absorption values in marine ice (Figure 64) are about 10 times higher than in meteoric ice.

Enhanced absorption of electromagnetic waves as they cross a meteoric ice/marine ice boundary can often result in a misleading interpretation where the meteoric ice/marine ice interface is mistaken for the trace of the ice shelf bottom (ice - sea water interface). In turn, this can lead to serious underestimation of the ice shelf thickness and therefore of the ice shelf mass balance, a crucial input to ice-sheet stability. A safe diagnostic for total ice shelf thickness therefore requires, because of the potential occurrence of marine ice, that the RES measurements be cross-checked against alternative geophysical methods like seismic, GPS or satellite radar altimetry (e.g. Figures 17, 20 and 21).

#### 4.2.2. $\delta^{18}\text{O}$ as a geochemical tracer of the contribution of ice shelf melting to the ice shelf mass balance

Schlosser et al. (1990) used Oxygen-18 measurements in a series of 9 water profiles in front of the Filchner Ice Shelf (Figure 65a,b) to detect the fraction of glacial meltwater in the Ice Shelf Water flowing out at the front. Figure 65c plots the potential temperature<sup>8</sup>/ $\delta^{18}\text{O}$  relationship in all the profiles. Clearly, the relationship is linear for temperatures below the freezing point of seawater at atmospheric pressure (i.e. for samples of Ice Shelf Waters). The shift in  $\delta^{18}\text{O}$  between the surface water and ISW is about 0.3‰. Assuming a  $\delta^{18}\text{O}$  concentration of -50‰ for the glacial meltwater from the ice shelf, the fraction of meltwater contained in the ISW at potential temperatures below -2°C can be estimated to be about 6‰.

In analogy to the  $\delta^{18}\text{O}$  balance of the meltwater fraction contained in ISW, Schlosser et al. (1990) applied a salinity balance to the same problem. Assuming a salinity of the ISW of 34.65‰ observed at stations located in the western Filchner Depression and further assuming a salinity of Western Shelf Water (WSW, the local name of High Salinity Shelf Water (HSSW)) of 34.75‰ (Foldvik et al., 1985), the meltwater fraction is estimated to be about 2.9‰, i.e. half the value obtained using  $\delta^{18}\text{O}$ . Schlosser et al. (1990) suggest two possible explanations for that discrepancy:

- (a) In the  $\delta^{18}\text{O}$  balance, ISW is compared with near surface waters, instead of WSW (HSSW), which is used for the salinity balance, and more reliable since it is the one that really mixes with the glacial ice that it melts to produce ISW (see Figure 10). No HSSW  $\delta^{18}\text{O}$  was available to Schlosser et al. (1990) for comparison
- (b) The salinity method could yield a lower fraction of meltwater, because "...some of the ISW might freeze again at the underside in the front part of the ice shelf (Hellmer, 1989). Such a freezing process would affect  $^{18}\text{O}$  concentration only to a minor extent (relatively low fractionation coefficient for the freezing of water) but would release most of the salt contained in the freezing water..."

<sup>8</sup> The potential temperature ( $\theta$ ) refers to the temperature that the water mass would indicate if it was located at the surface (atmospheric pressure).



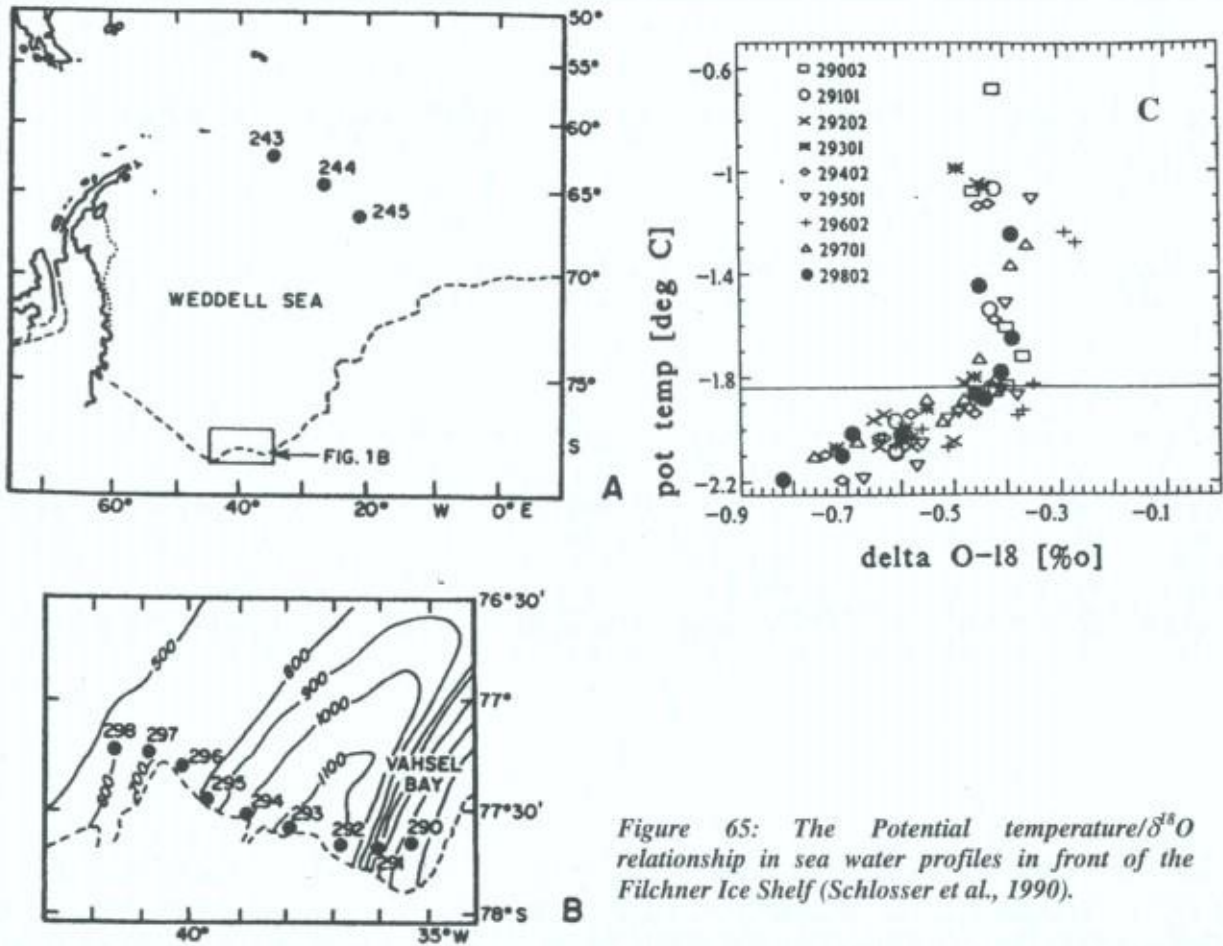


Figure 65: The Potential temperature/ $\delta^{18}\text{O}$  relationship in sea water profiles in front of the Filchner Ice Shelf (Schlosser et al., 1990).

The latter description is actually anticipating the later developments on marine ice formation discussed in this Thesis. However, although it is true that  $\delta^{18}\text{O}$  fractionation is of relatively low amplitude, it can still be an order of magnitude higher than the differences discussed by Schlosser et al. (1990). Therefore, our findings in section 3.4. lead us to recommend that salinity is used instead of  $\delta^{18}\text{O}$  to provide reliable estimates of the glacial melt contribution to ice shelf mass balance.

#### 4.2.3. Effect of impurities on ice rheology and potential rift welding efficiency in grounding and calving areas

The increased number of defects in the crystal lattice of marine ice, as compared to meteoric ice, is also likely to affect its rheological properties, by increasing the initial dislocation density. Softening of the ice through an increased impurity content has already been suggested as a source for the increased strain rate of Pleistocene (glacial) meteoric ice as compared to Holocene (interglacial) ice in the Barnes Ice Cap (Hooke et al., 1988). Thorsteinsson et al. (1999) observed an abrupt increase in strain rate at a height of 200m above the bed at Dye-3, Greenland, even though the temperature and fabric were smoothly varying functions of depth. They note a simple flow law and fabric development cannot account for the observed trends. However, they did find a statistical correlation between the higher strain rates and the levels of particulate and soluble impurities in the ice.

The peculiar properties of marine ice therefore make it prone to affect the rifts and crevasses welding efficiency in grounding and calving areas. Although Antarctic rifts and basal crevasses are common, their overall coverage area probably does not exceed a small fraction of that of a big ice shelf.



However, they could make a disproportionate contribution if they occur at the grounding line, which is a point of compulsory passage for continental ice on its way to the sea. There, fractures could be filled with marine ice and exported downstream before new fractures form at the same point again and the process is repeated. In this scenario, marine ice rheological properties cannot be neglected in understanding the ice shelf's behaviour, notably in a changing climate. Figure 66 shows the disintegrating Larsen B ice shelf, on 7<sup>th</sup> of March 2002. It is interesting to note, far inland from the front, the high density of individual icebergs delimited by a dense network of former rifts and crevasses, all potential locations for marine ice formation or disintegration, depending on oceanographic conditions.

Recently, Rignot and MacAyeal (1998) and MacAyeal et al. (1998), have used ERS (European Remote sensing Satellite) SAR (synthetic aperture radar) interferograms to study the Filchner-Ronne Ice Shelf dynamics near two ends (Lassiter Coast to the west and Hemmel Ice Rise to the east) of the iceberg-calving front (Figure 67). These authors note that many of the large rifts that appear to form the boundaries where tabular icebergs may eventually detach from the ice shelf are filled with a "melange" of sea ice, ice shelf debris and wind-blown snow. The continuity of the interferometric fringe patterns

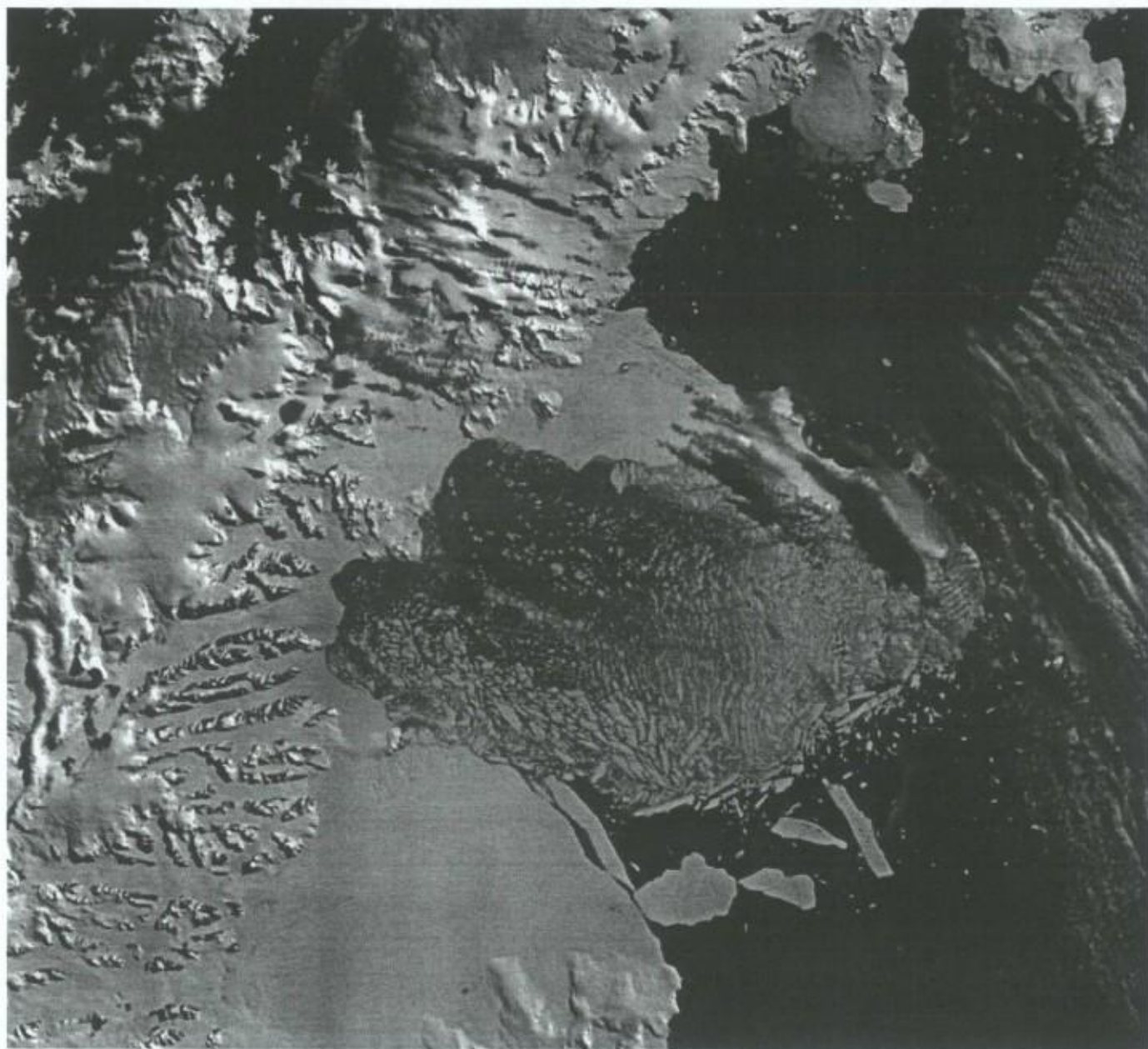


Figure 66: MODIS (Moderate Resolution Imaging Spectroradiometer) visible satellite image of the Larsen B ice shelf on the 7<sup>th</sup> March, 2002 during the total collapse. Source: National Snow and Ice Data Center – (<http://nsidc.org>)



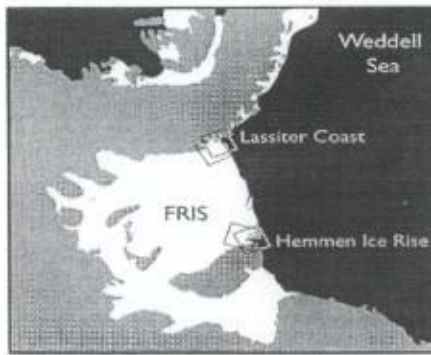
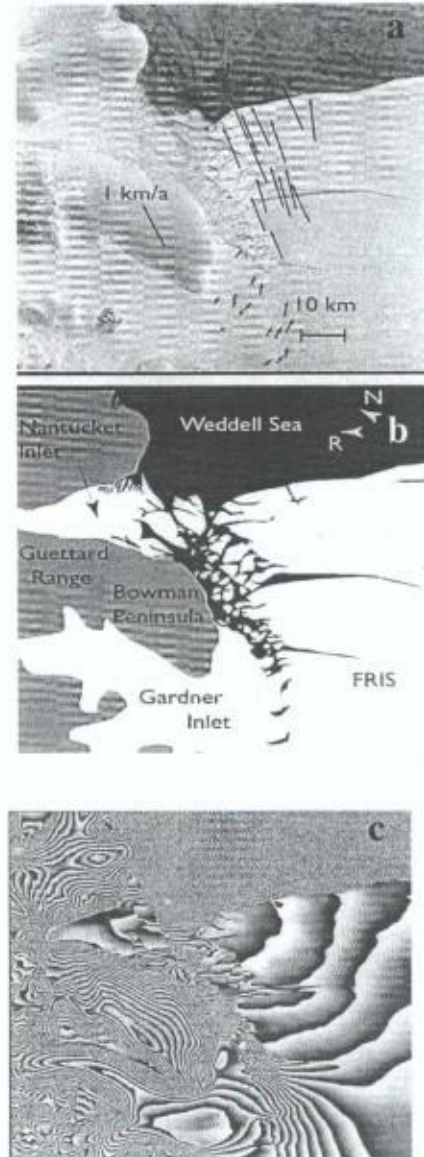
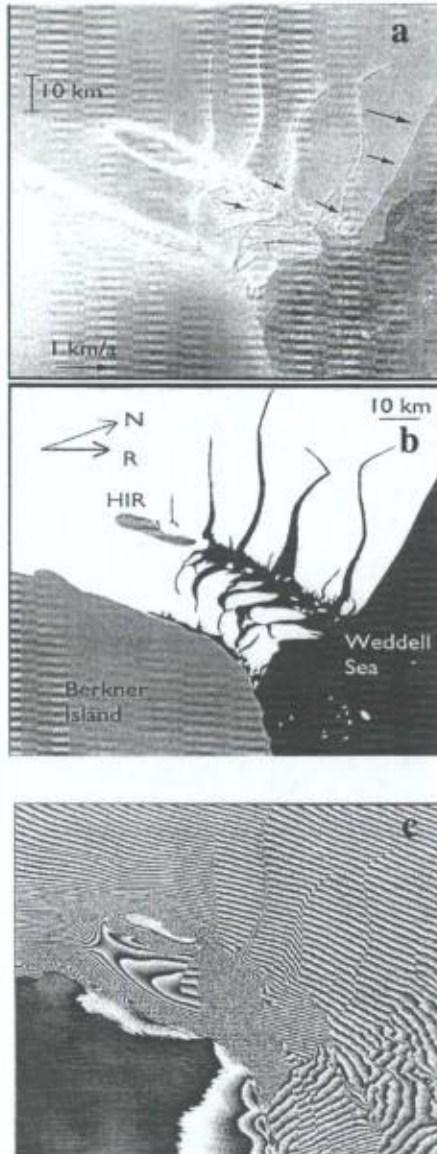


Figure 67: ERS SAR images (a), sketch maps (b) and interferograms (c) for the Hemmel Ice Rise (HIR, left column) and the Lassiter Coast (LC, right column) at the Filchner-Ronne Ice Shelf calving front. A location map is shown on top (after Rignot and MacAyeal, 1998).



(that can be interpreted as the expression of the ice displacement) within rifts shows that this *melange* tends to deform coherently in response to the ice-shelf flow and has sufficient strength to trap large tabular ice-shelf fragments for several decades before the fragments eventually become icebergs. This brings Rignot and MacAyeal (1998) to suggest two possible mechanisms by which climate could influence tabular iceberg calving:

- (a) Spatial gradients in oceanic and atmospheric temperature may determine where the *melange* melts and, thus, the location of the iceberg-calving margin



- (b) Melting or weakening of the ice *melange* as a consequence of climate change could trigger a sudden or widespread release of tabular icebergs and lead to rapid ice-shelf disintegration (the Larsen B scenario?)

Our work in the Nansen Ice Sheet area (Ross Sea) and in the George VI Ice Shelf area (Antarctic Peninsula), demonstrates that the filling of rifts is not always the ice *melange* described above, but possibly marine ice with variable thickness, depending on the sub-ice shelf oceanographic context. The stability of the ice shelf front could therefore, in those cases, depend on other variables like:

- (a) The existence of an ascending Ice Shelf Water plume below the rifting area, that would considerably increase the thickness of the welding unit, making it eventually less sensitive to oceanic or atmospheric warming
- (b) The rheological properties of the marine ice, as opposed to those of the ice "*melange*" hypothesized by Rignot and MacAyeal (1998)

#### 4.2.4. Marine ice production in a warmer climate

Nicholls (1997) studied sub-ice shelf water temperatures along the western flank of the Filchner – Ronne Ice Shelf. He demonstrated that the inflow of High Salinity Shelf Water (HSSW) shows a strong seasonality that is connected to the alternance of intense wintertime sea ice production and springtime warming. Nicholls (1997) argues that the seasonal springtime warming can be used as an analogue for climate warming. For the present mode of oceanographic circulation, the implication is that warmer winters (a climate warming leading to lower rates of sea ice formation) would cause a reduction in the flux of HSSW beneath the ice shelf. The resultant cooling in the sub-ice shelf cavity would lead, in turn, to a reduction in the total melting at the ice shelf's base. The author concludes that a moderate warming of the climate could thus lead to a basal thickening of the Filchner-Ronne Ice Shelf, perhaps increasing its longevity.

This scenario however neglects the impact of such a warming trend on the marine ice production under the Deep Thermohaline Circulation process. Indeed, as we have seen before, HSSW is responsible for Ice Shelf Water production in the Deep Thermohaline Circulation (mode-1 in Figure 10). A reduction of the amount of HSSW favouring melting at the grounding line will also reduce the amount of Ice Shelf Water produced and returning towards the front. The efficiency of the welding of basal crevasses and rift will be therefore accordingly reduced, and, although increased in thickness, the ice shelf will be weaker in its internal cohesion. One surely needs a further assessment of the relative importance of each of these two feedbacks mechanisms to assess the status of the ice shelf stability as the climate warms up.

### 4.3. Implications for sediment export during glacial vs. Interglacial times

Bond et al. (1993) studied correlations between climate records from North Atlantic sediments and the GRIP deep ice core from central Greenland, Summit (see location of both in Figure 68). A conspicuous feature common to both the ice  $\delta^{18}\text{O}$ <sup>9</sup> and ocean foraminiferal<sup>10</sup> records enabled these authors to correlate them in spite of their uncertain chronology. That feature is a bundling of the millennial-scale *Dansgaard Oeschger* cycles<sup>11</sup> into longer cooling cycles, each terminated by an abrupt shift from cold to warm temperatures. Bond et al. (1993) matched the records at the points of abrupt temperature shifts and then "stretched" the ice-core record linearly until points were aligned to produce the set of curves of Figure 69. Clearly, from Figure 69, *Dansgaard Oeschger* cycles are imprinted in the

<sup>9</sup> The  $\delta^{18}\text{O}$  in the ice is used as a proxy to the atmospheric temperature during the formation of the snow that initially deposited at the surface of the ice sheet, and from which the ice originated

<sup>10</sup> Planktic foraminifera (like *Neogloboquadrina pachyderma* (s.) used here) are strongly temperature sensitive and can therefore also be used as a proxy to sea surface temperature

<sup>11</sup> *Dansgaard Oeschger* cycles describe the millennial scale series of saw-tooth shaped temperature ( $\delta^{18}\text{O}$ ) cycles that characterize the last Glacial period



marine sediments of the North Atlantic. The temperature shifts, occur on a millennium timescales and have asymmetric shapes, sharp boundaries and strong amplitudes (up to a change in temperature of about  $5^{\circ}\text{C}$ ), features which characterize the *Dansgaard Oeschger* cycles.

Another remarkable finding from Bond et al. (1993) study is the evidence of an unexpectedly close relation between the ice-core temperature cycles and one of the most prominent features of North Atlantic sediments records, the *Heinrich events*. *Heinrich events* (H1 to H6 in Figure 69) occur during times of sea surface cooling, reduced fluxes of foraminifera and brief, exceptionally large discharges of icebergs from the Laurentide ice sheet that left conspicuous layers of detrital carbonate in deep sea sediments. Accompanying these events were large decreases in planktic  $\delta^{18}\text{O}$  (Figure 69, top), evidence of lowered surface salinities probably caused largely by melting of the drifting ice. Generally (H1 is an exception), the *Heinrich events* occur near the end of the bundled *Dansgaard Oeschger* cycles defined by a succession a progressively cooler interstadials that is during times of particularly cold stadials.

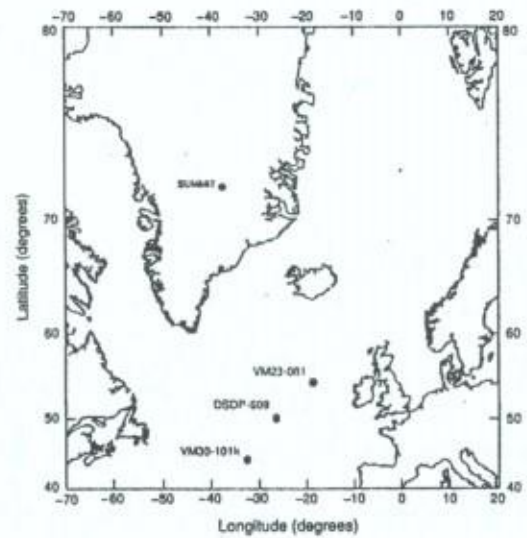


Figure 68: Location map of the GRIP (Summit) ice core and the North Atlantic sediment cores (Bond et al., 1993)

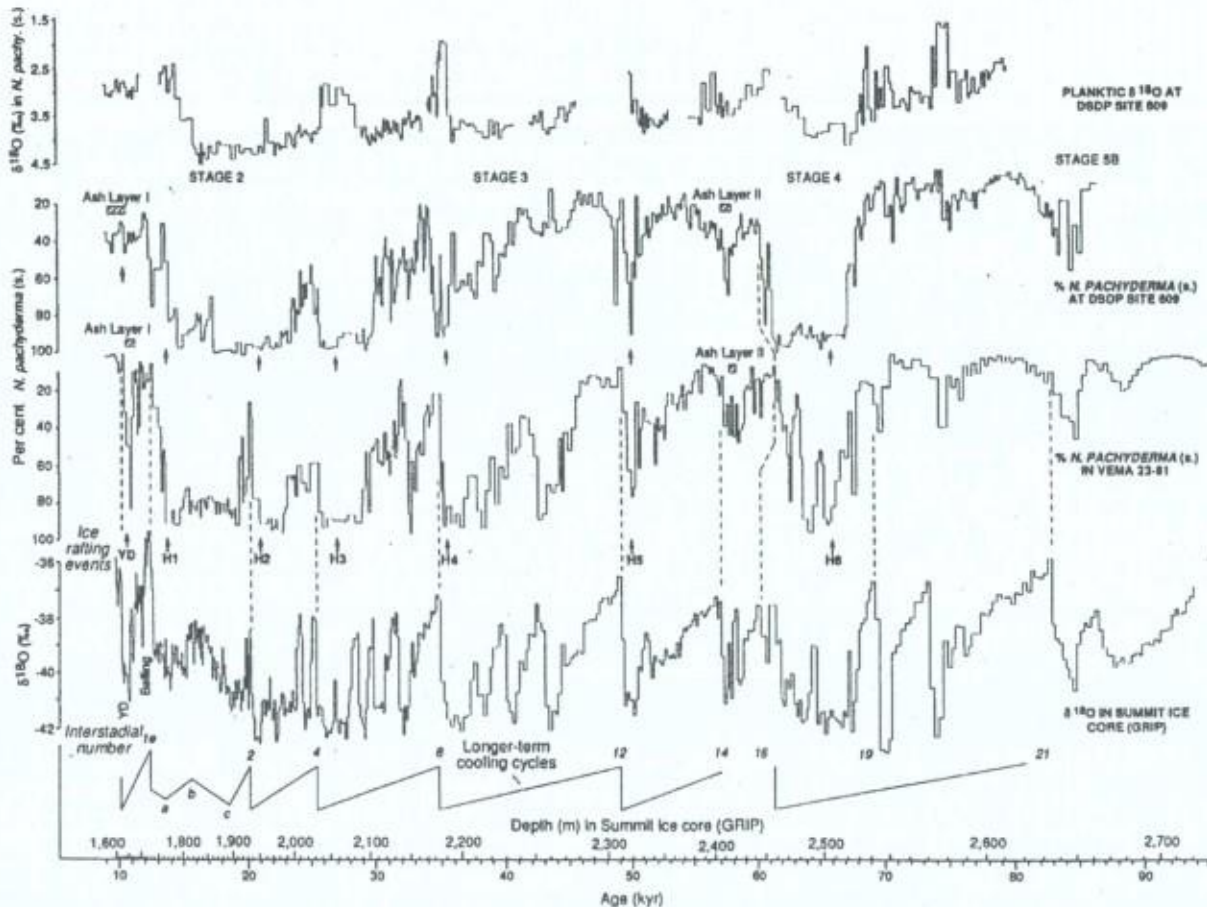


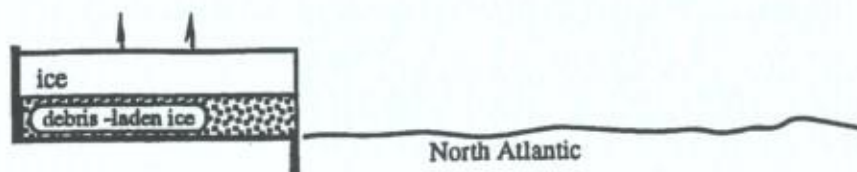
Figure 69: Correlation of the foraminiferal records from DSDP site 609 and V23-81 with the  $\delta^{18}\text{O}$  record from GRIP, Summit, Greenland. The dashed lines, corresponding to the abrupt changes towards interstadials were used as tie points for matching the ice core and marine records. The heavy arrows mark the locations of the IRD (Ice Rafted Debris) peaks within the Heinrich events (H1 to H6) and the peak concentrations of detrital carbonate IRD in the Younger Dryas event (Bond et al., 1993).



Following that stadial is a rapid termination-like shift to a prominent warm interstadial marking the beginning of the next cycle. It is still debated if the cooling cycles were caused entirely by internal oscillations of the ice sheet or whether they reflect a mode of climate forcing that caused ice sheets to grow, culminating each time in a prolonged, cold stadial, then ice-sheet instability and massive calving. The abrupt warmings that followed the Heinrich events could have been a direct consequence of the ice. Collapse of the ice sheet and landward retreat of ice streams after each event must have reduced the flux of icebergs to the open ocean. The resulting increase in surface salinity could have been large enough to strengthen thermohaline circulation rapidly bringing heat into the north Atlantic, therefore triggering the abrupt warming.

In the context of a process driven entirely by the ice sheets internal oscillations, Alley and MacAyeal (1994) investigated a simple conceptual model of ice stream instability (the binge/purge model) to suggest ways in which the ice stream could have entrained sufficient debris to account for the

#### Binge Phase:



#### Purge Phase:

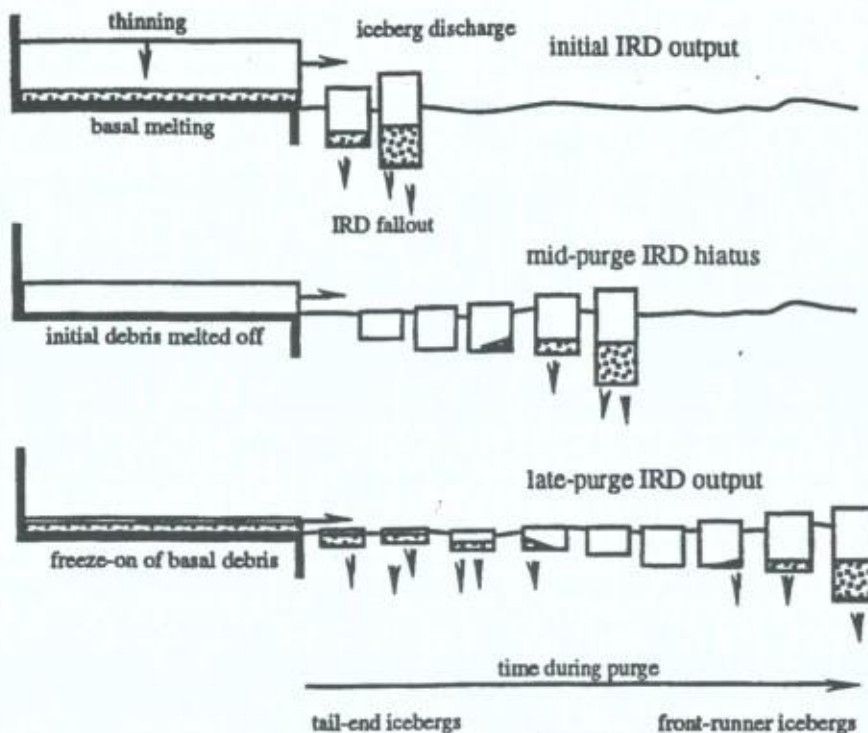


Figure 70: Schematic diagram of a Heinrich event displaying the IRD flux associated with a binge/purge cycle of the Laurentide Ice Sheet when debris is entrained into the ice stream by a simple freeze-on mechanism (Alley and MacAyeal, 1994).

estimated mass of IRD associated with a typical Heinrich IRD layer in the North Atlantic ( $1.0 \pm 0.3 \times 10^{15}$  kg). Alley and MacAyeal (1994) based their calculation on the binge/purge model developed for the Laurentide Ice Sheet (LIS), initially described by MacAyeal (1993 a, b), and illustrated in Figure 70.



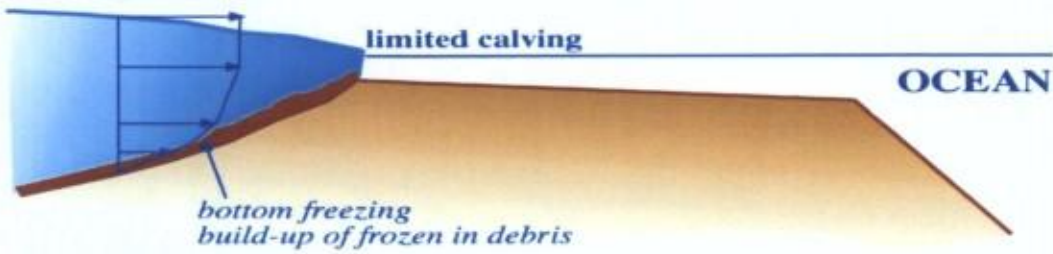
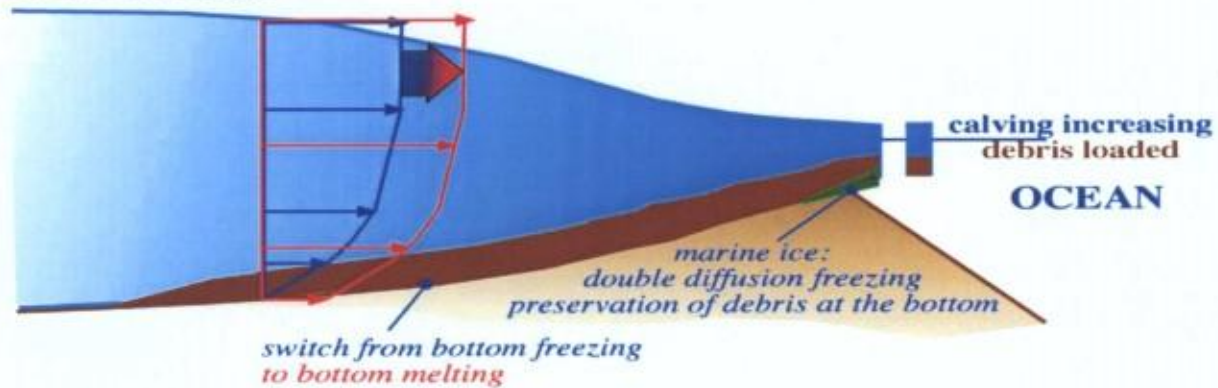
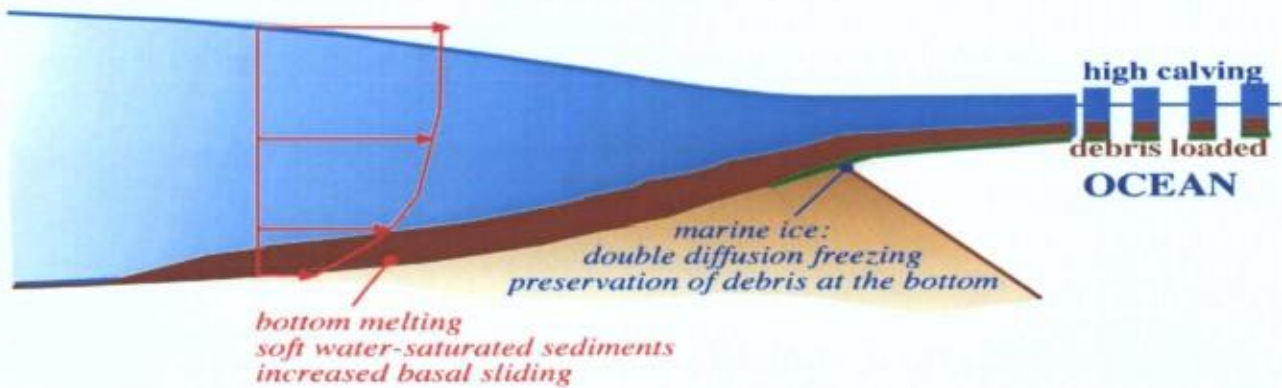
**1. Binge****2. end of Binge****3. Purge initiated****4. end of Purge**

Figure 71: Improved scheme of MacAyeal's binge/purge model for IRD production showing the potentially important role of ice-ocean interactions and marine ice production when the ice gets afloat. See text for details.



According to this model, the volume of the LIS suffers cyclic perturbations. Long periods of slow growth (binge) alternate with short periods of rapid discharge (purge). During the approximately 7700-year binge phase of the cycle, ice builds up gradually over Hudson Bay while geothermal heat slowly warms the glacial bed. Once thawed, the glacial bed becomes lubricated by soft, water-charged subglacial till derived from underlying sedimentary rock. This lubrication facilitates the rapid flow of an ice stream in Hudson Strait, which drains the central part of the LIS. During the brief 750-year purge of the ice stream, iceberg discharge into the Labrador Sea would account for IRD with affinities to bedrock conditions in Hudson Bay and Hudson Strait. The purge ends and a new binge begins when ice sheet thinning promotes the widespread refreezing of the glacial bed.

Outputs from the model show that freezing of the debris-laden ice at the bed of the ice stream during the surge phase of the ice stream's hypothesized binge/purge cycle can incorporate up to  $5.1 \times 10^{15}$  kg. This amount is sufficient to meet the constraints of the North Atlantic sediment record but, as acknowledged by the authors themselves, by no means verifies the binge/purge model as the cause of Heinrich events. Also, recent developments (Dowdeswell et al., 1999; Grousset et al., 2000; Scourse et al., 2000) indicate supply from European ice sheets as precursors to Laurentide Ice Sheet supply by up to 1.5 ka, thereby indicating a diversification of the sources for the total IRD mass.

Clearly, MacAyeal's binge/purge model (Figure 70) neglects the fact that the ice streams will commonly get afloat at one stage, either as part of an ice shelf (e.g. Ice Streams A, B and C at the Ross Ice Shelf) or as a floating ice tongue (e.g. Drygalski Ice Tongue). It therefore also neglects the potential impact of ice-ocean interactions and marine ice build-up on the IRD production mechanism. Using our increased knowledge of the diversity of marine ice formation processes described in the previous sections we can propose an improved version of the binge/purge process including the role of marine ice (Souchez et al., 1998). This is summarized in the sketches of Figure 71. The hypothesized impacts of marine ice are fourfold:

- (a) Initiation of double-diffusion freezing at the grounding line, when the thermodynamical regime at the bed of the Ice Stream switches from bottom freezing to bottom melting (Figure 71.2), will help preserving the layer of frozen debris from early release on the continental shelf
- (b) Initiation of the Deep Thermohaline Circulation (mode-1) as the sub-ice shelf cavity opens up at the middle to end of the purge phase will bring HSSW in contact with the frozen debris at the grounding line and favor early release of the debris to the continental shelf inside the cavity (Figure 71.4)
- (c) Initiation of the Shallow Thermohaline Circulation (mode-3) will favor melting at the ice shelf bottom near the front and further reduce the amount of debris left in the bottom ice of icebergs
- (d) Initiation of ice pump mechanisms in basal and frontal crevasses and rifts will transitionally stabilize the ice shelf flow, until increased warming eventually limits the HSSW production in front of the ice shelf, reduces the ISW associated marine ice production and finally weakens the welding marine ice units resulting in the ice shelf totally collapsing (Figure 71.4).

#### 4.4. Similarities with lake environments under large ice-sheets: the Vostok case

Investigating interactions at the ice-ocean interface has given us new tools to explore and understand processes occurring at other ice-water interfaces (Souchez et al., 2000). The most striking example is the formation of lake ice at the bottom of the Vostok ice core, in central Antarctica (Figure 72). The Vostok ice core has provided the longest record of past changes in climate and atmospheric composition, showing four glacial-interglacial cycles down to a depth of 3310 m (zone C in Figure 72). The ice at that depth is about 420 ky old. Between 3310 and 3350 m (Zone I), suggestions of complex ice deformation are difficult to interpret. Below zone I, the climatic record is no longer reliable, as shown by the Deuterium record. The decrease in magnitude (by a factor of at least 3) of this isotopic signal in zone



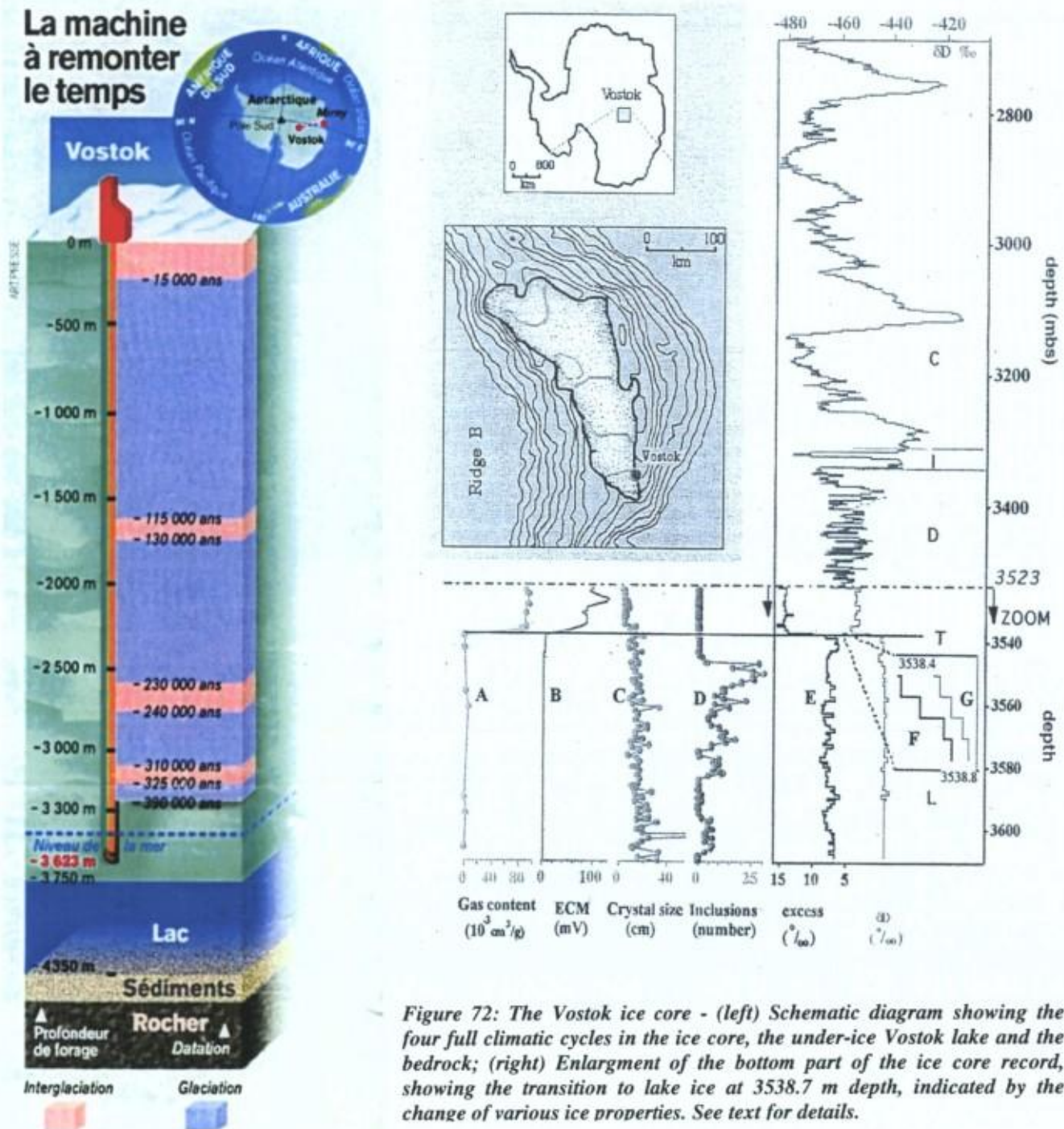


Figure 72: The Vostok ice core - (left) Schematic diagram showing the four full climatic cycles in the ice core, the under-ice Vostok lake and the bedrock; (right) Enlargement of the bottom part of the ice core record, showing the transition to lake ice at 3538.7 m depth, indicated by the change of various ice properties. See text for details.

D (between 3350 and 3538.3 m) cannot be of climatic origin, but rather must result from ice flow disturbances.

The lower part of the ice core, however, provides interesting and unique information. Jouzel et al. (1999) have shown using the changes in multiple variables (Figure 72) like the total gas content, the electrical conductivity (ECM - dc current), the crystal size, the solid impurity content and the stable isotopes, that the bottom 210 meters of the core actually consist of accreted lake ice. Stable isotopes probably provide the most decisive arguments. Samples from these bottom 210 meters are organized in a  $\delta\text{D}$ - $\delta^{18}\text{O}$  diagram in a cloud stretching along a straight line with a slope of 3.98 that Jouzel et al. (1999) show to be a "freezing slope" where ice samples resulting from the freezing of water would be located.



That freezing line intersects the Vostok precipitation line (corresponding to the ice samples from the past four climatic cycles, see footnote 3) at a point that is taken as the Vostok lake water isotopic composition.

An important observation made by Jouzel et al. (1999) is that the Deuterium and  $^{18}\text{O}$  enrichment of the lake ice in comparison to the lake water (6.6‰ in  $\delta\text{D}$  and 1.65‰ in  $\delta^{18}\text{O}$ ) is only about 60% of the corresponding isotopic equilibrium (11.4‰ in  $\delta\text{D}$  and 2.8‰ in  $\delta^{18}\text{O}$ ). This is in apparent contradiction with the fact that under such a large ice thickness, direct freezing under heat conduction through the ice shelf is bound to be extremely slow, i.e. to result in equilibrium isotopic fractionation at the interface. Jouzel et al. (1999) suggest that part of the liquid water may be trapped during ice accretion. Such water pockets would freeze completely afterward, and their bulk isotopic composition would not be modified. Therefore, the observed fractionation must be less than the true value, depending on how much water is included in water pockets in the ice during the course of freezing. This hypothesis however rests on unrealistic porosity values for known columnar/congelation ice resulting from the direct freezing of a liquid reservoir. Indeed, Cox and Weeks (1975) established the expression for brine volume in sea ice as a function of temperature and ice salinity as:

$$v_b = 1000 \left( \frac{S_i / \rho_b S_b}{S_i / \rho_b S_b + (1 - S_i / S_b) / \rho_i} \right) \quad (8)$$

where

$$\rho_i = 0.917 - 1.403 \times 10^{-4} T \text{ (}^\circ\text{C)} \quad (9)$$

$$\rho_b = 1.000 + 0.0008 S_b \quad (10)$$

$$S_b = \alpha_1 T + \alpha_2 T^2 + \alpha_3 T^3 \quad (11)$$

$$\alpha_1 = -17.573$$

$$\alpha_2 = -0.381246$$

$$\alpha_3 = -3.28366 \times 10^{-3}$$

$S_i$  = sea ice salinity

$T$  = temperature in  $^\circ\text{C}$

Applying these equations with an ice salinity of 6‰ (mean arctic sea ice salinity) and a temperature of  $-3.1^\circ\text{C}$  (ice water interface temperature deduced from linear extrapolation of the thermal gradient calculated at 3600 m depth in the Vostok core) gives a porosity of 10.5%, far from the value of about 40% required to explain the isotopic shift of 60% of the equilibrium fractionation. Furthermore, the maximum lake ice bulk salinity is only of about 2 ppm (Souchez et al., 2000), i.e. 0.0002%. With such low salinity values, a planar growth interface is certainly stable (as opposed to the cellular interface developed in sea ice because of constitutional supercooling (e.g. Weeks and Ackley, 1986)), and the relationships above probably breakdown to negligible brine volume values.

The presence of subglacial lake Vostok is related to the geothermal heat flux, the temperature of the ice at the ice-water interface being that of the melting point. The

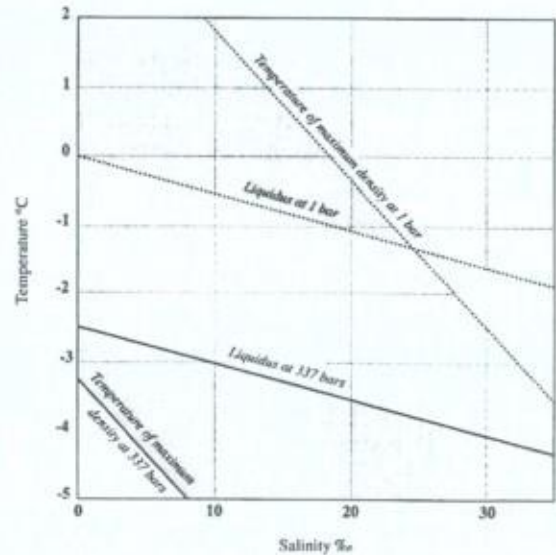


Figure 73: Temperature of maximum density of water and freezing temperature versus salinity at atmospheric pressure and at 337 bar. Values were computed from the general state equation of sea water (Souchez et al., 2000).



ice ceiling of the lake is tilted, being at 750 m below sea level under 4300 m of ice in the North and at 250 m below sea level under 3750 m of ice in the South near Vostok Station. Figure 73 gives, at a pressure of 337 bar corresponding to an ice thickness of 3750 m, the temperature of maximum density of water versus salinity and the freezing temperature versus the salinity. It can be clearly seen that, whatever the salinity, the freezing temperature is first reached when water is cooled so that, closer to the freezing point, water has a higher density. The consequence of this fact is an unstable water column for geothermal heating from below since warmer water is less dense. Wüest and Carmack (2000) combine this notion with the fact that a temperature gradient must exist along the ice-water interface, because of the tilted ceiling, to construct a model of water circulation in the lake. In this model, salinity is not considered as a factor. However, we have shown (Souchez et al., 2000) that a rough estimation of the Lake Vostok salinity can be reconstructed from the lake ice impurity content (about 1 ppm at 3600 m depth), using reasonable estimates of the effective fractionation coefficient for diluted waters ( $k_{eff} \approx k_{eq}$  given the very slow consolidation freezing rate— see discussion in section 3.4.). Taking a  $k_{eff}$  range of 0.0008 to 0.0028 results in a lake water salinity prediction between 0.4 and 1.2 ‰. Although a 0.4 ‰ salinity will not change the general behaviour of lake waters, it will strongly enhance the water circulation pattern. At a pressure of 337 bars, a difference of 0.37 °C in temperature corresponding to the difference in the pressure melting temperature between the northern and the southern part of the lake at the ice-water interface gives a difference in  $\sigma_w$  of about 0.03.  $\sigma_w$  is equal to  $1000 (\rho_w - 1)$  where  $\rho_w$  is the water density. By contrast, at the same pressure, a difference in salinity of 0.4 ‰, like that between lake water and pure glacial meltwater, gives a difference in  $\sigma_w$  of about 0.32. Even a weak salinity must therefore be taken into account to complete the picture of water circulation in lake Vostok.

Water circulation in the Vostok lake clearly shows strong similarities with the Deep Thermohaline circulation observed below ice shelves. The question then arises if an equivalent to the ice pump mechanism associated with the oceanic DTC is not a reasonable alternative to the direct congelation process under heat conduction through the ice sheet, to explain the formation of Vostok lake ice. Let us consider rising meltwaters from the ice-water interface from the northern part of the lake where melting occurs. The rising plume is the consequence of thermal and also probably salinity effects. Such waters will become supercooled as they rise. The maximum water supercooling would be the difference in melting points between the deeper and the upper parts of the lake at the ice-water interface. Nucleation will however start in the rising water for lower supercooling levels. A reasonable range of supercooling is between 0.01°C and 0.1°C. For such values, growth velocities of frazil ice crystals in fresh water are between  $10^{-6}$  and  $5 \cdot 10^{-5} \text{ m s}^{-1}$  (Hobbs, 1974). As we have seen in section 3.4., observed isotopic fractionation between ice and water in open systems ( $k_{eff}$ ) can be described by Burton's equation (5). Using the supercooling range and the associated growth rates mentioned above with a reasonable boundary layer thickness of 0.1 cm, calculations indicate that the frazil ice crystals will have an isotopic enrichment in  $\delta D$  between 4.56 ‰ and 0 ‰ respectively, compared to the lake water (Table 4). A higher supercooling will of course lead to higher growth rate and thus, a fortiori, to no isotopic enrichment in the frazil ice crystals.

Table 4: Calculated proportion of frozen host water in lake ice deduced from its isotopic composition. Burton's equation (5) is used with boundary layer thickness = 1 mm;  $\alpha_{eq} = 1.0208$ ;  $D = 1.1 \times 10^{-9} \text{ m}^2 \text{ sec}^{-1}$ ;  $\delta D_{\text{bulk lake ice}} = -442.7\text{‰}$ ;  $\delta D_{\text{water}} = -449.3\text{‰}$ ;  $\delta D_{\text{frazil host water}} = -437.9\text{‰}$  (Souchez et al., 2000)

Water supercooling	Crystal growth rate	Effective fractionation coefficient	$\delta D_{\text{frazil}}$	Frazil	Frozen host water
(°C)	(m sec <sup>-1</sup> )	( $\alpha_{eff}$ )	(‰)	(%)	(%)
0.01	$10^{-6}$	1.0083	-444.74	70	30
0.1	$5 \times 10^{-5}$	1.0000	-449.3	42	58



Now, consolidation of loose frazil ice crystals by freezing the host water is a very slow process, thus at isotopic equilibrium. The isotopic composition of the bulk lake ice, can therefore be understood by a simple mixing between the composition of the individual frazil ice crystals and the one of the frozen host water, in which the frozen host water represents between 30 and 58 % of the bulk lake ice (Table 4). Such values are comparable to those obtained in experimental and field studies of frazil ice formation (Andersson and Daly, 1992; White, 1991). The characteristics of the isotopic composition of the lake ice thus strongly support the occurrence of a mechanism similar to marine ice formation under an ice shelf, involving consolidation of loose frazil ice crystals accreted at the ice ceiling of the lake.

#### 4.5. Challenge for the future

We hope to have shown with this Thesis that ice-ocean interactions play an important role in the processes controlling ice shelves stability. Despite the fact that we believe to have unveiled part of the picture, there is still a fair way to walk towards a fully quantitative assessment of the impact of these various complex processes and feedbacks on ice sheet stability in a warming climate. We would therefore like to close this exercise by suggesting a few directions that we consider as first order priority for future work on the topic.

##### 4.5.1. Field work

Our major effort in the coming field seasons should focus on documenting the ice accumulation in the major rifts fringing the border of the Filchner-Ronne, the Amery and the Ross Ice Shelves in order to get a better estimate of ice thicknesses, ice types and properties (marine ice vs. "ice melange"). This would provide further validation of Khazendar's rift model and improve our perception of the "weak links" in these major ice shelves. Repeated visits to a few strategic areas (like the Antarctic Peninsula) of more sensitive ice shelves would also be quite valuable to follow a potential degradation of the "welding" efficiency inside those rifts, and better understand the underlying weakening processes (surface atmospheric vs. bottom oceanic warming). These glaciological investigations should obviously be supported by oceanographic measurements to build a complete picture.

Further exploration of those rare opportunities we have to see marine ice rift filling processes in action as close as possible to grounding lines, like in the Nansen Ice Sheet area, would help us in understanding the early stages of the process and therefore provide a sound basis for future modelling developments.

##### 4.5.2. Experimental work

Clearly, tackling the difficult problem of welding efficiency of the rift fillings relies on a better perception of the rheological properties of both marine ice and the composite rift *melange* considered by Rignot and Mac Ayeal (1998). Experimental settings for testing the mechanical properties of meteoric and sea ice in a wide range of stress configurations are well documented in the literature. It shouldn't therefore be a major problem to adapt those to study the rift ice rheology in realistic stress conditions.

Our first attempt to model the acquisition of the stable isotope composition and the bulk salinity in marine ice from the Nansen Ice Sheet (section 3.4.), with a boundary layer type of approach, has brought up the need for a better knowledge of some fundamental variables, like, for example, the equilibrium fractionation factor in granular media (including its possible dependency on the freezing rate). More fundamentally, the detailed process of coarsening and sintering of frazil ice discs in a water suspension submitted to pressure and/or a heat sink needs to be better understood. Our experience is that a lot can be gained from simple and well-designed laboratory experiments dedicated to those questions. This should be another priority in our research activity.



#### 4.5.3. *Modelling work*

We have started this exercise by underlining how performing present-day 3-D models of the Antarctic Ice Sheet show it as rather insensitive to the expected temperature changes for the next century (3-5 °C). Our investigations on marine ice diversity, both spatially and in terms of genetic processes, and the discussion on the potential implications of its occurrences call for explicitly including ice-ocean interactions in our predictive models for ice-sheet stability and sea level rise. This involves the difficult tasks to:

- (a) Solve the problem of modelling temporary discontinuities to account for the peculiar stress transition at the grounding line involving crevasses and rift generation
- (b) Couple glaciological and oceanographical models on a reasonably small scale to account for surface and bottom melting and freezing processes along the ice shelf flow line
- (c) Use the outputs from those meso-scale models as inputs for the large-scale models (nested grids?)



**Paper 13**

**Freezing at the Grounding Line in East Antarctica: Possible Implications for Sediment Export Efficiency**

**Authors**

**R. Souchez, A. Khazendar, D. Ronveaux, J.-L. Tison**

**Journal**

**Annals of Glaciology, Vol. 27**

**Year**

**1998**



## Freezing at the grounding line in East Antarctica: possible implications for sediment export efficiency

R. SOUCHEZ,<sup>1</sup> A. KHAZENDAR,<sup>1</sup> D. RONVEAUX,<sup>2</sup> J.-L. TISON<sup>1</sup>

<sup>1</sup>Département des Sciences de la Terre et de l'Environnement, Faculté des Sciences, Université de Bruxelles, B-1050 Brussels, Belgium

<sup>2</sup>Department of Geography, Temple University, Philadelphia, PA 19122, U.S.A.

**ABSTRACT.** A study of the  $\delta D$  and  $\delta^{18}O$  composition of ice formed at or near the grounding line was undertaken in Terra Nova Bay, East Antarctica. The results indicate that a double-diffusion mechanism is responsible for freezing at the grounding line in areas sheltered from the sub-ice cavity circulation. Freezing at the grounding line is unlikely to be prevalent today, but the situation may have been different in the past when the ice reached the outer limit of the continental shelf and there was no sub-ice cavity. The implications for sediment export in the polar oceans are explained.

### INTRODUCTION

Ice-rafted debris from icebergs derives mostly from subglacial entrainment by glaciers or ice sheets. The ice-substratum interface is a place where particles can be incorporated into the glacier sole. The basal debris can then be carried by glacier flow and reach the ocean if the ice mass begins to float. In order for the debris to be preserved in the basal ice at the front of a floating glacier or of an ice shelf, it must not have been released at the grounding line. If the melting point is reached at the glacier base in the coastal region and if melting prevails at the grounding line, subglacial meltwater loaded with sediments discharges there into the sea. The probability of preservation of basal debris in the frontal zone greatly increases if freezing occurs at or near the grounding line.

This paper investigates conditions for freezing at the grounding line. It uses stable isotopes to give evidence that such a situation occurs in Terra Nova Bay, East Antarctica.

### PRESENT-DAY CONDITIONS AT GROUNDING LINES

The grounding line is usually defined as a line across the glacier where it goes afloat. However, it can also be considered as the limit between grounded ice and floating ice. Therefore, a grounding line exists if the glacier goes afloat or becomes grounded again. With such an extended definition in mind, the grounding line is in fact a transition zone between a grounded glacier or ice sheet and a floating glacier or ice shelf where the ice repeatedly loses and regains contact with the subglacial bed before eventually floating. It is relevant to consider such a transition zone in a work focusing on possible phase changes.

Drillings through ice shelves show evidence of accretion of marine ice layers under ice of meteoric origin (Zotikov and others, 1980; Oerter and others, 1992). In the upper part of marine shelf ice from the Filchner-Ronne Ice Shelf, Oerter and others (1992) showed the existence of particle inclusions in conjunction with horizontal layering. The inclusions most probably result from scavenging during marine

ice formation. However, the overwhelming absence of debris layers between meteoric ice and marine ice suggests the absence of adfreezing at the grounding line. In general, available evidence favors melting rather than freezing.

Today, the frontal zone of most of the medium-sized and small ice shelves in Antarctica is well upstream of the maximum extent of the ice during the Last Glacial Maximum (LGM). Since glacio-isostatic loading of the crust has resulted in a depression of the coastal zone upstream of the continental slope or since overdeepening by ice flows has occurred, a cavity usually exists between the ice shelf and the ocean floor. This sub-ice cavity is subject to a specific oceanic circulation (Jacobs and others, 1992). Surface sea water in front of the ice shelf plunges because its density increases by release of sea salts during sea-ice formation. This water, at depth (high-salinity shelf water, HSSW), is above its pressure-melting point since the freezing point of sea water is lower when pressure increases (Lewis and Perkin, 1986). Therefore, this water has at depth sensible heat to transfer to the base of the floating ice. Melting occurs and the less dense water so produced leaves the cavity as ice-shelf water (ISW). Hence, melting rather than freezing must prevail today at or near the grounding line. If marine ice forms, it is mainly by accretion of frazil-ice crystals generated in the supercooled ISW as it rises towards the surface. The absence of plunging waters is thus a prerequisite for possible freezing at the grounding line.

### EVIDENCE FOR FREEZING CLOSE TO GROUNDING LINES IN TERRA NOVA BAY

The Hells Gate Ice Shelf in Terra Nova Bay (Fig. 1) was studied in detail. Because of the action of katabatic winds, the ice surface is losing ice, mostly by sublimation. Since top-surface ablation is prevalent, an upward velocity component exists and the marine ice formed at the ice-shelf-ocean interface ultimately appears at the surface. Debris-rich ice is present under the moraine ridges which appear at the separation between different ice flows. The western moraine ridge is located along a flowline that connects with



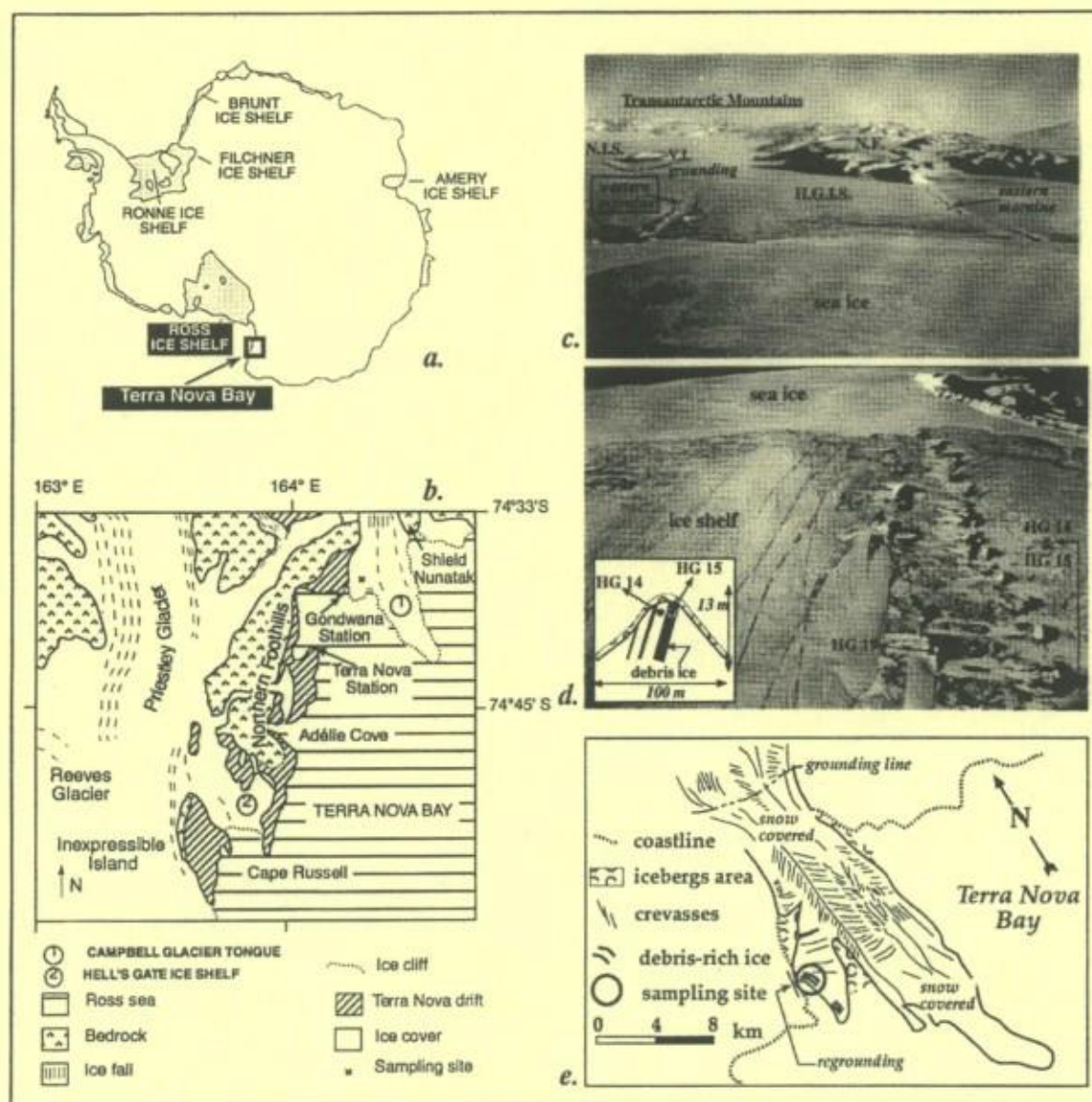


Fig. 1. Sampling sites in Terra Nova Bay area: (a, b) general location; (c) oblique view of Hells Gate Ice Shelf (HGIS) looking upstream; N.I.S., Nansen Ice Sheet; VI, Vegetation Island; NF, Northern Foothills; (d) closer view of the western moraine from HGIS looking downstream, with ice-core locations and detailed sketch for cores HG 14 and HG 15; (e) detailed sketch of Campbell Glacier Ice Tongue with sampling site.

Vegetation Island, a pinning point of the ice shelf. There is little doubt that the debris forming the ridge has been entrapped into the ice at the base. Like the marine ice, because of ablation, the debris appears at the surface and forms an ice-cored ridge.

A detailed investigation of the ice at the level of the western moraine ridge shows not only debris and clear-ice layers but also sponge remains in growth position and serpulid worm tubes. It is difficult to interpret the significance of the presence of these serpulid worm tubes since Adélie penguins, which are numerous in the area, are known to build small hillocks from them. As shown by photographs from a robotic submarine, sponges are growing near a grounding line (Powell and others, 1996). Sponge remains in growth position can be incorporated into the ice shelf

because of anchor-ice formation on the sea floor. Dayton and others (1969) indicated that, in McMurdo Sound, anchor ice develops to about 33 m depth on the sea floor. When it becomes detached, because of inherent buoyancy, it floats to the undersurface of an ice cover, carrying with it portions of the substratum which can weigh at least 25 kg. By this process, sponges can be incorporated into the ice shelf. Because of their location well upstream in the ablation zone of the Hells Gate Ice Shelf, these sponge remains must have been incorporated near the grounding line. The bottom water where the sponges were growing must not have been above the pressure-melting point in order for anchor ice to be formed. Therefore, the area where the sponges have grown must have been sheltered in some way from the influence of HSSWs, which would be above their freezing point at depth.



*Souchez and others: Freezing at grounding line in East Antarctica*

Other evidence supporting the possibility that certain areas are sheltered from sub-ice cavity circulation can be inferred from temperature and salinity measurements made in front of the ice shelf (Tison and others, in press). Oceanic profiles down to 600 m depth show a transition between ISW and HSSW below 440 m. However, typical high-salinity shelf waters were not observed in the profiles. This suggests that plunging of HSSW affects only a narrow central trough more than 700 m deep that exists beneath the ice shelf (Stocchino, 1991). Since a maximum ice thickness of about 200 m (personal communication from I. E. Tabacco, 1997) was observed immediately downstream of Vegetation Island, there must be sheltered sea-floor areas where anchor ice can develop away from the influence of HSSW.

Bathymetric information available (Stocchino, 1991) in the Campbell Glacier Ice Tongue area also suggests a sheltering effect where the debris-rich ice formed near the grounding line originated (Souchez and others, 1995).

**FREEZING BY A DOUBLE-DIFFUSION MECHANISM AT THE GROUNDING LINE**

Zotikov (1986) discussed at length the various possible processes controlling the mass balance at the bottom of an ice shelf. Using the Amery Ice Shelf as a case-study, this author suggested heat transfer between a water layer of reduced salinity and sea water to explain the abnormally high freezing rates deduced from temperature profiles across the ice shelf. Lambert outlet glacier, at the bottom of which melting takes place because of enhanced ice thicknesses, is seen as a connection between the basin of subglacial runoff from the ice-sheet center and the sea. It provides the source for out-flowing waters of reduced salinity under lithostatic load. A rough calculation assuming no mixing between the two water layers, salinity differences of about 20‰ and relative flow velocities of about  $10 \text{ cm s}^{-1}$  provided freezing rates of about  $1 \text{ m a}^{-1}$ , in accordance with the observed rates. This mechanism, however, requires the sea water to be at its local freezing point, which precludes areas under the influence of a sub-ice cavity circulation. On the other hand, the "no-mixing hypothesis" is a rather constraining one, especially given the fact that there is evidence (MacAyeal, 1984) of efficient tidal mixing near grounding lines. A double-diffusion process within the pores of subglacial sediments, in areas sheltered from the Deep Thermohaline Convection, is therefore worth considering. In these areas, at some distance upstream from the actual decoupling of the glacier from its bed, sea water seeping through the sediments will come into contact with continental meltwaters (Fig. 2). Because the freezing point of sea water is lower than that of continental meltwater, heat diffusion will occur. Heat will diffuse through both liquid and solid fractions from upstream to sea water. On the other hand, the salinity of sea water being higher than that of continental meltwater, salts will diffuse from the sea-water-saturated sediment into the meltwater-filled subglacial sediment. Salts can diffuse only through liquid, unlike heat. Thermal diffusivity is also an order of magnitude higher than salt diffusion. The meltwater-filled sediment loses heat more rapidly than it gains salt, and freezing occurs, welding the sediments to the bottom of the ice. Since this mechanism occurs within the subglacial sediments, rapid mixing between continental meltwater and sea water is precluded.

If the extended definition of the grounding line is considered, freezing can occur at different places, depending on variable water fluxes. Also, if the ice makes contact with a protuberance of the substratum in this critical area, pressure melting and regelation is likely to take place.

Such a double-diffusion mechanism leading to freezing at the grounding line would explain not only incorporation of debris into the glacier sole but also preservation of debris-rich ice already present upstream in the basal zone.

Is there evidence that such a process really occurs? The isotopic composition of debris-rich ice sampled in the region of Terra Nova Bay gives information on this question.

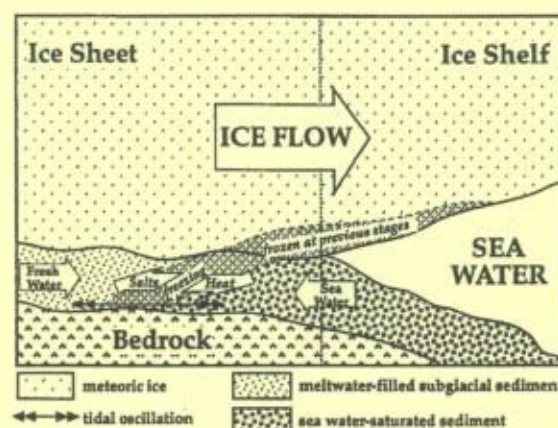


Fig. 2. Sketch of the suggested freezing mechanism by double diffusion at the grounding line.

**ISOTOPIC EVIDENCE OF THE DOUBLE-DIFFUSION MECHANISM**

Samples of bubbly glacier ice which reaches the sea in Terra Nova Bay (Fig. 3, inset), are aligned on a straight line in a  $\delta D$ - $\delta^{18}O$  diagram with equation  $\delta D = (7.91 \times \delta^{18}O) + 2.59$

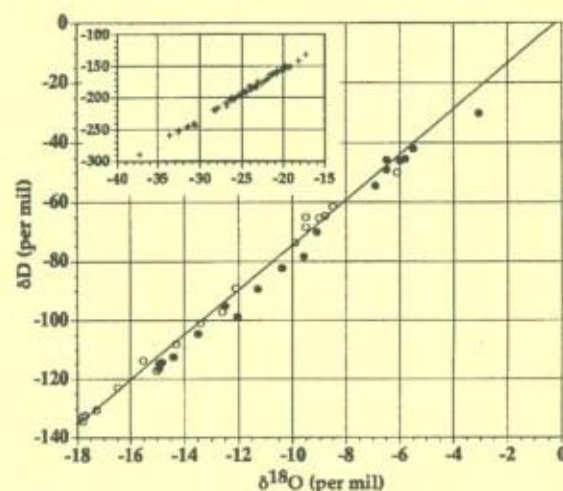


Fig. 3.  $\delta D$ - $\delta^{18}O$  diagram of the studied basal ice samples from Terra Nova Bay. Black circles: ice samples; open circles: initial water samples computed from  $\delta$  values of ice samples and equilibrium fractionation coefficients. The straight line represents the best-fit line for the waters. Inset shows the  $\delta D$ - $\delta^{18}O$  diagram of glacier ice samples from the area.



(correlation coefficient 0.997; 55 samples). The  $\delta$  values are more negative than  $-17\text{‰}$  in  $\delta^{18}\text{O}$  and  $-130\text{‰}$  in  $\delta\text{D}$ . The straight line which can be considered as a local Meteoric Water Line or precipitation line goes close to Standard Mean Ocean Water. The  $\delta$  values of the meltwaters from glacier ice will have the same isotopic composition since there is no fractionation on glacier ice melting.

By contrast, the debris-rich ice layers, thought to have been formed near the grounding line, from the western moraine ridge of Hells Gate Ice Shelf and from the site studied in Campbell Glacier Ice Tongue (Souchez and others, 1995) have  $\delta$  values of  $-15\text{‰}$  to  $-3\text{‰}$  in  $\delta^{18}\text{O}$ , and  $-120\text{‰}$  to  $-30\text{‰}$  in  $\delta\text{D}$ . Detailed sampling locations at both sites are shown in Figure 1. A thorough description of the samples collected at Campbell Glacier Ice Tongue is given in Souchez and others (1995). The samples from Hells Gate Ice Shelf are from three shallow (2 m) ice cores drilled below the surficial dirt layers of two major dirt-ice cones located on the western moraine (Fig. 1). The textures of the cores were similar to those described for ice type 2 at Campbell Glacier, showing interlayering of debris layers with bubbly- and clear-ice layers at centimetric to decimetric scales. The bubbly-ice layers show typical meteoric-ice values, and the clear-ice/dirt-ice values are in the range  $-3.07\text{‰}$  to  $-12.50\text{‰}$  in  $\delta^{18}\text{O}$  and  $-30.03\text{‰}$  to  $-98.90\text{‰}$  in  $\delta\text{D}$ . Samples from all cores are well aligned in a  $\delta\text{D}-\delta^{18}\text{O}$  diagram on a straight line (Fig. 3), the equation for which is  $\delta\text{D} = (7.71 \times \delta^{18}\text{O}) - 1.15$  (correlation coefficient: 0.993; 18 samples).

Progressive freezing downwards in a water mass or in a subglacial sediment produced, for example, by ice-thickness variations cannot explain this last distribution. Indeed, the observed slope is steeper than a freezing slope would be, and the ranges of  $\delta$  values are such that near-complete freezing of the reservoir (99%) would be required to understand the most negative  $\delta$  values (Souchez and Jouzel, 1984). Ice intrusion of a subglacial sediment by pressure-induced regelation past grains is also precluded since the isotopic signature of such a process would have been different (Iverson and Souchez, 1996). On the other hand, pressure melting and regelation do not significantly modify the isotopic properties of the ice submitted to this process (Souchez and others, 1988).

If glacier-ice meltwater within the subglacial sediment enters into contact with sea water at the grounding line, diffusion will occur. Like salts, heavy isotopes of oxygen and hydrogen will diffuse from sea water, where they are less impoverished, to continental meltwater, where they are more depleted. Diffusion coefficients of stable isotopes and of salts in liquid water have the same order of magnitude, so that the double-diffusion mechanism described above also leads to isotopic diffusion. Therefore, the isotopic composition of the debris-rich ice layers formed by freezing will be dependent on the magnitude of the diffusion process prior to freezing. Isotopic composition is likely to be a better indicator of the process than the salt content since the different isotopes are within the lattice of the ice formed and only subjected, on very long time-scales, to solid-state diffusion.

From the isotopic composition of the ice layer formed, it is possible to reconstruct that of the initial water. Freezing at the subglacial site near the grounding line is most probably very slow, so that equilibrium fractionation can be considered. Therefore, taking into account the equilibrium fractionation coefficients for deuterium and oxygen-18 and the respective  $\delta$  values of the ice, it is possible to compute the

*Souchez and others: Freezing at grounding line in East Antarctica*

isotopic composition of the water which was later partially frozen. The best-fit line for the waters (Fig. 3) has the following equation:  $\delta\text{D} = (7.63 \times \delta^{18}\text{O}) + 1.9$  ( $r = 0.993$ ). This line goes close to points representing  $\delta$  values of sea water in the area and  $\delta$  values of meltwaters from glacier ice.

Isotopic diffusion within the water-filled subglacial sediment submitted to freezing by a double-diffusion mechanism seems thus to be the process explaining the peculiar distribution in the  $\delta\text{D}-\delta^{18}\text{O}$  diagram.

## IMPLICATIONS

Field observations from the present Interglacial indicate prevailing melting conditions at the base of the major Antarctic ice shelves (Jacobs and others, 1992). Models of the Deep Thermohaline Convection in sub-ice-shelf cavities have provided estimates of melt rates and growth rates (marine ice) under various areas of the Filchner-Ronne and Amery ice shelves (Bombosch and Jenkins, 1995; Jenkins and Bombosch, 1995; Grosfeld and others, 1997; Williams and others, 1998). Using a modeled mean bottom melting rate of  $0.20 \text{ m a}^{-1}$  over 400 km in a downstream direction from the grounding line (Jenkins and Bombosch, 1995) and mean surface velocities of  $500 \text{ m a}^{-1}$  (Jenkins and others, 1994), the bottom 160 m of the Ronne Ice Shelf will be lost before marine-ice accretion begins. Considering that observed basal debris-rich sequences at the bottom of ice tongues at the grounding lines do not exceed a few tens of meters, it is not surprising to find meteoric/marine ice interfaces devoid of significant sediment loads. During the glacial stages, however, the Antarctic ice sheet must have partly or fully refilled the sub-ice-shelf cavities and submarine trenches carved during the previous stages, thereby strongly inhibiting the Deep Thermohaline Convection. Therefore, conditions for freezing by a double-diffusion effect, i.e. conditions for preservation of basal debris to the frontal zone in contact with the ocean, would have been more prevalent than today. To what extent this mechanism will allow transport of basal sediments through iceberg drifts off the continental shelves is still conjectural. Recent work in the Prydz Bay area (Domack and Harris, 1998) shows that the grounding line did not make it to the continental shelf edge during the LGM. However, the situation may have been somewhat different in the Northern Hemisphere or for previous glacial stages in Antarctica. The present work points to the need to include grounding-line adfreezing processes in the development of the general picture, in order to fully understand typical events of sediment export to the Deep Sea, like the "Heinrich events" in the North Atlantic. The grounding line is indeed a spot of compelled passage for subglacial debris on its way to the ocean.

## ACKNOWLEDGEMENTS

The authors would like to acknowledge the help received from the Italian Antarctic Program which made possible the ice sampling in Terra Nova Bay. This paper is a contribution to the Belgian Antarctic Program (Science Policy Office). J.-L. Tison is Research Associate at the Fond National de la Recherche Scientifique.



*Souchez and others: Freezing at grounding line in East Antarctica*

## REFERENCES

- Bombosch, A. and A. Jenkins. 1995. Modeling the formation and deposition of frazil ice beneath Filchner-Ronne Ice Shelf. *J. Geophys. Res.*, **100**(C4), 6983-6992.
- Dayton, P. K., G. A. Robilliard and A. L. DeVries. 1969. Anchor ice formation in McMurdo Sound, Antarctica, and its biological effects. *Science*, **163**(3864), 273-274.
- Domack, E. W. and P. T. Harris. 1998. A new depositional model for ice shelves, based upon sediment cores from the Ross Sea and Mac. Robertson shelf, Antarctica. *Ann. Glaciol.*, **27** (see paper in this volume).
- Grosfeld, K., R. Gerdes and J. Determann. 1997. Thermohaline circulation and interaction between ice shelf cavities and the adjacent open ocean. *J. Geophys. Res.*, **102**(C7), 15,595-15,610.
- Iverson, N. and R. Souchez. 1996. Isotopic signature of debris-rich ice formed by regelation into a subglacial sediment bed. *Geophys. Res. Lett.*, **23**(10), 1151-1154.
- Jacobs, S. S., H. H. Hellmer, C. S. M. Doake, A. Jenkins and R. M. Frolich. 1992. Melting of ice shelves and the mass balance of Antarctica. *J. Glaciol.*, **38**(130), 375-387.
- Jenkins, A. and A. Bombosch. 1995. Modelling the effects of frazil ice crystals on the dynamics and thermodynamics of ice shelf water plumes. *J. Geophys. Res.*, **100**(C4), 6967-6981.
- Jenkins, A., D. Vaughan and C. Doake. 1994. Numerical modelling of Filchner-Ronne Ice Shelf. In Oerter, H., ed. *Filchner-Ronne Ice Shelf Programme. Report 8*. Bremerhaven, Alfred Wegener Institute for Polar and Marine Research, 36-38.
- Lewis, E. L. and R. G. Perkin. 1986. Ice pumps and their rates. *J. Geophys. Res.*, **91**(C10), 11,756-11,762.
- MacAyeal, D. R. 1984. Thermohaline circulation below the Ross Ice Shelf: a consequence of tidally induced vertical mixing and basal melting. *J. Geophys. Res.*, **89**(C1), 597-606.
- Oerter, H. and 6 others. 1992. Evidence for basal marine ice in the Filchner-Ronne Ice Shelf. *Nature*, **358**(6385), 399-401.
- Powell, R. D., M. Dawber, J. N. McInnes and A. R. Pyne. 1996. Observations of the grounding-line area at a floating glacier terminus. *Ann. Glaciol.*, **22**, 217-223.
- Souchez, R. A. and J. Jouzel. 1984. On the isotopic composition in  $\delta D$  and  $\delta^{18}O$  of water and ice during freezing. *J. Glaciol.*, **30**(106), 369-372.
- Souchez, R., R. Lorrain, J.-L. Tison and J. Jouzel. 1988. Co-isotopic signature of two mechanisms of basal-ice formation in Arctic outlet glaciers. *Ann. Glaciol.*, **10**, 163-166.
- Souchez, R. and 6 others. 1995. Investigating processes of marine ice formation in a floating ice tongue by a high-resolution isotopic study. *J. Geophys. Res.*, **100**(C4), 7019-7025.
- Stocchi, C. 1991. *Carta batimetrica, Mare di Ross — Baia Terra Nova. Second edition*. Genova, Istituto Idrografico della Marina. (Scale 1:50 000).
- Tison, J.-L., C. Barbante, A. Bondesan, R. Lorrain and A. Capra. In press. Ice shelf-ocean interactions at the front of Hells Gate Ice Shelf (Terra Nova Bay, Antarctica). *Terra Antarctica*.
- Williams, M. J. M., R. C. Warner and W. F. Budd. 1998. The effects of ocean warming on melting and ocean circulation under the Amery Ice Shelf, East Antarctica. *Ann. Glaciol.*, **27** (see paper in this volume).
- Zotikov, I. A. 1986. *The thermophysics of glaciers (Teplofizika lednikovyykh pokrovov)*. Dordrecht, D. Reidel Publishing Co.
- Zotikov, I. A., V. S. Zagorodnov and J. V. Raikovsky. 1980. Core drilling through the Ross Ice Shelf (Antarctica) confirmed basal freezing. *Science*, **207**(4438), 1463-1465.



**Paper 14**

**Ice Formation in Subglacial Lake Vostok, Central Antarctica**

**Authors**

**R. Souchez, J.-R. Petit, J.-L. Tison, J. Jouzel, V. Verbeke**

**Journal**

**Earth and Planetary Science Letters, Vol. 181**

**Year**

**2000**





EPSL

Earth and Planetary Science Letters 181 (2000) 529–538

www.elsevier.com/locate/epsl

## Ice formation in subglacial Lake Vostok, Central Antarctica

R. Souchez<sup>a,\*</sup>, J.R. Petit<sup>b</sup>, J.-L. Tison<sup>a</sup>, J. Jouzel<sup>c</sup>, V. Verbeke<sup>a</sup>

<sup>a</sup> *Département des Sciences de la Terre et de l'Environnement, Faculté des Sciences, CP 160103, Université Libre de Bruxelles, 50, avenue F.D. Roosevelt, B-1050 Brussels, Belgium*

<sup>b</sup> *Laboratoire de Glaciologie et de Géophysique de l'Environnement, CNRS, Grenoble, France*

<sup>c</sup> *Laboratoire des Sciences du Climat et de l'Environnement, CEA, Saclay, France*

Received 4 February 2000; accepted 17 July 2000

### Abstract

The investigation of chemical and isotopic properties in the lake ice from the Vostok ice core gives clues to the mechanisms involved in ice formation within the lake. A small lake water salinity can be reasonably deduced from the chemical data. Possible implications for the water circulation of Lake Vostok are developed. The characteristics of the isotopic composition of the lake ice indicate that ice formation in Lake Vostok occurred by frazil ice crystal generation due to supercooling as a consequence of rising waters and a possible contrast in water salinity. Subsequent consolidation of the developed loose ice crystals results in the accretion of ice to the ceiling of the lake. © 2000 Elsevier Science B.V. All rights reserved.

**Keywords:** stable isotopes; glacial geology; ice; Vostok Station; Antarctica

### 1. Introduction

Subglacial Lake Vostok in Central Antarctica has an area of about 14 000 km<sup>2</sup> and a water depth of about 600 m in its southern part. Gorman and Siegert [1] showed that it was shallow in its northern part in a few places. The presence of subglacial Lake Vostok is related to the geothermal heat flux, the temperature of the ice at the ice–water interface being that of the melting point.

The ice ceiling of the lake is tilted, being at 750 m below sea level under 4300 m of ice in the north

and at 250 m below sea level under 3750 m of ice in the south near Vostok Station. Therefore a gradient of the pressure-dependent melting point must exist at the base of the tilted ice ceiling [2,3]. Wüest and Carmack [4] indicate that, at a glacio-static pressure of more than 3350 m of ice, the temperature of maximum density of fresh water is lower than the freezing temperature. Therefore, subglacial Lake Vostok behaves as an ocean. The gradient of the freezing point along the ice–water interface and the geothermal heat flux are responsible for convection. In such a situation, melting occurs at the ‘thick-ice’ side and freezing at the ‘thin-ice’ side [5]. At the scale of the lake, there must be a dynamic equilibrium between melting and freezing.

The aim of this paper is to derive ice formation processes in subglacial Lake Vostok from a study

\* Corresponding author. Tel.: +32-2-650 22 16; Fax: +32-2-650 22 26; E-mail: glaciol@ulb.ac.be



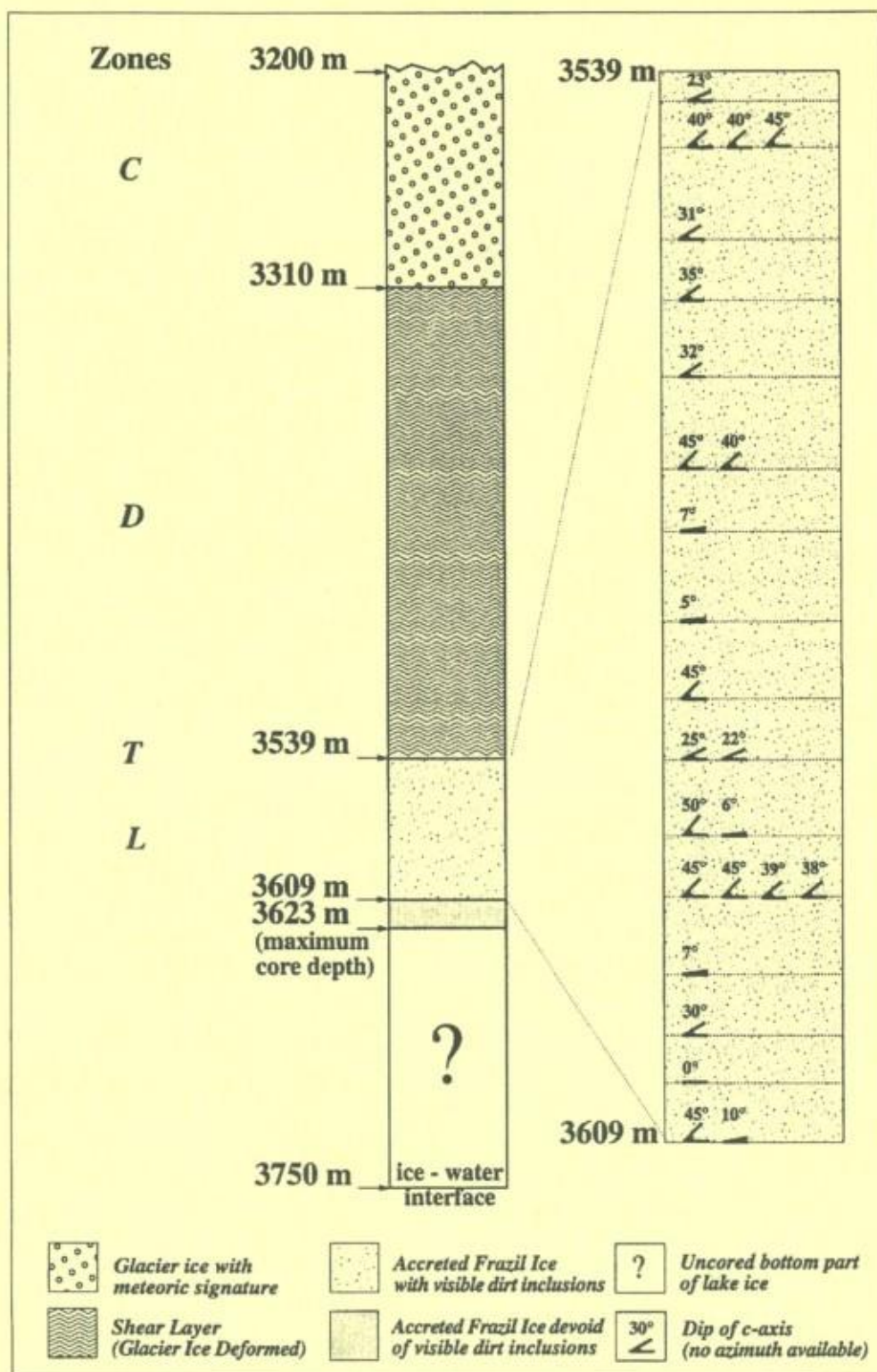


Fig. 1. The different ice types in the Vostok ice core. The dip of each ice crystal measured is indicated by the angle with the horizontal.



of the lake ice retrieved by deep drilling at Vostok Station.

## 2. Relevant information from ice core studies

In the Vostok ice core, there are two distinct types of ice separated by a very sharp transition at a depth of 3539 m (Fig. 1). The ice just above that depth is typically ice of glacial origin from the ice sheet although it is disturbed and its climatic record has been modified. The ice below that depth is lake ice accreted at the bottom of the ice sheet. Jouzel et al. [6] showed that this is clearly indicated by a change in isotopic properties. The  $\delta D$  values exhibit a 10‰ increase at the transition, from about  $-452.5$ ‰ to  $-442.5$ ‰, and remain stable in the lake ice profile underneath (Fig. 2). The deuterium excess similarly decreases from a value of about 14‰ in glacial ice to a near constant value of about 7‰ in lake ice. Other ice properties also change at this 3539 m transition. Crystal size increases dramatically, electrical conductivity (ECM) decreases and reaches the detection limit and total gas content changes from a value of about  $80 \times 10^{-3} \text{ cm}^3/\text{g}$ , typical for glacier ice, to a value of about  $6 \times 10^{-5} \text{ cm}^3/\text{g}$  in the lake

ice. Drilling stopped at a depth of 3623 m but the total ice thickness is estimated to be 3750 m. There is no reason to believe that the deeper ice down to the water interface would not also be refrozen lake water. Therefore, a total thickness of 210 m of lake ice can be reasonably assumed.

The deduced isotopic composition of lake water is  $\delta D = -449.3$ ‰,  $\delta^{18}\text{O} = -57.9$ ‰ [6]. Such an isotopic composition implies that most of the water constituting Lake Vostok comes from glacial melt. Jouzel et al. [6] indicate that the lake water isotopic composition differs significantly from that of the overlying glacier ice. These authors suggest that it may be the result of a warmer average Antarctic climate before 420 000 years ago. It must, however, also be said that glacier ice is richer in heavy isotopes 200 km north of Vostok Station, above the northern part of the lake. As will be seen later in this paper, melting at the ice–lake interface is concentrated in this area influencing in that way the lake water isotopic composition.

Fig. 3 gives the concentration in ppb versus depth of different chemical compounds in the basal part of the Vostok ice core. Since the sampling resolution is much less than for the previous variables studied, concentrations are indicated by

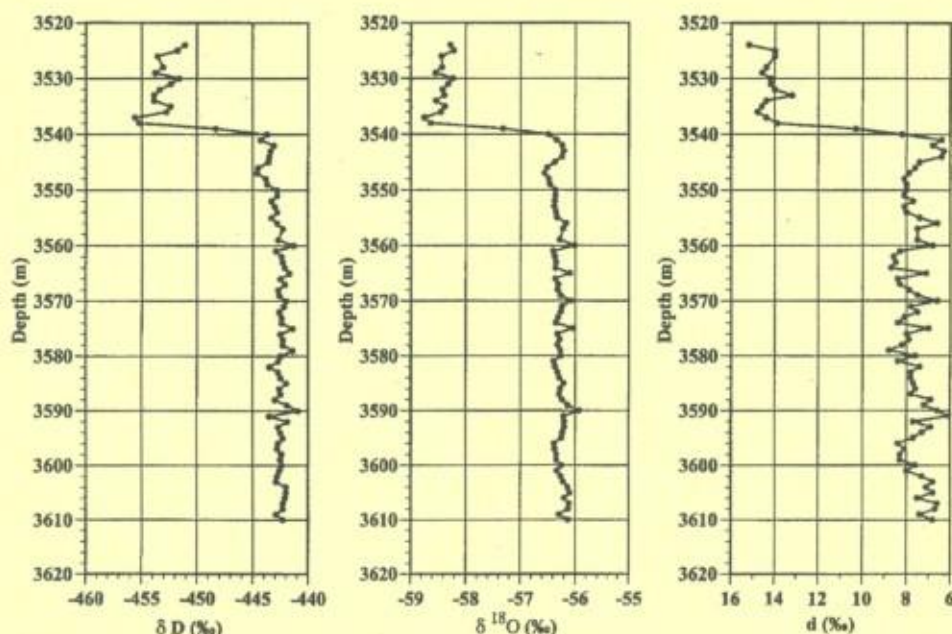


Fig. 2.  $\delta D$ ,  $\delta^{18}\text{O}$  and deuterium excess in the basal part of the Vostok ice core.



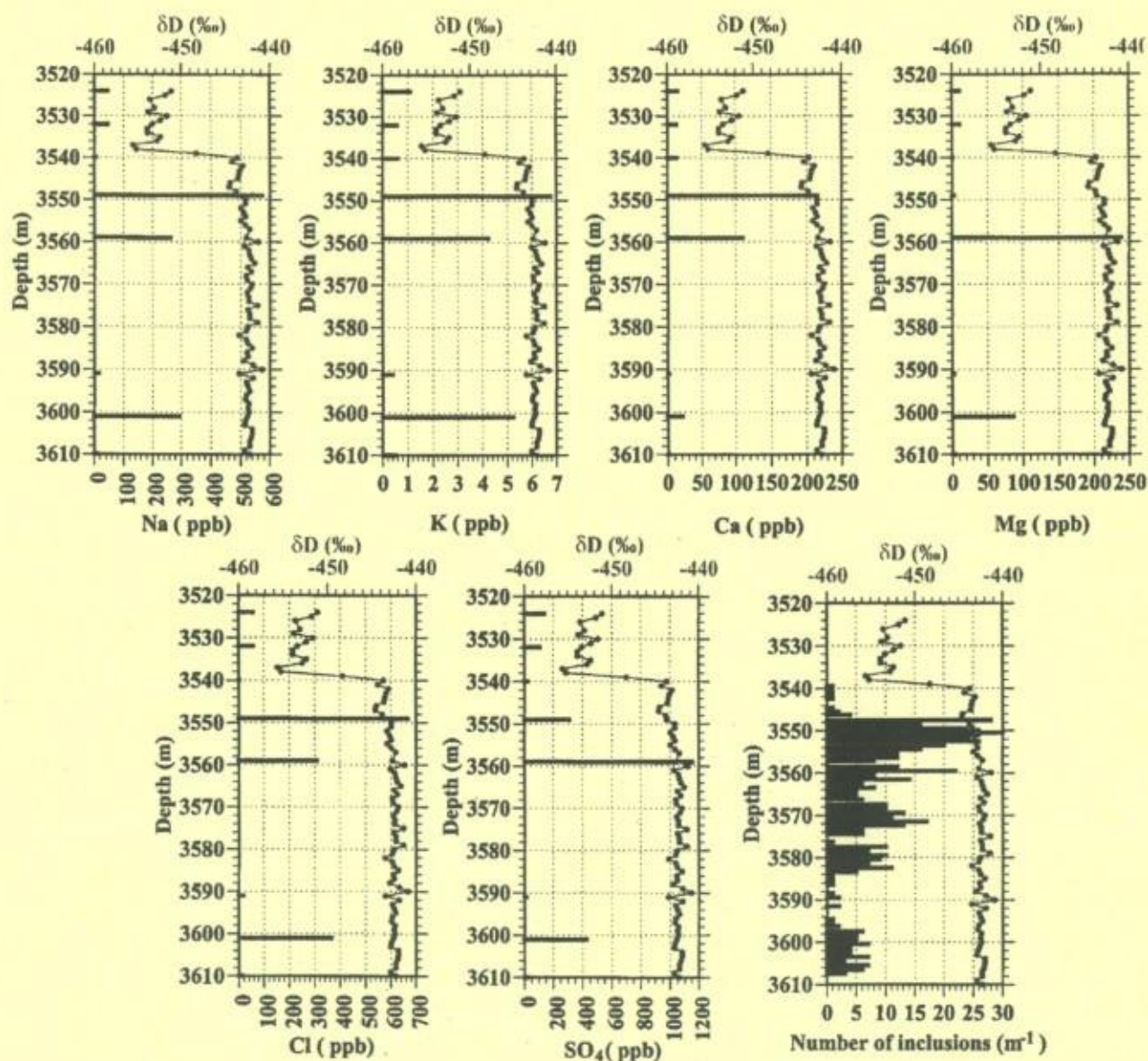


Fig. 3. Concentration in ppb of different chemical compounds in the basal part of the Vostok ice core. The  $\delta D$  vs. depth data are plotted on all graphs as a reference.

bars at the depth where sampling occurred. Results indicate three major features:

1. major elements represented in Fig. 3 are clearly enriched in lake ice, compared with glacial ice above;
2. lake ice shows very strong variations in concentration of major compounds with, at the level of sampling resolution, peak values at about 3550 m, 3560 m and 3600 m depth respectively;

3. the relatively high concentration of major compounds in some lake ice layers compared to glacial ice above is an indication that the waters of Lake Vostok are chemically not just pure glacial melt. As suggested by Siegert et al. [5], impurities are transferred to Lake Vostok water upon melting but are not transferred in the same concentrations back to the relatively pure refrozen ice above the lake. This is very important in connection with water circulation in the subglacial lake because, at the



melting point, salinity has a major impact on water density. However, Gorman and Siegert [1] showed that radar reflections are present across the northern end of Lake Vostok. For VHF radar penetration to be possible in water to 20 m, the water must be fresh but it is difficult from the deduced value of electrical conductivity ( $3\text{--}5 \times 10^{-4}$  mhos  $\text{m}^{-1}$ ) to derive a value of water salinity. The northern end of the lake could also be influenced by meltwater of low salinity as suggested below.

Also indicated in Fig. 3 is the profile of solid, mineral inclusions within the ice versus depth. These solid inclusions mainly consist of a rock core on which dirt particles are attached; they reach a few mm thickness in diameter. Solid inclusions are more numerous in the upper part of the lake ice profile and seem to be absent below 3609 m. Ice accretion close to the grounding line allows the trapping of dirt particles in the ice, which is impossible once the lake becomes deeper. Is there some relationship between the dirt concentration profile and the different chemical profiles displayed in Fig. 3? Although the difference in resolution hampers such a comparative study, there seems to be some correlation from visual inspection of the profiles. The microparticles present in the ice could in part be soluble and therefore would affect the chemical results obtained on melted samples, but they must come principally from the lake waters. It must also be said that at the depth of 3600 m the number of inclusions is about 5 per meter of core. This small number barely affects the chemical results at that level where major chemical elements are in significantly higher concentrations than in the glacier ice above.

### 3. A rough estimation of Lake Vostok salinity

A first approach to estimating Lake Vostok salinity is by studying the thermal gradient in the ice. The thermal gradient in the ice at Vostok Station measured at 3600 m depth where the drilling stopped is 0.02 K/m. Kapitsa et al. [2] used detailed radio-echo soundings to derive the depth

of the ice–water interface at the Vostok drilling site: 3750 m deeper than the ice sheet surface, at about 250 m below sea level. This allows calculation of a temperature of  $-3.1^\circ\text{C}$  at the interface by extrapolating linearly the gradient mentioned above.

Now, at a pressure of 337 bar corresponding to the glaciostatic pressure of this column of ice, the pressure melting temperature of pure water is  $-2.5^\circ\text{C}$ , i.e.  $0.6^\circ\text{C}$  higher than the value calculated from the temperature gradient in the ice. Can this difference in temperature be attributed to the salinity of Lake Vostok? In that case, a difference of  $0.6^\circ\text{C}$  in the pressure melting–freezing temperature leads to a value of 12‰ in salinity. This is probably too high in view of the results of Gorman and Siegert [1].

Furthermore, the validity of linear extrapolation of the thermal gradient to the ice–water interface can be questioned in cases where phase changes occur at the interface. During both melting and freezing heat diffuses away from the boundary into the cold ice sheet. The flux is generally higher during melting because the removal of the warmest ice tends to steepen the temperature gradient, whereas during freezing the addition of warm ice to the ice sheet base reduces the gradient [7,8].

Another possible approach to estimate Lake Vostok salinity is by studying lake ice chemistry and applying a reasonable distribution coefficient between ice and water so that a deduced lake water salinity can be obtained. Let us take the ice salinity of the sample at 3600 m depth as an example. The ice salinity of this ice layer is about 1 ppm. In order to deduce the water salinity, knowledge of a partitioning coefficient called the effective distribution coefficient ( $k_{\text{eff}}$ ) in the literature is required. The effective distribution coefficient is the ratio between the observed concentration in the ice and the concentration in the liquid far from the interface.  $k_{\text{eff}}$  is dependent on the freezing rate and on the importance of liquid convection which can homogenize the liquid and suppress chemical gradients near the interface [9]. Gross et al. [10] showed experimentally a linear relationship between the concentration of NaCl in the ice and the concentration of NaCl in the water



up to a few permil salinity if the solution is stirred in order to avoid concentration gradients near the interface. This indicates that, in that range of water salinities, the effective distribution coefficient is independent of the concentration. Since concentration gradients near the interface were suppressed in the experiments, such a distribution coefficient is equivalent to the thermodynamic equilibrium coefficient  $k_{eq}$ , the ratio of solute concentration in the ice to solute concentration in the liquid at the interface, which is independent of the freezing rate. Gross et al. [10] obtained experimentally a value of 0.0028 for  $k_{eq}$ .

For higher salinities of the reservoir, the set up of constitutional supercooling induces the development of a dendritic or cellular interface, often described as the 'skeletal layer' in the bottom layer of sea ice [11,12]. This results in the incorporation of brines within every single crystal and leads to the development of a typical intra-crystalline substructure of brine layers between ice plates (clearly illustrated in horizontal thin sections in Gow et al. [13], for example). The whole process seriously enhances chemical fractionation and increases  $k_{eq}$  values up to 0.12, as has been derived from field measurements on first-year sea ice [11,14]. Theoretical considerations [11,15] allow one to define a stability criterion for an interface having planar grooves with steep walls (a good proxy for the 'skeletal layer'), for water salinities of the order of a few permil, in natural conditions of convection. This is corroborated by experimental observations of 'interface breakdown' for salinities of NaCl solutions between 1 and 3‰ [10,16,17]. No intra-crystalline substructure is visible in the thin sections from Vostok lake ice, suggesting that the water salinity is such that it did not lead to constitutional supercooling and the development of a skeletal layer at the ice–water interface. Therefore a  $k_{eff} \approx k_{eq}$  value similar to the one obtained by Gross et al. [10] should apply.

As will be discussed below, we suggest that the lake ice at the base of the Vostok core developed in a way similar to marine ice at the bottom of ice shelves, and not as ice growing by progression of a freezing front at the interface. Marine ice mainly results from the consolidation of loose frazil ice

crystals that were formed as individuals in the water column under peculiar oceanic circulation conditions and subsequently accreted under buoyancy at the bottom of ice shelves. Eicken et al. [18] obtained a value of  $k_{eff}$  of about 0.0008 for marine ice at the base of the Ronne Ice Shelf and Tison et al. [19] a  $k_{eff}$  of 0.0009 for orbicular frazil ice at the base of Hell's Gate Ice Shelf in Terra Nova Bay. These even lower values of the distribution coefficient result from the fact that marine ice is a complex medium where the mean ice salinity is partly controlled by the proportion of initial individual frazil ice crystals which can be considered, in a first approximation, as devoid of salt impurities.

It thus seems that a reasonable range of  $k_{eff}$  values between 0.0008 and 0.0028 would apply for the Vostok case study where the freezing rate is quite low and the lake water not stagnant. This results in lake water salinity prediction between 0.4 and 1.2‰.

A 0.4‰ lake water salinity estimate is considered as a minimal rough approximation. Let us noted here that Dry Valley's perennially frozen lakes receiving only meltwaters from direct glacial runoff reach salinities higher than 1‰ [20]. It will, however, be shown that, for the purposes of this paper, the difference in salinity between glacier ice melt and lake water is much more important to consider than a precise value of lake water salinity. It is, moreover, quite possible that the salinity of Lake Vostok water is higher in the deeper parts of the lake.

The salinity of glacier ice melt is of the order of 0.001‰ but, if this water is in contact with the subglacial floor, the salinity may increase to 0.1‰, depending on the particle/water ratio. This latter value has been obtained by several chemical studies of subglacial waters in different environments [21–23].

#### 4. Water circulation

Fig. 4 gives, at a pressure of 337 bar corresponding to an ice thickness of 3750 m, the temperature of maximum density of water versus salinity and the freezing temperature versus salinity.



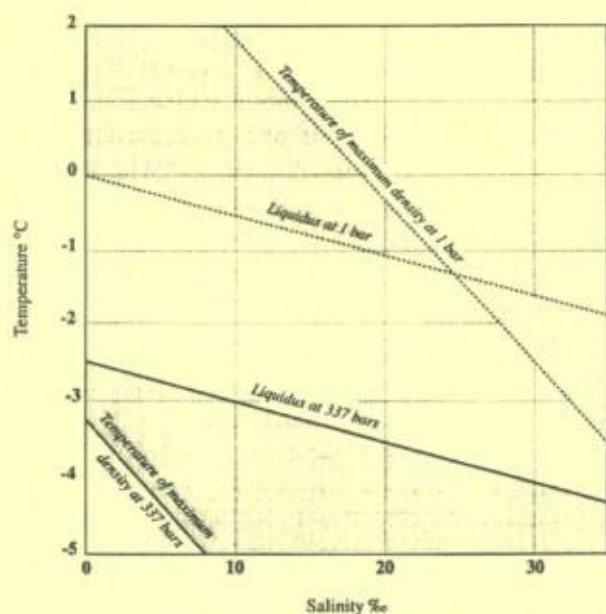


Fig. 4. Temperature of maximum density of water and freezing temperature versus salinity at a pressure of 337 bar. Values were computed from the general state equation of sea water.

It can be clearly seen that, whatever the salinity, the freezing temperature is first reached when water is cooled so that, closer to the freezing point, water has a higher density. The consequence of this fact is an unstable water column for geothermal heating from below since warmer water is less dense. Wüest and Carmack [4] combine this notion with the fact that a temperature gradient exists along the ice–water interface to construct a model of water circulation in the lake. In this model, salinity is not considered as a factor. It is true that a 0.4‰ salinity will not change the general behavior of lake waters. However, as indicated below, a difference in salinity could have far greater consequences in Lake Vostok than a contrast in temperature. At a pressure of 337 bar, a difference of 0.37°C in temperature corresponding to the difference in the pressure melting temperature between the northern and the southern parts of the lake at the ice–water interface gives a difference in  $\sigma_w$  of about 0.03.  $\sigma_w$  is equal to  $1000(\rho_w - 1)$  where  $\rho_w$  is the water density. By contrast, at the same pressure, a difference in salinity of 0.4‰, like that between lake water and pure glacial meltwater, gives a difference in  $\sigma_w$  of about 0.32. Even a weak salinity

must therefore be taken into account to complete the picture of water circulation in Lake Vostok.

Information gained by the study of medium-sized Antarctic ice shelves is worth considering in this context. Today, melting generally occurs at the grounding line. Less dense water at the pressure melting point at depth is produced in this way since glacier ice melt has a much lower salinity than sea water. This less dense water rises along the ice shelf–ocean interface. Since the freezing point is higher when pressure decreases, the rising water becomes supercooled. Frazil ice crystals are generated in the rising plume and, because of their lower density, accrete at the bottom of the ice shelf consolidating as a layer of marine ice. Lewis and Perkin [24] called this process the ice pump mechanism.

The situation in Lake Vostok is not, however, identical to that found beneath ice shelves. Firstly, along the glacier flow line in the southern part of the lake passing through Vostok Station the highest point of the lake is close to the grounding line, where the ice sheet leaves contact with its solid substratum and becomes floating on the lake. Along this line, the ice–water interface does not change very much in altitude between the grounding line and the place where the ice sheet makes contact again with its solid substratum at the south-eastern end of the lake. By contrast, along a north–south profile, the ice–water interface is at a much lower altitude in the northern part of the lake than in the surroundings of Vostok Station in the south. Secondly, Lake Vostok is a closed system whereas an ice shelf is open on one side to the ocean [25].

## 5. Ice formation in the subglacial lake

The isotopic characteristics of the lake ice present at the bottom of the Vostok ice core were given in Jouzel et al. [6]. It was shown in this paper that the deuterium and oxygen-18 enrichment of the lake ice in comparison to the deduced values of lake water (6.6‰ in  $\delta D$  and 1.65‰ in  $\delta^{18}O$ ) is only about 60% of the corresponding isotopic equilibrium (11.4‰ and 2.8‰ respectively). Freezing rate and reservoir effects



were discarded as possible explanations. It was suggested that, if freezing itself occurs at equilibrium, water pockets may be trapped during ice accretion. Such water pockets would freeze completely afterwards, and their bulk isotopic composition would not be modified. Therefore the observed fractionation must be less than the true value, depending on how much water is included in water pockets in the ice during the course of freezing. It is now possible with the developments given above to develop such a process in the light of water circulation in the lake.

Let us consider rising meltwaters from the ice–water interface from the northern part of the lake where melting occurs. The rising plume is the consequence of thermal and also probably salinity effects. Such waters will become supercooled as they rise. The maximum water supercooling would be the difference in melting points between the deeper and the upper parts of the lake at the ice–water interface. Nucleation will, however, start in the rising water for lower supercooling levels. A reasonable range of supercooling is between 0.01 and 0.1°C. For such values, growth velocities of frazil ice crystals in fresh water are between  $10^{-6}$  and  $5 \times 10^{-5}$  m/s [26]. Now, observed isotopic fractionation between ice and water in open systems can be described by an equation similar to Burton's equation [27]:

$$\left( \frac{1000 + \delta_s}{1000 + \delta_i} \right) = \frac{\alpha}{\alpha - (\alpha - 1)e^{-\frac{hv}{D}}}$$

where  $\delta_s$  and  $\delta_i$  are the respective  $\delta$  values of the ice and of the initial water,  $\alpha$  is the appropriate equilibrium fractionation coefficient,  $v$  the freezing rate,  $h$  the boundary layer thickness and  $D$  the appropriate diffusion coefficient. This equation

can be solved either for deuterium or oxygen-18. Using the supercooling range and the associated growth rates mentioned above with a reasonable boundary layer thickness of 0.1 cm, calculations indicate that the frazil ice crystals will have an isotopic enrichment in  $\delta D$  between 4.56 and 0‰, compared to the lake water (Table 1). A higher supercooling will of course lead to higher growth rate and thus, a fortiori, to no isotopic enrichment in the frazil ice crystals. Now, consolidation of loose frazil ice crystals by freezing the host water is a very slow process, thus at isotopic equilibrium. The isotopic composition of the lake ice, which is not at equilibrium freezing taking into account the lake water isotopic composition (enrichment of 6.6‰ instead of 11.4‰ in [6]), can be understood if the frozen host water represents between 30 and 58% of the bulk lake ice. Such values are comparable to those obtained in experimental and field studies of frazil ice formation [28,29]. The characteristics of the isotopic composition of the lake ice thus strongly support the occurrence of a mechanism similar to marine ice formation under an ice shelf, involving consolidation of loose frazil ice crystals accreted at the ice ceiling of the lake.

In addition, Priscu et al. [30] found at 3590 m, the core depth they studied, a much higher proportion of micas in the particles of micrometer size than in crystalline and metamorphic rocks. This is probably an indication of capture by scavenging during frazil ice accretion, the geometry of mica crystals allowing them to float more easily in the lake waters. Ice crystals are fairly big in the lake ice: > 20 cm to 1 m. It is therefore not possible to compare the azimuths of their *c*-axes and so unambiguous information on their formation process cannot be obtained. The variability in the dip (Fig. 1) does not, however, favor a single pro-

Table 1  
Proportion of frozen host water in lake ice deduced from its isotopic composition

Water supercooling (°C)	Crystal growth rate (m/s)	Effective fractionation coefficient ( $\alpha_{\text{eff}}$ )	$\delta D_{\text{frazil}}$	Frazil (%)	Frozen host water (%)
0.01	$10^{-6}$	1.0083	-444.74	70	30
0.1	$5 \times 10^{-5}$	1.0000	-449.3	42	58

Burton's equation is used with boundary layer thickness = 1 mm;  $\alpha_{\text{eq}} = 1.0208$ ,  $D = 1.1 \times 10^{-9}$  m<sup>2</sup> s<sup>-1</sup>,  $\delta D_{\text{bulk lake ice}} = -442.7$ ‰,  $\delta D_{\text{water}} = -449.3$ ‰,  $\delta D_{\text{frozen host water}} = -437.9$ ‰.



cess of freezing front progression in the lake water from the ice–water interface.

An additional mechanism is the possibility of glacial meltwater seeping at the grounding line at selected places of the ice–bedrock–water contact, for example up-glacier from Vostok Station. If seeping glacial meltwater with a salinity of the order of 0.1‰ or less enters into contact with Lake Vostok water of 0.4‰ salinity, a peculiar situation occurs. Let us consider that both waters are at their respective pressure freezing points. At a given pressure, the freezing point temperature is dependent on the salinity of the water, being higher if the salinity is lower. Thus the freezing point of lake water is lower than that of seeping glacial meltwater. Heat diffusion will occur locally from the seeping meltwater to the lake. On the other hand, the salinity of lake water being higher than that of glacial meltwater, salts will diffuse from the lake to the meltwater. Thermal diffusivity is an order of magnitude higher than salt diffusion. The seeping glacial meltwater loses heat more rapidly than it gains salt so that supercooling followed by freezing occurs, incorporating into the ice mineral particles present in this locality. This double-diffusion mechanism is responsible for the presence of aggregates of millimeter sizes into the frazil ice. A small water quantity which freezes is enough for mineral inclusion into the frazil ice. Diffusion coefficients of stable isotopes and of salts in liquid water have the same order of magnitude, so that the double-diffusion mechanism described above also leads to isotopic diffusion. The isotopic composition of the ice formed at the grounding line is thus likely to be a good indicator of the process. This is the background of the study undertaken in Terra Nova Bay [31]. In the case studied here, however, there is no significant difference in isotopic composition between glacial meltwater and lake water.

On the time scale for ice to pass over the width of the lake, changes in lake volume and in position of the lower boundary of the ice sheet due to changes in ice thickness are likely to occur. Therefore, there could well be periods where lake ice formation is promoted. There is, however, no information yet for constraining such a hypothesis. It is probably true that freezing will be favored if

the ice thickness is less. Freezing rates determined by Siegert et al. [5] from radar data could well be not correct if the frazil ice mechanism is retained. Lake ice once formed is entrained by glacier flow and can be exported outside the lake area where ice makes contact again with its substratum at the downstream end of the lake.

## 6. Conclusion

Ice formation in subglacial Lake Vostok is related to the tilted surface of the ice–water interface. Because the lake behaves as an ocean, water circulation is likely to occur. Supercooling in rising waters along the tilted ice–water interface is considered to be the mechanism responsible for lake ice formation. This produces loose frazil ice crystals which will accrete at the ice ceiling with subsequent freezing of the host water.

The isotopic composition of the lake ice corroborates ice formation in two steps: loose frazil ice crystals produced in supercooled plumes followed by slow freezing of the host water in which the ice crystals accrete at the ice ceiling.

## Acknowledgements

The authors thank M. Jaffrezo for the chemical analyses. This paper is a contribution to the Belgian Antarctic Program (S.S.T.C.-Science Policy Office). J.-L.T. is a Research Associate of the Belgian National Fund for Scientific Research (F.N.R.S.).[EB]

## References

- [1] M.R. Gorman, M.J. Siegert, Penetration of Antarctic subglacial lakes by VHF electromagnetic pulses: Information on the depth and electrical conductivity of basal water bodies, *J. Geophys. Res.* 104 (1999) 29311–29320.
- [2] A. Kapitsa, J. Ridley, G.d.Q. Robin, M.J. Siegert, V. Zotikov, A large deep fresh water lake beneath the ice of Central East Antarctica, *Nature* 381 (1996) 684–686.
- [3] M.J. Siegert, J. Ridley, An analysis of the ice sheet surface and subsurface topography above the Vostok station subglacial lake, central East Antarctica, *J. Geophys. Res.* 103 (1998) 10195–10207.



- [4] A. Wüest, E. Carmack, A priori estimates of mixing and circulation in the hard-to-reach water body of lake Vostok, Ocean Model., submitted.
- [5] M.J. Siegert, R. Kwok, C. Mayer, B. Hubbard, Water exchange between the subglacial Lake Vostok and the overlying ice sheet, *Nature* 403 (2000) 643–646.
- [6] J. Jouzel, J.R. Petit, R. Souchez, N. Barkov, V. Lipenkov, D. Raynaud, M. Stievenard, N. Vassiliev, V. Verbeke, F. Vimeux, More than 200 meters of lake ice above subglacial lake Vostok, Antarctica, *Science* 286 (1999) 2138–2141.
- [7] A. Jenkins, A. Bombosch, Modeling the effects of frazil ice crystals on the dynamics and thermodynamics of Ice Shelf Water plumes, *J. Geophys. Res.* 100 (1995) 6967–6981.
- [8] W.S.B. Paterson, *The Physics of Glaciers*, Elsevier Science Ltd., Oxford, 1994, 480 pp.
- [9] B. Özüm, D. Kirwan, Impurities in ice crystals grown from stirred solutions, S.S. International Association of Chemical Engineers, ed. 153-72, 1976, pp. 1–6.
- [10] G.W. Gross, P.M. Wong, K. Humes, Concentration dependent solute redistribution at the ice–water phase boundary. III. Spontaneous convection, chloride solutions, *J. Chem. Phys.* 67 (1977) 5264–5274.
- [11] W.F. Weeks, S.F. Ackley, The growth, structure and properties of sea ice, in: N. Untersteiner (Ed.), *The Geophysics of Sea Ice*, ed. 146, Martinus Nyhoff, Dordrecht (Nato ASI Series B, Physics), 1986, pp. 9–164.
- [12] H. Eicken, Deriving modes and rates of ice growth in the Weddell Sea from microstructural, salinity and stable-isotope data, in: M.O. Jeffries (Ed.), *Antarctic Sea Ice: Physical Processes, Interactions and Variability*, ed. 74, American Geophysical Union, Washington, DC, 1998, pp. 89–122.
- [13] A.J. Gow, S.F. Ackley, K.R. Buck, K.M. Golden, Physical and structural characteristics of Weddell Sea pack ice, *CRREL Rep.* 87-14, 1987, 70 pp.
- [14] M. Nakawo, N. Sinha, Growth rate and salinity profiles of first-year sea ice in the high Arctic, *J. Glaciol.* 27 (1981) 315–330.
- [15] W.A. Tiller, Effect of grain boundaries on solute partitioning during progressive solidification, *J. Appl. Phys.* 33 (1962) 3106–3107.
- [16] K. Nagashiwa, Y. Furukawa, Solute distribution in front of an ice/water interface during directional growth of ice crystals and its relationship to interfacial patterns, *J. Phys. Chem. B* 101 (1997) 6174–6176.
- [17] W.F. Weeks, G. Lofgren, The effective distribution coefficient during the freezing of NaCl solutions, in: H. Oura (Ed.), *Physics of Snow and Ice: International Conference on Low Temperature Science*, Institute of Low Temperature Science, Hokkaido, 1967, pp. 579–597.
- [18] H. Eicken, H. Oerter, H. Miller, W. Graf, J. Kipfstuhl, Textural characteristics and impurity content of meteoric and marine ice in the Ronne Ice Shelf, Antarctica, *J. Glaciol.* 40 (1994) 386–398.
- [19] J.-L. Tison, D. Ronveaux, R. Lorrain, Low salinity frazil ice generation at the base of a small antarctic ice shelf, *Antarct. Sci.* 5 (1993) 309–322.
- [20] W.J. Green, M.P. Angle, K.E. Chave, The geochemistry of Antarctic streams and their role in the evolution of four lakes of the McMurdo Dry Valleys, *Geochim. Cosmochim. Acta* 52 (1988) 1265–1274.
- [21] R. Raiswell, Chemical models of solute acquisition in glacial melt waters, *J. Glaciol.* 30 (1984) 49–57.
- [22] R. Reynolds, N. Johnson, Chemical weathering in the temperate glacial environment of the Northern Cascade Mountains, *Geochim. Cosmochim. Acta* 36 (1972) 537–554.
- [23] N. Eyles, D. Sasseville, R. Slatt, R. Rogerson, Geochemical denudation rates and solute transport mechanisms in a maritime temperate glacier basin, *Can. J. Earth Sci.* 18 (1982) 1570–1581.
- [24] E.L. Lewis, R.G. Perkin, Ice pumps and their rates, *J. Geophys. Res.* 91 (1986) 11756–11762.
- [25] C. Mayer, K. Grosfeld, M.J. Siegert, Water circulation and mass exchange within subglacial Lake Vostok, submitted.
- [26] P.V. Hobbs, *Ice Physics*, Clarendon Press, Oxford, 1974, 837 pp.
- [27] J.A. Burton, R.C. Prim, W.P. Slichter, The distribution of solute in crystal growth from the melt. Part I: Theoretical, *J. Chem. Phys.* 21 (1953) 1987–1991.
- [28] A. Andersson, S.F. Daly, Laboratory investigations of trash rack blockage by frazil ice, *CRREL Rep.* 92-16, Hanover, 1992, 11 pp.
- [29] K.D. White, Determining the intrinsic permeability of frazil ice – Part I. Laboratory investigations, *CRREL Rep.* 91-23, 1991, 15 pp.
- [30] J. Priscu, E. Adams, W. Lyons, M. Voytek, D. Mogk, R. Brown, C. McKay, C. Takacs, K. Welch, C. Wolf, J. Kirshtein, R. Avci, Geomicrobiology of subglacial ice above lake Vostok, Antarctica, *Science* 286 (1999) 2141–2147.
- [31] R. Souchez, J.-L. Tison, R. Lorrain, C. Fléhoc, M. Stievenard, J. Jouzel, V. Maggi, Investigating processes of marine ice formation in a floating ice tongue by a high resolution isotopic study, *J. Geophys. Res.* 100 (1995) 7019–7025.



## 5. Conclusions





This Thesis is an overview of more than 10 years of our research activity in the field of ice-ocean interactions in the polar regions, during which we believe we have successfully contributed to unravelling the complexity and the diversity of processes that were clearly underestimated before. It is however only one of our fields of interest that are more generally dealing with the study of initial and boundary conditions at ice interfaces (be it the ice-bedrock, the ice-ocean or the ice-atmosphere interface).

In most glaciological models of ice sheet dynamics, ice shelves are generally reduced to a floatation criterion and a transition from simple shear dominated to vertical pure shear dominated stress fields. Even though the most sophisticated of those models explicitly take into account the complex transition from one regime to the other at the grounding line, they are not actually able of representing discontinuities such as basal crevasses or rifts opening in the ice. Simulation of global warming impact on the ice shelves is approached in those models by artificially forcing the surface mass balance to decrease, therefore reducing the ice shelf thickness and observing the impact on grounding line retreat, increasing floatation and, ultimately, potential sea level rising.

We have shown that ice shelves mass balance is not only reduced to its surface mass balance and a simple assumption of direct melting/refreezing at the ice ocean interface. Combining (a) field observations in a suitable environmental setting, where high surface ablation allow easier observation of ice bodies initially formed at the ice-ocean interface, and (b) landfast sea ice studies at the front of ice shelves or in rifts, we have demonstrated the existence of a variety of ice-ocean interaction processes affecting the ice shelves in their whole 3-D structure. The main working area is located south of the Italian Antarctic station of Terra Nova, along the Terra Nova Bay coast in South Victoria Land, Ross Sea. This is a region renown for its intense katabatic wind regime, which is responsible for the high surface ablation rates inducing an upward vertical component of the ice particles path, therefore bringing ice from depth to the ice shelf surface. Earlier work from the rift area in the southern part of the George VI Ice Shelf in the Antarctic Peninsula is also considered.

Five different mechanisms were detected by which ice-ocean interaction processes actually increase or redistribute ice in the ice shelf body, in the form of marine ice:

- (a) Crack metamorphism at grounding lines
- (b) Double diffusion between basal continental fresh meltwater and sea water in (re-) grounding areas
- (c) Deep Thermohaline Circulation in the whole of the sub-ice shelf cavity
- (d) Shallow Thermohaline Circulation in the frontal zone of the ice shelf
- (e) Rift Thermohaline Convection

We have then shown the potential implications of these various processes on predictions for ice shelf mass balance and stability under a warming climate. The peculiar chemical properties of marine ice are affecting its dielectric and rheological characteristics, as compared to meteoric ice, sea ice or sea water. When present below meteoric ice, marine ice can therefore jeopardize a safe ice shelf thickness evaluation through radio echo-sounding methods alone. When filling the rifts that prepare the calving of large tabular icebergs, marine ice welding efficiency is likely to be very different from that of an "ice melange" made of a mixture of sea ice, meteoric ice blocks and drifted snow. Because  $\delta^{18}\text{O}$  fractionation occurs on marine ice formation within the Ice Shelf Water, it is unsafe to use this isotope as a geochemical tracer of glacial melt contribution to the outflow at the ice shelf front. In a warming climate scenario it is also unsafe to associate the decrease in HSSW production in front of ice shelves to increased stability. Although this would indeed probably limit glacial melting at the grounding line, it would also hamper the filling of basal crevasses and rifts with marine ice, and therefore reduce internal cohesion.



We have also demonstrated how the ice ocean interaction processes described above come in support of the binge/purge model proposed by Alley and Mac Ayeal (1994) to explain the cyclic occurrence of Ice Rafted Debris (IRD) in the Heinrich events observed during the last glacial period.

Finally, our expertise on ice-ocean interactions processes below ice shelves helped us solving apparent discrepancies in the isotopic records of the lake ice forming the sole of the central Antarctic ice sheet at Vostok. There, we have shown that an ice pump mechanism very similar to the one occurring below ice shelves exists, that is associated to the water circulation pattern in the subglacial lake.

As is common in scientific research, the findings summarized in this work have generated new questions that led us to define pathways for future exploration. Among those, probably the most challenging will be the explicit description of the various ice-ocean interaction processes we have discussed in coupled glacio-oceanographical models simulating the response of the Antarctic system to the yet ongoing global warming.



## 6. References





- Alley R.B. and Mac Ayeal D.R., **1994**, Ice-rafted debris associated with binge / purge oscillations of the Laurentide Ice Sheet, *Paleoceanography*, 9: 503-511.
- Andersson A. and Daly S.F., **1992**, Laboratory investigation of trash rack blockage by frazil ice, *CRREL Report*, 92-16, 11 pp.
- Angrisano G., **1989**, Carta batimetrica Mare di Ross-Baia Terra Nova, Istituto Idrografico della Marina, Genova.
- Baroni C., **1990**, The Hells Gate and Backstairs Passage Ice Shelves, Victoria Land, Antarctica, *Mem. Soc. Geol. It.*, 43: 123-144.
- Baroni C., Frezzotti M., Giraudi C., Orombelli G., **1991a**, Ice flow and surficial variation inferred from satellite image and aerial photograph analysis of Larsen Ice Tongue, Hells Gate and Nansen Ice Shelves (Victoria Land, Antarctica), *Mem. Soc. Geol. It.*, 46: 69-80.
- Baroni C., Stenni B., Iacumin P., **1991b**, Oxygen isotopic composition of ice samples from the Hells Gate and Backstairs Passage ice shelves (Victoria Land, Antarctica): Evidence of bottom freezing, *Memorie della Società Geologica Italiana*, 46, 45-48.
- Baroni C., **1996**, Mount Melbourne quadrangle, Antarctic geomorphological and glaciological, *Museo Nazionale Dell'Antartide*, Siena.
- Ben-Yaakov S., **1972**, Diffusion of sea water ions - I. Diffusion of sea water into a dilute solution, *Geochimica and Cosmochimica Acta*, 36: 1395-1406.
- Blindow N., **1994**, The central part of the Filchner-Ronne Ice-Shelf, Antarctica: internal structures revealed by 40 MHz monopulse RES., *Ann. Glaciol.*, 20, 365-371.
- Bombosch A. and Jenkins A., **1995**, Modeling the formation and deposition of frazil ice beneath Fichner-Ronne Ice Shelf, *J. Geophys. Res.*, 100: 6983 -6992.
- Bond G., Broecker W., Johnsen S., McManus J., Labeyrie L., Jouzel J., Bonani G., **1993**, Correlations between climate records from North Atlantic sediments and Greenland ice, *Nature*, 365: 143-147.
- Bondesan A., Capra A., Gubellini A., Tison J.-L., **1994**, On the use of static GPS measurements to record the tidal response of a small antarctic ice shelf (Hells Gate Ice Shelf - Victoria Land), *Geog. Fis. Dinam. Quat.*, 17, 123-129.
- Bondesan A. and Tison J.-L., **1997**, The glaciological map of Hells Gate Ice Shelf (Terra Nova Bay, Antarctica), *Terra Antartica Reports*, 1: 9-11.
- Bouvette A., **1995**, Contribution à l'étude des interactions ice shelf-océan dans la Baie de Terra Nova, Antarctique, Univ. Libre de Bruxelles, *Master Thesis*, 64 pp., unpublished.
- Budd W.F., Jenssen D., Radok U., **1971**, Derived physical characteristics of the Antarctic ice sheet, *ANARE Interim Report*, Series A (IV), Glaciology Publ., 120, 178 pp.
- Budd W.F. and Smith I.N., **1982**, Large-scale numerical modelling of the Antarctic ice sheet, *Ann. Glaciol.*, 3, 36-41.



- Budillon G. and Spezie G., **2000**, Thermohaline structure and variability in the Terra Nova Bay polynya, Ross Sea, *Antarctic Science*, 12 (4): 493-508.
- Burton J.A., Prim, R.C. and Slichter W.P., **1953**, The distribution of solute in crystal growth from the melt. Part I: Theoretical, *J. Chem. Phys.*, 21 (1), 1987-1991.
- Carmignani L., Ghezzi C., Gosso G., Lombardo B., Meccheri M., Montrasio A., Pertusati P.C., Salvini F., **1987**, Geological Map of the area between David and Mariner glaciers, Victoria Land, Antarctic, *Mem. Soc. Geol. It.*, 33.
- Corr H., Popple M., Robinson A., **1995**, Airborne radio echo investigations of a marine ice body, *Filchner-Ronne Ice Shelf Programme (FRISP) Report 8*, AWI - Bremerhaven, 14-17.
- Cox G.N.F. and Weeks W.F., **1975**, Brine drainage and initial salt entrapment in sodium chloride ice, *CRREL Res. Rep.*, 345, 85 pp., Cold Reg. Res. And Eng. Lab., Hanover, N.H.
- Cragin J.H., Gow A.J., Kovacs A., **1986**, Chemical fractionation of brine in the McMurdo Ice Shelf, Antarctica, *Journal of Glaciology*, 32: 307-313.
- Craig H., **1961**, Isotopic variations in meteoric waters, *Science*, 133 (3465): 1702-1703.
- Dahl-Jensen D., **1989**, Steady thermomechanical flow along two-dimensional flow lines in large grounded ice sheets, *J. Geophys. Res.*, 94 (B8): 10355-10362.
- Daly S.F., **1984**, Frazil ice dynamics, *CRREL Monograph*, 84-1, 44 pp., Cold Reg. Res. And Eng. Lab., Hanover, N.H.
- Dansgaard W., **1964**, Stable isotopes in precipitation, *Tellus*, 16 (4), 436-468.
- Dayton P.K., Robilliard G.A., DeVries A.L., **1969**, Anchor ice formation in McMurdo Sound, Antarctica, and its biological effects, *Science*, 163: 273-274.
- Determann J. and Gerdes R., **1994**, Melting and freezing beneath ice shelves: implications from the three-dimensional model, *Annals of Glaciology*, 20: 413-419
- Dieckmann G.S., Rohardt G., Hellmer H., Kipfstuhl J., **1986**, The occurrence of ice platelets at 250m depth near the Filchner Ice Shelf and its significance for sea ice biology, *Deep-Sea Res.*, 21 (3): 169-174.
- Dowdeswell J.A., Elverhøi, A., Andrews and Hebbeln, D., **1999**, Asynchronous deposition of ice-rafted layers in the Nordic seas and North Atlantic Ocean, *Nature*, 400: 348-351.
- Eicken H. and Lange M.A., **1989**, Development and properties of sea ice in the coastal regime of the Southeastern Weddell Sea, *Journal of Geophysical Research*, 94 (C6): 8193-8206.
- Eicken H., **1994**, Structure of under-ice melt ponds in the central Arctic and their effect on the sea-ice cover, *Limnol. Oceanogr.*, 39 (3): 682-694.
- Eicken H., Oerter H., Miller H., Graf W., Kipfstuhl J., **1994**, Textural characteristics and impurity content of meteoric and marine ice in the Ronne Ice Shelf, Antarctica, *Journal of Glaciology*, 40 (135): 386-398.



- Eicken H., **1998**, Deriving modes and rates of ice growth in the Weddell Sea from microstructural, salinity and stable-isotope data, in *Antarctic sea ice: physical processes, interactions and variability*, edited by M.O. Jeffries, pp. 89-122, American Geophysical Union, Washington, D.C.
- Fabiano M., Povero P., Catalano G., and Benedetti F., **1991**, Hydrological data collected during the biological, chemical and geological sampling in Terra Nova Bay, *Nat. Sc. Com., Ocean. Camp. 1989-90, Data Rep.*, 35-71.
- Foldvik A., Gammelsrod T., Slotsvik N., Torresen T., **1985**, Oceanographic conditions on the Weddell Sea Shelf during the German Antarctic Expedition 1979-1980, *Polar Research*, 3: 209-226.
- Frezzotti M., **1993**, Glaciological study in Terra Nova Bay, Antarctica, inferred from remote sensing analysis, *Annals Glaciol.*, 17, 63-71.
- Frezzotti M., Tabacco I.E., Zirizzotti A., **2000**, Ice discharge of eastern Dome C drainage area, Antarctica, inferred from airborne radar survey and satellite image analysis, *J. Glaciol.*, 46, 253-264.
- Fricker H.A., Popov S., Allison I., Young N., **2001**, Distribution of marine ice beneath the Amery Ice Shelf, East Antarctica, *Geophysical Research Letters*, 28 (11): 2241-2244.
- Golden K.M., Ackley, S.F. and Lytle, V., **1998** The Percolation Phase Transition in Sea Ice, *Science*, 282, 2238-2240.
- Gow A.J. and Epstein S., **1972**, On the use of stable isotopes to trace the origins of ice in a floating ice tongue, *Journal of Geophysical Research*, 77 (33): 6552-6557.
- Gow A.J., Ackley S.F., Buck K.R., Golden K.M., **1987**, Physical and structural characteristics of Weddell Sea pack ice, *CRREL Report*, 87-14: 70 pp.
- Gow A.J., Ackley S.F., Govoni J.W., Weeks W.F., **1998**, Physical and structural properties of land-fast sea ice in McMurdo sound, Antarctica, in *Antarctic sea ice: physical processes, interactions and variability*, edited by M.O. Jeffries, A.G.U., Antarctic Research Series, 74, 355-374.
- Grosfeld K., Gerdes R., Determan J., **1997**, Thermohaline circulation and interaction between ice shelf cavities and the adjacent open ocean, *J. Geophys. Res.*, 102: 15595 -15610.
- Grosfeld K., Hellmer H., Jonas M., Sandhäger H., Schulte M., Vaughan D.G., **1998**, Marine ice beneath Filchner Ice Shelf: evidence from a multi-disciplinary approach, *Antarct. Res. Ser.*, 75, 319-339.
- Gross G.W., Wong P.M., Humes K., **1977**, Concentration dependent solute redistribution at the ice-water phase boundary. III. Spontaneous convection, chloride solutions, *The Journal of Chemical Physics*, 67 (11): 5264-5274.
- Grousset F.E., Pujol C., Labeyrie L., Auffret G., Boelaert A., **2000**, Were the North Atlantic Heinrich events triggered by the behavior of the European ice sheets?, *Geology*, 28 (2): 123-126.
- Hellmer H.H., **1989**, Ein zweidimensionales Modell zur Thermohaline Zirculation unter Schelfeisen, *Ph.D. Thesis*, 87 pp., Univ. Hambourg, Hambourg, Federal Republic of Germany.



- Hellmer H.H. and Jacobs S.S., **1992**, Ocean interactions with the base of the Amery Ice Shelf, Antarctica, *Journal of Geophysical Research*, 97 (20): 305-320.
- Hellmer H.H. and Olbers D.J., **1989**, A two-dimensional model for the thermohaline circulation under an ice shelf, *Antarc. Sci.*, 1 (4), 325-336.
- Hellmer H.H. and Olbers D.J., **1991**, On the thermohaline circulation beneath the Filchner-Ronne ice shelves, *Antarc. Sci.*, 3 (4), 433-442.
- Hindmarsh R.C.A. and Hutter K., **1988**, Numerical fixed domain mapping solution of free-surface flows coupled with an evolving interior field, *Int. J. Numer. Anal. Met.*, 12 (4): 437-459.
- Hindmarsh R.C.A., Boulton G.S., Hutter K., **1989**, Modes of operation of thermo-mechanically coupled ice sheets, *Ann. Glaciol.*, 12, 57-69.
- Hobbs P.V., **1974**, *Ice Physics*, 837 pp., Clarendon Press, Oxford.
- Hooke R.L.B., **1998**, *Principles of glacier mechanics*, Prentice Hall, New Jersey, 248pp.
- Hooke R.L.B., Gao X.Q., Jacka T.H., Souchez R.A., **1988**, Rheological contrast between Pleistocene and Holocene ice in Barnes Ice Cap, Baffin Island, N.W.T., Canada: a new interpretation, *J. of Glaciol.*, 34 (118): 364-365.
- Houghton J.T., Jenkins G.J., Ephraums J.J., **1990**, *Climate change: The IPCC scientific assessment*, Cambridge University Press, 365 pp.
- Hutter K., Yakowitz S., Szidarovsky F., **1986**, A numerical study of plane ice sheet flow, *J. Glaciol.*, 32 (111): 139-160.
- Huybrechts P., **1992**, The Antarctic ice sheet and environmental change: a three-dimensional modelling study, *Reports on Polar Research*, 99, 241 pp., Alfred Wegener Institute for Polar and Marine Research, Bremenhaven.
- Huybrechts P., **1993**, Glaciological modelling of the late Cenozoic East Antarctic Ice Sheet: stability or dynamism?, *Geografiska Annaler*, 75 A (4): 221-238.
- Jacobs S.S., Gordon A.L., Ardai Jr. J.-L., **1979**, Circulation and melting beneath the Ross Ice Shelf, *Science*, 203: 441-443.
- Jacobs S.S., **1991**, Sea-level response to ice sheet evolution: an ocean perspective, in Bindshadler R.A., ed., *West Antarctic Ice Sheet Initiative. Volume 2: discipline reviews. Proceedings of a workshop... Goddard Space Flight Center, Greenbelt, Maryland, October 16-18, 1990*, Washington, DC, National Aeronautics and Space Administration, 23-47. (NASA Conference Publication 3115)
- Jacobs S.S., Fairbanks R.G., Horibe Y., **1985**, Origin and evolution of water masses near the antarctic and continental margin: evidence from  $H_2^{18}O/H_2^{16}O$  ratios in sea water, in *Oceanology of the Antarctic Continental Shelf*, edited by S.S. Jacobs, pp. 59-85, A.G.U., Washington.
- Jacobs S.S., Helmer H.H., Doake C.S.M., Jenkins A., Frolich, R.M., **1992**, Melting of ice shelves and the mass balance of Antarctica, *Journal of Glaciology*, 38 (130): 375-387.



- Jeffries M.O., Weeks W.F., Shaw R., Morris K., **1993**, Structural characteristics of congelation and platelet ice and their role in the development of Antarctic land-fast sea ice, *J. of Glaciol.*, 39 (132): 223-238.
- Jenkins A. and Bombosch A., **1995**, Modelling the effects of frazil ice crystals on the dynamics and thermodynamics of Ice Shelf Water plumes, *J. Geophys. Res.*, 100: 6967 -6981.
- Jenkins A. **1991**, A one-dimensional model of ice shelf-ocean interaction, *J. Geophys. Res.*, 96 (C11): 20791-20677.
- Jenkins A. and Doake C.S.M., **1991**, Ice-ocean interaction on Ronne Ice Shelf, Antarctica, *J. Geophys. Res.*, 96: 791-813.
- Jenssen D., **1977**, A three-dimensional polar ice sheet model, *J. Glaciol.*, 18 (80): 373-389.
- Jezek K.C., Bentley, C.R. and Clough, J.W., **1979**, Electromagnetic sounding of bottom crevasses on the Ross Ice Shelf, Antarctica, *J. Glaciol.*, 24 (90), 321-330.
- Jezek K.C. and Bentley C.R., **1983**, Field studies of bottom crevasses in the Ross Ice Shelf, Antarctica, *J. Glaciol.*, 29 (101): 118-126.
- Jouzel J. and Souchez R., **1982**, Melting-refreezing at the glacier sole and the isotopic composition of the ice, *J. Glaciol.*, 28: 35-42.
- Jouzel J., Petit J.- R., Souchez R., Barkov N., Lipenkov V., Raynaud D., Stièvenard M., Vassiliev N., Verbeke V., Vimeux F., **1999**, More than 200 meters of lake ice above subglacial lake Vostok, Antarctica, *Science*, 2138-2141.
- Khazendar A., **2000**, Marine ice formation in rifts of Antarctic ice shelves – A combined laboratory study and modeling approach, Univ. Libre de Bruxelles, *Ph.D. Thesis*, 153 pp., unpublished.
- Khazendar A., Tison J.-L., Stenni B., Dini M., Bondesan A., **2001**, Significant marine-ice accumulation in the ablation zone beneath an Antarctic ice shelf, *Journal of Glaciology*, 47 (158) : 359-367.
- King E.C., **1994**, Observation of a rift in the Ronne Ice Shelf, Antarctica, *J. Glaciol.*, 40 (134): 187-189.
- Kipfstuhl J., **1991**, Zur entstehung von unterwassereis und das wachstum und die energiebilanz des meereises in der Akta Bucht, Antarktis. On the formation of underwater ice and the growth and energy budget of the sea ice in Atka Bay, Antarctica. *Ber. Polarforsch.*, 85.
- Lange M.A., **1988**, Basic properties of Antarctic sea ice as revealed by textural analysis of ice cores, *Annals of Glaciology*, 10: 95-101.
- Lewis E.L. and Perkin R.G., **1986**, Ice pumps and their rates, *J. Geophys. Res.*, 91: 11.756 -11.762.
- Lorrain R., Tison J.-L., Bondesan A., Ronveaux D., Meneghel M., **1997**, Preliminary results from 60 shallow cores and from one 45-m deep marine ice core at Hells Gate Ice Shelf, Victoria Land, Antarctica, *Terra Antarctica Reports*, 1: 19-24.
- MacAyeal D.R., **1984**, Thermohaline circulation below the Ross Ice Shelf : a consequence of tidally induced vertical mixing and basal melting, *J. Geophys. Res.*, 89: 597-606.



- Mac Ayeal D.R., **1993a**, A low-order model of growth/purge oscillations of the Laurentide Ice Sheet, *Paleoceanography*, 8, 767-773.
- Mac Ayeal D.R., **1993b**, Binge/purge oscillations of the Laurentide Ice Sheet as a cause of the North Atlantic's Heinrich events, *Paleoceanography*, 8, 775-784.
- MacAyeal D.R., Rignot E., Hulbe C.L., **1998**, Ice-shelf dynamics near the front of the Filchner-Ronne Ice Shelf, Antarctica, revealed by SAR interferometry: model/interferogram comparison, *J. Glaciol.*, 44 (147), 419-428.
- Manzoni M., **2000**, *La natura dell'Antartide*, Springer-Verlag Italia, Milano, 346 pp.
- Martin S. and Kauffman P., **1981**, A field and laboratory study of wave damping by grease ice, *Journal of Glaciology*, 27: 283-313.
- Moore J.C., Reid A.P., Kipfstuhl J., **1994**, Microstructure and electrical properties of marine ice and its relationship to meteoric ice and sea ice, *J. Geophys. Res.*, 99 (C3): 5171-5180.
- Morgan V.I., **1972**, Oxygen Isotope Evidence for Bottom Freezing on the Amery Ice Shelf, *Nature*, 238: 393-394.
- Nicholls K.W., **1997**, Predicted reduction in basal melt rates of an Antarctic ice shelf in a warmer climate, *Nature*, 388, 460-462.
- Oerlemans J., **1982a**, Response of the Antarctic ice sheet to a climatic warming: a model study, *J. Climat.*, 2, 1-11.
- Oerlemans J., **1982b**, A model of the Antarctic ice sheet, *Nature*, 297, 550-553.
- Oerter H., Kipfstuhl J., Determann J., Miller H., Wagenbach D., Minikin A., Graf W., **1992**, Evidence for basal marine ice in the Filchner-Ronne Ice Shelf, *Nature*, 358: 399-401.
- Oerter H., Eicken H., Kipfstuhl J., Miller H., Graf W., **1994**, Comparison between ice core B13 and B15, *Filchner-Ronne Ice Shelf Programme (FRISP) Report n°7* (1994) - AWI - Bremerhaven, pp. 29-36.
- Orheim O., **1986**, Glaciological research on Riiser-Larsenisen and nearby ice-shelves in Antarctica, *Norsk Polarinstitutt Skrifter*, 187: 5-22.
- Paterson W.S.B., **1994**, *The physics of Glaciers*, 480 pp., Elsevier Science Ltd., Oxford.
- Petit J., Jouzel J., Raynaud D., Barkov N., Barnola J.M., Basile I., Bender M., Chappellaz J., Davis M., Delaygue G., Delmotte M., Kotlyakov V., Legrand M., Lipenkov V., Lorius C., Pépin L., Ritz C., Saltzman E., Stievenard M., **1999**, Climate and atmospheric history of the past 420,000 years from the Vostok ice core, Antarctica, *Nature*, 399, 429-436.
- Philberth K. and Federer B., **1971**, On the temperature profile and age profile in the central part of old ice sheets, *J. Glaciol.*, 10, 3-14.
- Potter J.R. and Paren J.G., **1985**, Interaction between ice shelf and ocean in George VI Sound, Antarctica, in *Oceanology of the Antarctic Continental Shelf*, edited by J. S.S., pp. 35-58, A.G.U., Antarctic Research Series.



- Reimnitz E., Kempema E.W., Weber W.S., Clayton J.R., Payne J.R., **1990**, Suspended-matter scavenging by rising frazil ice as observed in tank experiments, in Ackley, S.F. & Weeks, W.F. eds., *Sea ice properties and processes*, CRREL Monograph, 90-1: 97-100.
- Richardson C., **1976**, Phase relationships in sea ice as a function of temperature, *Journal of Glaciology*, 17, 507-519.
- Rignot E. and MacAyeal D.R., **1998**, Ice-shelf dynamics near the front of the Filchner-Ronne Ice Shelf, Antarctica, revealed by SAR interferometry, *J. Glaciol.*, 44 (147): 405-418.
- Robin G.d.Q., **1955**, Ice movement and temperature distribution in glaciers and ice sheets, *J. Glaciol.*, 2, 523-532.
- Robin G.d.Q., **1979**, Formation, flow, and disintegration of ice shelves, *J. Glaciol.*, 24, 259-271.
- Ronveaux, D., **1992**, The dynamics of a small antarctic ice shelf as indicated by an ice composition study, Univ. Libre de Bruxelles, *Ph.D. Thesis*, 391 pp., unpublished.
- Schlosser P., Bayer R., Foldvik A., Gammelsrød T., Rohardt G., Munnich K.O., **1990**, Oxygen 18 and Helium as Tracers of Ice Shelf Water and Water/Ice Interaction in the Weddel Sea, *J. Geophys. Res.*, 95 (C3): 3253-3263.
- Scourse J.D., Hall I.R., McCave I.N., Young J.R., Sugdon C., **2000**, The origin of Heinrich layers: evidence from H<sub>2</sub> for European precursor events, *Earth and Planetary Science Letters*, 182 (2): 187-195.
- Seattle Workshop, **1985**, Glaciers, Ice Sheets, and Sea Level: Effects of a CO<sub>2</sub>-Induced Climatic Change (Report of a Workshop Held in Seattle, Washington, 13-15 September 1984), *Polar Board Research publication*.
- Seidensticker R.G., **1972**, Partitioning of HCl in the water-ice system, *J. Chem. Res.*, 56, 2853-2857.
- Serikov M.I., **1963**, Structure of Antarctic sea ice, *Information Bulletin of the Soviet Antarctic Expedition*, 4 (5), 265-266.
- Shabtaie S. and Bentley C.R., **1982**, Tabular icebergs: implications from geophysical studies of ice shelves, *Journal of Glaciology*, 28 (100): 413-430.
- Souchez R., Khazendar, A., Ronveaux, D. and Tison, J.-L., **1998**, Freezing at grounding line in East Antarctica: Possible implications for sediment export efficiency, *Annals of Glaciology*, 27: 316-320.
- Souchez R. and Jouzel J., **1984**, On the isotopic composition in  $\delta D$  and  $\delta^{18}O$  of water and ice during freezing, *Journal of Glaciology*, 30 (106): 369-372.
- Souchez R., Lemmens M., Lorrain R., Jouzel J., Sugden D., **1990**, Influence of hydroxyl-bearing minerals on the isotopic composition of the ice from the basal zone of an ice-sheet, *Nature*, 345 (6272): 244-246.
- Souchez R. and Lorrain R., **1991**, Ice composition and glacier dynamics, Springer Series in the Physical Environment, *Springer Verlag*, Heidelberg, New-York, 207 pp.



- Souchez R., Meneghel M., Tison J.-L., Lorrain R., Ronveaux D., Baroni C., Lozej A., Tabacco I., Jouzel J., **1991**, Ice composition evidence of marine ice transfer along the bottom of a small Antarctic ice shelf. *Geophys. Res. Lett.*, 18, 849-852.
- Souchez R., Petit J.-R., Tison J.-L., Jouzel J., Verbeke V., **2000**, Ice formation in subglacial lake Vostok, Central Antarctica, *Earth and Planetary Science Letters*, 181: 529-538.
- Souchez R., Tison J.-L., Jouzel J., **1987**, Freezing rate determination by the isotopic composition of the ice, *Geophysical Research Letters*, 4 (6): 599-602.
- Souchez R., Tison J.-L., Jouzel J., **1988**, Deuterium concentration and growth rate of Antarctic first-year sea ice, *Geophysical Research Letters*, 15 (12): 1385-1388.
- Souchez R., Tison J.-L., Lorrain R., Fléhoc C., Stiévenard M., Jouzel J., Maggi V., **1995**, Investigating processes of marine ice formation in a floating tongue by a high resolution isotopic study. *Journal of Geophysical Research*, vol.100, n°C4, p.7019-7025.
- Thorsteinsson, T., Waddington, E.D., Taylor, K.C., Alley, R.B. and Blankenship, D.D., **1999**, Strain-rate enhancement at Dye 3, Greenland, *J. Glaciol.*, 45 (150), 338-345.
- Thyssen F., **1988**, Special aspects of the central parts of Filchner-Ronne Ice Shelf, Antarctica, *Annals of Glaciology*, 11: 173-179.
- Thyssen F., Bombosch A., Sandhäger H., **1993**, Elevation, ice thickness and structure mark maps of the central part of the Filchner-Ronne Ice Shelf, Antarctica, *Polarforschung*, 62 (1): 17-26.
- Tison J.-L., Barbante C., Bondesan A., Lorrain R., Capra A., **1997b**, Ice shelf/Ocean interactions at the front of Hells Gate Ice Shelf (Terra Nova Bay, Antarctica), *Terra Antarctica Reports*, 1: 29-32.
- Tison J.-L., Bondesan A., Delisle G., Lozej A., Merlanti F., Janssens L., **1997a**, A dynamical approach to explain ice structures and complex morainic genesis on a partially grounded ice shelf (Hells Gate Ice Shelf - Victoria Land, Antarctica), *Terra Antarctica Reports*, 1: 33-37.
- Tison J.-L., Khazendar A., Roulin E., **2001**, A two-phase approach to the simulation of the combined isotope/salinity signal of marine ice, *Journal of Geophysical Research*, 106 (C12) : 31387-31401.
- Tison J.-L., Lorrain R., Bouzette A., Dini M., Bondesan A., Stiévenard M., **1998**, Linking landfast sea ice variability to marine ice accretion at Hells Gate Ice Shelf, Ross Sea, in Antarctic Research Series, "Antarctic Sea Ice Physical Processes, Interactions and Variability", Ed. M. O. Jeffries, AGU, Washington, 74: 375-407.
- Tison J.-L., Morris E.M., Souchez R., Jouzel J., **1991**, Stratigraphy, stable isotopes and salinity in multiyear sea ice from the Rift area, South George VI Ice Shelf. *Journal of Glaciology*, 37 (127): 357-367.
- Tison J.-L., Ronveaux D., Lorrain R.D., **1993**, Low salinity frazil ice generation at the base of a small antarctic ice shelf, *Antarctic Science*, 5 (3): 309-322.
- Wakahama G., **1974**, Structures and textures of the Amery Ice Shelf, Wilkes Ice Cap and Cape Folger, Antarctica, in Japanese Science Foundation, ed. *Physical and chemical studies of ice from glaciers and ice sheets*, Tokyo, Japanese Science Foundation, 99-108. [In Japanese]



- Warren S.G., Roesler C.S., Morgan V.I., Brandt R.E., Goodwin I.D., Allison I., **1993**, Green icebergs formed by freezing of organic-rich seawater to the base of Antarctic ice shelves, *J. Geophys. Res.*, 98 (C4), 6921-6928.
- Weeks W.F. and Ackley S.F., **1986**, The growth, structure, and properties of sea ice, in *The Geophysics of Sea Ice*, edited by N. Untersteiner, pp. 9-164, NATO ASI Series : Physics, 146, Plenum Press, New York.
- Weertman J., **1968**, Comparison between measured and theoretical temperature profiles of the Camp Century, Greenland, borehole, *J. Geophys. Res.*, 73: 2691-2700.
- White K.D., **1991**, Determining the intrinsic permeability of frazil ice - Part 1. Laboratory investigations, *CRREL Report*, 91-23: 15 pp.
- Williams M.J.M., Warner R.C., Budd W.F., **1998**, The effect of ocean warming on melting and ocean circulation under the Amery Ice Shelf, East Antarctica, *Annals of Glaciology*, 27: 75-80.
- Wilson C.J.L. and Zhang Y., **1994**, Comparison between experiment and computer modelling of plane strain simple shear ice deformation, *J. Glaciol.*, 40 (134): 46-55.
- Wilson C.J.L., Burg J.P., Mitchell J.C., **1986**, The origin of kinks in polycrystalline ice, *Tectonophysics*, 127 (1-2): 27-48.
- Worner G., Viereck L., Hertogen J., Niephaus H., **1989**, The Mount Melbourne volcanic field (Victoria Land, Antarctica) II, *Geochemistry and magma genesis. Geol. Jb.*, E 38: 395-433.
- Wüest A. and Carmack E., **2000**, A priori estimates of mixing and circulation in the hard-to-reach water body of Lake Vostok, *Ocean Model.*, 2: 29-49.
- Zotikov I.A., **1986**, *The thermophysics of glaciers*, Reidel, Dordrecht, 275pp.
- Zotikov I.A., Zagorodnov V.S., Raikovsky J.V., **1980**, Core drilling through the Ross Ice Shelf (Antarctica) confirmed basal freezing, *Science*, 207 (4438): 1463-1465.